IAEA-TECDOC-709

Fuel failure in normal operation of water reactors: experience, mechanisms and management

Proceedings of a Technical Committee Meeting held in Dimitrovgrad, Russian Federation, 26–29 May 1992

INTERNATIONAL ATOMIC ENERGY AGENCY IAEA

June 1993

The IAEA does not normally maintain stocks of reports in this series. However, microfiche copies of these reports can be obtained from

INIS Clearinghouse
International Atomic Energy Agency
Wagramerstrasse 5
P.O. Box 100
A-1400 Vienna, Austria

Orders should be accompanied by prepayment of Austrian Schillings 100,— in the form of a cheque or in the form of IAEA microfiche service coupons which may be ordered separately from the INIS Clearinghouse.

FUEL FAILURE IN NORMAL OPERATION OF WATER REACTORS:
EXPERIENCE, MECHANISMS AND MANAGEMENT
IAEA, VIENNA, 1993
IAEA-TECDOC-709
ISSN 1011–4289

Printed by the IAEA in Austria
June 1993

FOREWORD

The Technical Committee Meeting on Fuel Failure in Normal Operation of Water Reactors: Experience, Mechanisms and Management was convened by the International Atomic Energy Agency upon a proposal of the International Working Group on Water Reactor Fuel Performance and Technology (IWGFPT).

The meeting focused on reviewing the present knowledge of the causes and mechanisms of fuel failure and discussed the methods for detecting failure and management of failed fuel during and after operation. A previous IAEA meeting on this topic was held in Chalk River, Canada, in 1979.

At the invitation of the Government of Russia, the meeting was held in Dimitrovgrad and organized by the IAEA and the Research Institute of Atomic Reactors in Dimitrovgrad.

About 50 specialists from 13 countries attended the meeting and 25 papers were presented in five sessions. A poster session was organized where 12 Russian papers were presented and discussed. Working Groups composed of the session chairmen and authors of papers prepared the summary of each session with conclusions and recommendations for future work.

The fuel for water cooled reactors has become a highly standardized and reliable industrial product over the past years. Nevertheless, requirements for the fuel are still increasing with respect to burnup, neutron economy, thermohydraulics and thermal efficiency of the nuclear power plant. Advanced and improved fuel utilization in commercial LWRs, such as higher burnup, load following operating mode, MOX fuel and extended fuel cycle periods, requires special attention on reliable designs and higher quality fuel fabrication, as well as larger thermal margins for flexible operating capability.

The knowledge about fuel failure today is spread over many countries and to some extent differs for the various types of water reactors, such as BWRs, PWRs, WWERs. RBMKs and HWRs.

The meeting has been useful in reviewing and discussing the status of fuel failure problems for water reactors and in identifying directions where further work would be valuable.

EDITORIAL NOTE

In preparing this material for the press, staff of the International Atomic Energy Agency have mounted and paginated the original manuscripts as submitted by the authors and given some attention to the presentation.

The views expressed in the papers, the statements made and the general style adopted are the responsibility of the named authors. The views do not necessarily reflect those of the governments of the Member States or organizations under whose auspices the manuscripts were produced.

The use in this book of particular designations of countries or territories does not imply any judgement by the publisher, the IAEA, as to the legal status of such countries or territories, of their authorities and institutions or of the delimitation of their boundaries.

The mention of specific companies or of their products or brand names does not imply any endorsement or recommendation on the part of the IAEA.

Authors are themselves responsible for obtaining the necessary permission to reproduce copyright material from other sources.

Throughout the text names of Member States are retained as they were when the text was compiled.

CONTENTS

Summary of the Technical Committee Meeting 7

GENERAL OVERVIEW OF PRESENT STATUS OF EXPERIENCE (Session I)

A review of recent LWR fuel failures 17
A. Strasser, D. Sunderland
VVER fuel operation under normal conditions and analysis of damage causes 26
Yu.K. Bibilashvili, A.I. Belosokhov, V.P. Velyukhanov, A.G. Ioltukhovskij, A.I. Kushmanov, G.L. Lunin, V.D. Onufriev, Yu.V. Pimenov, V.N. Proselkov, D.A. Chirov
Operating experience of RBMK fuel under normal conditions and analysis of its damage causes 39
V.G. Aden, B.A. Vorontsov, V.V. Kalinin, G.S. Krivoshein, V.A. Nikolaev, V.V. Noskov, A.V. Robot'ko, A.N. Ryabov
FRAGEMA fuel reliability: From detection of fuel failures to the feedback on design and fabrication 46
A. Dumont
SIEMENS KWU experience with LWR fuel: Failure evaluation, mechanisms and remedies ... 50
R. von Jan
ABB Atom fuel failure — An overview 57
L. Lundholm, B. Grapengiesser, D. Schrire, L. Hallstadius

DETECTION AND MONITORING OF FUEL FAILURES (Session II)

Correlation between fission product activity in PWR primary water and characteristics of defects in fuel cladding 67
C. Leuthrot, A. Brissaud, A. Harrer
Experience with the Fission Products Monitoring System in Japanese reactors 72
K. Ono
A review of fuel performance and fission product release studies for defected fuel elements .. 79
B.J. Lewis, R.D. MacDonald, N.V. Ivanoff, F.C. Inglesias
Application of the PES–PEPA expert system at the Dukovany nuclear power plant 100
F. Pazdera, M. Valach, O. Bárta, L. Novák, V. Štech
Data on leaking fuel assemblies in LWRs operated in the former USSR 106
K.P. Dubrovin, N.L. Fatieva, V.P. Smirnov
Failed fuel monitoring at nuclear power plants with RBMK reactors: Operating parameters, requirements and decision making criteria 113
I.V. Zhukov

CAUSES AND MECHANISMS FOR FUEL FAILURE AND DAMAGE (Session III)

Overview of defect mechanisms in CANDU fuel 121
T.J. Carter, A.M. Manzer
Fuel failure at Hamaoka Unit 1 128
Y. Hayashi, T. Matsumoto, M. Kuzushima, T. Muramoto, T. Okubo
Westinghouse fuel performance experience 133
H.W. Wilson, R.S. Miller, H. Kunishi
Evaluation of debris fretting failures and preventive methods 138
A. Strasser, J. Gingold

MANAGEMENT OF FAILED FUEL (Session IV)

Management of failed fuel during operation: French policy and experience 147
P. Bournay
Features of operating a VVER reactor core containing leaking fuel rods 152
V.P. Velyukhanov, L.M. Voronin, A.G. Ioltukhovskij, A.I. Kanatov, V.K. Chistyakova
Experience with defect fuel at the Kernkraftwerk Leibstadt; detection, inspection, handling and management 156
S. Lundberg

Debris induced fuel failures on uranium and MOX fuel in Beznau I 168
H. Bay, D. Boulanger, P. Deramaix, H. Bairiot

SPECIFIC EXPERIMENTAL APPROACHES (Session V)

Mixed oxide fuel in defective experimental rod Edithmox 1: Irradiation results and metallographic PIE 179
D. Parrat, Y. Musante, A. Brissaud
Studies in the R2 test reactor of secondary damage formation in LWR fuel rods with simulated defects 184
H. Mogard, M. Grounes, H. Tomani, G. Lysell
Experimental study on the WWER fuel behavior in research reactors and shielded hot cells .. 192
A.F. Grachev, V.B. Ivanov, V.V. Konyashov, V.P. Smirnov
Search for ways of reducing VVER fuel damage by optimizing design and operating conditions 205
Yu.K. Bibilashvili, A.V. Medvedev, V.V. Novikov, V.D. Onufriev, I.N. Vasilchenko, E.D. Demin, G.L. Lunin, V.N. Proselkov, A.F. Grachev, V.A. Kuprienko, A.G. Ioltukhovskij
Study on stress corrosion cracking of fuel cladding tube 211
Y.H. Kang, W.S. Ryu, K.S. Rheem, S.H. Kim

POSTER SESSION

Experimental investigation of out-reactor methods of failed fuel detection 217
V.P. Elizarov, V.V. Konyashov, A.M. Krasnov
Geometry variety of VVER fuel rods 219
B.A. Kanashov, V.I. Kuzmin, G.D. Lyadov, V.S. Polenok, A.V. Smirnov, V.P. Smirnov, A.V. Sukhikh
Measurement methods of gas fission products quantity under fuel element claddings by means of deep cooling 225
A.V. Sukhikh, E.P. Klochkov
Investigations of radioactive fission product release from fuel elements with initial cladding defects during operation of the VK-50 reactor 228
V.P. Elizarov, V.V. Konyashov, A.M. Krasnov
Method for calculating fission product release from the fuel cladding gap of a failed fuel element to the coolant 233
V.V. Konyashov, A.M Krasnov
Some results of post-irradiation investigations of VVER-1000 unsealed fuel assembly 238
K.P. Dubrovin, A.V. Sukhikh, V.I. Kuzmin, A.V. Mestnikov, A.V. Smirnov, V.P. Smirnov
Results of post-reactor investigations of VVER-1000 untight fuel assembly 240
K.P. Dubrovin, A.V. Sukhikh, V.I. Kuzmin, A.V. Smirnov, V.P. Smirnov
Effect of inner surface preliminary oxidation on stress corrosion cracking susceptibility of Zr-1%Nb tubing 246
Yu.K. Bibilashvili, Yu.N. Dolgov, V.V. Novikov, A.P. Gryazev
Mechanism of fuel cladding failure in PCI 255
V.V. Novikov
Analysis of trends in fuel rod depressurization and determination of 'gas leak' and 'pellet–water interaction' type failures using radiation monitoring techniques of fuel rod leak tightness 263
E.A. Panov, Yu.M. Shestakov, V.N. Miglo
Operation and radiation monitoring of water cooled reactors with faulty fuel rods 272
Yu.M. Shestakov, E.A. Panov
Influence of water chemistry regimes on fuel cladding failure in LWRs 282
V.G. Kritskij

List of Participants 286

SUMMARY OF THE TECHNICAL COMMITTEE MEETING

This meeting was organized within the IAEA programme on Reactor Fuel Technology and Performance and was hosted by the Research Institute of Atomic Reactors in Dimitrovgrad, Russia. This institute comprises a number of research and prototype reactors, hot and radiochemistry laboratories, fuel fabrication facilities, and is one of the largest nuclear research and experimental nuclear centers in Russia and Europe. Scientific visits were organized during the meeting which provided the opportunity of getting to know the facilities and approaches to the studies.

The papers were presented in five sessions:

- General Overview of Present Status of Experience
- Detection and Monitoring of Fuel Failures
- Causes and Mechanisms for Fuel Failure and Damage
- Management of Failed Fuel
- Specific Experimental Approaches.

A significant number of the presentations gave overviews of fuel failure over a substantial period of time (5 to 7 years). Data presented in these overviews showed that in spite of the increasing demands placed upon fuels in LWRs during recent years, such as higher burnups, load-following, increased cycle periods and more extensive use of MOX fuels, the rate of fuel failures continued to fall. The reduction in failure rates underlines the effectiveness of the countermeasures that have been taken so far. Nevertheless, further progress towards the ideal aim of zero defects will not be reached easily. Even though failure rates have been reduced significantly, the failure modes characteristic of the different reactor systems persist. To overcome the remaining barriers in the approach towards a zero fuel failure rate in power reactors, the cross-fertilization of ideas promoted by the IAEA through its ongoing programmes in international collaboration and information exchange will be of benefit to all concerned.

Session I. General Overview of Present Status of Experience

Summary

In the first paper a review of USA defect fuel experience was presented. It pointed out that the margin to economic performance was smaller in most cases than the margin to a licensed safety limit. It gave typical cost comparisons for two degrees of leakers – large and small. The failure causes were divided into 3 groups, those releasing activity to the coolant, those likely to release activity and those not releasing activity (but still regarded as failures such as excessive rod growth).

Earlier large scale defects for pellet–cladding interaction (PCI) had been effectively remedied by imposing operating restrictions, the introduction of Zr-liner cladding, the introduction of 9×9 and 10×10 fuel array or a combination of these.

In spite of a reduction in failure rates over the last decade, those residual failures that still occur in BWRs can be divided into two categories those due to unknown causes (including unspecified manufacturing defects) and some debris failures. CILC (crud induced localized corrosion) failures have been brought under control. In the USA, as in Europe, debris induced fretting has now been recognized as the major cause of failure in PWRs, which is being countered by the introduction of debris filters on the inlet nozzles. All in all, the aim is still to

achieve a zero defect rate and continued investigation of failure causes will help to come as close as possible to this goal.

The next paper dealt with failures in Russian type reactors WWER-440 and WWER-1000. The nuclear safety regulations aim to limit defective rods to 0.2% for release of fission gases and to <0.02% for defects with 'fuel–coolant contact'. This is a factor of 5 below any safety concerns. For WWER reactors fuel have operated successfully to 4–5 cycles (48 MW·d/kg U) with integrity better than 0.007%.

In WWER-1000 reactors, higher numbers of leaking defects occurred; 3.7% of all discharged fuel elements had as a rule one or more leaking rods. After introduction of a new 3 cycle rod design, these rates were reduced. Causes of failures were analysed as being due to inadvertent departure from operating limits and debris induced failures which included the presence of organic impurities in the coolant. Measures which led to improved reliability included better control of the manufacturing process by automation, higher control of operating limits and (unspecified) design changes. Post-irradiation examination (PIE) is being carried out on some defective rods in order to better determine failure causes.

The second Russian paper dealt with the reliability of RBMK fuel under normal operation. Here, the failure rates are significantly higher than in the WWER plants and an extensive programme of analysis, PIE and instrumented tests is under way, which is leading to improvements in design, fabrication and operation. Increased automation of the fabrication process – reducing human error, changes in rod designs (chamfered pellets, annular pellets, closer tolerances, He pressurization) as well as more control over the operating requirements (restriction of the on-line refuelling mode to prevent local overpower transients) are being introduced resulting in failure rates of 0.02% (the ratio of defective fuel rods to all rods discharged) for the RBMK 1500. In future, the introduction of liner cladding and getters in the fuel rod will further reduce the likelihood of failure.

In the French paper techniques for coolant activity analysis (MORGANE model) and on-site facilities for detection of leaking fuel assemblies and rods (on-line and in-cell sipping test, ultrasonic test) and for determination of fuel failure causes were described. As in the USA, 70% of the PWR defects are debris related, 10% grid fretting and only some 7% are fabrication defects. For the latter, more automated fabrication processes and filters against debris-related failures are also being introduced. With these remedies a leaking fuel rate near to 5×10^{-6} rods per cycle is expected. FRAGEMA intends to intensify leaking fuel rod investigations in order to continuously improve the fuel reliability. In France, severe secondary hydriding has been seen in defective rods with high powers (hydride blisters and large longitudinal cracks).

In the German paper experience with PWRs and BWRs was described. Unlike in the USA, fuel failures in BWRs were still dominated by PCI for the 50% of currently operating fuel without barrier claddings. This could be attributed to a special phenomenon of pellet chipping and was mitigated by changes in pellet shape and fabrication procedures. The US CILC experience was not repeated in Germany thanks to early measures to control copper ingress via the feedwater, after the effect had been documented in the USA. In PWRs, debris-fretting was the principal cause of failure. Overall the failure rates had been reduced to low levels thanks to the well known remedy measures. An important feature was a five point plan to evaluate and control fuel failures beginning with coolant activity monitoring, comprehensive and extensive poolside evaluations, failure analyses, experience feedback and follow-up monitoring.

Failure rate (failed/total inserted) for ABB-Atom(Sweden) fuel rods since 1979 is 6×10^{-5} from all causes and $<2 \times 10^{-5}$ neglecting known debris and other non-fuel related causes. As

in Germany, the Swedish policy is to identify all fuel failure mechanisms and determine failure rate improvements. The Xe-133 leakage rate is the preferred monitoring indicator although other isotopes give additional information. Anticipated leakers are determined before shutdown by flux tilting methods but inspection and repair is done off the critical path after the reactor returns to operation. Hot cell examinations are also performed where necessary.

Swedish experience with large secondary failures has been mixed one large release followed a major secondary failure of a Zr-line/sponge cladding but a second failure of a Sn-alloy liner rod was more benign. In both cases debris fretting was the primary cause.

High debris-fretting failure rates in BWRs in Sweden can be attributed to specific plants.

Conclusions

- Rates of defective fuel continue to reduce thanks to various remedy measures and are approaching values below 10^{-5} per cycle.

- Defective fuel mitigation, control and management meets an economic need of the plant operators, and contributes to dose reduction but is not a safety issue.

- There is general agreement on the main causes of defective fuel remaining in LWRs – apart from some specific individual plant or fabrication related causes. These are debris-fretting and unknown, possibly fabrication related, failures. CILC (BWRs) and PCI now seem generally under control, although not completely eliminated.

- There remains a low percentage of LWR failures due to fabrication defects which are being reduced by increased automation and control of the fabrication and inspection procedures.

- In WWER reactors and more particularly in the RBMK, the defect rates are being reduced by more restrictive operating controls, tighter control over fabrication and design changes.

- All programmes seeking a zero defect rate need to have the support of a comprehensive and complete monitoring, inspection and failure analysis regime. Examples of these are the German, Swedish and French programmes and the measures being undertaken for the RBMK and WWER fuel.

Recommendations

- Continued monitoring, analysis and inspection of failed fuel is needed to approach a zero defect rate.

- With the solution of the debris-related defects by the addition of filters, fabrication defects may become the principle cause of failure and this should be matched by appropriate control of fabrication processes and materials. Automatic measures in fabrication may become increasingly important, reducing human error.

Session II. Detection and Monitoring of Fuel Failures

Summary

The papers presented in this session describe a number of different station specific installations. The following experience described in this session vary each reactor, depending on the reactor design:

- A comprehensive review of fuel performance in CANDU reactors and of the mechanisms of defective fuel rod deterioration.

- The corrections used in the French PWRs in order to predict the characteristics of cladding failures from fission product activities in the primary coolant and also to calculate the fission product activities when defected assemblies are refuelled.

- Fission Product Monitoring System, FPMS, installed in several Japanese PWRs and its ability to provide real-time analyses for continuous primary coolant activity estimates.

- The PES-PEPA Expert System used at the Dukovany reactor (CSFR) to predict the probability of fuel damage and data showing a comparison between calculated and measured data. The method offers a possibility to decrease the released gaseous activity.

- A statistical compilation of data on the quantity of leaking fuel assemblies in all operating NPP units in the former USSR, indicating that modern WWER reactor fuel has a satisfactory reliability, while the RMBK fuel failure rate needs to be decreased.

- A procedure for estimating the number of failed fuel rods and prediction of their radioactivity discharge during NPP with RBMK reactor operation. The procedure is based on the FFM data base and I-131 and Xe-133 activities in the coolant.

Session III. Causes and Mechanisms for Fuel Failure and Damage

Summary

In the Canadian paper it was stated that fuel fabrication performance has been excellent in CANDU with over 99.9% of loaded bundles performing well. Of the small number of defected bundles, the defect mechanisms are: fabrication defects constituting incomplete end closure results and porous end-plug bar-stock material. Smaller numbers of defects have been attributed to fretting and vibration damage which is a reactor operating problem.The existence of occasional excursion in fabrication quality along with the decreased tolerance for iodine in the primary coolant from licensing requirements emphasize the need for continued surveillance of fuel performance.

In the second paper, the Japanese experience was presented. Fuel failure at Hamaoka Unit-1 in 1990 originated from corrosion whose cause was inferred to be the combined effect or irregular water chemistry and use of more corrosion susceptible cladding material.

In the next cycle, the reactor was operated using new and irradiated sound fuel under strong control of coolant chemistry. The cycle was successfully completed without any fuel failure or accelerated corrosion. The use of important methods of condensate demineralizer resin treatment and modified clad fabrication methods for improved corrosion resistance are recommended.

The first USA paper indicated that field examinations of leaking fuel rods have shown that debris induced fretting is the dominant leakage cause in Westinghouse fuel, accounting for approximately 70% of observed leakers. Corrective actions have taken the form of control measures taken by the utilities to keep debris out of the system and a design change to the fuel assembly. These steps have significantly reduced debris related defects. To reach zero defects, additional changes are needed.

In the second USA paper specific items discussed included the source of debris, the types of debris and the interaction of debris with fuel assemblies. Differences in failure histories between BWRs and PWRs were discussed. Preventive measures include improved maintenance procedures to preclude introduction of debris into the primary system and fuel assembly design features that make the fuel cladding less likely to be exposed to through-wall fretting. The improved maintenance procedure guidelines and the fuel design modifications were discussed as well. Continued improvements in operating and maintenance programmes are recommended to preclude debris, and the effectiveness of debris resistant fuel designs should be monitored.

Session IV. Management of Failed Fuel

Summary

The first paper of this session gave information on the French policy and experience in the management of failed fuel during operation. Fore more than ten years and with the agreement of the French safety authorities, Electricité de France (EDF) has been applying a policy of reinserting the leaking assemblies which fulfill the following criteria:

- equivalent diameter of the defects less than 35 μm, measured by 'quantitative sipping test';
- no solid fission products in liquid samples during sipping test;
- limited impact of reloaded leaking assemblies, at the beginning of cycle activity level: D.E. I-131 less than 1.1 GBq/t.

Under these conditions the feedback from EDF experience is the following:

- no significant release of UO_2 and no important enhancement of activity in the coolant with up to three times reinsertion of a leaker;
- acceptable stability of equivalent diameter for reloaded defects.

This policy induces significant savings in time and money, does not impact the units availability, and is compatible with safety requirements.

The operational experience of WWER fuel is considered in a Russian paper and high reliability of this fuel has been confirmed. In particular, the number of leaking fuel rods does not exceed 0.01% for both WWER-400 and WWER-1000. The main failure causes are: deviation from design operational conditions, debris, and deposition of organic compounds on fuel rod and assembly surfaces.

Emphasis is given to justify the possibility of reinsertion of fuel with microleaks for one more fuel cycle. The successful experience with 20 reinserted leakers has been accumulated at three WWER-1000 units.

The paper on the Leibstadt NPP experience (Switzerland) gave an overview of all failures having occurred in the reactor (BWR). In addition to the failed fuel operating history,

the methods for detection and identification of defective rods as well as the operation with failures and post-irradiation handling were described. Results of non-destructive examinations of the failed rods were presented. Special emphasis was given to the two severe barrier failures in the reactor. These failures resulted in large activity release and severe cladding deterioration, probably caused by delayed hydrogen cracking. The main conclusion of the paper is the need to understand the mechanism for these types of failures. Such understanding can then lead to means to avoid or mitigate the effects and consequences. These consequences can be severe, especially in reactors with high power densities.

The Belgian paper dealt with details of debris induced failures in U and MOX fuel in the Beznau-1 plant. During operation of Beznau-1 from July 1989 to May 1990, primary circuit activity indicated that several fuel assemblies developed leaks. The core was constituted during that cycle of 24 MOX fuel assemblies and 97 U assemblies. Sipping identified five leaking fuel assemblies: one U fuel assembly in its first irradiation cycle, two U assemblies in the second irradiation cycle, one U fuel assembly in its third irradiation cycle and one MOX fuel assembly (with two failed rods) in its second irradiation cycle. On-site examination during repair indicated that the failures were caused by debris induced fretting resulting subsequently in secondary hydriding failures. Coolant activity measurements were analysed to correlate primary and secondary failures for U fuel and MOX fuel.

The following can be concluded:

- the failure is not affected by the type of fuel;
- the lag time between primary defect detection and secondary defect occurrence ranges between 200 and 300 days, similar for both UO_2 and MOX fuel;
- the activity releases were not worse for the MOX failures than for U failures.

Conclusions

- The French experience with controlled reinsertion of leaking fuel up to three times showed that this policy did not result in severe fuel rod degradation and is acceptable in PWRs from a radiological point of view. A similar conclusion can be drawn from the WWER experience.

- A second failure of a barrier fuel rod in Leibstadt showed similarly severe degradation (60 cm split) as the first one, reported earlier, and provided additional evidence that the probability of such degradation is higher for pure Zr barrier cladding than for non-barrier cladding. The resulting uranium washout can cause significant problems in plant maintenance during operation and with higher than desired exposure during outages.

  From the Beznau-1 experience it can be concluded that the behaviour of leaking MOX fuel is very similar to that of leaking U fuel with respect to both, development of secondary damage of the fuel rod and the overall activity release to the coolant. However, it is possible to distinguish U and MOX failures by some differences in release behaviour by careful analysis of the activities.

Recommendations

- The mechanisms of degradation for different types of claddings (standard, sponge, Zr-barrier and other remedies) in BWRs and the influence of parameters (power, burnup, gap, etc.) should be further investigated.

- The increasing experience with reinserted leakers in PWRs should be further analysed with respect to the validity of the well known Locke curve for secondary damage as a function of heat flux and time of operation.

- The sources of organic contamination of primary circuit in WWERs should be analysed with the purpose of preventing contamination of the fuel.

Session V. Specific Experimental Approaches

Summary

The aim of the paper from France was to study the behaviour of a defective MOX rod under irradiation and especially the release rate of fission products. An experimental fresh rod has been irradiated in a research loop between 8 and 27 kW/m. Fission product release was measured by on-line gamma spectrometry and sampling.The results of this experiment show a release rate of fission product comparable to that obtained with uranium oxide. Metallographic analyses performed after irradiation show an appreciable evolution of microstructure, with fission gas precipitation bubbles, due to fuel oxidation under water vapour conditions. This evolution is not usually observable on UO_2.To cover the entire range of MOX fuel operating conditions in PWRs, these results should be validated for higher burnup levels and long irradiation time.

The Swedish paper discusses a new test method for comparative investigations of the defected fuel degradation process under simulated primary defect conditions, describes the first explorations tests performed and a proposed international fuel R&D project, the Defect Fuel Degradation Experiment (DEFEX).

The first Russian paper starts with a review of the requirements for an experimental programme on failed fuel. The paper covers the methodology which should be adopted for both the experimental tests and the post test examinations, including the full range of measurements to be carried out for the detection and characterization of defects. The rest of the paper is a description of the test facilities at the Research Institute of Atomic Reactors , Dimitrovgrad. These consist of the MIR reactor with several pressurized loop facilities, the SM-2 reactor, also with loop facilities, and both with the capability for transient experiments, the VK-50 reactor and loop, and hot cells.

The second Russian paper recognizes the important goal of achieving high reliability of power reactor fuel. It identifies a number of failure mechanisms and describes areas of the design of WWER-440 and 1000 fuel assemblies to improve performance and reliability, and emphasizes the need to optimize operating conditions. The paper includes a detailed discussion of the need to optimize operating conditions for a daily load follow schedule in order to minimize clad stress. The paper then considers the importance of controlling cladding defects during manufacture in order to improve the resistance of the cladding to SCC. A maximum defect depth of 35 μm is recommended.

In the final paper in this session from the Republic of Korea, iodine induced stress corrosion cracking (ISCC) tests on Zircaloy-4 tubes were undertaken using an internal pressurization method to elucidate the mechanisms and to find out remedies of pellet–cladding interaction failure. FeI_2, AlI_3 and CsOH acted as active corrosive agents for SCC of Zircaloy-4, showing almost the same critical concentration as that of I_2. CsI and CsC1, however, were found to be not active for SCC. The fabrication process of each company brought out certain characteristics of mechanical and metallurgical properties of Zircaloy-4 tubes, resulting in a different ISCC behaviour. Tubes with high toughness in burst tests and with textures in a

radial direction showed a good behaviour of ISCC. In addition, the welding process made ISCC resistance decrease up to 40% as compared with that of tubes as-received. An annealing treatment and/or a modified welding process showed some effects to recover the ISCC resistance, but welded parts still had a potential risk of ISCC. Graphite or siloxane was found to be so effective to improve the ISCC resistance which seemed to be acting as a getter of iodine and/or a lubricant, or a protective barrier, respectively.

Conclusions

- Experimental measurements of gaseous and airborne fission product release from a mixed oxide fresh fuel stack under steady state conditions show them to be similar to those for UO_2 fuel at least at low burnup. Significant evolution of the MOX microstructure was observed, which was not visible in early UO_2 life.

- An experimental technique has been developed and tested to simulate a primary defect and to allow the development of secondary defects under irradiation to be studied.

- Significant work is being carried out to improve the SCC behaviour of cladding materials. The Russians are proposing a maximum initial defect size of 35 μm for WWER-440 and 1000 cladding.

- A programme of the Republic of Korea on iodine induced SCC for CANDU type Zircaloy-4 tubes investigates at the effect of several variables including welding, and graphite and siloxane coatings.

- Programmes to reduce or eliminate failures from debris or fretting are already well advanced within the commercial arena.

Recommendations

- Post-irradiation investigations aimed at finding an explanation of defective fuel occurrences in power reactors should be pursued with the aim of reducing 'unknown causes'.

- Special irradiation experiments, aimed at a most complete understanding of the mechanisms of degradation of defective fuel , are desirable. It is recommended to initiate a special task aimed at reviewing the state of the art and recommending whether further experimental activities are needed in this area.

- The interest in understanding the basic mechanisms of stress corrosion cracking should continue.

- More experimental data are needed to study the behaviour of a defective MOX rod under irradiation, especially at higher burnup and for a larger irradiation time.

Next page(s) left blank

GENERAL OVERVIEW OF PRESENT STATUS OF EXPERIENCE

(Session I)

Chairmen

F. PAZDERA
Czechoslovakia

R.W. STRATTON
Switzerland

A REVIEW OF RECENT LWR FUEL FAILURES

A STRASSER, D SUNDERLAND
The S M Stoller Corporation,
Pleasantville, N Y ,
United States of America

Abstract

Increasing attention to improved fuel reliability has reduced the failure rates significantly A review of the failure rates and failure causes in the past approximately four years, are given in this paper, including those resulting from

- design
- manufacturing
- corrosion
- pellet-clad interactions
- hydraulic vibration
- debris fretting

and combinations of these effects Corrective actions instituted to minimize or eliminate these problems are described The discussion of the failure causes addresses those observed in all nuclear nations, but the failure statistics are limited to U S plants

1 0 INTRODUCTION

The reliability of nuclear fuel is not only of importance to the health and safety of the public but has a substantial impact on protecting the large financial investment in the fuel and plant Fuel reliability has a significant effect on the economics of the nuclear fuel cycle, and in fact, fuel failures have a greater impact on plant economics than on the licensed margin to safe operation

A large spectrum of cost parameters is impacted by fuel failures, and these are listed below

- Cost components associated with identification and discharge or repair of failed fuel

  - Direct inspection costs
    Incremental exposure cost-inspection
    Energy loss costs inspection (if on the critical path)
    Direct reconstitution costs
    Incremental exposure costs - reconstitution
    Energy loss costs reconstitution (if on the critical path)
    Spent fuel storage expansion costs - premature discharge
    Cost of energy loss - premature discharge
    Cost of calculation of new fuel loading scheme
    Off optimum fuel loading cost
    Cause of failure determination

- Cost components associated with continued operation of failed fuel

  Energy Losses

  - Derate
  - Ramp rate limitations
  - Increased demineralizer flow
  - Containment entry delay
  - Premature shutdown

  - Increased operating costs due to higher coolant activity levels and greater contamination of plant systems and components

  - *Incremental O&M costs - radwaste systems*
  - Incremental O&M costs - plants
  - Incremental non-specific exposure costs
  - Loss of personnel efficiency

The sensitivity of plant operating costs to these parameters varies greatly, but the largest effect on cost is due to events that result in loss of energy production, such as derates or shutdowns required due to high coolant activity Examples of such cost evaluations are shown in Figures 1 and 2

These analyses made by a US utility show the comparison of costs for continued operation with failed fuel versus inspection and repair following the cycle in which the failures occurred, as a function of the number of failed rods These analyses are very sensitive to the input assumptions and are utility specific

The analysis in Figure 1 for small leakers indicates that reconstitution is the more economic route at greater than 10 failed rods For large leakers, resulting in power losses due to derates or shutdowns, the economics favor reconstitution at 1 or 2 failed rods as shown in Figure 2

A computer model COFFEC, has been developed by the Stoller Corporation for the Electric Power Research Institute to evaluate the cost of failures [1]

The term failure is generally used to indicate a clad breach that releases radioactive fission products into the coolant However, failure" should be considered in the broader concept of any event that results in the need to repair or remove a fuel assembly from the core By that definition, one can have failures that are unlikely to release activity and failures that do not leak yet, but are likely to do so with continued service Failure types are shown by these categories in Table I and discussed subsequently

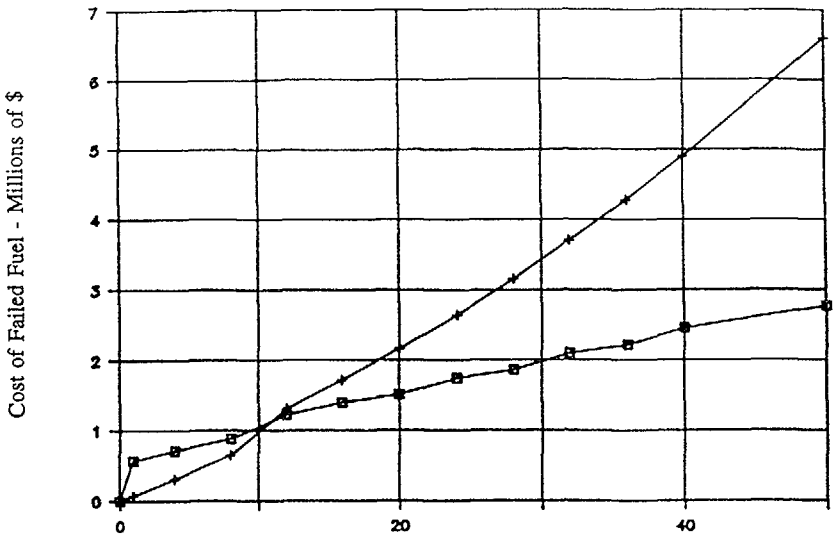

Figure 1: FUEL FAILURE COST ANALYSIS (SMALL LEAKERS)

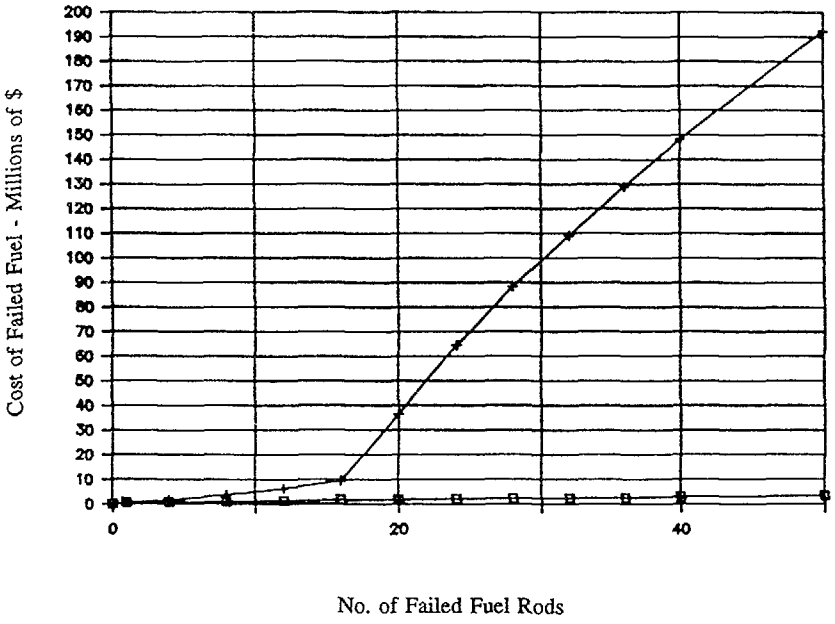

Figure 2: FUEL FAILURE COST ANALYSES (LARGE LEAKERS)

2.0 FAILURES THAT RELEASE ACTIVITY

2.1 CLAD FRETTING BY DEBRIS

One of the largest failure causes has been the fretting of fuel clad by debris in the coolant. This type of failure occurred in some early nuclear plants but then did not recur again until about 10 years ago, when plant maintenance operations increased. A detailed discussion of debris failures is given in another paper at this conference [2].

2.2 SPACER-CLAD FRETTING

Fuel failures can result from vibration of the fuel rod against the spacer tabs and springs, if the rod is improperly supported. The fretting can result from flow induced vibrations during operation or, less frequently, during shipping of poorly supported fuel rods. The resulting fretting is easy to identify visually.

Clad failures due to this mechanism have occurred almost entirely in PWRs and have been increasing recently. They have been traced primarily to inadequate control of spacer fabrication and the assembly of fuel rods into the spacers. Some of the remedies for the problem have been increasingly automated fabrication, inspection and assembly procedures. The pulling, instead of pushing, the fuel rods into the assembly, is one example of improved fabrication techniques.

2.3 PELLET-CLAD INTERACTIONS (PCI)

Primary Failures

Failures due to PCI have occurred almost exclusively in BWRs. The cause of a large number of failures about 15-20 years ago, the frequency of these failures has decreased significantly due to a series of increasingly effective remedies, including:

- Operating recommendations that required clad pre-conditioning and limited the rate of rise to power
- Zirconium liner, or barrier, on the clad inner diameter to increase the margin to failure
- Subdivision of 8x8 fuel array to 9x9 and 10x10 to reduce the linear heat generation rate (LHGR)
- Combination of the barrier with the 9x9 and 10x10 fuel.

Recent primary PCI failures were limited to non-barrier fuel rods in BWRs and with the overwhelming use of the PCI remedies listed above, this failure cause should diminish further.

TABLE I. IDENTIFIED FAILURE CAUSES

	BASIC CAUSE					
	FUEL		PLANT			
	Design	Fabrication	Design	Operation	Maintenance
Failures that Release Activity					
• Clad fretting by debris		X	X	X	X
• Spacer to clad fretting			X	X	
• Pellet clad interaction (PCI)	X			X	
• Clad corrosion		X	X	X	
• Corrosion of end plug welds		X			X
• Leaking end plugs		X			
• Primary hydriding of clad		X			
• Baffle jetting			X		
Failures Likely to Release Activity					
• Fuel rod vibration	X		X	X	
• Damaged spacers	X			X	
• Collapsed clad		X			
Failures Unlikely to Release Activity					
• Broken screws and bolts	X	X			
• Broken holddown screws	X	X			
• Guide tube wear			X		
• Limits of differental Zircaloy growth	X	X			

Secondary Failures

Nearly 100 barrier clad rods have failed due to CILC corrosion manufacturing defects in the clad, and debris in the coolant Several of these, however, had long PCI type cracks in the cladding and their failure was associated with unusually high off gas activity [3] [4]

Most of these types of failures are believed to be due to secondary PCI The primary failure cause is non-PCI, such as debris fretting, and this permits coolant inside the fuel rod The failure can then propagate in the following steps

- Fuel oxidizes and expands
- Lower thermal conductivity uranium oxide increases fuel temperatures
- Steam blanketing increases fuel temperatures further and the fuel expands further
- The clad is stressed sufficiently for a secondary PCI failure
- High off-gas results from the high fuel temperatures
- Secondary hydriding under certain fuel rod internal chemistry conditions can propagate the crack

In the event an undetected defect exists in the clad, a primary PCI defect could occur if stresses exceed the failure threshold at the defect location This is true of any type of clad of course

Key questions at this time are whether any differences exist between the barrier and non-barrier rod behavior, and what failure mechanism causes the extensive fuel oxidation and crack propagation in a few instances and not in most of the others A current project is evaluating these failure mechanisms at the authors' organization

2 4 CLAD CORROSION

BWR

The recent corrosion failures in BWRs have been due to crud induced localized corrosion (CILC) The CILC mechanism is very complex in detail, but generally is a function of the water chemistry, the characteristics of the clad, and the power history of the fuel rod Each one of these factors is subject to a very large number of variables and most importantly changes in variables as a function of time

The development of CILC requires three items at a minimum Cu in the coolant, corrosion susceptible cladding and heat flux Dense, high Cu crud deposits with circumferential cracks and steam blanketing raise the clad temperature to a level at which oxidation through the clad occurs relatively rapidly

The condensers are the principal source of Cu, but plants with deep bed demineralizers remove the Cu adequately prior to the feedwater system Powder demineralizers do not have as good a Cu removal efficiency and the CILC failures have been restricted to plants with this type of equipment Chemical intrusions other than Cu can also induce CILC corrosion Cladding with poor nodular corrosion resistance appears to be most susceptible to CILC

The CILC failures from the condenser Cu source were first observed in 1978 in General Electric plants using General Electric fuel Significant efforts on the part of the utilities to improve coolant chemistry control and on the part of General Electric to improve clad quality gradually reduced this problem Several utilities with CILC susceptible plants have replaced their Cu alloy condenser tubes with titanium alloys which, in combination with the above, is expected to eliminate the CILC problem

PWR

The corrosion failures in PWRs are in two categories

- Corrosion by high temperature coolant in high efficiency PWRs
- Corrosion susceptible, fabrication related Zircaloy metallurgical structure

High coolant exit temperature plants in the range of 320°C to 330°C have been coming into service over the past decade, and the performance of Zircaloy 4 under these demanding conditions is not as good as at lower temperatures

Standard Zircaloy 4 operates satisfactorily at the high temperatures up to the former, standard burnup goals of 33-36 GWD/MT batch average burnups The first plant to operate at high temperature conditions, KKGosgen in Switzerland, found that above about 40 GWD/MT and heat flux of 68 w/cm^2 the oxidation rate was sufficiently high to fail the clad before the scheduled discharge of the fuel

Remedies are under intensive development by the fuel vendors and utility organizations Improved corrosion resistant materials include modified Zircaloy 4 compositions, new zirconium base alloys and "duplex" clad consisting of a Zircaloy 4 base with a thin corrosion resistant zirconium alloy outside liner

In a few isolated instances, Zircaloy 4 has suffered severe corrosion at normal coolant temperatures and heat fluxes These were traced to fabrication methods, specifically thermal treatments that decreased the annealing parameter below about 10^{18} hrs (Q/R = 40,000°K), a point of steep transition to increased uniform corrosion susceptibility in PWRs

The remedy for this situation is increased attention to process control during thermal treatment so that the desired annealing parameter range is maintained The search for a good quality control test to identify corrosion susceptible material is still in progress

2 5 CORROSION OF END PLUG WELDS

The tungsten inert gas welding process for Zircaloy end plugs is conducted either in a vacuum or inert atmosphere Poor control of the gas purity, or leaky vacuum chambers, have led to nitrogen contamination of the welds and the resulting corrosion was sufficient in some cases to breach the weld integrity

The remedy is clearly better atmosphere control and monitoring by impurity sensors

2 6 LEAKING END PLUGS

The fabrication of zirconium alloy end plugs can result in defects that provide a leakage path for gases through the end plug

Chloride stringers present in some zirconium products are one such defect that could be aligned longitudinally along the axis of the bar stock by the fabrication process Cold swaging of barstock has also resulted in internal voids at the ends of the bars, by deforming the outer surfaces more than the center and eventually leaving central voids

Failures of this type have been rare The remedies are clearly careful fabrication process control and inspection Ultrasonic inspection of finished barstock is necessary

2 7 PRIMARY HYDRIDING OF CLAD

Hydriding of zirconium alloy clad by residual moisture in the pellets, once the cause of extensive fuel failures, is all but eliminated today Occasional failures due to lapses in quality control still occur, but rarely

The tendency to ever higher UO_2 pellet densities, up to 96% of theoretical, have decreased pellet open porosity and increased pellet resistance to moisture absorption significantly This, combined with good degassing procedures, hydrogen analysis methods and even a hydrogen getter in the plenum of General Electric BWR fuel rods, have been an effective remedy

2 8 BAFFLE JETTING

Cross flow (jetting) from inadequately sealed core baffle joints has caused vibration, fretting, and some fuel rod failures in the peripheral row of the assemblies This condition has existed in Siemens, Westinghouse and Westinghouse licensee PWRs The phenomenon was first observed in the Zorita plant in Spain some years ago and has since affected many assemblies that resided in core peripheral positions near baffle joints with crossflow Failures occurred regardless of the design or origin of the fuel

Sealing the baffle joints by peening did not prove to be entirely satisfactory An interim, but successful remedy was applied by Siemens Nuclear Power, and consisted of a steel clip applied to the outside of the fuel rod at the point of jet impingement to restrain the rods from vibration The ultimate remedy is to reduce the pressure drop across the baffle, by rerouting flow in the baffle region Several plants have made this rather extensive change

3 0 FAILURES LIKELY TO RELEASE ACTIVITY

3 1 FUEL ROD VIBRATION

Extensive ex-reactor hydraulic loop testing of fuel assemblies by the vendors generally precludes in-reactor failures Shortcomings in process control or quality control can result in vibration and fuel rod-spacer fretting Similarly, minor design changes or changes in hydraulic conditions can also result in fuel rod vibration These are significantly less frequent and have not normally resulted in clad breach because they were discovered in time

However, the Oskarshamn 1 BWR [5] experienced fretting of the lower end cap of the spacer capture rod due to hydraulic vibrations The cause was traced to excessive pressure fluctuations caused by lateral oscillations of a water jet at the inlet orifice directly below the lower tie plate The changes that induced the vibration included increased core flow for uprated plant operation, re orificing of the flow, and the extension of the end cap length

The remedies included modifying the orifice and the end plug shape, but the plant uprating was maintained

3 2 DAMAGED SPACERS

Handling of fuel assemblies during receipt, inspection core loading and unloading can result in interference, or "hang-up" between spacers in PWRs Interference between adjacent PWR fuel assemblies during fuel shuffling has occurred with essentially every PWR fuel vendor's fuel, resulting in damaged grid spacers The tight clearances between PWR assemblies, combined with potential changes in assembly straightness during irradiation, require careful handling

To minimize "hang-up" between assemblies, PWR vendors have chamfered the corners of their spacers, and minimized protrusions that could cause interference Improved fuel shuffling techniques and better monitoring of handling tools have all contributed to minimize this problem Nevertheless, even though less frequent, the problem is a reoccurring one

3 3 COLLAPSED CLAD

Fuel densification combined with no fuel rod prepressurization resulted in clad collapse of PWR fuel rods in the early 1970s Occasional instances of clad collapse still occur, but these are due to quality control lapses which result in the omission of one or more pellets in the fuel column The remedy is clearly good surveillance at the gamma scanning step for completed fuel rods

4 0 FAILURES UNLIKELY TO RELEASE ACTIVITY

4 1 STRESS CORROSION CRACKING OF HIGH STRENGTH COMPONENTS

The performance of the variety of high strength nickel alloys, such as Inconel 718, 800 and X-750, which are used as nuts, bolts, and springs in the fuel assembly has been less than perfect. Some failures have occurred in almost every application, primarily in PWRs but in BWRs as well In contrast, nickel alloy spacers and springs have performed without known stress corrosion failures

Stress corrosion cracking or fatigue has been the cause of essentially all the failures Typical examples are Inconel X-750 BWR channel springs and bolts [6], PWR holddown springs[7], and, most recently, the bolts that clamp the PWR holddown leaf springs

The detailed causes are a combination of excessive stress, component vibration, inadequate metallurgical structure or heat treatment, and perhaps the choice of an alloy with inadequate stress corrosion resistance The vendors have changed alloys in several cases, but more importantly modified their designs to reduce localized stress concentrations as well as improving the metallurgical treatment This author's review of nickel alloy failures indicates that each type of component has its own combination of failure causes, but that excessive stress has been an overriding failure cause, and its reduction is the most effective way to increase reliability

The cracked components have stayed in place most of the time and only occasionally have pieces of these components become debris To the authors' knowledge, there is no direct evidence that any of these have resulted in clad breach

4 2 GUIDE TUBE WEAR

Vibration of the PWR control rods has resulted in the wear of Zircaloy guide tubes at the location of the rodlet tips. The vibration is induced by hydraulic conditions to which the control rods are exposed in the upper core and upper internals These are most severe in the Combustion Engineering and Babcock and Wilcox 17x17 type (Mark C) plants Chromium plated steel sleeves have been inserted in the upper end of the guide tubes as a successful remedy to prevent wear.

Similar vibration exists in other plants, notably Westinghouse-type NSSS, however, in these, the wear is relatively slight on the guide tube but greater on the control rodlet, requiring remedies for the control rod but not the guide tube

4 3 LIMITS OF DIFFERENTIAL ZIRCALOY GROWTH

The differential growth between Zircaloy components has limited the life of fuel assemblies in the past. Redesign of the assemblies has always provided additional margin for such growth The margins decrease, however, with extended burnups, and could change as a result of changes to the assembly design or the Zircaloy fabrication procedures

The limiting conditions for the differential growth between the following components are as follows

Component	Condition	Potential Failure
• Fuel rod - assembly (upper tie plate)	Holddown spring completely compressed	Rod bow - rods in contact
	Upper end plug disengagement	Rod vibration clad fretting
• Water rod assembly (upper or lower tie plate)	Water rod disengagement	Rod vibration - clad fretting
• Channel - assembly	Uncover finger spring seal	Bypass flow - decreased CPR margin

The first two events have occurred infrequently and required repair or reconstitution of the assembly The third item has been noted but has not reached a limiting condition

The remedy is clearly a good irradiation growth data base related to the exact process used for the fabrication of the component, combined with statistical design procedures that take into account the full range of the available data

5 0 FUEL FAILURE STATISTICS

The failures discussed in this section relate only to those that breached the clad and released activity to the coolant Further, they are limited to LWRs in the USA

Developing fuel failure statistics fairly, and on a basis which makes comparison meaningful, is not an easy task The bases of the statistics developed by the authors and the assumptions which had to be made in the process, are

- The time period considered for each review is two years A snapshot in time, or a period of only one year, is potentially misleading, and tends to be unduly influenced by those cases where a fairly large number of failures occur in only a few plants Periods longer than a few years are unduly influenced by fuel of older designs fabricated by non-current methods A two year period encompasses at least one shutdown considering most plants in the US are on 18 month cycles

- The number of rods which operated during this period is not easy to determine Best estimates, rather than exact values have been used

- In PWRs, most inspections have been with UT, yielding the number of both rods and assemblies failed When no inspections were made, the number of failed rods has generally been estimated by the utility or the authors

- In BWR investigations, the number of failed bundles is often known but the number of failed rods is not The number of failed rods has been estimated based on similar occurrences

- Failed rods are often carried over from one cycle to the next. An attempt has been made not to double count such incidents

The uncertainty in the fuel statistics should be recognized, based on the need for the above listed estimates

The failure rates represent the total of the US vendors' experience The BWR vendors are General Electric and Siemens Nuclear Power The PWR vendors are ABB-Combustion Engineering, B&W Fuel Company, Siemens Nuclear Power and Westinghouse

The BWR failure rate trend is shown in Figure 3 and percent failures by cause in Figure 4 The PWR data are shown similarly in Figures 5 and 6

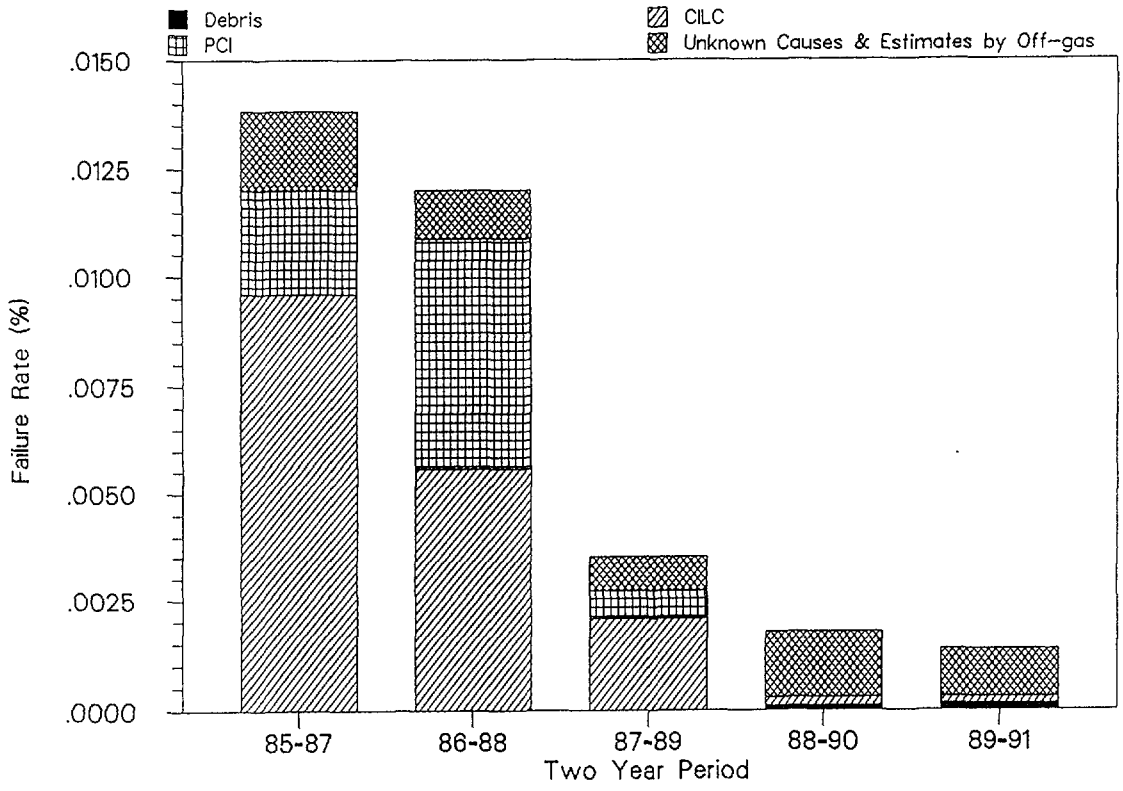

Figure 3: BWR FAILURE RATES

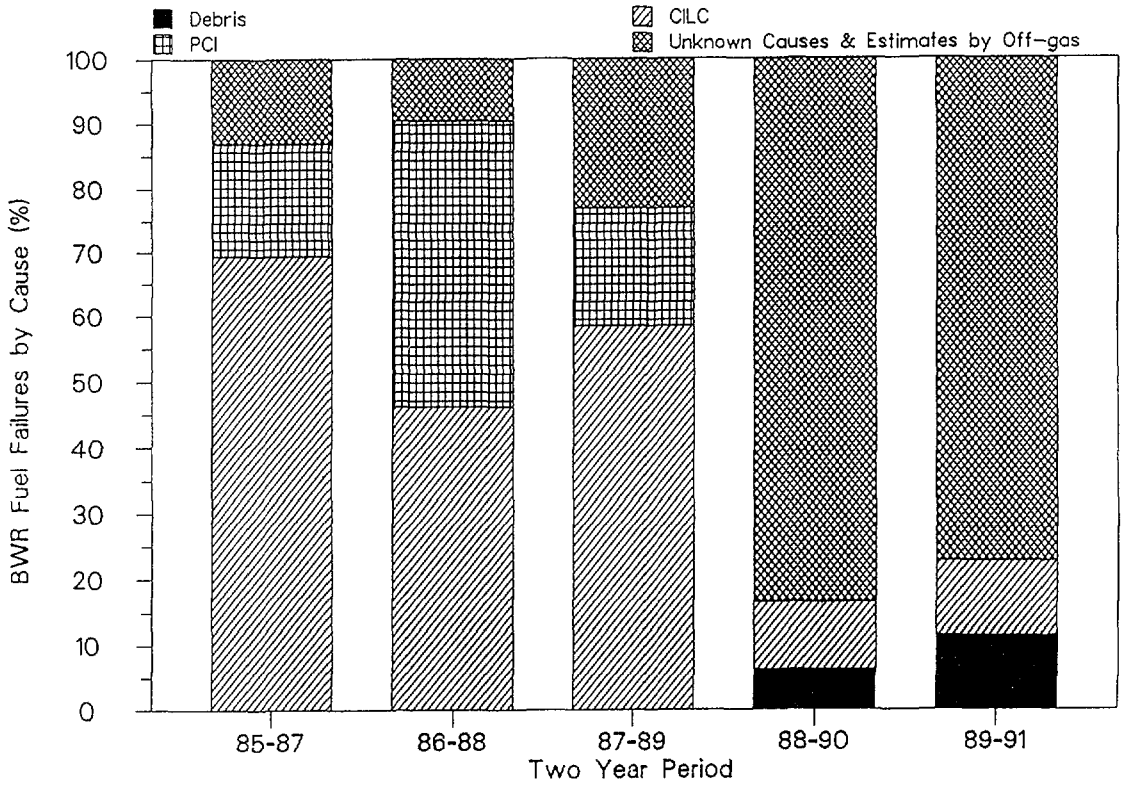

Figure 4: BWR FAILURE CAUSES

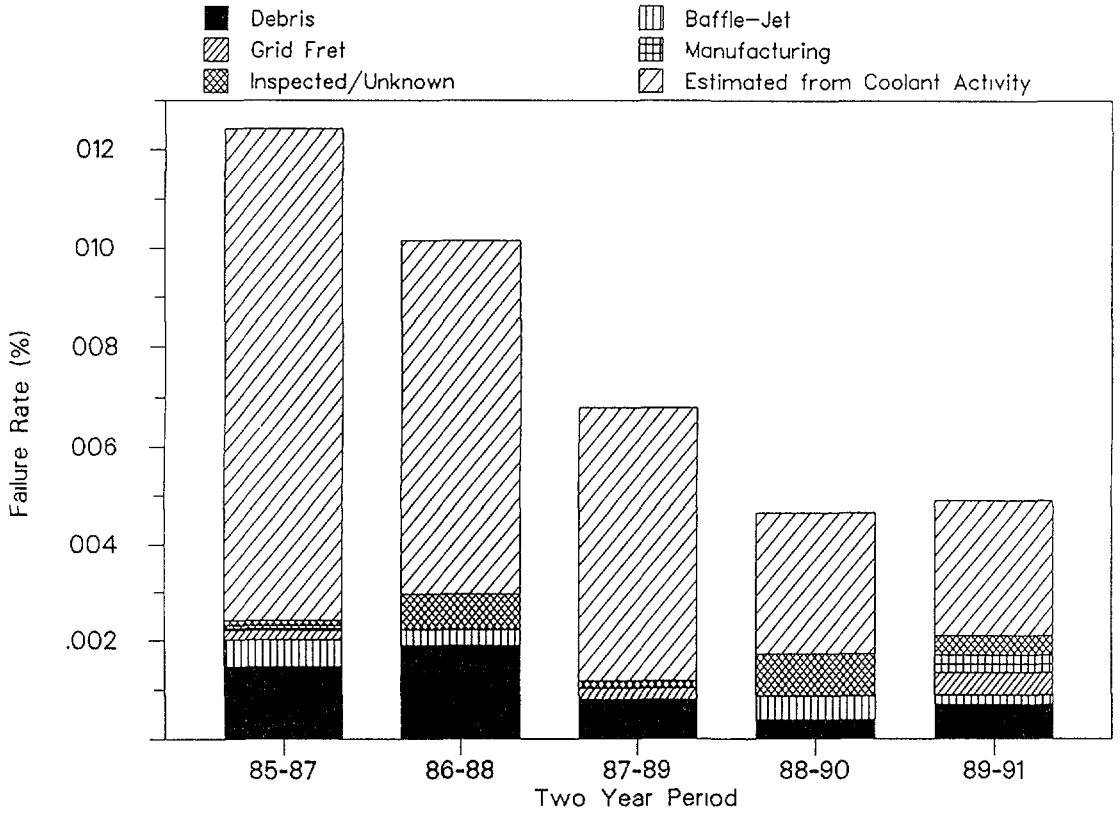

Figure 5: PWR FAILURE RATES

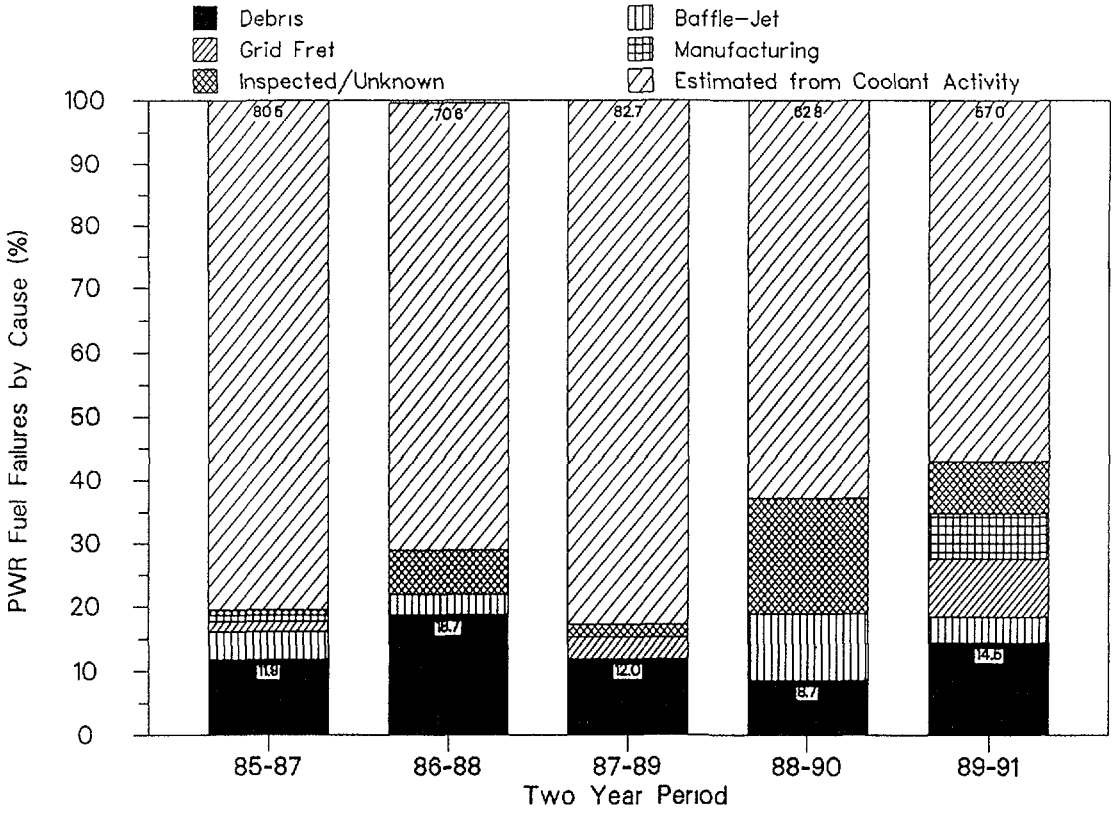

Figure 6: PWR FAILURE CAUSES

Failure causes are noted where they are sufficiently large in number to appear on the bar charts The failure causes are unknown for several inspected failures and for failures estimated from coolant or off gas activity they are clearly unknown The two categories are noted separately for the PWRs and are combined for the BWRs

The observations that can be made from the BWR Figures 3 and 4 are

- Failure rates have decreased significantly due to the elimination of PCI failures and virtual elimination of CILC failures
- A small but increasing number of debris failures have occurred recently
- The failure rates are less than in PWRs
- The number of unidentified failure causes has stayed essentially constant over the years

The observations that can be made from the PWR Figures 4 and 5 are

- Failure rates decreased significantly until about 1989 and then leveled off
- Debris failure rates have been consistently high over the period surveyed
- Grid fretting failures are increasing
- % Failures estimated from coolant activity are decreasing, indicating increased fuel inspection

The increased trend to remove all failed fuel from the core prior to startup and to strive for zero failure levels, has led to increased inspection and determination of failure causes Continued efforts in this direction will eventually eliminate many of the failure causes and reduce failures to the lowest practical level

REFERENCES

[1] R. EPSTEIN, K. SHEPPARD and A STRASSER, "COFFEC Cost of Fuel Failure Evaluation Code", EPRI NP-5458-CCML, Volume 1, (August 1988)

[2] A STRASSER, J GINGOLD, "An Evaluation of Debris Fretting Failures and Preventive Methods' This conference

[3] J DAVIES, G POTTS, "Post-Detect Behavior of Barrier Fuel" International Topical Meeting on LWR Fuel Performance Vol 1 Avignon, France April 1991

[4] A JONSSON, L HALLSTADIUS, B GRAPPENGIESSER, "Failure of A Barrier Rod in Oskarshamn 3' International Topical Meeting on LWR Fuel Performance Vol 1 Avignon France April 1991

[5] A REPARAZ, S NORDLOF, An Innovative Solution to an End Cap Fretting Problem in Oskarshamn Unit 1' International Topical Meeting on LWR Fuel Performance Vol 1 Avignon, France April 1991

[6] O BERNANDER, G VESTERLUND, 'Performance Experience of the ASEA-ATOM BWR Fuel ANS Topical meeting on Light Water Reactor Fuel Performance April 1985, Orlando, Florida DOE/NE/34/30-1

[7] D L BATY, et al , "Metallurgical Factors Affecting the Failure of Alloy X-750 Holddown Springs" International Symposium on Environmental Degradation of Materials in Nuclear Power Plants Myrtle Beach, South Carolina, August 1983

VVER FUEL OPERATION UNDER NORMAL CONDITIONS AND ANALYSIS OF DAMAGE CAUSES

Yu.K. BIBILASHVILI*, A.I. BELOSOKHOV**,
V.P. VELYUKHANOV***, A.G. IOLTUKHOVSKIJ***,
A.I. KUSHMANOV**, G.L. LUNIN+, V.D. ONUFRIEV*,
Yu.V. PIMENOV*, V.N. PROSELKOV+, D.A. CHIROV++

* Scientific Research Institute for Inorganic Materials, Moscow

** Novosibirsk Plant of Chemical Concentrates, Novosibirsk

*** Research Institute for Nuclear Power Plant Operation, Moscow

\+ I.V. Kurchatov Institute of Atomic Energy, Moscow

++ PU Machine Building Plant

Russian Federation

Abstract

Pressurized water reactors VVER-440 and VVER-1000 are and will remain the basis of the nuclear power of the CIS (Commonwealth of Independent States) and some East-European countries for the nearest future. In this connection much attention is paid to an increased utilization of nuclear fuel and NPP safety, including irradiation safety at a NPP site and off-site. One of the aspects of this job is to increase fuel element and assembly serviceability under normal operational conditions including a higher fuel burn-up.

The paper analyzes the experience gained in VVER-440 and -1000 fuel operation both in design fuel cycles and on convertion to more efficient four- and three year fuel cycles. The VVER fuel operational conditions are discussed.

The results of the fission gas activity measurements primary circuit coolant and the control of the fuel cladding tightness in a shut-down reactor were used to analyze the loss tightness by fuel elements and assemblies vs normal operation conditions and the fuel burn-up.

The data given using mainly as an example 3^{d} unit of Kola NPP with VVER-440 and 5^{th} unit of Novovoronez NPP and 1^{st} unit of Kalinin NPP with VVERs-1000 and their analysis show that the VVER fuel is highly reliable, the amount of leaky (gas) fuels (e.g. for VVER-1000 is less than 0.01% of the total number) meets the world-wide level. No increase in the amount of damaged fuels with burn-up to ~50 MW.day/kg is observed.

INTRODUCTION

Nuclear power development puts forward problems of improving nuclear and radiation safety of NPP as well as fuel element reliability. Alongside the challenge is issued to increase the efficiency of fuel utilization through extension of fuel burn-up.

To resolve the problems a number of technological, design and experimental studies are under way:

1. Design-experimental studies to validate improvements of fuel cycle (optimization of core, grid and fuel parameters, analysis of fuel cycle characteristics on switching to fuel of higher enrichment, study of fuel behaviour with FA averaged burn-up increase up to 50 MW.day/kg etc).

2. Design-methodical work to validate improvements of fuel cycle (development of computer programmes, check-up of design and operation data, improved accuracy of preparation of data on burn-up and isotope composition of discharged FAs etc).

3. Optimization of methods and algorithms of reactor power control.

4. Up-date of fuel manufacture processes (fuel parameter optimization).

5. Analysis of VVER reactor and fuel operation experience, including fuel operation conditions, burn-up, distribution of burn-up, coolant activity, results of full leak tightness control in a shut-down reactor.

6. Post-irradiation studies of spent FAs.

This paper deals with one of the important aspects - analyses of VVER-440 and -1000 fuel operation experience.

1. CHARACTERISTICS OF VVER FUEL

1a. Fuel Assemblies (FAs)

VVER-440 core has 312 (276) standard assemblies (SA) and 37 (73) FAs SUZ(the values for the design of the 3^{d} and 4^{th} units at the Novovoronezh NPP are given in the brackets). The FA wrappers are fabricated from Zr-2.5% Nb.

Hexagonal SAs with a perforated wrapper and FAs SUZ have 126 fuel rods. The mass of U in SA is ~120 kg and that of FAs SUZ is ~115 kg. The fuel column height of SA is 2420 mm, and that of the fuel element of FA SUZ is 2320 mm. Hexagonal FAs of VVER-1000 are of two types, viz., with a perforated wrapper (the Novovoronezh NPP Unit 5) and without wrapper (for all the other units of VVER-1000). Wrapped FAs contain 317 fuel elements, the number of FAs per a core is 151, those without wrappers have 312 and 163, respectively. For FAs the "key turn" dimension is 234 mm, the FA length is 4570 mm, the fuel bundle length is 3840 mm, that of the fuel column is 3530 mm, the fuel mass of an FA is 430 kg.

The fuels in FAs are separated with stainless steel Х18Н10Т spacer grids of a honeycomb type. Presently introduction of Zr- 1 % Nb spacer grids is under consideration.

1b. Fuel Rods (FRs)

VVER-440 and -1000 fuel claddings are fabricated from Zr+1% Nb. The outer cladding diameter is 9.1 mm, the inner one is ~7.7 mm.

VVER type FRs consist of cladding, enriched uranium dioxide fuel pellets, end pieces (plugs) and a hold-down device. Prior to sealing fuel elements are filled with He, the pressure of which is presently ~0.5 MPa and ~2.5 MPa in VVER-440 and -1000, respectively. As a result of experimental-design work and generalization of operation experience the fuel design and fuel and its constituent part fabrication processes were improved and meet the up-to-date requirements.

2. FABRICATION OF FUEL

At the plants of CIS fuel is produced having different enrichments with U-235, % mass, including that for VVER-440: 1.6, 2.4, 3.6, 4.4 and for VVER-1000: 1.6, 2.0, 3.0, 3.3, 3.6 and 4.4. FA can contain FRs of the same enrichment only, or two groups of FRs of two different enrichments (profiled). In this case, e.g., FRs in

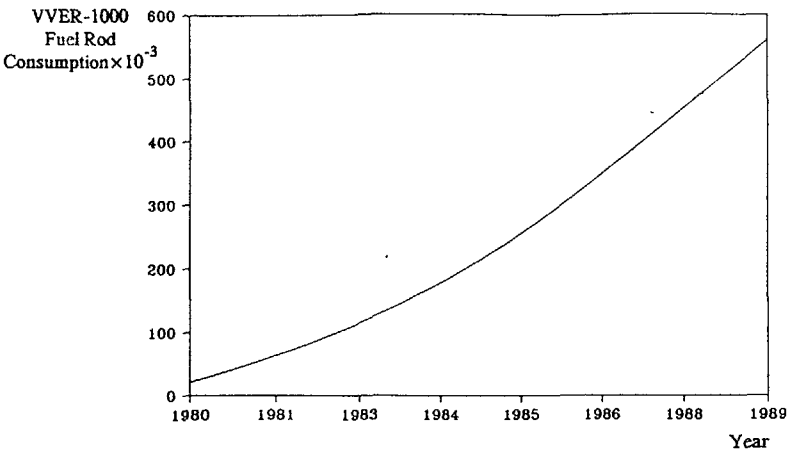

Fig. 1. Fuel Rod Consumption by NPPs with VVER-1000 Units.

the circumferential row and FRs at the angles of the subsequent row are of lower enrichment (3.6% mass U-235) and the rest in VVER-1000 fuel assembly are more enriched (4.4% mass U-235).

The industry fully meets the demands of NPP with VVER-440 and -1000. In the period from 1969 to 1989 ~49 thousand FAs or ~6.2 mln fuels were fabricated and loaded into VVER-440 in CIS and East European countries. In the period from 1980 to 1989 ~8000 FAs or ~2.5 mln fuels were fabricated and loaded into in 17 units of VVER-1000 (16 units - in CIS and one - in Bulgaria). Fig.1 shows graphically the consumption of VVER-1000 fuel elements during 1980-89.

3. MAJOR PERFORMANCE PARAMETERS AND STEADY-STATE FUEL CYCLES OF VVER-440 AND -1000

All NPPs with VVER-1000 operate under base-load conditions at load factor (LF) ~70-75%, those with VVER-440 also operate for the most part under base load conditions at the LF ~70-80%, although some experiments are under way for load follow conditions.

Initially, the fuel cycles of serial VVER-440 and -1000 were oriented to annual reloading, respectively, 1/3 and 1/2 part of a core. Presently they operate under or being transferred to conditions of reloading 1/4 and 1/3 portions of cores of VVER-440 and -1000, respectively.

The major design parameters of operation and steady-state fuel cycles of VVER-440 and -1000 are listed in table 1.

Table 1

Major Design Parameters of Operation and Steady-State Fuel Cycles of VVER-440 and -1000

Parameter \ Reactor	VVER-440	VVER-1000
Heating power, MW	1375	3000
Electric power, MW	440	1000
U load, t	42	70
Fuel fraction removed on reloading	0.33/0.25	0.5/0.33
Enrichment of make up fuel, % mass U-235	2.4-3.6/4.4	3.3/4.4
Average fuel burn-up, MW.day/kg	31/40-42	28.6/40-43
Mean heat generation rate, W/g	28.5/28.5	45.0/52.0
Life-time, eff.h	21000/28000	14000/21000
Mean linear heating, W/cm	129	167
Maximum linear heating, W/cm	325	448
Maximum temperature of cladding outer surface, °C	335	350
Coolant pressure in core, MPa	12.5	15.8

As it was mentioned above, initially the serial VVER-440 was oriented to a three year fuel cycle at the enrichment of 2.4 and 3.6% with 1/3 portion of core removed on each reloading. At the average enrichment of make-up fuel ~3.3% and with the scheme of fuel motion in the direction from circumference to centre (Out-In) all parameters of a three-year fuel cycle are realized.

Enrichment of make-up fuel of VVER-440 increased to 3.6% made it possible to reduce the number of annually reloaded FAs to 1/4 of a core without any alterations in the scheme of in-reactor fuel motion Out-In, and to attain the average burn-up of discharged fuel of 36.5 MW.day/kg. However, the efficient time of FC (between reloads) was decreased to ~6500 h.

Enrichment increased to 4.4% with four reloads of fuel per cycle allows an almost 25% increase of burn-up and an increase of fuel cycle time to ~8000 h.

The commercial operation of the first VVER-1000 (the 5th unit at the Novovoronez NPP) started in May 1980. The decision was taken to use initially fuel intended for a two-year operation. The characteristics of this fuel cycle are listed in table 1. The composition and characteristics of typical fuel loads of the first (2N-S-1, i.e., the first year of unit operation under conditions of non-stationary two-year FC), the second year (2N-S-2, i.e, the second year of a unit operation under non-stationary two-year FC) and the subsequent years (2S-usually beginning with the third year of operation the steady-state conditions of a two-year FC were reached) are tabulated in table 2. It also indicates the number of FAs after particular FC and their batch averaged discharge burn-up.

Table 2

Composition and Characteristics of Spent Fuel Loads (FL)

Number of FA / Enrichment, % mass U-235	Type of FL, unit, number of FC, end of FC, year					
	2N-S-1 Bal.3-1 1989	2N-S-2 Kal.2-2 1989	2S S-U,2-3 1989	3T Kal.1-5 1989	3N-S Zap.5-1 1990	3S Novovor. 5-9 1990
2.0	79(79)	6(6)	1(1)	0	54(54)	
3.0	42	42(42)	1(1)	7(1)	55	12
3.3	36	91(25)	149(65)	48(48)		
3.3+3.0(3.26)	6	24	12	0		
4.4				48	24	
4.4+3.6(4.23)				60(1)	30	139(50)
Batch averaged discharge burn-up after particular FC	12.76	26.1	28.8	~33.0	~11.5	42.8
Number of discharged FAs after particular FC	79	72	67	50	54	50

Notes: The following abbreviations are used:
5th unit of Novovoronezh NPP: NV5; Zaporozhie NPP - Zap.
South Ukranian NPP: S-U; Balakovo NPP - Bal.
Kalinin NPP: Kal.; Khmel'nitsk NPP - Khm.

VVER-1000 make-up fuel enrichment increased to 4.23*-4.4% resulted in reduction of annually discharged FAs to 1/3 of a core and an increase of the batch averaged discharge burn-up to 42-44 MW.day/kg (in steady-state 3 year FC - 3S in table 2). Certainly, to convert a unit that early operated in a two year mode two transient cycles

*FA averaged profiled enrichment.

(index 3T in table 2) are needed. An exception was the 5th unit at the Zaporozhie NPP, where the first and second fuel loads were constituted partially with 4.4% enriched fuel (3N, i.e., unit operated in non-stationary 3 year mode - table 2).

4. ASSESSMENT OF FA CONDITION IN OPERATING AND SHUT-DOWN REACTORS

"Nuclear Safety Regulations for NPP Reactor Units" [1] establish the following operation limits for fuel damage in VVER cores: number of defective fuels (gas leakage) must not exceed 0.2% fuel elements while that having a defect of a "fuel-coolant contact" type must be 0.02% of the whole number of fuels in a core. The NPP safe operation limit is reached when the above numbers are 5 times exceeded, i.e., 1 and 0.1% fuels, respectively, which corresponds to the coolant specific activity of 1.5×10^{-2} Ci/l iodine radionuclides [1,2]. This activity level of the primary circuit coolant has never been reached while the normal operation of units is paralleled by the activity several orders of magnitude less.

After the reactor is shut down the fuel elements are subject to inspection of fuel integrity (IFI). The need in IFI and number of FAs to be checked are determined by the activity level of the primary circuit. The control is based on measuring the leakage of fission products from leakers by analyzing I-131, Cs-134 and -137 activities in water samples of IFI facility. The measured results are used for the analysis of the statistical radionuclide distribution in all discharged FAs. All FAs are considered to be leaky if the I-131 activity in them exceeds the average value by not less than tripled squared deviation("three sigma" criterion).

5. OPERATION EXPERIENCE AND INCREASE OF VVER-440 FUEL BURN-UP

In December 1971 the commercial operation of the 3d unit of the Novovoronez NPP - the first serial VVER-440 unit - started. Presently the total number of the units in operation with VVER-440 is 26 (8 in CIS and 18 in East European countries). The VVER-440 units in operation in CIS, including the 1st and 2nd units of the Armenian NPP that are not in operation now, had operated about 130 fuel cycles by 01.01.92, i.e., about 15000 FAs had been discharged. In the main they operated in a steady-state three year mode. The fraction of leaky FAs did not exceed 1.5-1.6%, that of fuels was 0.007% [3].

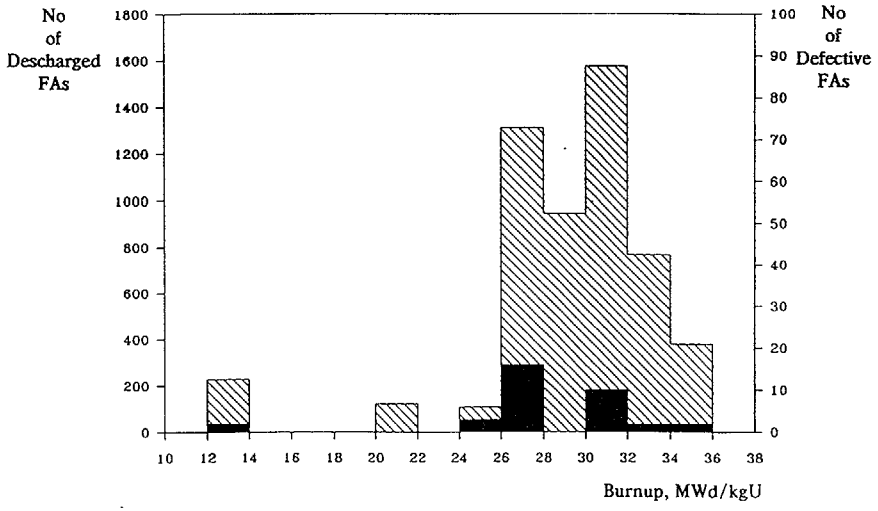

Fig. 2. Burnup Distribution of Discharged (Including Defective) VVER-440 FAs.

Fig.2 is histogramme of distribution of discharged, leakers included, FAs vs fuel burn-up . It generalizes the operation experience of the 1^{st} and 2^{nd} units at the Rovno NPP, 1^{st}-4^{th} units at the Kola NPP and 3^{d}-4^{th} units at the Novovoronez NPP during 1980-90. The total number of discharged FAs was 5429, including 35 leakers; the number of fuel cycles (years of operation) was 48. For the same group of FAs fig.3 shows distribution of leaky FAs in years per 1 GW(e) of installed capacity.

It can be seen from figs.1-2 that with an increase of fuel burn-up the fraction FAs that lost their tightness during operation is not increased. In 1986 the maximum relative number of leaky FAs per installed capacity was 3.4 1/y per 1 GW(e) at the mean value of 1.1.

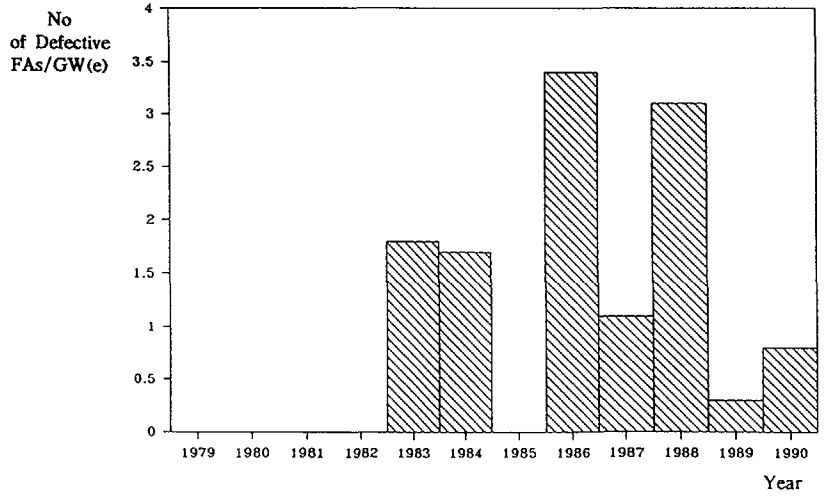

Fig. 3. Number of Defective FAs per GW(e) Installed Capacity for VVER-440.

The causes of VVER-440 FA leakage especially if a group of leaky FAs appears in a core are subject to careful study. Some of the causes are discussed in [3]. At the early stages loss of tightness by fuels was related to an increase of fuel pellet moisture content and this disadvantage was eliminated. As is shown by figs.2-3 the reliability of VVER-440 fuel elements and assemblies is assessed to be high.

As the analysis of the primary coolant activity and hot cell investigations of fuel condition show the recently found out instances of fuel leakage are likely to be due to departure from design operation conditions or other causes that are difficult to generalize because of the low extent of loss of tightness.

The high reliability of "the three year mode" fuel of VVER-440, experience in its operation in a 4 year mode [2], experimental and design work to improve fuel elements and assemblies as well as a whole complex of neutron-physics calculations of the core allowed validation of the conversion of the 3^{d} unit at the Kola NPP to a 4 year mode of operation at the 4.4% enrichment of the make-up fuel in standard FA (SA) and 3.6% mass U-235 enrichment of fuel in FA SUZ. In 1990 the work was completed, i.e., the whole core was fully made up of higher enrichment fuel assemblies. The average discharge fuel assembly burn-up was 42 MW.day/kg, the maximum one was 48 MW.day/kg.

Table 3 presents the characteristics of the FAs of the Kola NPP 3^{d} unit that were discharged during 1986-90, i.e., from the 5^{th} to 8^{th} fuel cycle, some parameters of the unit operation (the number of scrams and transients with a power change by more than 50% of $P_{nom.}$) the specific activity of iodine radionuclides in the coolant and IFI results in the shut-down reactor.

Table 3

Performance of Kola NPP 3^{d} Unit during 5-8 FC and Results of IFI

N of FC	Beginning/End	FC time, eff. days	Average discharge burn-up, MW.day/kg	Number of FA discharged	Mean enrichment of FA discharged, % U-235	Number of screens	Number of transients	I activity, total, Ci/l x10^{5}	Results of IFI	
									number of FA investigated	number of in-leak FA
5	beginning	246	28.1	90	3.30	3	4	1.4	12	0
	end							2.5		
6	beginning	336	30.1	91	3.19	2	8	0.7	12	0
	end							1.8		
7	beginning	300	34.7	88	3.50	1	7	1.2	12	0
	end							1.2		
8	beginning	370	42.0	79	4.27	0	6	0.84	12	0
	end							0.84		

During the reactor unit operation special attention was paid to the analysis of the fuel cladding condition. Table 3 tabulates the results of measurements of the primary coolant activity due to fission products (5-8 FC). The total activity of iodine isotopes varied within 0.7×10^{-5} and 2.5×10^{-5} Ci/l;as a rule, the variations were related to reactor transients (decrease and increase of power, start-up after maintenance etc). After the reactor had operated at the constant power for 4-5 days the specific fragment activity became stabilized and remained constant. Even during transients when the process of fission products release to coolant is significantly intensified there was a two order margin as compared to the established value of the specific fragment activity.

The results of the fuel tightness control in some FAs enriched to 4.4% attested their integrity.

Thus, the longer time of the FA operation and extended burn-up reached at the end of the four year cycle did not result in loss of tightness by fuel claddings.

Introduction of the four year fuel cycle improves the fuel utilization by ~12% of the design one.

To validate the switching of VVER-440 to a five year mode of operation 12 FAs of the 3^{d} unit at the Kola NPP were left in the core to operate for the fifth year (the 9th fuel cycle). This experiment pre-checked by thermal physics and neutron physics calculations was successful. The burn-up ~50 MW.day/kg was reached. To receive additional data on the 10th fuel cycle (5th year of operation) 12 more FAs were left in the core.

To-date there is positive experience in the long-term steady-state operation of the 4th unit at the Kola NPP and the 2nd unit at the Rovno NPP at the power of 107% of nominal. The core performance at the power of 107% of nominal meets the main design requirements. The specific activity of the primary circuit coolant did not significantly change which attests the high serviceability and reliability of the VVER-440 fuels [2].

The following conclusions can be drawn based on experience in the VVER-440 fuel operation:

1. Fuel elements and assemblies remain serviceable for 4-5 years of operation to reach the FA averaged burn-up ~48 MW.day/kg.

2. Maximum loss of tightness by fuels (gas leakage), does not exceed 0.007%.

3. No fuel assembly having enrichment of 4.4% mass U-235 that operated for 4-5 years did not lose its tightness.

4. No interrelation between fuel leakage and burn-up has been revealed.

5. Relatively low number of leaky VVER-440 fuel elements makes it difficult to generalize the causes of their loss of tightness, among them there is a departure from design operation conditions and others.

6. OPERATION EXPERIENCE AND EXTENSION OF VVER-1000 FUEL BURN-UP

Table 4 lists the fuel cycle characteristics of 16 VVER-1000 units, in operation in CIS during the period up to 01.01.92. It follows from the table that at the beginning of 1992 the VVER-1000 units have operated 72 fuel cycles (fuel charges) including the schedule of the first year of the non-stationary 2 year cycle - 15 FC, the 2nd year of the non-stationary 2 year cycle - 14 FC, the steady 2 year cycle - 18 FC, under transient conditions from 2 and 3 year cycle - 17 FC, in non-stationary 3 year cycle - 2 FC and steady 3 year cycle - 6 FC.

Until 01.01.92 altogether 4210 FAs have been discharged from VVER-1000 reactors; 156 FAs were acknowledged leaky based on the results of IFI, 154 of them have operated their life time and only two FAs were discharged based on the "ahead of time" criterion. Some of the reloads did not contain leaky FAs at all. The realive number

Table 4
Characteristics of VVER-1000 Fuel Cycles

Unit	Beginning	Total FC as of 01.01.92	N and type of FC; number of leaky FAs per given cycle										Number of FAs discharged in all FC	Number of leaking FAs in all FC	% of leaking FAs relative to number of FAs discharged
			1	2	3	4	5	6	7	8	9	10			
Novovoronez 5	05.80	10	2N-S-1 1	2N-S-2 2	2S 4	2S 1	3T 5	3S 0	3S 1	3S 4	3S 8	3S 1	513	27	5.26
South-Ukrainian 1	12.82	8	2N-S-1 6	2N-S-2 3	2S 3	2S 9	2S 0	2S 0	2S 0	2S 0			467	18	3.85
- " - " - 2	01.85	4	2N-S-1 5	2N-S-2 0	2S 2	3T 2							260	9	3.46
- " - " - 3	09.89	2	2N-S-1 0	2N-S-2 2									115	2	1.74
Kalinin 1	05.84	7	2N-S-1 0	2N-S-2 3	2S 3	3T 4	3T 4	3S 4	3S 2				382	20	5.24
- " - 2	12.86	4	2N-S-1 1	2N-S-2 7	2S 15	3T 0							255	23	9.02
Zaporozhie 1	12.84	5	2N-S-1 11	2N-S-2 0	2S 3	3T 2	3T 0						296	15	5.07
- " - 2	06.85	5	2N-S-1 0	2N-S-2 3	2S 1	3T 1	3T 1						279	6	2.15
- " - 3	12.86	4	2N-S-1 1	2N-S-2 1	2S 2	3T 5							236	9	3.81
- " - 4	12.87	4	2N-S-1 0	2N-S-2 0	3T 0	3T 3							205	3	1.46
- " - 5	08.89	2	3N-S 0	3N-S 0									96	0	0.00
Balakovo 1	12.85	4	2N-S-1 1	2N-S-2 1	2S 0	3T 0							272	2	0.74
- " - 2	10.87	4	2N-S-1 3	2N-S-2 1	3T 3	3T 0							247	7	2.83
- " - 3	12.88	2	2N-S-1 1	3T 0									121	1	0.83
Rovno 3	12.86	4	2N-S-1 3	2N-S-2 1	2S 1	3T 7							279	12	4.30
Khmelnitsk 1	12.87	3	2N-S-1 1	2N-S-2 1	2S 0								187	2	1.07
Total for all units		72	Total FC: 2N-S-1 -15; 2N-S-2-14; 2S-18; 3T-17; 3N-S-2; 3S-6										4210	156	3.71

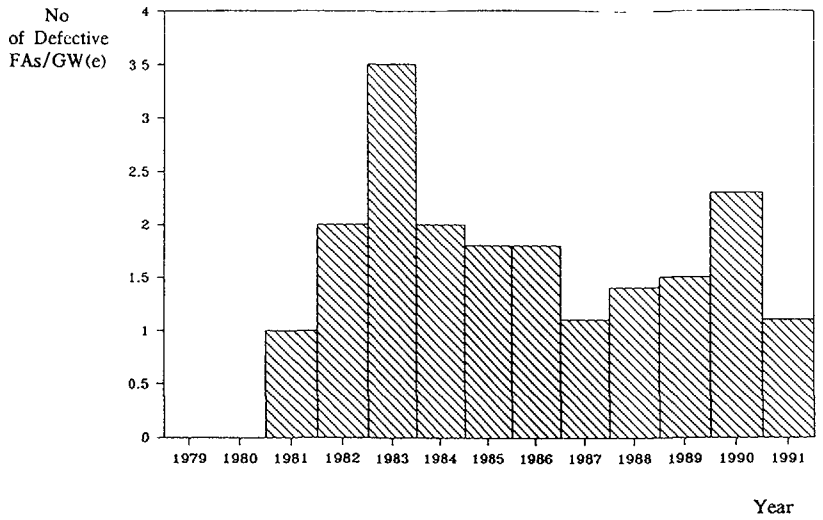

Fig. 4. Number of Defective FAs per GW(e) Installed Capacity for VVER-1000.

of leaky FAs in relation to the total number discharged was ~ 3.7%, and to the number of the loaded FAs was ~ 2.6%.

Fig.4 shows a histogram of year distribution of leaky (1) FAs per 1 GW (e) of the installed capacity. The maximum (3.6) was observed only in the fuel discharged in 1983; the average value is ~ 1.6, i.e., it is within the operation experience gained in West European countries and USA.

Fig.5 shows a histogram of fuel burn-up distribution of the number of the discharged (leakers included) VVER-1000 FAs. Of the total number (4210) of the FAs discharged before 01.01.92 a group of 2842 FAs with a large extent of leakage was taken (135 leaky FAs) in relation to the whole massive of leaky bundles (156). It can be seen that the absolute number of leaky FAs is lowered with an increase of burn-up.

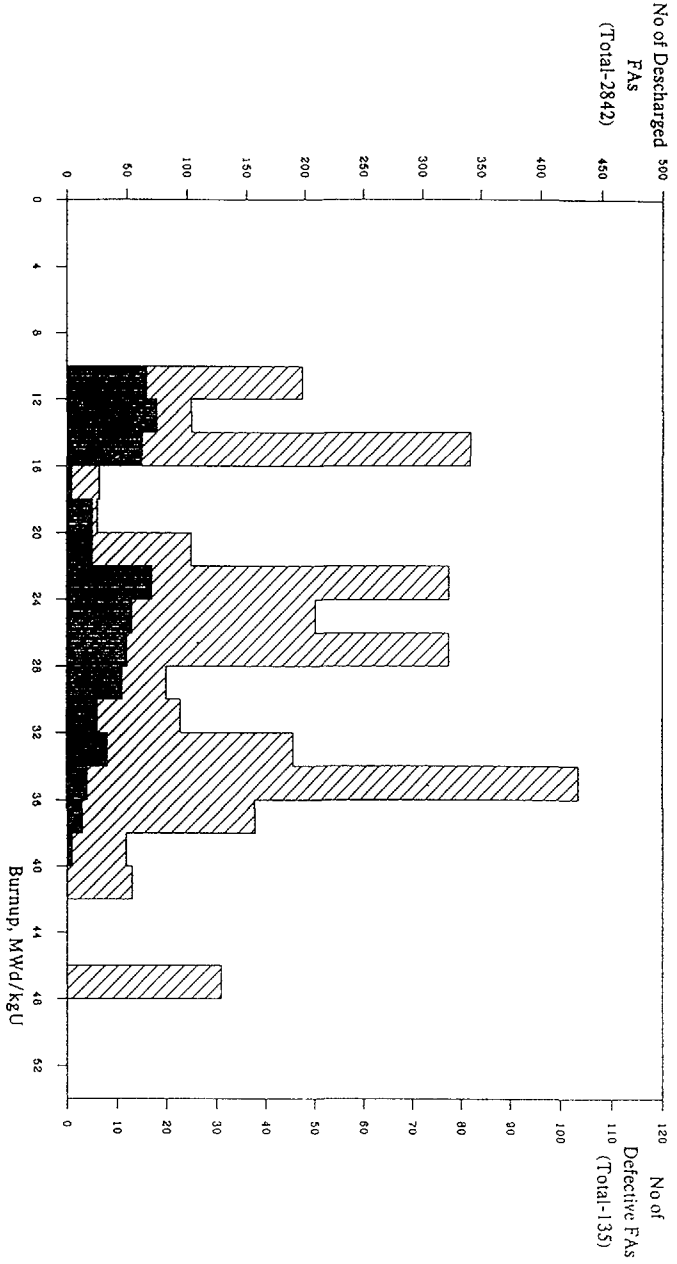

Fig. 5. Burnup Distribution of Discharged (Including Defective) VVER-1000 FAs.

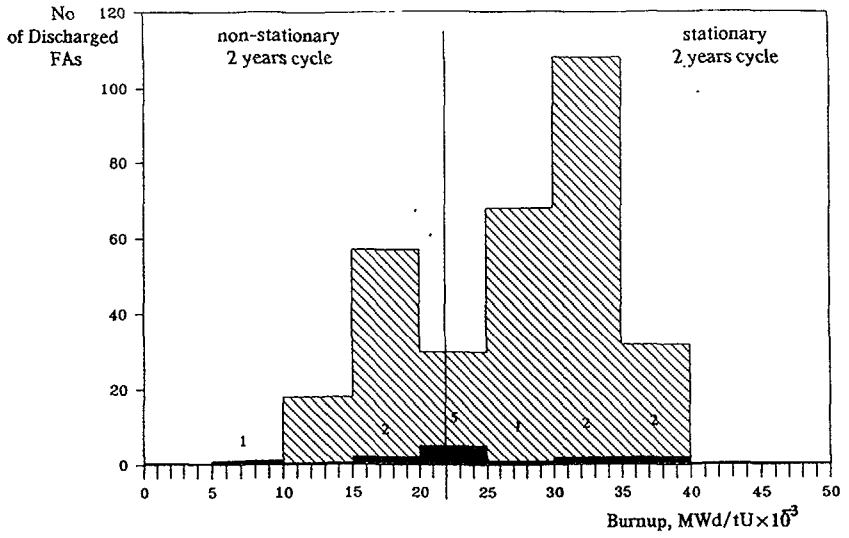

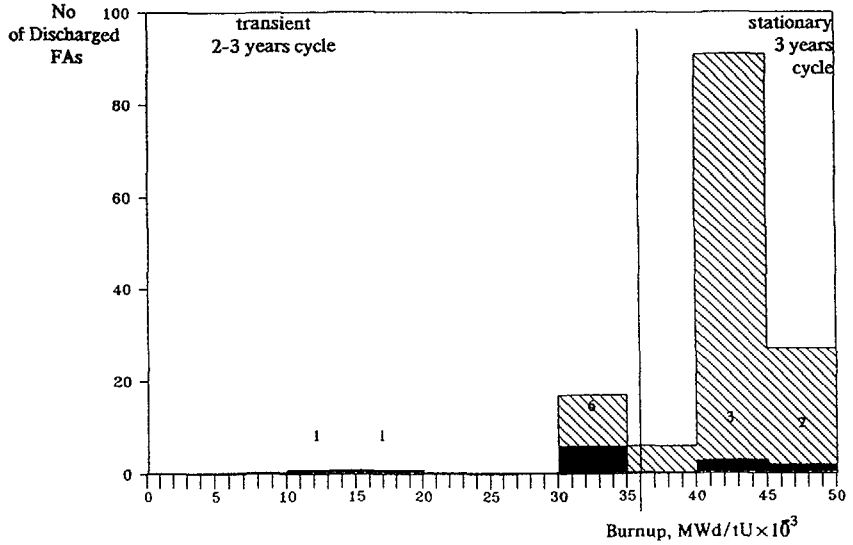

Fig. 6. Burnup Distribution of FAs Discharged from Novovoronez NPP Unit 5 until 01.01.1991 (thin lines and numbers indicate quantity of Defective FAs)

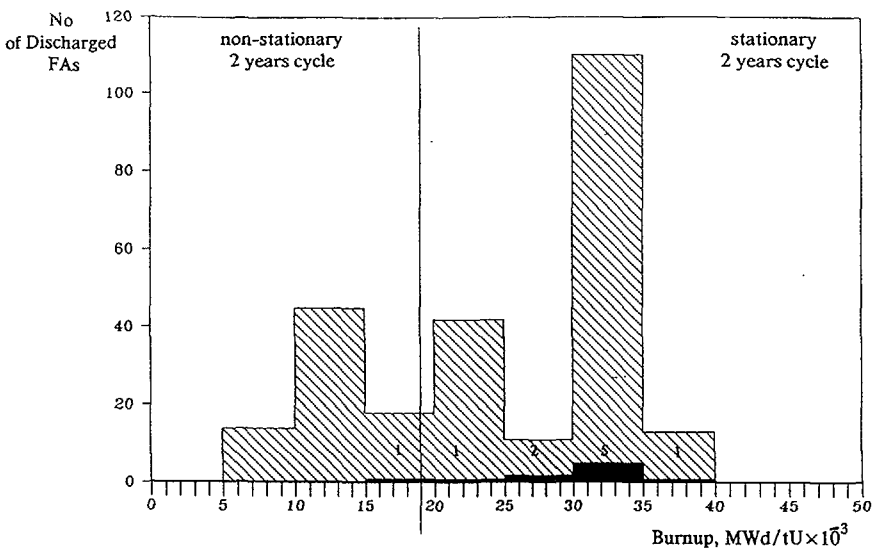

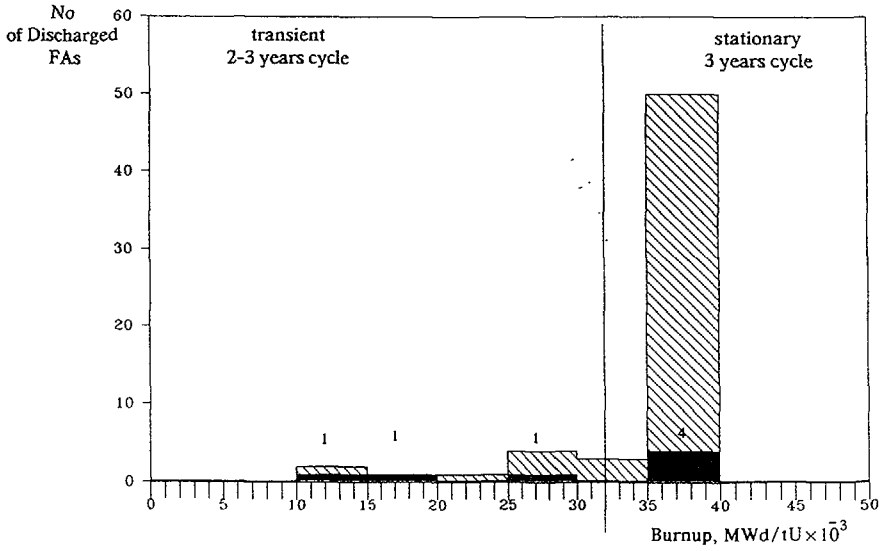

Fig. 7. Burnup Distribution of FAs Discharged from Kalinin NPP Unit 1 until 01.01.1991 (thin lines and numbers indicate quantity of Defective FAs)

The analysis of the coolant activity variations during the fuel cycle (the relations are given for all units in [3]) the results of IFI after the end of the fuel cycle and of post-irradiation studies allowed a conclusion to be drawn of leakage of an essentially single fuel element in each FA acknowledged to be leaky by IFI. Then the number of leaky fuels in relation to all discharged will be ~0.01% and that in relation to all loaded will be ~0.008%.

The analysis of the data on the coolant radio-chemistry shows that on the whole the radiation conditions in the primary circuits of the stations are normal. In the recent cycles the stable conditions were observed for the 5^{th} unit at the Novovoronezh NPP, the 1^{st} and 2^{nd} units at the South-Ukranian NPP, the 2^{nd} unit at the Kalinin NPP, the 1^{st} and 2^{nd} units at the Zaporozhie NPP, the 1^{st}, 2^{nd} and 3^{d} units at the Balakovo NPP, where the iodine radionuclide activity of the primary coolant did not exceed $(1.5\text{-}2.0)\times10^{-5}$ Ci/l.

In the other units the coolant activity as dependent on the number of leaky FAs varies within 1×10^{-6}-2.8×10^{-4} Ci/l and tends to decrease with the time of operation.

The conversion to a three year mode of operation was first accomplished for the 5^{th} unit at the Novovoronez NPP and the 1^{st} unit at the Kalinin NPP and then for other units (table 4). The unit operation under the particular conditions pointed to the high reliability of the fuel (fig.4). The acknowledgement of eight FAs of the 5^{th} unit at the Novovoronez NPP to be leaky after the 9^{th} fuel cycle can be assessed ambiguously, since the primary coolant activity did not exceed 2×10^{-5} Ci/l (iodine radionuclides) during this cycle.

The average fuel discharge burn-up after the 3 year steady-state cycle is 42-44 MW.day/kg for the 5^{th} unit at the Novovoronez NPP and ~40 MW.day/kg for the 1^{st} unit at the Kalinin NPP (figs.6,7). The maximum FA burn-up in the 5^{th} unit at the Novovoronez NPP was ~50 MW.day/kg.

The three-year mode operation of the VVER-1000 cores showed that the improved so-called "three year" fuel was more serviceable and reliable as compared to the previously used "two-year" fuel (table 5).

Table 5

Number of VVER-1000 FAs with "Two" and "Three" Year Fuel that Losttheir Tightness during Three Year Operation

Fuel quality \ Number of leaky FA operated for year	1	2	3
"Two-year"	49	56	21
"Three-year"	3	7	9

The work is under way now to validate the four year cycle of VVER-1000 fuel.

It is interesting to discuss the dependence of the average burn-up and initial enrichment of discharged fuel on the year of fuel discharge from the VVER-1000 units (fig.8). It can be seen that within 80-90 a higher burn-up was accompanied by an increase of the initial fuel enrichment. However, the calculation shows that beyond 1990 it is feasible to reach at least 55 MW.day/kg burn-up in fuel enriched to 4.4% [4]. This is due to a partial or complete

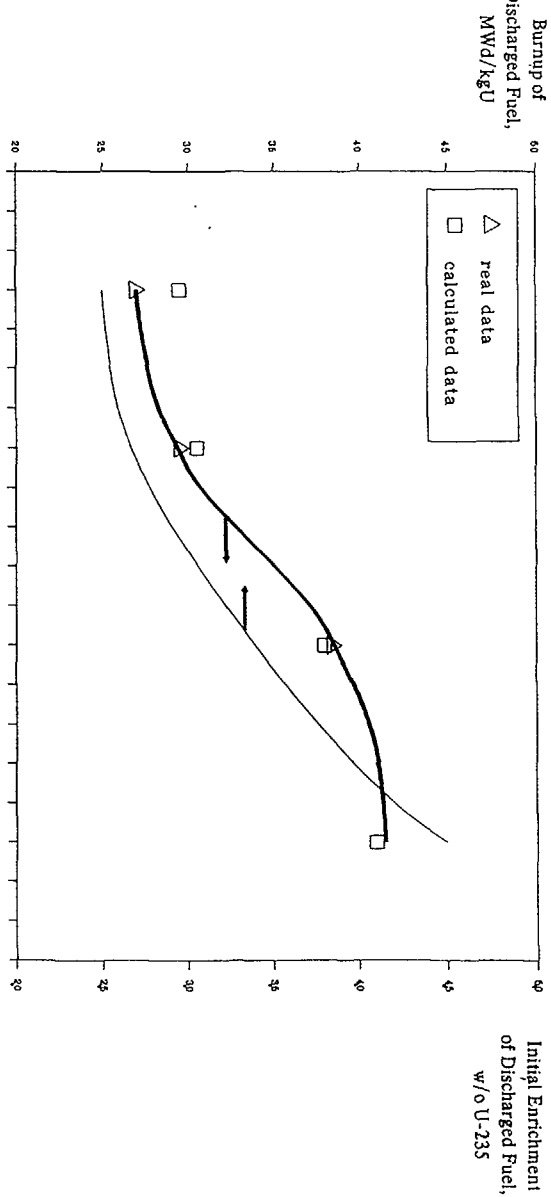

Fig. 8. Real and Calculated Data for Burnup and Initial Enrichment of Discharged VVER-1000 Fuel.

introduction of the scheme of the in-reactor motion of fuels that reduces neutron leakage (In-In-Out). The use of Zr-alloy spacer grids and substitution of steel guide tubes by zirconium ones will increase the fuel burn-up.

The statistical analysis of the radiation conditions in the primary circuits of the plants, the results of IFI and post-irradiation hot cell studies show that the main causes of loss of tightness by VVER-1000 fuels are:

1. No-optimized (accelerated) rate of reactor going to power, especially after loops are switched on [5], and departures from design operation conditions (e.g., increased number of scrams).

2. Debris getting into the primary circuit coolant; they are organic compounds (possibly,ion-exchange resin particles from a water clean-up system, residues of dissolvents employed to clean piping and steam generators from activated corrosion products and oth) and foreign particles (different dispersity steel turnings from friction parts, carbon dust from pump bearings etc).

In some cases these impurity particles can give rise to a higher hydraulic resistance of FA and to fuel rod superheat, score of their surfaces, formation of heat insulation cruds at the surface and their local superheat. Similar phenomena took place in the 1st unit at the South Ukranian NPP and in the 4th unit at the Zaporozhie NPP.

The analysis of the results of the operation of 72 fuel loads in VVER-1000 and a series of experimental design and research and development work to validate the technology of fuel element and assembly fabrication and their characteristics shows that:

1) Fuel elements and assemblies retain the high serviceability level during a three year cycle and reach the batch averaged discharge burn-up of ~42-44 MW.day/kg and the maximum FA one of ~50 MW.day/kg.

2) As of 01.01.92 VVER-1000 reactors have operated for 72 fuel cycles (years), 4210 spent FAs were discharged, only 156 of them were supposed to contain a single leaker and only 2 from them revealed FR's defect of type "fuel-coolant contact". The number of such fuel elements does not exceed 0.008%.

3) A considerably higher reliability has been demonstrated by the "three year" fuel as compared to the "two year" one.

4) Higher burn-up does not lead to an increased frequency of events of loss of tightness by fuel elements and the tendency for its reduction is noted in FAs with the "three year" fuel.

5) It is established that in some cases loss of tightness (gas leakage) is due to departures from the design operation conditions, indequately optimized methods and algorithms of power control and organic substances and solid particles getting into coolant.

6) To further find out and generalize the causes of loss of tightness by standard VVER-1000 FAs an analysis was performed of the irradiation history and operation conditions of leaky FAs; the most representative ones were taken for post-irradiation fill-scale investigations.

References

1. Nuclear Safety Regulations for NPP Units (NSR RU NPP-89) PN-AE-G-1-024/90, Gospromatomnadzor SSSR. M., Energoatomizdat, 1991.
2. Proselkov V.N. et al. "Increase of Power at VVER-440 NPP", Atomnaya Energiya, t.69, vyp.2, 1990, s.78-81.
3. Dubrovin K.P., Fatieva N.L., Smirnov V.P. "Data on Loss of Tightness by Fuel of Water Cooled Reactor NPP in USSR", Paper presented at TC of IAEA, Dimitrovgrad, 26-29 May, 1992.
4. Bibilashvili Yu.K., Onufriev V.D., Proselkov V.N., Pazdera F. et al. "Incentives for Extended Burnup for VVER Reactors", TCM on Fuel Performance at High Burnup for Water Reactors, IWGFPT/36, pp.24-32., 1991
5. Reshetnikov F.G. et al. "Problems in Pressurized Water Reactor (VVER-1000) Fuel Fabrication for Operation under Load Follow Conditions and at Extended Burn-up", IAEA Conference on Nuclear Power and Safety, IAEA-CN-48/244, 1988, s.537-547.

OPERATING EXPERIENCE OF RBMK FUEL UNDER NORMAL CONDITIONS AND ANALYSIS OF ITS DAMAGE CAUSES

V.G. ADEN, B.A. VORONTSOV, V.V. KALININ,
G.S. KRIVOSHEIN,V.A. NIKOLAEV, V.V. NOSKOV,
A.V. ROBOT'KO, A.N. RYABOV
Research and Design Institute of Power Engineering,
Moscow, Russian Federation

Abstract

Data on RBMK-1000 and RBMK-1500 fuel are presented in this paper. The analysis of the fuel assembly failure describes reasons and measures for the improvement of fuel reliability (by introducing new fabrication methods, more severe requirements for operating conditions, and improvement of fuel designs). All these measures made it possible to reach a failure level of 0.02% of the total discharged fuel from the RBMK-1500 reactor.

Currently, there are 13 power units with RBMK-1000 reactors and 2 units with RBMK-1500 ones to be in operation Fig.1 presents the RBMK-1000 fuel assemblies designs. At the first stage of the RBMK-1000 reactor construction the fuel assemblies with 1.8 % enriched U-235 fuel were loaded. Then, since 1.07.77 there was performed the convertion to 2 %-enriched fuel and since 1986 year the convertion to 2.4 %-enriched U-235 fuel was realized with the aim of improving the technical and economic RBMK-1000 characteristics.

The fuel enrichment in RBMK-1500 fuel assemblies is 2 %.

Table 1 presents the main characteristics of the RBMK-1000 and 1500 fuel assemblies The values of fuel burn-up depth are given for the state before the implementation of measures for safety improvement.

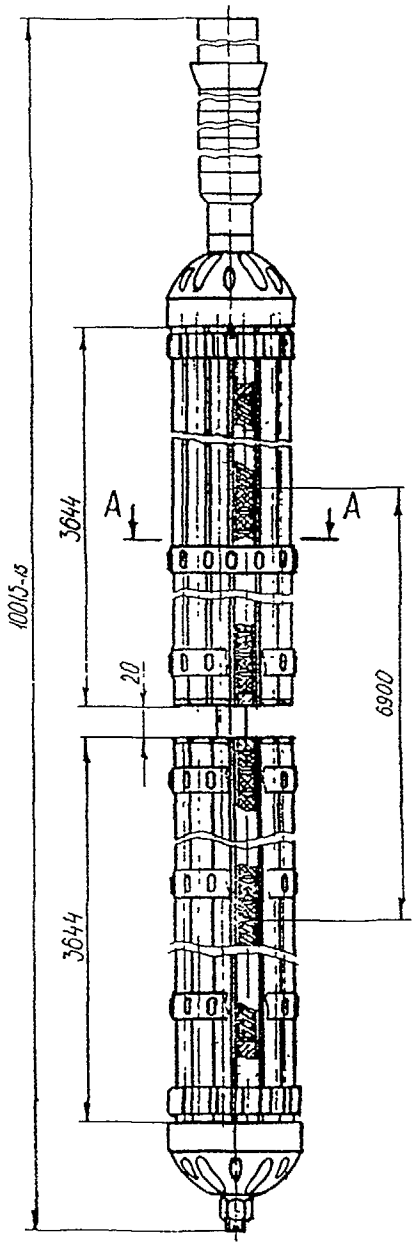

Fig.1 RBMK-1000 FUEL ASSEMBLY. GENERAL VIEW

As a result of measures implemented in 1986 for RBMK-1000 safety improvement, there were installed the additional absorbers in amount of 80-100 absorbers and the reactivity margin was increased by 15 manual control rods (from 30 to 45 manual control rods). It resulted in decrease of 2 % enriched U-235 fuel depth up to 15 MW days/kg U.

TABLE 1. MAIN FA CHARACTERISTICS

Parameter	RBMK-1000 FA	RBMK-1500 FA
Maximum rated power of FA, kW	2850	4140
Nonuniform power density distribution factor:		
- in core height	1.4	1.4
- along the FA section	1.07	1.06
Maximum linear power of fuel element, W/cm	328	485
Fuel enrichment, %	2.0	2.0
The fuel burn-up depth in fuel assembly being unloaded, MW days/kg U:		
- average in reactor	22.4	21.6
- in plato zone	24.6	23.0
- maximum in fuel element	26.4	25.0
- maximum in the point	34.3	32.0
Fuel cycle duration of FA, days eff	1290	860
Neutron fluence with energy of > 1 MeV, n/cm^2	$1,3 \cdot 10^{21}$	$1,3 \cdot 10^{21}$

There were about 55 additional absorbers to be installed in the RBMK-1500 reactor and the reactivity margin was increased by ~ 55 manual control rods. It resulted in decrease of burn-up depth up to ~ 17 MW days/kg U. Simultaneously with the implementation of measures the RBMK-1000 was converted to 2.4 %-enriched fuel in 1986. In this case, the planned fuel burn-up was increased up to 22.4 MW days/kg U Since July 1988 the RBMK-1500 power was decreased down to 4200 MW(th) (by ~ 13 %).

By the present time about 57000 fuel assemblies have been unloaded from the RBMK-1000, units including ~ 2770 failed fuel assemblies and about 6000 and 267 fuel assemblies from RBMK-1500 power units, respectively. The total loss of fuel burn-up, the value of which is lower than the predicted one and is resulted from the FA failure was equal to 360 fresh fuel assemblies.

Figs. 2 and 3 present data on loss of FA tightness for Ignalina NPP Units 1 and 2, respectively during the whole period of their lifetime. Besides, Figs. 2 and 3 show the failure rate λ, which is the ratio between the number of failed FAs within the chosen range of burn-ups and the total number of the exposed fuel assemblies, i.e.

$$\lambda = \frac{\Delta N_F}{N \cdot \Delta B} \quad \frac{1}{(\text{MW days/FA})}$$

where ΔN_F - the number of failed FAs within the chosen burn-up range of ΔB, N - the total number of the exposed FAs.

Fig. 2 presents the data on the failure rate of the fuel assemblies for four units of the Leningrad NPP during the whole period of operation. The comparison shows that on the average the characters of FE failure rate for the RBMK-1000 and 1500 are practically in agreement

To go into greater detail the operation time of the Ignalina NPP unit 1 should be devided into 4 stages:

- stage N 1 (12.83-0 485) - the period of bringing power to the design figure from 0 to 4400 MW(th);
- stage N 2 (4 85-10.86) - the period of rated power operation of 4800 MW(th);
- stage N 3 (10 86-12 88) - the transient period during which a number of organizing and technical measures for increasing the reactor safety and reliability, was implemented;

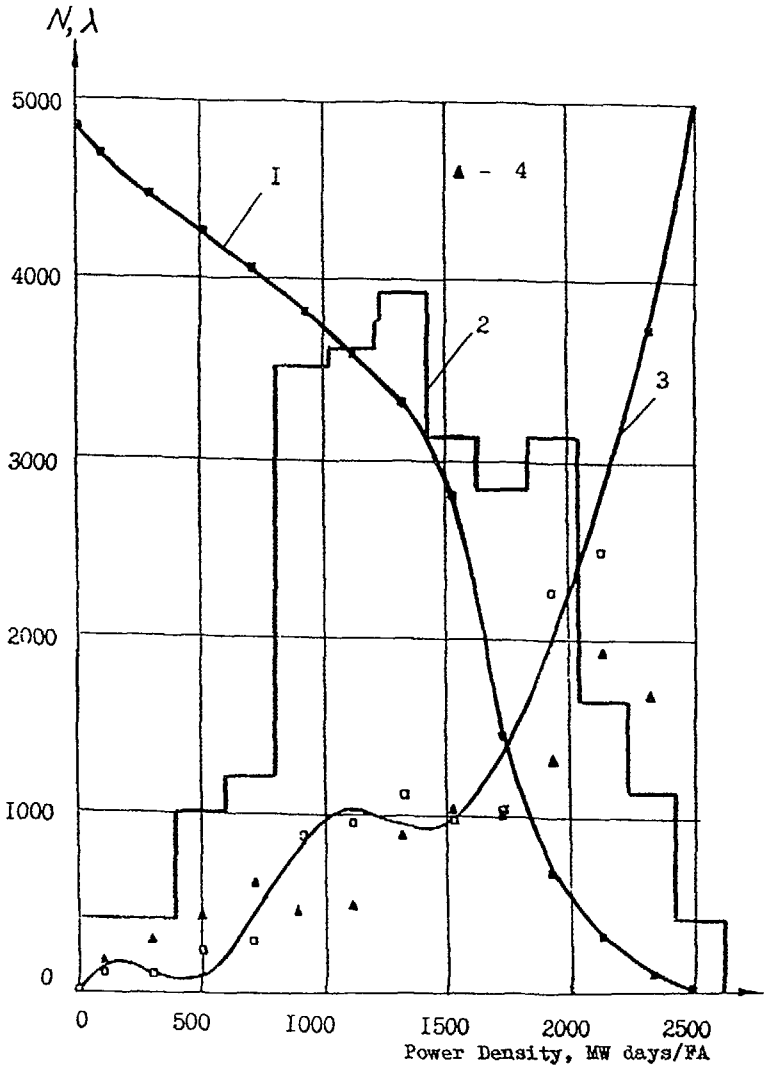

Fig.2. WITHDRAWAL OF FAILED FUEL ASSEMBLIES AT INPP UNIT I
1 - Total number of the exposed fuel assemblies
2 - Number of failed fuel assemblies, $N \cdot 10^{-2}$, qnt
3 - Failure rate, $\lambda \cdot 5 \cdot 10^{-8}$(MW days/FA)$^{-1}$
4 - Failure rate LNPP, $\lambda \cdot 5 \cdot 10^{-8}$ (MW days/FA)$^{-1}$

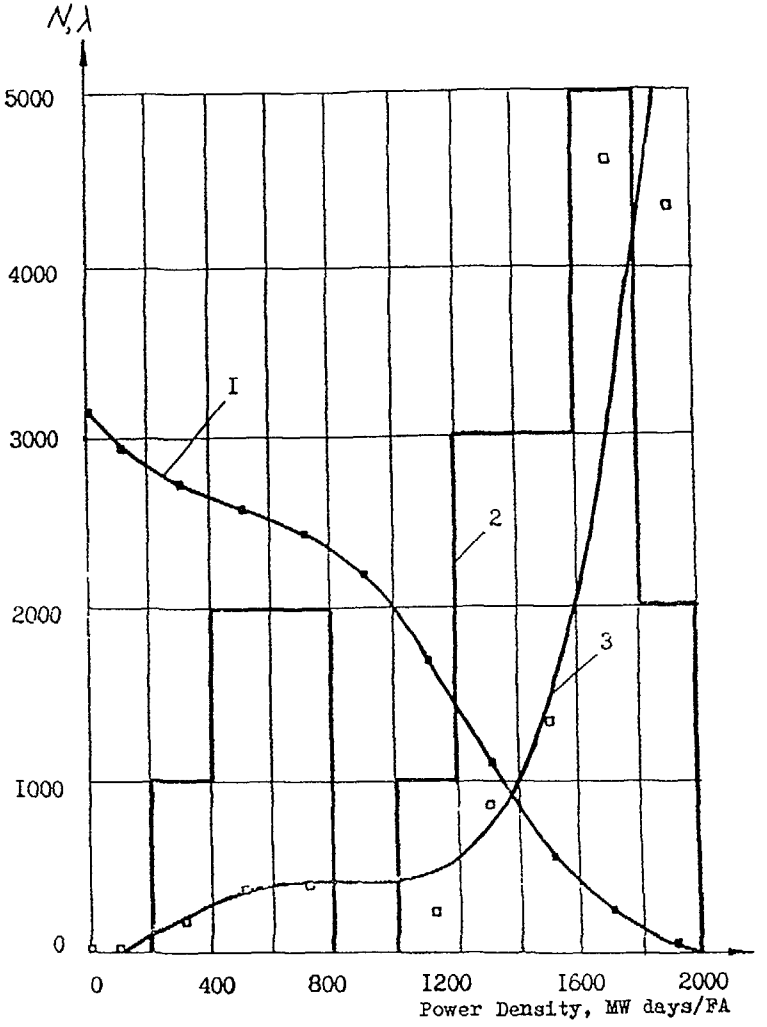

Fig.3 WITHDRAWAL OF FAILED FUEL ASSEMBLIES AT INPP UNIT 2
1 - Total number of the exposed fuel assemblies
2 - Number of failed fuel assemblies, $N \cdot 10^{-3}$, qnt
3 - Failure rate, $\lambda \cdot 10^{-8}$ I/(MW days /FA)

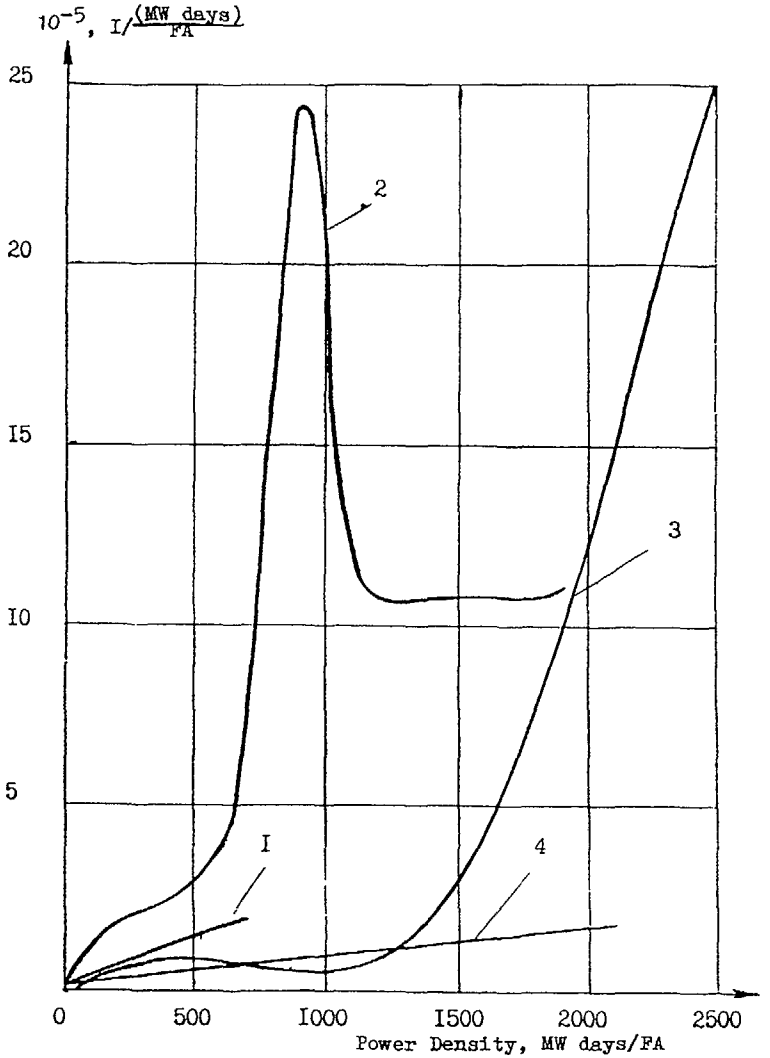

Fig.4 FAILURE RATE OF FUEL ASSEMBLIES AT NPP UNIT 1
1 stage - since 12.83 to 04.85
2 stage - since 04.85 to 10.86
3 stage - since 10.86 to 12.88
4 stage - since 12.88 to 12.90

TABLE 2

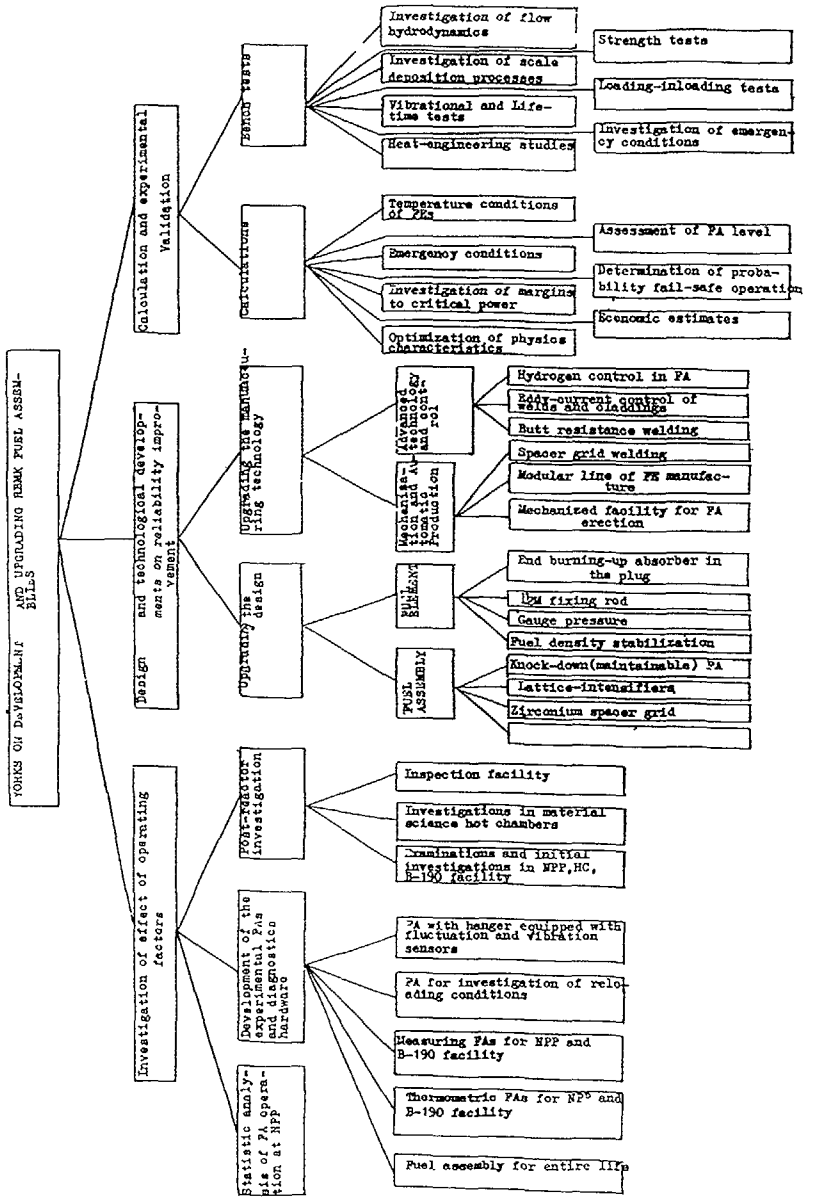

TABLE 3

In-pile studies at operating channel-type NPPs by means of measuring fuel assemblies (FA)

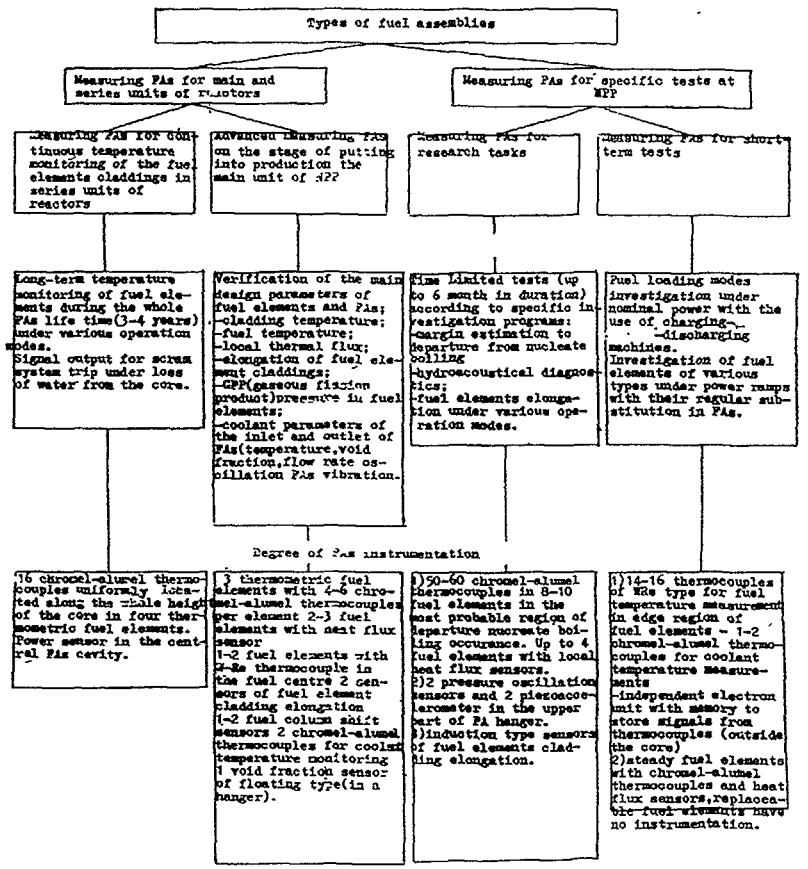

Main performance characteristics

1) Nominal coolant parameters in channel with measuring FA: water and steam-water mixture (x up to 0,4)
   - temperature up to 290 C;
   - pressure 7 MPa
2) Operating measurement range of Measuring FA: - fuel element cladding temperature - 25—380 C(up 800 C - momentary);
   - fuel temperature - up to 1800 C (2000 C);
   - fuel element cladding elongation - 0-6 mm,
   - fuel column shift - 0-25 mm;
   - pressure inside fuel element cladding - 0,1-1,5(2,0) MPa;
   - local heat flux - 200-500 W/cm (700 W/cm);
   - mass steam fraction - 0,1-0,6;
   - pressure oscillation - 40-800 Pa.

- stage N 4 (12.88-12.90) - operation at 4000 MW(th) power level under steady-state reloading conditions.

The failure rate was calculated for each stage. Fig. 4 presents the results of the calculations.

It is seen from Fig. 4 that the failure rate at the first and forth stage increased gradually with the power density field growth. At second stage there was observed the drastic increase in failure rate over the power density distribution range from 850 to 950 MW days/FA. In this case the failure rate reached its maximum value which is equal to about $(23-24)\cdot10^{-5}$ 1/(MW days/FA). The above character of the variation in the failure rate permits to conclude that there were significant disturbing factors in FA operation at this period of time which promoted the increase in failure rate of the fuel elements.

As it is known, the operating reliability of fuel assemblies is determined by the design and quality of FA and FE manufacture, as well as by the operating factors. The works on improvement of the RBMK FA reliability were carried out in this directions (Table 2). The investigations of effect of the operating factors were carried out in three directions. They are as follows:

a) statistic analysis of FA operation at the NPP;

b) study of modes of operation with the aid of FAs instrumented by different sensors (Table 3);

c) post-reactor investigations.

The design and technological developments concerning the reliability improvements were performed in the following directions:

a) upgrading the FA and FE designs;

b) upgrading the manufacturing methods including the mechanization and automatic production, as well as the advanced technologies.

A complex of design and experimental studies permitted to define the boundaries of the safe operation of fuel assemblies, to determine the operating factors affecting their serviceability

From the considered 120 failed fuel assemblies there are.

- 5 % of FAs with the detached plug, as a rule it is the plug of the upper beam;

- 20 % of FAs with flaws in the form of longitudinal and annular cracks. And the crack can be observed not only in the cladding part contacting with the fuel column, but also in the pressurizer;

-75 % of FAs without flaws.

The post-reactor investigations of the fuel assemblies (in general, there were tested about 30 fuel assemblies in the material science laboratories at the different fuel burn-up levels under normal and emergency conditions) were carried out in the following directions:

- investigation of fuel elements and FA structural components behaviour at power cycling under emergency conditions related with the dryout effect;

- substantiation of limiting serviceable lifetime of the RBMK fuel assemblies;

- investigation of failed fuel assemblies with the aim of revealing the failure causes and mechanisms of through cracks developments.

The material science investigations of fuel assemblies which have already achieved maximum burn-up of ~ 40 MW days/kg U give quite favourable results with reference to residual strength characteristics of fuel elements, fuel status and FA structural components.

So, the mechanical properties of the specimens tested at 25 C were within the range:

Initial values:	End of lifetime:
σ_{τ} = 280-300 MPa	σ_{τ} = 500-570 MPa
$\sigma_{0,2}$ = 220-250 MPa	$\sigma_{0,2}$ = 450-510 MPa
δ - 28-33 %	δ - no less than 12 %

The hydrogenation of FE pipe metal was no more than 0.01 % (mass) with the favourable (annular) orientation of hydride plates At the same time the emphasis was placed on the significant corrosion growth in the form of local increased thickness of oxyde on the outer surface of the fuel element cladding under spacer grids.

The depth of the corrosion damage was equal to 36 % (in maximum) of the initial thickness of the "actual" cross-section of the cladding. As the experience of post-reactor material science investigations of the fuel elements and FA structural components shows, the main factors responsible for the premature failure of fuel assemblies under normal operating conditions are the local volumetric hydrogenation and the stress corrosion cracking of FE claddings in the presence of the aggressive fission products (J, Cs). The effect of the first factor is usually in the RBMK fuel elements with fuel burn-up of ~ 200-600 MW days/t U. The cracks in plugs arranged in the core centre, present an example of the corrosion process mentioned above. The formation of zirconium hydride penetrating through the whole thickness of the cladding was observed in the crack zone at the concentration of hydrogen dissolved in the FE cladding of no more than $(2\text{-}4)\cdot10^{-3}$ % (mass). In this case the content of hydrogen dissolved in the FE cladding is similar, as a rule, to that of the leak-tight fuel elements even at the distance of ~ 25-50 mm of the crack.

The second factor - stress corrosion cracking (SCC) of claddings occurs at higher burn-up fraction.

In the RBMK reactor where the refuelling takes place at power operation the stress corrosion cracking can be caused by:

- the flash-up of linear power of the fuel elements on fuel and additional absorbers reloading;

- the fluctuations of linear power of fuel elements due to the skewness of axial power density distribution.

Fig 5 presents the axial power density distributions obtained from the calculations for the reactor states corresponding to the onset of unloading the additional absorbers, to the most skewness of power density distribution

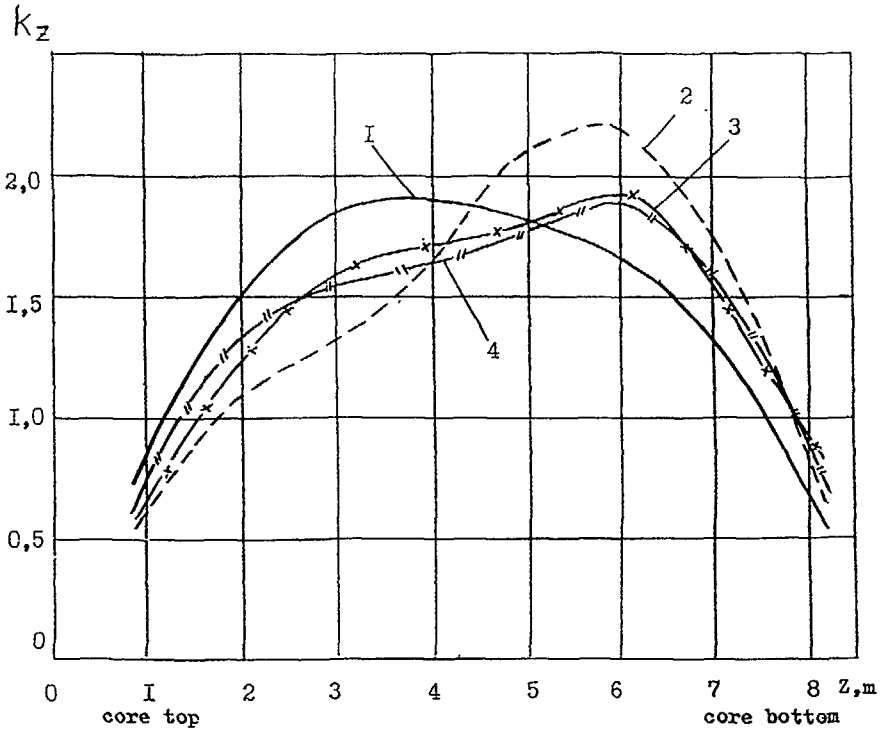

Fig.5. AXIAL POWER DENSITY DISTRIBUTION DURING UNLOADING THE ADDITIONAL ABSORBERS
1 - Additional absorber is inserted by 7.0 m, manual control rod is inserted by 0.58 m
2 - Additional absorber is inserted by 3.59 m, manual control rod - by 3.39 m
3 - Additional absorber is inserted by 1.45 m, manual control rod - by 4.43 m
4 - Additional absorber is inserted by 0.51 m, manual control rod - by 4.43 m

by the time when the unloading of the additional absorbers is completed.

The experiments performed with fuel assemblies which are equipped with sensors for cladding alongation, fuel column displacement, as well as the calculations have shown the risk of such a condition from the viewpoint of FE serviceability.

A variety of the works has been carried out to increase the quality of fuel elements manufacturing and their stability in thermomechanical interaction of the fuel with cladding:

a) automized modular line for manufacturing the fuel elements was introduced in 1988. This made it possible to eliminate the potentially dangerous operations resulting in the pellet failures and fuel column locking. At the same time eddy-current monitoring of the claddings was additionally introduced to ultrasonic one. Moisture content in fuel was reduced up to 2 ppm;

b) in a part of fuel element design the facets were introduced to the fuel pellet, central opening of 2 + 0.3 mm in dia. was made in the RBMK-1500 fuel element pellet, the geometrical fuel pellet dimension and density tolerances became tougher, initial helium pressure under cladding was increased up to 0.5 MPa.

In 1989 the new regulations of refuelling that eliminate increase in linear fuel element power due to axial power density distribution skewnesses, were introduced at NPPs with the RBMK-type reactors.

All the above-mentioned measures made it possible to reduce the fuel element failures up to 0.02 % for RBMK-1500 and up to 0.05 % of the number of fuel elements that are annually unloaded from the reactors, for RBMK-1000. The subsequent improvement of the fuel element designs (introduction of cladding with pure zirconium sublayer, getters, absorbers in plugs) will make it possible to increase additionally the fuel element reliability.

FRAGEMA FUEL RELIABILITY: FROM DETECTION OF FUEL FAILURES TO THE FEEDBACK ON DESIGN AND FABRICATION

A. DUMONT
Fragéma/Framatome Division Combustible,
Lyon, France

Abstract

FRAGEMA fuel reliability is excellent and we are constantly working to improve it and bring it to an as high as achievable level. This objective concerns all the aspects related to leaking fuel in PWR. The detection and the evaluation of the leaking fuel during reactor operation through coolant activity analysis are carried out by using the MORGANE model. On-site facilities allow to detect the leaking fuel assemblies (sipping test devices) and the leaking fuel rods (ultrasonic test device). The determination of the fuel rod failure causes is carried out by on-site examinations (Eddy Current examination and macroscopic visual examination of the leaking fuel rods) and for some selected leaking rods by hot cell examinations. The main fuel failure origin is the presence of debris in the primary coolant (70 % of the examined rods are damaged by debris). As a feedback on the fuel design, the new FRAGEMA fuel assembly (AFA 2G) is equipped with an anti-debris filter and is expected to have a leaking fuel rate near 5 x 10^{-6} rods per cycle compared to 1.5 x 10^{-5} presently. Concerning fabrication related defects, the quality control and the efficiency of non destructive examination methods are being continuously improved.

Keywords : PWR - FUEL FAILURES - FUEL RELIABILITY - SIPPING TEST.

1. COOLANT ACTIVITY ANALYSIS

The coolant activity analysis is based on the MORGANE model which is a semi-empirical model using simplifying hypotheses and benchmarked to FRAGEMA experience. The analytical form of the model was determined from theoretical equations and the unknown coefficients were determined from PWR experimental data. One of the main simplifying hypotheses is that all the fuel rods operate at nominal power.

MORGANE uses I131, I133, I134, Xe133 and Kr85m coolant activities to evaluate the number and the severity of the defects. For each isotope, the measured coolant activities are corrected for tramp uranium contribution by using I134 activity.

The coolant activity analysis in PWR shows that two types of defect can be distinguished :

- defects releasing only gaseous fission products ("G-Defects")
- defects releasing both iodine and gaseous fission products ("I-Defects").

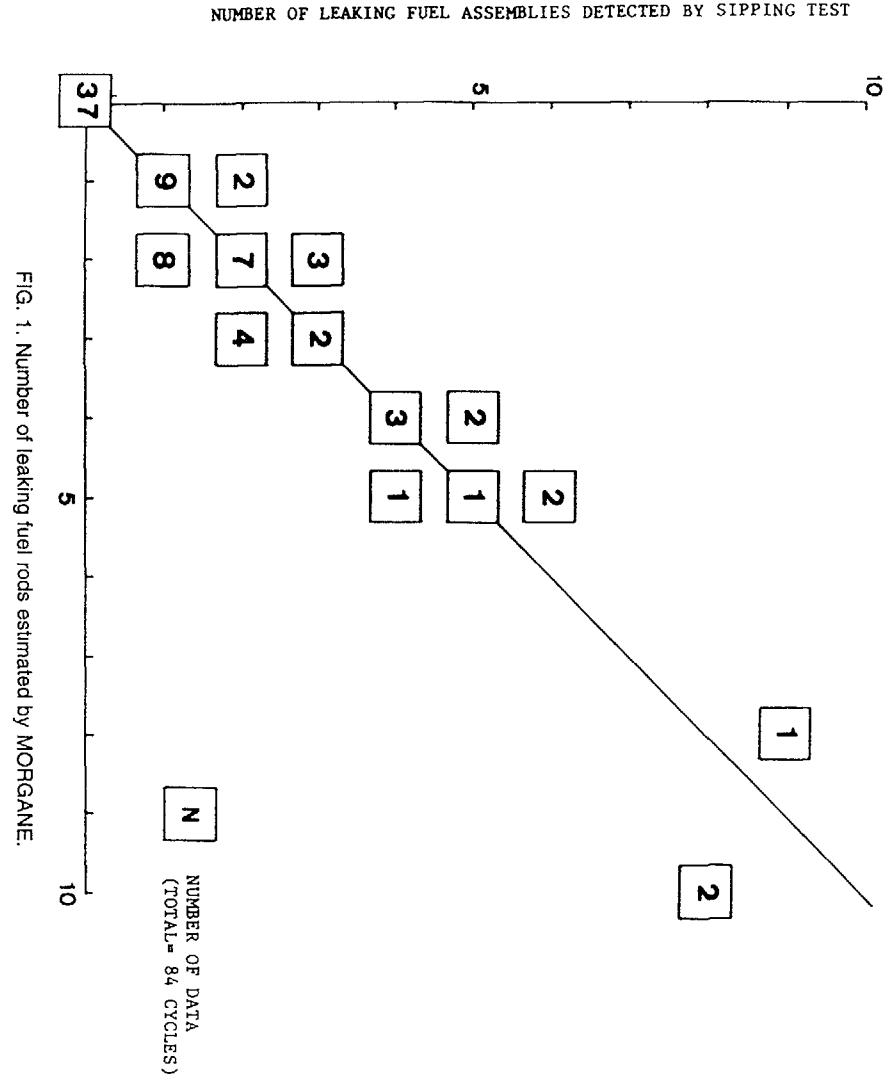

FIG. 1. Number of leaking fuel rods estimated by MORGANE.

MORGANE calculates the number of the "I-Defects" from I131 and I133 activities, the ratio I131/I133 giving an estimation of the severity of these defects Then, MORGANE calculates the number of the "G Defects" from the difference between the measured Xe133 and Kr85m activities and the calculated Xe133 and Kr85m released by the "I-Defects"
For most cases, the MORGANE results allow to assess satisfactorily the fuel rod condition (see Figure 1)

2. ON-SITE FACILITIES FOR DETECTION AND EVALUATION OF THE LEAKING FUEL RODS

2.1 Leaking fuel assembly detection

The leaking fuel assemblies can be detected by an on-line sipping test device inside the refuelling machine mast or by conventional sipping test cells in the spent fuel pool

The on-line sipping test device (DRMC), the process of which was developed by CEA, detects leaking fuel assemblies during core unloading operation in the reactor building, and thus provides a significant refuelling outage time saving [1] When the core is unloaded or shuffled, each assembly is raised from the core inside the fuel manipulator crane mast if one rod is leaking, the differential pressure caused by raising the assembly from the core cavity entails the release of the fission products through the cladding The device collects gaseous fission products (mainly Xenon 133) by means of an air stream which routes them to a gamma activity measurement unit The top gripper position of the assembly inside the mast corresponds to the optimum detection configuration the air stream covers the entire assembly and the internal-external pressure difference is at its maximum Two minutes in this position are needed before moving the mast

The advantages of the on-line sipping test system are as follows

- only two days are needed for the initial installation,
- the mast equipment is installed on the machine without modifications to the mast mechanical structure,
- no additional operator is required for driving the system which is a self-operated equipment,
- only one modification to the unloading sequence is needed two additional minutes with the assembly in the top gripper position,
- in case of leaking fuel assembly, a sound alarm informs the manipulator crane operator

Figure 2 presents the main characteristics of the on-line sipping test system The gamma activity detection limit is 1 2 x 10^{-6} Ci/m^3, measured in CEA laboratory with calibrated source

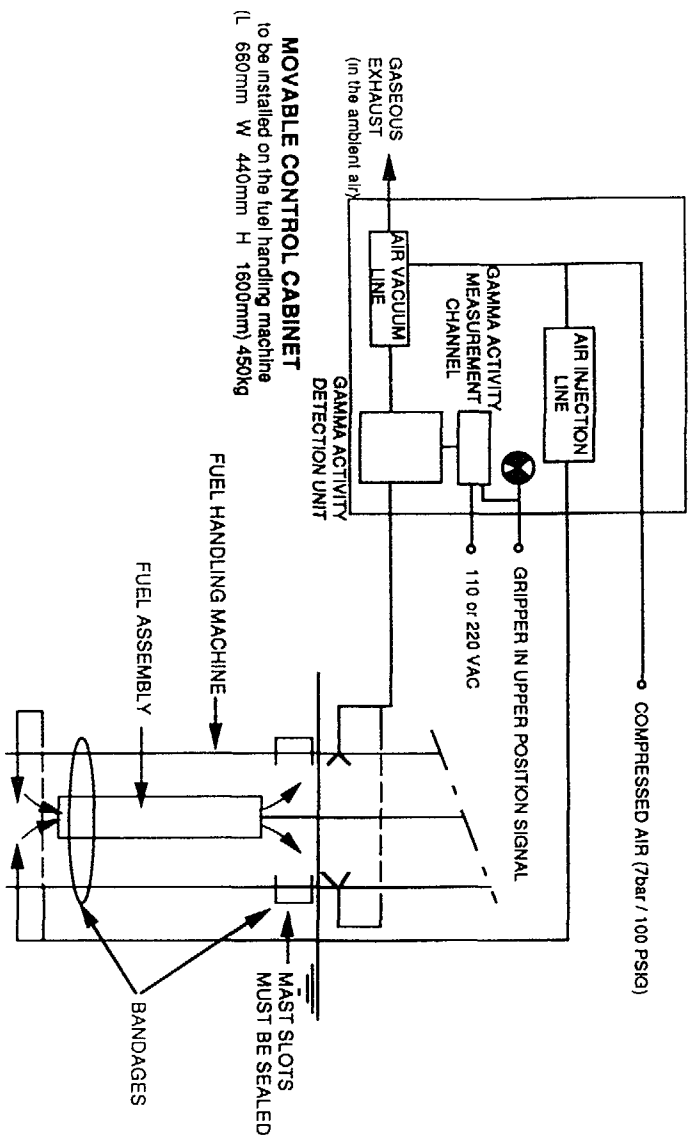

FIG 2 Main characteristics of the on-line sipping system

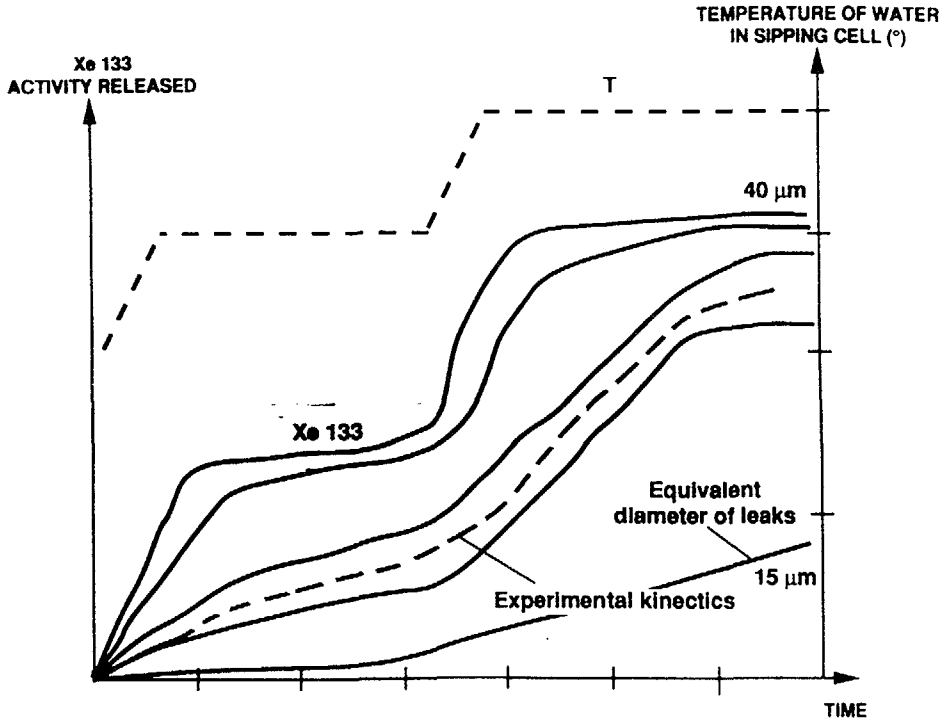

FIG. 3. Quantitative sipping test: Example of result.

A total of 55 on-line sipping test systems were installed by FRAGEMA (France, Belgium, Sweden, China). In France, all EDF plants are equipped with this on-line sipping test system, which is used routinely to detect the leaking fuel assemblies. The conventional sipping test cells in the spent fuel pool are only used by EDF to perform quantitative sipping test in the framework of the French policy of reloading selected leaking fuel assemblies [2].

Sipping test cells can be used for qualitative inspection (detection of Xe133 or Kr85 during 10 to 20 minutes per assembly) or for quantitative inspection : determination of the stabilization kinetics of the Xe133 release during two constant levels of temperature (total time per assembly : 2 to 3 hours) in order to evaluate fuel assembly equivalent leak size (see Figure 3). A total of 31 sipping test cells were installed by FRAGEMA (France, South Africa, China).

In addition, a removable sipping test cell (AXCELL) has been developed by FRAGEMA.

2.2 Leaking fuel rod detection and examination

On-site ultrasonic tests are performed with the ECHO 330 device (developed by BWFC) in order to identify the leaking fuel rods inside the leaking fuel assemblies. The ECHO 330 device is a system of 17 blades equipped with ultrasonic probes and allowing to scan the bottom or any wanted level of 17 rods at once. When a fuel rod is leaking, the water inside the fuel rod induces the absorption of the ultrasonic signal and no echo of the signal is detected for this rod.

After removing the leaking fuel rods out of the leaking fuel assemblies, single rod examinations are performed to characterize the fuel defects and to determine the causes of the defects. Eddy Current examinations allow to identify the axial position of the defects. Macroscopic visual examinations with a high definition camera allow to characterize the shape and the aspect of the defects and in most cases to identify their cause.

In case of need a single rod sipping test can be performed to check if the rod is leaking.

When no evidence of the fuel defect cause is obtained during on-site examinations, the leaking fuel rods may be sent to an hot cell laboratory for further non destructive examination, and destructive examination if necessary [3].

3. CAUSES OF DEFECTS

FRAGEMA, with the cooperation of the utilities (EDF, TRACTEBEL, VATTENFALL), has undertaken investigations to identify the causes of leaking fuel since 1986. The first leaking rod examinations were carried out for fuel assemblies which released high fission product activities in the primary coolant. Afterwards, leaking fuel rod examinations were performed during repair campaigns. Up to now, most of the repaired fuel assemblies concern Inconel Grid Assemblies. For these previous design fuel assemblies, repair campaigns are carried out in France only when several of them are in one pool [4]. In addition, the French policy of reloading some leaking fuel assemblies [2] induces very few assemblies to be repaired.

As a consequence, baffle jetting failures being excepted, only about 10 % of the FRAGEMA 17x17 leaking fuel assemblies were examined for fuel defect investigation. The baffle jetting failure mode will not be detailed since it is well-known and appropriate actions were taken to minimize the baffle jetting incidence on the reactor operation (stainless steel rods, supplementary partial grids, up-flow conversion).

At the present time, the investigations performed on twenty three 17x17 assemblies containing thirty leaking fuel rods have allowed to identify the following causes :

. Debris induced failures	=	15 assemblies containing	21 leaking rods	=	70 %
. Grid-cladding fretting	=	2 assemblies containing	3 leaking rods	=	10 %
. Fabrication related failures	=	2 assemblies containing	2 leaking rods	=	7 %
. Unknown cause	=	4 assemblies containing	4 leaking rods	=	13 %

3.1 Debris induced failures

Seventy percent of the examined leaking rods were related to the cladding wear by debris such as little springs or wires, metallic chips. The debris induced defects present typical wear patterns on the cladding surface : comma shape wears are typically related to metallic chips, springs induce cladding wear corresponding to each spring coil and metallic wires can induce large breaches in the cladding [3].

Most of the debris-induced defects are observed under the bottom grid. They generally occur early in the cycle and concern indiscriminately one, two or three cycle assemblies.

In most cases, secondary hydriding defects are observed : severe secondary hydriding is observed especially for rods operating at high power (hydride blisters and longitudinal cracks).

3.2 Fretting induced by grid/cladding interaction

Fretting was observed on two fuel rods in one fuel assembly and on one fuel rod in another fuel assembly. In both cases, the phenomenon occurred at the bottom spacer grid level. A very extensive programme of investigations was performed on the fuel assembly containing the two affected fuel rods, yielding detailed grid cell dimensional information. The results of dimensional measurements on the bottom grid cells (distance between dimple and spring in 2 orthogonal directions) show very little difference between the cells where the fuel rods were securely held and the two cells where fretting wear took place.

In both fuel assemblies, the defect occurrence is estimated to take place either at the end of the second irradiation cycle or during the third one.
The conditions for such a defect occurrence might plausibly be the conjunction of :
- specific transverse flow condition located at the bottom end grid,
- initial grid cell characteristics in excess of their specification values, inducing an excessive relaxation of the restraining force.

3.3 Fabrication - induced defects

Two rods presented fabrication related defects. The first one exhibited a longitudinal sinusoïdal crack and at the back of this first defect a radial crack. Such defect is typical of a cladding pilgering problem. The second one was concerned by a defective weld at bottom end plug. In both cases, the defective products were inadvertently not rejected during fabrication.

3.4 Other investigation results

For four rods, the failure cause is still unknown after investigations. This is mainly due to the difficulty of identifying the primary defect once the rod has been irradiated for a long time after primary defect occurrence.

Waterside corrosion as a failure mode was not identified, nor an excessive rod bow or pellet-cladding interaction or internal hydriding.

4. FUEL RELIABILITY AND FEEDBACK TO FUEL DESIGN AND FABRICATION

FRAGEMA fuel, all designs included, is or has been in operation in 68 commercial PWRs. Irradiation experience is nearly 6.5 millions of fuel rods in about 25 000 fuel assemblies, the main experience being related to the 17x17 fuel design.

The fuel failure rate has been stable for 4 years at about 1.5×10^{-5} rods per cycle [5]. More than two thirds of the examined leaking fuel rods are related to debris-induced defects. So the fuel failure rate attributable to fabrication is likely around 5×10^{-6} rods per cycle.

As a remedy for debris-induced defects, FRAGEMA is now proposing for the 2nd generation of Advanced Fuel Assembly (AFA 2G) a bottom nozzle equipped with an anti-debris filter. This anti-debris filter is designed to trap the debris below the bottom nozzle with the same efficiency as a fuel assembly spacer grid : debris larger than approximately 3 mm are retained. It is a very thin plate made of Inconel 718 with a final aging treatment providing the hardness needed to withstand the debris impact effect. Flow holes are made by punching.

Concerning fretting corrosion defects induced by grid/cladding interaction, so far a few cases of occurrence were observed and are related to Inconel grid design fuel assemblies manufactured before 1986. No design problem was related to these few observations. Significant fretting problems may exist only if the fuel rods are not well supported by the grids. Special care is maintained throughout the fabrication process to provide fuel rods with sound support conditions. Up to now, no such defect was observed on Advanced Fuel Assemblies (AFA).

For the fabrication related defects, the defective fuel rods were inadvertently not scrapped. To avoid such human errors, more and more automatic controls are implemented. In this way, an automatic visual control of the claddings has been recently added to the automatic ultrasonic and Eddy Current control. Also, all the AFA 2G rod welds are controlled by an automatic X-Ray device (EIDOMATIX), in order to avoid human errors during weld controls.

5. CONCLUSION

FRAGEMA, with the cooperation of the utilities (EDF, TRACTEBEL, VATTENFALL), carries out investigation on fuel defects in order to :

- determine the fuel defect causes
- implement changes in fuel design and fabrication
- improve fuel reliability

The main fuel failure origin is the presence of debris in the primary coolant. The new FRAGEMA fuel assembly (AFA 2G) equipped with an anti-debris filter is expected to have a leaking fuel rate near 5×10^{-6} rods per cycle.
For the few other remaining causes, intensifying leaking fuel rod investigations, with the related feedback to design and fabrication, should lead to an as high as achievable fuel reliability target.

REFERENCES

[1] BORDY, M , PARRAT, D , "On-line sipping test", IAEA Technical Commitee Meeting on Poolside Inspection, Repair and Reconstitution of LWR Fuel Elements, LYON (October 21-23, 1991)

[2] BOURNAY, P , "Management of failed fuel during operation, french policy and experience", to be presented at this meeting

[3] BOURGOUIN, J et al "Enseignement tiré des résultats d'expertises de crayons de combustible non étanches", International Symposium Contribution of Materials Investigation to the Resolution of Problems Encountered in PWR plants, FONTEVRAUD II (September 10-14, 1990) - Volume 1, 131-141

[4] BOURNAY, P , "Inspection and restoration, EDF experience, policy and needs" IAEA Technical Committee Meeting on Poolside Inspection, Repair and Reconstitution of LWR Fuel Elements, LYON (October 21-23, 1991)

[5] BLANC, C., DUMONT, A , BOURNAY, P , DANGOULEME, D , "FRAGEMA fuel reliability", ANS-ENS International Topical Meeting on LWR Fuel Performance Fuel for the 90's, AVIGNON (April 21-24, 1991)

SIEMENS KWU EXPERIENCE WITH LWR FUEL: FAILURE EVALUATION, MECHANISMS AND REMEDIES

R VON JAN
Siemens AG,
Unternehmensbereich Kraftwerk Union,
Erlangen, Germany

Abstract

After a brief survey of available operating experience with Siemens KWU LWR fuel, the causes and mechanisms of recent fuel failure and damage including the respective remedies are discussed The results are based on a systematic fuel failure evaluation, which is divided into five stages, (i) monitoring coolant activity, (ii) pool–side examinations, (iii) failure analysis, (iv) experience feedback, and (v) monitoring the success of remedies Details and experience for each of these topics are presented The continuous efforts of Siemens and the support of plant operators in all stages have been essential to achieve and maintain high fuel reliability, and to implement measures for further improvements

1 SURVEY OF OPERATING EXPERIENCE

The discussion and understanding of fuel failures requires some background information on fuel designs and development including the available operating experience Since the mid 60ies Siemens has accumulated operating experience with commercial Zircaloy clad UO_2 and MOX fuel in LWRs, covering 33 000 fuel assemblies with 4 million fuel rods inserted in 45 plants of different types and generations (30 PWRs, 15 BWRs) in Germany and other countries About 60% of this experience has been gained with fuel in Siemens built plants, 40% with Siemens fuel supplied to plants from other vendors As a consequence the variety of different Siemens fuel designs is unusually large as shown in table I

In the last decade the average discharge burnups for many plants have been increased from the earlier standard values, i e 28 MWd/kgU in BWRs and 33 MWd/kgU in PWRs, to about 40 MWd/kgU in both types of plants, and currently inserted fuel batches will operate to even higher exposures A peak assembly burnup of 52 MWd/kgU has been successfully reached with PWR and with BWR fuel During the same time period advanced fuel assembly types with enhanced fuel utilization and optimized spacer types, cladding and structural material with improved corrosion resistance, and more economic core loading and operating strategies have been developed and introduced /1–3/ Some important features and the approximate time of their introduction are summarized in figs 1 and 2

Parallel to these developments which were accompanied with increasing fuel duties, a very high operating reliability has been achieved with average fuel rod failure rates near 10^{-5} per reactor cycle i e 1–2 failed rods per 100 000 rods in operation /4/ During the last three years higher failure rates were exclusively caused by a particular type of PCI failure in some non–barrier BWR fuel to be described below

Table I: Overview on the Cumulative Operating Experience with Siemens/KWU LWR Fuel (Status 02/92)

Reactor Type	Assembly Type	Fuel Rod Diameter [mm]	Number of Fuel Assemblies / Rods				Maximum FA-Burnup [MWd/kgU]
			in Operation		accumulated		
SIEMENS-PWR (first cores, reloads)	14x14–16	10.75	109	19.620	883	158.940	41
	15x15–20	10.75	628	128.740	3.700	758.500	50
	16x16–20	10.75	995	234.820	3.927	926.772	45
	16x16–20–4	10.75	100	23.200	136	31.552	41
	18x18–24	9.50	579	173.700	1.039	311.700	43
Third-Party-PWR (reloads)	14x14–(16+1)	10.75	212	37.948	936	167.544	43
	15x15–(20+1)	10.75	157	32.028	493	100.572	51
	16x16–(20+1)	9.50	80	18.800	120	28.200	35
	17x17–(20+1)	9.50	235	62.040	1.402	370.128	52
SIEMENS-BWR (first cores, reloads)	6x6	14.30	0	0	1.200	43.133	28
	7x7	14.30	0	0	1.742	85.358	38
	8x8–1	12.50	17	1.071	3.497	220.311	38
	8x8–2	12.30	1.441	89.342	4.022	249.364	41
	9x9–1	10.75	788	63.040	1.728	138.240	52
	9x9–5	11.00	342	25.992	376	28.576	44
	9x9–9Q	11.00	638	45.936	644	46.368	42
	9x9–9QA	11.00	152	10.944	152	10.944	24
Third-Party-BWR (reloads)	6x6–1	13.45	81	2.835	82	2.870	20
	8x8–2	12.30	4	248	128	7.936	40
	9x9–1	10.75	500	40.000	755	60.400	40
	9x9–5	11.00	470	35.720	673	51.148	41
	9x9–9Q	11.00	16	1.152	16	1.152	38
Total			7.556	1.048.504	27.642	3.799.384	52

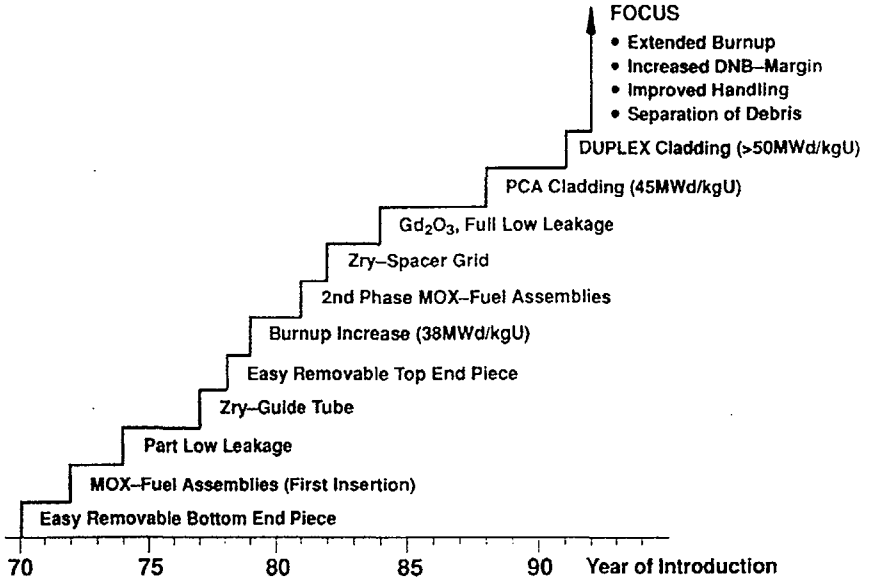

Fig. 1. Development of Siemens Fuel Technology for Pressurized Water Reactors.

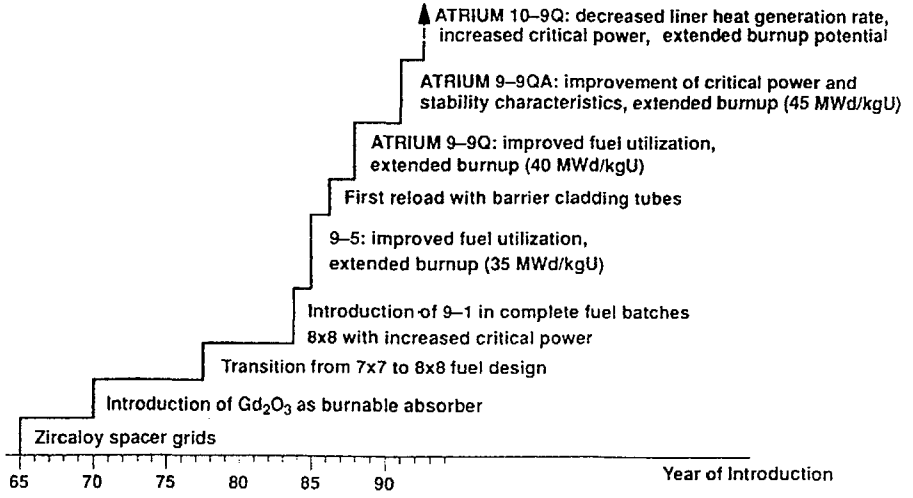

Fig. 2. Development of Siemens Fuel Technology for Boiling Water Reactors

2. CAUSES AND REMEDIES OF FUEL FAILURE AND DAMAGE

2.1. Introductory Remarks

Since the last international reviews on fuel failures, e.g. in Ref. /5,6/, the obvious world–wide change has been a drastic reduction of failure rates by successful countermeasures against all failure categories, although many of them still persist even at todays low failure level. In some cases, as e.g. with the phenomenon of crud induced localized corrosion (CILC) in the field of cladding corrosion, a larger variability in acting mechanisms as well as in contributing factors have been recognized.

In Siemens fuel no new generic type of failure was found and not all types of failures reported in the literature were encountered. In particular, there were never failures by clad collapse, CILC or dryout. Although in several PWRs with high coolant temperature the design limits for clad corrosion are fully exploited to reach high burnup goals, corrosion failures did not occur in commercial fuel due to permanent surveillance programs and optimized refueling schemes. (In experimental high power assemblies some corrosion failures were observed above 140 µm circumferentially averaged oxide thickness.)

2.2 Recent Experience with Siemens KWU Fuel

2.2.1 General

In the following we shall discuss the mechanisms and remedies of failure and damage of Siemens KWU fuel in recent years. An overview on the causes of fuel rod failures and their relative importance is given in fig. 3.

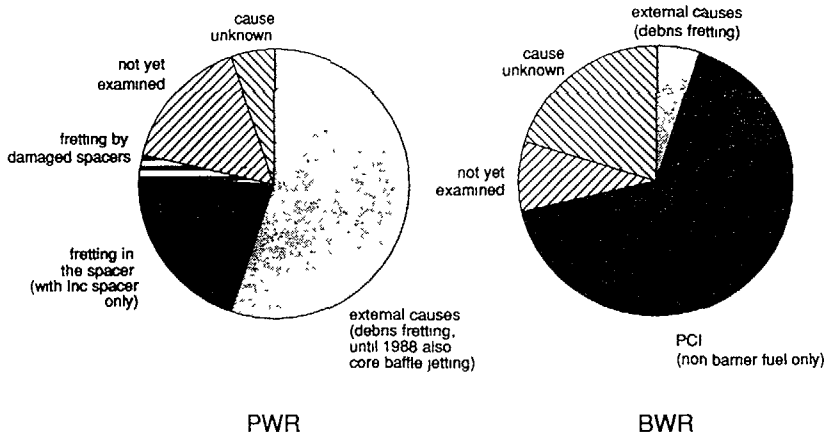

Fig. 3: Causes of Fuel Rod Failures and Their Relative Importance in SIEMENS/KWU Fuel (1985–91)

In both, PWRs and BWRs, only for a small fraction of rod failures the exact cause remained unknown inspite of detailed rod examination and other analyses. In the case of BWR this fraction has been somewhat larger and may contain unidentified PCI failures which typically occur in the 2nd or 3rd irradiation cycle. The percentages of early failures with unknown cause are equally low in BWRs and PWRs and are attributed to undetected deficiencies during manufacturing. Repeated checks and improvements in manufacturing procedures and quality control to eliminate all potential sources of impurities or other deficiencies led to a continuous decrease of those failures.

Further discussion has to be separated between PWR and BWR fuel, since all other features are different in the two types of plants.

2.2.2 PWR fuel

Up to 2/3 of the rod failures in PWRs had external causes, i.e. core baffle jetting and debris fretting. The former mechanism could be eliminated by repairing baffle joints and temporarily placing solid dummy rods on endangered positions; since 1989 only debris fretting was observed in this category. In future designs a debris separation grid at the lower end piece will provide significant improvements.

Rod failures due to fretting by vibration within spacer cells occurred sporadically in 15x15 and 16x16 fuel with Inconel spacers, preferentially in the bottom grid. So far the effect was not observed in assemblies with Zircaloy spacers. Nevertheless, the effect needs further attention, particularly at extended burnup.

With the exception of an early event (Obrigheim 1974), which had initiated the introduction of PCI limits in PWRs, not a single PCI failure has been observed in PWR operation, although the linear heat generation rates and burnups have been increased, and most plants are performing load follow operation. For this reason, and because of the fact that the PCI criteria for PWRs practically do not restrict load follow operation, there was never an incentive to use Zr–liner (barrier) cladding in PWR fuel.

Occasional spacer damage was observed in connection with assembly bow. The main effect is damage of spacer corners during loading or unloading fuel assemblies, but fuel rod failures by such damage have been extremely rare (see fig. 3). As initial modifications of spacer corner designs could not fully eliminate the problem, recommendations for loading and unloading procedures are still maintained and were successful in preventing this type of damage. Future fuel designs will be further optimized to reduce the potential of both, assembly bow and spacer corner interaction.

A remark should be made to the mechanism of assembly bow in PWRs, which predominantly had been attributed to cross flow in the core. A cross flow model, however, could not explain fretting effects by spacer corner interaction (fig. 4) recently seen in mixed cores of 18x18 fuel (more specificly in assemblies with Zry spacers having diagonal neighbours with Inconel spacers). The interaction must have occurred during operation and was more pronounced in assemblies with strong radial power gradients near the core periphery. It was concluded and is supported by a theoretical model that such gradients may contribute to in–pile bow under certain conditions and had been responsible for the observations in this fuel type.

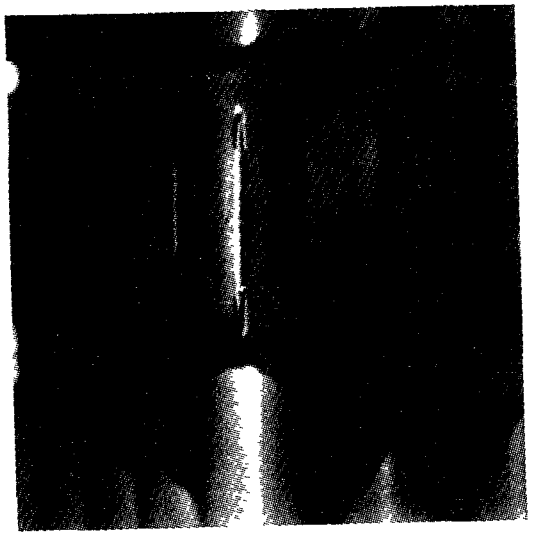

Fig.4. Fretting Mark on a Zry Spacer of a PWR 18x18 Fuel Assembly by Diagonal Spacer Corner Interaction

An isolated event of bow of some Zircaloy guide thimbles in a foreign plant (which in two cases led to damage during handling in the fuel pool) was found to be caused by unusual early hydrogen take–up from the coolant Since the effect is not generic, it will not be further discussed at this place. A brief description is given in Ref. /7/.

2.2.3 BWR fuel

A majority of fuel rod failures in BWRs was caused by PCI–induced stress corrosion cracking in 8x8 and 9x9–1 fuel not using the recommended remedy of a Zr–liner cladding. According to detailled analyses of power histories of affected 9x9–1 assemblies (from LPRM signals as well as recalculations), and of the correlation to increases in activity release into the coolant, the failures occurred under local ramping conditions which had not been experienced to a larger extent before but still maintained the given PCI operating recommendations. Since the failures could not be explained by relevant tests and earlier experience, several rods were examined in the hot cells under a joint program of the German utility group RWE and Siemens. The result was that an especially unfavourable type of pellet chipping and gap geometry had caused these failures, obviously by reducing the failure threshold compared to gap geometries with the usual patterns of pellet fracture. Out–of–pile pressure tests on pellet columns could reproduce this particular chipping effect and were also able to prove that a modified shape of the pellet end face and other measures to improve the fracture resistance of the pellets could prevent it. The introduction of these improved pellets is expected to solve the problem.

Rod failures by debris fretting occurred in BWRs with a much lower frequency than in PWRs. Smaller flow holes in the lower tieplate will be used in future designs and will further reduce the probability of such failures. Significant damage of structural parts was not observed in BWR fuel.

Channel deformation is monitored by measurements and calculuations with theoretical models, and an optimized "channel management" is applied for each refueling to avoid undue local power peaking and control rod/channel interference.

3. MANAGEMENT OF FUEL FAILURES

From the beginning of nuclear energy production in Germany in the mid 60ies, the general policy of Siemens and of plant operators was not to reinsert intentionally leaking fuel nor damaged fuel with the potential of developing a leak in the subsequent cycle. Therefore, Siemens was leading in providing all necessary fuel services to identify leakers, failure causes and remedies, as well as in designing repairable fuel assemblies and performing fuel repairs and reconstitutions. Nearly all fuel assemblies which failed before having reached their design burnup, have been repaired and successfully reused, which is an important contribution to optimum fuel utilization. This policy has been of great help to identify failure causes due to the possibility of closer examination of fuel rods and structural parts during repair.

Of course, inadvertent reinsertion of a leaking fuel assembly did occur occasionally, when a leak was not detected by sipping. There is no evidence for more severe damage of the fuel rods due to secondary hydriding in these cases when compared to fuel rods operating only up to one cycle in a defective condition.

All finally discharged fuel assemblies with leaking rods are repaired before shipment for final disposal, as reprocessing plants would require encapsulation of such assemblies. This circumstance provides for a very high percentage of fully examined fuel failures.

A major goal derived from the Siemens Quality Policy for the nuclear fuel is a systematic and continuous evaluation of the failure mechanism with immediate countermeasures to eliminate or at least to minimize the risk of failure in future operation. The corresponding procedures can be subdivided into five stages which will be described in more detail in the following chapter. Fig. 5 shows the typical sequence for these partly overlapping activities.

4. STAGES OF FUEL FAILURE EVALUATION

4.1. Monitoring coolant activity

The 1st stage is monitoring fuel performance during operation by evaluating coolant acticivities (and off–gas activities in BWRs). The relevant nuclides for this purpose are Xe–133,135, Kr–85m,87, I–131,133, Cs–134,137, and Np–239. Fairly continuous (e.g. daily) measurements over extended periods of steady–state operation are required to obtain reliable interpretations.

Today with over 90% of reactor cycles with Siemens fuel having zero or just one leaking fuel rod, one of the most important tasks is the unequivocal determination of a zero leaker condition. This task is easy to solve for clean reactor cores, but can be difficult in the presence of tramp uranium from failures in earlier cycles. The best way we found is an empirical one. Firstly one has to

1) based on sipping and inspections 2) based on detailed examination during repair

Fig. 5: Typical Sequence for Fuel Failure Evaluation

monitor the activity levels over the full cycle lengths including periods where the zero-leaker condition has been confirmed. Secondly one can take credit of the experience that most of the tramp uranium is deposited on fuel surfaces, which means that after refueling the activity from tramp uranium is diminished by a factor approximately corresponding to the fraction of fresh fuel assemblies loaded into the core. Practically a 100% successful prediction of zero leaker condition is feasible on the basis of this information.

If the activity levels indicate a leaker in the core, an estimate of the number of leaking fuel rods is routinely done by Siemens. Table II shows typical activities per leaker for several nuclides for current 1300 MW Siemens type plants /8/. However, one has to be careful in application, since the activity releases of different nuclides are dependend on the type, size, and axial location of a failure as well as on the linear heat generation rate. Very often a simple application of such values produces contradictory results for different nuclides, and special expertise with the evaluation of additional nuclides and nuclide ratios respectively are required for a good leaker estimate, which is generally more reliable with noble gas nuclides than with iodine nuclides.

Table II. Typical Activity Concentrations in the Coolant and Release Rates (rounded values) for one Leaking Fuel rod /8/

	Kr-85m	Xe-133	I-131
PWR*	4-6 E8 Bq/m³	1-2 E10 Bq/m³	1-2 E8 Bq/m³
BWR*	2-6 E6 Bq/s	2-6 E6 Bq/s	2-4 E6 Bq/m³

*1300 MWe plants with typical purification rates
Lower values for smaller fuel rod diameters (18x18 and 9x9 fuel respectively),
higher values for larger rod diameters (16x16 and 8x8 fuel respectively)

Without knowledge of the core position and power of the leaking assemblies, the accuracy of leaker estimates is limited to about a factor of 2. But if (e.g. by flux tilting or after sipping) this information is available, an accurate prediction of the number of leaking rods is usually obtained.

Continuous activity measurements allow the determination of the time when a failure occurs and the assessment of the further operational behaviour of the leaking fuel rod. It can also provide early hints on the failure mechanism (e.g. PCI and fretting type failures are often distinguishable at this stage). The details, however, are fairly complicated and have been summarized in Ref. /9/.

Flux tilting methods by evaluating the effect of moving control rods on the coolant activity are applied in several German BWRs to localize the region of leaking fuel in the core, which can save substantial time in sipping.

Task	Methods and *Equipment Used*
Checking for leaking fuel rods	Wet sipping technique *Pool-site and in-core sipping equipment* Ultrasonic detection of leaking fuel rods *ULTRATEST equipment*
Evaluation of general appearance (surface condition, deposits, wear integrity of connections)	Visual inspection *Underwater TV camera (monochrome and color) with manipulator*
Reconstitution of defective fuel assemblies	Removal of defective rods transfer of fuel rods to another skeleton recon ditioning of structural components *Fuel assembly reconstitution equipment automatic positioning system for fuel rod exchange device, EDM-cutting equipment*
Examination on fuel assemblies, individuel fuel rods and structural components for evaluation of operational performance	Measurement of dimensions and forces, eddy current methods *Accessory equipment to the inspection equipment for e g* *measuring length bow, rod position (axial and radial)* - *measuring oxide layer thickness on fuel rods and spacers* *collection and analysis of CRUD* *Accessory equipment to the reconstitution equipment for e g* *measuring fuel rod length and diameter* *measuring fuel rod oxide layer thickness circumferentially* *determination of spacer spring force* *Individual equipment for e g* *length and integrity of guide tubes* *assembly hold-down spring force*

Fig. 6 SIEMENS/KWU Nuclear Fuel Service Tasks and Methods for Examination of Fuel Assemblies

4 2 Pool–site examinations /10/

Extensive pool–site examinations as outlined in fig 6 define the 2nd stage, starting with sipping if the coolant activity indicates a leaker Fuel inspections are performed routinely during refueling to check fuel performance and include visual inspection as well as specific measurements e g for length growth, bow, and corrosion as desired The scope of inspection includes leaking fuel assemblies and can provide preliminary information on the extent and mechanism of the damage

With respect to fuel failure evaluation, the most valuable information is coming from the fuel repair which is usually performed during the subsequent operating cycle of the plant It includes a rod–by–rod examination by eddy current measurements and detailed visual inspection of the defective rods with a high–resolution underwater TV camera, allowing videotape and photographic documentation Also ultrasonic tests are used to identify the leaking rods in the assembly The repair campaign also provides an opportunity of closer inspection of inner structural parts and other examinations e g of the residual spacer spring forces

Based on the results of inspections and repair (sometimes supplemented by additional investigations as discussed in section 4 3), the failures can normally be uniquely attributed to one of the categories shown in fig 3 The sections "not yet examined" in fig 3 refer to fuel assemblies, where the fuel inspection has been insufficient to clarify the cause, and repair is still pending Nevertheless todays high percentage (nearly 100 %) of full examinations makes sure that there are no undetected failure mechanisms

4 3 Failure analysis

The 3rd stage is further failure analysis in order to fully understand the root cause and contributing factors This task starts with a detailed evaluation of the documentation from inspection and repair, since it requires expertise to interprete the visual observations and measuring results (e g to distinguish between primary and secondary failure or partial and through–wall damage in the case of a damaged fuel rod) In such cases a group of Siemens experts from different disciplines meet to find the correct interpretations with a reconstruction of the most likely sequence of events which had led to the damage

Depending on the individual case, further analysis has to be done by evaluating and/or recalculating fuel duties, power histories and burnup characteristics during earlier operation, by checking the detailed procedures of core operation or fuel handling, by analysing the influence of thermalhydraulic and water chemistry data, and of course by looking for correlations to specific fuel design and manufacturing features In some cases additional laboratory tests and analytical work, or even hot cell examinations are required for final clarification

A full description of these activities is not feasible in this paper, as the detailed procedure varies from case to case The analyses of recent PCI failures in BWRs and of assembly bow in PWRs as discussed in chapter 2 provide good examples for more complex situations

4 4 Experience feedback

As a result of the stages 2 and 3, adequate remedies can be defined to prevent reoccurrance of failures, and to mitigate the effects on affected assemblies during further operation The experience feedback by introducing such remedies is the task of stage 4 It comprises (i) immediate countermeasures in plant operation if required (e g modified operating recommendations or fuel handling procedures), (ii) the implementation of identified improvements in fuel design and manufacturing, and (iii) the long–term feedback into future development of fuel designs and materials Important is that this feedback is done as an indispensible part of quality assurance and of the efforts to improve fuel performance

Beyond the examples given in chapter 2, the following story can illustrate the importance of feedback In the mid 70ies fretting in spacer cells had been the main contributing factor to PWR fuel rod failures The root cause was found to be the low frequency event of inadvertent deformation of spacer springs during manufacturing Tighter quality control in spacer fabrication and improved assembling procedures were able to reduce the failure rate of new assemblies by

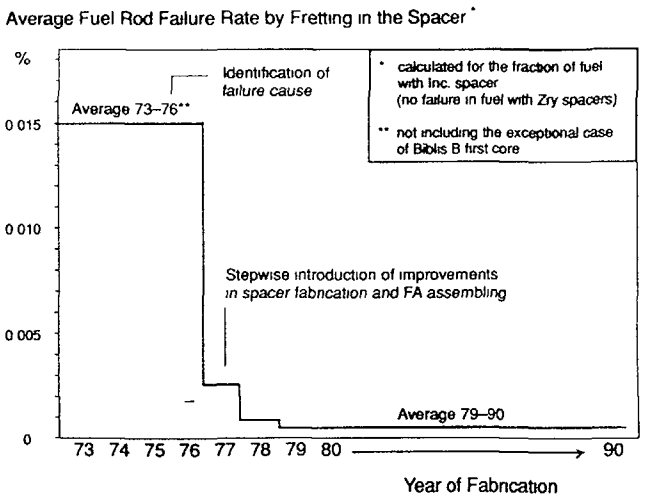

Fig. 7: PWR Fuel Rod Defect Rate by Fretting within the Spacer Cell for Assemblies with Inconel Grids

more than one order of magnitude (fig 7) Further reduction of the failure rate was achieved by optimizing the spring characteristics, which has been particularly successful in Zry spacers with no failure in over 3 300 fuel assemblies (corresponding to about 750 000 fuel rods) supplied up to now.

The experience feedback also includes the evaluation of the world-wide fuel performance to take preventive actions if necessary An excellent example is available. When General Electric had reported CILC failures in several plants and had identified Cu impurities in the water as a major contributing factor, Siemens contacted the German BWR operators with "CILC susceptible" plants and recommended stringent control and limitation of Cu ingress by the feedwater In this way the CILC phenomenon was not observed in German BWRs

4 5 Monitoring the success of remedies

The 5th and final stage is monitoring the success of the remedies This is mainly a repetition of the procedures of the stages 1 through 3 with the specific aim to quantify the improvements in fuel behaviour and reliability after the introduction of a remedy However, this aim has the consequence, that not only fuel failures have to be evaluated In addition to this a quantitative follow-up of operating experience with *all* fuel assemblies is necessary in order to obtain the statistical data base for evaluating the long-term development of failure rates from different causes and of other performance features

For Siemens KWU fuel this task is solved by storing the relevant information on design operation and performance for each individual fuel assembly in a common data base This approach provides quick access to the data and facilitates the necessary evaluations Another advantage of this data base is of course, that summaries on relevant aspects of operating experience (as e g table1, fig 3, fig 7) can easily be made and updated

5 CONCLUSIONS

Inspite of the very low fuel failure rates the systematic and permanent evaluation of operating experience and fuel failures plays an important role today The continuous efforts of Siemens and the full support of the plant operators in all stages of fuel failure evaluation, with permanently accumulating expertise and improving the methods of investigations, have been essential to keep fuel performance fully under control, and to achieve and maintain high fuel reliability The resulting detailled knowledge of the failure mechanisms and their relative importance are also the basis to implement effective measures for further improvements

REFERENCES

/1/ KREBS, W-D , HOLZER, R , WINNIK, S , Activities of a fuel supplier for European nuclear power plants, Kerntechnik 55 (1990, No 2) 87

/2/ LILL, G , KNAAB, H , URBAN, P , Advanced BWR fuel designs incentives, implementation, performance verification, Proc ANS/ENS International Topical Meeting on LWR Fuel Performance, April 21–24, 1991, Avignon France "Fuel for the 90 s , Vol 1, p 74,
see also SIEMENS Nuclear Fuel Report No 2 (March 1992) 11

/3/ HOLZER, R , GARZAROLLI, F , ZIMMERMANN, R , Fuel design advancements by application of Siemens FOCUS technology, presented at the 7th KAIF/KNS Annual Conference, April 21–22, 1992, Seoul Korea,
see also SIEMENS Nuclear Fuel Report No 2 (March 1992) 16

/4/ SIEMENS Nuclear Fuel Report No 2 (March 1992) 19

/5/ ROBERTSON, J A L , Nuclear fuel failure, their causes and remedies, (Proc ANS/CNA Topical Meeting of Commercial Nuclear Fuel Technology Today, April 28–30,1975, Toronto Canada), p 2–1

/6/ GARZAROLLI, F , von JAN R STEHLE, H , The main causes of fuel element failure in water cooled power reactors, ATOMIC ENERGY REVIEW (IAEA Vienna) 17 (1979) 31

/7/ SIEMENS Nuclear Fuel Report No 2 (March 1992) 42

/8/ BLEIER, A , FISCHER, G , SIEMENS AG KWU, Department Radiochemistry, personal communication

/9/ SCHUSTER, E., von JAN, R., FISCHER, G., Evaluation of fuel performance from coolant activity data, Proc. ANS/ENS International Topical Meeting on LWR Fuel Performance, April 21–24, 1991, Avignon France, "Fuel for the 90 s" Vol.1, p. 285.

/10/KNAAB, H., KNECHT, K., JUNG, W., Pool–site inspection and repair techniques, Atomwirtschaft–Atomtechnik 37 (April 1992) 194;
see also SIEMENS Nuclear Fuel Report No.2 (March 1992) 33.

ABB ATOM FUEL FAILURE – AN OVERVIEW

L. LUNDHOLM, B. GRAPENGIESSER,
D. SCHRIRE, L. HALLSTADIUS
ABB Atom AB,
Västerås, Sweden

Abstract

This paper presents the recent experience of ABB Atom fuel failures, inspection results and failure remedies. The failure frequency for fuel rods supplied since 1979 is $6x10^{-5}$ (all causes), and $<2x10^{-5}$ when proven debris fretting and other non fuel-related causes are excluded. ABB Atom aims to identify the cause of every failed rod, to help achieve a zero failure goal. Reactor cores are assured free from failures at start up after refuelling.

ABB Atom carefully follows the monitored leakage. Up to 1986 the number of leaking rods could usually be estimated from leakage levels of radio-isotopes of xenon, cesium, iodine and neptunium. However, these correlations are not always accurate, since the power rating has been upgraded. Xe-133 leakage rate is still as the best measure of the number of fuel failures in the core. The Cs-137/Cs-134 ratio is useful for assessing the burn-up of the leaker. Np-239 is used to determine the amount of fuel in direct contact with the coolant, and is used together with different iodine isotopes to follow the development of secondary defects. Anticipated leakers as determined from flux tilting and in-core or out of core sipping are subjected to pool-side inspection. This includes visual inspection, eddy current testing and sometimes gamma-scanning, in order to determine the location and primary cause of failure. If the cause cannot be determined with certainty in the poolside inspection, or in other exceptional cases, hot cell examination is performed.

Fretting by foreign debris has been determined as the predominant cause of failure (at least 39 of 58 failed rods since 1979). Debris fretting occurs close to or within a spacer, and can be positively identified by the appearance and exact location of the fretting hole. Severe secondary degradation may hide the primary failure, and it is believed that most of all of the 14 unidentified cases are also caused by fretting. Only one rod is known to have failed as a result of a fabrication fault: this was a PWR rod of early design which is thought to have failed due to low spring force. In 1988 in Oskarshamn 2 four rods failed due to dry-out.

Remedies are being implemented to minimize the risk of fuel failure, as well as to ameliorate the effect of failure. Debris filters have been designed and verified out of pile for both BWR and PWR fuel, and will be tested in power reactors from 1992. A new corrosion-resistant liner cladding has been proven effective in reducing the extent of secondary hydriding failure in BWR liner fuel.

1. INTRODUCTION

ABB Atom defines fuel failure as penetration of the cladding, although in practice fuel failure is only identified by activity release. This paper presents a brief overview of our recent experience with fuel failure causes, detection, behaviour, management and remedies, covering fuel loaded after 1979, or fuel delivered since 1978.

2. DETECTION AND CHARACTERIZATION OF FUEL FAILURES

2.1 Monitoring of fission product release

The utilities carefully follow the activity in the coolant and offgas. Noble gases are measured "on-line" in the offgas system. The offgas measurements are performed at the turbine condenser ejectors (system 552) or at the plant main stack (553), as shown in Figure 1.

The "Σ6" (sum of the six most important noble gas radionuclides) is frequently quoted as a measure of release rates. However, these six krypton and xenon isotopes have very different production ("birth") rates and half-lives (Table I).

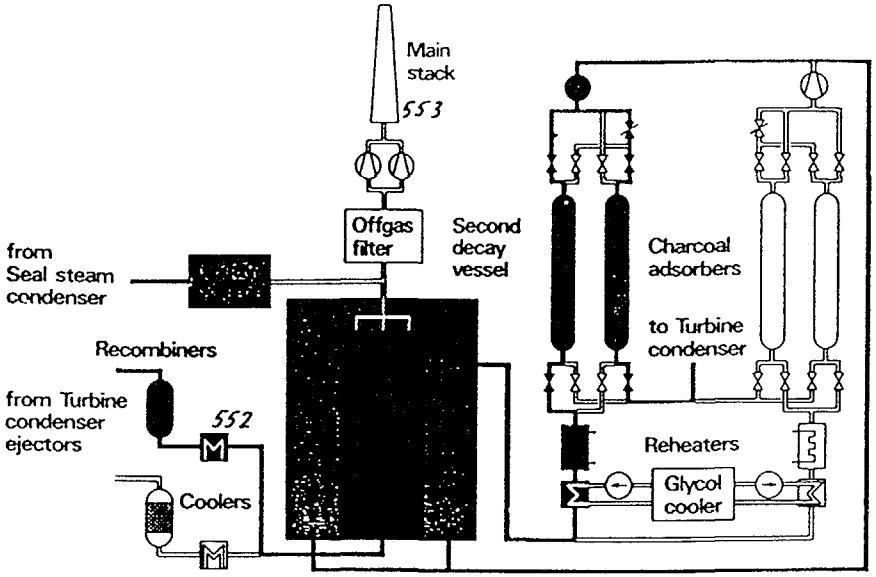

FIG. 1. The ABB Atom offgas system.

Table I. Sum-of-six

Isotope	Half-life	Production rate relative to Xe-133 Bq/s
^{85m}Kr	4,5 h	4
^{87}Kr	76 min	25
^{88}Kr	2,8 h	16
^{133}Xe	5,3 d	1
^{135}Xe	9,1 h	10
^{138}Xe	14 min	359

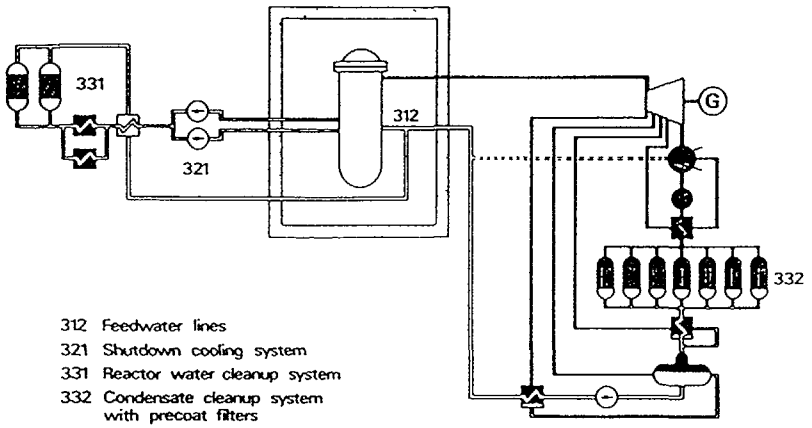

FIG. 2. Primary water cleanup system.

Due to their different half-lives, these isotopes also have very different detection-to-birth ratios, depending on the overall transport time from birth to detection. This transport time includes diffusion and transport within the fuel and fuel rod, excepting when the fuel is in direct contact with the coolant.

The ^{133}Xe leak rate is probably the best measure of the number of fuel failures in the core. ^{133}Xe has a comparatively long half-life (5,3 days), which means that it is relatively unaffected by the transport time within the fuel rod prior to release to the system. Activity levels of short-lived isotopes are on the other

hand strongly affected by the time for diffusion out of the rods. These isotopes thus dominate the measured noble gas activity when there is extensive exposure of fuel to the coolant, as is the case with tramp uranium, or severely degraded secondary defects leading to fuel exposure, since they dominate the production (Table I), and recoil release from fuel surfaces is essentially instantaneous. In addition, the recoil release from tramp uranium has a release/birth ratio of about 0,5 (50% release), with the rest firmly embedded in the cladding. The ratio of a short-lived isotope (ABB Atom uses ^{138}Xe with a half-life of 14 minutes), to a long-lived isotope (^{133}Xe) indicates the degree of degradation. This ratio is especially sensitive to the increase in the diffusional release stimulated by the oxidation of the UO_2. It should be noted, however, that transportation delays within the primary circuit before detection can still make a large difference to the detection-to-birth ratios of the different isotopes and must be corrected for when comparing failures in different reactors.

Non-volatile isotopes are measured in the reactor water cleanup system (321) as shown in Figure 2. ^{239}Np (with a 2,4 d half-life), daughter activity to an activation product of ^{238}U, indicates the amount of fuel in direct contact with the coolant. It is released by dissolution together with uranium, as well as by β-recoil when essentially only the decaying nuclide (^{239}U) itself is transferred to the coolant. Together with different iodine isotopes, it can be used to follow the development of secondary defects, and is also used to assess fuel erosion.

^{131}I (8 d) is of interest from a radiological standpoint: refuelling outages may occasionally be delayed by high levels of ^{131}I in connection with core depressurisation, resulting in large additional costs . However, iodine is a quantitatively poor indicator of fuel failures. It is distributed in a complicated manner between both water and steam, and it's volatility ratio depends on reactor design. Iodine also shows a different behaviour in water compared to steam.

A correlation has been found between secondary failures with cladding deposits of fissile material and the activity level of ^{60}Co. It is believed that fission recoils from the thin layer of fissile material, which plates out on the cladding, ejects ^{60}Co from the crud layer. This effect is thought to be large enough to increase the ^{60}Co release to the degree observed, and is thus an example of an indirect radiological consequence of severe secondary fuel rod defects.

Since ^{137}Cs is proportional to burnup and ^{134}Cs is proportional to the square of the fluence, the $^{134}Cs/^{137}Cs$ ratio is useful for assessing the burn-up of the leaker. Many BWR utilities use flux-tilting at reduced power prior to shutdown at the end of a cycle, in order to locate the leaking assembly by correlating leakage response to control rod movement. This technique is usually successful in localising the leak at the "supercell" level (i. e. the four assemblies adjacent to the same cruciform control blade). Additional information on the burnup level of the leaking rod can sometimes then be used to identify the individual leaking assembly, when the four assemblies in the supercell have different average burnups. This practice leads to efficient use of the short Nordic BWR annual refuelling outages, since a limited number of assemblies have to be checked by sipping in order to assure a failure free core at the start of the next cycle.

2.2 Poolside Inspection

Anticipated leaking assemblies, as determined from flux tilting during operation, undergo in-core or out of core sipping after reactor shut-down. ABB Atom has developed advanced sipping techniques, which provide enhanced sensitivity and speed of operation. After the leaking assembly has been identified, the individual rods are subjected to pool-side inspection. This includes visual inspection and eddy current testing. Gamma-scanning has been used to determine the amount of uranium lost by erosion in a severely degraded defect rod. Gamma-scanning has also been used to locate regions with extensive Cs-137 release, and thereby determine the axial location of penetrations.

2.3 Hot-cell examinations

If the failure cause cannot be determined with reasonable certainty in the poolside inspection, or when additional valuable information on failure and degradation mechanisms is desirable, hot cell examinations are performed. A relatively large number of the failed rods have been shipped to the Studsvik hot cells for PIE; this work has largely been financed by the Swedish utilities.

Visual inspection, neutron radiography, profilometry, eddy current testing and axial gammascanning have been used to locate and identify the cause of failure, as well as the extent of cladding damage and fuel and fission product loss. In addition to these techniques, metallography, ceramography, microgammascanning, scanning electron microscopy of the fuel and cladding, pellet-clad gap and fuel density measurements, and cladding hot extraction hydrogen measurements, are some of the methods which have been employed at Studsvik to clarify the mechanisms of failed fuel behaviour.

3. EXPERIENCE

3.1 Failure causes

Fretting by foreign objects (debris fretting) has been identified as the primary cause for at least 39 of the 58 failed rods since 1979, and is thus the predominant failure mechanism (Figure 3). Debris fretting occurs close to or within a spacer grid, and can often be positively identified by the appearance and exact location of the fretting hole. It is likely that most of the 14 remaining unidentified cases are also caused by debris fretting.

Four rods failed in Oskarshamn 2 in 1988. Pool-side inspections including gamma measurements quite clearly indicated that the cause was dry-out, which was later confirmed by hot-cell examinations in Studsvik. The axial distribution of ^{137}Cs revealed a loss of cesium in the "dry-out zone" indicating excessive temperatures in that region. This technique was also valuable for

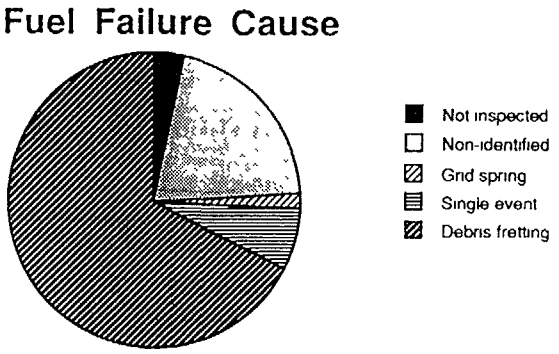

FIG. 3. ABB Atom fuel rod failure experience.

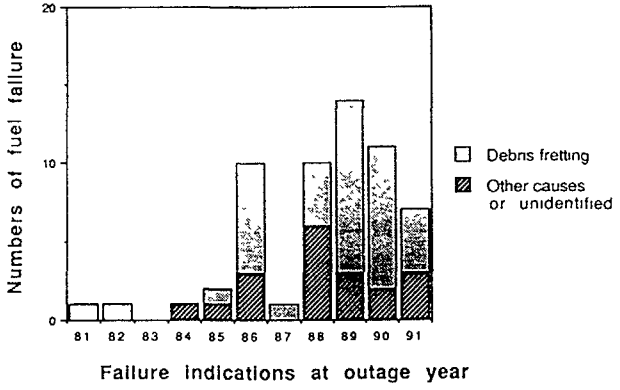

FIG. 4. Debris fretting and other fuel failure causes versus outage year.

experimental power characterization in the dry-out region, which showed that non-failed neighbouring rods had operated at excessive power ratings due to channel bow.

Only one ABB Atom rod is known to have failed since 1979 as a result of a fabrication error; this was a PWR rod of an early design and it is believed to have failed due to an insufficient spacer spring force.

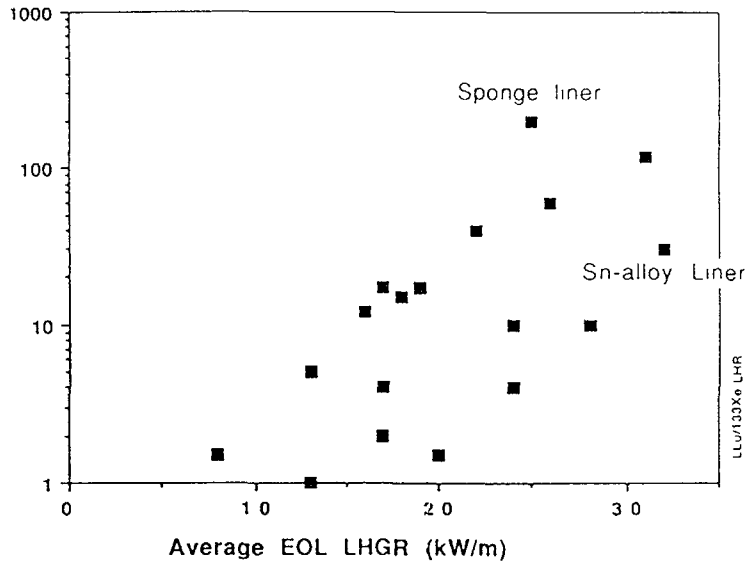

FIG. 5. Average ^{133}Xe leak rate (MBq/s).

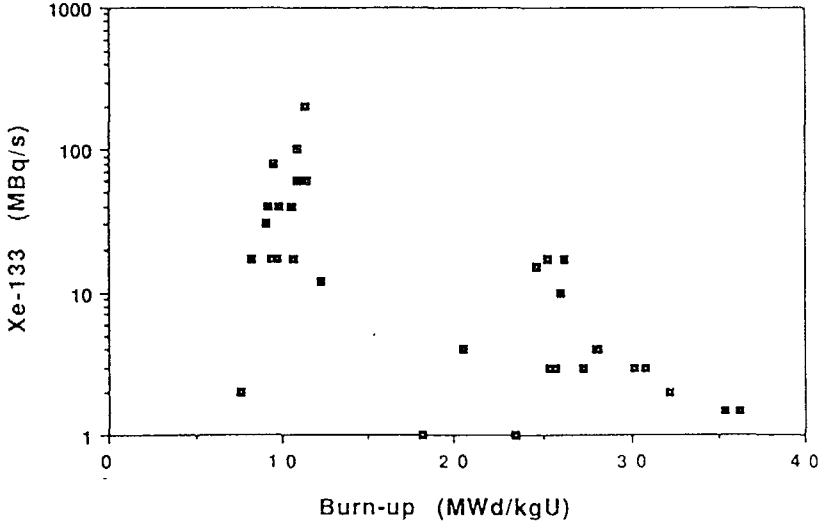

FIG. 6. Leak rate of ^{133}Xe versus burnup

Table II.

Failures on fuel loaded after 1979

Unit	Failure indications at outage year											
	Σ	81	82	83	84	85	86	87	88	89	90	91
BWR 1	1	0	0	0	0	0	0	0	0	0	1	0
BWR 2	4	0	0	0	0	0	1	0	0	2	0	1
BWR 3	5	1	1	0	0	1	0	0	0	0	1	1
BWR 4	3	-	0	0	1	0	0	0	0	1	1	0
BWR 5	25	-	-	-	-	0	3	0	3	10	5	4
BWR 6	0	0	0	0	0	0	0	0	0	0	0	0
BWR 7	4	0	0	0	0	0	0	0	4	0	0	0
BWR 8	4	-	-	-	-	0	3	0	1	0	0	0
BWR 9	5	0	0	0	0	1	2	0	2	0	0	0
PWR 1	2	-	-	(2)	(2)	0	(3)	(1)	0	(1)	2	(1)
PWR 2	1	-	-	0	0	0	0	1	(2)	(1)	0	0
BWR 10	0	0	0	0	0	0	0	0	0	0	0	0
BWR 11	2	0	0	0	0	0	1	0	0	0	0	1
BWR 12	0	-	-	-	-	-	-	-	0	0	◊	0
BWR 13	0	-	-	-	-	-	0	0	0	0	0	0
BWR 14	0	-	-	-	-	-	-	-	0	0	0	0
PWR 3	2	-	-	-	-	-	-	-	-	1	1	0
BWR 15	0	-	-	-	-	-	-	0	0	0	0	0
PWR 4	0	-	-	-	-	-	-	-	-	-	0	0
BWR 16	0	-	-	-	-	-	-	-	-	-	0	0
PWR 5	0	-	-	-	-	-	-	0	0	0	0	0
PWR 6	0	-	-	-	-	-	-	0	0	0	0	0
Σ	58	1	1	0	1	2	10	1	10	14	11	7

Bold face	Final data
Numbers in brackets	ABB Atom rods in W skeleton.
◊	No outage

3.2 Leakage

ABB Atom has performed several studies of activity leakage rates. These have shown that the number of leakers and leakage levels of radio-isotopes of xenon, cesium, iodine and neptunium are not always well correlated, due to power uprating and non-homogeneous axial power distributions. However, certain trends are evident.

The leakage rate increases with the linear heat generation rate (LHGR), since vital mechanisms such as diffusion and chemical reactions accelerate with temperature. The effect of power on activity release rates is seen in Figure 5, where the release rate is plotted against the rod average LHGR for different rod failures.

When the primary cause, normally fretting from foreign debris, results in a penetration of the rod cladding, steam enters the rod and the internal pressure equilibrates with the system pressure. It is easier for the fission gas (both the previously released gas in the rod free volume, as well as ongoing gas release), to leave the rod after pressure equilibration. Earlier released fission gases leave the rod by diffusion and pumping ("breathing") due to small power-induced temperature and pressure changes. Leakage from a single minor hole must be pulsed, since fission gas (normally) cannot escape from the rod unless an overpressure is generated all the time.

An open pellet cladding gap is a prerequisite for efficient dispersion of water and fission products along the rod. Hence, low burnup would be expected to favour large leak rates. This effect can be clearly seen in Figure 6; although the decrease in release with increasing burnup is mainly due to the lower power levels at higher burnups, correction for the LHGR reveals a residual burnup effect which is independent of the power. PCI failures should therefore only slowly lead to extensive secondary damage and leak rates, since the gap is closed (by definition) when the penetration occurs. On the other hand, a large primary hole, such as those caused by fretting, with a large gap (early in life) may be expected to lead to rapid detoriation of large axial parts of the rod and considerable leakage.

Local oxidation of the fuel from $UO_{2.00}$ to more hyperstoichiometric states leads to an increase in the self-diffusion and fission product diffusion rates, as well as a decrease in the thermal conductivity. These effects lead to a marked increase in the local fission gas swelling and release, as well as grain growth.

3.3 Secondary failures

There is no certain way, other than experience, to predict precisely if and when a secondary defect will form.

Due to oxidation of the fuel, and radiolysis of the steam entering the rod, the H_2/H_20 ratio is changed, eventually leading to rapid local hydrogen pick-up by the cladding at some location (some distance away from the primary leak) with a favourable H_2 and H_20 partial pressure. Areas of the cladding with little protective oxide, as well as Zircaloy with locally reduced resistance (such as heat affected zones near welds), are particularly susceptible to hydriding. Having established a secondary hydride defect, a steamflow ("chimney effect") can be created through the rod, which in turn exposes much more of the fuel stack to steam, and causes even more fission product release as well as direct fuel erosion in severe cases.

The steamflow can limit any further hydriding between the two leak sites, but the conditions required for hydriding may again be established at a new site. A secondary hydride defect may also propagate by a delayed hydrogen cracking

mechanism, if sufficient cladding hoop stresses are built up by fuel swelling or cladding oxidation and hydriding.

3.4 Liner rods

Only two ABB Atom liner-cladding rods have failed, both due to debris fretting. In recent years, ABB Atom has been supplying Sn-alloyed liner with improved corrosion resistance. Ramping tests in the R2 reactor at Studsvik verified that the PCI advantages were the same as for zirconium liner. A sponge liner rod failed in Oskarshamn 3 with severe degradation leading to a very large release, while a rod which failed in Barsebäck 2, with the optimized liner proved its effectiveness in reducing the extent of secondary hydriding propagation in BWR liner fuel (Figure 5).

4. MANAGEMENT

Since the leakage rate increases with LHR, reducing the local power in an assembly with a leaking rod is helpful in reducing the activity leak rate, as well as the onset of secondary defects.

When a severe fuel failure is present, avoiding power cycling (such as daily or weekly load following) can alleviate secondary degradation.

The Nordic utilities avoid reinserting defected fuel (i. e. assemblies known or strongly suspected of containing one or more defected fuel rods), a practice which ABB Atom strongly recommends. Rapid location of the leaking assembly, and efficient ICFM routines, have enabled the Nordic utilities to implement this policy without impacting on their short annual refuelling outages, and thus maintain their high plant capacity factors. The failed fuel rod can then be identified in the poolside inspection, removed and replaced, so that the assembly can be reinserted at a later stage.

ABB Atom and the utilities share the common goal of identification of the primary failure cause. Only by identifying the cause of failure is it possible to take steps to prevent its reoccurrence. A deliberate policy of failure cause identification is implemented by the utilities in Sweden, and is facilitated by relatively easy access to hot cell facilities at Studsvik.

5. REMEDIES

Remedies are being implemented to minimize the risk of fuel failure, as well as to minimize the effect of a failure if it still appears. Changing from 8x8 fuel to the SVEA concept is, in itself, efficient in reducing fuel failure due to debris fretting, since the bottom tie plate stops wires better than the old 8x8 bundle.

5.1 Debris filter

Debris filters have been designed and verified out of pile for both BWR and PWR fuel, and will be tested in power reactors from 1992. For BWRs the design is made up of four separate debris filters mounted in the bottom tie plate of the bundle (Figure 7). In laboratory tests the debris filter has been shown to trap 65-100 % depending on the type of debris, and together with the bottom plate,

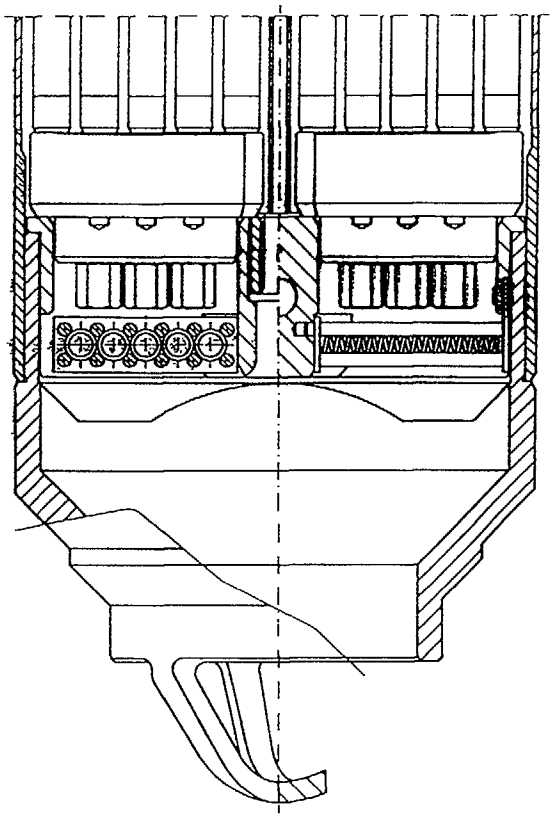

FIG. 7. Debris filter SVEA-96.

catches 85-100%. It traps all the swarf, and almost all of the wires, which are typical fretting debris.

ABB statistics show that about 70% of PWR fuel failures are caused by debris. ABB Atom supplies the ABB CE Guardian™ grid for PWR fuel (Figure 8). The debris tend to be trapped between the lower end fitting and the grid. If trapped debris vibrates here, it will harmlessly contact only the solid end cap which goes into the Guardian™ grid. The debris stays within the fuel assembly and is eventually discharged with the spent fuel.

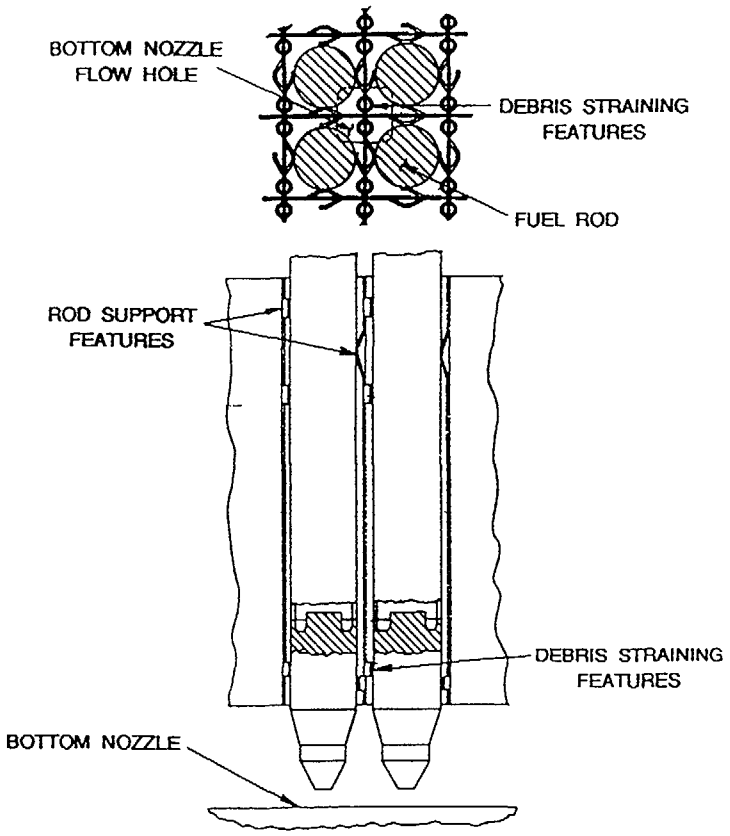

FIG. 8. The Guardian ™ design.

5.2 SVEA 10x10

SVEA 10x10 is a more favourable design as regards of leakage due to its lower linear heat rate and the fact that there is a smaller amount of fuel in each rod. No ABB Atom 10 x 10 rod has failed to date.

ACKNOWLEDGEMENTS

We are grateful to the utilities without whose efforts the data and information, on which our understanding of fuel failures is based, would not have been possible. In particular, we would like to mention OKG, SSPB, Sydkraft and TVO, who financed most of the in-pool and hot cell examinations.

Next page(s) left blank

DETECTION AND MONITORING OF FUEL FAILURES

(Session II)

Chairmen

M. GROUNES
Sweden

T.J. CARTER
Canada

CORRELATION BETWEEN FISSION PRODUCT ACTIVITY IN PWR PRIMARY WATER AND CHARACTERISTICS OF DEFECTS IN FUEL CLADDING

C. LEUTHROT
Direction des réacteurs nucléaires,
Commissariat à l'énergie atomique,
Saint-Paul-lez-Durance

A. BRISSAUD, A. HARRER
Service Etudes et projets thermiques et nucléaires,
Electricité de France,
Villeurbanne

France

Abstract

Modeling of the behavior in the primary circuit of fission products released by fuels with cladding failures, carried out at the CEA in connection with EdF feedback on the subject, has made it possible to develop and validate correlations between the spectrum of volatile fission products (rare gases, iodines and cesiums) in the primary coolant of PWRs under stable operating conditions and the characteristics of fuel cladding failures ; these correlations are presently used in France for monitoring the state of PWR fuel cladding. New developments, which take into account various operating modes of the reactors (stable operating conditions, shutdown transients, network monitoring transients) produce new correlations allowing a more precise and more complete characterization of cladding failures. Formalization of these developments has led to the writing of failure characterization software concerning fission product activity in the primary coolant ; optimal use of this software will be obtained by coupling it to an on-line gamma spectrometry device measuring primary activity.

INTRODUCTION

The design of pressurized water reactors does not allow the use of selective equipment for detecting failures in fuel cladding. Attempts have always made been to overcome this drawback by devising methods for characterizing the state of reactor cladding using the spectrum of fission products emitted by defected fuels. These attemps have particularly concentrated on those chemical species whose behavior in the primary circuit is easiest to model and whose activity is relatively easy to measure using gamma spectrometry of the primary water. The chemical species that meet these criteria are fission gases, iodines and cesiums.

Until the 1970s, the reliability and accuracy of the gamma measuring systems installed in reactors as well as understanding of fission product release mechanisms were inadequate for accurate characterization of cladding failures. Only correlations involving a few easily measured istopes (^{131}I, ^{133}I and ^{133}Xe) could be used to obtain qualitative characterizations of the state of deterioration of the cladding (failure free, presence of micro-failures, major failures). Improvements in equipment, measuring methods and theoretical understanding, together with the considerable number of measurements taken by the EDF on electronuclear reactors, both under stable operating conditions and during operational transients, have allowed considerably more accurate correlations to be developed between the spectrum of fission products and the characteristics of cladding failures. In many cases, selective characterization of the various defected rods present in the core at a given time has been possible. These correlations can also be used in reverse, i.e. to predict primary circuit activity for given cladding states and reactor operating conditions. This application of the correlations is of particular interest in decision-making concerning the refuelling of defected reactor assemblies as part of the EDF's fuel management policy.

1. PRINCIPLE OF CALCULATION METHODS

Activity in primary coolant due to fission products released by defected fuels are the result of an equilibrium between the release rates of the uranium oxide where they originate and their disappearance due to radioactive decay, neutron capture and reactor purification. Activity levels of nuclides with different radioactive periods are therefore dependent on these release rates. The release rates are in turn dependent on migration speeds within the oxide and inside the clearance between the fuel and the cladding in the defected rods, and consequently on the characteristics of the rods :

- Oxide temperature
- Dimensions of the defect
- Physico-chemical characteristics of the fuel/cladding clearance
- Quantity of fissile material disseminated in the primary circuit

Theoretical modeling of release mechanisms performed using the CEA PROFIP IV code [1] shows that some nuclides are more sensitive to one or other of these characteristics and that the various characteristics of the defects can usually be selectively determined from the activity of carefully selected nuclides.

To break away from the reactor operating parameters that are independent of the failure characteristics but have an influence on the activity levels of fission products in the primary coolant (such as the CVC rate or water make-up), all the correlations described in this presentation concern instantaneously released fractions of nuclides in the water and not their activity levels. These released fractions are calculated using the activity balance of each nuclide in the primary water and the operating parameters of the reactor. Among other notions used is the mean instantaneously released fraction for a nuclide, i, defined as:

$$(F_i)_m = R_i/(B_i)_m$$

where:

R_i is the instantaneous release (at/s) of the nuclide into the primary water from all the defected rods

$(B_i)_m$ is the instantaneous production of the nuclide i (at/s) in one rod subject to the mean linear power density of the reactor.

1.1. Chemical families of fission products used for diagnosis:

Quantitative characterization of the state of the fuel cladding of PWRs and the resulting contamination of the primary circuit is based on studies of 3 chemical families that do not present

significant deposit mechanisms on the circuit walls and for which correlations between defected rod release and activity in the water are consequently easily implemented

rare gases
iodines
cesiums

The radionuclides from these different families that are easy to measure by gamma spectrometry and can be used in diagnosis are as follows

gases ^{133}Xe ^{133m}Xe ^{135}Xe ^{138}Xe ^{85m}Kr ^{87}Kr ^{88}Kr
iodines ^{131}I ^{133}I, ^{134}I ^{135}I
cesiums ^{134}Cs, ^{137}Cs

1 2 Correlations with fission gases Number of defects

Gaseous nuclides are easily diffused by uranium oxide and are not trapped during their migration from the oxide to the primary coolant. Gases are the chemical family for which released fractions into the primary coolant are the most significant Moreover, at least as concerns French PWRs, their migration is little affected by the size of the defect As first approximation, released fractions of these nuclides are only dependent on the temperature of the defected fuel It follows that if the power of the defected rods can be established, models can be used to calculate real released fractions for each rod into the water from fission gases A comparison of this calculation with the measured values of mean released fractions will yield the number of cladding defects present in the core

Theoretical models of gas migration [2], including grain boundary diffusion, and athermal mechanisms such as knock-out and recoil, show that, within the utilization limits of PWR fuel and for the radionuclides under consideration, the instantaneous released fraction of a fission gas, i, with radioactivity constant, λ_i, can be expressed as follows

$$F_i = k \cdot \lambda_i^{\,n} \qquad (1)$$

where k and n are only dependent on the fuel temperature (n is usually close to 0.5, which is consistent with a diffusion mechanism) If ^{133}Xe is taken as a reference, equation (1) can be written

$$F_i = F133_{Xe} \cdot (\lambda_i / \lambda 133_{Xe})^{\,n} \qquad (2)$$

1 2.1 Correlations under stable operating conditions

Calculations for a particular type of fuel, performed using the PROFIP code can be used theoretically to establish the relations

$$F_{133Xe} - f(T_{fuel})$$

$$n - f(T_{fuel})$$

The relation $F_{133Xe} = f(n)$ can be deduced in which the implicit parameter T_{fuel} no longer appears (see figure 1)

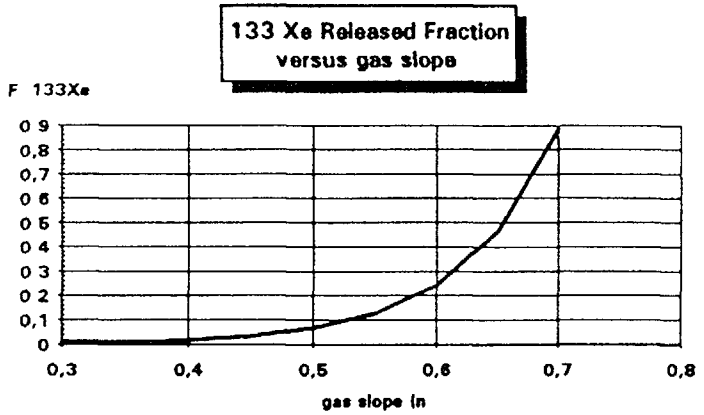

FIG 1

Experimental determination of n enables the number of defects to be calculated using the relation.

$$\text{number of defects} = [(F_{133Xe})_m / F_{133Xe}] \cdot (P_m / P) \qquad (3)$$

where P is the linear power density of the defected rods
Pm is the mean linear power density of the core

The power P of the defected rods is obtained from the same study carried out using the PROFIP code to link F_{133Xe} to the fuel power as a function of the opening period of the defects (see figure 2)

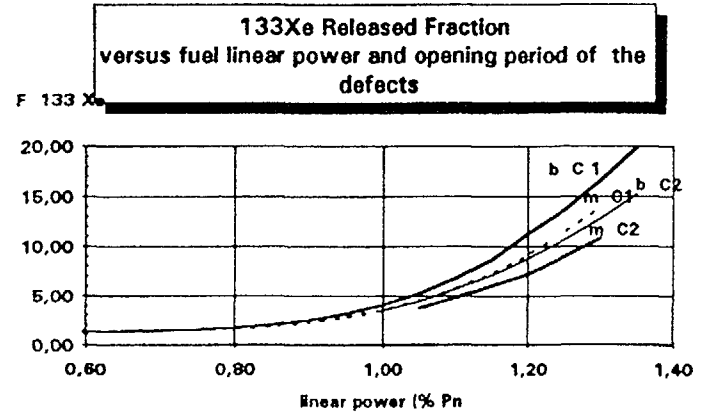

FIG 2

1 2 2 Correlations using power plateaux at different levels

It will be seen from figure 1 that a slight variation in slope n produces significant deviations in values for F_{133Xe} Moreover, the size of the defect, even though only operating in the second order, can also disturb relation (1) The method of establishing the number of defects described in 1 2 1 is thus not very accurate Wherever possible, the method described below in 1 2.3 is used instead

The ratio $(F_{133Xe})_{P1} / (F_{133Xe})_{P2}$, expressing released fractions of ^{133}Xe during 2 power plateaux at different levels, P1 and P2, is a function of the radial power factor of the defected rod This ratio can be measured either directly or by extrapolating F_i for gases with shorter radioactive periods and then deducing the real released fraction, F_{133Xe} of a defected rod The value of the higher plateau P1, is usually the nominal power, Pn Figure 3 shows the theoretical development of the real fraction of ^{133}Xe released per rod as a function of the ratio of mean fractions released in the primary coolant for different power levels compared with the nominal power The values in figure 3 can be reduced to a single curve as follows (see figure 4)

$$F_{133Xe} = f[(F_{133Xe})_{mP1} / (F_{133Xe})_{mPn} * (Pn/P1)^{**}0.4] \quad (4)$$

The number of defects is then determined using the method described in 1 2 1 (relation (3))

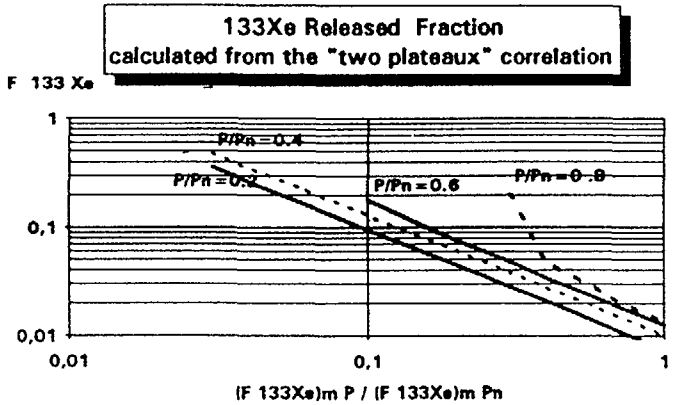

FIG. 3

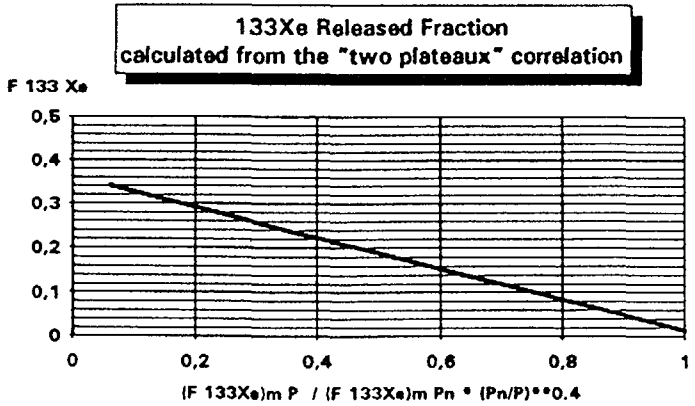

FIG 4

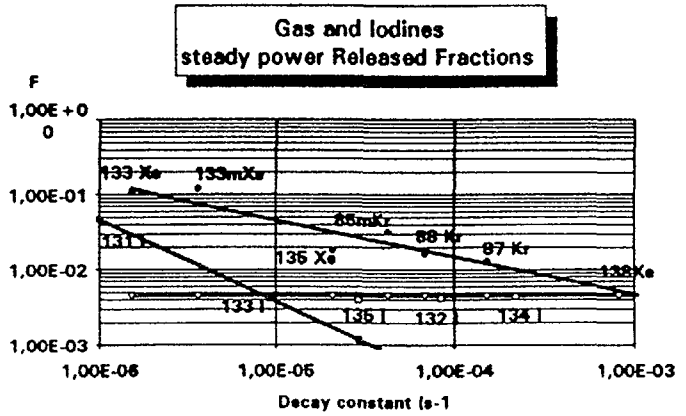

FIG 5

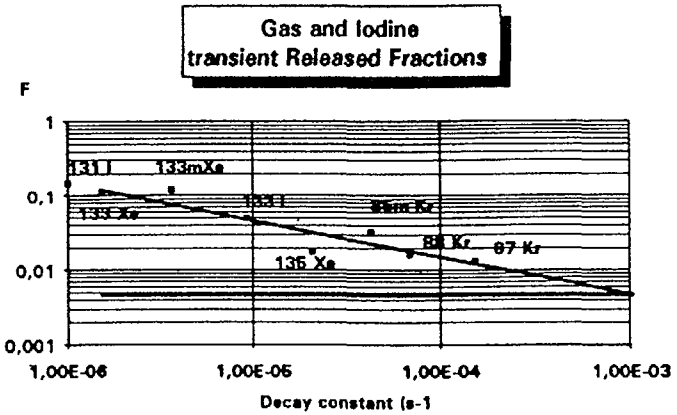

FIG 6

1 3 Correlation using iodines Number and size of defects Uranium contamination of cladding

(a) Number of defects

Fission iodines migrate inside the oxide in exactly the same way as gases They can, however, be trapped during migration in the cold sections of the fuel and the fuel/cladding clearance The fractions released into the primary coolant are therefore usually lower than those of gases (figure 5) However, during long power transients, particularly shutdown transients, these trapped fractions are redissolved in the primary coolant following penetration of water into the clearance Experience shows that detrapping is usually total and that overall released iodine fractions, including release under stable operating conditions and during transients, are equal to those of gases with the same radioactive periods (figure 6) All the values for released gas and iodine fractions enable the parameters of equation (1) to be established with considerably greater accuracy than that obtained using gases under stable operating conditions This is because this estimation

concerns a larger number of nuclides
- is independent of the size of the defect.

(b) Size of defects

It is very difficult to produce theoretical modeling of iodine trapping and detrapping in relation to the thermohydraulic conditions of the clearance At the present time, we only use an experimental, empirical approach in our models. The numerous radiochemical measurements taken by the EdF, in conjunction with quantitative measurements of defect size during quantitive sipping tests on fuels at the end of cycle, have been used to demonstrate a relation between defect size and the ratio of fractions released of iodine and fission gases under stable operating conditions at nominal power Figure 7 shows the development of the ratio of released fractions of ^{131}I and ^{133}Xe in terms of the equivalent size of the defect measured during quantitive sipping tests. This relation has been used to establish an empirical correlation between this ratio and the size of the defects

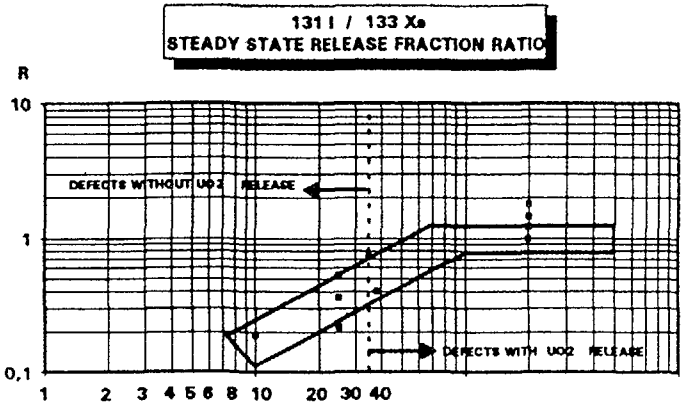

FIG 7

It should, however, be noted that this correlation between the ratio of released fractions of ^{131}I and ^{133}Xe and the size of cladding defects also depends on the physical state of the water in the clearance and therefore on the surface temperature of the fuel This dependence is currently being studied at CEA but has not yet been taken into account in our modeling

(c) Uranium contamination of the cladding

There are two sources of fission products in the primary circuit of a PWR

migration from the oxide in defected rods as described above

discharge by direct recoil into the primary water of fission products created in the uranium and deposited on the outer surface of the cladding. This results in erosion of fuel rods with major defects either during the current cycle or in previous cycles.

The released fractions of fission gases can be expressed as follows.

$$F_i = F_{133Xe} \cdot (\lambda_i / \lambda_{133Xe})^{n} + F_{contamination} \quad (5)$$

where $F_{contamination}$ is the released fraction of the nuclide due to contamination It is independent of the radioactive period of the nuclide under consideration Similarly for iodine, the following equation can be written

$$F_i = F_{131I} \cdot (\lambda_i / \lambda^{131}I)^{n'} + F_{contamination} \quad (6)$$

The value of n' (of the order of 1) is greater than the slope of the gases, leading to a negligible value for the first term of equation (6) for iodines with low radioactive periods

For ^{134}I in particular, the following approximation can be written

$$F^{134}I = F_{contamination} \quad (7)$$

Modeling of phenomena realised using the PROFIP code enables $F_{contamination}$ to be linked to the mass of uranium deposited on the cladding.

$$\text{Mass U} = k_1 \cdot F_{contamination} \cdot f_{(combustion\ rate)} \quad (8)$$

where
k_1 is a constant determined by the calculation
f is a function of the combustion rate outside the cladding of the contamination that takes the individual contaminations of fissile isotopes (particularly ^{239}Pu) into account

1 4 Correlations using cesiums

The 134 and 137 isotopes of cesium are usually only measurable during major power transients such as shutdown transients when, like the iodines,they are detrapped by water penetrating into the fuel/cladding clearance During these periods, $^{134}Cs/^{137}Cs$ activity ratios in the water are equal to that of the oxide of the defected rod. This ratio in the fuel is a function of the combustion rate of oxygen, which we can calculate using our models We use this property to establish the combustion rate and to give the approximate location of the leaking rod.

2. VALIDATING CHARACTERIZATION METHODS

Wherever possible, all the correlations described in chapter 1 are used to characterize PWR cladding defects. It will be understood that the accuracy of this characterization is greater the more calculation data is available, even to the point of redundancy, to offset the uncertainties of radiochemical measurements This is why optimum use of these correlations is obtained when the development of these activities is monitored closely using, for example, a gamma spectrometry device in the primary coolant line Since this type of monitoring is only in current use on a few reactors, we have usually validated our models using radiochemical measurements taken on samples from nuclear plants and measuring campaigns carried out by the CEA on primary circuit activity We give some examples of validation of our methods below In particular, we cite cases where simplified diagnosis methods gave highly erroneous forecasts

Reactor	Defects number		
	Measured	Diagnosis	
		CEA method	simplified method
A	2	1 à 2	2
B	2	1 à 2	30
C	6	8 à 10	17
D	2	1	20
E	5	6	18

There is a considerable improvement in diagnosis reliability compared with the simplified methods that have been used in the past

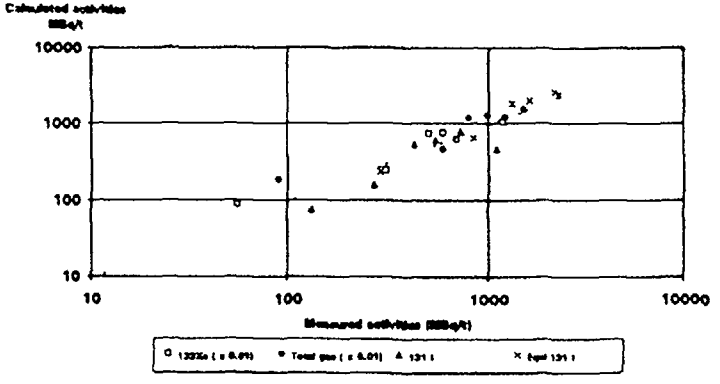

FIG 8 Forecast of F P activities in French PWRs

3 FORECASTING PRIMARY ACTIVITY WHEN REFUELLING DEFECTED ASSEMBLIES

During refuelling of defected assemblies with known characteristics, the models for release of fission products included in the PROFIP IV code can be used to forecast the activities in gas and fission iodines in the primary water when the reactor is restarted Figure 8 below shows examples of this type of forecast carried out for the EdF over 6 reactor cycles

Deviations between predictive calculations and measurements taken after reactor restart were less than 50% for all nuclides The only exceptions were for forecasts made for very low power defected assemblies where gas releases were underestimated and iodine releases were overestimated These deviations are due to gaps in the modeling for the behavior of fission products in the fuel/cladding clearance during the liquid phase

4 CONCLUSION

All the correlations established by the CEA using its models for the release of fission products into defected PWR fuels enable realistic forecasts to be made of the state of the fuel cladding throughout reactor operating cycles. They also give estimates of activity in the primary water at the start of a cycle for reactors containing refuelled defected assemblies with known characteristics. Improvements continue to be made to these models and correlations in order to give greater reliability and accuracy of diagnosis

REFERENCES

[1] OLANDER, D R., Fundamental Aspects of Nuclear Reactor Fuel Elements. Technical Information Center Energy Research and Development Administration (1976)

[2] BESLU, P , LEUTHROT, C., FREJAVILLE, G , The PROFIP Code A Model to Evaluate the Release of Fission Products from a Defected Fuel in PWR IAEA specialists' meeting on the behavior of defected Zirconium alloy clad ceramic fuel in water-cooled reactors, Chalk River, Canada, 1979

EXPERIENCE WITH THE FISSION PRODUCTS MONITORING SYSTEM IN JAPANESE REACTORS

K ONO
Nuclear Fuel Industries, Ltd,
Osaka, Japan

Abstract

In the event of increased levels of iodine fission products (an indication of failed fuel) frequency of radiochemical analysis of radioactivity for primary coolant is increased to monitor radioactivity in detail In order to watch change of radioactivity in the primary coolant continuously we have developed the Fission Product Monitoring System (FPMS) in cooperation with Japanese PWR utilities The FPMS was developed originaly by the US company of Babcock & Wilcox Company Japanese PWR utilities and Nuclear Fuel Industries Ltd (NFI) improved the system to apply it to the Japanese reactors form 1980 to 1981 and performed validation test compaign in the Japanese commercial reactor A in the event of increased levels of iodine fission products in 1983 In 1985 trial operation of the FPMS in Japanese reactor B was performed to prove equivalency with radiochemical analysis and ability of compensation for it
Since 1985 the system has been installed to some Japanese reactors temporarily in order to monitor radioactivity in detail Characteristics of FPMS are as follows

1) Prompt real – time analyses for radioativity continuously
2) Automatic operation (unmaned measurement)
3) There is no need to improve any equipment of a plant
4) Radiation exposure for workers during measurement and analyses can be reduced because the system works automatically

FPMS was installed to monitor radioactivity of coolant at some Japanese commercial reactors form 1986 to 1992 at 7 times The lowest level of radioactivity for I – 131 to be able to detect by the FPMS in our experience was about 15 Bq/cm^3 but it depends on the conditions of circumstances for measurement location Of course the FPMS can detect other fission products such as cesium krypton xenon and other radionuclides

1 Introduction

The fission products monitoring concept was conceived and designed by Bobcock and Wilcox (B & W) in 1976 Nuclear Fuel Industries LTD (NFI) and B & W had performed research and development to apply it to the Japanese commercial reactors with Japanese PWR utilities in 1980 and 1981

In the event of increased level of iodine fission products at the reactor A in 1983 validation test of the fission products monitoring system (FPMS) was performed by NFI and utilities
According to these operative experiences at the commercial reactors FPMS was improved and was recognized to be able to fulfill the following requirements

1) Perform a gamma isotopic analysis on reactor coolant continuously passing through a pipe in the letdown system upstream of the purification demineralizers
2) Have sufficient sensitivity so that activity level changes occuring during fuel failures can be monitored and quantified
3) Produce a coutinuous reliable record of specific parameters of interest so that incidents occurring while the equipment is unmanned can be recorded and easily retrievable for later analysis

2 Description of The FPMS

2 1 Description of Equipment

The Fission Products Monitoring System (FPMS) hardware can be subdivided into two groups radioactivity measuring equipment and data processing equipment

2 1 1 Radioactivity Measuring Equipment

The radioactivity measuring equipment is the portion of the FPMS that measures the radioactivity and produces a hgih – voltage power
The compornents are

- A high – purity germanium (Ge) detector with factory mounted preamplifier
- A bin power supply which provide high – voltage bias to preamplifier
- Lead shieding for detector as bricks
- A frame which supports shielding and detector in order to keep appropriate position for a detector
- A weighing machine to measure quantity of liquid nitrogen

Figure 1 shows rough sketch of measuring equipment
Photograph 1 shows assembling process of measuring equipment near a pipe in the letedown system at a commercial reactor
Lead shieding is subdivided into many bricks because of easy transportation assembling disassembling and protection from streaming of gamma – ray

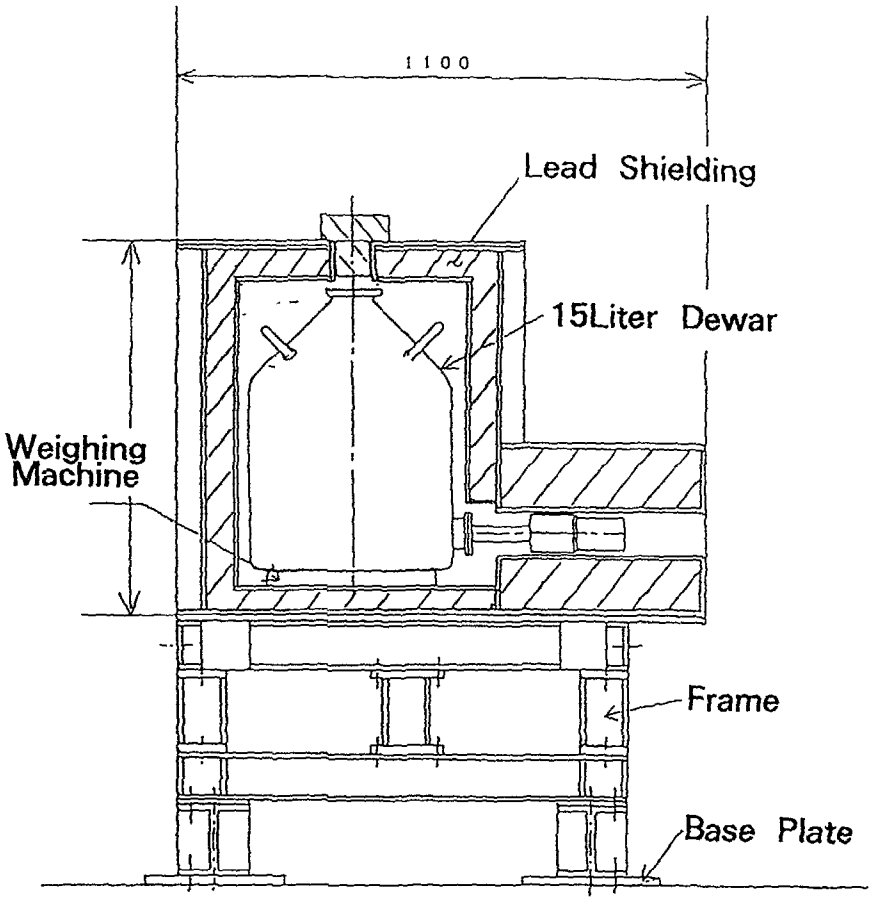

Figure. 1 Measuring Equipment

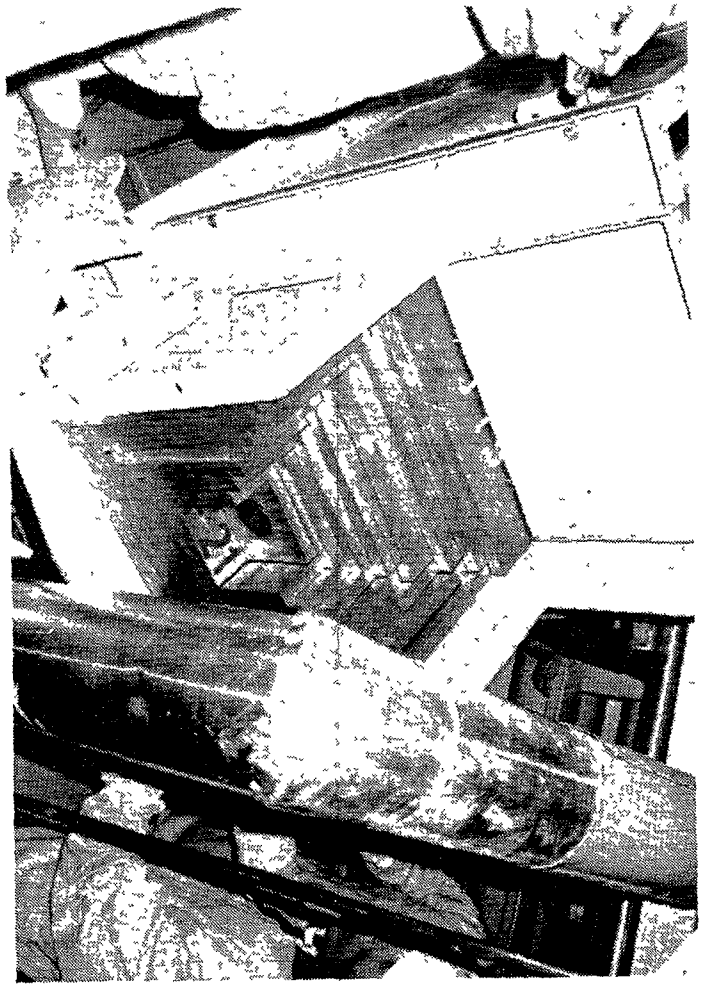

Photo 1. Lead shielding for Ge detector.

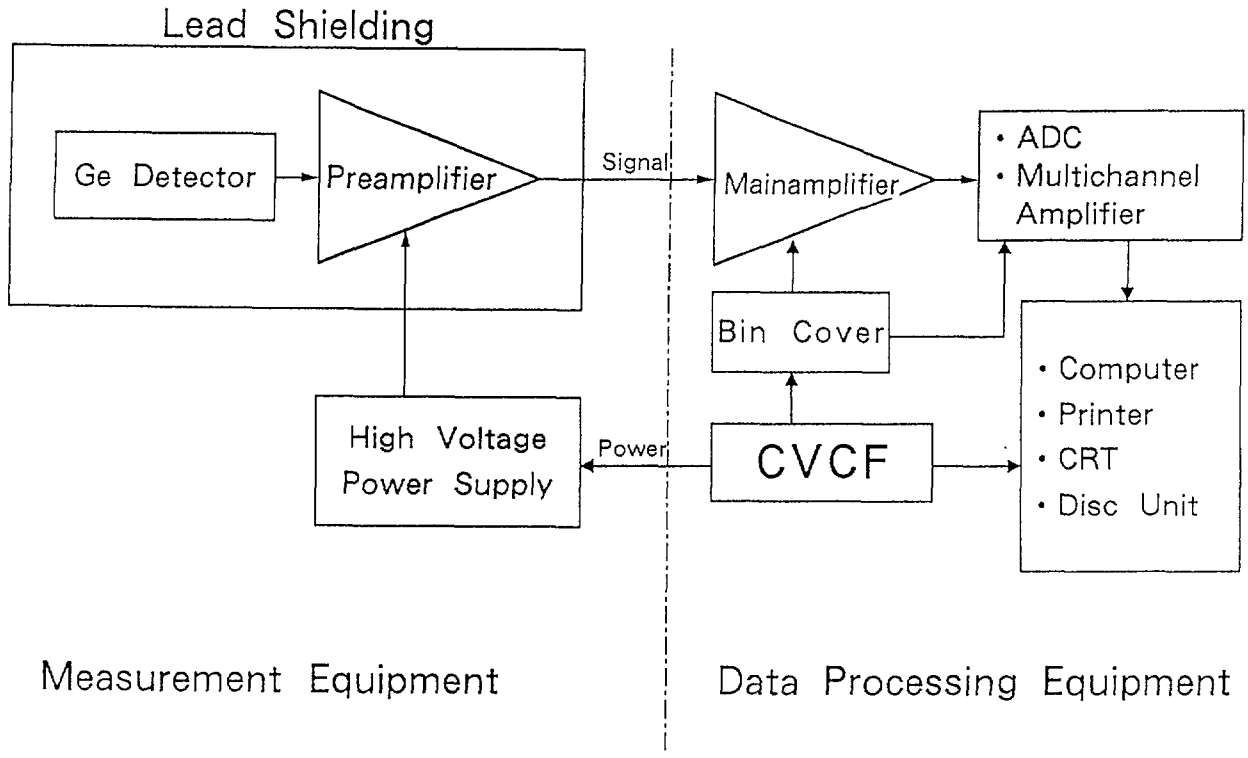

Figure. 3 Block Diagram of FPMS

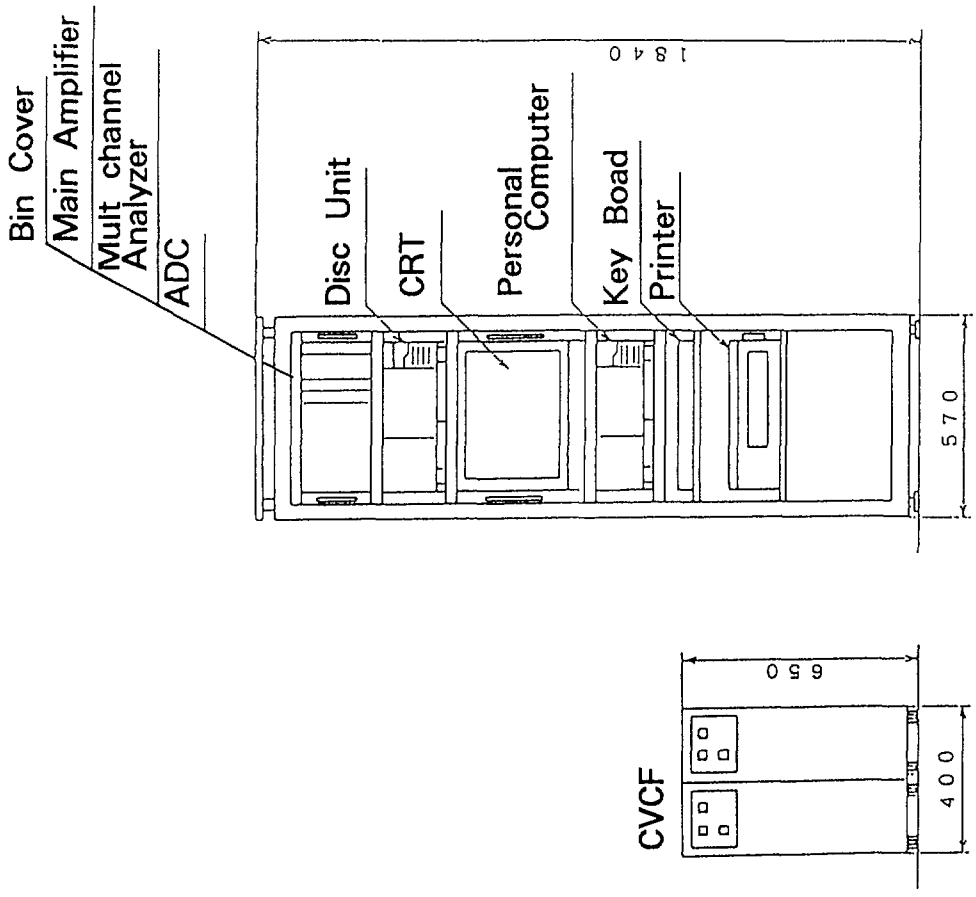

Figure. 2 Data Processing Equipment

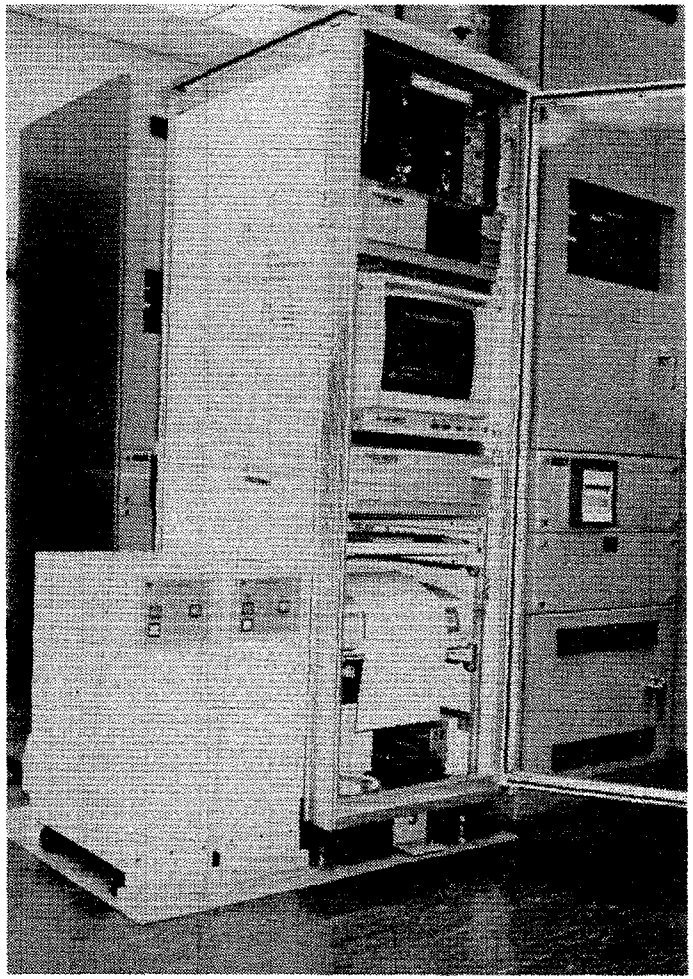

Photo 2. Data processing equipment.

2.1.2 Data Processing Equipment

The data processing equipment is mounted in a rack because of easy handling and transportation. The compornents are :

- Main amplifier
- ADC
- Multichannel analyser with 4096 channels
- Personal computer with CRT display, key board and disc unit
- Printer for reports
- CVCF.

Figure 2 shows rough sketch of data processing equipment and Figure 3 shows a block diagram of the FPMS which shows relationship of these compornents.

Photograph 2 is data processing equipment in a centeral control room at a reactor.

2.2 System Software

Important functions of the FPMS are acquisiton and analyses of data. The system software was developed and improved by NFI. The main application programs are as follows :

- Data aquisition
- Storage of data
- Analysis of data
- Report generation
- Automatic peak search
- Energy calibration
- Automatic self diagnosis

Figure 4 to 6 show sample outputs of the FPMS.

2.3 Features of The FPMS

Features of the FPMS are as follows :

1) Prompt real – time analyses for radioactivity are provided.
2) The system is operated automatically.
3) There is no improvement for the existing plant equipment.
4) Operator can get trend graph of radioactivity and another type of reports easily.
5) Germanium detector can detect various isotopes such as, iodine (I – 131, I – 132, I – 133, I – 134, I – 135), rare gas (Xe – 133, Xe – 135, Kr – 85m, Kr – 87, Kr – 88) and others (Co – 58, Co – 60, Fe – 59 etc.).

▽ Radiochemical Analysis
▼ FPMS

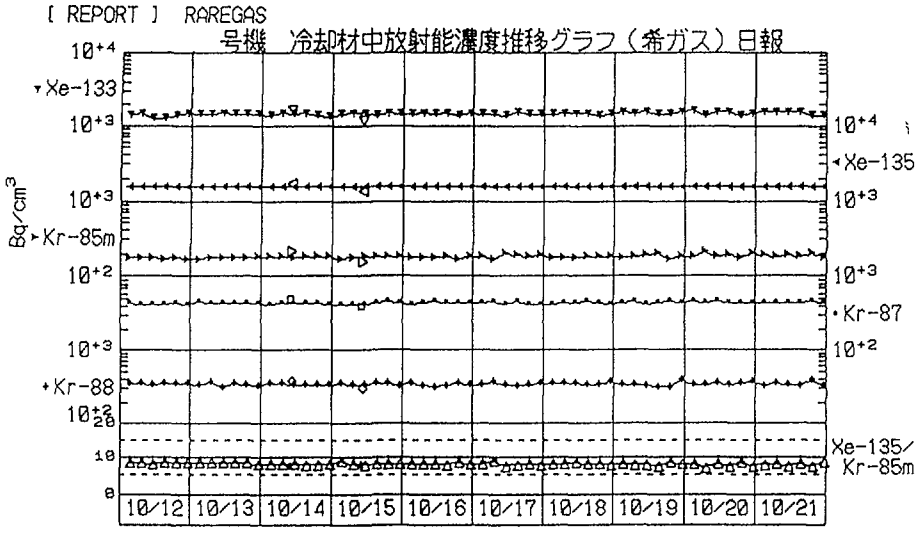

Figure. 4 Sample Output of FPMS for Rare Gas

▽ Radiochemical Analysis
▼ FPMS

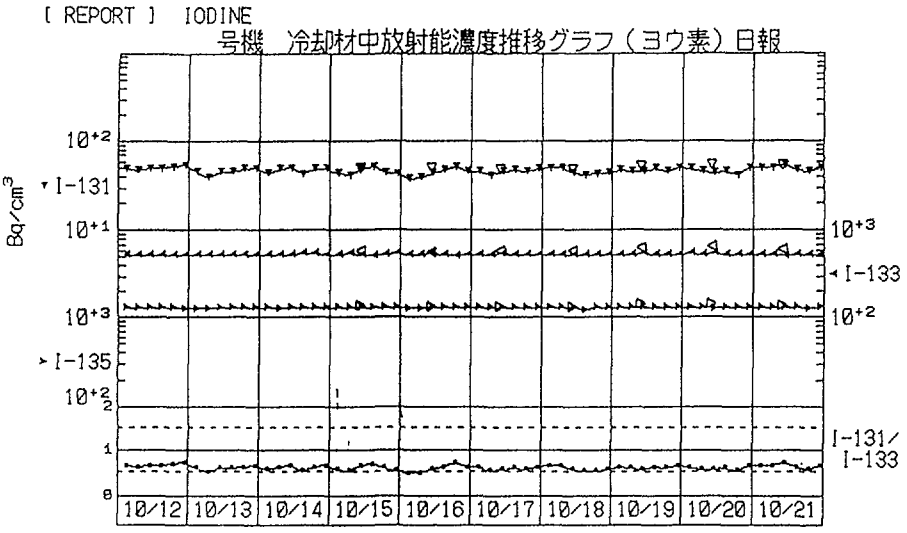

Figure. 5 Sample Output of FPMS for Iodine

F.P.M.S FUEL ASSEMBLY REPORT

号機 冷却材中放射能濃度推移表

DATE [91/01/25 - 91/05/04]

DATE	TIME	Xe-133	Xe-135	Kr-85m	Kr-87	Kr-88	Xe-135/ Xe-133 Kr-85m	ERROR (%)	COUNT-TIME (H)
		Bq/cm³							
91/03/15	03 00	1 28E+03	1 26E+03	1 73E+02	3 72E+02	2 84E+02	7 271	4 716	4
	07 00	1 15E+03	1 25E+03	1 65E+02	3 96E+02	3 43E+02	7 586	5 238	4
	11 00	1 16E+03	1 26E+03	1 72E+02	3 85E+02	2 98E+02	7 352	5 223	4
	15 00	1 17E+03	1 27E+03	1 66E+02	3 80E+02	2 91E+02	7 677	5 167	4
	19 00	1 25E+03	1 27E+03	1 69E+02	3 94E+02	3 12E+02	7 482	4 852	4
	23 00	1 22E+03	1 27E+03	1 75E+02	4 04E+02	3 07E+02	7 260	4 961	4
91/03/16	03 00	1 29E+03	1 26E+03	1 64E+02	3 81E+02	3 17E+02	7 677	4 672	4
	07.00	1 23E+03	1 26E+03	1 73E+02	3 97E+02	2 99E+02	7 331	4 919	4
	11:00	1 20E+03	1 26E+03	1 89E+02	4 06E+02	3 40E+02	6 675	5 023	4
	15·00	1.30E+03	1 26E+03	1 72E+02	3 90E+02	3 20E+02	7 313	4 665	4
	19:00	1.25E+03	1 26E+03	1 76E+02	4 03E+02	3 12E+02	7 154	4 825	4
	23.00	1 33E+03	1 27E+03	1 73E+02	3 98E+02	3 12E+02	7 325	4 565	4
91/03/17	03.00	1.26E+03	1 26E+03	1 58E+02	3 89E+02	3 38E+02	7 994	4 808	4
	07.00	1.22E+03	1 27E+03	1 75E+02	3 98E+02	3 16E+02	7 226	4 953	4
	11:00	1.26E+03	1.26E+03	1.54E+02	3 81E+02	3 26E+02	8 207	4 798	4
	15·00	1.16E+03	1.27E+03	1.65E+02	3 95E+02	2 93E+02	7 710	5 218	4
	19·00	1 29E+03	1 26E+03	1 67E+02	3 95E+02	3 32E+02	7 564	4 691	4
	23·00	1 25E+03	1 27E+03	1 68E+02	3 95E+02	2 97E+02	7 532	4 833	4
91/03/18	03.00	1.30E+03	1.28E+03	1.68E+02	3 97E+02	3 09E+02	7 634	4 666	4
	07.00	1.12E+03	1 26E+03	1.64E+02	3.87E+02	2 85E+02	7 714	5 390	4
	11:00	1.16E+03	1.26E+03	1 60E+02	3.80E+02	2.98E+02	7 909	5 227	4
	15:00	1.31E+03	1 27E+03	1 62E+02	3 83E+02	3 28E+02	7 791	4 611	4
	19·00	1.20E+03	1 27E+03	1.64E+02	3 95E+02	3 09E+02	7 747	5 036	4
	23.00	1.14E+03	1.20E+03	1.58E+02	3.83E+02	2.86E+02	7 607	5 330	4
91/03/19	03:00	1.13E+03	1 17E+03	1.43E+02	3 85E+02	2.92E+02	8 185	5 345	4
	07:00	1 13E+03	1 17E+03	1 55E+02	3 93E+02	3 01E+02	7 549	5 364	4
	11:00	1 17E+03	1 18E+03	1.58E+02	3 76E+02	2 97E+02	7 481	5 161	4
	15:00	1.14E+03	1.21E+03	1 65E+02	3 88E+02	2 98E+02	7 295	5 308	4
	19:00	1.19E+03	1.20E+03	1.58E+02	3 88E+02	3.12E+02	7 613	5 076	4
	23:00	1.16E+03	1.22E+03	1.58E+02	3.93E+02	2.93E+02	7.678	5.240	4
91/03/20	03:00	1.28E+03	1.21E+03	1.58E+02	3.80E+02	3.14E+02	7 686	4 734	4
	07·00	1.08E+03	1.22E+03	1.66E+02	3.67E+02	3.22E+02	7 325	5 620	4
	11:00	1.26E+03	1.23E+03	1.67E+02	3.86E+02	3.06E+02	7 376	4 805	4
	15:00	1.20E+03	1.22E+03	1.65E+02	3 90E+02	3.12E+02	7.368	5.042	4
	19:00	1.19E+03	1.23E+03	1.54E+02	3.89E+02	2.90E+02	7.943	5 084	4
	23:00	1.16E+03	1.24E+03	1.63E+02	3.82E+02	2.86E+02	7.600	5.228	4
91/03/21	03:00	1.20E+03	1.23E+03	1.63E+02	3.97E+02	3.10E+02	7.572	5.056	4
	07:00	1.20E+03	1.24E+03	1.65E+02	3.94E+02	3 02E+02	7 485	5 073	4
	11:00	1.34E+03	1.24E+03	1.71E+02	3.71E+02	3.23E+02	7.230	4.522	4
	15:00	1.17E+03	1 25E+03	1.86E+02	3.91E+02	2.88E+02	6 736	5 214	4
	19:00	1.27E+03	1.25E+03	1.75E+02	3.75E+02	3.13E+02	7.143	4.787	4
	23:00	1.27E+03	1 26E+03	1.75E+02	3.96E+02	3.15E+02	7.179	4 771	4
91/03/22	03·00	1.28E+03	1 25E+03	1.81E+02	3.89E+02	2.85E+02	6 889	4 737	4
	07:00	1.21E+03	1.27E+03	1.69E+02	3.90E+02	3 01E+02	7 489	5 012	4
	11:00	1.19E+03	1.28E+03	1.75E+02	3.86E+02	2 86E+02	7 271	5 091	4
	15.00	1.27E+03	1.27E+03	1.83E+02	4 00E+02	2.82E+02	6 981	4 794	4
	19 00	1.25E+03	1.28E+03	1.88E+02	3 82E+02	3 12E+02	6 789	4 881	4
	23 00	1.18E+03	1.28E+03	1.95E+02	3 92E+02	3.21E+02	6 560	5 175	4

Figure 6 Sample Output of FPMS for Rare Gas

3 Gneneral Criteria for The FPMS Compornents Installation

3 1 Criteria for Ge Detector Location

Criteria can be classified into four groups

1) Piping
- Constant flow of primary coolant
- Upstream of demineralizer beacause of same composition of coolant
- Diameter is less than 10cm because of avoiding self absorption and scattering of gamma – ray
- Perpendicular arrangement of piping is desirable because of avoiding CRUD accumulation

2) Space
- Sufficient space for equipment and working about 1m × 1 2m × 1 5m
- Sufficient floor strength is required because weight of lead shieding is very heavy , > 1ton/m²

3) Enviroment
- Low background radiation because of reduction of radiation exposure during installation and maintenance
- Temperature and humidity are limited for electronics temperature is less than 35℃ and humidity is less than 35 %

4) Working
- Easily accessible location for installation calibration, maintenance and liquid nitrogen filling

3.2 Criteria for Data Processing Equipment

Criteria can be classified into three groups

1) Space
- Sufficient space for equipment and working , about 2m × 2m × 1 8m

2) Enviroment
- Temperature and humidity are limited for electronics temperature is less than 25℃ and humidity is less than 35 %

3) Working
- Easily access
- Power supply of AC 110V is required

3.3 Example of Installation Location

Measuring equipment is always installed near a piping in the room of letdown heat exchanger in CVCS line and data processing equipment is installed at central control room because of daily access to get analyses

Figure. 7 Installation Location for Measuring Equipment

Figure. 8 *Gamma – ray Energy Spectrum of Primary Coolant in PWR at Fuel Failure*

4. Experience of The FPMS in Japanese Reactors

The FPMS has been installed to monitor radioactivity of primary coolant at some Japanese commercial reactors from 1985 to 1992 at seven times temporarily. Table 1 shows a list of installation experience of the FPMS in Japanese reactors from 1985 to 1992.

Iodine – 131 is the most remarkable nuclide from the viewpoint of human health in monitoring of radioactivity. But energy of gamma – ray from I – 131 is relatively low (364.48KeV) and there is disturbed energy peak from Krypton – 88 near it So it is relatively difficult to measure radioactivity of I – 131 Sensitivity for radioactivity of I – 131 by the FPMS in our experience is about 15 Bq/cm³ in the lowest case, but it depends upon the conditions of circumstances for germanium detector The effective factor for sensitivity of I – 131 is radioactivity quantity of CRUD nuclides such as Cobalt – 58 and Cobalt – 60, which are accumulated *on the inside wall of the piping and solved or flowed in coolant*

The worst case in our experience is the case of reactor D which is shown in Table 1. In that case the lowest level of I – 131 is about 60 Bq/cm³ with 24 hours accumulation of data Accumulation time of other cases in Table 1 is less than four hours.

Selection of location for measuring equipment installation is the most important for keeping sensitivity of I – 131 radioactivity

Table 1 Experience of The FPMS in Japanese Reactors

Plant	Year	Period (Months)	Radioactivity of I − 131 (Bq/cm³)	
A	1985~1986	8	40~280	
	1988~1989	10	15~800	
B	1988	5	30~60	
C	1988~1989	11	30~50	
	1989~1990	13	30~60	
	1991	11	30~55	
D	1991~1992	6	~60	*

* It was difficult to measure Iodine − 131 under the level of 60 Bq/cm³ in case of D, because there was high backgrounds by CRUD nuclides.

5. Conclusion

In general, the FPMS can be installed at any nuclear power plant. The principal problem which must be solved for specific installations is finding suitable locations for the detector, electronics modulus, and computer.

Through our experience the FPMS has proved to be able to have the following functions ;

1) Prompt real − time analyses of radioactivity.
2) Continuous analyses for various nuclides.
3) Reduction of radiation exposure for plant radiochemists at measurement during fuel failure.

without any inprovement or change of the existence plant equipment.

A REVIEW OF FUEL PERFORMANCE AND FISSION PRODUCT RELEASE STUDIES FOR DEFECTED FUEL ELEMENTS

B.J. LEWIS
Royal Military College of Canada,
Kingston, Ontario

R.D. MACDONALD
Chalk River Laboratories,
Atomic Energy of Canada Limited,
Chalk River, Ontario

N.V. IVANOFF
Ontario Hydro,
Pickering, Ontario

F.C. IGLESIAS
Ontario Hydro,
Toronto, Ontario

Canada

Presented by T.J. Carter

Abstract

Results from numerous in-reactor experiments with uranium-dioxide fuel elements that contain defects in the Zircaloy cladding are reviewed. The various factors which influence the rate of physical deterioration of a defected element are examined. Experimental and theoretical investigations into the release behaviour of radioactive noble gases and iodine are considered for both the steady-state and transient situation, focusing on the relationship between the release behaviour and the state of deterioration of a fuel element. Application of this work to power reactor operation is discussed.

1. INTRODUCTION

Fuel performance in Canada Deuterium Uranium (CANDU) reactors has been excellent with an overall fuel-bundle defect rate of typically less than 0.1 percent.[1-3] Fuel failures have generally been attributed to four distinct causes: stress-corrosion-cracking (SCC) in association with pellet/clad interaction (PCI) during power ramping manoeuvres; delayed-hydrogen-cracking near end cap welds due to hydrogen diffusion to areas of high stress and low temperature in the cladding; fuel fabrication flaws (e.g. end-cap porosity and faulty end-cap welds); and fretting of the fuel cladding from small pieces of debris in the heat transport circuit. Similar defect statistics have been observed in light-water reactors (LWRs) with defect rates typically less than 0.04

Table 1: Summary of Experiments With Defective Fuel at Chalk River

A NATURALLY DEFECTIVE FUEL

Experiment	Description of Experiment	Element Identity	Primary Defect Size (μm)	Average Linear Power (kW/m)	Accumulated Burnup (MWh/kgU)		Accumulated Days of Irradiation (Full Power Days)		Fuel Element Degradation	
					Initial	Final	Onset of Damage	In Core	Fuel Loss (g)	Description of Sheath Deterioration
FF0 102 1	Irradiation of elements with porous end caps	A7A,A7B A7C A7D A7F A7E A7H,A7J A7K A7X	0 4 0 9 0 3 1 6 1 4 1 4 1 1 1 2 1 5 1 5	16 62 64 56 61	0 0 0 0 0	68 65 37 33 30	 32 14 14 8	153 43 24 24 19	 No loss N/A No loss No loss	Incipient sheath hydriding Cracks Open hydride blister Open hydride blister/cracks Pin hole defect (no hydriding)
FF0 102 2	Re irradiation of an element with through wall hydriding at high power	A7E	1 4	67	37	67		43	3 5	Sheath hydriding and deterioration increased †
FF0 102 3	Re irradiation of an element with incipient hydriding at low power	A7A	0 4	23	68	130	155	263	N/A	No significant deterioration following the occurence of through wall hydriding at a burnup of 70 MWh/kgU †
FF0-104	Power ramp failure by stress-corrosion cracking	A2F		26 (soak) 58 (ramp)	255	278		16	≤10	Sheath hydriding Sheath deterioration continually progressed (inferred from release behaviour) †
FF0 105	Irradiation of elements with faulty end welds	A8F,A8J,A8N A8H A8M A8K A8L	0 9 0 4 1 1 0 4 0 7 0 9 0 6	44 62 65 62	0 0 0 0	101 142 23 121		92 92 14 78		No sheath hydriding or deterioration
FF0-109 (Phases 1 & 3)	Power uprating of an element with incipient hydriding	A7C	0 3	31 40	68 82	82 133		171 246		No through wall hydriding in either phase
FF0-110 FF0-109 (Phase 2)	Power-cycling of an element with through wall hydriding	A7A	0 4	14 26 22 38	130 140	140 155		281 300	N/A <0 1	Little or no increase in sheath hydriding and/or deterioration †

B ARTIFICIALLY DEFECTIVE FUEL

Experiment	Description of Experiment	Element Identity	Primary Defect Size	Average Linear Power (kW/m)	Accumulated Burnup (MWh/kgU)		Accumulated Days of Irradiation (Full Power Days)	Fuel Element Degradation	
					Initial	Final		Fuel Loss (g)	Description of Sheath Deterioration
FD0-681 (Phase 1) (Phase 2) (Phase 3)	Irradiation of elements with drilled hole(s)	 RPL LFZ RPP	 1 3 mm hole* 1 2 mm hole* 1 3 & 0 4 mm holes*	 48 48 48	 140** 0 140**	 158 20 173	 15 24 35	 <0 1 <0 1 0 17	No (massive) sheath hydriding or deterioration
FD0-687 (Phase 1) (Phase 2) (Phase 3)	Irradiation of elements with drilled hole(s)/single slit	 RPR NSZ RPR	 2 0 mm hole* 10 mm x 0 6 mm slit 2 additional 1 6 mm holes (one at each end of the element)	 55 55 55	 43** 0 85	 85 28 90	 40 26 44	 N/A ≤0 1 ≤0 1	No (massive) sheath hydriding or deterioration
FF0-103	Irradiation of an element with 23 slits	A3N	36 mm x 0 3 mm (each slit)	48	0	18	15	~60	No (massive) sheath hydriding Slits at the top of the element enlarged †

† The UO_2 exposure for the single rod experiments is summarized in Fig 16
* Holes drilled at mid length
** Irradiated intact to this burnup
N/A Not available (no metallography was performed following this stage of irradiation)

percent in the past several years [4] The defective fuel elements can deteriorate further during operation as a result of hydriding of the Zircaloy cladding [5-13] This deterioration and the associated activity release may present economic penalties to the power utility from lost burnup due to premature discharge of the fuel, and from increased occupational exposures

When a fuel rod defects due to any of the above mechanisms, the cladding no longer provides a barrier between the fuel and the primary coolant A leak path then exists so that the primary coolant can enter into the fuel rod, and radioiodine, gaseous and solid fission products, as well as fuel debris, can escape into the primary heat transport system (PHTS) Recent investigations in Canada, based on an in-reactor research program at the Chalk River Laboratories (CRL), have provided a better understanding of the performance of defected-fuel elements This study has yielded data on the rate of fuel-element deterioration and the associated fission-product release [14-25]

In this paper, the results of the Chalk River study are reviewed The application of this work to fuel failure monitoring in the power reactor is also discussed

Table 2: Fuel Element Design

	Fuel Element Classification[a]	
	Class I	Class II
Fuel description		
Sintered UO_2 density (Mg/m^3)	10 7	10 7
Enrichment (wt% ^{235}U in uranium)	4.5	5 0
Pellet diameter (mm)	13 7	12 1
Pellet length (mm)	18 0	16.5
Pellet end dishing	One end	Both ends
Land width (mm)	0.56	0 46
Depth (mm)	0 64	0 23
Fuel stack length (mm)[b]	179	477
Sheath description		
Material	Zircaloy-4	Zircaloy-4
Outside diameter (mm)	15 2	13 1
Wall thickness (mm)	0 71	0 43
Clearances		
Diametral (mm)	0 10	0 10
Axial (mm)	1 0	2 2

a) Class I elements include RPL, LFZ, RPP RPR and NSZ.
Class II elements include A3N A7A A7B A7C A7D A7E A7F A7H A7J A7K A7X, A8F A8H A8J A8K A8L, A8M, A8N and A2F
The Class II design is typical of those elements used in the CANDU-6, Bruce and Darlington power reactors

b) Elements LFZ and NSZ had fuel stack lengths of 168 mm Element A3N had a fuel stack length of 470 mm

2. EXPERIMENTAL DETAILS

An experimental program with defective CANDU type fuel elements was carried out at CRL from 1975 to 1983 Failed elements with various degrees of sheath damage were irradiated in separate tests in an experimental loop of the NRX reactor A brief summary of the fuel operating parameters for each experiment is given in table 1 The fuel element design is detailed in table 2 The experiments involved the irradiation of fuel elements which were either artificially or naturally defective Several elements were defected prior to irradiation with artificially drilled holes or machined slits in the fuel sheathing In other experiments, however, the defects in the elements were characteristic of failures found in the power plant fuels These failures arose as a result of small manufacturing flaws during fuel fabrication, or by SCC of the fuel sheathing after a power ramp

A schematic diagram of the defect loop facility is shown in Fig 1 This loop is capable of operating at the coolant conditions specified for the CANDU pressurized heavy water reactor

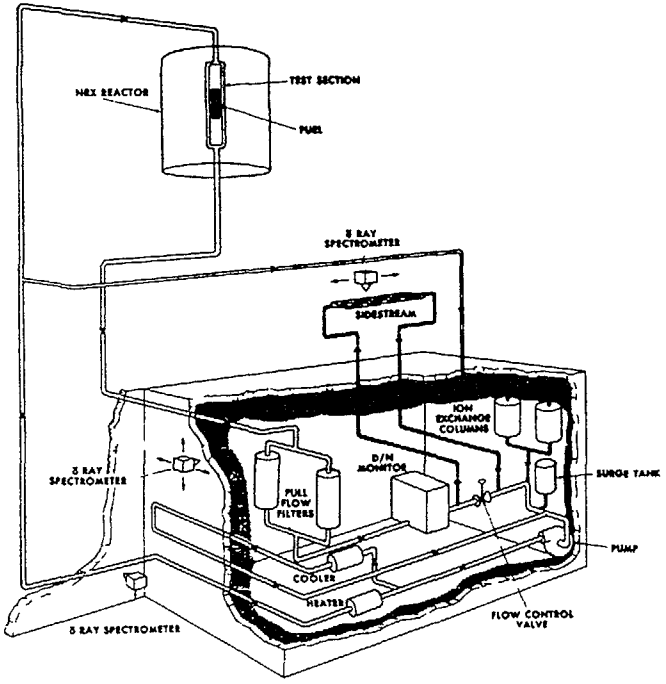

Figure 1 Schematic diagram of the X 2 Loop Facility

Table 3: Loop Operational Parameters

Thermal flux (axially-averaged) (n/cm^{2}s)	5.5 x 10^{13}
Temperature (°C)	240 - 260
Pressurized water (MPa)	7.7 - 10.5
Flow rate (kg/s)	0.6 - 1.1
Recirculation time (s)	105
Coolant pH (LiOH controlled)	10 - 11
Hydrogen content (mL/kg)	5 - 20
Graphite filters (μm)	6
Coolant volume (m^3)	0.15

Details of the operational parameters are given in table 3. This facility is designed to cope with high activity levels as a result of fission product release and fuel loss through large defects. The full flow graphite filters prevent significant UO_2 fuel recirculation. Separate sidestream circuits for the ion-exchange mixed-bed resin columns, and degassing system, provide an optional coolant-cleanup capability for both radioiodine and noble gases.

3. FUEL-ELEMENT DETERIORATION

A comprehensive study to correlate the deterioration of a defective fuel rod with the fuel operating parameters was performed by the United Kingdom Atomic Energy Authority (UKAEA).[6,7] As shown in Fig. 2(a), data was collected for fuel fabrication defects and those rods with severe hydriding damage were differentiated from pins with minor damage. One notable feature of this boundary is that it is almost independent of surface heat flux above 1750 kW/m^2, indicating that sheath hydriding takes place very quickly above this value. The CRL experiments that involved fabrication defects (table 1) are plotted on Locke's performance curve in Fig. 2(b). These experiments are in general agreement with the UKAEA work.

As depicted in Fig. 3(a), the UKAEA study indicated that most defects go through an initial period with low fission-product leakage (Stage I), followed by the development of secondary damage (as a result of sheath hydriding), and a slowly increasing release rate (Stage II).[8] Defects eventually deteriorate to the point (Stage III) where the fission-product release has increased significantly as a consequence of sheath breakage and/or multiple-failure sites. It has also been shown that PCI and fretting defects can deteriorate more rapidly (in weeks or days) than elements operating under the same conditions with fabrication defects.[8]

Secondary deterioration to the zirconium alloy sheath of a defected fuel element (see Fig. 4) is usually caused by a combination of massive localized hydriding and stresses in the sheath. In this process, available hydrogen enters the sheath at preferred locations and forms local areas of high concentrations of hydride or sunbursts [see Fig. 3(b)]. These locations may become sinks for further hydrogen pick-up, leading to more massive localized hydriding. Hydride blisters, which form in areas of solid zirconium hydride, result from a 16 percent expansion in volume of the δ-hydride phase. Since the hydrided sheath is very brittle, failures eventually occur from further sheath stress.

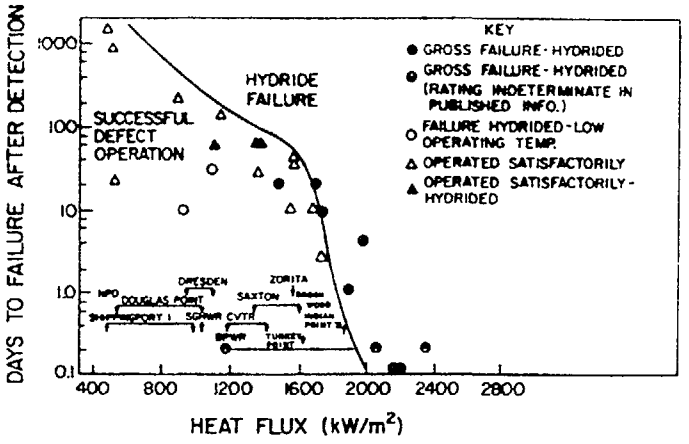

(a)

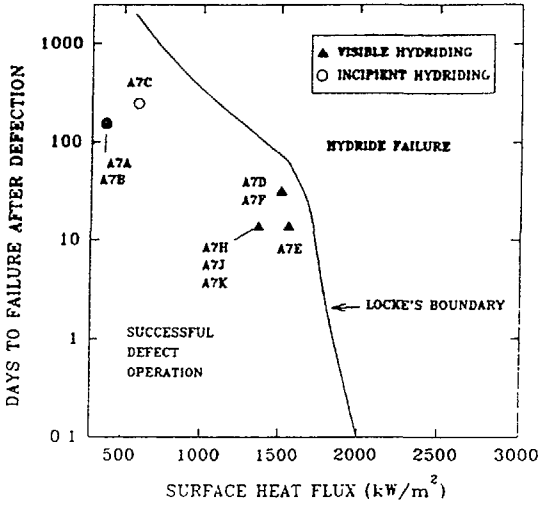

(b)

Figure 2: (a) Locke's defect performance curve for Zircaloy-sheathed fuel.
(b) Hydriding experience in CRL experiments FF0-102-1, FF0-102-3, and FF0-109 for fuel elements (as labelled) with fabrication defects.

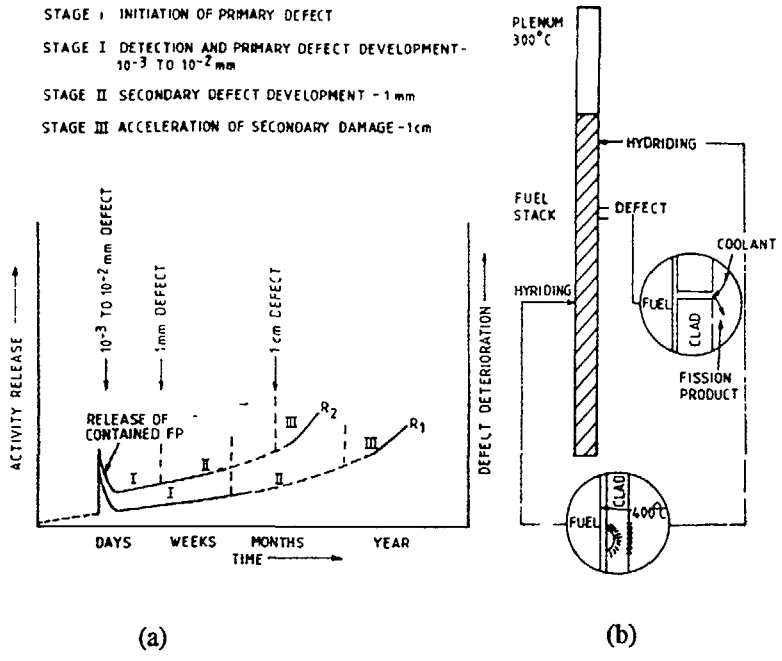

Figure 3: Stages of defective fuel rod operation. (Taken from Ref. 8).
(a) Curves relating stages of fuel rod deterioration to the activity release as a function of time and fuel rod rating $R_1 < R_2$.
(b) Conditions in a defective rod.

3.1 Hydriding Mechanism

Hydriding is a complex phenomenon with a number of variables controlling the rate, the location, and the amount of hydrogen pick-up by the sheath:

(a) Element Power

As indicated in Fig. 2, the number of days to failure through gross hydriding of the sheath decreases with increasing surface heat flux. The surface heat flux, in turn, determines the radial thermal gradient and the inside temperature of the sheath for a given geometry and coolant temperature.[12] Although the pick-up of hydrogen by the sheath is clearly dependent on element power (i.e. the hydrogen liberating reactions are both flux and temperature dependent), the degree of damage is also affected by localized stresses on the sheath for elements operating at high specific powers. In the present study (see table 1), hydriding progressed during further irradiation of an element at high power (FF0-102-2) even after sections of the sheath had broken away [see

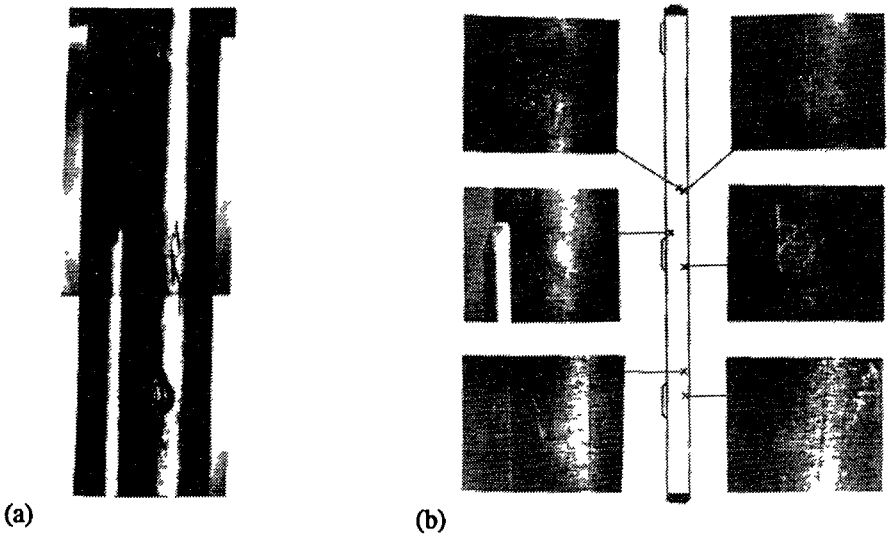

Figure 4: Zirconium hydriding and sheath degradation for:
(a) Defective fuel element A7E after irradiation in experiment FF0-102-1. The upper and lower blisters have broken open exposing the underlying fuel; the centre blister has cracked.
(b) Defective fuel element A7A after irradiation in experiment FF0-109 (Phase 2).

Fig. 4(a)]. The increased damage to the sheath had resulted from localized sheath stresses during a reactor trip, as inferred from a stepped increase in the coolant activity levels. On the other hand, neither hydriding nor sheath degradation significantly progressed for an element irradiated at low power (FF0-102-3), following the onset of through-wall hydriding at a burnup of 70 MW·h/kgU. Power-cycling of this hydrided element at low and intermediate powers on a daily basis at a ramp rate of 14 percent of full power per hour (FF0-109 and FF0-110), did not significantly increase the amount of sheath cracking [see Fig. 4(b)]. In an axial power gradient, more hydriding occurred in the maximum power region of the higher-powered elements irrespective of the primary defect location (FF0-102-1). The hydriding was generally confined to the heat affected zones around the brazed spacer pads of the fuel elements.

(b) Primary Defect Size

The initial source of the internal hydrogen is the water or steam that enters the defective element through the primary defect. As discussed in Section 3.2, hydrogen is generated in the fuel-to-sheath gap of a fuel element by the four possible mechanisms of: (i) radiolytic decomposition of the water; (ii) internal clad corrosion that provides a "protective oxide film" of ZrO_2 on the inside surface of the cladding (see, for example, table 4); (iii) water vapour

Table 4 Zirconium Oxide Thicknesses for CRL Defect Experiments

Element	Distance from High Powered Bottom End (mm)	Zirconium Oxide Thickness (μm)	
		Inside Sheath Surface	Outside Sheath Surface
LFZ	92	6 to 56	0.5 to 2
	125 Primary Defect	4 to 30	0 5 to 2
	174	4 to 64	0 5 to 2
A7E	8 to 38 Secondary Defect	up to 30 (remote from defect) 100 (at defect site)	up to 36
	63 to 88 Secondary Defect	same as above	up to 76
	235	1 to 4 (oxide pockets up to 70)	1 to 4 (oxide pockets up to 26)
	390	1	1
A3N	0 to 485	5 to 12 (remote from slits) 2 to 8 (at slits maximum near bottom, downstream end)	2 to 4

oxidation of the fuel, and (iv) dissolved coolant hydrogen The liberated hydrogen from these various processes is then free to enter the sheath where there is a local breakdown of the protective oxide film

Davies has demonstrated that the ratio of hydrogen to oxidant in the fuel-to-sheath gap is critical to the hydriding process [10] In a review article, Cox has reported critical ratios of hydrogen/oxidant ranging between 10^2 to 10^6 [11] These ratios are consistent with the theory that a critical hole size exists above which hydriding is inhibited In elements with small defects, water ingress is limited not only by the small hole size, but also because the hole may plug up with zirconium oxide or with fission products Consequently, as hydrogen is produced from the various reactions, the hydrogen partial pressure will increase so that if there is a local breakdown in the protective oxide film, localized hydriding may result. The film may be broken by either fission-product attack or by mechanical stresses that are introduced during power transients

In the present study (see table 1), experiments with porous end caps (FF0-102-1) indicated that a critical hole size of about 1 μm was necessary to promote sheath hydriding, however, in a similar experiment with faulty end welds (FF0-105), the nature of the defect was such that it plugged up before hydriding could be initiated In contrast, for elements with large defects produced by mechanical drilling or machining (e g hole diameters ≥ 1 mm) (FD0-681, FD0 687 and FF0-103), no massive hydriding or deterioration of the sheath was observed This observation is in agreement with in reactor tests with Light Water Breeder Reactor (LWBR) fuel where rods containing intentionally-drilled holes of diameters 0 13 mm were too large to duplicate the slow ingress rate of coolant through an operational defect [12] With larger defects, the protective oxide film may be in a state of continuous repair Thus, a hole size of about 1 μm is necessary for the initiation of massive sheath hydriding resulting from a critical hydrogen to oxidant ratio, whereas a large defect (≥ 0 13 mm) will not promote sheath hydriding

The primary defect sizes in experiments FF0-102 1 and FF0 105 were estimated by high pressure, helium leak testing of the empty fuel sheaths containing a single (suspect) end cap An equivalent" hole size was determined for each element with the use of a Hagen-Poiseuille flow law Each element required a differential pressure (ΔP) before a leak was detectable, e g differential pressures of between 0 2 to 8 MPa were required for the porous end cap rods The fuel elements were then back-filled with helium at atmospheric pressure in the final fabrication process Standard helium leak-testing techniques (as employed by the commercial fuel fabricators) could not pick up this size of leaker However, during the FF0 102 1 loop test, the coolant pressure was sufficiently high (10 MPa) to permit a critical ΔP for coolant leakage leading to massive hydriding

(c) Fission Product Attack

It has been suggested that fission products in the fuel-to-sheath gap can accelerate the hydriding process,[7 9 10 12] and perhaps account for the faster rate of hydriding of elements defected by power ramp than comparable elements with manufacturing defects For instance, in an out-of-pile experiment, the hydriding process was enhanced in a vapour environment containing iodine [26] It is believed that the protective zirconium oxide film can be damaged by bombardment by highly energetic and massive fission products, allowing for hydrogen penetration In addition corrosive fission products such as iodine can react with the Zircaloy cladding Furthermore, the amount of fission products in the gap is also related to element power since the mechanisms of fission product release from the fuel depend on both the fission rate and temperature The defect size may also play an important role, since the flushing of water into the gap may reduce the critical" inventory of fission products (see Section 4)

3 2 Sources of Hydrogen

Hydrogen can be introduced into, or generated in, a defected fuel rod by the following mechanisms radiolysis of water, fuel oxidation, Zircaloy corrosion, and dissolved coolant hydrogen For illustrative purposes in the following calculations, it has been assumed that a typical defective fuel rod (with the dimensions of a class II element in table 2) is operating at a linear power of 50 kW/m in a pressurized coolant of 10 MPa, the temperature characteristics of the fuel rod are listed in table 5 (see Ref 22)

Table 5 Fuel-Element Temperature Calculation*

Linear Power (kW/m)	Temperature (K)				Radial Gap (μm)
	Fuel Centreline T_{fc}	Fuel Surface T_{fs}	Sheath Inside, T_s	Fuel to-Sheath Gap T_g	
50	2231	867	591	729	13

* Estimated with the ELESIM fuel performance code for a fuel burnup of 16 MW h/kgU (see Ref 22)

(a) Radiolysis of Water

Fission-product radiolysis can be a direct source of hydrogen as a result of the reaction:[5,12]

$$2\ H_2O \longrightarrow H_2O_2 + H_2. \qquad (1)$$

Since the rate of formation of hydrogen peroxide and hydrogen greatly exceeds their radical-induced recombination rate, the above reaction does not reach equilibrium. However, the highly-reactive hydrogen peroxide molecule can equilibrate with the fuel (in the presence of a large excess of hydrogen) with the liberation of still more hydrogen:[5,12]

$$H_2O_2 + (2/x)\ UO_2 = H_2 + (2/x)\ UO_{2+x}. \qquad (2)$$

The rate of production of molecular hydrogen from fission-product recoil can be estimated as follows. The molecular hydrogen yield (Y_{H_2}) from the highly energetic fission fragment has been experimentally determined to be about 18 gas molecules/keV of dissipated kinetic energy.[5] In addition, for fission product recoils with an average kinetic energy of 80 MeV, the stopping power (dE/dx) in a steam medium (at a density of 0.035 g/cm^3) is about 220 keV/μm.[27] Hence, the rate of hydrogen production (S_{H_2}) (in molecules per second) is given by[5]

$$S_{H_2} = R^{rec}\ Y_{H_2}\ (dE/dx)\ z. \qquad (3)$$

where R^{rec} is the rate of release of fission fragments (atoms/s) from the solid fuel body, and z is the average path length (in microns) of the fission fragment in the fuel-to-sheath gap. The recoil release rate R^{rec} is given by the well-known relation:[19,28,29]

$$R^{rec} = \tfrac{1}{4}\mu(S/V)\dot{F}Y_{ff}, \qquad (4)$$

where μ = average range of the fission fragment in the UO_2 fuel (density of 10.7 g/cm^3) (see table 6) = 7.6 μm
(S/V) = surface-to-volume ratio of the uranium dioxide fuel (= 331 m^{-1})
$\dot{F}$ = fission rate (= 6.28 x 10^{14} fissions/s)
Y_{ff} = fission-fragment yield = 2 particles/fission.

Table 6: Range of Br-88 and I-135 Fission Fragments in Different Media

Medium	Range* (mg cm^{-2})	
	Br-88	I-135
He	2.385	1.735
Ar	4.677	3.369
H_2O	2.545	1.841
UO_2	9.330	6.831

* Calculated with the TRIM Code (see Ref. 27). It is assumed that the Br and I fragments carry 100 and 67 MeV of the available fission energy.[19]

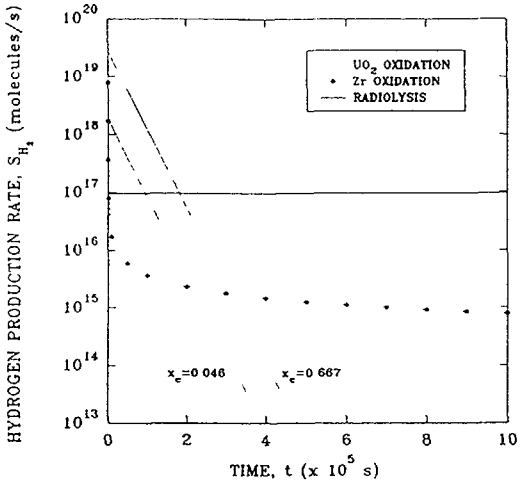

Figure 5: Hydrogen production rate as a function of time for a Class II fuel element (see table 2) irradiated at 50 kW/m in a pressured coolant of 10 MPa.

The calculation of the fission rate assumes that each fission event liberates 200 MeV of energy. Since the average range of the 80 MeV particles in the steam-filled gap is about 620 μm (see table 6),[27] most of these particles can traverse through the small gap (thickness of 13 μm in table 5), and embed themselves in the adjacent sheath. Therefore, z can be reasonably approximated by the mean chord length in the gap. In general, for any concave cavity of volume V_c and surface area S_c, the mean chord length (ζ) can be given by:[19,29,30]

$$\zeta = 4\ V_c/S_c. \qquad (5)$$

Hence, for the geometry of a cylindrical fuel rod with a radial gap of thickness t,

$$z \approx 2t. \qquad (6)$$

Finally, using Eqs. (3), (4) and (6), the hydrogen production rate is estimated as 9.6 x 10^{16} molecules/s (see Fig. 5).

(b) Fuel Oxidation

Although no data exist on the kinetics of oxidation of UO_2 by gas-phase hydrogen peroxide, the oxidation of uranium dioxide in steam has been studied by a number of investigators in experiments performed out-of-pile.[31-35] In the early work of Bittel et al.,[31] it was suggested that the oxidation process was controlled by oxygen diffusion through the fuel matrix.

However, Carter and Lay[32] subsequently showed that this process was controlled by a reaction at the solid/gas interface. Based on these results, an expression for the oxidation rate was proposed:

$$dx/dt = \alpha[x_e - x(t)](S/V) \quad (7)$$

where α = surface exchange coefficient of oxygen (m/s)
x_e = equilibrium deviation from stoichiometry
$x(t)$ = deviation from stoichiometry in UO_{2+x} at time t
(S/V) = surface-to-volume ratio of the solid (m^{-1}).

The surface exchange coefficient, α (in metres per second), has been determined experimentally by Cox et al.,[34,35] in the temperature range 1073 to 1873 K:

$$\alpha = 36.5 \times 10^{-2} \exp(-23500/T), \quad (8)$$

where T is the temperature in K. The analytic solution of Eq. (7) can be readily obtained if the temperature is constant:

$$x(t) = x_e [1 - \exp\{-\alpha(S/V)t\}], \quad (9)$$

where it has been assumed that the fuel is initially stoichiometric (i.e. x(0)=0).

The equilibrium deviation from stoichiometry (x_e) is defined by the oxygen potential of the gas phase.[22] At a total system pressure of p_t (atm), the oxygen partial pressure pO_2 (atm) can be obtained from equilibrium thermodynamics where (see Ref. 36)

$$pO_2 = X\, p_t, \quad (10)$$

and X is the mole fraction of oxygen in the gas. The mole fraction X is given by the solution of the transcendental equation

$$K(p_t\, X)^{1/2} [(Q/2 - 1) + (Q/2 + 1)X] = 1 - (Q + 1)X. \quad (11)$$

The parameter K is derived from the law of mass action that can be evaluated as a function of temperature

$$K = pH_2O/[pH_2(pO_2)^{1/2}] = \exp(-\Delta G^0/RT)$$

$$\Delta G^0 = -250.8 + 57.8(T/10^3) \quad kJ/mol, \quad (12)$$

where R is the ideal gas constant (= 8.314×10^{-3} kJ/mol·K). The parameter Q in Eq. (11) is defined as the hydrogen-to-oxygen (H/O) atom ratio of the gas environment such that

$$Q = (pH_2 + pH_2O)/(pO_2 + \tfrac{1}{2}\, pH_2O). \quad (13)$$

For example, Q = 2 for a pure steam environment, Q = 2.02 if the steam contains 1% excess hydrogen, and Q = 1.98 if the mixture is oxygen-enriched by 0.5%. In general $X \ll 1$, and Eq. (11) can be reasonably approximated as:

$$X = [K(p_t)^{1/2} (Q/2 - 1)]^{-2}, \quad Q > 2.001,$$

$$X = (4K^2 p_t)^{-1/3}, \quad Q = 2,$$

$$X = (1 - Q/2)/(1 + Q/2), \quad Q < 1.996. \quad (14)$$

With the calculation of X, the oxygen potential of the gas mixture can then be evaluated from

$$\overline{\Delta GO_2} = RT \ln(pO_2) = RT \ln (Xp_t). \quad (15)$$

The oxygen potential, or equivalently the partial molal free energy of oxygen in the solid per mole of O_2, can also be expressed in terms of the partial molar enthalpy $\overline{\Delta HO_2}$ (in kJ/mol) and entropy $\overline{\Delta SO_2}$ (in J/mol·K) of oxygen in the solid such that:

$$\overline{\Delta GO_2} = \overline{\Delta HO_2} - \overline{\Delta SO_2}\,(T/10^3) \quad (16)$$

where the thermodynamic parameters are given in Figure 6 as a function of x (see Ref. 37).

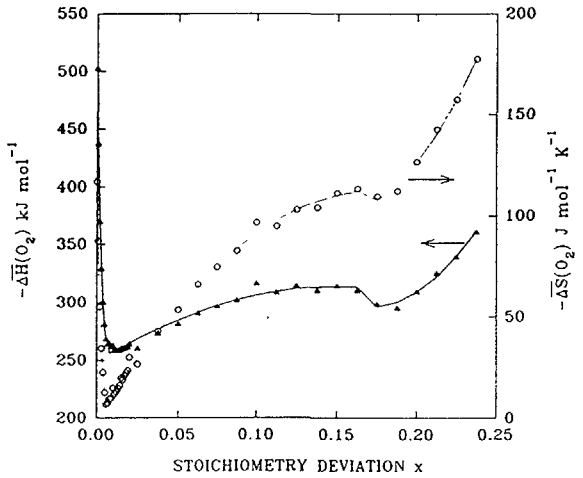

Figure 6: Partial molar entropy and enthalpy of oxygen in UO_{2+x} (see Ref. 37). The solid fitted curves are given by the polynomial expressions in Eq. (17).

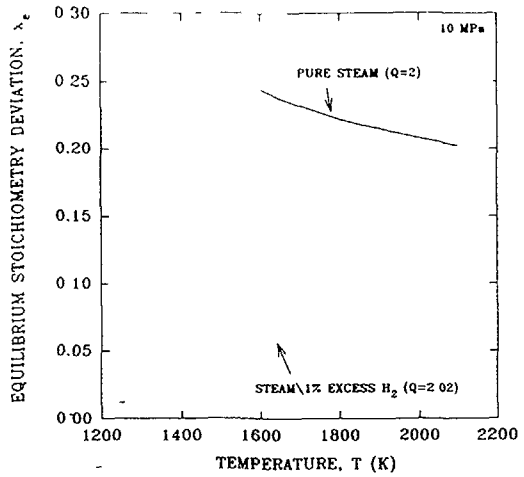

Figure 7: Equilibrium stoichiometry deviation (x_e) for UO_{2+x} in pure steam and in steam containing 1% excess hydrogen as a function of temperature.

These parameters can also be described by a polynomial correlation in x based on a non-linear least squares fit to the data (see Figure 6):

$$
\begin{aligned}
-\Delta\overline{HO_2} &= 501.9 - (7.392 \times 10^4)\,x + (5.779 \times 10^6)\,x^2, && 0 \le x \le 0.007,\\
&= 249.1 + 849.5\,x - (2.779 \times 10^3)\,x^2, && 0.007 < x \le 0.1625,\\
&= 695.8 - (4.737 \times 10^3)\,x + (1.402 \times 10^4)\,x^2, && x > 0.1625,\\
\\
-\Delta\overline{SO_2} &= 118.1 - (3.715 \times 10^4)\,x + (3.224 \times 10^6)\,x^2, && 0 \le x \le 0.005,\\
&= 3.698 \times 10^{-2} + (1.270 \times 10^3)\,x - (3.568 \times 10^3)\,x^2, && 0.005 < x \le 0.1625,\\
&= 333.4 - (3.066 \times 10^3)\,x + (1.016 \times 10^4)\,x^2, && x > 0.1625.
\end{aligned}
\qquad (17)
$$

The equilibrium stoichiometry deviation (x_e) is therefore obtained as the solution of the quadratic equation for x on equating Eqs. (15) and (16), where the thermodynamic parameters are given by the correlations in Eq. (17). For example, the results of this calculation are shown in Figure 7 where x_e is given as a function of temperature (at a system pressure of p_t = 10 MPa) for pure steam (Q = 2), and for 1% excess hydrogen in the gas mixture (Q = 2.02).

The hydrogen production rate can now be calculated as follows. The overall oxidation reaction is

$$x\,H_2O + UO_2 = UO_{2+x} + x\,H_2. \qquad (18)$$

Given that the atomic number density of oxygen in the fuel before and after oxidation is:

$$NO^{before} = 2\rho UO_2 N_o/MUO_2$$

$$NO^{after} = (2+x)\rho UO_{2+x} N_o/MUO_{2+x},$$

the number of oxygen atoms consumed by the fuel during oxidation is

$$\{[(2 + x)\,\rho UO_{2+x} VUO_{2+x}/MUO_{2+x}] - [2\,\rho UO_2 VUO_2/MUO_2]\}N_o, \qquad (19)$$

where ρ = density of the fuel (kg/m^3)
M = molecular weight of the fuel (kg/mol)
V = volume of the fuel (m^3)
N_o = Avogadro's constant (= 6.022 x 10^{23} atoms/mol).

If the number of moles of the hyperstoichiometric fuel is equal to that of the uranium dioxide fuel, i.e $(\rho V/M)UO_{2+x} = (\rho V/M)UO_2$, Eq. (19) reduces to

$$\text{number of oxygen atoms consumed during fuel oxidation} = x(\rho UO_2 VUO_2/MUO_2)N_o, \qquad (20)$$

Thus, using Eqs. (18) and (20), the production rate of molecular hydrogen is

$$SH_2 = (dx/dt)(\rho UO_2 VUO_2/MUO_2)N_o. \qquad (21)$$

Finally, differentiating Eq. (9) and using this expression in Eq. (21) yields

$$SH_2 = x_e\,\alpha\,S\,e^{-\alpha(S/V)x}(\rho UO_2/MUO_2)N_o. \qquad (22)$$

Equation (22) has been plotted in Fig. 5, assuming the fabrication values for the surface and volume of the solid fuel in table 2, and an average fuel temperature of 1549 K (see table 5). These calculations are shown for both pure steam (x_e = 0.667) and for a 1% hydrogen excess in the gas mixture (x_e = 0.046). In the case of pure steam, it has been conservatively assumed that the equilibrium phase is U_3O_8 (see Ref. 36).

(c) Zircaloy Corrosion

The water corrosion of Zircaloy proceeds through the reaction

$$Zr + 2H_2O = ZrO_2 + 2H_2. \qquad (23)$$

Part of the hydrogen generated in this reaction diffuses into the metal. At the start of the oxidation process, all of the hydrogen may be absorbed. However, the rate of absorption steadily decreases from a maximum during the first 10 mg/dm^2 oxidation to a typical plateau.[12,38] The pick-up fraction (defined as the amount of hydrogen in the metal to the total amount produced during the corrosion reaction) for Zircaloy-4 is usually between 5 and 25 percent. The hydrogen that is not absorbed by the sheath is released into the fuel-to-sheath gap of the defected rod, thereby enriching the steam atmosphere in hydrogen.

The kinetics of this reaction have been extensively studied (see, for example, Refs 39-42) In the temperature range 523 to 673 K, the corrosion process of Zircaloy starts with the formation of a thin protective oxide that grows with an approximate cubic rate law After a certain thickness is reached, a transition occurs where cracks develop in the oxide film structure These cracks provide easier access of the oxygen to the oxide-metal interface, resulting in a breakaway regime that is characterized by linear kinetics

The kinetics of the weight gain for the pre-transition period is given by

$$w^3 = k_{pre} F t \qquad (w \le w_t) \tag{24}$$

where w = weight gain per unit area of Zircaloy reacting with steam (mg/dm^2)
w_t = weight gain per unit area of Zircaloy at transition (mg/dm^2)
k_{pre} = pre-transition reaction rate constant (mg^3/dm^6 d)
F = fitting factor for in-reactor corrosion enhancement
t = exposure time (d)

At a weight gain of ~30-40 mg/dm^2, the post-transition kinetics follow a linear rate law

$$w = k_{post} F (t-t_t) + w_t \qquad (w > w_t), \tag{25}$$

where k_{post} is the post-transition reaction rate constant (mg/dm^{2}d) For an exposure of the cladding at a temperature T (in Kelvins), the time to transition, t_t, (in days) is given by[39]

$$t_t = 6\,50 \times 10^{11} \exp(-0\,035T)/F \tag{26}$$

The reaction rate constants are given by an Arrhenius form [39]

$$k_{pre} = 5\,07 \times 10^{13} \exp(-32{,}289/RT)$$

$$k_{post} = 2\,21 \times 10^{9} \exp(-28{,}200/RT), \tag{27}$$

where R is the universal gas constant (=1 987 cal/mol K) The oxide layer thickness is also related to the weight gain by

$$S_{ox} = 1\,56\,(A_{Zr}/MO_2)\,(w/\rho_{Zr}) \tag{28}$$

where A_{Zr} = atomic weight of zirconium (= 91 22 x 10^3 kg/mol)
MO_2 = molecular weight of oxygen (= 32 00 x 10^3 kg/mol)
ρ_{Zr} = Zircaloy-4 density (= 6 49 g/cm^3)

The constant of 1 56 is the Pilling-Bedworth ratio (i e the volume of oxide formed per unit volume of metal) Using Eqs (24) to (28), a fitting factor of F equal to 49 is obtained for the internal corrosion of defected fuel elements irradiated at about 50 kW/m in the CRL loop experiments (see Table 4) This value is larger than that observed for water-side corrosion in pressurized water reactors (F = 1 to 3), and in boiling water reactors (F = 10) (see Ref 39), because of bombardment by energetic fission fragments on the inside cladding surface

Finally, using Eqs (24) and (25), the corrosion rate for the pre- and post-transition regimes are given by

$$dw/dt = (k_{pre} F)^{1/3} t^{2/3}/3 \qquad (t \le t_t)$$

$$dw/dt = k_{post} F \qquad (t > t_t) \tag{29}$$

Since a weight gain of 32 x 10^3 kg (corresponding to 1 mole of oxygen) produces 2 moles of hydrogen, the production rate of molecular hydrogen (in molecules/s) is

$$S_{H_2} = 2(N_o/MO_2)S_{ci}\,(dw/dt)\,C, \tag{30}$$

where S_{ci} = inside cladding surface area (m^2)
C = 1 16 x 10^9 (kg/m^{2}s)/(mg/dm^{2}d)

Equation (30) has also been plotted in Figure 5 at the temperature of the inside cladding surface (table 5) This calculation assumes an unlimited supply of steam (i e no steam starvation)

(c) Dissolved Coolant Hydrogen

The amount of dissolved hydrogen in the coolant of pressurized water reactors is typically 10 to 60 cm^3/kg [12] The dissolved hydrogen in the defect loop experiments is 5 to 20 cm^3/kg (see Table 3) As shown in Ref 5, this amount of hydrogen would provide a much smaller contribution to internal hydriding of the cladding than that produced by radiolytic decomposition This process can therefore be ignored

3 2 1 Discussion of Results

The results of the above calculations for the production of hydrogen by coolant radiolysis, fuel oxidation, and Zircaloy oxidation in the defective fuel rod are summarized in Fig 5 The rate of hydrogen production by oxidation of the uranium dioxide fuel and Zircaloy cladding are only important at the beginning of the irradiation period. After about 3 days, coolant radiolysis in the gap becomes the major component.

3.3 Fuel Loss

As the integrity of the sheath deteriorates with secondary hydriding, fuel is released from the defective element into the coolant. Loss of UO_2 is probably caused by erosion from the thermalhydraulic effects of the coolant after individual grains are loosened by oxidation along their boundaries Figure 8 shows individual grains separating along boundaries from the bulk of the UO_2 at the surface of a pellet underneath a defect This phenomenon has been observed in CRL steam oxidation tests at low-temperature (773 to 1073 K) where a U_3O_8 layer is initially formed along the grain boundaries of the lower oxide material (such as U_4O_9) [35]

Fuel loss for defective fuel in the CRL loop irradiations is given in table 1 The fuel losses for the various experiments are estimated by visual and metallographic examination at the

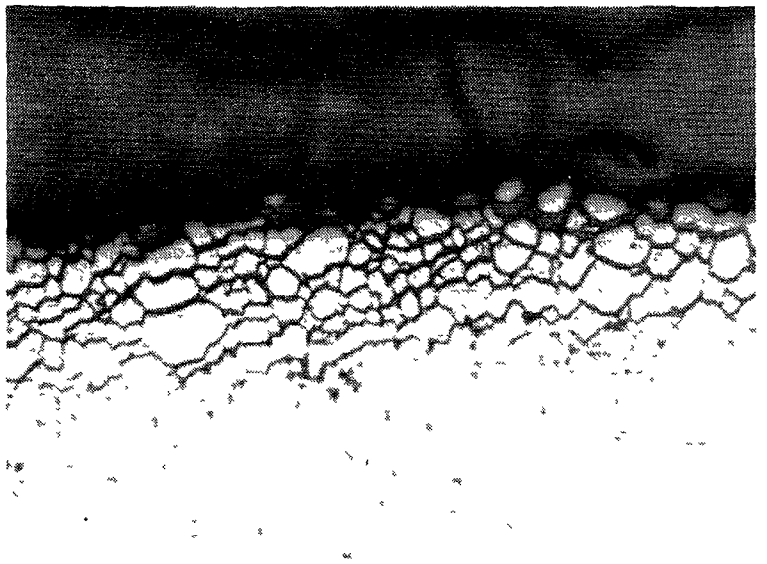

Figure 8: Oxidation of UO_2 under a defect hole in the Zircaloy sheath. Oxidation is progressing along the grain boundaries causing the grains to separate from the bulk of the pellet.

end of the irradiation. These values are upper-bound estimates as inevitably some fuel loss was incurred during the post-discharge handling of the elements. As a consequence of the grain-boundary oxidation process, the fuel loss depends on the amount of time that the fuel is exposed to the coolant. Other factors which are believed to influence the amount of fuel loss include:

(i) The size and shape of the defect and its orientation to the coolant flow. A larger size of defect generally results in greater fuel loss. Defects oriented with their long axis parallel to the coolant flow also lose more UO_2.

(ii) The operating power of the fuel since the oxidation rate is dependent on the UO_2 temperature (see Section 3.2, item b). For example, the greatest amount of fuel loss (and oxidation) occurred in the lower-powered region of the multi-slit element (FF0-103), in accord with Eq. (9) and Fig. 7 for a pure steam environment.

(iii) The amount of restructured fuel (which is also power dependent). Oxidation is slower in restructured fuel possibly because there are fewer and longer grain boundaries, or because of the higher temperature in this region of the fuel (see item ii). This observation can be seen in Figure 9; here, the UO_2 loss follows the as-sintered portion of the pellet while the area that has experienced grain growth is relatively untouched.

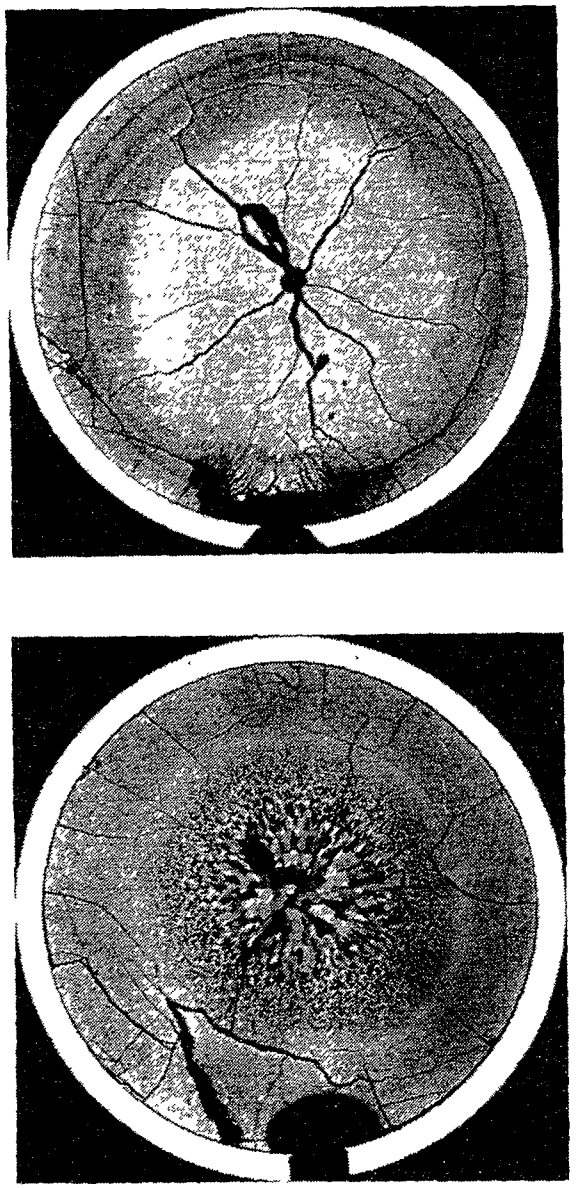

Figure 9: UO_2 missing from a pellet under a defect hole in the sheath. In the vicinity of the defect, the UO_2 that has undergone columnar grain growth in element RPR (left figure) is more resistant to attack than the UO_2 with the equiaxed grain structure in element LFZ (right figure). (Taken from Refs. 43 and 44.)

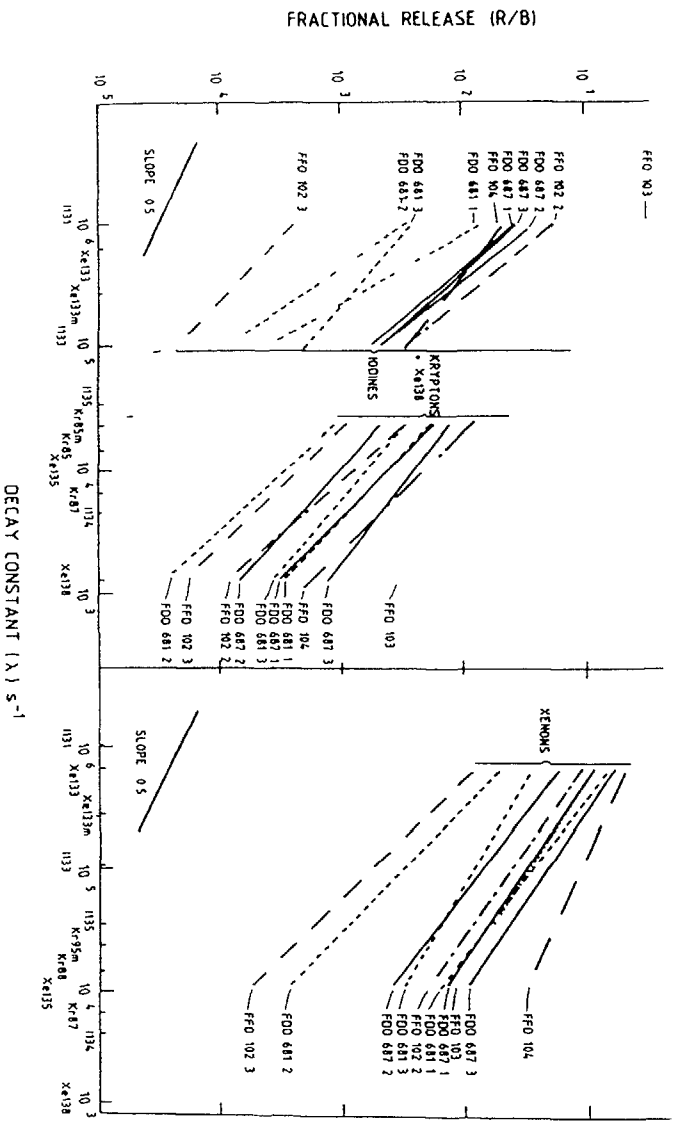

Figure 10 Steady-state R/B versus decay constant plot for noble gas and iodine for various defect experiments at Chalk River

4 FISSION PRODUCT RELEASE

4 1 Experimental Results

The dependence of the release-to-birth rate ratio, R/B, on the decay constant, λ, for both the iodine and noble gas species, has been obtained for the various defect experiments, as shown in Fig 10 Inspection of this figure reveals release dependencies between $\lambda^{1/2}$ and $\lambda^{3/2}$ Early theoretical considerations by Booth predicted an R/B proportional to $\lambda^{1/2}$ for purely diffusive release from the bulk UO_2 [45,46] This latter dependence has been confirmed in recent sweep gas experiments with intact fuel at CRL at high linear powers (40 to 62 kW/m),[47-49] and Halden at low linear power (23 kW/m) [50] A similar dependence was also found in experiment FF0-103 where the element had been machined with many slits along its sheath to minimize the holdup of fission products in the fuel-to-sheath gap (see table 1) Therefore any delay in release from elements with defects of a smaller size (i e a steeper release curve in Fig 10) can be attributed to additional trapping in the gap as the fission products migrate toward the defect site The relatively steeper slope for iodine also indicates a chemical retention of this species in the gap

4.2 Steady-State Fission Product Release Model

Historically, a number of models have been proposed to describe the transport behaviour of fission products in the fuel-to-sheath gap of a defective fuel element during steady-state reactor conditions The early work of Helstrom suggested that the rate-determining process of transport in the gap was atomic diffusion of fission gases within a bulk steam environment.[51,52] The empirical model of Allison and Rae estimated the effect of the axial path length on the holdup of the radioactive noble gases [53] In other treatments, a first-order rate process was assumed, where the coolant release was proportional to the total inventory in the gap (the proportionality constant was defined as an "escape-rate" coefficient) [54-56] In addition, the chemical holdup of iodine, presumably on the internal sheath surface, was modelled with an adsorption isotherm This latter approach provided the basis of the PROFIP code for determining the number of failed fuel rods in Pressurized Water Reactors (PWRs) based on coolant activity analyses [55-57] The treatment of Kalfsbeek also considered competing diffusive and bulk-convective transport processes in Boiling Water Reactor (BWR) fuel pins [58] A number of multi-step models have attempted to account for the release of fission products from both the fuel and the gap using separate escape-rate coefficients [59,60] More recently, a kinetic model[61,62] was used in the CHIRON code for estimating the number of defective fuel pins in Pressurized and Boiling Water Reactors [63,64] Based on the experimental program at CRL, models have been developed for CANDU fuel to describe the source of release into the gap, and the subsequent transport into the primary coolant by diffusion and first-order kinetics [17,20,22]

A generalized treatment has also been used to describe the transport of volatile fission products in the gap, leading to a unification of the previous diffusive and first-order kinetic approaches [23] This treatment considers axial diffusion along the gap in which release into the coolant is modelled as a surface-exchange process This model is shown to contain (as special cases) all previously reported results In particular, the R/B ratio for release into the primary coolant for an element containing n symmetrical defects along the sheath is

$$\frac{R}{B} = \left(\frac{2nL}{\ell}\right)\alpha\left(\frac{\tanh(\ell/2nL)}{(D/L)\tanh(\ell/2nL) + \alpha}\right)\left(\frac{R}{B}\right)_f , \qquad (31)$$

where α = surface exchange coefficient between the gap and the coolant (m/s)
L = diffusion length = $(D/\lambda)^{1/2}$
D = diffusion coefficient in the fuel-to-sheath gap (m^2/s)
ℓ = fuel element length (m)
$(R/B)_f$ = fission-product source term in the gap.

Here it is assumed that the defects are located at a distance ℓ/n from each other, and $\ell/2n$ from the ends of the element. Equation (31) is also applicable for the following special cases: n = 1 for a mid-rod defect, n = ½ for an end rod defect, and n = ℓ/b for a longitudinal slit where b is the inner circumference of the fuel sheath.

When the cladding-defect offers little holdup compared to the axial path length along the gap, $\alpha >> (D/L)\tanh(\ell/2nL)$, and Eq. (31) becomes (see also Ref. 20):

$$R/B = (2nL/\ell)\tanh(\ell/2nL)\,(R/B)_f . \qquad (32)$$

If the diffusion length of the fission product is much shorter than the fuel element length, $L << \ell/2n$, Eq. (32) reduces further to (see also Ref. 17):

$$R/B = (2nL/\ell)\,(R/B)_f . \qquad (33)$$

For the case of a single longitudinal slit (i.e. n = ℓ/b), Eq. (32) becomes

$$R/B = (2L/b)\tanh(b/2L)\,(R/B)_f , \qquad (34)$$

as previously developed by Helstrom.[51] On the other hand, if the diffusion length is much greater than the fuel element length, $L >> \ell/2n$, Eq. (31) yields

$$R/B = \frac{\varepsilon}{\varepsilon + \lambda}\,(R/B)_f \qquad (35)$$

where $\varepsilon = 2n\alpha/\ell$. Equation (35) has been proposed by a number of investigators as a first-order kinetic model where ε is termed an escape-rate coefficient.[17,20,54-56,59-64] If diffusion is the dominant mechanism of release from the fuel matrix:[45,46]

$$(R/B)_f = 3(D'/\lambda)^{1/2} , \qquad (36)$$

where D' = empirical diffusion coefficient of fission products in the fuel matrix (s^{-1}).

In this case, the diffusion model in Eq. (32) yields a release dependence on the decay constant of $\lambda^{-1/2}$ to λ^{-1}; the kinetic model in Eq. (35) yields a behaviour of $\lambda^{-1/2}$ to $\lambda^{-3/2}$. These dependencies are in excellent agreement with the observed results in Fig. 10.

Table 7: Oxygen-to-Uranium Ratios for CRL Experiments

Metallographic Sample Location	Distance From Bottom (High-Powered) End	Oxygen-to-Uranium (O/U) Ratio*	
		FF0-102-2 (A7E)	FF0-103 (A3N)
Lower-Plane Section**	43 - 63	2.15	N/A***
Mid-Plane Section	195 - 215	2.11	2.28
Upper-Plane Section	365 - 275	2.16	N/A***

* O/U ratios were determined by gravimetric analysis.
** This sample was located between two large secondary defects.
*** N/A = Not Available

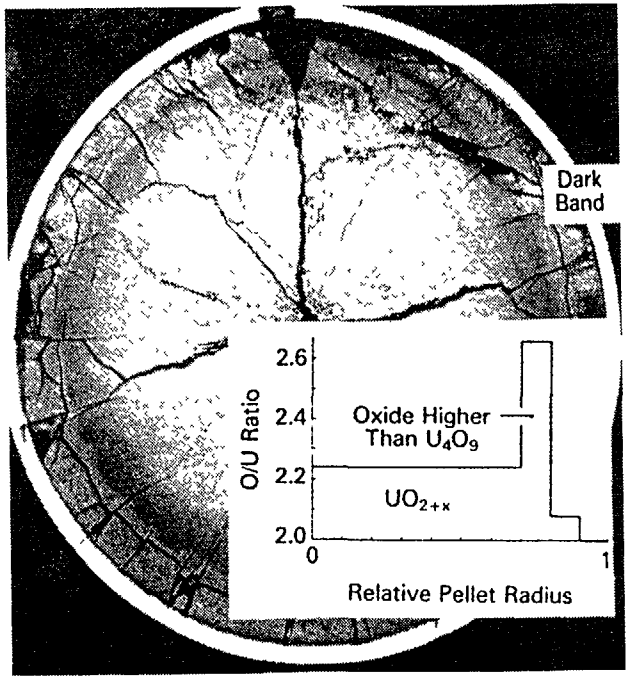

Figure 11: Comparison of the metallographic cross section and predicted O/U ratio distribution for experiment FF0-104. (Taken from Ref. 22.)

4 2 1 Fission Product Release and Fuel Oxidation

With defected fuel, a transport path exists in which the coolant can enter into the internal element atmosphere As discussed in Section 3 2 (b), steam is capable of oxidizing the UO_2 fuel resulting in an increased oxygen to uranium (O/U) ratio (see table 7) The oxidation model in Eq (7) has been applied to a defective fuel element to provide an estimate of the O/U radial distribution [22] This calculation suggests that a characteristic band structure observed in the metallographic examination is due to the presence of a higher oxide phase (see Fig 11)

In oxidized fuel the fuel thermal conductivity is reduced,[65] leading to an average temperature increase in the fuel pellet, which, in turn enhances the fission product release More importantly, an increase in the O/U ratio results in a direct enhancement of the diffusional release of fission products from the fuel matrix [66,67] These effects have been incorporated into the ELESIM fuel performance code (Ref 68) to predict the release of radioactive noble gases from defective fuel elements [22] This treatment employs the fuel oxidation model of Eq (7), and a diffusion coefficient that depends on both the stoichiometry deviation and the temperature profile in the fuel pellet. The diffusion coefficient itself is based on the assumption that diffusion takes place on vacant cation lattice sites in which Frenkel and Schottky equilibria govern the isolated point defects [69-71] In contrast, more recent work suggests that xenon diffusion occurs as a neutral trivacancy (Schottky trio) in UO_2 [66 72,73] However, the present model of the diffusion coefficient is in agreement with annealing test results in CO/CO_2, and with the experimental work of Lindner and Matzke for xenon diffusion in hyper-stoichiometric UO_{2+x} [69] The defective fuel model in ELESIM also accounts for the diffusional transport of fission products in the gap in accord with Eq (32), where the gap diffusivity is calculated with the Chapman Enskog kinetic theory [17]

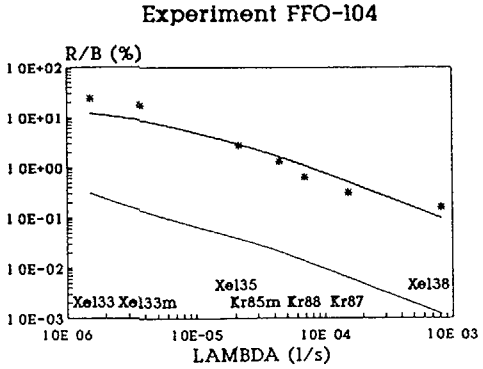

Figure 12 Comparison of measured versus predicted release for CRL defect experiment FFO-104 The asterisks indicate the measured data, the solid line corresponds to the model prediction without fuel oxidation, and the dark solid line indicates the use of the model with fuel oxidation (Taken from Ref 22)

Figure 12 shows a typical comparison of the measured versus predicted R/B ratios for CRL experiment FFO-104 as function of decay constant at steady state conditions When fuel oxidation effects are ignored, the noble gas releases are under-predicted by at least an order of magnitude, however, excellent agreement is generally obtained for all experiments when fuel oxidation effects are considered.[22] Similar enhancement factors have been experimentally observed by Schuster et al [74] based on studies of defective and intact fuel pins in LWRs

4 3 Transient Fission Product Release

Transient operation includes such manoeuvres as reactor startup and shutdown, as well as the cycling of the reactor power An understanding of the release behaviour for the transient situation is important because there is generally a greater burden of fission products in the coolant. Figure 13 shows the release from a defective fuel element power-cycled between 22 and 38 kW/m in experiment FFO-109 (Phase 2) [21] The short-lived isotopes display a greater sensitivity to changes in the fuel element power The increase in the noble gas concentrations occur during the power-uprating portion of the cycle For experiment FDO-681, the concentration of iodine steadily increased during the shutdown period in Figs 14(a) and (b) (see discussion below), in contrast, the noble gas concentrations decreased as a result of radioactive decay in the coolant.[43] On start-up, the activity levels increased for both iodine and noble gases with the shorter-lived isotopes exhibiting the greater increase

Inspection of Fig 10 shows that only a small fraction of the fission-product iodine in a defective pin is released into the coolant while the reactor is operating at constant power Most of the iodine available for release is present as a liquid-water soluble deposit (such as cesium iodide) on the UO_2 fuel surface or inner surface of the Zircaloy sheath If the temperature in the fuel to sheath gap drops below that of coolant saturation, as during reactor shutdown, the water

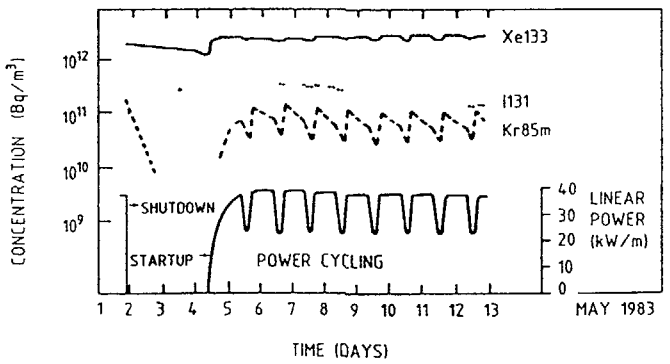

Figure 13 Concentration of fission products in the coolant versus time for a reactor cycling mode of operation in experiment FFO-109 (Phase 2) (Taken from Ref 21)

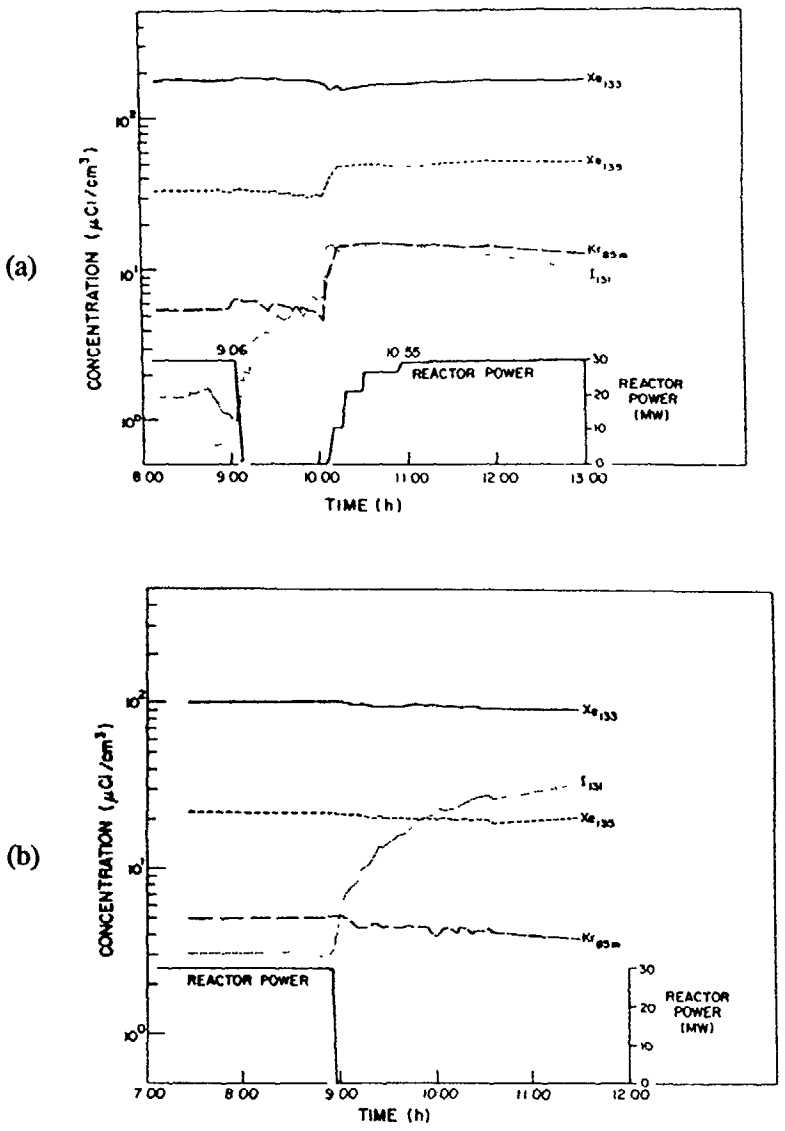

Figure 14. Concentrations of fission products in the coolant versus time in experiment FD0-681 for:
(a) a reactor trip and subsequent startup (Ref. 43)
(b) a scheduled reactor shutdown (Ref. 43).

which has entered the element remains in the liquid phase (see Ref. 75), and leaches these deposits. The dissolved iodine then migrates along the water-filled gap to the defect site, resulting in an increased release to the primary coolant. This "iodine-spiking" phenomenon has been widely discussed in the literature.[18,20,21,76-85] The behaviour of the iodine release on shutdown in Fig. 13 has been modelled by both diffusion and first-order kinetics according to the expression (see Fig. 15):[18,20,21]

$$N_c(t) = (N_{co} + N_{go}\{1 - \exp[-(\varepsilon - L)\,t]\}\varepsilon/(\varepsilon - L)) \times \exp[-(\lambda + L)\,t], \quad (37)$$

where $N_c(t)$ = inventory of iodine in the coolant at time t (atoms)
N_{co} = initial inventory of iodine in the coolant (atoms)
N_{go} = initial inventory of iodine in the gap (atoms)
ε = gap escape-rate coefficient (s^{-1})
= $n^2\pi^2D/\ell^2$, where D is the effective diffusion coefficient for iodine in the gap, and n is the number of defect sites (see Section 4.2)
L = loss-rate constant for coolant leakage and ion-exchange purification (s^{-1}).

On reactor shutdown, only the water-soluble species (e.g. iodine and cesium) are released into the coolant.[83] The liquid water present in the gap blocks the release of noble gas by either trapping the gas at the top of the element or by surface tension effects in the fuel cracks.[21] As the reactor returns to full power, the iodine-rich water is expelled from the element (at low power), giving a second distinctive spike as the fuel thermally expands and the size of the gap is reduced. The noble gases are expelled from the element after the water in the gap has vapourized.

4.4 Fission Product Release From Uranium Contamination

In a reactor, traces of uranium compounds may be found on the surfaces of the heat transport system. This contamination is the result of a previous loss from defective fuel (see

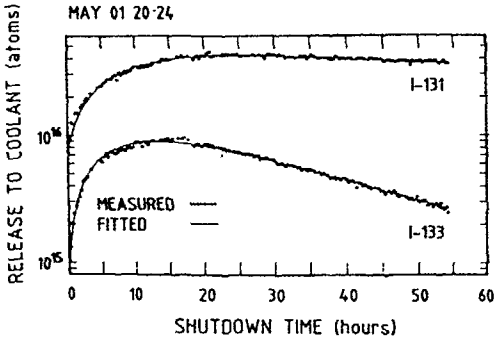

Figure 15: Fitting of iodine-spiking model [Eq. (37)] to data for reactor shutdown in experiment FF0-109 (Phase 2) (Ref. 21).

Section 3 3), and from the original uranium traces deposited on fuel pin external surfaces during fuel fabrication As a consequence of grain boundary oxidation, the uranium contamination is generally in the form of very fine particles (see Figs 8 and 9), except in the circumstance of a severe failure where a portion of the fuel pellet may be released Hence, for small particles of fuel at low temperature, fission product release will occur by direct recoil where the range of the fission fragment ($\mu \sim 8$ μm) is comparable to the size of the UO_2 fuel particle [19,20] For instance, experimental ratios of release rates of ^{88}Kr to ^{138}Xe were between 0 4 and 0 7 in a pressurized-water loop containing fuel debris on the piping surface [86] This range is in excellent agreement with the theory of recoil where the ratio of the release rates (R^{88}/R^{138}) is equal to that of the fission-product yields ($y^{88}/y^{138} = 0\ 55$) In particular, the release expression for a small particle of fuel of diameter d, deposited onto a solid surface, is[19 20]

$$R/B = \frac{1}{2}\left\{\frac{1}{\alpha^3} + \frac{3\mu}{2d}\left(1 - \frac{1}{\alpha^2}\right)\right\} \qquad (38)$$

where $\alpha = 1$ or d/μ whichever is greater Thus, $R \propto y$ since the right hand side (RHS) of Eq (38) is a constant and B is proportional to y Furthermore, if $d \ll \mu$ (see Fig 8), Eq (38) reduces to $R/B = ½$

5. POWER REACTOR APPLICATIONS

The present understanding of defective fuel performance and fission-product release have led to a number of analytical tools for the monitoring of failed fuel in commercial power reactors of the LWR[55-57 60-64,83,87] and CANDU[3 15,24,25,88-91] design Based on a gamma-ray spectrometry analysis of the primary coolant, such tools can provide an estimate of the core condition (e g the number of defective fuel rods, the average defect size, and the amount of tramp uranium deposited on the in-core surfaces) In some CANDU reactors, defective fuel bundles can also be detected and located by exploiting the on-power refuelling capability of the reactor with the use of delayed-neutron monitoring techniques [3 92,93]

Many of the analysis programs for fuel-failure monitoring are based on the methodology presented in Section 4 [25,56,61-64] For example, the release-to-birth rate ratio (R/B) of fission products released into the primary coolant is given by the model [25]

$$\frac{R}{B} = \left(\frac{\varepsilon}{\varepsilon + \lambda}\right)\frac{A}{\sqrt{\lambda}} + c \qquad (39)$$

where A = x 3 (D)$^{1/2}$,
ε = escape rate constant in the fuel-to-sheath gap (s^{-1}),
λ = radioactive decay constant (s^{-1}),
D = empirical diffusion coefficient in the UO_2 fuel (s^{-1}),
c = ½ F_t/F,
F_t = fission rate in the tramp uranium,
F = average fission rate per defective fuel rod

The first term on the RHS of Eq (39) pertains to the fission-product release from x failed fuel rods [see Eqs (35) and (36)], while the second term describes the recoil release from the tramp uranium deposited on in reactor surfaces of the PHTS [Eq (38)] The measured coolant activity concentration C_m (Bq/L) is converted into an R/B ratio given the average fuel-element power

$$\left(\frac{R}{B}\right) = \left(\frac{\lambda + \beta}{\lambda}\right)\frac{C_m V_L}{Fy}\exp(\lambda T) \qquad (40)$$

where β is the purification rate constant (s^{-1}), V_L is the PHTS loop volume, T is the transport time from the core to the data sampling location, and y is the fission product yield Equation (39) is fit using a non-linear least squares analysis to the measured R/B ratios for a given fission product species

The condition of the core can now be determined from the fitting parameters of the model (ε, A and c) [25] These parameters can be compared to the well-characterized data of the CRL experiments (table 1) By fitting Eqs (35) and (36) to the release data in Fig 10, the diffusion coefficient can be expressed as a function of the fuel element linear power, P (in kW/m), according to the correlations $D'_{Iodine} = 10^{9\,857\ logP\ 25\,1314}$ and $D'_{Noble} = 10^{8.632\ logP\ 23\,4091}$ Thus, the number of fuel failures in the power-reactor core can be determined by·

$$x = \frac{A}{3\sqrt{D'}} \qquad (41)$$

where D is evaluated at the average fuel-rod power The average size of defect for these failures can also be estimated with the previous relation (see Section 4 2)

$$\varepsilon = (2\,n\,\alpha)/\ell, \qquad (42)$$

where the escape rate constant ε depends on both the fission-product chemistry, and the defect geometry (i e transport path length) in the fuel rod As shown in the CRL experiments (see Fig 16), the surface exchange coefficient, α, can be expressed as a function of the defect size E in square millimetres $\alpha_{Iodine} = 10^{0\,7046\ logE\ 7\,5173}$ and $\alpha_{Noble} = 7\ 14 \times 10^{-6}$ m/s In fact, α is strongly dependent on the defect size for iodine due to the chemical effects of water/steam in the fuel-to sheath gap, whereas, it is relatively constant for the inert noble gases Thus, the average defect size for the power-reactor failures can be estimated in which the geometry (n) is determined from Eq (42) given the experimental value of α_{Noble} and the fitted value of ε from the power-reactor data Using this information, the size of the sheath defect, E, can in turn be calculated from the correlation for α_{Iodine} and the fitted value of ε for the iodine species Finally, the amount of tramp uranium m_U in the power reactor core can be determined from the fitted value of c such that [19,20,25]

$$m_U = \frac{cF}{N_o \psi \langle \phi_T \rangle}, \qquad (43)$$

where N_o is Avogadro's constant, ψ is a function that depends on the isotopic fissile content of the fuel, and $\langle \phi_T \rangle$ is the volumetrically-averaged thermal neutron flux

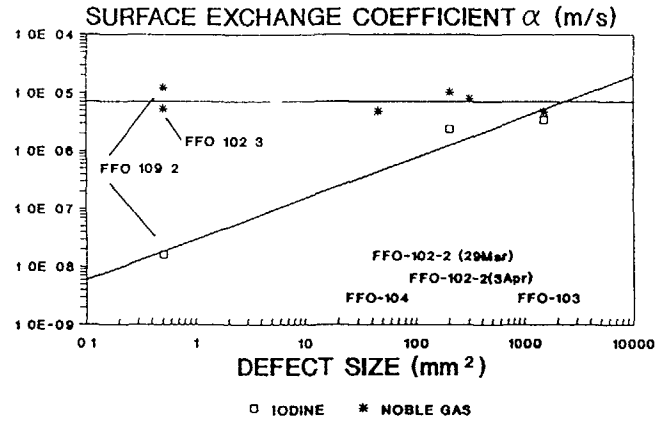

Figure 16 Surface exchange coefficient α for iodine and noble gases versus defect size for CRL experiments. The surface exchange coefficient was evaluated assuming (a) a mid-rod defect (n = 1) for elements A7A and A2F, (b) an end-rod defect (n = ½) for element A7E, and (c) a longitudinal slit (n = ℓ/b) for element A3N (see table 1)

The present analysis package has been validated against fuel failure data obtained from CANDU power-reactor experience For instance, the package is able to predict the number of failures within a factor of two for the iodine analysis, with a much better agreement (i e within 25 per cent) for that of the noble gases [25]

6. SUMMARY

1 Studies based on in-reactor loop experiments and nuclear power plant experience have provided a better understanding of the performance of defective nuclear fuel rods For example, an in-reactor research program at the Chalk River Laboratories (CRL) has involved the irradiation of fuel elements containing various sizes and types of sheath failure, operating at linear powers ranging from 14 to 67 kW/m up to a maximum burnup of 278 MW h/kgU

2 For the initiation of sheath hydriding, a primary hole size of about 1 μm will provide a critical hydrogen/oxidant ratio, whereas hydriding will not occur for defect sizes greater than about 130 μm The rate of internal hydrogen production by the oxidation of the uranium dioxide fuel and Zircaloy cladding are only important at the beginning of the irradiation period, after which coolant radiolysis becomes the predominant source Both hydriding and degradation of the sheath progress faster at higher power in accord with a previous UKAEA study Increased element damage can result from mechanical stresses during transient reactor operation An average fuel loss rate of up to 4 g of UO_2/day has been observed

3 The release-to-birth rate (R/B) ratio, at steady-state reactor operation, increases with the power and burnup of the fuel element, as well as with the size of defect (see Fig 10) For defective fuel elements operating above 20 kW/m, the R/B dependence on the decay constant is directly related to the defect state, with a dependence between $\lambda^{1/2}$ to $\lambda^{3/2}$ This behaviour is consistent with theoretical models based on simple diffusion in the fuel matrix, and diffusion or first order kinetics in the fuel-to-sheath gap Transport of iodine in the gap is more restricted than that of noble gas

4 Physically-based models have been developed to predict the activity release of radioactive noble gases from defected fuel elements during steady-state reactor conditions In particular, a model implemented in the ELESIM fuel-performance code accounts for the various interrelated phenomena that can affect the prediction of fuel temperature and fission-product release including the kinetics of fuel oxidation, and the diffusion of fission products in the fuel matrix and along the gap

5 The transient release is dependent on the half-life of the isotope (shorter-lived isotopes are more sensitive to changes in the fuel power), and the chemical nature of the fission product. Iodine is released on both reactor startup and shutdown, whereas noble gas is only released in quantity on reactor startup On prolonged reactor shutdown, iodine deposits are leached by the liquid water resulting in an enhanced release to the primary coolant. In this "iodine-spiking" process, the transport of iodine in the gap can be described by diffusion or first-order kinetics

6 Recoil is the dominant mechanism of fission-product release from fuel debris found on in-core reactor surfaces This source of activity release in the primary heat-transport system can be distinguished from that of fuel pin failure, allowing for a more accurate assessment of the core condition Analytical tools, based on a number of defective-fuel studies, have been developed for fuel-failure monitoring in power reactors

ACKNOWLEDGEMENTS

The authors would like to acknowledge the contributions of J J Lipsett, R D Delaney, R L da Silva, M R Floyd, J J Judah, A M Manzer, D D Semeniuk, D F Shields, and NRX Reactor Branch personnel, to the defect program The assistance provided by J C Wood, H E Sills, D G Hardy, D S Cox, M J Notley, P J Fehrenbach, J M. Bunge, and E P Penswick of CRL is greatfully acknowledged The authors would also like to thank C R Phillips (U of T), P T Truant (OH), C E Beyer (BPNL), Y H Kang (KAERI), E Gheorghiu (INPR), R J Green (RMC), and D R Olander (UC) for many helpful discussions

The experimental program was funded by a cooperative program between Atomic Energy of Canada Limited (AECL) and Ontario Hydro The current work was funded by the Academic Research Program of the Department of National Defence of Canada under allocations 3705-882 and 3705 4, and AECL

REFERENCES

1. P.T. Truant and I.J. Hastings, "CANDU Reactor Experience: Fuel Performance", Atomic Energy of Canada Limited report AECL-8774, July 1985.

2. A.J. Hains, R.L. da Silva and P.T. Truant, "Ontario Hydro Fuel Performance Experience and Development", Proceedings of the International Conference on CANDU Fuel (ISBN 0-919784-13-5), Chalk River, Canada, October 6-8, 1986, p. 79.

3. R.D. MacDonald, M.R. Floyd, B.J. Lewis, A.M. Manzer and P.T. Truant, "Detecting, Locating and Identifying Failed Fuel in Canadian Power Reactors", Atomic Energy of Canada Limited report AECL-9714, IAEA Coordinated Research Program on the Examination and Documentation Methodology for Water Reactor Fuel (ED-WARF), February 1990.

4. R.L. Yang, O. Ozer and H.H. Klepfer, "Fuel Performance Evaluation for EPRI Program Planning", Proceedings of the International Topical Meeting on LWR Fuel Performance, Avignon, France, April 21-24, 1991, p. 258.

5. J.M. Markowitz, "Internal Zirconium Hydride Formation in Zircaloy Fuel Element Cladding Under Irradiation", Bettis Atomic Power Laboratory report WAPD-TM-351, May 1963.

6. D.H. Locke, "Defected Zircaloy Fuel", Nucl. Eng. Inter., August 1969, p. 648.

7. D.H. Locke, "The Behaviour of Defective Reactor Fuel", Nucl. Eng. Design 21 (1972) 318.

8. D.H. Locke, "Mechanisms of Deterioration of Defected LWR Fuel", Proc. Specialists' Mtg. Defected Zirconium Alloy Clad Ceramic Fuel in Water Cooled Reactors, Chalk River, Canada, September 17-21, 1979, IWGFPT/6, p. 101, International Atomic Energy Agency (1980).

9. R.A. Proebstle, J.H. Davies, T.C. Rowland, D.R. Rutkin and J.S. Armijo, "The Mechanism of Defection of Zircaloy-Clad Fuel Rods by Internal Hydriding", Proc. Of the Joint ANS-CNS Topical Mtg. on Commercial Nuclear Fuel Technology Today, Toronto, Canada, April 1975.

10. J.H. Davies, "Secondary Damage in LWR Fuel Following PCI Defection - Characteristics and Mechanisms", Proc. Specialists' Mtg. Defected Zirconium Alloy Clad Ceramic Fuel in Water Cooled Reactors, Chalk River, Canada, September 17-21, 1979, IWGFPT/6, p. 135, International Atomic Energy Agency (1980).

11. B. Cox, Mechanism of Hydrogen Absorption by Zirconium Alloys", Atomic Energy of Canada Limited report AECL-8702, November 1984.

12. J.C. Clayton, "Internal Hydriding in Irradiated Defected Zircaloy Fuel Rods", Zirconium in the Nuclear Industry: Eighth International Symposium, STP 1023, American Society for Testing and Materials, Philadelphia, 1989, p. 266.

13. J.H. Davies and G.A. Potts, "Post-Defect Behaviour of Barrier Fuel", Proceedings of the International Topical Meeting on LWR Fuel Performance, Avignon, France, April 21-24, 1991, p. 272.

14. R.L. da Silva, "Irradiation of a CANDU UO_2 Fuel Element with Twenty-three Machined Slits Cut Through the Zircaloy Sheath", Atomic Energy of Canada Limited report AECL-8260, September 1984.

15. M.R. Floyd, "Characterisation of Defective CANDU Fuel Using Gaseous and Dissolved Fission Product Data", Ontario Hydro report CNS-IR-37351-2, October 1985.

16. R.L. da Silva, D.R. McCracken and K.J. Monserrat, "Behaviour of Depositing Fission Products Released from Defective Fuel", Advances in Ceramics, Vol. 17, Fission Product Behaviour in Ceramic Oxide Fuel, American Ceramic Society (1986), p. 107.

17. B.J. Lewis, C.R. Phillips and M.J. Notley, "A Model for the Release of Radioactive Krypton, Xenon, and Iodine from Defective UO_2 Fuel Elements", Nucl. Technol. 73 (1986) 72.

18. B.J. Lewis, D.B. Duncan and C.R. Phillips, "Release of Iodine from Defective Fuel Elements Following Reactor Shutdown", Nucl. Technol. 77 (1987) 303.

19. B.J. Lewis, "Fission Product Release from Nuclear Fuel by Recoil and Knockout", J. Nucl. Mater. 148 (1987) 28.

20. B.J. Lewis, "Fundamental Aspects of Defective Nuclear Fuel Behaviour and Fission Product Release", J. Nucl. Mater. 160 (1988) 201.

21. B.J. Lewis, R.D. MacDonald and H.W. Bonin, "Release of Iodine and Noble Gas Fission Products from Defected Fuel Elements During Reactor Shutdown and Start-Up", Nucl. Technol. 92 (1990) 315.

22. B.J. Lewis, F.C. Iglesias, D.S. Cox and E. Gheorghiu, "A Model for Fission Gas Release and Fuel Oxidation Behaviour for Defected UO_2 Fuel Elements", Nucl. Technol. 92 (1990) 353.

23. B.J. Lewis, "A Generalized Model for Fission-Product Transport in the Fuel-to-Sheath Gap of Defective Fuel Elements", J. Nucl. Mater. 175 (1990) 218.

24. M.J.F. Notley and J.H.K. Lau, "A Model for Estimating the Pre- and Post- Shutdown I-131 Coolant Inventories in CANDU Reactors", Proceedings of the International Topical Meeting on LWR Fuel Performance, Avignon, France, April 21-24, 1991, p. 419.

25. B.J. Lewis, R.J. Green and C.W.T. Che, "A Prototype Expert System for the Monitoring of Defected Nuclear Fuel Elements in CANDU Reactors", Nucl. Technol., in press.

26. J.C. Wood, "Interactions Between Stressed Zirconium Alloys and Iodine at 300°C", J. Nucl. Mater. 23 (1974) 63.

27. J.F. Ziegler, J.P. Biersack and U. Littmark, "The Stopping and Range of Ions in Solids", Vol. 1, Pergamon Press, New York, 1985. (See also the computer code: "TRIM-89: The Transport of Ions in Matter - Version 5.1", International Business Machines, Radiation Science Group, User's Manual, November 1988.)

28. D.R. Olander, "Fundamental Aspects of Nuclear Reactor Fuel Elements", US Department of Energy, TID-26711-p1, 1976, p. 303.

29. C. Wise, "Recoil Release of Fission Products from Nuclear Fuel", J. Nucl. Mater. 136 (1985) 30.

30. G.I. Bell and S. Glasstone, "Nuclear Reactor Theory", Robert E. Krieger, Huntington, New York, 1979, p. 120.

31. J.T. Bittel, L.H.Sjohdal and J.F. White, "Steam Oxidation Kinetics and Oxygen Diffusion in UO_2 at High Temperatures", J. Amer. Ceram. Soc. Vol. 52, No. 8, 446 (1968).

32. R.E. Carter and K.W. Lay, "Surface-Controlled Oxidation-Reduction of UO_2", J. Nucl. Mater. 36 (1970) 77.

33. J.A. Meachen, "Oxygen Diffusion in Uranium Dioxide: A Review", Nucl. Energy, 28 (1989) 221.

34. D.S. Cox, F.C. Iglesias, C.E.L. Hunt, N.A. Keller, R.D. Barrand, J.R. Mitchell and R.F. O'Connor, "Oxidation of UO_2 in Air and Steam with Relevance to Fission Product Releases", Proc. Symp. Chemical Phenomenon Associated with Radioactivity During Severe Nuclear Plant Accidents, Anaheim, California, 9-12 September 1986, NUREG/CP-0078, pp. 2-35, U.S. Nuclear Regulatory Commission.

35. D.S. Cox, F.C. Iglesias, C.E.L. Hunt, R.F. O'Connor and R.D. Barrand, "High-Temperature Oxidation Behaviour of UO_2 in Air and Steam", Proc. Int. Symp. High-Temperature Oxidation and Sulphidation Processes, Hamilton, Ontario, Canada, August 26-30, 1990.

36. D.R. Olander, "Oxidation of UO_2 by High Pressure Steam", Nucl. Technol. 74 (1986) 215.

37. P.O. Perron, "Thermodynamics of Non-Stoichiometric Uranium Dioxide", Atomic Energy of Canada Limited report AECL-3072, May 1968.

38. B. Cox, "Some Factors Which Affect the Rate of Oxidation and Hydrogen Absorption of Zircaloy-2 in Steam", AERE-R4348, 7 November 1963.

39. G.W. Parry and P.G. Smerd, "Review of PWR Fuel Rod Waterside Corrosion Behaviour", NP-1472, Electric Power Research Institute", August 1980.

40. H. Stehle, F. Garzaolli, A.M. Garde and P. Smerd, "Characterization of ZrO_2 Films Formed In-Reactor and Ex-Reactor to Study the Factors Contributing to the In-Reactor Waterside Corrosion of Zircaloy", Proc. 6th Int. Symp. on Zirconium in the Nuclear Industry, ASTM-STP 824 (1984) 483.

41. H.R. Peters, "Improved Characterization of Aqueous Corrosion Kinetics of Zircaloy-4", Proc. 6th Int. Symp. on Zirconium in the Nuclear Industry, ASTM-STP 824 (1984) 507.

42. A.I.A. Almarshad and A.C. Klein, "A Model for Waterside Oxidation of Zircaloy Fuel Cladding in Pressurized Water Reactors", J. Nucl. Mater. 183 (1991) 186.

43. R.D. MacDonald and J.J. Lipsett, "The Behaviour of Defected Zircaloy-Clad-UO_2 Fuel Elements with Graphite Coatings Between Fuel and Sheath Irradiated at Linear Powers of 48 kW/m", Atomic Energy of Canada Limited report AECL-6787, May 1980.

44. R.D. MacDonald, J.J. Lipsett, E.E. Perez and P.K. Kos, "Purposely Defected UO_2 Zircaloy Fuel Elements Irradiated in Pressurized Light Water at Linear Powers of 55 kW/m", Atomic Energy of Canada Limited report AECL-7751, May 1983.

45. A.H. Booth, "A Suggested Method for Calculating the Diffusion of Radioactive Rare Gas Fission Products from UO_2 Fuel Elements and a Discussion of Proposed In-Reactor Experiments that may be used to Test its Validity", Atomic Energy of Canada Limited report AECL-700, September 1957.

46. B.J. Lewis and H.E. Sills, "Fission-Product Transport and the Diffusion Approximation", J. Nucl. Mater. 184 (1991) 107.

47. I.J. Hastings, C.E.L. Hunt and J.J. Lipsett, "Release of Short-Lived Fission Products from UO_2 Fuel: Effects of Operating Conditions", J. Nucl. Mater. 130 (1982) 407.

48. B.J. Lewis, C.E.L. Hunt and F.C. Iglesias, "Source Term of Iodine and Noble Gas Fission Products in the Fuel-to-Sheath Gap of Intact Operating Nuclear Fuel Elements", J. Nucl. Mater. 172 (1990) 197.

49. B.J. Lewis, D.B. Knight and F.C. Iglesias, "Comparison of the ANS 5.4 Fission Product Release Model with Sweep Gas Experiments", Proceedings of the International Topical Meeting on LWR Fuel Performance, Avignon, France, April 21-24, 1991, p. 605-619.

50. A.D. Appelhans and J.A. Turnbull, "Measured Release of Radioactive Xenon, Krypton and Iodine from UO_2 during Nuclear Operation and a Comparison with Release Models", Proc. 8th Water Reactor Safety Research Information Meeting, Gaithersburg, Maryland, October 27-31, 1980, US Nuclear Regulatory Commission.

51. C. Helstrom, "Emission Rate of Fission Products from a Hole in the Cladding of a Reactor Fuel Element", AECU 3220, July 1956.

52. B. Lustman, "Irradiation Effects in Uranium Dioxide", Chapter 9, in: J. Belle, "Uranium Dioxide: Properties and Nuclear Applications" U.S. Government Printing Office, Washington D.C. (1961), pp. 431-666.

53. G.M. Allison and H.K. Rae, "The Release of Fission Gases and Iodine from Defected UO_2 Fuel Elements of Different Lengths", Atomic Energy of Canada Limited report AECL-2206, June 1965.

54. P. Bourgeois and J.P. Stora, "Behaviour of Fission Products in PWR Primary Circuits and Defected Fuel Rod Evaluation", presented at the 5th Int. Conf. Structural Mechanics in Reactor Technology, Berlin, FRG, March 20, 1979.

55. P. Beslu, C. Leuthrot, and G. Frejaville, "PROFIP Code: A Model to Evaluate the Release of Fission Products from Defected Fuel in PWRs", Proc. Specialists' Mtg. Defected Zirconium Alloy Clad Ceramic Fuel in Water Cooled Reactors, Chalk River, Canada, September 17-21, 1979, IWGFPT/6, p. 23, International Atomic Energy Agency (1980).

56. R. Beraha, G. Beuken, G. Frejaville, C. Leuthrot, and Y. Musante, "Fuel Survey in the Light Water Reactors Based on the Activity of the Fission Products", Nucl. Technol. 49 (1980) 426.

57. C. Leuthrot, A. Brissaud and J.P. Missud, "Relationships Between the Characteristics of Cladding Defects and the Activity of the Primary Coolant Circuit and Aid for the Management of Leaking Fuel Assemblies in PWR", Proceedings of the International Topical Meeting on LWR Fuel Performance, Avignon, France, April 21-24, 1991, p. 324.

58. H.W. Kalfsbeek, "The Abundance of Fission Gases in the Off Gas of a Boiling Water Reactor", Nucl. Technol. 62 (1983) 7.

59. J.T. Mayer, E.T. Chulick, and V. Subrahmanyam, "B&W Radiochemical Analyses for Defective Fuel", Proc. Specialists' Mtg. Defected Zirconium Alloy Clad Ceramic Fuel in Water Cooled Reactors, Chalk River, Canada, September 17-21, 1979, IWGFPT/6, p. 221, International Atomic Energy Agency (1980).

60. H. Zänker, "Defective Fuel Rod Detection in Operating Pressurized Water Reactors during Periods of Continuously Decreasing Fuel Rod Integrity Levels", Nucl. Technol. 86 (1989) 239.

61. D.L. Burman, "Methods for Estimating Numbers of Failed Rods from Coolant Activity Analysis", presented at the EPRI Workshop on Fuel Integrity Monitoring by Coolant Activity Analysis, Charlotte, North Carolina, May 21, 1986.

62. D.L. Burman, O.A. Correal, H.W. Wilson, H. Kunishi, L.H. Boman, "Development of a Coolant Activity Evaluation Model and Related Application Experience", Proceedings of the International Topical Meeting on LWR Fuel Performance, Avignon, France, April 21-24, 1991, p. 363.

63. C.E. Beyer, "Methodology Estimating Number of Failed Fuel Rods and Defect Size", Electric Power Research Institute, EPRI NP-6554, September 1989.

64. C.E. Beyer, "An Analytical Model for Estimating the Number and Size of Defected Fuel Rods in an Operating Reactor", Proceedings of the International Topical Meeting on LWR Fuel Performance, Avignon, France, April 21-24, 1991, p. 437.

65. "MATPRO-Version 11 (Revision 1)-A Handbook of Materials Properties for Use in the Analysis of Light Water Reactor Fuel Rod Behaviour", NUREG/CR-0497, Rev. 1 [TREE 1280 (Rev. 1)], U.S. Nuclear Regulatory Commission 1980.

66. H. Matzke, "Gas Release Mechanisms in UO_2-A Critical Review", Radiation Effects 53 (1980) 219.

67. G.T. Lawrence, "A Review of the Diffusion Coefficient of Fission-Product Rare Gases in Uranium Dioxide", J. Nucl. Mater. 71 (1978) 195.

68. M.J.F. Notley, "ELESIM: A Computer Code for Predicting the Performance of Nuclear Fuel Elements", Nucl. Technol. 44 (1979) 445.

69. J.C. Killeen and J.A. Turnbull, "An Experimental and Theoretical Treatment of the Release of ^{85}Kr from Hyperstoichiometric Uranium Dioxide", Proc. Workshop Chemical Reactivity of Oxide Fuel and Fission Product Release, Gloucestershire, England, April 7-9, 1987, p. 387, Central Electricity Generating Board.

70. J.V. Sharp, "Radiation Enhanced Diffusion", Report 6267, Atomic Energy Research Establishment (1969).

71. A.B. Lidiard, "Self-Diffusion of Uranium in UO_2", J. Nucl. Mater. 19 (1966) 106.

72. H. Matzke, "Diffusion in Ceramic Oxide Systems", Advances in Ceramics, Vol. 17, 1986, p. 1, American Ceramic Society.

73. R.A. Jackson and C.R.A. Catlow, "Trapping and Solution of Fission Xenon in UO_2; Part 1: Single Gas Atoms and Solution from Underpressurized Bubbles; and Part 2: Solution from Small Overpressurized Bubbles", J. Nucl. Mater. 127 (1985) 161-169.

74. E. Schuster, F. Garzarolli, A. Kersting, K.H. Neeb and H. Stehle, "Escape of Fission Products from Defective Fuel Rods of Light Water Reactors", Nucl. Eng. Des. 64 (1981) 81.

75. G. Kurka, A. Harrer and P. Chenebault, "Fission Product Release from a Pressurized Water Reactor Defective Fuel Rod, Effect of Thermal Cycling", Nucl. Technol. 46 (1979) 571.

76. R.J. Lutz, Jr., "Iodine Behaviour Under Transient Conditions in the Pressurized Water Reactor", WCAP-8637, Westinghouse Electric Corporation (1975).

77. N. Eickelpasch and R. Hock, "Fission Product Release After Reactor Shutdown", Proc. Symp. Experience from Operating and Fueling Nuclear Power Plants, Vienna, October 8-12, 1973, CONF-731083, IAEA-SM-178/19, STI/Pub-351, International Atomic Energy Agency.

78. R.J. Lutz and W. Chubb, "Iodine Spiking - Cause and Effect", Trans. Am. Nucl. Soc. 28 (1978) 649.

79. K.H. Neeb and E. Schuster, "Iodine Spiking in PWRs: Origin and General Behaviour", Trans. Am. Nucl. Soc. 28 (1978) 650.

80. N. Eickelpasch, R. Seepolt and R. Hock, "Iodine Release Mechanism and its Verification in Plant Operation", Trans. Am. Nucl. Soc. 28 (1978) 652.

81. R.R. Bellamy, "A Regulatory Viewpoint of Iodine Spiking During Reactor Transients", Trans. Am. Nucl. Soc. 28 (1978) 651.

82. W.N. Bishop, "Iodine Spiking", EPRI NP-4595, Electric Power Research Institute (1986).

83. W. Chubb, "On-Line Assessment of LWR Core Integrity", Trans. Am. Nucl. Soc. 56 (1988) 508.

84. P.G. Voillequé, "Measurement of Radioiodine Species in Samples of Pressurized Water Reactor Coolant", Nucl. Technol. 90 (1990) 23.

85. J.P. Adams and C.L. Atwood, "The Iodine Release Rate During a Steam Generator Tube Rupture", Nucl. Technol. 94 (1991) 361.

86. G.M. Allison and R.F.J. Robertson, "The Behaviour of Fission Products in Pressurized-Water Systems (A Review of Defect Tests on UO_2 Fuel Elements at Chalk River)", Atomic Energy of Canada Limited report AECL-1338, September 1961.

87. W. Hüttig, H. Zänker and M. Forberg, "In-Core Surveillance of Defective PWR Fuel Elements in the Case of Fuel-to-Water Contact", J. Nucl. Mater. 175 (1990) 147.

88. A.M. Manzer, "In-Core Assessment of Defective Fuel in CANDU-600 Reactors", IAEA Specialists' Meeting on Post-Irradiation Examination and Experience, Tokyo, Japan, November 26-30, 1984.

89. A.M. Manzer and N. Macici, "Fuel Defect Detection by Radioiodine Monitoring", 8th Annual Conference of the Canadian Nuclear Society, Saint John, New Brunswick, June 14-17, 1987.

90. A.M. Manzer, R.W. Sancton and N. Macici, "Canadian CANDU-600 Perspective on Fuel Integrity Performance Indicators", (AECL-9602), International Meeting on Nuclear Power Plant Operation, Chicago, Illinois, August 30 - September 3, 1987.

91. B.J. Lewis, "A Model for Calculating the I-131 Release from Defective Fuel for Steady-State and Reactor Shutdown Conditions", to be presented at the Third International Conference on CANDU Fuel, Pembroke, Canada, October 4-8, 1992.

92. A.M. Manzer, "Transport Mechanisms of Uranium Released to the Coolant from Fuel Defects", International Conference on CANDU Fuel, Chalk River, Canada, October 6-8, 1986.

93. A.M. Manzer, J.W.D. Anderson and C.W. So, "Defect Detective: An Expert System for the Detection and Evaluation of Fuel Defects in CANDU 600 Nuclear Power Reactors", 9th Annual Conference of the Canadian Nuclear Society, Winnipeg, Manitoba, June 12-15, 1988.

APPLICATION OF THE PES–PEPA EXPERT SYSTEM AT THE DUKOVANY NUCLEAR POWER PLANT

F. PAZDERA, M. VALACH
Nuclear Research Institute,
Řež

O. BÁRTA, L. NOVÁK
Chemcomex Limited,
Prague

V. ŠTECH
Nuclear Power Plant Dukovany,
Dukovany

Czechoslovakia

Abstract

The report summarizes practical experience obtained by the application of the expert system PES-PEPA developed for WWER 440, type V230/V213 nuclear power plants. As an example, it shows its ability to identify, independently on the personnel activity, the presence of a damaged FE in the core, to optimize transients with the aim to limit radioactivity releases and to assess burnup of the damaged fuel assembly.

1. Introduction

Since 1990, a simple Fuel Expert System has been in operation at all units of Dukovany NPP which enables to:

- optimize transients with the aim to minimize the probability of damage to fuel elements as a result of pellet-cladding interaction;
- identify, independently on personnel activity, the beginning of dehermetization of the FE cladding;
- quantify the number of damaged FE's and the degree of their damage by evaluating the measured values from on-line gamma spectrometer monitoring primary coolant;
- optimize transients with regard to total released radioactivity from the damaged fuel element;
- estimate probable burnup of damaged fuel elements.

The developed expert system is implemented directly to *existing Dukovany NPP information system.*

A similar expert system is at present being implemented also in the information system of the Bohunice NPP.

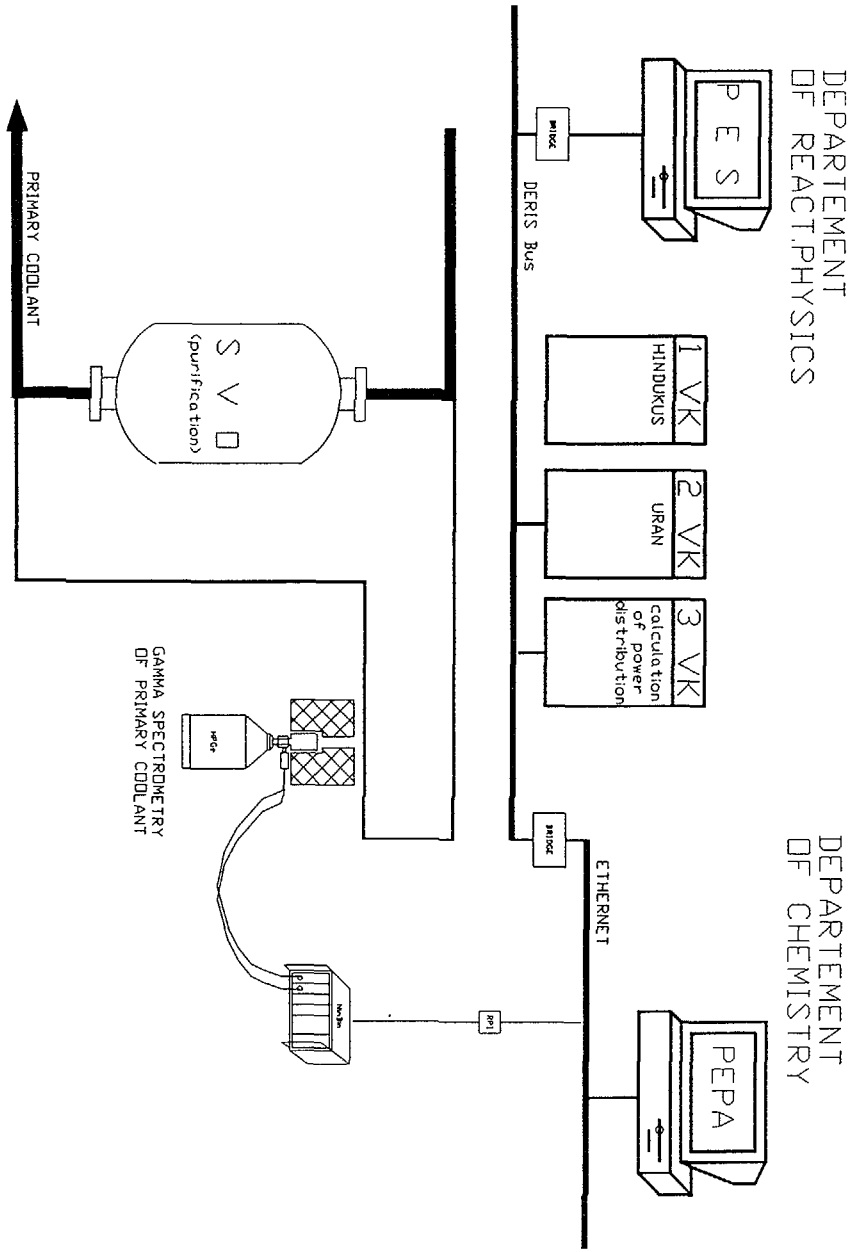

Fig. 1 - The Dukovany Fuel Expert System structure

2. The Fuel Expert System features

The expert system structure as well as its implementation in existing information systems of V230/V213 units is presented in Fig.1.

The description of the algorithm of individual modules used to build the system can be found in reports [1-4]. It should be emphasized that the Fuel Expert System comprises two independent subsystems (PES-Bu and PEPA).

The subsystem PES-Bu is installed in the so-called 3rd calculation set of the V213 unit which, besides other, performs calculation of instantaneous spatial distribution of core power during operation. These results serve as an input for real-time calculations of so-called "conditioned power" in 10 horizontal planes of the core with 365 points to each plane. At the same time PES-Bu subsystem calculates maximum allowable power jump for all these points.

The operator receives current information on:
- maximum permissible increase of the unit power;
- exceeding of permissible local power jump, if any, with its exact position within the core and some other information

On request the operator obtains:
- complete list of individual core assemblies along with the instantaneous value of the conditioned power and maximum allowable local power increase for each assembly;
- at the end of the fuel cycle: a map of fuel damage probability distribution caused by the pellet-cladding interaction (PCI).

The other subsystem, PEPA, has been installed into the Chemistry Department information system as a software supplement to the on-line gamma spectrometry of each unit's primary coolant. It provides:
- reports on the state of fuel cladding, including the number of damaged fuel elements;
- distribution of the damaged fuel elements into three groups according to the rate of fission products release (small, medium, large defects);
- the level of contamination of the primary circuit surface by fission products.

The operator can interactively enter the parameters of a planned transient, i.e. change of the unit output, coolant temperature and pressure, water parameters, as flow rate at the SVO-1 (coolant purification system). He will also receive the prediction of coolant radioactivity increase (i.e. up to 27 chosen radionuclides). Thus, system provides simple procedure for off-line optimization of the planned transients, the objective being to minimize the amount of fission product release from a damaged FE.

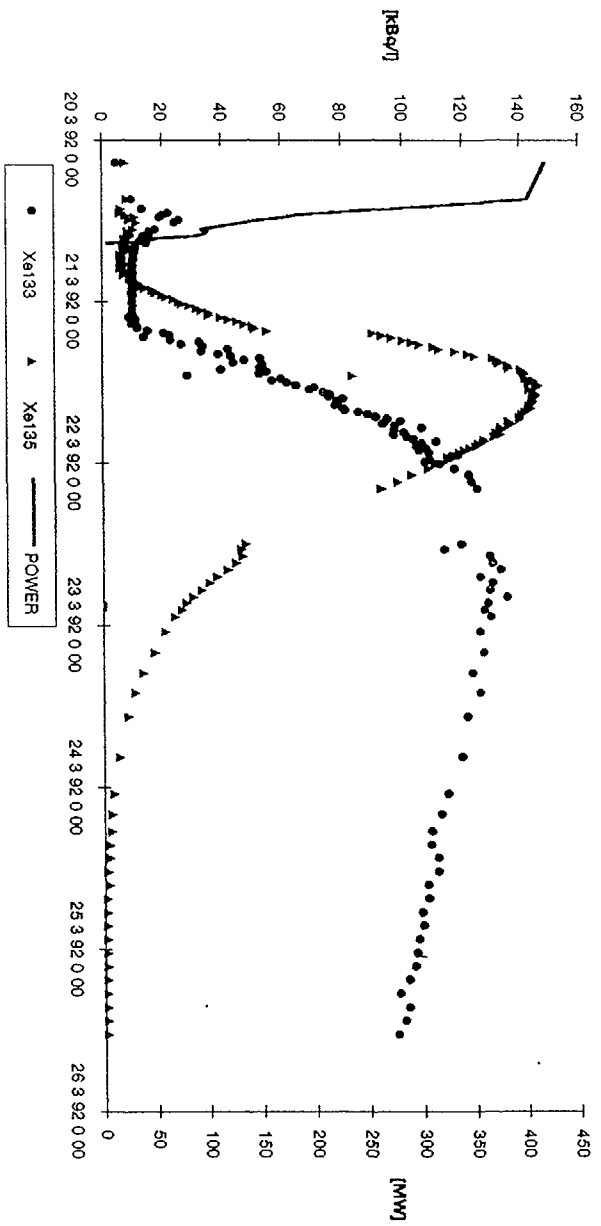

Fig. 2 - Radionuclides activity in primary coolant Dukovany NPP unit 2, period 20.3.92 - 25.3.92

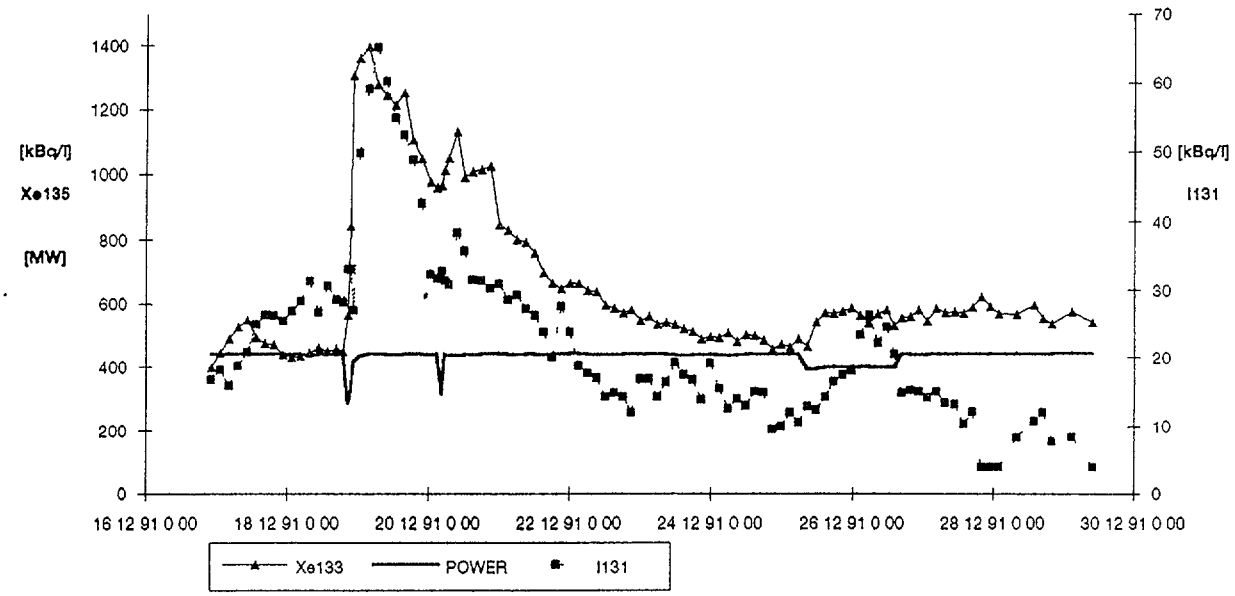

Fig. 3 - Radionuclides activity in primary coolant
Dukovany NPP unit 1, period 1.12.91 - 31.12.91

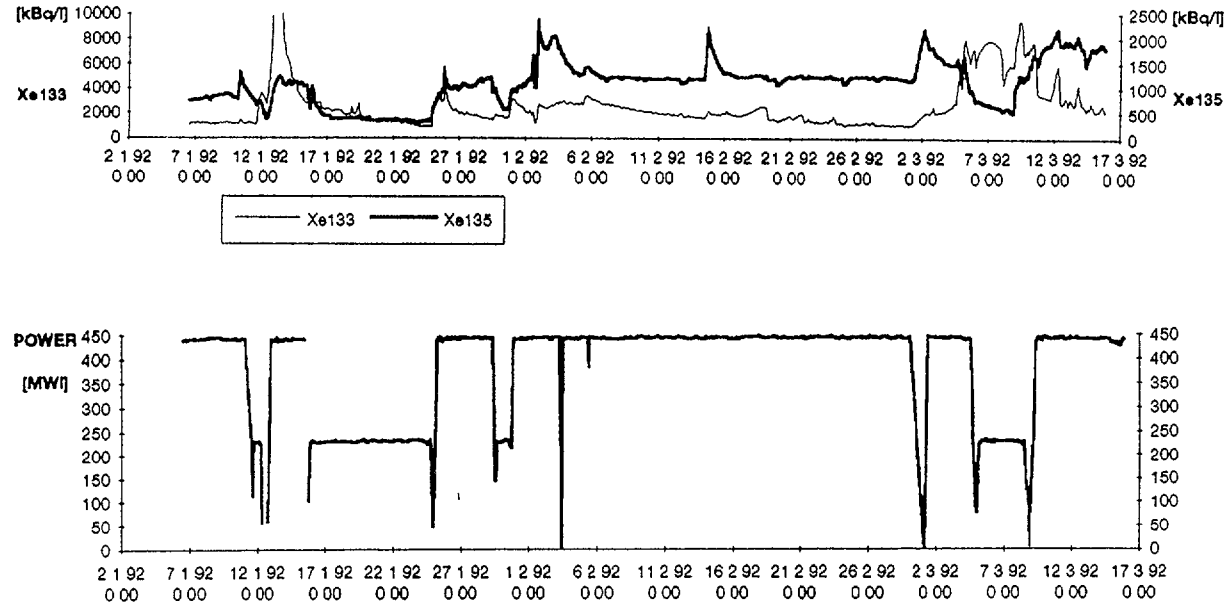

Fig. 4 - Radionuclides activity in primary coolant
Dukovany NPP unit 1, period 5.1.92 - 15.3.92

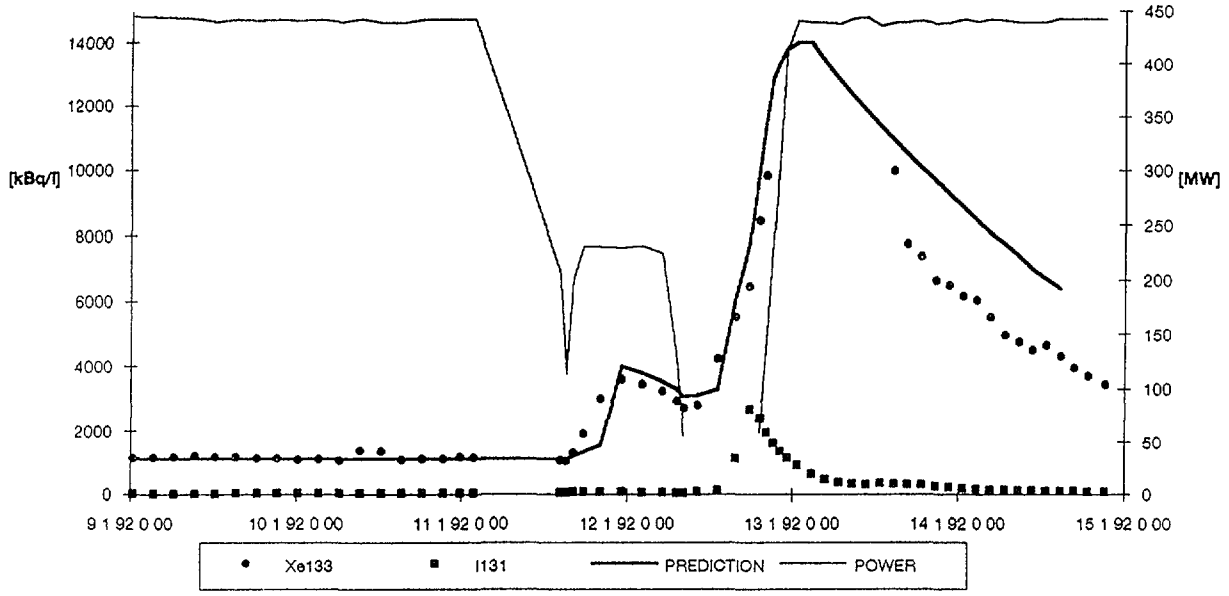

Fig. 5 - Radionuclides activity prediction in primary coolant
Dukovany NPP unit 1, transient, period 8.1.92 - 10.1.92

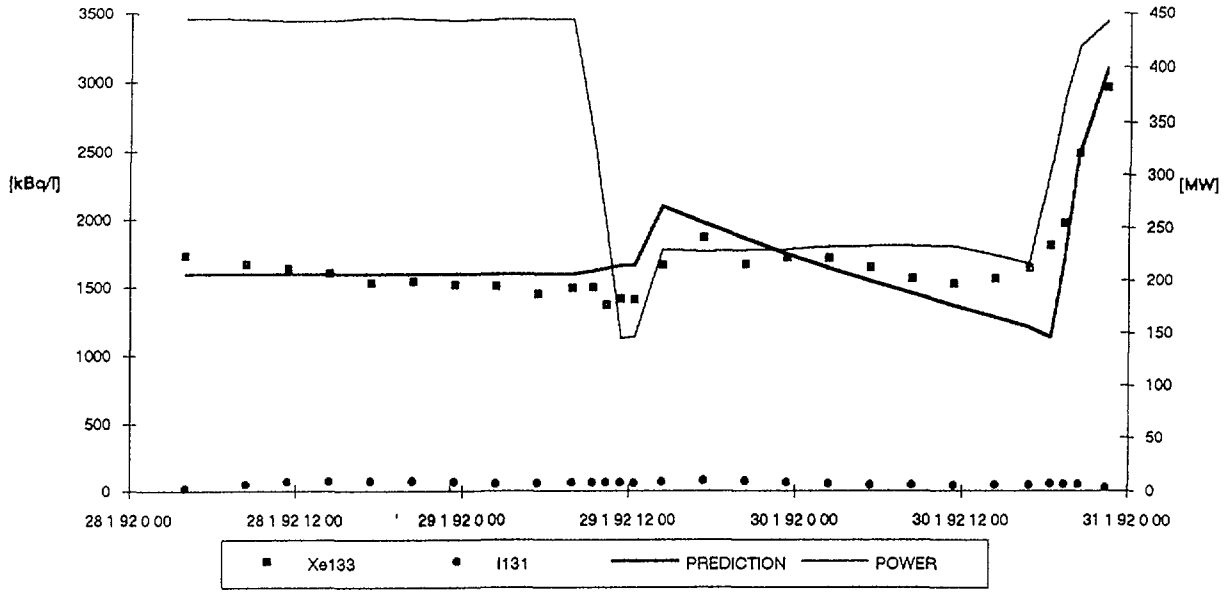

Fig. 6 - Radionuclides activity prediction in primary coolant
Dukovany NPP unit 1, transient, period 28.1.92 - 30.1 92

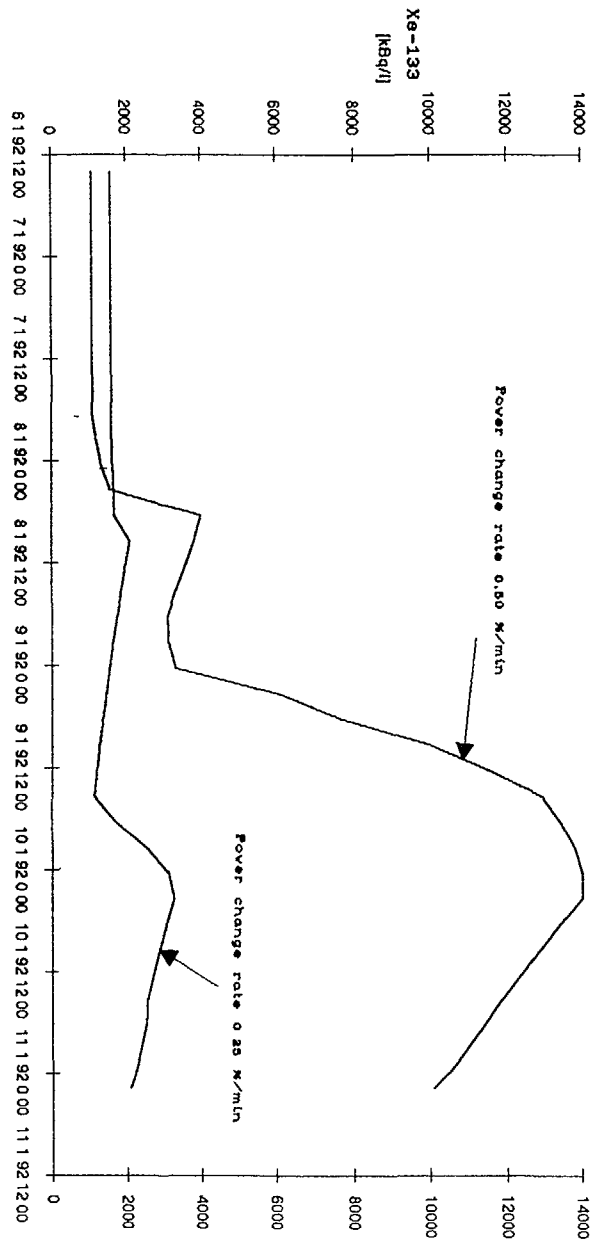

Fig. 7 - An example of possible radiation situation development optimization

3. The results of the Fuel Expert System application at the Dukovany NPP

The results for the first and second units for the period Jan 5, 1992 - March 15, 1992 are in Figures 2-7.

3.1 The damage identification

The determination of leaking a fuel element is based on two independent criteria:

a) stationary state primary coolant radiation analysis - obtained by the KGO (cladding tightness check) procedure results (i.e. after more than three days of stabilized unit performance characterized by zero output and pressure gradient)

b) identification of the spikes of Xe-133, Xe-135, I-131, I-132 at each transient

The KGO procedure is automatically activated at each finished on-line radioactivity measurement of primary coolant or on request. The calculation is performed only under the stationary state conditions. If this is the case (the transient is still in process) personnel receives a message on screen. (The analysis results are written in a file that serves as an input for possible optimization of the planned transient.)

A heuristic algorithm of spike identification is activated automatically at each transient, i.e. with each change of power output. After the power change, the frequency of on-line primary coolant activity measurement is automatically changed. Whenever the excess of radioactivity is found, spike of either Xe-133 / Xe-135 or I-131 / I-132, personnel receives a pertinent information on the monitor.

A typical example of the heuristic module application can be seen in Fig. 2. The coolant radiation during the whole fuel cycle of Dukovany NPP unit 2 has been very low, especially as to noble gases activity level. The KGO procedure has not identified a damaged FE during the whole cycle. However, at a short-time unit shutdown, by HO-1 (emergency protection), the heuristic module has identified a noble gases spike (Xe-133, Xe-135) and thus a defect present. After the transient, the noble gases activity levels have been stabilized at the previous level corresponding to the primary circuit surface contamination only, the damaged FE having no significance. These conclusions have been later confirmed during the unit 2 shutdown. Based on the results of of the spike evaluation it has been decided not to use the in-core sipping test to find the damaged assembly for the following reasons:

- the noble gases spike has been identified only due to the extreme gamma spectrometry monitor sensitivity at the SVO-1 by-pass, and its maximum has not reached the activity levels typical for a damaged FE;
- the pressure pulse at the planned unit shutdown accompanied by the pressurizer test has not cause the iodine/cesium spike. Therefore the probability of finding the damaged assembly by the in-core sipping test was considered as nearing zero.

A typical example of the KGO module application can be seen in Fig. 3. Here, under the stationary state, the noble gases activity has risen gradually from the level near the detection limit to values ≥ 10^2kBq/l and the automatically activated KGO module has reported the presence of a damaged FE. During the next transient, the damaged assembly burnup was estimated on the basis of primary coolant Cs-137 / Cs-134 activity. The value of burnup was determined 12,606 ± 860 MWd/tU. The obtained number of damaged FE and their distribution then served for the primary coolant radiation situation development prediction.

3.2 Prediction of coolant's radioactivity

Possibilities to influence the amount of radioactivity released during operation transients can be seen in Fig. 4-7.

The primary coolant radiation during first three months of this year is pictured in Fig. 4. At this part of the fuel cycle, the regime of the unit shutdown and startup was modified according to the prediction results with the aim to verify the predictive part of the Fuel Expert System.

3.3 The power regime optimization

The influence of an optimization (during power changes) on the radiation situation is demonstrated in Fig. 5-6.

The Fig. 5 shows the primary coolant and ventilation system radioactivity changes after the standard procedure of power regulation, when the power was decreased and increased with the rate of 0.5%/min.during 15 min. and then remained unchanged for 10 minutes.

The Fig. 6 shows the same picture but after extremely slow rate of power change, i.e. 0.25 % / min. during 15 min. and then unchanged for 20 minutes.

The results show:
- relatively small radioactivity release from the damaged FE to the coolant during power decrease. In accordance with the prediction, the influence of the chosen power rate change was negligible;
- significant decrease of the radioactivity release as a result of the proposed power rate change for the transient. The actual decrease was estimated as an order of magnitude, which was in compliance with the predicted value.

4. Summary

The Fuel Expert System which predicts the probability of fuel damage and minimizes the radioactivity releases into the primary coolant has been developed and verified in operation of the Dukovany unit.

The experience gained show that this expert system provides values which are reasonably close to the measured data.

The most important results is the possibility to reduce the radioactivity of gaseous releases at least by 10% by regulating unit's power, and by at least 20% when employing primary coolant treatment.

References

[1] F.Pazdera, L. Novák, O. Bárta: Fuel Rod Expert System, Report UJV-8734 M, 1989

[2] O.Bárta, J. Beňa, V.Kapišovský: Simple Checking Method of the Fuel Rods at the Core of the Power Reactor during the Irradiation, Report ÚJV-7382 M, 1985

[3] O.Bárta, J.Beňa, V.Kapišovský, I.Smieško: Evaluation of the Cladding Integrity on the basis of the Radiation Set-up in Primary Circuit of PWRs, Report ÚJV-7866 M, Oct.1986

[4] O.Bárta, V.Kapišovský, J.Beňa, R.Berndt, U.Hageman: Gamma-spectrometry for the Evaluation of Fuel Rod Integrity and for the Minimization of Fission Products Activity during Transients, Co-ordination Research Meeting on Examination and Documentation Methodology for Water Reactor Fuel, 24-27 March, 1987, Řež, Czechoslovakia

DATA ON LEAKING FUEL ASSEMBLIES IN LWRs OPERATED IN THE FORMER USSR

K.P. DUBROVIN, N.L. FATIEVA
I.V. Kurchatov Institute of Atomic Energy,
Moscow

V.P. SMIRNOV
Research Institute of Atomic Reactors,
Dimitrovgrad

Russian Federation

Abstract

The paper presents data on the quantity of leaking fuel assemblies discovered in all the operating NPP units in the USSR with VVER-440, VVER-1000, RBMK-1000 and RBMK-1500 reactors from the moment of start-up and up to the scheduled refueling in 1991. The failure rate of fuel assemblies and fuel rods manufactured in different periods of time and operated in different NPP units is considered. A brief discussion is also given of post-irradiation examinations performed to investigate the reasons for relatively poor reliability of fuel assemblies produced during period of transition from the extrusion technology of VVER-440 pellet fabrication to a technology of individual pressing. Some data on primary circuit coolant activities at VVER reactor NPP units is given.

The results presented in the paper indicate a satisfactory reliability achieved with modern VVER-440 and VVER-1000 fuel.

1. Introduction

The researchers at Kurchatov Institute hot cell have been collecting and analyzing information on the performance of fuel assemblies operated at all NPP units in the USSR with VVER-1000, VVER-440, RBMK-1500 and RBMK-1000 reactors. This information includes some data on the fabrication and operation of charged, discharged and leaking assemblies (assembly identification number, assembly type, enrichment, core cell number in which the assembly was operated, fuel burnup etc.), data on radiological situation at the units and other parametrs which affect the fuel performance.

The paper presents a brief review of results of post-irradiation examination aimed at elucidation of the reasons for poor performance of the fuel rods fabricated in 1972-76. The data on the relative number of leaking fuel assemblies produced in different periods of time and operated in all types of reactors is discussed and some information about primary circuit coolant activities at VVER units is given.

The start-up dates for all NPP units with water cooled reactors, VVER and RBMK, with electrical power from 440 to 1500 MW are listed in Table 1. The performance data under consideration date from the unit start-up and up to scheduled refueling of 1991 for VVER reactors and up to the end of 1991 for RBMK reactors.

2. Reasons of poor performance of VVER-440 fuel rods produced in 1972-76

The data of Table 2 shows that reliability of VVER-440 fuel assemblies manufactured in 1972-76 was poor. Failure rate of fuel assemblies produced in that period reached 6%. This was caused by a change in the pellet fabrication technology.

Table 1

Date of starting of the power units considered

Ser No	NPP name	Unit No	Start date	Ser No	NPP name	Unit No	Start date
	VVER 1000			23	Rovno	I	12 80
				24		II	12 81
1	Novovoronezh	V	05 80				
				25	Armenian *	I	12 76
2	South Ukrainian	I	12 82	26		II	01 80
3		II	01 85				
4		III	09 89		RBMK 1500		
5	Kalinin	I	05 84	27	Ignalina	I	12 83
6		II	12 86	28		II	08 87
7	Zaporozhje	I	12 84		RBMK 1000		
8		II	06 85				
9		III	12 86	29	Leningrad	I	12 73
10		IV	12 87	30		II	07 75
11		V	08 89	31		III	12 79
				32		IV	02 81
12	Balakovo	I	12 85				
13		II	10 87	33	Kursk	I	12 76
14		III	12 88	34		II	01 79
				35		III	10 83
15	Rovno	III	12 86	36		IV	12 85
16	Khmelnitskij	I	12 87	37	Chernobyl *	I	09 77
				38		II	12 78
	VVER 440			39		III	12 81
				40		IV	12 83
17	Novovoronezh	III	12 71				
18		IV	12 72	41	Smolensk	I	12 82
				42		II	05 85
19	Kola	I	06 73	43		III	01 90
20		II	11 74				
21		III	03 81				
22		IV	10 84				

* Armenian NPP was stoped in 1989 Data collection about Chernobyl NPP was ceased in 1986

Table 2

Number of charged and leaking VVER-440 and VVER-1000 fuel assemblies

Year of assembly production	VVER 440 Charged assemblies	VVER 440 Leaking Assembl	VVER 440 Leaking %	VVER 440 Prematurely discharged assembl	VVER 1000 Charged assemblies	VVER 1000 Leaking Assembl	VVER 1000 Leaking %	VVER 1000 Prematurely discharged assembl
1969	177	2	1,13					
1970	203	2	0,99					
1971	331	2	0,60	1				
1972	524	30	5,73	24				
1973	273	10	3,66	2				
1974	969	59	5,33	3				
1975	536	12	2 24					
1976	561	14	2,50					
1977	650	6	0,92					
1978	490	10	2,04		151	7	4,64	
1979	869	14	1,61	1				
1980	1483	17	1,14	1	208	7	3,36	1
1981	756	6	0,79		130	2	1,54	
1982	770	9	1,17		313	19	6,07	
1983	1204	20	1,66	8	383	7	1,83	
1984	957	12	1,25	2	504	17	3,37	
1985	892	0	0,00		705	23	3,26	1
1986	1097	4	0,36	2	1053	35	3,32	5
1987	1262	8	0,63	3	1102	27	2,45	
1988	678	10	1,48	4	711	11	1,55	2
1989	823	0	0,00		604	1	0,17	
1990	311	0	0,00		58	0	0,00	
Total	15816	247	1,56	51				
Total from 1977	12242	116	0,94	21	5922	156	2,63	9
Fuel rod failure rate								
	0,007%				0,008%			

Historically it so happened that up to 1972 fuel for VVER reactors was produced in the USSR according to a unique procedure which differed from that applied all over the world According to this procedure small amounts of oxides of metals (other than uranium) and plasticizer were added to uranium dioxide powder and the resulting mixture was subjected to extrusion forming a long rod having central hole The rod was then cut into extruded pellets about 30 mm long Then pellets were sintered and cylindrical surface was polished so that pellet external and internal diameter were 7 7 mm and 1 5 mm, respectively The fuel prepared in this way had high density and operated successfully in VVER 440 reactors

The high reliability of assemblies with extruded fuel pellets is highlighted by the experience of operation of two units of Loviisa NPP. Up until 1987 they used only extruded fuel manufactured in USSR. To this day the Lo-1 unit has been in operation for 14 complete fuel cycles, while Lo-2 unit - for 11 fuel cycles. The total number of leaking assemblies for this period was 16, which corresponds to fuel rod failure rate of less then 0.004%.

In 1972 an technology was developed for producing pellets about 12 mm long by means of individual pressing (without other oxide additions). In 1973 in the course of the scheduled refueling 69 and 100 experimental assemblies with pressed pellets and 75 and 26 assemblies with extruded pellets were loaded at Novovoronezh NPP (NVNPP), Units 2 and 3, respectively.

Twenty days into the fuel cycles at NVNPP-2 and 3 the coolant activities increased by 10 times compared to those at the end of the previous fuel cycles. During refueling in 1974 24 and 19 leaking assemblies with the pressed pellets were discharged from NVNPP-2 and 3, respectively. All assemblies with extruded pellets were found to be leak-tight. In 1975 and 1976 13 and 11 leaking assemblies with pressed pellets were discharged additionally from these units. Thus, after three years of operation about 40% of experimental assemblies with pressed pellets failed.

Two leaking assemblies discharged from NVNPP-2 and 3 in 1974 were investigated at NVNPP and at the Kurchatov Institute. In this assemblies were found 19 and 1 leaking fuel rods respectively. Leaks were primarily detected in the regions of welded joints (13 fuel rods), although through holes and transverse cracks were also found. In all cases claddings were heavily hydrided in the areas of leaks.

Metallografic studies of welded joints of the 136 leak-tight fuel rods of these assemblies revealed 20 rods with regions of local internal hydriding of claddings and plugs of various intensity. Fig.1 shows the area of heavy hydriding of the cladding and the plug of leak-tight fuel rod.

The fuel rods of assemblies analyzed differed in the weights of the fuel stacks and fluorine contents in fuel batches. It was found that all failed fuel rods and leak-tight fuel rods where local hydriding of the claddings was observed differed from the remaining of the fuel rods in low weights of the fuel stacks (1050-1063 g) and relatively high fluorine contents (up to 0.02 wt %). The mass of the fuel stack and the maximum fluorine contents as stipulated by the specifications in force at that time was 1050-1100 g and 0.02 wt %, respectively.

The density of all pressed pellets extracted from four unirradiated fuel rods contained in the first experimental batches was determined by the method of hydrostatic weighing. Table 3 illustrates the measurement results. It is seen that fuel stack weight correlates well with the average density of the pellets loaded in the rod. The average pellet density in "light" fuel rods (1054-1062 g) was about 10.3 g/cub.cm, while that in the relatively "heavy" ones (1093 g) was 10.5 g/cub.cm. From 33 to 46 % of pellets in light fuel rods had density lower than 10.2 g/cub.cm. Two rods were loaded with pellets of two or three batches having high and low density. The density of some

Fig.1 The area of heavy hydriding of cladding (right) and plug (left) in leak-tight fuel rod of the assembly discharged from Unit II of Novovoronezh NPP

Table 3

Density distribution of pressed pellets extracted from the fuel rods of different weights

Density range, g/cub.cm	Pellet number in fuel stack of given weight, g			
	1093	1062	1056	1054
10.71 - 10.80	1			
10.61 - 10.70	4		7	
10.51 - 10.60	50		51	39
10.41 - 10.50	109	12	26	44
10.31 - 10.40	27	62	4	19
10.21 - 10.30	3	57	5	17
10.11 - 10.20	5	51	33	5
10.01 - 10.10	1	12	9	8
9.91 - 10.00		4	11	18
9.81 - 9.90		2	16	13
9.71 - 9.80			10	5
9.61 - 9.70				7
9.51 - 9.60				2
Total	200	200	172	177
Average density, g/cub.cm	10.50	10.30	10.32	10.32

pellets in one of this rods was only 9.6 g/cub.cm, while according to specifications it should not have been less than 10.2 g/cub.cm. Experiments on moisture absorption by pellets of various densities showed that the amount of moisture sorbed from even relatively dry air depends essentially on fuel pellet density and increases sharply with the decrease of density below 10.2 g/cub.cm.

From the whole body of results considered it was concluded that intense failure of the first experimental batches of assemblies with pressed pellets was caused by local internal hydriding of the claddings under the action of moisture sorbed by low-density (lower than 10.2 g/cub.cm) pellets from the air in manufacturing of the fuel rods.

This conclusion resulted in a revision of the specifications for pressed pellet and the manufacturing procedure. The revision concerned, in particular, the requirements to density, weight of fuel stacks, moisture and fluorine contents in the fuel, methods of density control, pellet charging, defluorination of uranium dioxide power and also requirements to many other parameters and manufacturing processes affecting fuel rod performance.

3. Quantitative data on leaking VVER-440 and VVER-1000 fuel assemblies

The data on the quantity of leaking VVER-440 and VVER-1000 fuel assemblies is listed in Table 2. The reasons for the increased VVER-440 fuel rod failure rate were discussed in the previous chapter.

Table 2 shows that VVER-440 fuel assemblies produced in 1977 and later provided a satisfactory level of reliability. On the average, number of leaking assemblies was less than 1% and the number of assemblies that had to be discharged prematurely - less than 0.2%.

Table 4 presents data on leaking fuel assemblies discovered at different VVER-440 units. The reliability is shown to be the lowest for Unit II Kola NPP as well as Units III and IV Novovoronezh NPP (the assembly failure rate of up to 2%). At other units the reliability of fuel assemblies was quite satisfactory. In 8 years of Unit IV Kola NPP operation only two fuel assemblies leaked (a rod failure rate of less than 0.002%).

Table 4

Number of leaking assemblies operated at different VVER-440 units

Year of assembly production	NPP name and unit number										Total
	Novovoronezh		Kola				Rovno		Armenian		
	3	4	1	2	3	4	1	2	1	2	
1977				2					2	2	6
1978	1	5	1	3							10
1979	2	2		2			5			3	14
1980	3	4		1	3		3	1	2		17
1981	1	1	1						3		6
1982	4									5	9
1983	2	1		12		2	1	1	1		20
1984		3	3	4			1			1	12
1985											
1986	1		2	1							4
1987	2			6							8
1988		8		2							10
1989											
1990											
Total	16	24	7	33	3	2	10	2	8	11	116
%	1,19	1,67	0,47	2,13	,25	,20	,75	,15	1,03	1,01	

Out of the 116 leaking assemblies 18 were SUZ assemblies (the assemblies of control and protection system). Considering that VVER-440 reactor cores contain 37 or 73 SUZ assemblies it is possible to conclude that SUZ assemblies have approximately the same reliability as working assemblies.

The employees of Loviisa NPP in Finland found that 6 assemblies out of 10 assemblies developed leaks in core cells

located next to the cells of automatic control system. With our fuel 19 assemblies out of 116 leaking assemblies were operated in such cells. There are 42 such core cells, therefor going on assumption of equal probability of leaks from all assemblies only about 14 (not 19) out of 116 leaking assemblies should have been located next to the cells of automatic control system. Thus in our case we also see a tendency of accelerated failure of fuel assemblies operated next to the cells of automatic control system.

The data in Table 2 on leaking VVER-1000 fuel assemblies indicate a satisfactory reliability of VVER-1000 fuel. The average fuel rod-failure rate is 0.008%. The worst assembly reliability was observed at Unit V of Novovoronezh NPP, Units I and II of Kalinin NPP and Unit I Zaporozhje NPP (Table 5). The fuel rod failure rate reached up to 0.02 %. With the rest of units it was substantially lower than 0.01%. In the 6 years of Unit I Balakovo NPP operation only two assemblies developed leaks (the fuel rod failure rate less than 0.002%).

4. Data on number of leaking RBMK-1000 and RBMK-1500 fuel assemblies

Table 6 lists data on the number of RBMK-1000 and RBMK-1500 assemblies charged and the number of leaking assemblies manufactured in different periods of time. It is apparent that the failure rate of RBMK fuel rods is about an order of magnitude higher than for VVER fuel rods. More than 3000 leaking fuel assembly were discharged from all RBMK-1000 reactors before reaching the project fuel burnup.

Table 5

Number of leaking assemblies operated at different VVER-1000 units

Ser No	NPP name	Unit No	Date of start	Charged assemblies	Leaking assembl.	Leaking %
1	Novovoronezh	V	05.80	639	27	4,22
2	South-Ukrainian	I	12.82	575	18	3,13
3		II	01.85	368	9	2,44
4		III	09.89	224	2	0,89
5	Kalinin	I	05.84	507	20	3,94
6		II	12.86	363	23	6,34
7	Zaporozhje	I	12.84	411	15	3,65
8		II	06.85	381	6	1,57
9		III	12.86	333	9	2,70
10		IV	12.87	320	3	0,93
11		V	08.89	217	0	0,00
12	Balakovo	I	12.85	380	2	0,52
13		II	10.87	297	7	2,36
14		III	12.88	230	1	0,43
15	Rovno	III	12.86	381	12	3,15
16	Khmelnitskij	I	12.87	296	2	0,67
Total				5922	156	2,63

The data in Table 7 shows that the failure rate depends strongly on the operating conditions. The worst performance was shown by Chernobyl NPP assemblies. The number of leaking fuel assemblies at Unit I of Chernobyl NPP was in excess of 10%. The assembly failure rate at Leningrad NPP was also high and was on average for the four units about 5%. The fuel assemblies of Unit I of Kursk NPP had a similar failure rate. The rest of the units of this NPP and at all units of Smolensk NPP the relative quantity of leaking assemblies was 2-5 times less.

Table 6

Number of charged and leaking RBMK-1000 and RBMK-1500 fuel assemblies

Year of assembly production	RBMK-1000			RBMK-1500		
	Charged assemblies	Leaking		Charged assemblies	Leaking	
		Assembl.	%		Assembl.	%
1973	1628	116	7,13			
1974	1678	34	2,03			
1975	3024	227	7,51			
1976	2617	116	4,43			
1977	2857	249	8,72			
1978	3706	410	11,06			
1979	4713	338	7,17			
1980	5419	354	6,53			
1981	5327	240	4,50			
1982	6324	237	3,75			
1983	4227	148	3,50	1636	195	11,92
1984	4355	120	2,76	1293	60	4,64
1985	4531	140	3,09	232	2	0,86
1986	3462	110	3,18	1999	21	1,05
1987	5500	95	1,73	366	5	1,37
1988	5471	88	1,61	973	4	0,41
1989	4426	34	0,77	1312	1	0,08
1990	2949	3	0,10	1204	1	0,08
1991	1362	0	0,00	306	0	0,00
Всего	73576	3059	4,16	9321	289	3,10
Fuel rod failure rate						
	0,11%			0,09%		

The assembly failure rate at Unit I of Ignalina NPP operating a RBMK-1500 reactor was 4.84% as of the end of 1991. A vary large number of assemblies failed during the start-up period as the Unit was taken up to its nominal electrical power of 1500 MW and operated at this power. After about 3 years of operation at nominal level the power of Unit I was reduced and now each unit of Ignalina NPP is operated at power not more than 1300 MW.

Table 7

Number of charged and leaking assemblies operated at different RBMK-1000 and RBMK-1500 units

RBMK-1000 units

Number of assembl.	NPP name and unit number														
	Leningrad				Kursk				Chernobyl*				Smolensk		
	1	2	3	4	1	2	3	4	1	2	3	4	1	2	3
Charged	8084	8114	6139	5744	7839	6666	4455	3709	4345	3912	2358	1587	4768	3990	1866
Leaking	415	333	316	273	383	193	48	54	468	338	106	11	71	46	4
%	5,13	4,10	5,15	4,75	4,89	2,90	1,08	1,46	10,8	8,64	4,49	0,69	1,49	1,15	0,21
Date of unit starting	12. 73	07. 75	12. 79	02. 81	12. 76	01. 79	10. 83	12. 85	09. 77	12. 78	12. 81	12. 83	12. 82	05. 85	01. 90

RBMK-1500 units

Unit	Charged assemblies	Leaking assemblies	%	Date of unit starting
Ignalina-1	5435	263	4,84	12.83
Ignalina-2	3886	26	0,67	08.87

*Data on Chernobyl NPP are given as of the end of 1985 and on the other units - as of the end of 1991.

On the other hand 4 years of operating experience with Unit II of Ignalina NPP indicate that the performance of RBMK fuel rods may be practically the same as the performance of VVER fuel. The fuel rod failure rate at this unit is less than 0.02%.

5. VVER reactor coolant activity

The coolant activity is to be below the allowable level and for most of the units was in the range of 0.01-1.0 mCi/l.

The reasons for separate cases of a more adverse radiological situation at reactor units due to leaks from a relatively large number of fuel assemblies are probably treated in other presentations. Presently we should note only that the coolant activity increase at Unit IV of Novovoronezh NPP during 13th fuel cycle (1985-86) by two order of magnitude was due to an experiment with "two-storey" assemblies when 33 fuel assemblies developed leaks.

6. Conclusions

The data presented above indicate a satisfactory reliability of the modern VVER fuel and that the RBMK fuel rod failure rate should be reduced, particularly through optimization of the operating conditions.

FAILED FUEL MONITORING AT NUCLEAR POWER PLANTS WITH RBMK REACTORS: OPERATING PARAMETERS, REQUIREMENTS AND DECISION MAKING CRITERIA

I.V. ZHUKOV
Research and Design Institute of Power Engineering,
Moscow, Russian Federation

Abstract

The procedure for estimating the number of failed fuel rods in the core and the prediction of their discharge efficiency during operation is presented The procedure is based on the FFM data base and the I-131 and Xe-133 coolant activity

The observance of the principles and codes of radiation safety is one of the main requirements imposed on all NPPs design and operation. Introduction of the safe NPP operation criteria results from this requirement. Among these criteria are the operational limit of the fuel element failures under normal operating conditions, dose limits for exposure of NPP personnel and population, maximum permissible release of radionuclides into the atmosphere, annual permissible disposal of radionuclides with liquid wastes,etc.

The operational limit of the fuel elements damage equals to 0,2% for gas-permeable elements and 0,02% for those with the fuel-coolant interaction of the total fuel elements loaded into the reactor, is specified for NPP with RBMK reactor.

The value of the above limit is determined by the efficiency of the system for the NPP process medium decontamination from radionuclides of fission products (FP) that released from the unsealed fuel elements to the coolant.

As a matter of fact, regulation of the number of unsealed fuel elements in the reactor results in regulated levels of some FP activity in the primary coolant using the different models of FP release from the unsealed fuel elements and their build-up in the primary circuit.

The reference operational level of I-131 activity in water of the primary circuit is prescribed proceeding from the fact that the operational limit of the unsealed fuel elements should not be exceeded, i.e. it should be no more than 2*10-6 Ci/kg at the steady-state reactor power. In this case radioactive noble gas (RNG) and iodine nuclide releases into the atmosphere should be no more than 500 Ci/(day x 1000 MW(e)) and 0,01 Ci/(day x 1000 MW(e)), respectively

The strategy of indentification and discharge of the fuel assemblies (FA) with the unsealed fuel elements takes into account the design features of the PBMK reactor as unscheduled discharge of the unsealed fuel elements at NPP with the channel-type reactors can be implemented at operating reactor without reduction in its power.

In this connection under NPP operation there arises the problem of identification and confining the FAs with the unsealed fuel elements in the RBMK reactor . The problem concerning discharge of the identified FAs is solved depending on radiation state of the reactor core that is determined as a totality of FAs with unfailed and unsealed fuel elements with the different degree of seal failure. In this case the core state can vary from highly good state when there are no unsealed fuel elements in the reactor, to unsatisfactory one from the viewpoint of radiation safety.

Monitoring of radiation state of the reactor core is carried out as follows:

- continuous monitoring of gas-aerosol release rate into the atmosphere;
- - continuous monitoring of RNG activity in drum-separator steam;
- periodic measurements of reference FP activities in the primary coolant.

Qualitative classification of the unsealed and failed fuel elements according to the degree of cladding seal failure includes four classes.

- fuel elements with direct fuel-coolant interaction;
- fuel elements with developed gas-permeability;
- fuel elements with the initial phase of gas-permeability;
- fuel elements with microflaws like a pin-hole.

The probability of reliable identification of FAs with the unsealed and failed fuel elements primarily depends on two parameters, i.e. the sensitivity of the channel-by-channel failed fuel monitoring (FFM) system and degree of fuel element cladding seal failure. As the sensitivity of any failed fuel monitoring system has an own threshold beyond which the system does not able to detect the unsealed fuel elements, there are always several non-identified FAs with the unsealed fuel elements in the reactor. The sensitivity threshold of the failed fuel monitoring system corresponds to minimum rate of the fission product release from the unsealed fuel elements to the coolant that can be reliably fixed in the real conditions and generally specified by the design and physical principles of the system operation.

Diagnostics of FAs with the unsealed fuel elements is carried out using the channel-by-channel failed fuel monitoring system that provides periodic without-sampling measurement of collimated γ- radiation from the steam-water pipelines in the section that is upstream of cutting-in into the drum-separator.

In this case a valid signal of the failed fuel monitoring system, i.e. γ- radiation intensity, caused by the fission products released from the unsealed fuel elements, should be detected in highly large background caused by short-lived activated isotope 16N with half-life period of about 7s and energy of γ-quanta of 6.13 MeV.

The mathematic model of FFM system signals generation which are actuated from the fuel channel steam-water line containing FAs with leak-tight fuel elements, was used to minimize the FFM system signal fluctuations. With such a model the FA with unsealed fuel elements is detected by the statistically significant deviation of the measured signal of the FFM system from the calculated one according to the model.

As a result of the statistic analysis of the FFM system signals being actuated from the steam-water line of the same technological row, by applying the statistic criterion derived on the basis of the concept of the most normalized selective deviation,

$$\delta_{max} = \frac{\Delta_{max} - \bar{\Delta}}{\sigma\sqrt{\frac{K-1}{K}}} \qquad (1)$$

the FA was classified according to the possible states

$\delta_i \leq 2\sigma$ - FA with unfailed fuel elements

$2\sigma < \delta_i < 3\sigma$ - FA with fuel elements which are suspected to be unsealed;

$\delta_i \geq 3\sigma$ - FA with unsealed fuel elements;

$\delta_i \geq 4\sigma$ - FA with fuel elements having the claddings with large flaws.

The FE, FA and core failure concepts are the necessary components to ensure the safe and cost-effective operation of the nuclear power plant The failure definitions are as follows:

- FE failure - impossibility of fuel element operation due to the risk of primary circuit contamination with fuel, as a result of direct interaction of the coolant with fuel;

- FA failure - impossibility of FA operation with failed fuel element;

- reactor core failure - impossibility of the reactor core operation due to:

a) the excess in allowed rate of gas and aerosol releases and/or in values of the allowed activity of fission products in the coolant at steady-state power reactor operation, when the clean-up systems and facilities are operated under the design-basis conditions;

b) the presence of failed FAs in the core and the impossibility of their timely unloading from the operating reactor due to the technical reasons.

The main failure cause of the fuel element and fuel assembly, as well, is loss of tightness in its cladding, i.e. the formation of flaw. In the reactor engineering practice by "flaw" one usually understands the FE cladding break, when the fuel interacts directly with the coolant

Based on the above definition of failure the fuel elements with microflaws and gas permeable ones cannot be considered to be failed.

Note, that the leak-tight fuel elements are not failed in the failed fuel assembly and can be reused. The mechanisms of radioactive fission products releases from the failed fuel elements and of their accumulation in the coolant were investigated with actual physical and process parameters of fuel elements, core and primary circuit to predict the effect of operation and unscheduled unloading of FA with failed fuel elements on the radiation state of the RBMK NPP.

For this purpose, the sampling devices allowing to control the fission products release into the coolant from the failed and unsealed fuel elements specially loaded into the reactor, were installed at the Chernobyl NPP Unit 2.

The analysis of the results of the experimental investigations has shown that:

- the process of ingress of the RNG and iodine nuclides into the coolant from the failed fuel elements was described by the diffusion model irrespective of the absolute values of the release rates The parameters of the model include the FA power and the effective size of the flaw in the fuel element cladding,

- for the gas permeable fuel elements and those with the direct interaction between the fuel and coolant at average linear power over the range of 140-220 W/cm, the release rate parameter $(R/B)_\lambda$ for RNG nuclides does not depend on fuel element power within the experiment error range and equals to $2.8 \cdot 10^{-8}\ s^{-1}$ and $2.0 \cdot 10^{-7}\ s^{-1}$, respectively;

- the parameter of the iodine release rate $(R/B)_\lambda$ is on the average, by an order of magnitude lesser than for the radioactive noble gases and is proportional to the linear power of the fuel element.

The comparative analysis between the FFM system data and the results of the simulation of fission products release into the coolant from the failed fuel elements shows that:

- the physical and design features of the system for channel-by-channel monitoring of the failed fuel at the NPP with the RBMK reactor permit to detect only those failed fuel elements from which the fission products with half-life period of 10^{3} s or less can release;

- the contibution of short-lived fission products into the total rate of FP release into the coolant is predominant when the effective equivalent flaw area in the FE cladding is 0.01 cm^2 or more;

- the threshold of sensitivity of the channel-by-channel failed fuel monitoring system at average linear power of 160-240 W/cm is equal to 1.0 cm^2 of the effective bare surface of the fuel.

The classification of quality assessments of fuel elements cladding loss-of-tightness degree has received the supplementary quantitative characteristics:

- the FA, which FFM signal $\delta \geq 4.0\sigma$, involves the seal failure of the direct fuel-coolant interaction type, corresponding to the equivalent effective flaw area in the fuel element cladding of ~10 cm^2; the contribution of a fuel element having such a flaw to I-131 activity in the coolant and to Xe-133 discharge through the stack (at delay time of 15 hours) amounts to ~ 10^{-6} Ci/kg and ~ 20 Ci /day, respectively;

- the FA, which FFM signal $3.0\sigma < \delta < 4.0\sigma$ involves the seal failure of the developed gas-permeable type, corresponding to the equivalent effective flaw area in the fuel element cladding of ~ 1.0 cm^2. The contribution of a fuel element having such a flaw to I-137 activity in the coolant and to Xe-133 discharge through the stack amounts to ~ 10^{-7} Ci/kg and ~ 6 Ci/day, respectively;

- the FA, which FFM signal can not be recorded due to high noise, may have:

a) the loss-of-tighness of the initial stage of gas-permeable type, correspoding to the effective equivalent flaw area in the fuel element cladding of ~ 0,1 cm^2; the contribution of a fuel element having such a flaw to I-131 activity in the coolant and to Xe-133 discharge through the stack amounts to ~ $2.5 \cdot 10^{-8}$ Ci/kg and ~ 2 Ci/day,or;

b) the pin-hole type loss-of-tighness, corresponding to the effective equivalent flaw area in the fuel cladding of 0,01. cm^2; the contribution of a fuel element having such a flaw to I-131 activity in the coolant is practically absent, and to Xe-133 discharge through the stack amounts to 0.5-1.0 Ci/day.

The experimental data obtained under conditions of apriori uncertainty of the failed fuel elements number in the FA and a flaw location along the core height have shown that:

- unloading the FAs with fuel elements having a direct fuel-coolant interaction has resulted in decrease in I-131 activity in the coolant and Xe-133 discharge into the atmosphere by $(0.4 - 4.0)10^{-6}$ Ci/kg and 20-25 Ci/day, respectively;

- unloading the FAs with developed unsealed gas permeability of fuel elements claddings has resulted in decrease in I-131 activity in the coolant and Xe-133 discharge into the atmosphere by $(0.7\text{-}5.0)*10^{-7}$ Ci/kg and 4-6 Ci/day, respectively;

- unloading the FAs with the initial stage of fuel elements cladding gas permeability has resulted in decrease in I-131 activity in the coolant and Xe-133 discharge into the atmosphere by $(1.0\text{-}3.2)10^{-6}$ Ci/kg and 1 Ci/day, respectively.

A good agreement of experimental data and model calculations has given an objective possibility to develop an algorithm for the RBMK core radiation state control and its implementation in the form of the regulations.

The reactor core radiation state control is a procedure based on:

- reactor core radiation state monitoring;
- diagnostics of the FAs with failed fuel elements;

- prediction and arranging the contribution values of the FAs with failed fuel elements to the reactor radiation state;

- discharging the FAs with maximum unsealed and failed fuel elements, i.e. those fuel elements which are producing the release of FPs and/or fuel into the coolant.

The FAs are subjected to the unscheduled discharge from the reactor according to following succession:

- failed fuel elements with direct fuel-coolant interaction;

- failed fuel elements with developed gas-permeability;

- failed fuel elements with the initial stage of gas permeability.

The duration of unloading for the FAs having a direct fuel-coolant interaction does not exceed 5 days regardless the reactor core radiation state to prevent the primary circuit contamination with fuel. The necessity of unscheduled discharge of FAs with gas-permeable fuel elements is determined in each specific case.

The leak-tightness of fuel elements claddings for each disharged FA is checked by the "sipping" method in the cooling pool case. The FAs are identified as the failed ones if in the case water after three days sipping the specific activities of the following nuclides are exceeded:

I-131 - 10^{-3} Ci/kg

Cs-137 - 10^{-4} Ci/kg

Np-239 - 10^{-5} Ci/kg

A repeated loading of failed FAs into the reactor is prohibited.

The performed investigations of laws for the FPs release out of the failed fuel elements claddings into the coolant, the study of efficiency of unloading for the FAs with failed fuel elements from the reactor core, the estimation of the quantitative interaction between the signals of the channel-by-channel FFM system and the rate of FPs release into the coolant, have permitted to develop a method for quantitative assessment of failed fuel elements number in the core during reactor power operation.

The assessment algorithm consists in:

- assessment of the number of fuel elements with direct fuel-coolant interaction and fuel elements with developed gas permeability by data of the channel-by-channel FFM system;

- assessment of the number of fuel elements with initial stage of gas permeability by the I-131 value;

- assessment of the number of fuel elements with microdefects by the Xe-133 activity value in the drum-separator steam.

Next page(s) left blank

CAUSES AND MECHANISMS FOR FUEL FAILURE AND DAMAGE

(Session III)

Chairmen

V.D. ONUFRIEV
Russian Federation

A.A. STRASSER
Unites States of America

OVERVIEW OF DEFECT MECHANISMS IN CANDU FUEL

T.J. CARTER
Chalk River Laboratories,
AECL Research,
Chalk River, Ontario

A.M. MANZER
AECL CANDU,
Mississauga, Ontario

Canada

Abstract

The CANDU -PHW reactor uses horizontal pressure tubes to contain the fuel and primary coolant. An 800 MW reactor contains more than 6 000 fuel bundles, and the low defect rate emphasizes the excellent fabrication quality control achieved with the 460 000 end-closure welds and end-plugs that are within the reactor at any one time. Although quality control is excellent, defects that do occur fall mainly into the two categories of incomplete end-closure welds and the less-frequent end-plug barstock porosity. Incomplete end-closure welds may give early or later defect indications, depending upon the defect hole size, whereas the porous end-plugs are generally very small defects, which have a distinct incubation period before secondary damage allows fission-product release to the coolant. A third category of defect, which could be considered fabrication-dependent, is primary hydriding failure. This mechanism had never been indicated in CANDU fuel until a defective fuel incident occurred during 1991/1992 at one of the 600 MW Generating Stations. There, post-irradiation examination eliminated most other possible defect causes, and the fabricator determined that an undetected shift in raw material characteristics allowed fuel to be produced with up to 4 mg hydrogen per element, rather than the specified <1 mg hydrogen per element. Two further mechanisms of fuel damage are caused by reactor operating conditions rather than fabrication quality. Pellet/cladding interaction defects generally require a power ramp after a period of lower power operation. This provides sufficient stress from the expanding fuel pellet and freshly released fission-product corrodents to crack the cladding. Fretting damage generally occurs from debris or foreign objects in the primary coolant, which are caught up in the fuel. Fretting damage may also be caused by vibration, which may result from hydraulic instability of a fuel bundle or column of bundles.

1. INTRODUCTION

The CANDU* reactor uses pressurized heavy water (PHW) as both the primary coolant in the pressure tubes, which contain the fuel, and as the moderator in the calandria tank, which surrounds the pressure tubes. The pressure tube, surrounding calandria tube, and end-fittings comprise the fuel channel. The reactor is fuelled with 500-mm-long fuel bundles with elements clad in Zircaloy-4 and containing natural UO_2 pellets. The use of natural uranium with very little excess reactivity necessitates the use of on-power refuelling with remotely controlled fuelling machines, which add fresh bundles and remove spent bundles from the channels. Two types of fuel bundles are currently used in Canadian CANDU-PHW reactors: 28-element bundles (used in the Pickering reactors) and 37-element bundles (used in the Bruce, Darlington and 600 MW reactors). The element diameter is 15.2 mm for the 28-element bundle, and 13.1 mm for the 37-element bundle. The Zircaloy-4 fuel cladding is thin (about 0.4 mm) and is designed to operate in intimate contact with the pellets at a coolant pressure of about 10 MPa. The inside surface of the cladding is coated with a thin layer of CANLUB graphite to improve power ramping performance. The 37-element bundle is shown in Figure 1.

The on-power fuelling system of a CANDU reactor uses two fuelling machines, one at each end of the channel. During refuelling, the machines operate in pairs, locking onto opposite ends of the same channel. One machine inserts new fuel bundles into the channel, while the other accepts the same number of discharged bundles. Each of the fuel channels contains 12 fuel bundles in-core.

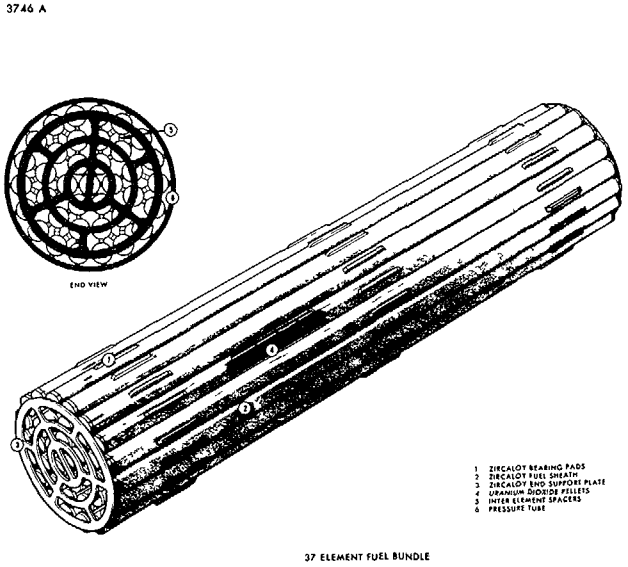

FIGURE 1. The CANDU 37-Element Fuel Bundle

* CANDU: CANada Deuterium Uranium is a registered trademark.

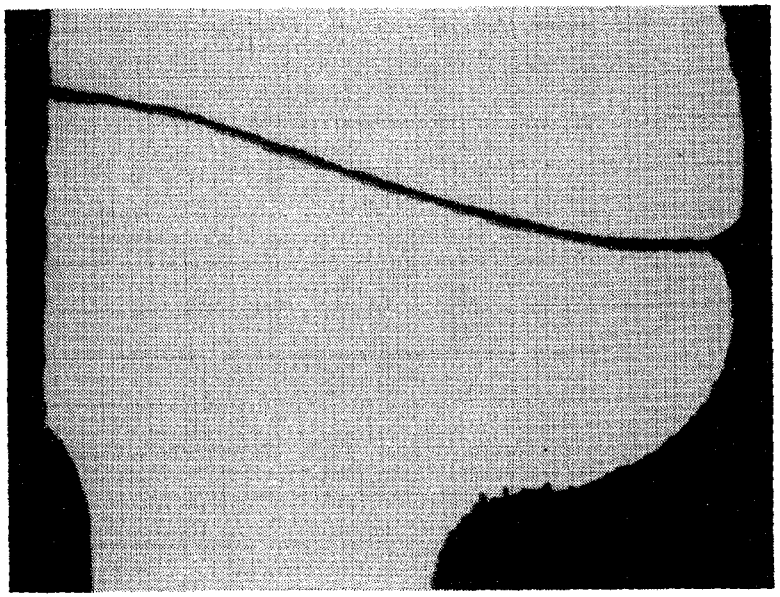

FIGURE 2. A Metallographic Cross-section through an Incomplete Weld

The number of bundles replaced in a channel during refuelling depends on the fuel-management scheme used by the utility; commonly, 2, 4, 8, and 10 bundle shifts are in use.

Fuel performance in Canadian CANDU reactors has been excellent; 99.9% of the close to 600 000 fuel bundles irradiated to date have operated as designed. The fuel defects that have occurred in Canadian CANDU reactors fall into four main categories, listed below in probable order of importance:

- fabrication defects,
- pellet/cladding interaction (PCI) defects,
- fretting and vibration defects, and
- primary hydriding defects.

These four categories of defects are discussed in detail in the following sections, with comments on deterioration rate where possible.

2. FABRICATION DEFECTS

While Canadian fuel fabricators have achieved an excellent level of quality in fuel production, faults occasionally elude normal surveillance procedures and cause a defective fuel element. Element end-closure resistance welding provides an example of the high quality standards achieved with a simple mass-

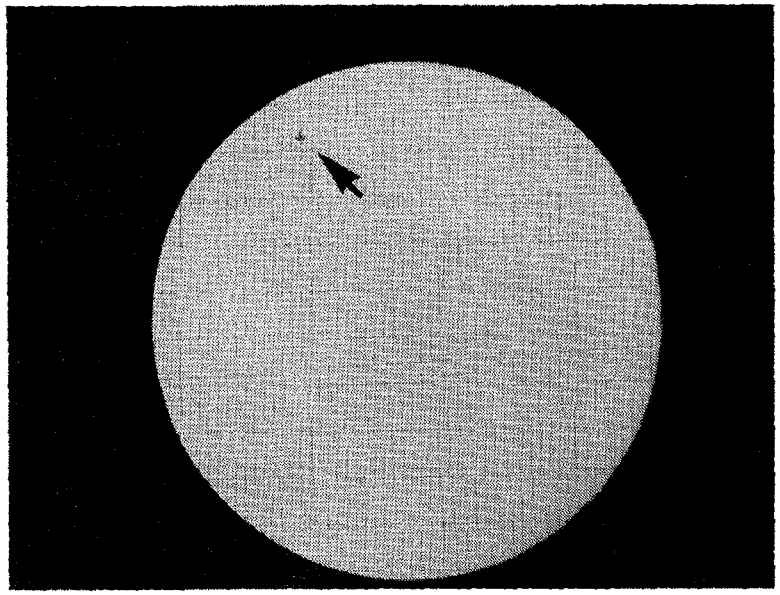

FIGURE 3. A Macroscopic View of a Polished Section of an End-Plug With a Porosity Defect (Arrowed)

production product. Each 850 MW reactor core contains 6 240 bundles, each with 74 end-closure welds. Thus, there are 461 760 welds in the reactor core at any one time. The very low frequency of leaking welds testifies to the consistency of the technology. When incomplete welds do occur, they typically show the metallographic appearance depicted in Figure 2. The residence time in-reactor before leakage and release of fission products can vary enormously, depending upon the size of the leak path and the operating power. In one Chalk River irradiation of a commercially produced Bruce-type bundle, the first emission of fission products from an incomplete weld occurred after more than 16 GW.d/Te U of burnup. Deterioration after leakage is critically dependent upon operating power.

A further type of fabrication defect that has occasionally been seen (but rarely, compared to incomplete end-closure welding) is porosity in the barstock used to machine end-plugs. This is a coring type of metallurgical defect, resulting from the original ingot used to produce the barstock. In a few cases, the porosity has eluded the ultrasonic detection method used by the fabricator. Because these defects are small, often only a few micro-metres in diameter, there is a significant operational period before fission products in the coolant signal the presence of a defect. Typical end-plug porosity is shown in Figures 3 and 4.

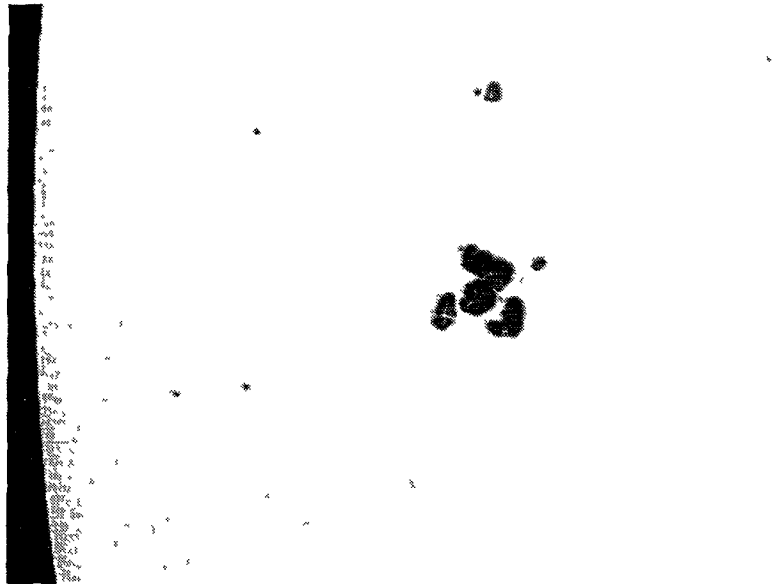

FIGURE 4. As for Figure 3, Porosity Defect at Higher Magnification

Primary hydriding defects, which can also be regarded as fabrication-related defects, are very rare in the CANDU system; a recent occurrence is discussed in Section 6.

3. PELLET/CLADDING INTERACTION (PCI) DEFECTS

Since the early 1970s, it has been recognized that the mechanical interaction of the Zircaloy cladding with the expanding fuel pellet could give rise to cracking. PCI defects are generally characterised by a power history showing a power increase after significant burnup at lower power. Corrosive fission products, such as iodine or cesium, have been indicated as the probable corrodents causing Stress-Corrosion Cracking (SCC) of the Zircaloy, activated by the high cladding stress from PCI. CANDU reactor and Chalk River power-ramp defect statistics were used by Penn, Lo and Wood [1] to pioneer the power-ramp defect threshold diagram for CANDU fuel. This has since been modified, using the massive statistics for fuel power-ramp performance available from operating CANDU reactors, for use with CANLUB-coated fuel in current reactor types. Figures 5 and 6 show the recommended threshold diagrams for the CANDU 6 reactor [2]. The curves labelled 1979 are initial curves recommended for use in CANDU 6 reactors, where bundle powers peak at about 900 kW. In 1982, the curves were

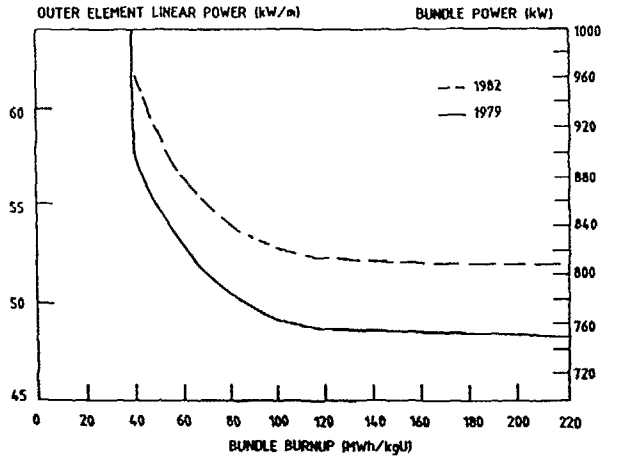

FIGURE 5. Threshold for Final Ramped Power for SCC Defects in the CANDU 6 Reactor

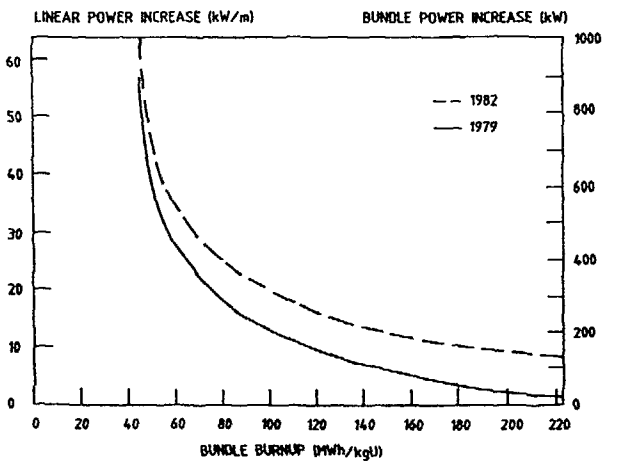

FIGURE 6. Threshold for SCC-Defects for Power Increase During Ramping in the CANDU 6 Reactor

adjusted upwards to reflect good fuel performance during 4 bundle shifts at the Bruce "A" Generating Station. To use these diagrams, the final power of the fuel, after a power increase at a given burnup, is compared with Figure 5. If the point falls above the threshold line, it lies in a region of finite defect probability. Figure 6 must be used to compare the power increase in the ramp with the

threshold for power increase. Only if both thresholds are violated is the fuel indicated to fail. In the investigation of fuel defects, a fuel power history showing a power increase that violated the thresholds of the power-ramp defect diagrams would strongly suggest PCI/SCC defects.

In CANDU fuel, the SCC cracks occur predominantly at pellet interface positions, and in rarer cases, due to high fuel expansion, they occur alongside the brazed bearing pads. Pellet interfaces are generally the highest stress positions in the cladding. SCC cracks can often be located in hot-cell examination by cutting the element, adding a gas-pressure fitting, and pressurizing with gas while holding the element under water. Bubbles can generally be seen at crack locations. Metallographic examination of SCC defects in Zircaloy often reveals very characteristic branching (see Figure 7).

Fission-product release to the coolant from PCI defects is usually very rapid. In NRU loop power-ramp tests, the gamma defect signal from the coolant was often seen within minutes or seconds of achieving full power. However, in one power ramp in the NRU reactor, the coolant gamma signal was not seen until 9 days after the ramp. In general, in CANDU reactors, PCI defects due to power ramping have deteriorated more rapidly with continued operation in the defective condition than have fabrication defects.

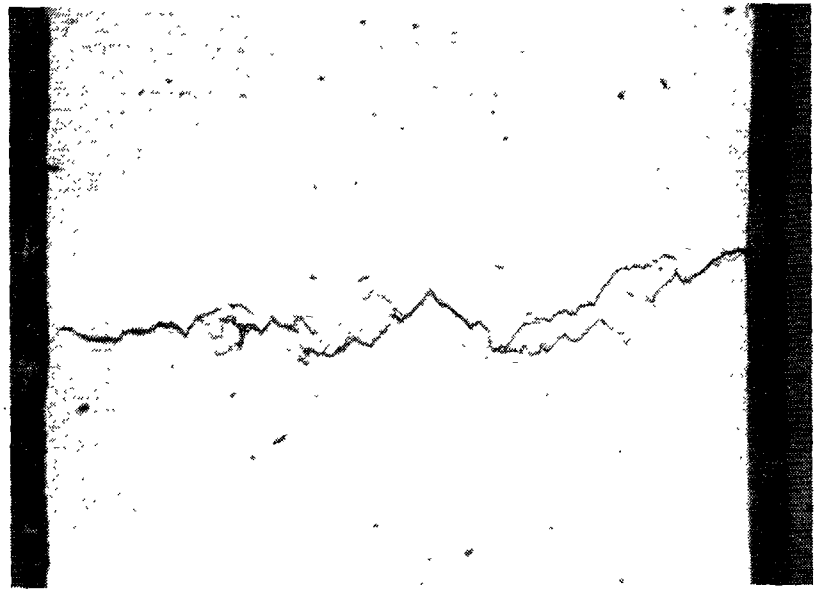

FIGURE 7. A Metallographic Cross-Section through a Typical Branching SCC Crack

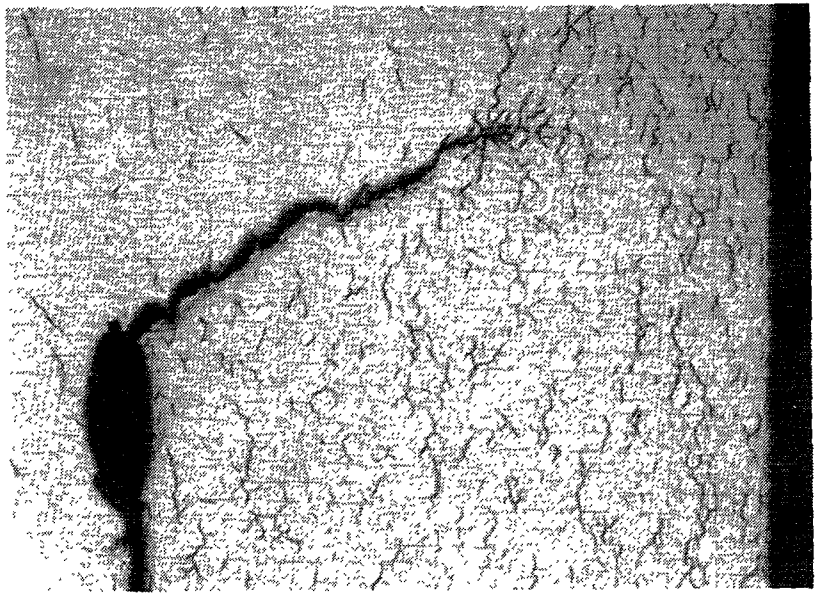

FIGURE 8. A Typical Crack through the Weld Heat-Affected-Zone of a Defective Fuel Bundle

As well as cladding cracks at the pellet interface locations resulting from power ramps, a further type of PCI cracking has been experienced in Canadian reactors. The mechanism was first noted in the Bruce Generating station, Unit 3, around 1984 [3]. This cracking occurs at the closure weld heat-affected zone and is thought to result from high stress caused by pellet expansion with either hydrogen or iodine as the crack initiator. Hydride/deuteride flakes have been seen at the crack tips in some of these cases, giving rise to the theory that cracking originates and/or is propagated by Delayed Hydrogen Cracking (DHC). This is limited to high-powered bundles, where one might equally have expected SCC from fission products. Thus it is difficult to separate DHC and SCC for the weld-region cracks. A typical weld-region crack is shown in Figure 8.

4. FRETTING AND VIBRATION DEFECTS

4.1. Fretting from Debris in the Coolant

Fretting from debris in the coolant is perhaps the most common cause of fuel defects in LWRs [4 to 6], and CANDU reactors can also be affected. Often the foreign objects or debris result from construction or maintenance work on the

reactor. In this situation, the debris become caught in the fuel and frequently result in fretting of the cladding and fuel defects. Figures 9 and 10 show typical fretting holes in the cladding of a CANDU element. Figure 11 shows a bunch of turnings caught in a fuel bundle.

4.2. Coolant-Induced Vibration and Fretting

Coolant-induced vibration of a fuel bundle or a column of fuel bundles can occur either by hydraulic flow instabilities in the fuel column or by pressure pulsations carried by the coolant from the pumps. Hydraulic instability or "flutter" at the upper end of 10 bundle vertical fuel assemblies caused damage to the Gentilly-1 reactor (now de-commissioned). In Gentilly-1, the top (number 10) bundle of the vertical fuel assembly oscillated in the up-flowing coolant and caused damage to both bundle and pressure tube. This effect was sensitive to operating power, steam quality and flow rate. As a remedial measure, a stiffer fuel-bundle design was recommended, along with stiffening of the fuel carriage by using a stiffer central support rod and increased retaining-spring force.

Another mechanism for fuel damage by fretting is the response of bundles to turbulence or other flow instabilities. This may cause both axial and transverse motion of the elements, leading to inter-element spacer wear and, eventually, to cladding contact between elements. Figure 12 shows inter-element spacer fretting wear, and wear of the cladding due to element-to-element fretting contact.

FIGURE 9. A Macroscopic View of a Fuel Element with a Fretted Hole (Arrowed)

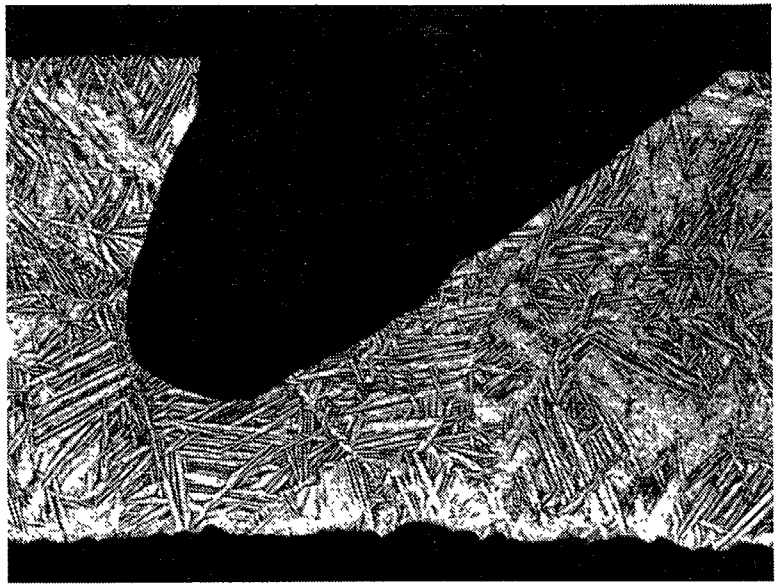

FIGURE 10. A Metallographic Cross-Section of a Fretted Hole Partly through the Cladding

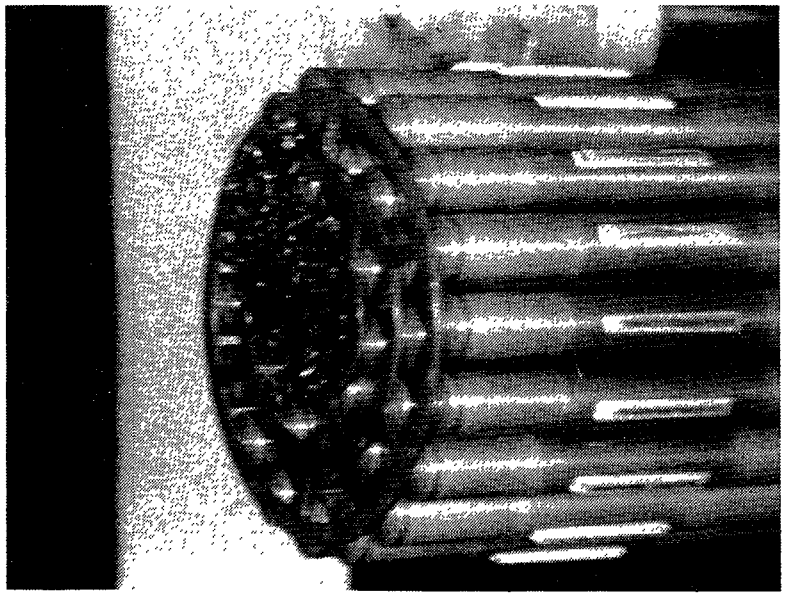

FIGURE 11. Turnings Trapped in the End-Plate of a Fuel Bundle

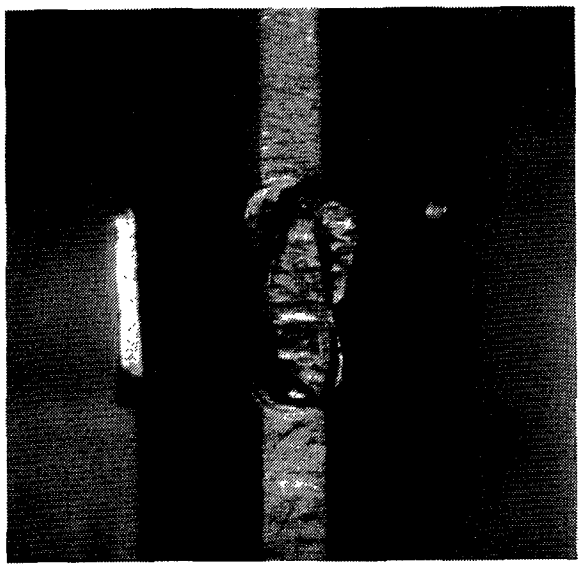

FIGURE 12. Severe Fretting Wear of a Spacer-Pad (Centre) and a Worn Strip from Element-to-Element Contact

5. PRIMARY HYDRIDING DEFECTS

Even in the early 1970s, when the first CANDU reactors were commissioned, there were no problems with primary hydriding of CANDU fuel. The reason lies in the required high density for CANDU fuel pellets to support the collapsible cladding. The fuel pellets are the main source of hydrogen in fuel elements [7]. CANDU UO_2 fuel pellets have always had a specified density of about 10.6 Mg/m^3, or greater than 96% of theoretical density. The higher density fuel has very little inter-connected porosity to retain moisture for subsequent release in-reactor. Thus the problems experienced in light-water reactors in the 1970s [7] were not experienced in CANDU reactors. However, isolated incidents with enriched UO_2 experimental fuel at Chalk River led to the imposition of a limit of 1 mg hydrogen per element for protection against potential primary hydriding defects from hydrogen included in the fuel.

The first fuel defects attributed to primary hydriding in a Canadian CANDU reactor occurred at one of the 600 MW stations in 1991 and 1992. A quantity of 37-element fuel was fabricated with insufficient vacuum-baking of the graphite CANLUB sheath coatings. This allowed an excessive amount of hydrocarbon binder to remain in the elements. The fabricator's internal investigation as a result of the fuel defects revealed a probable hydrogen level of up to 4 mg per element in the affected fuel.

Primary hydriding failure is very difficult to prove from post-irradiation examination of defective fuel, since a primary hydride "sunburst" in the cladding is masked by secondary hydriding or deuteriding damage. Theoretically, in heavy-water-cooled fuel, such as CANDU fuel, it should be possible to differentiate isotopically between hydrogen-rich and deuterium-rich sunbursts in the cladding. In particular, neutron radiography shows a marked difference in attenuation of the neutron beam between zirconium hydride and zirconium deuteride. The investigation of the suspected hydriding defects is still ongoing (1992 May) and neutron radiography of selected elements is planned for a later date. Post-irradiation examination was able to eliminate other possibilities, such as incomplete closure welds, porous end-plugs and SCC. A bundle suspected of having failed from primary hydriding is shown in Figure 13 and a metallographic section through a deuterided area is shown in Figure 14.

Detection of fuel defects in CANDU reactors depends on the kind of equipment installed at the station. Some stations, including CANDU 6 stations, use Delayed Neutron (DN) monitors, which count the neutrons from short-lived

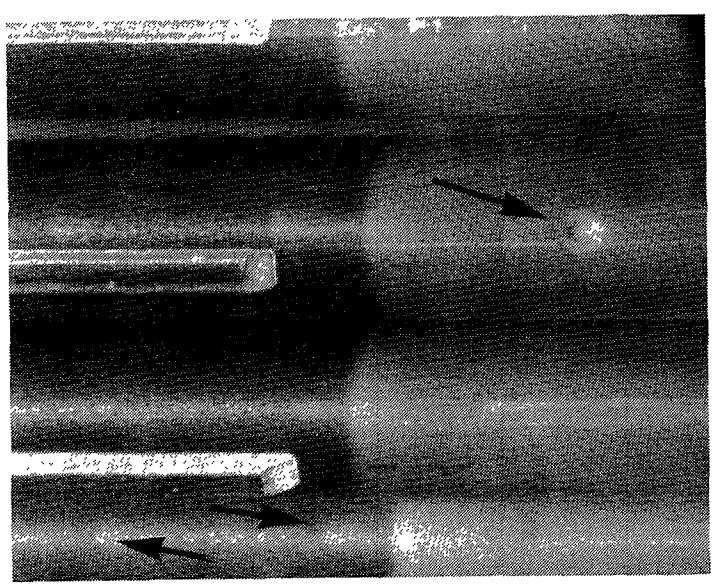

FIGURE 13. Fuel Bundle Showing Defects (Arrowed) Suspected of Primary Hydriding Defects

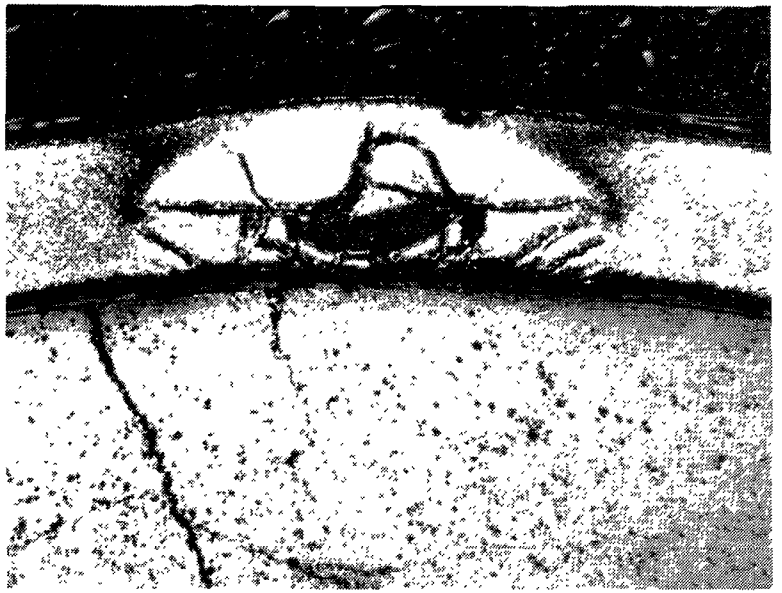

FIGURE 14. Metallographic Cross-section through a Heavily Deuterided Area on an Element Suspected of Primary Hydriding Failure

fission products, such as I-137 and Br-87. Scrutiny of the DN detection data indicated that the fuel bundles suspected of having failed from primary hydriding began to emit fission products very shortly after being loaded into the reactor. This is consistent with a primary hydriding mechanism in high-powered bundles (having ruled out other defect mechanisms). Operating power data for defected bundles indicated a dependency of defect deterioration on operating power. From the ongoing investigation, it appears that little deterioration would be expected at peak powers of less than about 40 kW/m.

6. CLOSURE

In this report, we have discussed the four principal categories of fuel defects that occur in CANDU-PHW fuel. The occurrence of fabrication defects is a comparatively rare event and represents a small statistical probability in a very reliable mass-production product. Other defects, such as SCC or fretting damage, challenge both the fuel fabricator and the operating utility to avoid conditions that may allow defects to occur. The tendency of occasional excursions in fabrication quality or operational procedures to give rise to fuel defects demands reliable failed-fuel detection procedures, and the capability for verification of the defect mechanism by post-irradiation examination. This is even more important given the sharply decreasing coolant activity burden limits being imposed by licensing authorities, and the implicit reduction in allowable fuel defects.

REFERENCES

1. PENN, W.J., LO, R.K., and WOOD, J.C., "CANDU Fuel-Power Ramp Performance Criteria", ANS, Nuclear Technology, 1977 July.

2. MANZER, A.M., DENNIER, D., HU, R.H., and YOUNG, E.G., "CANDU 6 Reactor Shim Operation: Fuel Performance Guidelines", Proceedings, Canadian Nuclear Society, Annual Conference, Saskatoon, 1991.

3. JUDAH, J., "Defective Fuel Location by Dry Sipping: Experience at Bruce NGS-A During the 1984 Fuel Defect Excursion", International Conference on CANDU Fuel, Chalk River, 1986 October 6-8.

4. LUNDHOLM, L., GRAPENGIESSER, B., SCHRIRE, D., and HALLSTADIUS, L., "ABB Atom Fuel Failure: An Overview", This Meeting.

5. BAY, H., BOULANGER, D., DERAMAIX, P., BAIRIOT, H., "Debris Induced Fuel Failures on U and MOX Fuel in Beznau I", Ibid.

6. STRASSER, A., GINGOLD, J., "An Evaluation of Debris Fretting Failures and Preventive Methods", Ibid.

7. PROEBSTLE, R.A., DAVIES, J.H., ROWLAND, T. C., RUDKIN, D.R., and ARMIJO, J.S.," The Mechanism of Defection of Zircaloy-Clad Fuel Rods by Internal Hydriding", ANS-CNA Joint Meeting on Commercial Nuclear Fuel Technology, Toronto, 1975 April 27 to 30.

FUEL FAILURE AT HAMAOKA UNIT 1

Y. HAYASHI
Nippon Nuclear Fuel Development Company Ltd,
Ibaraki

T. MATSUMOTO
Toshiba Corporation,
Yokohama

M. KUZUSHIMA, T. MURAMOTO
Chubu Electric Power Company Inc.,
Nagoya

T. OKUBO
Sophia University,
Tokyo

Japan

Abstract

Five fuel assemblies failed during Cycle 11 at Hamaoka Unit 1 of Chubu Electric Power Company in 1990. A thick zirconium oxide layer formed on the fuel rods and was partially spalled off in many of the assemblies, including the failed ones. The failure was attributed to cladding corrosion, which was caused by a combination of cladding susceptible to corrosion and irregular reactor coolant chemistry. In Cycle 12, Hamaoka Unit 1 operated under better water chemistry and with fuels which were confirmed to be sound. Neither failure nor accelerated corrosion was found in the subsequent annual inspection.

1. Introduction

The number of fuel failures in Japanese boiling water ractors (BWRs) has been low, being 0-1 bundles during the 5 years from 1985 to 1989. But five fuel assemblies were identified as having leaked in Hamaoka Unit 1 in 1990. These were the first failures in Unit 1. Soon a extensive inspection program was started to reveal the cause of failure. This paper describes the progress of the program, its findings and the measures applied to prevent other failures.

2. Reactor operation

Hamaoka Unit 1 is a BWR with a capacity of 540 MWe. It has been operated since 1976. Its Cycle 11 operation was started in August 1989 after the 10th annual regular inspection. The iodine-131 activity in the reactor coolant started to increase in March 1990 under full power operation. The reactor operation was continued until June under more intense surveillance. The iodine-131 activity in the coolant and the off-gas monitor indication are given in Figure 1. The iodine-131 activity reached a maximum of 20 Bq/g which was 1/400 of the operating limit. The activity release to the environment

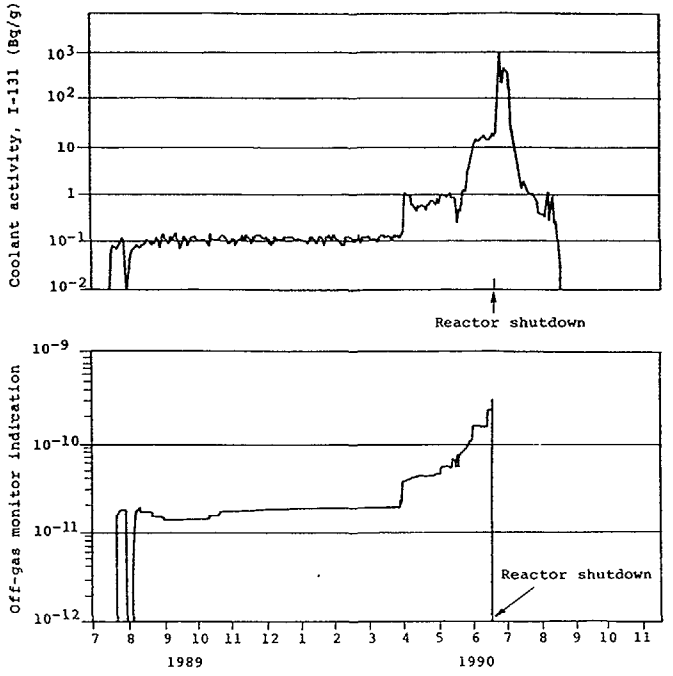

Figure 1 Coolant activity and off-gas monitor indication during Cycle 11

during operation was kept satisfactorily low through relevant treatment in the radioactive waste disposal system.

A total of 368 fuel assemblies were loaded. They were composed of two types of fuel assemblies, 8x8RJ and 8x8BJ. 8x8BJ used zirconium liner cladding with improved thermal processing. The reactor was shut down in June and all fuel assemblies were inspected by sipping test and 5 assemblies were identified as having leaked.

An extensive inspection program was subsequently planned and implemented. The probable cause of failure was identified and the countermeasures were determined.

The reactor operation was resumed in June 1991 after the appropriate measures were applied and Cycle 12 was completed in February 1992. Neither fuel failure nor accelerated corrosion was found in the subsequent annual inspection.

Studies are still going on; post irradiation examination of a failed bundle was started in October 1991.

3. Inspection

3.1 Fuel

a. Visual inspection

All fuel assemblies were observed by under water TV and fiber scope camera. Many assemblies had "spalling" on the surface of fuel rods. The spalling was like that shown in Figure 2. Crud and the outer surface of the oxide layer were spalled off and white oxide layers were exposed. The size and shape of the spalling was varied and some were dented due to multiple spallings. The number of assemblies with spallings is summarized in Table 1. Seventy-eight out of 368 bundles had spalling. The spalled rods belonged to fuels which were loaded from Cycle 8 or Cycle 9 and had experienced 3 or 4 irradiation cycles respectively. The fuels loaded from Cycle 10 or Cycle 11 did not have any spalled surfaces. The spalling started from the burnup of 19 GWd/t, as shown in Figure 3. Rods containing Gd did not show any spalling.

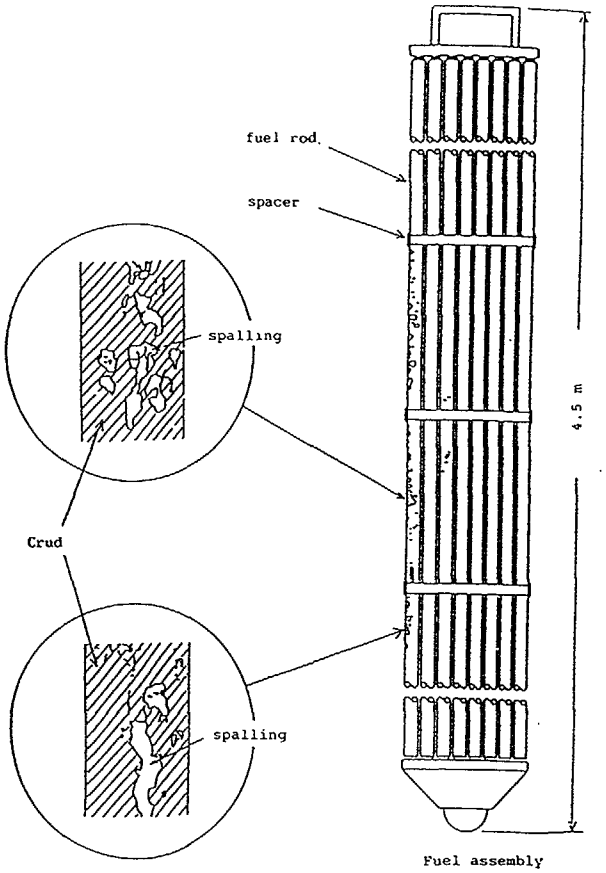

Figure 2 The appearance of a failed assembly

b. Ultrasonic inspection

Five fuel rods were identified as water immersed rods from 4 fuel assemblies. One leaked assembly was judged not to have any water immersed rods.

c. Visual inspection and oxide thickness measurements of rods

Twenty-seven assemblies were selected as typical in consideration of irradiation period, cladding tube manufacturer, manufacturing period and other factors. The visual

Table 1 Number of fuel assemblies with spalled oxide layer

Reload batch	Irradiation period (Cycle)	Type of fuel	Number of assemblies	Number of assemblies with spalling	Average burnup (GWd/t)
Cycle 8	8, 9, 10, 11	8x8RJ	8	8	29.8
Cycle 9	9, 10, 11	8x8RJ	128	70*	24.2
Cycle 10	10, 11	8x8RJ	116	0	16.3
Cycle 11	11	8x8RJ	20	0	9.5
Cycle 11	11	8x8BJ	96	0	8.8
Total			368	78	

*5 failed assemblies were included.

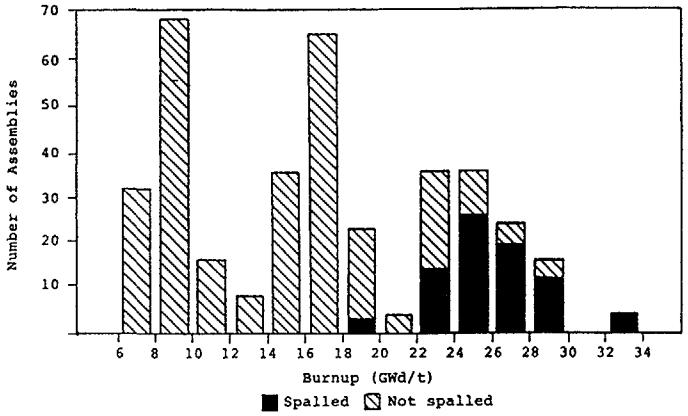

Figure 3 Number of spalled assemblies vs. burnup

inspection and oxide thickness measurements were performed on their outermost rods after the crud was removed. The oxide thickness vs bundle averaged burnup is shown in Figure 4. The fuel rods in the assemblies irradiated to 3 or 4 cycles were covered with white zirconium oxide the thickness of which was more than double that typically found on fuel rods irradiated in Japanese BWRs. Rods with 1 or 2 cycle irradiations were covered with ordinary nodular corrosion and did not have the white oxide layer. Their oxide thickness was as much as ordinary sound fuels.

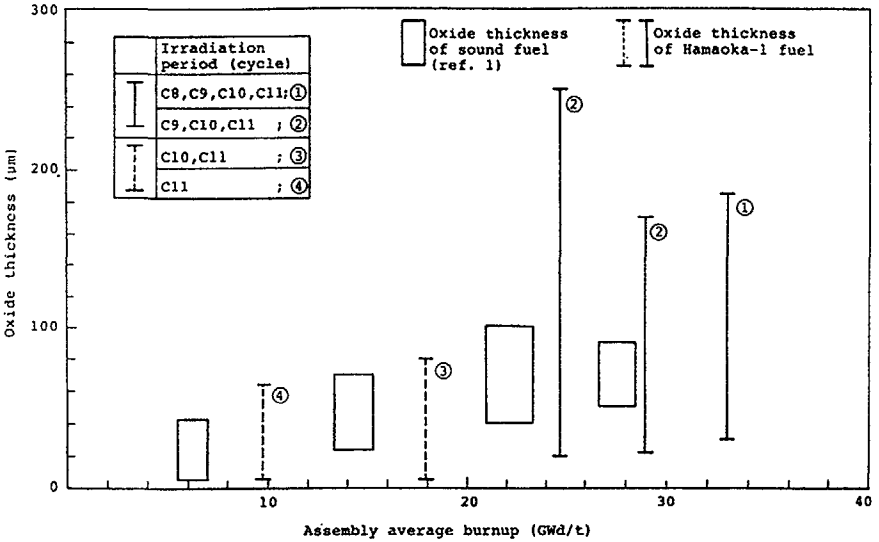

Figure 4 Oxide thickness measurements

3.2 Operation history

Rod power was kept below the operational limit (440W/cm) and power increase was also below PCIOMR (the guide line for power increase: less than 0.11kW/ft/h).

3.3 Manufacturing history

The manufacturing record from ingot-tubeshell-tubing to fuel assembly was surveyed. The manufacturing procedures and quality control for every process were properly followed.

3.4 Coolant chemistry

The coolant water from the condenser is purified through the condensate filter demineralizer (CFD) and condensate demineralizer (CD). The coolant water chemistry records from Cycle 1 to Cycle 11 were surveyed. All control items for coolant in the reactor and feed water were maintained within the water chemistry control limit during operation. The electrical conductivity of coolant at the startup of Cycles 9

Table 2 Coolant water chemistry and their causes

	Cycle 9	Cycle 10	Cycle 11	Causes
At the startup	Increase of electrical conductivity (1-1.2 μS/cm)		Increase of electrical conductivity (1 μS/cm)	Decomposition of organic compounds which were dissolved from CD and flowed into the core.
Under operation	High pH (7.8) Na^+ (18 ppb)	High pH (7.7) Na^+ (12 ppb)	High pH (7.7) Na^+ (17 ppb)	Na^+ which was dissolved from the cation exchange resin in CD.
At the shutdown		Increase of electric conductivity (0.86 μS/cm)	Increase of electric conductivity (0.89 μS/cm)	Na^+ and SO_4^{2-} which were dissolved from the fuel rod surface.

and 11 was higher than in the other cycles but low enough to be within the regulation limit. Though the coolant chemistry was well controlled, records were surveyed in detail to find any irregularity which could possiblly affect rod corrosion. The surveyed results are summarized in Table 2.

a. Reactor startup

The electrical conductivity of coolant was increased to 1-1.2 μS/cm early in the startup of Cycles 9 and 11 and sulfate ions (SO_4^{2-}) were detected.

This increase of electrical conductivity was thought to come from the presence of chemical species which were formed by decomposition of organic materials due to heat and radiation. The organic materials, which were usually monitored as Total Organic Carbon, dissolved from the ion exchange resin in the condenser demineralizer and flowed into the core.

b. Reactor operation

The average sodium ion content in the core during the most recent four cycles was 15 ppb under normal operation and pH was about 7.7. These values were slightly higher than in other Japanese BWRs.

The increase of Na^+ ions could be explained by the following process. In the chemical regeneration process of resin in the condenser demineralizer, a potion of cation resin was mixed with anion resin. The mixed cation resin was converted to the Na form, namely attached to Na^+, when anion resins were regenerated by sodium hydride. These Na^+ ions entered the core during normal operation.

c. Reactor shutdown

The electrical conductivity of coolant was high at reactor shutdown in Cycles 10 and 11. It had not increased at the previous shutdowns. Na^+ and SO_4^{2-} were detected at the reactor shutdown of Cycle 10. These ions were thought to be dissolved from Na_2SO_4 which had adhered to the oxide layer on the cladding tube surface.

3.5 Cladding tube material

The nodular corrosion susceptibility of BWR cladding is known to decrease with decreasing annealing parameter. The parameter is defined as:

$$A=\Sigma t_i \exp(-Q/RT_i)$$

where

t_i : time of i-th annealing step after β quench, h

T_i : temperature of i-th annealing step, K

Q/R: 40,000 K

This susceptibility was calculated for the tubes used in Hamaoka Unit 1 and found to be relatively large for the tubes used from Cycles 8 and 9 (Figure 5). A high temperature corrosion test was performed on the archive tubing samples. The corrosion weight gain of the tubings used from Cycles 8 and 9 was relatively large and widely distributed.

4. Cause of failure

PCI, fretting, burnout, defects caused on fuel handling, hydriding and manufacturing defects were judged not to be related to the fuel failure. Although the cladding surface appearance was similar to that of CILC failure, its possibility was small because coolant copper concentration, which was

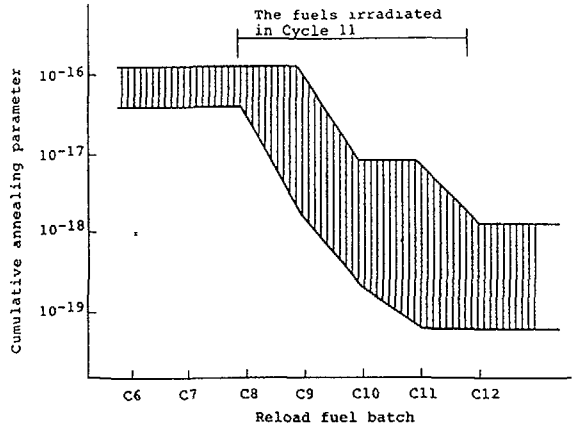

Figure 5 Cumulative annealing parameter of Hamaoka-1 reload fuel batch

comparable to other domestic BWRs, was 1-2 order of magnitude lower than foreign cases of CILC.

Finally it was decided that the fuel failure was caused by unique corrosion. The characteristics of the corrosion were as follows.

i. Extensive corrosion occurred only on the fuels loaded in Cycles 8 and 9.

ii. The oxide thickness was more than twice that of ordinary sound fuel.

This corrosion behavior could not be explained as due to use of corrosion susceptible materials or irregular coolant chemistry independently. One reason is that similar corrosion susceptible cladding tubes have been used in other Japanese BWRs but accelerated corrosion has not occurred. A second reason is that fuel using less susceptible cladding loaded in Cycles 10 and 11 experienced the irregular coolant chemistry, but their corrosion was normal. Therefore this corrosion was inferred to occur through a combination of the irregular coolant water chemistry and the relatively high corrosion susceptible cladding.

The following process leading to failure was proposed. Chemical species like SO_4^{2-} and others anions are present in the coolant at the start of operation, and Na^+ and organic compounds flow into the core during operation. These ions and organic compounds accelerate the start of corrosion on corrosion susceptible claddings. When corrosion has started, Na_2SO_4 and similar compounds condense on the cladding surface and speed up the corrosion even more. As the corrosion layer becames thicker, the cladding temperature rises and corrosion is accelerated further to cause spalling. Finally, multiple spallings produce holes in the cladding wall.

5. Countermeasures

5.1 Fuel assemblies

It was decided that fuel assemblies in Cycle 12 should be composed of fuels loaded from Cycles 10 and 11 and new fuels. Namely, fuel assemblies irradiated from Cycles 8 and 9 were not used in Cycle 12, even though they might have been found to be sound. The fuel assemblies loaded in Cycle 12 are shown in Table 3.

Table 3 The fuel assemblies in Cycle 12

		Number of assemblies
Used fuel	Irradiated in Cycles 10 and 11	113
Used fuel	Irradiated in Cycle 11	115
	Sub-total	228
New fuel		140
	Total	368

5.2 Coolant chemistry and its control

a. Prevention of sodium ion inflow

Used resins were replaced with new resins in the condensate demineralizer. The resins will not be regenerated after Cycle 12.

b. Suppression of electric conductivity increase at startup

Discharge of organic compounds from CD, bypassing the coolant water from the CD in the cleanup operation before startup and improvement of cleanup capacity in the reactor cleanup system were carried out.

c. Stronger control

Stronger controls of organic compounds (Total Organic Carbon) before startup, of coolant electrical conductivity at startup and of Na^+ during operation were set.

d. Other coolant quality improvement

The water in the primary coolant system was purified more by cleaning the system components before startup and the exchanging the water

6. Conclusions

The failure of rods and spalling of oxide layer originated from corrosion whose cause was inferred to be the combined effect of irregular water chemistry and use of more corrosion susceptible cladding material.

In the next cycle, the reactor was operated using new and irradiated sound fuels under stronger control of coolant chemistry. The cycle was successfully completed without any fuel failure or accelerated corrosion.

References

[1] Mishima, Y. et al., Proving Test on Reliability for BWR Fuel Assemblies, J. Atomic Energy Soc. Japan, 29, 90 (1987).

[2] Garzarolli, F. et al., Microstructure and Corrosion Studies for Optimized PWR and BWR Zircaloy, Zirconium in the Nuclear Industry, ASTM STP 1023 (1988) pp. 202-212.

WESTINGHOUSE FUEL PERFORMANCE EXPERIENCE

H.W. WILSON, R.S. MILLER, H. KUNISHI
Commercial Nuclear Fuel Division,
Westinghouse Electric Corporation,
Pittsburgh, Pennsylvania,
United States of America

Abstract

Nuclear fuel reliability is among the highest priority items in the nuclear industry today. Despite having fuel reliability unsurpassed in the PWR industry, Westinghouse has an aggressive program to identify the efforts needed to achieve defect-free operation. This program consists of monitoring fuel performance, detailed on-site examinations to identify leakage causes, and implementation of corrective actions. These efforts have identified debris-induced fretting as the dominant leakage mechanism, accounting for approximately 70% of observed leaking rods. Corrective actions, consisting of training of site personnel and fuel assembly design changes, have been implemented to minimize the impact that debris can have on fuel integrity. Evaluations of data obtained from site examinations show several interesting trends. The size of debris wear scars has become smaller over the past several years, implying that debris in the system is becoming smaller. Also, the majority of debris-induced fretting defects have been found to occur early in the fuel's operating life. This suggests that fuel rods have properties which make them more resistant to debris damage as burnup increases. The corrective actions implemented have been shown to be successful in reducing the occurrence of debris-related damage. Additional improvements are being developed to provide even further resistance to debris.

1. BACKGROUND

Maintaining excellent fuel reliability is among the highest priorities for nuclear power plant operators throughout the world. Despite the fact that Westinghouse fuel reliability is unsurpassed in the PWR industry, an aggressive program has been conducted since the early-1980s to identify and implement efforts needed to achieve defect-free operation in all reactors. Results of this effort are illustrated in Figure 1. Since the early 1980s when higher coolant activity levels were being experienced, principally due to the effects of baffle-jetting and debris-induced fretting, the coolant activity in Westinghouse fueled plants has decreased steadily. This paper will describe the structure of the Westinghouse program, the operative leakage mechanisms found through fuel examinations, and corrective actions implemented to reduce the dominant mechanism, debris-induced fretting.

Fuel leakers are currently very rare. In order to identify the causes for the small number of leakers and to implement corrective actions needed to eliminate them completely, a program incorporating coolant activity follow in operating plants, detailed on-site examinations, and root cause and corrective action evaluations has been pursued. Performing detailed fuel examinations at reactor

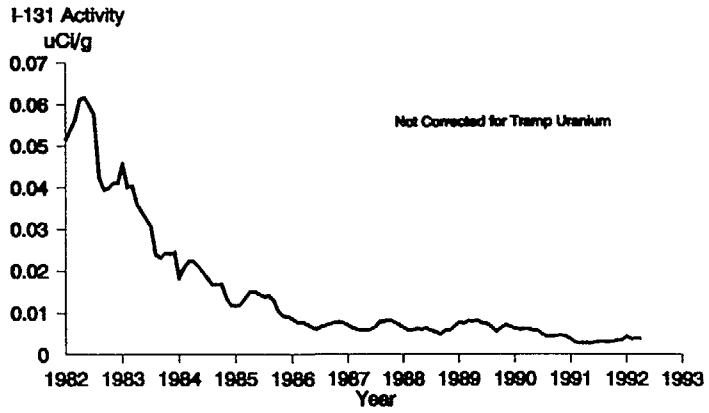

FIG. 1. Average coolant activity versus time.

sites during refueling outages is a key element of the Westinghouse program. Results from such examinations are used to direct follow-on efforts in product design, manufacturing, and reactor operation in order to eliminate the cause of the identified leakage mechanisms.

2. FUEL RELIABILITY PROCESS

The process for fuel performance monitoring and evaluation is summarized in Figure 2. Evaluation of coolant activity in operating plants is the first step in this program. The coolant activity from all operating plants is monitored and evaluated on a monthly basis. This effort allows an accurate assessment of overall performance and provides direction for examination efforts. On-site examinations typically start with the identification of specific leaking fuel rods by ultrasonic (UT) examination. Individual leaking fuel rods are then examined in detail at the site. In 1986 fuel reconstitution techniques became available to routinely allow the removal of leaking fuel rod(s) from an assembly during refueling outages and to allow reuse of the fuel assembly with such rod(s) replaced with solid stainless steel rods during the next cycle. This made possible a detailed evaluation of leaking rods outside the assembly to identify the leakage cause. Once a cause has been identified, the appropriate improvements can be implemented. Improvements implemented have been in the manufacturing, design, and reactor operational areas. In some cases on-site examinations are not successful in identifying a leakage cause (or confirming that the rod is actually leaking). A hot-cell program is being conducted to examine rods of this type. Following the identification of necessary corrective actions, fuel performance continues to be monitored in order to confirm that the corrective actions have been successful in eliminating the observed leakage-causing mechanisms.

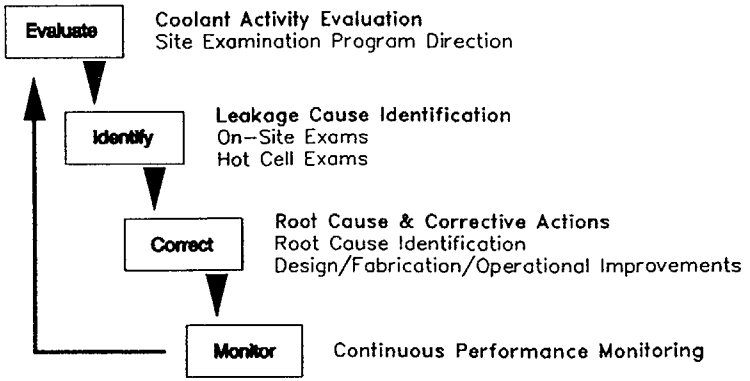

FIG. 2. Fuel performance program.

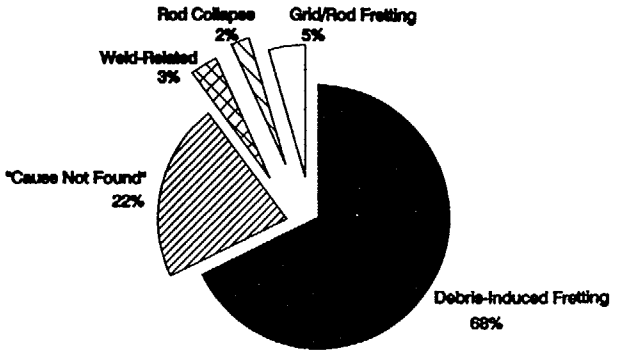

FIG. 3. Leakage mechanisms identified from on-site examinations for fuel of recent fabrication (after 1983).

3. EXAMINATION RESULTS

The leakage mechanisms confirmed by detailed examination of leaking fuel rods removed from the assembly are summarized in Figure 3. These results show that the current dominant leakage mechanism, accounting for approximately 70% of observed leaking rods in fuel of recent fabrication, is debris-induced fretting. Other mechanisms have been observed in the past, but are now generally very low in frequency of occurrence and non-systematic in nature. Successful actions have been put in place to eliminate the non-debris related leakage mechanisms which have been observed. A hot-cell examination program is underway to address the fuel rods with unknown leakage causes. As a result, effort is currently focused on debris-induced fuel rod fretting.

Debris-induced damage results from fretting wear on the outside of the fuel rod due to metallic material (debris) which has been introduced into the system during maintenance operations on the reactor system. Loose metallic debris can circulate in the reactor coolant system and become trapped in the fuel assembly, where it vibrates against the fuel rods (due to flow effects) and frets through the cladding. Observed debris has typically included turnings and shavings such as those which result from metal-working operations performed during primary system maintenance. In a few isolated cases, larger objects such as tools and screws have even been found in damaged fuel assemblies. Pictures of typical types of debris scars seen on fuel rods are shown in Figures 4 - 6.

4. CORRECTIVE ACTIONS FOR DEBRIS-INDUCED FRETTING

After the impact that loose debris in the system had on fuel reliability became well understood in the early-1980s, the industry took steps to control its introduction into the system. Utility and reactor service vendors helped assure that plant maintenance operations did not introduce new debris into the system and helped to remove debris already in the system. Extensive efforts in training and worker-awareness were focused on eliminating the introduction of debris into the system. These efforts were successful in significantly reducing the occurrence of debris-related leakers.

At the same time, Westinghouse introduced a new feature, the Debris Filter Bottom Nozzle (DFBN), to further prevent potentially damaging debris from entering the active core. Compared to the previous bottom nozzle, the DFBN has reduced

FIG. 4. Debris wear scar.

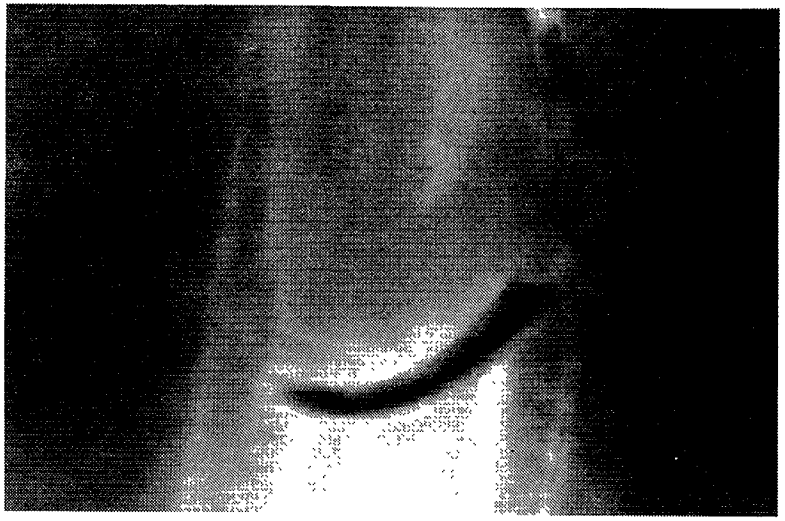

FIG. 5. Debris wear scar.

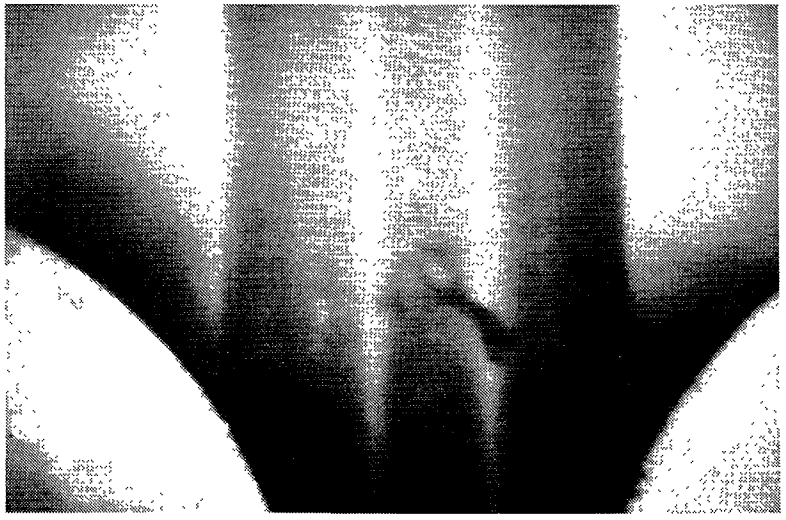

FIG. 6. Debris wear scar.

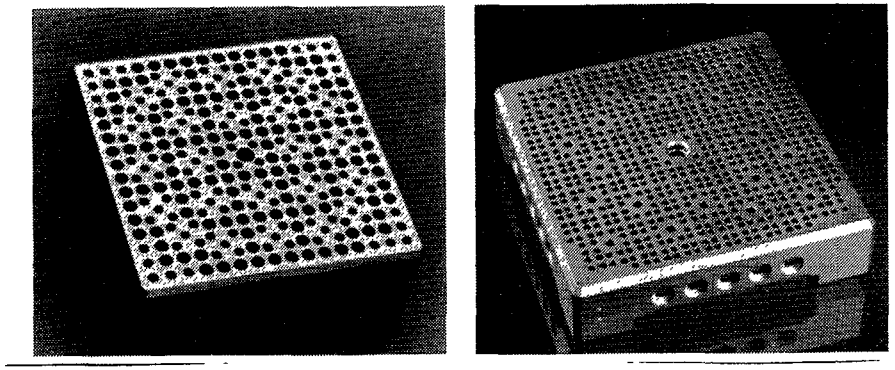

FIG. 7.Debris filter bottom nozzle.

diameter flow holes through which the coolant enters the fuel assembly. Figure 7 shows the DFBN compared to the previous bottom nozzle. The smaller flow holes limit the size of debris which can enter the assembly and prevent large, aggressive debris from coming into contact with the fuel rods. The selection of the size of the flow holes was a compromise between filter effectiveness, mechanical strength, and the hydraulic characteristics of the bottom nozzle. The Westinghouse DFBN was designed to have the same pressure drop as the previous bottom nozzle, resulting in no flow mis-matches between the two types. This allows an orderly transition to a complete core of DFBNs in operating plants as more DFBNs are brought in with each successive cycle. Testing showed that the nozzle was >90% effective in stopping debris that would pass through the previous bottom nozzle. The DFBN was introduced in 1988 and is now in operation in 44 Westinghouse-fueled plants.

The above actions to control the introduction of debris into the system and the implementation of DFBNs have significantly reduced the occurrence of debris defects. Figure 8 shows the number of debris-related leakers confirmed during on-site examinations since the early-1980s for Westinghouse-fueled plants. It is clear in Figure 8 that, although debris leakers are still present to a very small degree, the number seen at any particular plant after the initiation of industry efforts to eliminate debris (approximately 1986) has been greatly reduced. The most observed were typically in the 4 to 5 per plant range, whereas, before these efforts, it was common to see larger numbers, in one case as high as 83. The DFBNs have contributed to a further reduction in debris-induced leakers. As shown in Figure 8, over the last one to two years, the frequency of observed debris leakers has been even further reduced.

To date, four rods from DFBN assemblies have been confirmed to be leaking due to debris-induced fretting. Two of these rods were on the outside row of the assembly and were adjacent to non-DFBN assemblies. It is possible that the debris which caused these rods to leak may have come from the adjacent assembly and not through the DFBN. When this is taken into account, the leakage rate due

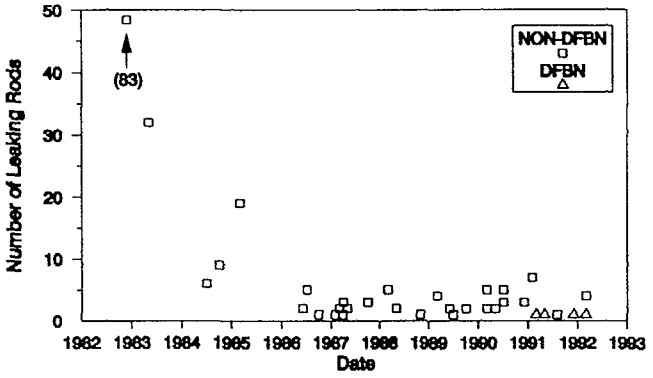

FIG. 8. Debris-related leaking rods versus time.

to debris in examined assemblies is about 7 to 8 times lower in DFBN assemblies than in non-DFBN assemblies.

5. DEBRIS CHARACTERISTICS

Evaluations of the debris wear scars show several interesting trends. When the impact of debris was first observed in the early-1980s, it was common to see very large wear scars, and occasionally multiple scars, on a single rod (Figure 4). As awareness of the adverse impact of debris increased and control measures were taken, not only has the frequency been reduced, but the size and nature of the observed defects has also changed. Typical debris scars became smaller and the frequency of multiple scars on the same rod decreased.

A large number of TV tapes showing debris-induced damage from the early-1980s to late-1989 were evaluated. The wear scars were categorized based on size (small, medium, large), shape (small hole, gouge, gross, and crescent), and whether there were multiple or single scars. Three trends were seen:

(a) The "small-hole" wear scars were not seen in the early-1980s, but became prevalent in the late-1980s.

(b) Single wear scars became dominant in the late-1980s. In the early-1980s, multiple scars were more prevalent.

(c) Greater than 95% of the debris-induced scars occurred below the bottom grid.

These observations imply that the debris which caused these scars in the late 1980s, after the efforts to minimize debris, were smaller in size than was the case in the early 1980s.

As the debris became smaller, another trend was observed. The majority of the debris-induced fretting defects were found to occur early in the fuel's operating

life. The frequencies of occurrence of debris-induced leakers found after one, two, and three cycles of operation were compared. This evaluation was performed by summarizing all cases where debris-induced fretting was found by detailed on-site examination. In order to address the specific issue of susceptibility to debris-induced fretting as a function of the number of irradiation cycles, the leaking rod data was carefully reviewed. Cases were removed from the data base where UT was performed only on part of the core. In addition, results from plants which had completed their first cycle of operation were deleted since they provide no information on the relative susceptibility of the number of cycles of operation. For the remaining cases, the number of cycles of irradiation of each confirmed leaker was tabulated. In many cases, fuel rods were first examined only after their second or third cycle of irradiation. The coolant activity history was reviewed for each of these cases to determine if the fuel rod could have been leaking in a previous cycle, was not inspected at the end of the earlier cycle(s), was reloaded for continued operation, and was tested for the first time and found leaking after its second or third cycle of operation. The specific examination results were reviewed and the number of observed debris leakers believed to be leaking in an earlier cycle and carried over into a subsequent cycle without examination (called "carryovers") was determined. The results of this evaluation is summarized in Table I. The number of rods leaking due to debris listed in Table I is the number after the "carryovers" are removed. The number of "carryover" leakers found at each plant site is also shown in parentheses in Table I.

Of all the debris-related leaking rods observed, approximately 70% were found to be in fuel that was in reactor for its first cycle of irradiation. This trend becomes even more pronounced when those leaking rods caused by the larger more aggressive debris seen in the early examinations (specifically Plant A-1 on Table I) are excluded from the evaluation. This cycle occurred in the early-1980s and involved debris that was very large and aggressive. It is reasonable to eliminate this data from the evaluation since it is not typical of what is currently observed and debris of this nature would be very effectively filtered out by the DFBN.

The above evaluation suggests that fuel rods have properties which make them become more resistant to debris damage as burnup increases. One possible reason for this is the oxide film which forms on the cladding surface as a result of corrosion during irradiation. This oxide layer is much harder than the base zircaloy and is also harder than typical debris. Therefore, it would be expected that the oxidized rods would be more resistant to debris-fretting than fuel rods early in their first cycle of irradiation which are not oxided.

6. FUTURE IMPROVEMENTS

Recent experience has shown actions taken by plant operators to minimize the introduction of debris into the system and the implementation of DFBNs has had a significant impact on reducing debris-related leakers. These actions, however, would not be expected to completely eliminate debris-related defects. The current objective throughout the world is to achieve zero defect fuel performance. In order to support this objective, Westinghouse is developing additional debris mitigation features.

Table I

Debris Obsevations vs
Number of Cycles of Operation

Plant-cycle	Number of Debris Observations 1 Cycle	2 Cycle	3 Cycle
A-1	39	27(10)	4(2)
A-2	8	0(1)	
B	18	0(8)	0(5)
C	2	0(1)	
D-1	1		
D-2	5		
E	1	2(0)	0(1)
F	2		
G	1		
H	1		
I	4	0(2)	0(1)
J		1(0)	
K	1		
L	5	0(1)	
M	1	1(0)	2(1)
N	3	2(0)	
O	1		
P	1		
Q	3	0(1)	
TOTAL	97	33(24)	6(10)
TOTAL W/O PLANT A-1	58	6(14)	2(8)

( ) - Number of carryovers

7. SUMMARY

Corrective actions have been taken to minimize the adverse impact that debris can have on fuel integrity. These actions have consisted of training personnel to minimize debris at the plant site and fuel assembly design changes. These efforts have been successful in substantially reducing the incidence of debris-related leaking rods. Additional changes are being developed to provide even further resistance to debris, so that the objective of no leaking fuel rods can be achieved at all operating plants.

EVALUATION OF DEBRIS FRETTING FAILURES AND PREVENTIVE METHODS

A. STRASSER, J. GINGOLD
The S.M. Stoller Corporation,
Pleasantville, N.Y.,
United States of America

Abstract

Metallic debris in the primary coolant has caused a significant fraction of the failures in LWRs. A review and evaluation of the failures is presented. Specific items discussed include the source of debris, the types of debris and the interaction of debris with fuel assemblies. Differences in failure histories between BWRs and PWRs are discussed. Preventive measures include improved maintenance procedures to preclude introduction of debris into the primary system and fuel assembly design features that make the fuel cladding less likely to be exposed to through-wall fretting. The improved maintenance procedure guidelines and the fuel design modifications are discussed.

1.0 INTRODUCTION

Of various mechanisms leading to failure of fuel rods in LWRs, debris is one of the most significant. Debris related failure seems to be primarily a PWR issue, although a modest, but growing, number of failed rods in several BWRs have been attributed to debris. In order to mitigate the debris problem, utilities have developed programs to identify and eliminate the sources of debris, and fuel vendors are now offering "debris-resistant" fuel designs.

This paper describes typical debris failures, the debris related failure rates, the source of the debris and methods of debris failure prevention.

2.0 STATISTICS OF DEBRIS FAILURE AND SURVEY OF EXPERIENCE

The overwhelming majority of debris failures have occurred in PWRs. The number of BWR debris failures has been limited, but appears to be increasing.

There is no single definitive reason for this, although the principal factor may be the difference in the velocity of the coolant flow in the two types of reactors. In BWRs, the coolant velocity at the single phase inlet to the core is on the order of about 2.1 m/sec at full rated flow. In PWRs, on the other hand, the flow velocity can range between about 3.5 and 5 m/sec depending upon the specific reactor design.

The higher flow velocity in the PWR is capable of supporting larger pieces of debris and carrying them into the core. A piece of debris which might sink to the bottom of a BWR reactor vessel and remain there during operation might be carried along by the higher velocity of the PWR coolant, become lodged in the grid of a fuel assembly and cause a failure. The size and weight of the debris which can be carried by the BWR coolant flow may be such that most of it is likely to pass through the core without doing any damage.

Other factors which may contribute to the lower debris failure rate in BWRs include the presence of the control rod guides underneath the core which can act as a filter for debris. The annular downcomer region around some BWR cores may also provide an opportunity for debris in the coolant to be deposited without entering the core.

Although a number of debris failures have been observed at the upper elevations of the PWR fuel rods, the vast majority of such failures, over 90%, occur at or below the bottom grid of the affected fuel assembly. This is due to the mechanisms by which most debris failures occur.

Based upon the experience to date, it appears that the great majority of the debris which enters a fuel assembly will either become lodged in the bottom grid spacer or it will pass through the fuel assembly without doing significant damage. Once the debris has been trapped by the grid, it frets against the fuel rod (or, perhaps, more than one fuel rod) until the clad is penetrated.

The elevation of fretting failures in BWR assemblies does not follow the PWR trend, and the failures have been found at various elevations over the axial lengths of the fuel rods. This would support the theory that only small pieces of debris will be carried into the BWR cores and these can pass through the larger flow areas available in a BWR assembly.

A higher incidence of debris failures has been found in the outer rows of PWR fuel rods than in the center of the PWR fuel assembly. This may be due to the flow patterns as the coolant enters the assembly or to the cycling of the flow. As the core flow decreases, debris may settle on the lower end fitting. As flow increases, there is a chance that the debris will work its way toward the outside of the assembly. As the flow cycles, the debris moves toward the intra-assembly gap. Thus, failures are found in the two peripheral rows of rods.

In some instances, the debris failures tended to be close to the corner of the assembly. This has been explained by an eddy in the flow pattern caused by the feet on the lower end fitting.

Debris failures can be identified visually with reasonable certainty, and as a result the debris failure statistics are quite reliable.

The number of identified debris failures in US and European LWRs during the past, approximately 10 years, is shown in Table I.

The largest debris failure incident in the past 10 years occurred with stainless steel clad fuel in the Connecticut Yankee reactor, where over 400 failed rods were identified in one cycle due to debris fretting. This is not included in the table since it would distort the Zircaloy clad fuel failure statistics significantly.

The figures indicate that debris is a significant contributor to the overall fuel failure rate and that PWRs are more prone to debris failures.

TABLE I. DEBRIS FAILURES IN PAST ~ 10 YEARS
NUMBER OF FAILED ZIRCALOY RODS (% OF IDENTIFIED FAILURES)

	BWR	PWR
ABB	30 (90%)	4 (80%)
CE	-	41 (85%)
FGA	-	13 (72%)
GE,	2 (1%)	
SNP (ANF)	5 (42%)	49 (39%)
W	-	47 (58%)
BWFC	-	32 (25%)
TOTAL	37	186

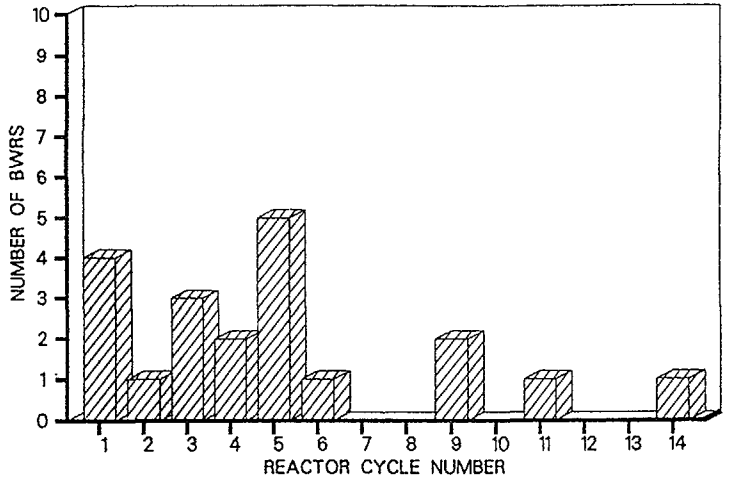

Figure 1: NUMBER OF BWRs vs. THEIR CYCLE NUMBER IN WHICH DEBRIS FAILURES OCCURRED

The number of debris failures as a function of the total failures has increased as a function of time, as other failure causes are remedied and as the sources of some of the debris, primary system maintenance and equipment wear out, increase.

The time at which debris failures occur in the life of the plant is shown on Figure 1 for BWRs and Figure 2 for PWRs. In the case of the BWRs the distribution is clearly skewed to the first cycle of the plant, and the incidents were most likely related to the construction of the plant. The data for PWRs do not show a specific trend. The decreased number of debris failures beyond Cycle 10 is more a function of the decreased number of reactors that have reached that age.

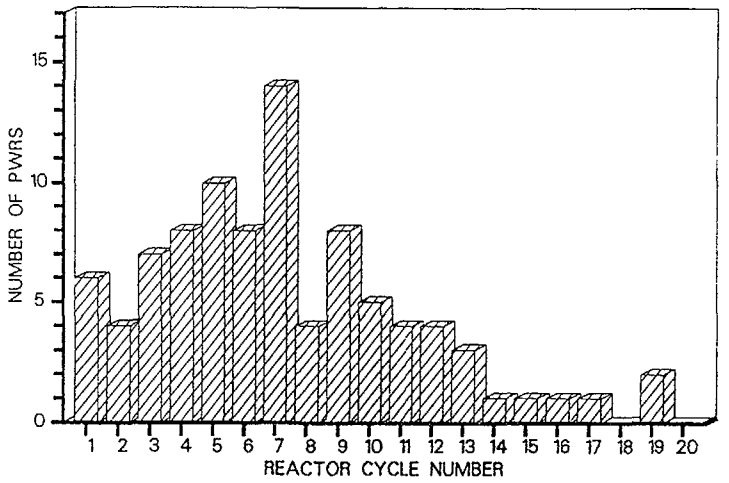

Figure 2: NUMBER OF PWRs vs. THEIR CYCLE NUMBER IN WHICH DEBRIS FAILURES OCCURRED

The relationship between the fuel exposure, i.e. number of cycles in-core, versus the time of debris failure has been examined also. Westinghouse has reported that the preponderance of the debris failures occur in the first operating cycle of the fuel; however, the experience of Fragema and Siemens do not support this trend. The reason for the higher failure rate in first cycle fuel is not known, but it has been suggested that the lack of a wear resistant ZrO_2 film on the cladding early in life, makes new fuel assemblies more susceptible to debris failures.

Perhaps the most consistent trend has been the location of the debris fretting failures at or below the first spacer on the bottom of PWR fuel assemblies. The small flow area spacer serves as a debris trap in PWRs. This has given clear directions to the designers of debris resistant fuel assemblies which are discussed later.

3.0 VISUAL APPEARANCE OF DEBRIS FRETTING FAILURES

Visual failure characteristics identified during poolside examinations can be used to differentiate debris failure from other types of fuel failure. The most striking feature is the presence of wear scars (or wear holes) in the cladding, of the type shown in Figures 3 and 4. The specific characteristics of these scars are that they are usually clean and show evidence of wear. The vibration of small, hard particles by flow-induced vibration, result in abrasion through the clad that is visibly detectable.

Secondary failure indications include secondary hydriding (blisters and failed end cap welds) or in the case of BWRs in secondary PCI splits.

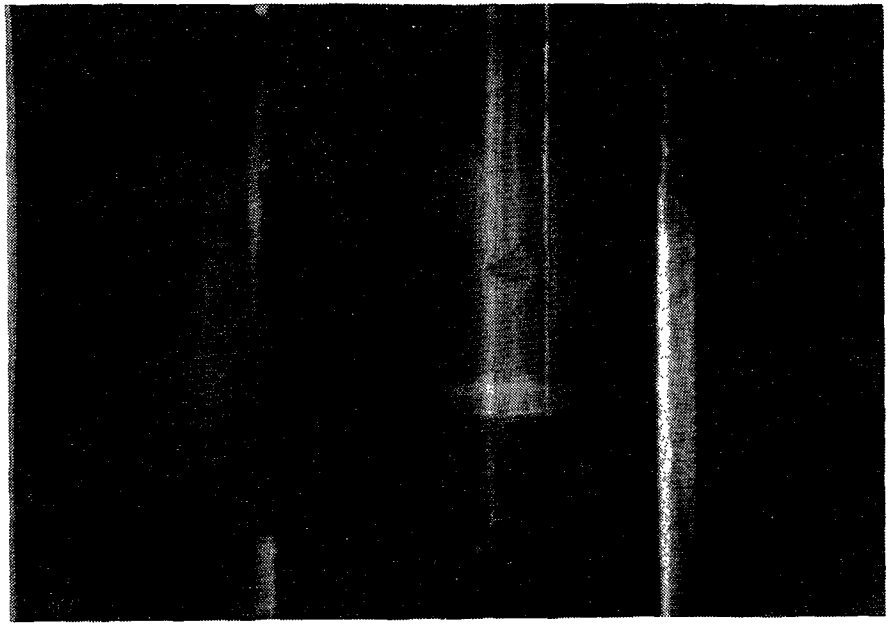

Figure 3: FRETTING FAILURES NEAR A BOTTOM END PLUG

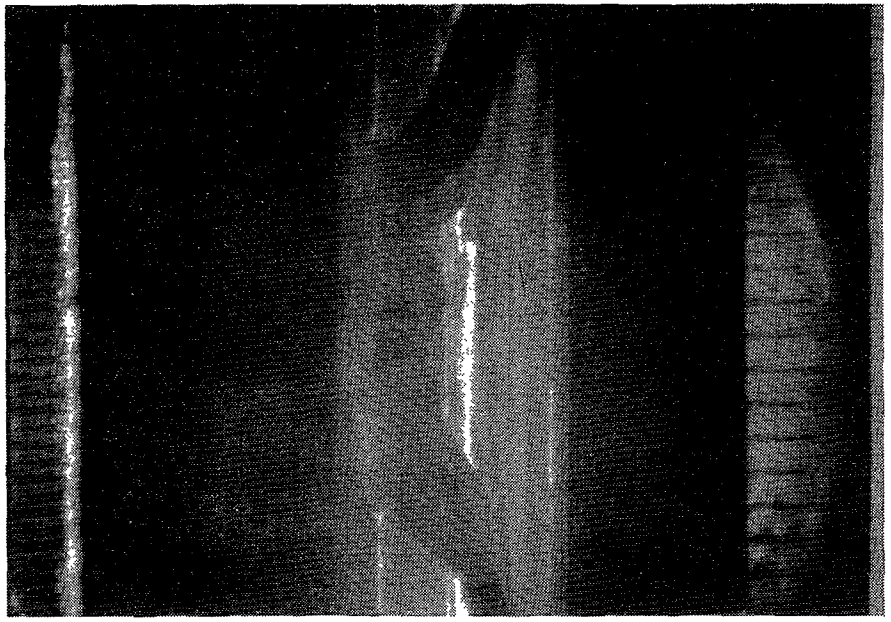

Figure 4: SEVERE FRETTING FAILURE

The debris that caused the fretting is, in most cases, no longer present at the failure location when the inspection is performed. Conversely, debris can be found in and around the assembly during poolside examination, which can not necessarily be associated with a specific failure.

4.0 DEBRIS SOURCES

4.1 INTRODUCTION

As noted before, observation of the actual piece of debris that caused clad fretting is the exception rather than the rule, since the debris can be moved from its position by the force of the coolant flow or drop from its position on shutdown.

Some debris is observed at fretting locations however, and a significant amount of debris has been collected during cleanup of the fuel assemblies and the reactor vessel. The debris identified away from fretting locations during core visual examinations or core cleanup may not have caused any fuel rod fretting, but does have a potential to do so.

Most debris found in reactors and fuel was from one or more of the following sources:

- primary system components
- fuel burnable absorber or control rod components
- primary system maintenance
- tools and equipment used within the containment

A review of these sources is most useful in implementing preventive actions.

4.2 PRIMARY SYSTEM COMPONENTS

Pieces of a variety of primary system components have been found in the primary system and in individual fuel assemblies. They have included:

- Wires from screens (new BWR components)
- Shavings from reactor coolant pump wearing ring
- Pieces from broken coolant pump shaft
- Failed nuts and bolts from thermal shields
- Stellite fragments (probably from valve seat)
- Metal tags from new components installed in the system
- Steam generator seal plugs
- Pieces from steam generator flow dividers

4 3 CORE COMPONENTS

Debris from fuel assemblies can develop due to handling, such as torn spacer straps or due to failures of the components Examples are

- Fragments of spacer grids broken during handling
- Fuel assembly or control rod nuts, bolts, or clamps failed due to IASCC
- Broken absorber rods
- Fuel rod end plugs

4 4 PRIMARY SYSTEM MAINTENANCE

As the plant ages increase, the required amount and degree of primary system maintenance increases as well The maintenance operations create debris and this has been the cause of the majority of the debris failures to date

The maintenance operations that have resulted in the greatest damage have come from machining operations that produce metal shavings during

- Replacement of steam generators
- Removal of thermal shields in PWRs
- Repair and replacement of spray headers in BWRs
- Repair and replacement of reactor coolant pumps

The actual debris identified, in addition to metal shavings, chips and filings has included

- Pieces of lock wire and other wires
- Pieces of welding rods
- Sawblades
- Parts of gaskets
- Pieces of nuts and bolts that were being removed

4 5 TOOLS AND EQUIPMENT USED WITHIN THE CONTAINMENT

The examples of debris found in this category represent the widest and most surprising array of items

- Eddy current test coils
- Ultrasonic test sensors
- Dosimeter
- Parts of pens and pencils
- Parts of tools
- Steel wool
- Keys
- Glass fragments from containment light bulbs
- Paint chips from containment walls

5 0 DEBRIS PREVENTION

The best way to prevent debris related failures is, obviously, to keep debris out of the primary system during operation First, to prevent debris from entering the system to begin with and, then, to remove whatever debris has unavoidably entered the system Over the past several years, utilities around the world have developed and refined their maintenance procedures to achieve these goals While each utility s program is unique in some of its aspects, there are certain principles which are common to almost all of them

There are three components to such a program,

1 Preventive maintenance on debris producing components
2 Improved maintenance and operating procedures that do not produce debris or reduce the quantity produced
3 Debris cleanup programs

The preventive maintenance should include the following steps,

- Worn equipment and components should be evaluated for their potential to produce debris, and preventive maintenance procedures instituted
- Fuel and control element handling procedures should be improved if they produce debris
- A debris identification program, visual and sampling for chemical analysis, should be established to identify debris sources directly and assist in their elimination

The improved maintenance procedure program should include the following elements

- A debris awareness training program should be implemented among the plant staff and workers responsible for maintenance work and other operations around the plant.
- An attempt should be made to maintain a stable staff for maintenance so that the benefits of accumulated experience can be taken advantage of
- Operating instructions should be developed for routine and special maintenance procedures that may cause debris, including,
  - Control and limit materials and tools brought to the work area.
  - Identify and control activities in sensitive areas, such as the fuel pool, reactor cavity, primary piping and system components, steam generators
  - Install covers, seals, etc over cavities and openings to keep debris out
    Implement appropriate work and cleanup procedures
- A maintenance debris inspection and cleanup program should be established

Some primary system maintenance procedures result in debris which may enter the system despite the best efforts of the maintenance workers Some debris results from failures of primary system components during operation and cannot be avoided Consequently, techniques have been developed to remove debris from the system

There have ben significant improvements in recent years to the equipment available for cleaning primary systems In addition to vacuuming devices operated directly from outside the reactor vessel, small remotely controlled vehicles have been developed These devices contain both television cameras and vacuuming or other debris removal devices and can gain access to portions of the reactors vessel which could not be reached with earlier equipment. Some such vehicles can also be used to inspect and clean primary system piping

The cleanup and debris prevention programs should consider all systems connected to the primary piping, including the spent fuel pool, where debris could hide out or be generated, and eventually work itself into the primary coolant

6 0 DEBRIS RESISTANT FUEL DESIGN FEATURES

6 1 INTRODUCTION

The increasing concern over debris related failures over the past decade has led essentially all of the PWR fuel vendors to develop fuel assembly design features which either prevent debris from entering the fuel assembly or prevent fuel rod failure if debris should find its way into the assembly Some of the BWR vendors have just started to offer specially designed debris resistant features as commercial products

There are three general approaches which have been used to prevent debris failures, including

- Longer solid lower end plugs
- Debris resistant lower spacer grids
- Modified lower end fittings

6 2 LONG LOWER END PLUGS

The vast majority of fuel failures due to debris have been located at the bottom of the fuel rod, between the end plug and the lower grid To combat this type of failure, several vendors offer fuel assemblies with a longer lower end plug, one which extends up into the bottom grid In this design, debris which becomes lodged in the bottom grid will fret against the solid end plug and will not damage or penetrate the active portion of the fuel cladding

Using a longer end plug requires some compromises in the balance of the fuel rod design Since the overall length of the rod cannot normally be increased, the extra end plug length must be accommodated by either reducing the volume of the fission gas plenum or reducing the length of the fuel pellet stack

The former case affects the end of life internal rod pressure which is a licensing limit when high exposures are desired Decreasing the length of the pellet stack, which is the method usually employed, will raise the linear heat generation rate and the temperature of the rod somewhat Some of the void volume has been regained by the use of low volume holddown springs, and hollow, thick walled end plugs

6 3 DEBRIS RESISTANT LOWER SPACER GRID

The debris resistant lower spacer grid is designed to prevent debris from entering the active part of the fuel assembly Assemblies containing these grids may also employ longer end plugs and the grids themselves are usually positioned closer to the lower end fitting than a conventional lower spacer grid A typical design is shown in Figure 5

These grids are designed so that the intersections of the grid straps are strategically located over the flow holes in the lower end fittings Additional structural components are added which project into the flow path The result is a component whose capability of acting as a strainer or filter of debris is significantly enhanced as compared to a standard grid

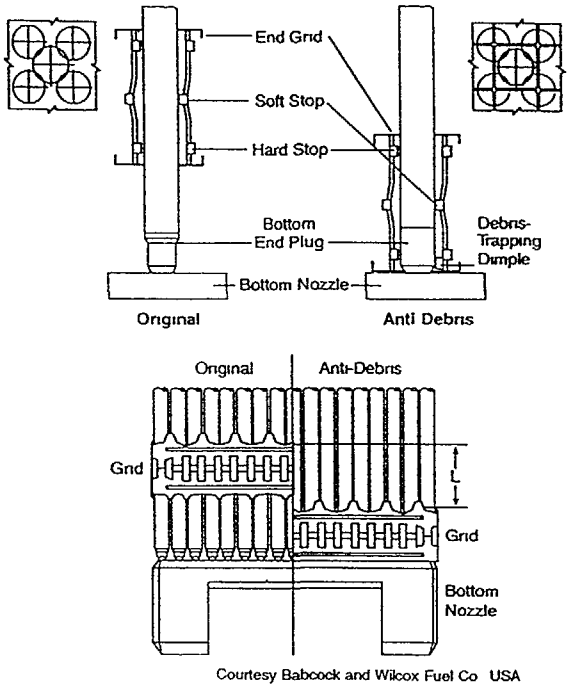

Figure 5 ANTI DEBRIS FUEL ASSEMBLY BOTTOM END GRID

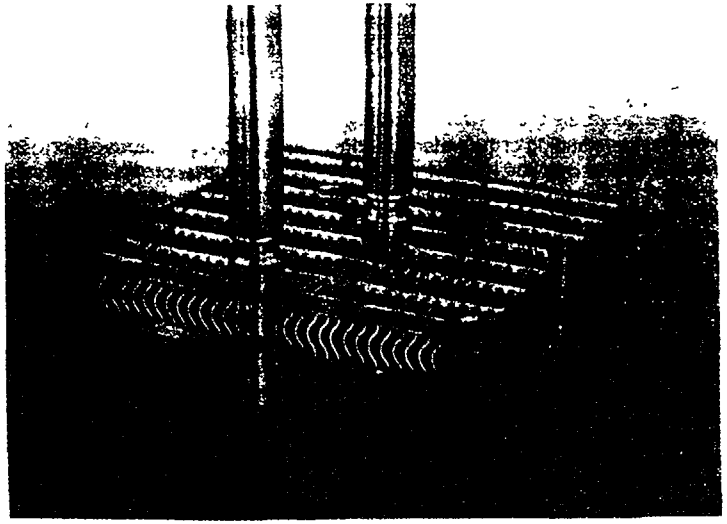

Courtesy of Siemens Nuclear Power Co., USA

Figure 6: DEBRIS FILTER BOTTOM END FITTING

Any debris which is trapped by the debris resistant grid will only fret against the end plug. The design is such that the probability of the debris passing through the grid into the active portion of the assembly is quite low.

6.4 MODIFIED LOWER END FITTINGS

PWR

The lower end fittings have been modified to screen out debris. Each vendor's design is somewhat different. Typical designs are:

- Decreased flow hole sizes in the lower plate (Westinghouse) (B&W Fuel Company)
- Screen added to lower plate (Fragema)
- Curved plate traps (Siemens Nuclear Power)

Figure 6 and 7 show some of these designs.

The challenge which faced the designers of debris resistant end fittings was that the smaller flow holes, screens and narrow channels tend to result in a greater pressure drop than conventional end fittings. However, the vendors offering each of these debris resistant features claim that the new designs are such that their pressure drop is essentially the same

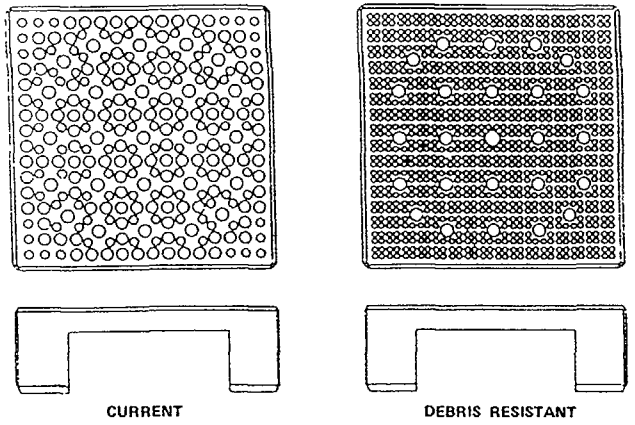

Courtesy Babcock and Wilcox Fuel Co , USA

Figure 7. DEBRIS FILTER BOTTOM NOZZLE

as in a conventional component. A large number of fuel assemblies containing this feature have been operated successfully.

BWR

The SNP curved plate design developed for PWRs and shown in Figure 6 has been adapted and is being offered for BWRs.

The lower tie plates of General Electric and ABBA fuel assemblies have been modified recently to increase their pressure drop for improved hydraulic stability. In the process, the flow hole size has been reduced improving the debris filtering capability as well.

6.5 DEBRIS RESISTANT DESIGN EFFECTIVENESS

To date, only partial core loadings of debris resistant design are in operation, and it is somewhat early to judge the effectiveness of the designs. Their performance will be monitored with great interest to determine how well they fulfill their intended function.

MANAGEMENT OF FAILED FUEL

(Session IV)

Chairmen

P. BOURNAY
France

R. VON JAN
Germany

MANAGEMENT OF FAILED FUEL DURING OPERATION: FRENCH POLICY AND EXPERIENCE

P. BOURNAY
Service de la production thermique,
Electricité de France,
Paris – La Défense, France

Abstract

Since more than 10 years, with the French safety Authorities agreement, EDF apply a policy consisting in re-insertion of the leaking assemblies which meet some convenient criteria.

During the shutdown period :
- leaky assemblies are identified on line with an in-mast sipping system,
- the equivalent diameter of defects is measured by "quantitative sipping test",
- the accepted assemblies according to our criteria are immédiately re-inserted. The rejected ones remain in spent fuel pool for futher repair or shipping for reprocessing.

Our criteria are the following :
- equivalent diameter less than 35 μm,
- no solid fission products in liquid sample during sipping test,
- impact of reloaded leaky assemblies, on the coming BOC activity level in D.E. I.131 less than 1,1 GBq/t.

In that conditions, we succeed to reach our main goal : no significant release of UO2 in the coolant due to leaking assemblies re-insertion.

Our experience feed back is the following :
- acceptable stability of equivalent diameter for the reloaded defects,
- no important activity evolution attributable to the re-inserted leaky assemblies,
- compatibility of this policy with the present scenarios of defects occurence and evolution in operation.

This policy induces significant time and money saving. It does not impact the units availability. It supposes convenient on-line means. It is compatible with safety requirements.

1) INTRODUCTION

As most of the utilities in the world, EDF adopted many years ago, a "zero defect" policy, in order to reach the objective of "no defect occurence in operation". This policy recommends conditions, actions, precautions to be taken in the different stages from design, manufacturing checking, handling, to operational limits.

At this point, EDF didn't choose a policy of "zero activity level in operation". Since 1981, with the French Safety authorities agreement, EDF re-insert leaking assemblies which meet some convenient criteria, trying to find the good balance between safety requirements and economical objectives.

In a safety point of view, as a result of our negociations with our safety authorities, the French technical specifications on the coolant activities levels, were lowered compared with the previous WESTINGHOUSE ones, as a counterpart of the re-insertion agreement.

In a technical and economical point of view, the benefits are time and money saving (no extra cost on the fuel, limited modifications of the refueling pattern, no impact on the critical path of the outage). But the "cost" is the acceptance that a reasonable but significant level of coolant activity could be invested in the possibility of re-insertion.

Nevertheless, the technical key point of our policy is the validy of our criteria in order to avoid the re-insertion of leaking assemblies which could release significant amount of UO2 through their defects, in the coming cycle.

By another way, the rejected leaking assemblies are repaired off shutdown periods.

2) CONDITIONS FOR RE-INSERTION

The first point to be determined is the capability of each reloadable leaky assembly to meet our main goal : no significant release of UO2 in the following cycle.

The corresponding criterion is based on the value of the equivalent diameter of the defect measured in what we call "quantitative sipping test". Physicaly, the equivalent diameter is the diameter of an hypothetic cylindrical hole through the cladding, which would allow the same dynamic release of the fission gases out of the defective rod, after a temperature step in the sipping cell. The fuel pool of each of our units is equiped with an adequate sipping cell to perform this measurement during the outage.

As a result of our experience, we don't identified any significant dissemination if the equivalent diameter of re-inserted defects is less than 35 μm.

More recently, we began to introduce a complementary condition to this first criterion : the absence of significant amount of solid fission products in the liquid sample taken during sipping test. The release of solid fission products in these conditions, could be an indication of the dissemination ability in operation.

The second point is to limit the impact of the re-inserted assemblies on the coolant activity level at a reasonable value. The corresponding criterion is DE I 131 less than 1,1 GBq/t (30 mCi/t), that is about 15 % of the specified limit for shutdown. The consequence is the possible limitation of the total number of leaking assemblies to be re-inserted. In that case, the re-insertion of some of them could be delayed.

3) MORE DETAILS ABOUT OUR PROCEDURES FOR RE-INSERTION

The implementation of our policy for inspection and re-insertion required convenient means and methods (Diagram 1).

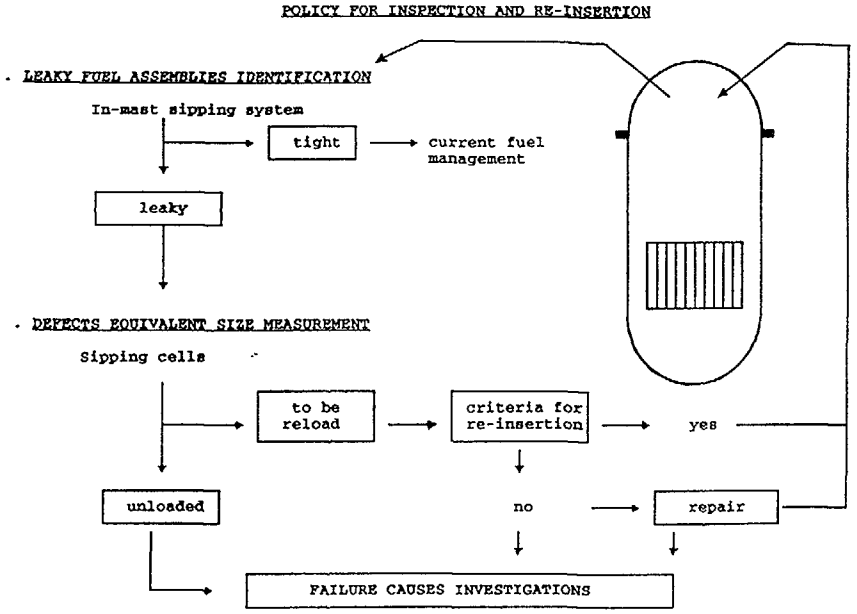

Diagram 1. Management of leaky fuel assemblies.

The leaky fuel assemblies identification was previously performed in the sipping cells in the spent fuel pool. This method was time consumming on the critical path. So, we developped, in cooperation with CEA an on-line monitoring system for fuel assembly integrity testing inside the handling machine mast (only two minutes per assembly on the critical path). This test allows a quick and reliable classification between the tight assemblies which follows the forecast management and the leaky ones.

In order to apply our criteria, the leaky assemblies are transfered to the sipping cells for equivalent size measurement of their defects. Those which are definitely unloaded, and those rejected according to our criteria remain available in spent fuel pool, for further failure cause investigation or repair. Those which meet our criteria are immediately re-inserted after a possible reloading pattern adjustment.

Besides, we have to mention the interest of a cladding integrity evaluation from the activities analysis in operation. It allows a prediction (number, severity position of defects) of what could be found at the time of investigations during the following outage. It allows a possible anticipation of necessary arrangements in case of predicted difficulties.

4) RE-INSERTED DEFECTS BEHAVIOUR

4.1 - Equivalent diameter evolution

One way to investigate the re-inserted assembly behaviour is the analysis of the successive results of the equivalent diameter measurements at each outages.

Our present experience concerns about 120 leaky re-inserted assemblies. Among them, 57 were re-inserted two times and 8 three times. Our conclusions are the following :

- no equivalent diameter change for 34 assemblies,
- increase for 23 assemblies,
- 11 among them reached the current criterion of 35 μm,
- two of them caused a slight UO2 release and were the origin of our recent criteria evolution.

4.2 - Activity evolution in operation

A second way is the analysis of the activity evolution along the cycles following a re-insertion. As a result, we didn't identify any important activity evolutions due to the re-inserted assemblies.

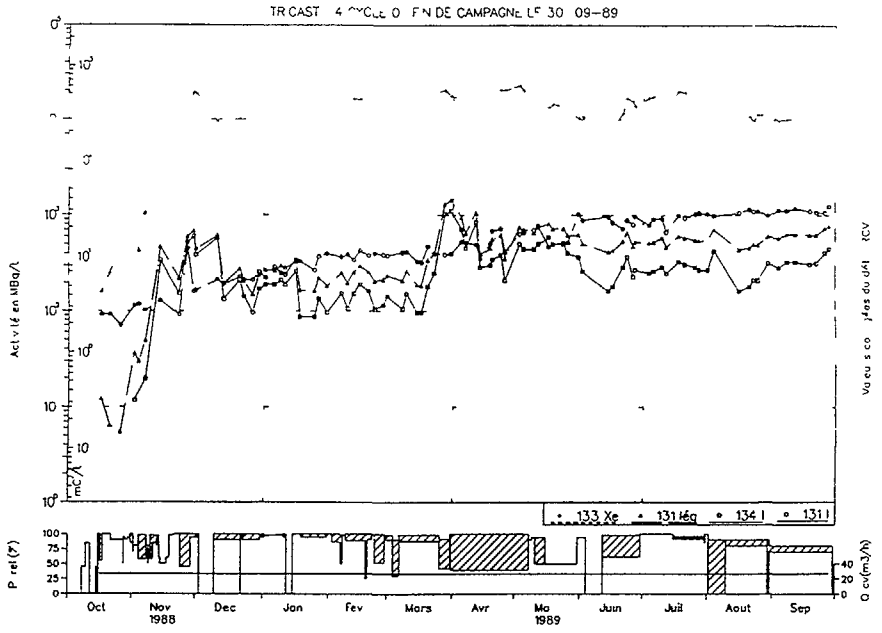

Diagram 2

We can give and comment an exemple of successive re-insertions we performed in TRICASTIN unit 4, from cycle 7 to cycle 9.

One month after the beginning of cycle 7 (Novembre 1988) a significant increase of activity occured (diagram 2). An other step on the iodines can be noticed on march 1989. I 134 activity level slowly but continuously increased all along the cycle, due to a slight release of UO2. The E.O.C. activities were lowered by coastdown period of operation.

During the outage, the on-line sipping test in the handling machine mast identified 8 failed fuel assemblies. Diagram 3 gives their positions in the core and the results of the quantitative sipping test. Assemblies A and B reached their nominal burnup. Assembly F was out of criteria. The five others were reinserted.

All along cycle 8, the activities levels remains globaly constant (diagram 4). The activity level in iodines at the BOC 8 are lower than at EOC 7 due to the unloading of

N OF ASS	END OF CYCLE 7		END OF CYCLE 8		END OF CYCLE 9
	eq diam (µm)		eq diam (µm)		
A	30	N R			
B	15/20	N R–			
C	15/20	R	20/25	R	N R
D	15/20	R		N R	
E	15	R	15/20	R	N R
F	> 35	O C			
G	15/20	R	20/25	R	N R
H	15/20	R	15/20	R	N R

N R Normaly rejected R re-inserted O C out of criteria

Diagram 3 Management of eight leaking assemblies identified at the end of cycle 7 (1989)

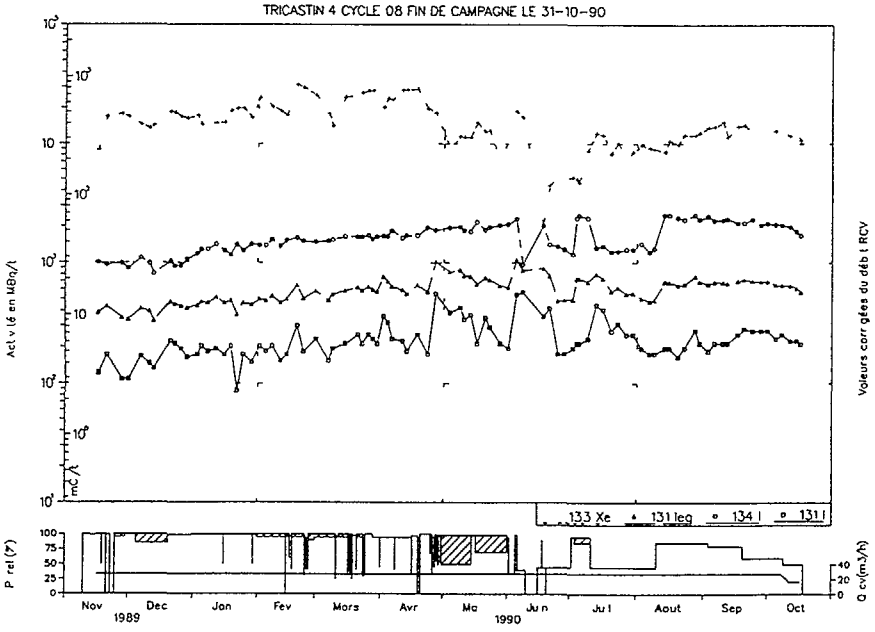

Diagram 4

the 3 leaky assemblies. Our second criterion DE I 131 < 30 mCi/t was respected. A slight increase of iodines can be noticed as a result of the activity contribution of UO2 deposit from the release of the previous cycle.

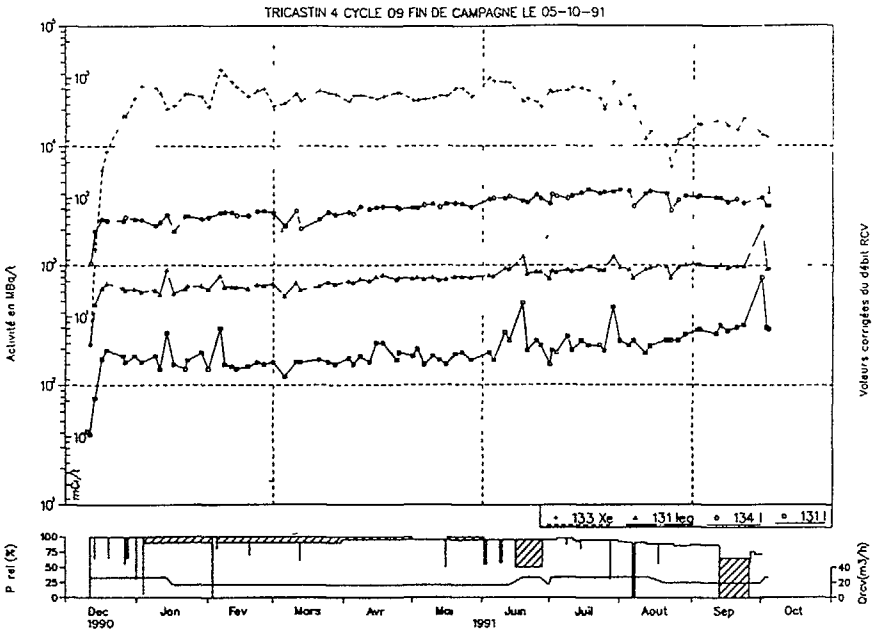

Diagram 5

At the following outage, D assembly reached his final burnup. The quantitative sipping test results showed stability or a slight increase of the equivalent diameter. The four assemblies were re-inserted for the second time.

During cycle 9 the activities remained globaly constant and far below our specified limits (Diagram 5).

4.3 - Compatibility between our policy and physical behaviour of defects in operation

A third way to know the re-inserted defects behaviour could be the leaky rods examination after each new cycle. But, for units availability reasons, it is impossible to plan the necessary investigations out of the critical path of the shutdown period.

Nevertheless, the possible scenarios for cladding failure occurence and evolution, are relatively well known. The worldwide most frequent one in PWRs, is an initial perforation of the cladding (wear by debris generally located under the lower spacer grid - fretting corrosion by grid/cladding interaction) and an optional secondary defects occurence (hydriding of the cladding) with possible UO2 release in the coolant. The secondary hydriding speed depends on two mains parameters : temperature of the cladding, related to the local linear power of the rod, and gap closure at the moment of the first perforation, related to the rod burnup. As a result of both activities evolutions analysis in operation and poolside or Hot Laboratories investigations, we observed a quick evolution when the initial perforation occured in the first cycle of the rod.

In this context, our re-insertion policy always induced the rejection of the defects which could release a significant amount of UO2. We never observed important evolution in operation, in terms of activity evolution or UO2 release, with re-inserted assembly meeting our criteria.

5) STATUS AFTER 10 YEARS OF EXPERIENCE

5.1 - Statistical results

Diagram 6 gives, at the end of 1991, the total number of leaking assemblies versus the cycle number of defects occurence. It also gives the distribution of those assemblies as a result of decisions during the outage following the defects occurence (reloaded - normaly rejected or delayed reloading).

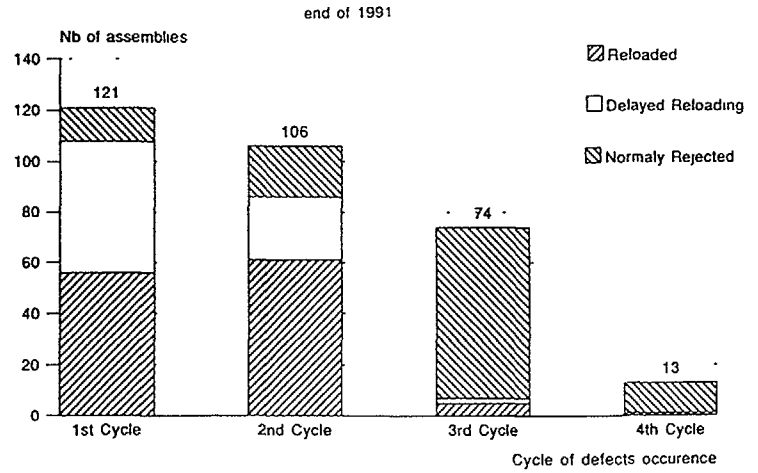

Diagram 6. Leaking assemblies management 900 MWe and 1300 MWe (314 assemblies)

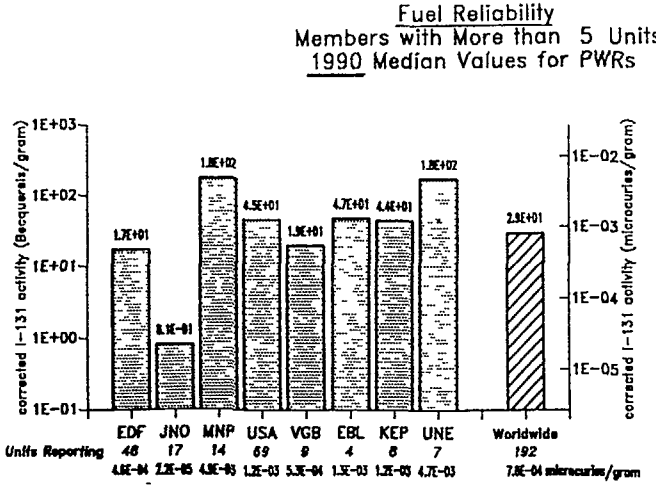

Diagram 7. WANO performance indicators

Among a total of 200 leaky assemblies to be reloaded, 120 of them were immediately re-inserted (60 %). The fuel saving corresponds to the available energy stored in about 60 fresh fuel assemblies (more than a batch).

5.2 - Impact on the activity levels in operation

Diagram 8 gives the distribution of the end of cycle activities for DE I 131 and sum of gases. In spite of our leaking fuel reloading policy which induces a part of the measured activity, the mean levels remained far from our specified limits.

Diagram 7 gives the 1990 values of the fuel reliability WANO indicator for members with more than 5 units. In spite of its re-insertion policy, the EDF level is lower than most of the others.

6) CONCLUSION

After more than 10 years of operating experience with our re-insertion policy, we can say that in all cases, we reached our main goal : no significant UO2 release during cycles with re-inserted leaking fuel assemblies.

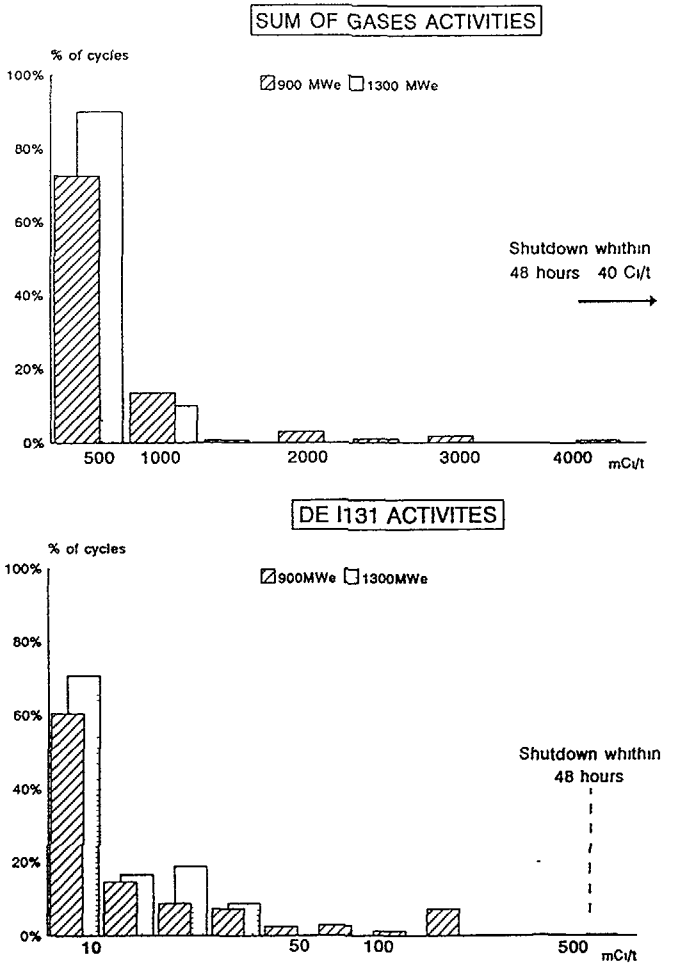

Diagram 8. End of cycles activities distributions for the 320 completed cycles (end of 1991) (272 cycles 900 MWe and 48 cycles 1300 MWe).

Up to now, the scenarios of defects occurence and evolution we experimented in operation, are compatible with our policy.

But we need more experience to completely confirm its validity, essentially in the field of high burnup and long times of residence.

FEATURES OF OPERATING A VVER REACTOR CORE CONTAINING LEAKING FUEL RODS

V.P. VELYUKHANOV, L.M. VORONIN, A.G. IOLTUKHOVSKIJ, A.I. KANATOV, V.K. CHISTYAKOVA
Research Institute for Nuclear Power Plant Operation, Moscow, Russian Federation

Abstract

The paper addresses criteria of performing in-service inspection of the leaking fuel rods (FR) of VVER-type reactors including assessment of the limiting content of iodine radionuclides in the primary circuit.

Experience of operating fuel assemblies, assessment of fuel assembly (FA) reliability indicators and dinamics of the primary coolant activity change during normal core charging have been summarized in the paper.

During the whole period of VVER reactors operation no unplanned reactor shutdown on exceeding the limiting coolant activity level has been reported. However, there were cases involving unscheduled fuel assembly withdrawal on a failure detected during reactor planned preventive maintenance outage.

Experience of operating reactor core containing leaking fuel assemblies as well as after-burning use of the leaking fuel assemblies is described in the paper.

The paper presents statistics on leaking fuel assemblies for VVER-1000 reactors during the whole operation period and dynamics of the primary coolant activity change during reactor campaign.

A number of examples involving operation of leaking fuel assemblies at the soviet NPPs are considered.

The authors discuss possible causes of cladding leakage, namely, violation of the technical specification (for example, as to power increase rate) inhomogeneity of power density distribution, overheating of fuel rods as a result of deposits on the spacer grid etc.

1. Criteria of FA depressurization estimate during the reactor operation.

In accordance with "Nuclear Safety Rules for NPPs" only < 0.2% of the fuel elements with the "gas leaks" and < 0.02% of the leaking rods with "pellet-water interaction" are permitted. Here the primary coolant activity should not exceed 1.5 x E-2 Ci/kg as to J isotopes. However, the first critical level (current level of the operational safety for VVER type reactors) is significantly lower, i.e. 1.0 x E-3 Ci/kg. Activity level is determined from the cleaning water flowrate of 30 t/h and 20 t/h for VVER-1000 and VVER-440 respectively. On exceeding the 2nd level a unit has to be shut down.

Inspections of fuel integrity (IFI) for the VVER type reactors are performed both in service and after reactor shutdown. In-service IFI are performed by measuring the total iodine radionuclides activity. Measurement of the coolant isotopic composition is performed on a weekly basis. On reaching the total iodine isotope activity of 1.E-3 Ci/kg analysis of the isotopic composition has to be performed on the dayly basis.

After reactor shutdown all the withdrawn FA, and on the primary coolant reaching 1.E-3 Ci/kg J activity level all the FA left for after-burning use, undergo IFI.

For the VVER-type reactors IFI are performed using container which is placed into the cooling pond. This method involves measurement of the fission products released from the leaking rods by analysing activity of J-131, Cs-134 and Cs-137 in water samples,based on the results of activity measurements for all the withdrawn assemblies analysis of the statistical distribution of radionuclides. FA are considered leaking if J-131 activity during IFI exceeds the mean square deviation three times. FA for which J -131 activity in the IFI container amounts to more than 1.E-4 Ci/kg are considered failured and have to be withdrawn from the reactor. The rest leaking FA can be kept on operating.

Presently IFI have been performed for 4000 fuel assemblies at 16 VVER-1000 power units. 119 FA were considered leaking, that is 0.009% of FR unloaded from the reactor. Two FA were recognized failed. Most leaking FA were unloaded from VVER-1000 reactors according to the schedule.

Activity level in the primary circuit of VVER-1000 reactors is rather low (does not exceed safety operation limits), i.e. in the range of 1xE-6 - 3. x E-4 Ci/kg and is tending to decline.

From VVER-440 reactors having been operated in the Commonwealth and Eastern Europe countries (32 units) 40000 spent

fuel assemblies have been unloaded. About 0.005 - 0.010% of them are the leaking fuel rods.

Consider the main causes of fuel leakage, severity of possible leakage and its impact on reactor operation

2. Main causes of the VVER reactor fuel leakage.

2.1. Design and process deficiencies of fuel rods and assemblies.

These causes mostly relate to VVER-440 FRs and FAs and to the first stage of operating this reactor type (1970s). One of the mentioned causes of fuel rod cladding cracking during operation is zirconium alloy hydrogenation from inside as a result of fuel pellets high humidity. Nowadays this cause is eliminated as a result of improved technology of fuel production. In some cases cracking cladding was the result of fretting-corrosion, caused by defects in spacer grids. Defects were observed as a result of the wrong mould of a fuel column (fuel pellet insertion with different fuel enrichment). All these deficiencies were eliminated and they had not been observed during VVER-1000 FA operation.

2.2. Latent process defects.

Transition to flow-line automatized production of fuel rods and assemblies of the type, in principle, has a potential for ommitting the latent defects in FR cladding (inclusions, cracks) or weldments. However, experience of VVER fuel operation points to extremely limited number of FA with such defects.

2.3. Power bursts.

More severe regimes for FR are those, accompanied by power bursts. Inspite of high plasticity of Zr-1%Nb alloy after high fluence (δ=15% after F=1.E22 N/cm2), fuel rods sensitivity to transients of operation is caused by zirconium alloys inclination to brittle corrosion cracking in the presence of cracking stresses in corrosive medium (in this case it is the products of uranium dioxide fission - iodine, cesium, tellurium etc.). Without taking special measures, cladding damage may occur in case of singal effect of transient. These may include loop connection, power restoration after extended operation at reduced power level.

The danger of such regimes can be illustrated by the experience of operation of VVER-1000 reactor at Novovoronezh NPP, 5 Unit. Thus, in 1985, the reactor power increase after the connection of an out of service turbine, was done with high speed. As a result of that, cladding internal stresses reached corrosion cracking limit, and fuel rods of four fuel assemblies developed leaks. It can be judged by iodine-131 isotope activity build-up from 7.3 x E-8 Ci/kg up to 2.3 x E-5 Ci/kg in the primary water. Inspection of one of the leaky FA in protective cells (hot cells) of NIIAR Institute revealed the depressurization of one of the fuel rods. Similar power burst may occur during a loop connection to the three operating loops. As a result, in reactor portion were the cooler water is supplied reactivity burst involving short-time (20 sec) increase of power density may occur; it leads to tensile stresses burst. This kind of situation occurred at Kozloduj NPP, Unit 5 (VVER - 1000) in 1990, it was followed by the depressurization of several FA and unplanned reactor shutdown due to extremely high level of the primary water activity. Repeatable power reductions and increases as a result of the scram system actuation during the first stage of VVER-1000 reactor unit power raising up to nominal (due to deficiencies in the primary and secondary equipment) may have the same effect (as well as power bursts) upon fuel rod depressurization. Statistics shows that such events had up to 30% of fuel leakage of reactors of this type in the period from 1980 to 1987. Nowadays the situation has slightly improved.

2.4. Carbon-containing impurity ingress into the core.

In 1990 during the operation of the 16th fuel load of VVER-440 reactor (60 effective days) at Kol NPP, Unit 2,

overheating of practically all the fuel assemblies of the third year of operation was detected. It was caused by coolant flowrate decrease (20-30%) in the FA. When this fact was revealed unit power was reduced up to 90% N nom. After 90 effective days of operation reactor was shut down for refueling. During the 17th campaign the condition of the mentioned FA has not changed and after operation during 142 effective days at 90% nominal power, reactor was shut down. IFI of 317 FA after 15th campaign revealed 5 leaky fuel assemblies, after 17th campaign - 3 leaky FA. During 16-17 campaigns specific total primary coolant activity (by the sum of iodine isotopes) fluctuated within the limits of (17-59)E-5 Ci/kg, which is one order of magnitude higher than the coolant activity level of the Kol NPP's other units. Post-reactor inspections of one of the mentioned fuel assemblies in the Novovoronezh NPP hot cell revealed deposits on the fuel rod surfaces, having filled the gaps between fuel rods and spacer grids. Maximum amount of deposits with the thickness of up to 1 mm, is on the periferal FRs in the zone of spacer grids 1 and 2 (from the low part of the fuel bundle) with damages in grids 1, 2 and 3. There are through-wall defects in some fuel rods. Chemical and spectral analysis showed that the composition of deposits includes carbon, as well as corrosion products of circuits and fuel rods (Fe, Cr, Ni, Co, Mn, Zr etc.), and also carbon and iron are the main elements (by mass). Inspection results allowed to suggest that the cause of the mentioned event is the deposition of organic compounds from the coolant into the zones with the high flow turbulence (spacer grids). These deposits are the base for structural materials corrosion products precipitation from the coolant flow. The cause of the organic elements appearance in the VVER-440 primary circuit coolant of the Kol NPP is not clear enough.

2.5. Foreign objects in the core.

During operation of Zaporozhye NPP, unit 4 (VVER-1000) in the fourth fuel charge (1991) the highest permissible value of the outlet water temperature was observed on several FA It was considered to be the result of the flowrate decrease through the 1st loop. After that the reactor power was reduced up to 60% and it had been operated for another 48 effective days. RCP inspection of the loop during the planned preventive maintenance showed that thermal barrier damage, resulting in penetration of fragments and particulates into the core, occurred (according to estimate nearly 86 kg of metal was transfered). After power reduction coolant activity of the primary circuit increased by the sum of iodine isotopes from (2.0 - 4.7) x E-6 Ci/kg up to (4.8 - 7.3)xE-5 Ci/kg. Therefore, depressurization of several fuel rods with the gas-leak type defects occurred. This was confirmed by further IFI of the 129 fuel assemblies, having operated during the second and the third campaigns. This IFI revealed 3 leaky FAs in the 1st loop sector. Among all the FA, subjected to IFI, these were not assemblies, having achieved the unload criterion. After flushing in a special test facility and visual inspection 115 FA, were returned to reactor for further operation. Comparison of water flowrate and pressure differential, measured at dummy fuel assembly with the same characteristics, served as a criterion of FA flushing. The condition of RPS rod cluster was also checked. Easy control rod movement served as a criterion for of the guide tube cleanness.

Analogous situation (with RCP vibration and thermal barrier damage) took place in 1983, at South Ukraine NPP, unit 1 (first charge), but in that case there was not FA depressurization because after RCP deficiencies detection the reactor was operating for no more than 3 days. After flushing in a special test facility FA were loaded into the core to achieve high burn-up. Experience of operating these flushed FA showed that the level of flushing was insufficient (or a lot of defects of FR claddings before flushing), because during further operation neptunium was detected in the coolant (i.e. depressurization, followed by fuel-coolant interaction), and while performing IFI 6 leaky FA were found after the first campaign, and 1 and 3 FA - after 2nd and 3rd campaigns respectively. Post-reactor inspections of one of the fuel assembly (1st campaign) in the hot cells at NIIAR Institute revealed deposits on a number of fuel rod surfaces, that contained a lot of carbon. Under the layer of deposits pittings were discovered (as a result of nodular

NPP unit	FA enrichment	FA operation prior to depressurization				Operation results for a fuel assembly loaded for the after-burning use			
		Number of fuel cycles	Burn-up Mwd/kgU	Activity in IFI cask, Ci/kgE-6	Primary circuit activity for J, Ci/kgE-6	Number of fuel cycles	Burn-up Mwd/kgU	Activity in IFI cask, Ci/kgE-6	Primary circuit activity for J, Ci/kgE-6
S. Ukraine NPP, 1 unit	3.0	1	16 01	3 0	285	2	28 1	17 0*	185
Kal NPP	3.0	1	13 16	3 4	78	2	23 9	3 2	145
1 unit	3.0	2	23.9	1 3	145	3	29 9	1 3*	300
	3.3 + 3 0	2	23.4	3 0	145	3	30 1	2 2*	300
	4.4 + 3.6	2	30 5	18 3	38	3	38 9	0 9	52
Zaporozhye	3.0	1	14.2	0.72	98	2	26 9	0 06	57
NPP, unit 1	3.3 + 3.0	1	13.0	0 52	98	2	25 7	0 02	57
	3.3 + 3.0	1	13.0	0 54	98	2	25 7	0 04	57
	3.0	1	15 6	0 46	98	2	27 7	0 03	57
	3.0	1	14.0	7 8	98	2	27 7	1 2	57

corrosion). The pitting depth was 50% of the FR cladding thickness. In this case fracture damage of the graphite inserts of one of the RCP bearings was considered to be the possible cause of the appearance of such deposits.

3. After-burning use of the leaking fuel assemblies.

Significant experience of after-burning use of fuel assemblies with gas leaks has been gained in the Commonwealth. Thus, at Zaporozhye NPP, South Ukraine NPP and Kalinin NPP with VVER-1000 reactors nearly 20 FA, developing insignificant level of depressurization (total activity of iodine isotopes during IFI was (0.5 - 7.0)xE-6 Ci/kg) were used after-burning. Some results of operating of FAs, having developed gas leaks, are shown in the table.

According to the results, FA after gas leak was found, can operate in a safe way during one more fuel cycle without defect propagation. It is proved by the fact, that iodine-131 water activity in IFI system, measured after final withdrawal of leaky FAs, as a rule , is lower than the activity, measured initially. Besides, during the final withdrawal of FAs, IFI revealed only 3 leaking FAs (marked *) among 10 checked FAs. The cause of this phenomenon is not clear enough, but it is possible to suggest that immobolization of a microdefect in the fuel rod cladding is connected with the deposition of products of uranium dioxide transmutation or their combinations.

The possibility of FA operation with FR, developing microdefects, is also proved by the fact that the dynamics of changes of primary coolant activity by the sum of iodine isotopes during campaigns, when leaky fuel assemblies were operated, has a smooth character and average coolant activity by the sum of iodine isotopes does not exceed the level of safe unit operation.

4. Conclusions.

1. Fuel operates rather reliably. The cases of FR depressurization make up for: VVER-440 - 0.005-0.010%
VVER-1000 - 0.005-0.009%.

As a rule depressurization has the character of gas leak.

2. The main causes of FA depressurization involve non-optimum conditions of operation, connected with multiple defects of the primary and secondary equipment and violation of the technical specification.

3. The possibility of after-burning use of fuel with micro leaks in the fuel rod claddings with the primary circuit water activity limitation was revealed.

EXPERIENCE WITH DEFECT FUEL AT THE KERNKRAFTWERK LEIBSTADT; DETECTION, INSPECTION, HANDLING AND MANAGEMENT

S. LUNDBERG
Kernkraftwerk Leibstadt AG,
Leibstadt, Switzerland

Abstract

The Leibstadt Nuclear Power Station, KKL, in Switzerland, is a General Electric Boiling Water reactor of the BWR/6 type with an output of 1050 MWe/3138 MWth.
The majority of the 648 bundles in the core are GE 8x8 barrier bundles. A small number of non barrier 8x8 bundles reside on the core periphery. Also one reload of ABB SVEA-96 10x10 non-liner bundles was loaded in 1991.

KKL has experienced fuel failures in 4 of the 8 cycles operated. These failures were detected by an increase in plant activity. The failures occurring in cycles 2 & 4 were typical PCI failures caused by overpowers during manoeuvres. The failure were located with partial and full core flux tilting methods.
To minimize handling of leaking bundles these rods have all been put together in a so called "superleaker bundle".

The cycle 5 & 7 barrier clad (GE sponge Zr) failures were classified as manufacturing defects due to presence of incipient cladding flaws not detected by the manufacturing control.
The failures showed severe secondary deterioration and caused unusually high activity releases. They were detected by the normal activity surveillance and finally located by In Core Sipping after shut-down.

All KKL failed fuel rods have been inspected both visually and with NDT directly after discharge.

The last two failures required special failed fuel management during operation, such as minimizing the number of power manoeuvrers and avoiding the planned feedwater temperature reduction. These actions were taken in order to minimize the power cycling of the failed rods.

The large activity release and Uranium-washout has caused major plant maintenance problems during operation and higher than desired exposures during outages.

Both the failed barrier rods have been put into a bundle skeleton for transport to PIE at The Paul Scherrer institute in Switzerland. Cladding samples will also be sent to the GE Valecitos Nuclear Centre, USA, for additional examinations.

1. Introduction

The Leibstadt Nuclear Power Station is located on the river Rhine on the German border. It is a General Electric (GE) BWR/6 1050 MWe type plant. The unit is currently operating in its 8th cycle.

A thermal output of 3138 MB is generated by 648 fuel bundles, mainly of the GE7B and GE8B (8x8 barrier) type. However bundles of the types GE6 & GE7 (non barrier) as well as GE10 (barrier) and one reload of ABB SVEA-96 10x10 bundles reside in the core. These later bundles have no Zr liner while they have a thinner rod diameter. They were loaded in 1991. The GE non barrier bundles are loaded on the core periphery, thus allowing the core to be operated as a barrier core without PCIOMRs (PreConditioning Interim Operating Management Recommendations).

The initial core loading and the first reload consisted of GE6 non barrier bundles.
KKL however early converted the reload contract to barrier elements with cladding having an inside thin pure sponge Zr layer. The main reason for this decision was to minimize the production losses caused by the PCIOMRs. The PCIOMR restrictions were not implemented on the barrier bundles.
Together with the non barrier introduction the CCC operational strategy was used.

The KKL plant is operated on an annual cycle basis with refuelling and maintenance outages in August/September.
The operating strategy include the control cell core (CCC) concept, using only predefined control cells for reactivity and power shape control.
The cycles are always ended with feedwater temperature reductions and power coast down.

2. KKL fuel failure power history.

KKL has experienced fuel failures in 4 of the 8 cycles so far operated. This section will summarize the failed fuel operational histories. **Table I** summarize some key data for the failed bundles.

2.1 Cycle 2

The first fuel failure in the KKL core occurred in cycle 2 and involved an initial core bundle. It reached an exposure of 17 MWd/kgU.
This failure was caused by PCI due to an overpower violating the PCIOMRs in connection to a control rod pattern change.

Table I: Failed Fuel Date

Bundle	Rod	Type	Bundle Enr. (	Rod Enr. w/o)	# of Cycle	E at Fail (MWd/kg)	E at EOC	Oper as failed (Days)
Cycle 2:								
LJN925	A1	GE6	2.19	1.30	2	15	17	~100
Cycle 4:								
KL0103	B4	GE6	2.84	3.95	3	25	22	~120
KL0142	C4	GE6	2.84	3.95	3	25	22	~120
KL0156	B1	GE6	2.84	2.40	3	25	22	~120
Cycle 5:								
LYE798	D6	GE7B	2.84	3.95	3	26	15	>300
Cycle 7:								
LYH200	E1	GE8B	3.02	3.00	4	32	28	~140

2.2 Cycle 4

Towards the end on the full power operation of the fourth cycle presence of new fuel defects in the core was identified. During the outage three failed non barrier rods, belonging to the second reload, were found. The exposure of all these bundles was 25 MWd/kgU.
All three failures were probably caused by PCI although the cladding defect of one of the rods resembled a fretting hole. All three bundles containing the three failed rods were located in active control cells after having been shuffled to these locations from peripheral corner locations. The shuffling history of the failed bundles, shown in **figure 1**, can very well have contributed to the failures. The overpowers according to the GE process computer were very moderate (0.6-1.0 kW/m). The real overpowers may however been larger due to the skewed radial exposure- and consequent radial power- shapes, resulting from their location in the large flux-gradients in the peripheral locations the previous cycle. The process computer is unable to track such power changes.

2.3 Cycle 5

One failed fuel rod was found after cycle 5. This rod was a GE7B barrier rod being in its third cycle of irradiation. The bundle average exposure at discharge was 25.9 MWD/kgU.
The bundle containing the failed rod was located in a control cell. The shuffling history of the bundle is shown in **figure**

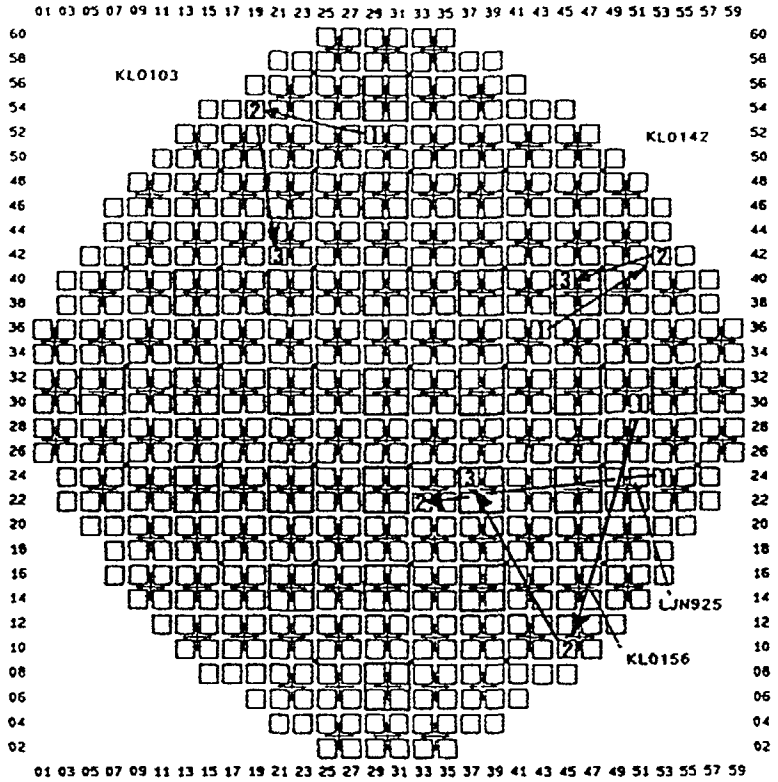

FIG. 1. Cycles 2 and 4 failed bundle shuffling history.

2. It experienced a relatively high power (41 kW/m peak LHGR) during its first cycle, moderate power during the second cycle (23-26 kW/m peak LHGR) and again higher powers (33-36 kW/m peak LHGR) during its third cycle of operation. The nodal power history of the failed rod over its life is shown in **figure 3**.
The slowly increasing off-gas activity over the first part of cycle 5 showed a dominant diffusion component, indicating the early stage of a deteriorating of a defect. After a scram recovery in January 1989 the off-gas activity however increased rapidly.(see below) During this scram recovery the failed rod experienced power increases in the order of 5 kW/m. Other sound rods of this bundle however experienced power increases in the order of 21-22 kW/m. Also no other ramps experienced during cycle 5 have been large enough to result in hoop stresses above the PCI limit.[4]

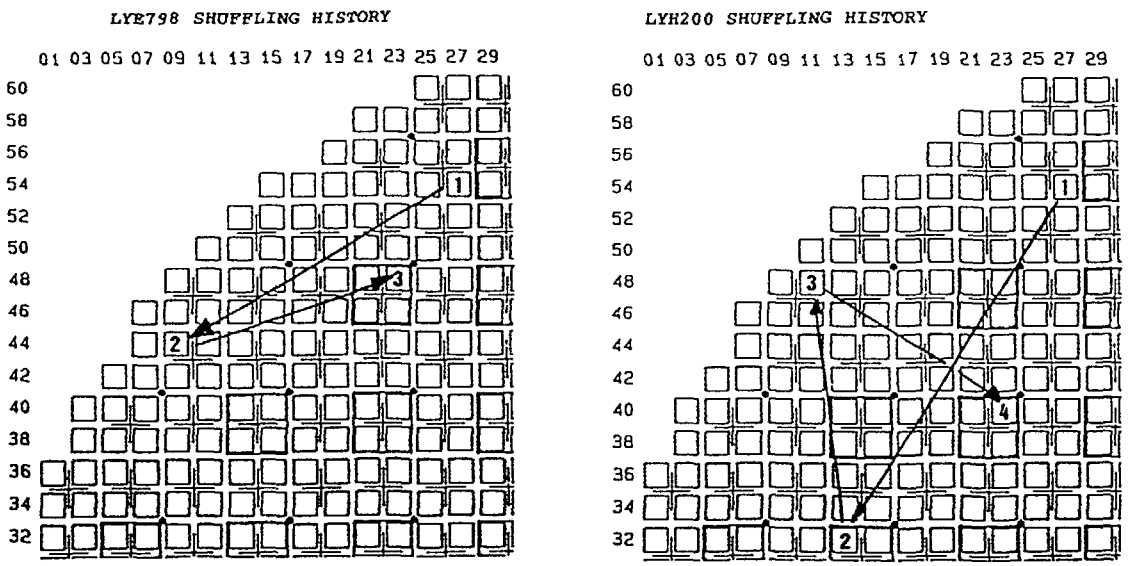

FIG. 2.

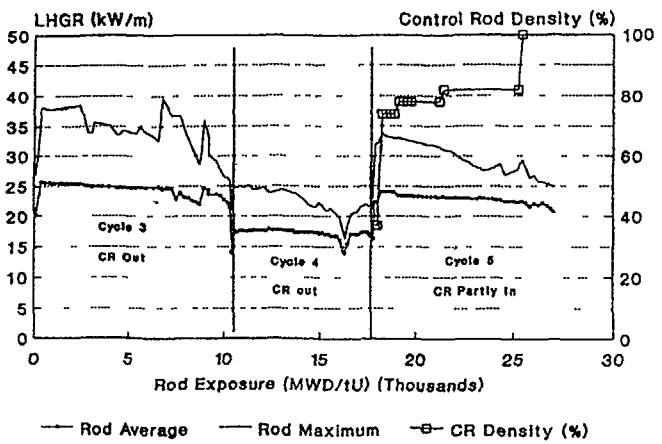

FIG. 3. LYE798 power history.

2.4 Cycle 7

After cycle 7, one failed barrier rod of the GE8B type was localized. The bundle containing this rod was in its fourth cycle and the EOC average exposure was 32 MWD/kgU. This bundle showed a similar shuffling history (figure 4) as the cycle 4 failure bundles; i.e. in-out-in shuffling.
The increased off-gas activity, identifying presence of fuel failures in the core, occurred after having pulled the last four control rods completely out of the core to an all-rods-out (ARO) state.
The maximum power increase during this manoeuvre occurred in the region of the cladding crack and was about 11 kW/m. The end power level was however only 27 kW/m. This is the same level as the PCI threshold for GE non barrier fuel. Therefore PCI was ruled out as the failure cause.

3. Detection of defect fuel

3.1 Activity measurements and analysis

All defect fuel in the KKL core have been primarily detected by the routine off-gas- and reactor water- activity surveillance.

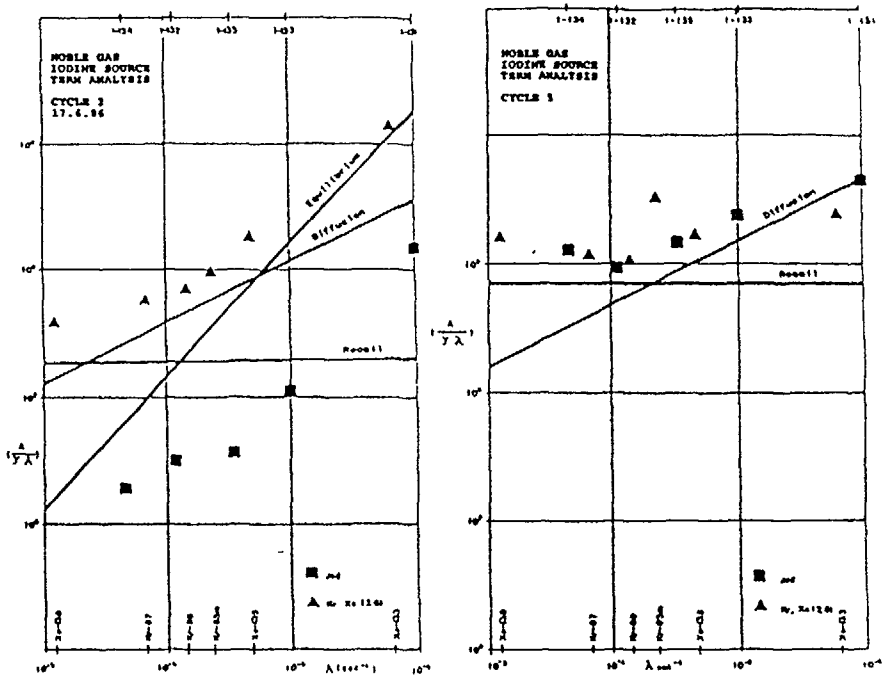

FIG. 4.

The off-gas activity is monitored online in the steam air ejection system and the reactor water samples are analysed once a week (more often after identified presence of defect fuel).

The activity data is analysed and plotted versus the decay constant of some important isotopes in order to determine the type of release, i.e. equilibrium, diffusion or recoil type of release. An example of this type of plot is shown in **figure 4** for the cycle 4 and the cycle 5 failures.

This type of information can, together with plots of the ratio I-131/I-133 activity versus the total Iodine activity, be used to determine (approximate) the stage of deterioration and the size of the defect, **figure 5**.

In addition to time behaviour if the Iodine isotopes the noble gases, Xe-133, Xe-135, Xe-138, Kr-85m, Kr-87, Kr-88, forming the "sum of six", are monitored.

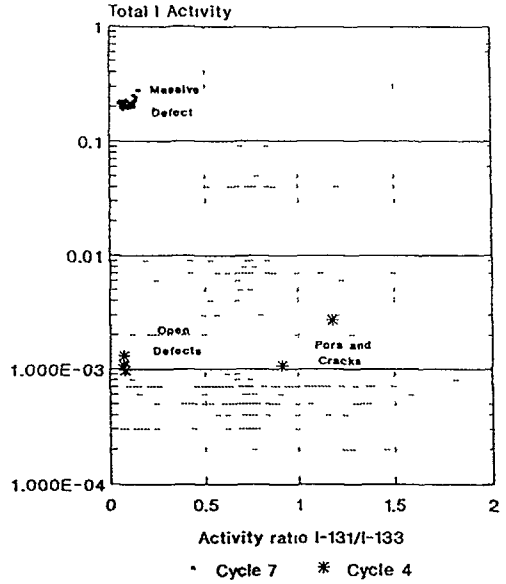

FIG. 5. Iodine relation.

The behaviour of the monthly average I-131 activity, over the life of the reactor, is shown in **figure 6** and the behaviour of the noble gases over the cycles containing fuel defect is shown in **figure 7a-d**.

Also other isotopes like for instance the Cs-134 and Cs-137 as well as the Np-237 are routinely monitored at KKL. The ratio of the Cs isotopes (137/134) are used as indicators of the failed fuel exposures and the presence of Np-237 in the reactor water indicates defects that are in contact with the cooling (wash out of Uranium). The Np-237 activity behaviour is shown in **figure 8**.

3.2 Flux Tilting

The control cells containing defect fuel in cycle 4 were successfully located by a flux tilting exercise performed before the end of the cycle.
The flux tilting was performed by single rod scrams at a reduced reactor power.
An example of an activity trace recorded and the resulting response map is shown in ***figures 9a & 9b***, [5].

The flux tilting was never employed to locate the cycle 5 defect. GE strongly recommended against a flux tilting

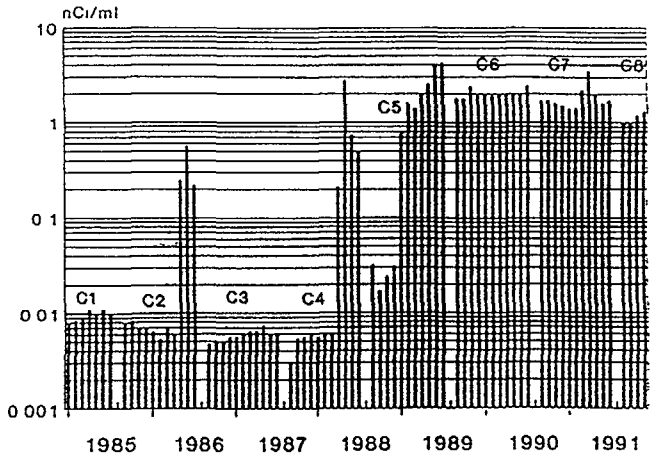

FIG. 6. KKL I-131 reactor water activity (monthly average 1985–1991).

utilizing single rod scrams due to the risk of further deteriorate the already heavily hydrided cladding. Also the high activity background (recoil release) would make it uncertain to find the expected 2-5 defects.

No flux tilting was perform after cycle 7 due to the high activity background. The location of the defects, in the last withdrawn control cells, was also known.

(a) Noble gas activity cycle 2 1985/1986

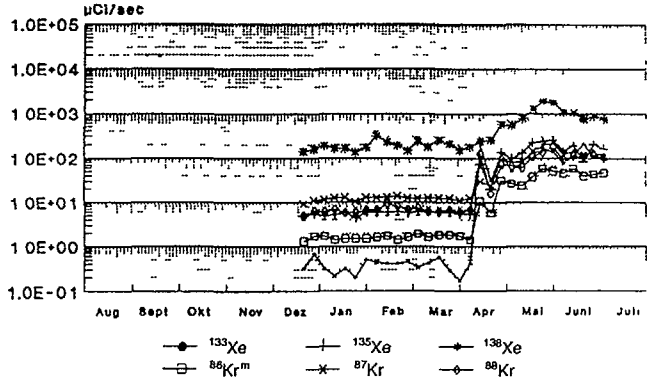

(b) Noble gas activity cycle 4 1987/1988.

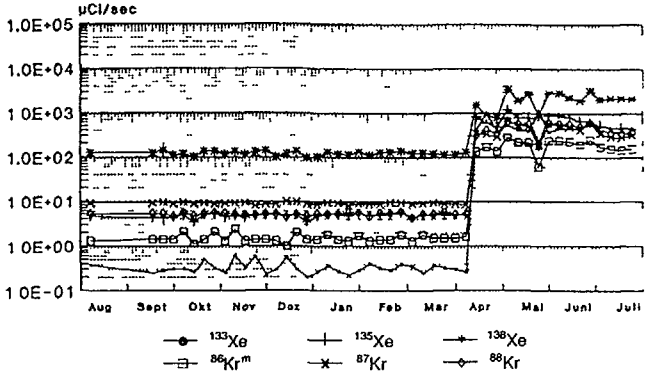

(c) Noble gas activity cycle 5 1988/1989.

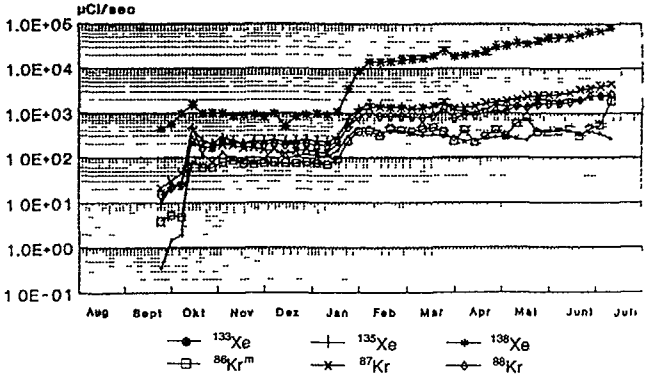

(d) Noble gas activity cycle 7 1990/1991.

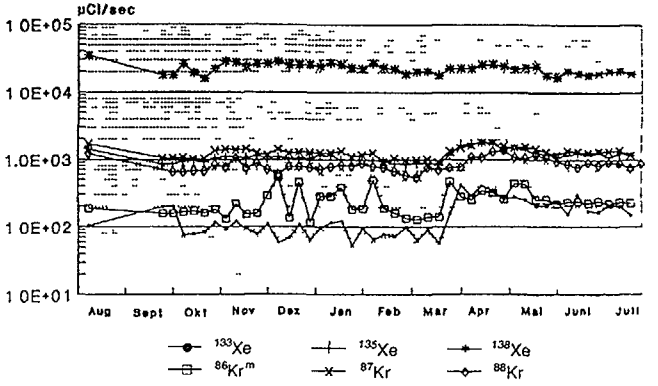

FIG 7

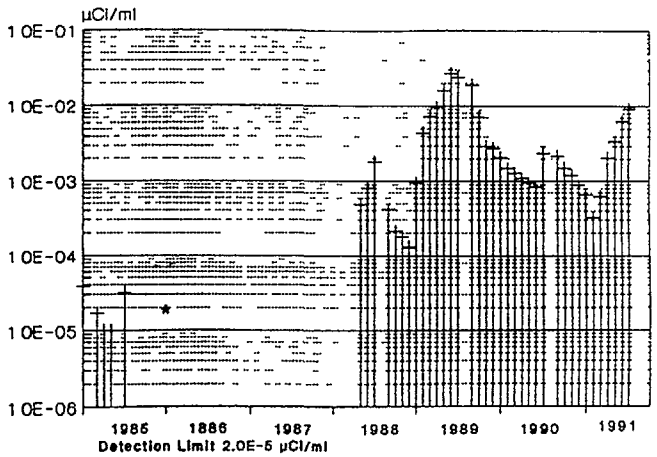

FIG. 8. Activity of Np-239 in the reactor water (monthly average 1985–1991).

3.3 Vacuum- and In Core- Sipping

After cycle 2 and 4 a limited vacuum sipping campaigns, based on the results of the flux tilting were performed. All expected failures were found. No barrier bundles were sipped, following GE recommendations.

After cycle 5 and 7 a new in core sipping (ICS) equipment, constructed by Siemens-KWU, was used to locate the leaking bundles. This equipment collects water samples from the bundles sipped. Both the cycle 5 as the cycle 7 failure were found by this ICS technique.
As, in cycle 5, more than one failure was expected all bundles that were reloaded for the cycle 6 core were also vacuum sipped. However no additional leakers were found.

After cycle 7 one failed bundle was identified by ICS.

4. Failed Fuel Inspection results

All failed fuel bundles, having been discharged from the KKL core after each leaker cycle, have been inspected by the vendor.
The purpose of these inspections has been to identify the failed rod(s) in each leaking bundle and to try to find the primary cause of the failure. This has so far been a requirement from the Swiss nuclear authorities, in order to give a release for startup of the next cycle.

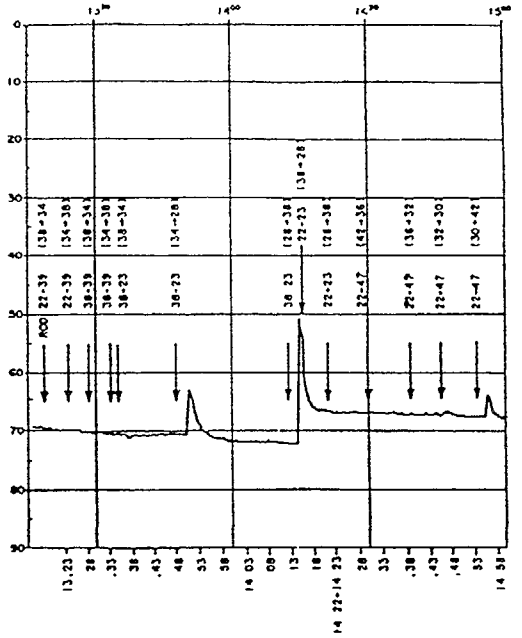

FIG. 9a. Example of cycle 4 flux tilting activity traces.

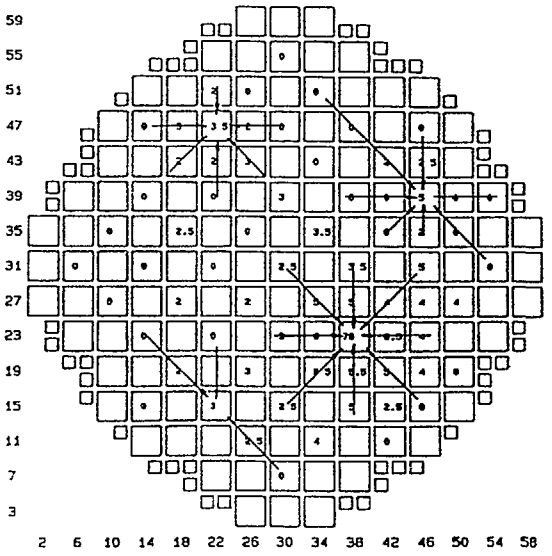

FIG. 9b. Cycle 4 flux tilting response map.

The inspections has utilized photographic visual inspections as well as non destructive (NDT) methods, such as Eddy Current (EC) Technique and Ultra Sonic Technique (UT).

Below follows a description of the findings of each KKL failure. **Table II** summarizes the inspection observations.

Table II: Summary of Failed Rod Pool Side Examinations

Bundle Identity	Rod	Failed Cycle	Inspection	Observation
LJN925	A1	2	Visual & NDT	- 1.27 cm longitudinal crack at 177.8 cm elevation - Small cracks at 46 and 68.5 cm elevation
KL0103	B4	4	Visual & NDT	- Circumferential crack below upper end-plug -NDT indicate penetration at 127 cm - Moderate corrosion
	Peri		Visual	- Foreign debris under first spacer
KL0142	C4	4	Visual	- Circumferential crack just above the lower end-plug
KL0156	B1	4	Visual	- 4cm longitudinal crack at 127 cm - 8cm longitudinal crack at 56 cm elevation - Small crack at 48 cm
LYE798	D6	5	Visual & NDT	- ~58cm longitudinal crack between 38cm and 96 cm elevation - Width ca 1.5 mm - 360° circumferential crack in heat treated End-plug weld - Moderate to heavy crud (fluffy) - Nodular corrosion
LYH200	E1	7	Visual	- ~60cm longitudinal crack between 36cm and 96cm elevation - Hydride Blister at 318 cm elevation - Both End-plugs intact

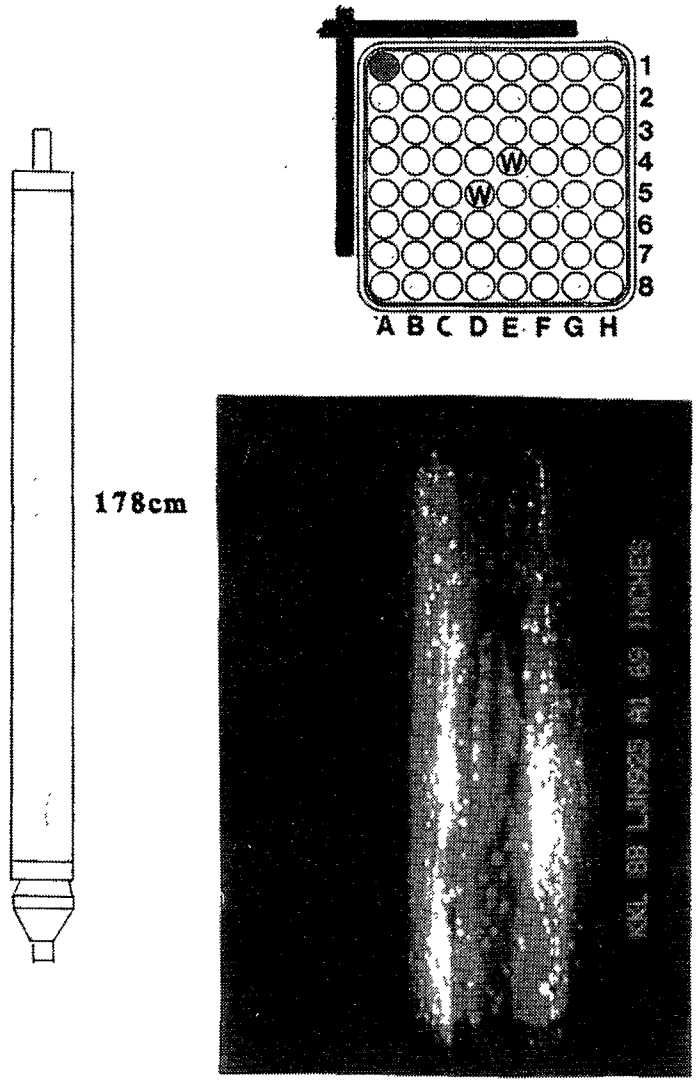

FIG. 10. Cycle 2 – LJN925/A1.

4.1 Cycle 2 (Reload 2, LJN925 rod A1)

The cycle 2 failure contained one failed rod in the A1 position (control rod corner), **figure 10**. A 1.5 cm longitudinal crack, typical to PCI, was found at the 175 cm level (from the bottom) of the rod. Additional secondary

hydrid cracks were found at the 44 and 68 cm levels of the rod. Both end-plugs of this rod were intact, [1].
The rod surface was in relatively good shape, with low nodular corrosion coverage. The crud deposition was however heavy.
This rod had been operated for about 100 days after its detection as defect, without causing larger increases in the activity release.

4.2 Cycle 4 (reload 3, KL0103/B4, KL0142/C4, KL0156/B1)

The B4 rod of the KL0103 bundle, **figure 11**, showed a circumferential crack below the upper end-plug weld. The end-plug fell of during the inspection handling of the rod. Also a clad penetration at the 127 cm level was found.

A foreign debris, originating from an initial startup instrumentation clip, was found under the first spacer. This debris did however not cause any damage, [1].

A circumferential crack, just above the lower end-plug weld was found on the C4 rod of bundle KL0142, **figure 12**. Also this end- plug was broken of during handling, thus making it extremely hazardous to remove the rod from the bundle structure, [1].

The B1 rod of bundle KL0156, **figure 13**, showed a 4 cm longitudinal crack at the 127 cm level and a 8 cm longitudinal open crack at the 56 cm level. This hole resembled what is normally seen in connection to fretting failures. There are however no clear evidence for fretting being the primary cause of this failure. Also a small crack was found at the 48 cm level, [1].

All three cycle 4 failed rods showed moderate corrosion but fairly heavy crud deposition, mostly fluffy. CILC as the failure cause was however ruled out, as KKL exchanged the original Admiralty Brass condenser against a condenser with Titan tubing after the first cycle of operation. The content of copper is also very low, a fact that has been found in other separate crud scrape campaigns at KKL. The crud at KKL consists to more than 95% of iron.
Sound UO_2 and Gd rods have also been examined. They showed no differences regarding the cladding corrosion status.

GE and KKL concluded that the most probable failure cause of these rods was PCI.

4.3 Cycle 5 (Reload 3, LYH798/D6)

The only failed rod found in this bundle, **figure 14**, was the D6 rod. This rod had a 1-2 mm wide longitudinal crack extending over a length of 58 cm between the axial levels of

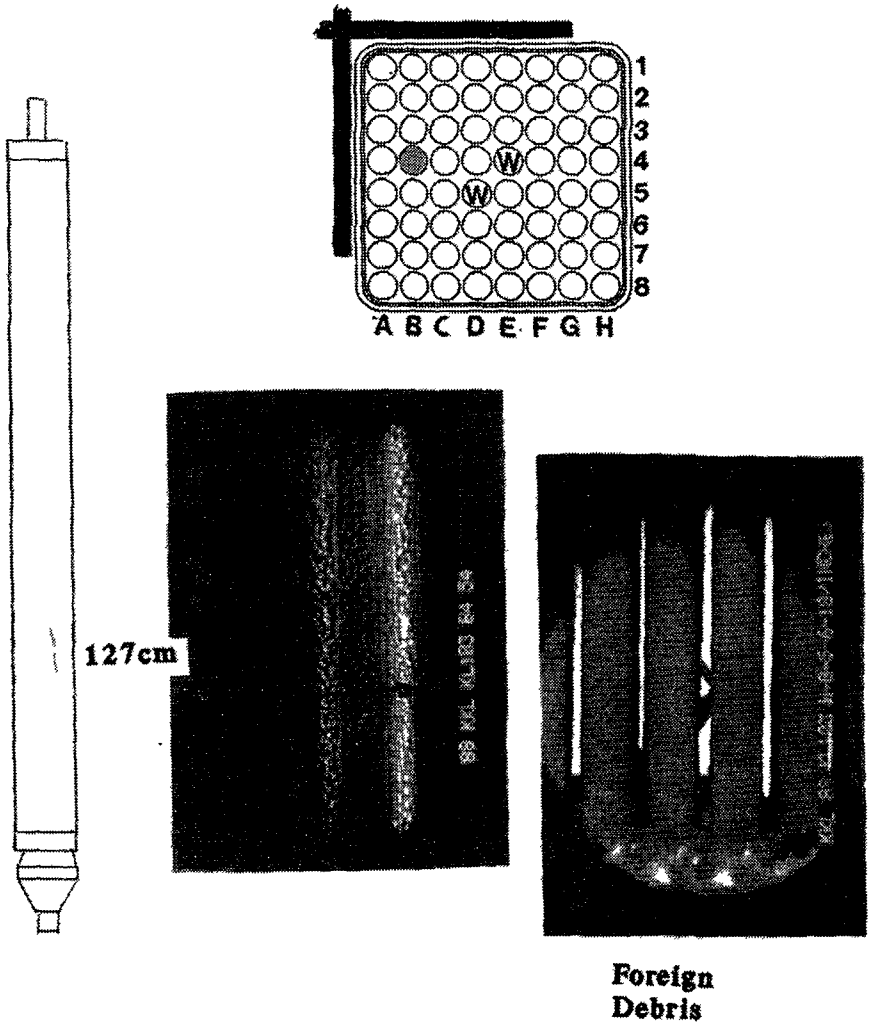

FIG. 11. Cycle 4 – KL0103/B4.

38 cm to 96 cm. The crack run trough the position of the first (lowest) spacer. The rod appeared black in the region of the crack, indicating severe washout of Uranium from the cladding. The amount of Uranium dissolved and washed out was estimated to about 70 g based on the Np-237 activity release data.

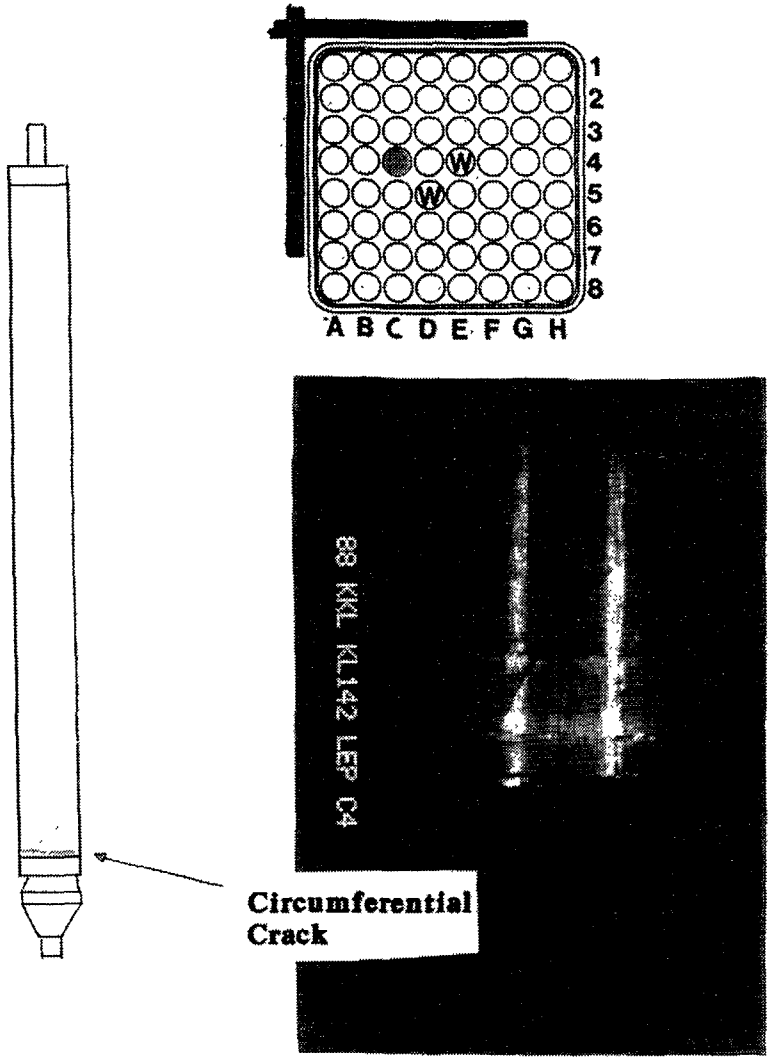

FIG. 12. Cycle 4 – KL0142/C4.

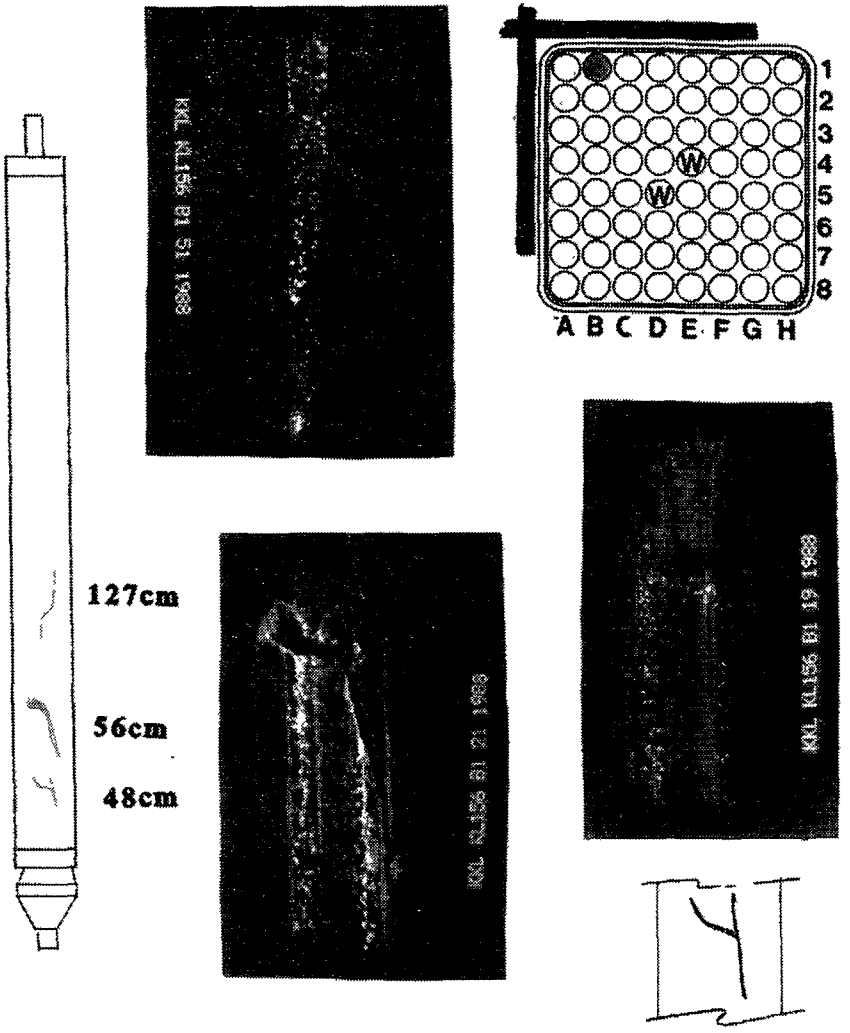

FIG. 13. Cycle 4 – KL0156/B1.

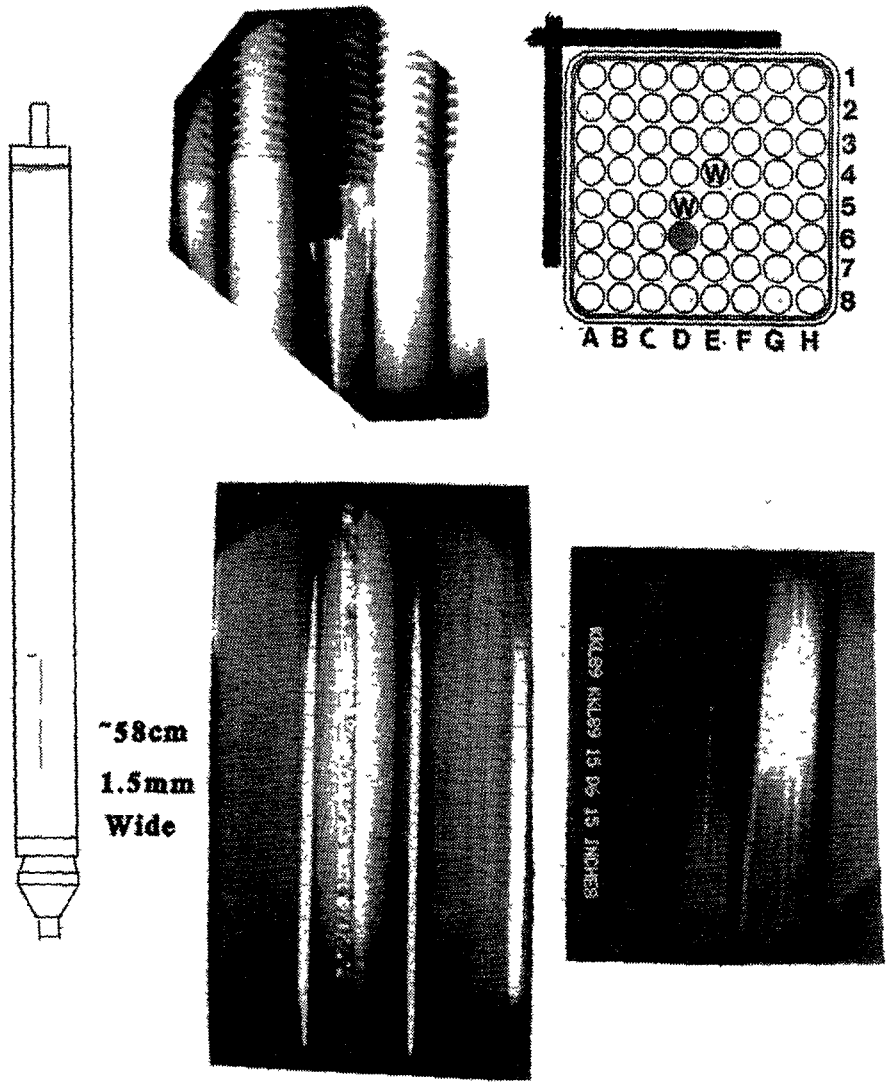

FIG. 14. Cycle 5 – LYE798/D6.

The upper end-plug, broken during operation, showed a circumferential crack in the heat treated zone of the weld. This zone was heavily hydrided.
All other rods in the bundle, except the tie rods were inspected with NDT and found to be sound. The tie rods were visually inspected, [2].

All rods had a very thin nodular coverage and the crud deposition was moderate to heavy. Most of the crud is however fluffy. The failure cause was not related to CILC

PCI was also ruled out as the failure cause. The reason for this is that other rods in the bundle had seen much higher power changes (22 kW/m) than the failed rod (5 kW/m). This has also later been confirmed by an independent review of the failure by the S.M.Stoller Corporation in New York [4]. Their PCI analyses showed that the peak hoop stress was below the stress threshold for this type of rods.

Instead the cause of the failure was attributed to a incipient manufacturing flaw, not detected by the manufacturing quality control.

GE has found that their manufacturing quality control at the time of the manufacturing of this lot was not optimum. They have however improved their manufacturing quality control since then.

4.4 Cycle 7 (Reload 4, LYH200/E1)

The failed E1 rod of this bundle, **figure 15**, was found by visual inspection. Both the upper and the lower end-plugs were intact.
The rod showed a 1-2 mm wide and 60 cm longitudinal crack, starting just below the first spacer and extending to just below the second spacer. Traces of washed out Uranium was found around the crack. A secondary hydride blister, probably trough wall, was also found at the 318 cm elevation of the rod, [3].
The longitudinal crack had a remarkable resemblance with the failed D6 rod in the cycle 5 leaker.

Also this failure was caused by an incipient manufacturing cladding flaw. The rod was manufactured at the time of the bad quality control at the GE Wilmington fuel manufacturing facility.

5. Post-irradiation handling of failed fuel

The cycle 4 leaker, having the defect lower end-plug, was chosen as a "super leaker". The failed rods in the other two cycle 4 leakers and the failed cycle 2 rod were removed from their respective mother bundles and placed in different positions of the "super leaker". The super leaker bundle thus created was then placed in a special closed flask in the spent fuel pool.

The failed barrier rods (cycles 5 and 7) could not be moved to the super leaker, as the end plugs of barrier rods do not fit the old GE6 lower tie plate.

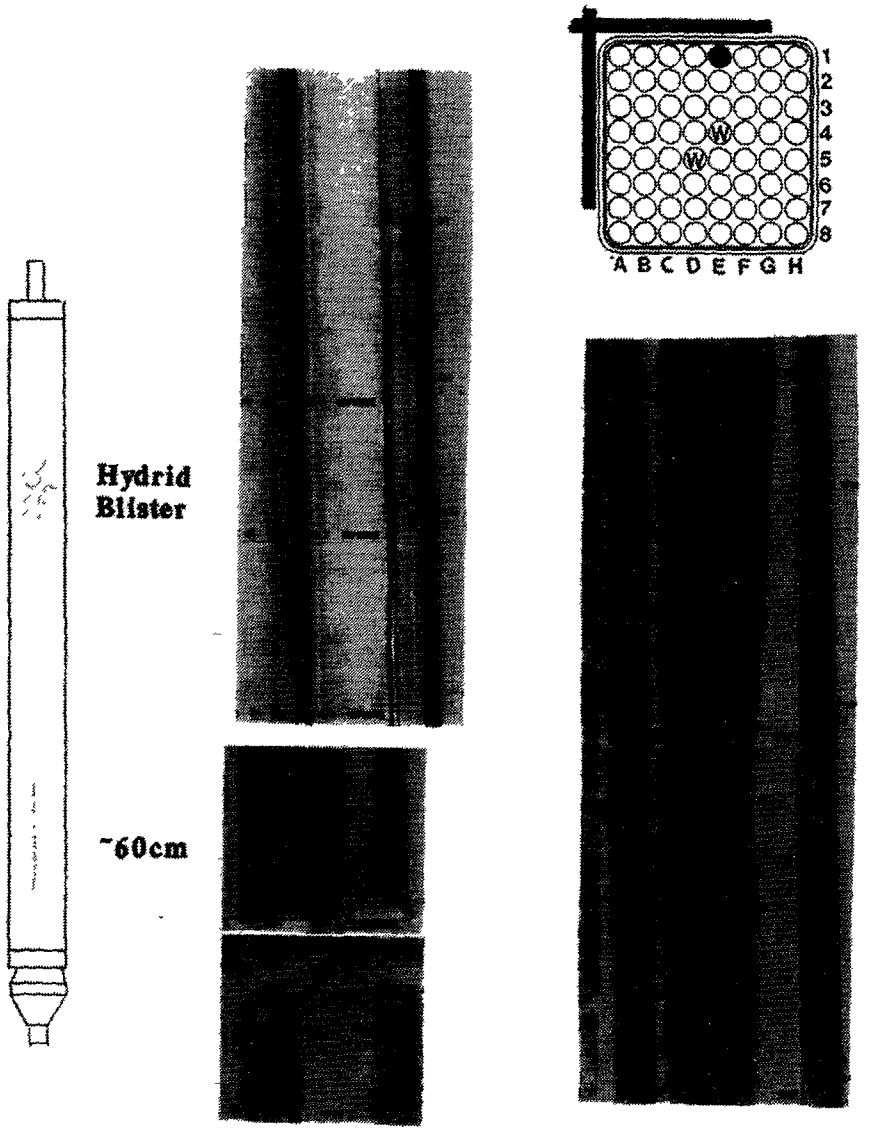

FIG. 15. Cycle 7 – LYH200/E1.

Instead all the sound rods of the cycle 5 leaker were moved to an empty unirradiated skeleton. The failed rod, that could not be removed, was left in the original bundle structure. The tie rods of the original bundle were replaced by inert rods. Additionally, the failed cycle 7 rod was also moved to the skeleton, thus containing two failed barrier rods.
The purpose of creating this "barrier super leaker" was to prepare the two rods for shipment to the Swiss Paul Scherrer Institute Hot Cell laboratory for non destructive and destructive examinations.

The general policy of KKL is to minimize the handling of failed fuel bundles in the pool in order not to stress the embrittled cladding and risk further activity release. Also from a reprocessing point of view, KKL wants to minimize the number of bundles containing failed rods.

6. KKL Failed Fuel Management

6.1 Operation with defect fuel

When the presence of defect fuel in the core during operation is identified the main objective is to mitigate further increase of the activity release and further deterioration of the defect cladding.
At KKL, attempts to achieve these goals were done by, in cycle 5, reducing the number manoeuvres affecting the local powers in the core. The necessary manoeuvres were performed at a slower rate in order to reduce the ramp rates as much as possible.

The cycle 7 failure was identified just after having pulled to an All Rods Out state (ARO). The originally planned feedwater temperature reduction, increasing the local power in the lower part of the core, was not performed. Instead the reactor entered the power coast down.

During the coast down phase of an operating cycle the power peaking of the bundles is slowly moved towards the top of the core, thus lowering the power in the region of the defects.

This had a positive, reducing, effect on the activity release of both noble gases and I-131. It most probably also slowed down the rate of cladding deterioration. An indication of this was that both the end-plugs of the failed rod were intact at EOC.

If presence of defect fuel is identified in the core, no load following is performed. This is in order not to impose any temperature gradients following a power change and thus to

avoid the pumping of water/steam into the failed rod through the defect. Avoiding this water/steam ingress will reduce the rate of secondary hydriding of the cladding from the inside.

6.2 Administrative activity surveillance guide-lines

The KKL plant has been designed for the possibility of operation with failed fuel. The maximum allowable noble gas activity has been set to 280,000 microCi/s (after 30 minutes delay) and 700 microCi/s I-131 activity in the reactor water. The I-131 source term leads to an equilibrium concentration in the reactor water of about 0.03 microCi/ml.
Although the activity levels experienced at KKL, in primarily cycle 5 and 7, have been well below the allowable limits (10% of the I-131 limit and 2% of the noble gas limit), failed rods like those experienced however lead to severe problems with maintenance of the secondary plant during operation as large parts of the condenser offgas system and the turbine systems will get contaminated.

Based on these problems KKL have defined new administrative alarm limits for the activity surveillance.

Normally the I-131 activity is primarily monitored and different alarm limits have been defined based on these activities. If, however, Np-239 is found in the reactor water sample analyses the surveillance focus on this isotope. At a specific Np-activity level a shut down of the plant in order to localize and remove the defect bundle must be planned. The performance
of this outage, at the next alarm limit, also takes the time to the next planned outage into account, in order to minimize the total doses to the personal. This follows the ALARA principle.

The new administrative alarm limits are shown in **figure 16.**

7. Conclusion and summary

One of the main objective when operating a nuclear power plant is to avoid fuel failures. One mechanism that have led to failures is the PCI phenomena. The remedy against PCI failures was the introduction of the Zircaloy cladding with an inner barrier of pure or alloy Zr. The liner cladding seems to have removed the PCI phenomena as a potential failure mechanism.

It is however more difficult to prevent fuel failures caused by debris fretting or presence of incipient manufacturing flaws.
This can, to some extent be done, by keeping good control of metal pieces and wires during the refuelling outage, when the reactor vessel is open.

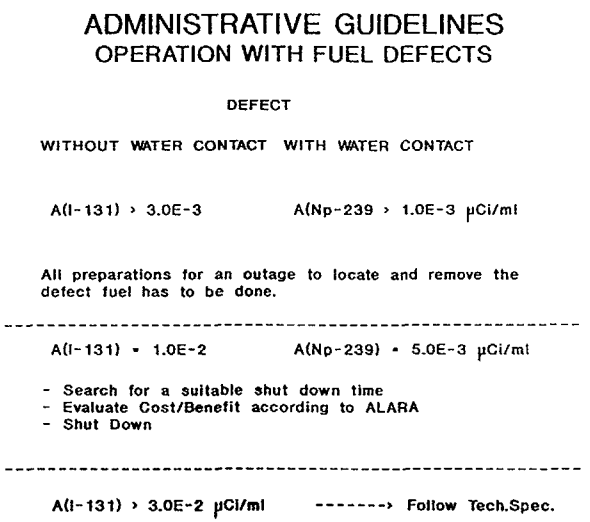

FIG. 16.

The frequency of manufacturing induced defects can be kept to an absolute minimum by improving the manufacturing quality control process as far as possible.

The Zr barrier is a remedy against PCI failures as long as the cladding remains intact. The question wether the Zr liner have a possible accelerating effect on fuel degradation and activity release of already defect rods is intensively discussed now days. Via PIE and attempts to analytically model the failure mechanism and especially the mechanism of the delayed secondary hydriding and the uranium and liner oxidation processes, answers to this questions are sought. It is very important, in light of the consequences for operation, to find those answers.

For high power density plants like KKL, operating with large fractions of liner fuel, it is very important to find means to effectively mitigate the effects of failures in such cladding, should they occur. One interim answer might be implementation of "secondary PCIOMRs" for failed barrier fuel.

Another area that need more attention is the localization of fuel defects in the core during operation by means of advanced flux tilting methods and more sophisticated activity release analyses methods.
When located, the power of a defect bundle can be suppressed by insertion of an adjacent control rod.

All mitigating actions have to be seen in light of the trends to increase the power densities of the cores, an action that will potentially increase the production of volatile fission products and the activity release in case of fuel defects.

References

Unpublished reports

[1] S.Lundberg, KKL Internal Report BET/88/140 "Untersuchung von beschädigten Brennelementen Revision 88"

[2] S.Lundberg, KKL Internal Report BET/89/334 "Cycle 5 Fuel Failure at KKL"

[3] S.Lundberg, KKL Internal Report BET/92/046 "KKL Cycle 7 Fuel Failure"

[4] The S.M.Stoller Corporation, Nwe York, U.S.A, personal communication.

Reports

[5] E.Obst, W.Blaser, "Einfluss von Brennelementdefekten auf den Betrieb", (Schweizerische Verienigung für Atomenergi Vertiefungsskurs, 6-8 Mai 1991, Brugg-Windisch.

[7] Post Defect Behaviour of Barrier Fuel, J.H.Davis, G.A.Pots, ENS/ANS Meeting in Avignon, France April, 1991

DEBRIS INDUCED FUEL FAILURES ON URANIUM AND MOX FUEL IN BEZNAU I

H. BAY
Nordostschweizerische Kraftwerke AG,
Switzerland

D. BOULANGER, P. DERAMAIX
Belgonucléaire SA,
Brussels, Belgium

H. BAIRIOT
FEX,
Mol, Belgium

Abstract

During operation of BEZNAU I from July 1989 until May 1990, primary circuit activity indicated that several fuel assemblies developed leaks. The core was constituted during that cycle of 24 MOX fuel assemblies and 97 U assemblies. Sipping identified five leaking fuel assemblies : one U fuel assembly in its first irradiation cycle, two U assemblies in there second irradiation cycle, one U fuel assembly in its third irradiation cycle and one MOX fuel assembly in its second irradiation cycle.

On site examination during repairs indicated that the failures were caused by debris induced fretting resulting subsequently in secondary hydriding failures.

Coolant activity countings taken throughout the period have been compared with those obtained during preceding cycles where similar types of fuel failures were identified on U fuel assemblies only and with the results obtained from cycles which did not contain failed fuel assemblies.

The data were analysed to correlate primary and secondary failure for U fuel and MOX fuel.

The fuel failures observed are used to assess the release of activity from a failed MOX fuel rod in comparison to a failed U fuel rod.

1. *INTRODUCTION*

At the BEZNAU site, located in the north-east of Switzerland, Nordostschweizerische Kraftwerke AG (NOK) operates two 350 MWe pressurized water reactors. BEZNAU 1 has been in operation since 1969. The core contains 121 fuel assemblies of 14 x 14 low parasitic design. Plutonium recycling was first started in 1978 with the loading of 4 MOX assemblies designed and built by WESTINGHOUSE in the USA. Since 1988 mixed oxide fuel assemblies (MOX assemblies) are loaded on a regular basis [ref. 1] [Fig.1]. Currently Uranium fuel assemblies are procured from WESTINGHOUSE in collaboration with ABB Atom and MOX fuel assemblies are procured from COMMOX in collaboration with WESTINGHOUSE. BEZNAU 1 is currently in its

Year	No.of fresh MOX Elements		Total MOX Elements in core	
	BEZNAU-I	BEZNAU-II	BEZNAU-I	BEZNAU-II
1984	-	4	-	4
1985	-	8	-	12
1986	-	4	-	16
1987	-	8	-	24
1988	12	8	12	28
1989	12	12	24	24
1990	12	-	32	36
1991	-	-	36	28
1992	24	-	41	20

Fig.1 SCHEDULE of MOX fuel elements in BEZNAU

21st cycle of operation. Starting in cycle 17 several debris induced fretting failures occurred including the MOX assembly M107. This paper attempts a correlation of the coolant activity during cycles 17 through 20 with the fuel rod failures as confirmed in a subsequent reconstitution campaign.

2. *INTERPRETATION METHODOLOGY*

Fission products like Iodine, Xenon and Krypton generated in the fuel are partially released into the fuel-cladding gap.

With defective fuel, these products migrate toward the defect site and eventually into the primary coolant, depending on the size of the defect and on the operating conditions.

A first step in the interpretation consists in a study of the absolute activity of the primary circuit.

Two elements are considered more particular

- Xenon as an indication of the gas releases from the failed rod
- Iodine, giving generally small amount of volatile steady release and washed out under water ingress conditions.

The activity of isotopes Xe 133 and I 131, with half lives of a few days, were analysed over the respective cycles of the BEZNAU 1 reactor, in order to

- assess the background level, given by a clean cycle.
- position in time and more or less in extent the rod failures.

A second step consists in a more specific analysis of the gas escaping from the fuel rod in order to determine the time at which MOX failed.

The study is based on the Xenon to Krypton production ratio, which is known to be about twice as high for Plutonium 239 than for Uranium 235 thermal fissions.

Two isotopes were chosen, characterized in the following table : Kr 85m and Xe 133, on the basis that the gas escaping from a MOX rod with low Kr content leads to an increase of the Xenon to Krypton ratio of the primary circuit.

ISOTOPE	Half-life	Fission Yield [3] (Recommended - Cumulated) U_{235}	Pu_{239}
Kr 85m	4.48 hours	1.311	0.550
Xe 133	5.29 days	6.770	6.973

Moreover, because of the purification of the Iodine 133 precursor of the Xenon 133 in the primary circuit, one could also expect a significant decrease of the Xenon to Krypton ratio of a "clean" cycle, compared to a cycle during which failure occurs (UO_2 failure and a fortiori MOX failure).

The study of the evolution of the ratio, over the different cycles, is to give the position and therefore time of the UO_2 and the MOX failures.

3. *PRIMARY CIRCUIT ACTIVITY EVOLUTION*

After multiple fuel failures in the early years of operation (densification and hydriding) fuel performance was good with generally stable primary circuit coolant activity at 100 to 150 MBq/m^3 I 131 and about 3 GBq/m^3 of Xe 133. Cycles 15 and 20 are typical for a core not containing defect fuel assemblies [Fig. 2 and 3]. During cycle 17 a leak developed after about 90 days of operation resulting in an increase in I 131 activity of 50 % and in Xe 133 activity of 100 %, once a new equilibrium was reached [Fig. 2]. The leaking fuel assembly was not identified during the following shut-down and was therefore reinserted in cycle 18. Both the I 131 and Xe 133 activity increased rapidly in cycle 18 confirming the presence of a leaking fuel assembly in the core and the development of additional leaks. Again the activity levels stabilized after about 1/3 of the cycle at an elevated level. Single rod UT examination after cycle 18 as well as the dry sipping of fuel assemblies failed to clearly identify the leaking fuel assemblies at this time.

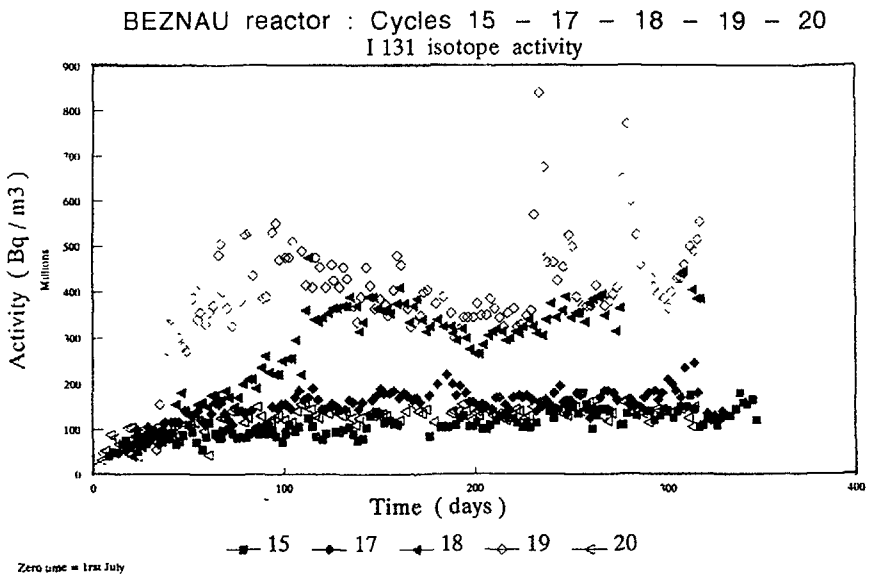

Fig.2

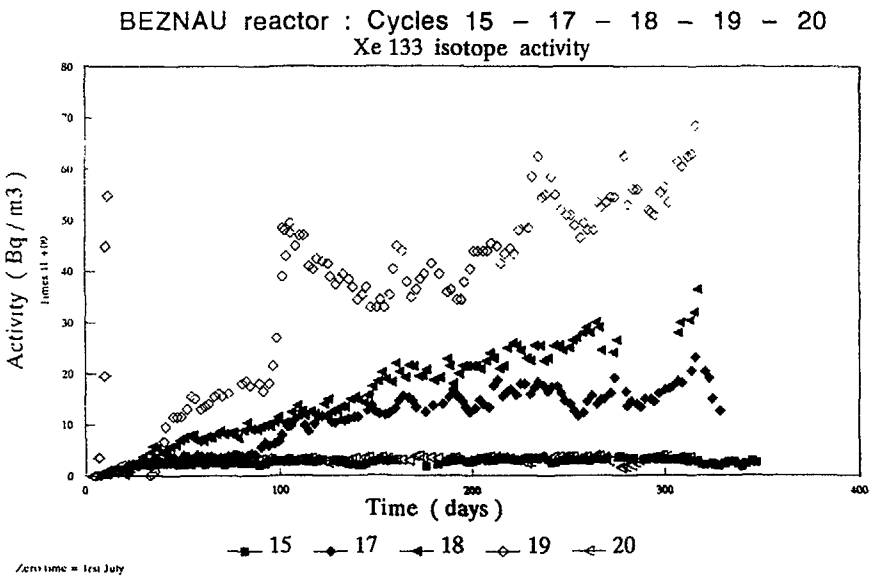

Fig.3

The rapid increase of activity in cycle 19 confirmed the presence of leaking fuel assemblies. Early in cycle 19 the plant was shut-down for steam generator repair. At this occasion the fuel assemblies were again leak tested with sipping and single rod UT examination. Fuel assembly 2004 was identified leaking and removed from the core. It was already suspected leaking at the previous shut-down but had been reloaded, due to the ambiguity of the test results obtained with the two detection methods.

The start-up of subsequent cycle 19A confirmed, that not all of the leaking fuel assemblies had been removed from the core. The I 131 activity stabilized in that cycle at about 2 - 3 times the value for a tight core with distinct bursts of Iodine releases while the Xe 133 activity steadily increased 20 times the background value, again with distinct bursts of activity at several times during the cycle.

Fuel sipping after the shut-down of cycle 19A identified 5 leaking fuel assemblies (assemblies 1704, 1915, 1926, 2019 and M107). Assembly M107 had been suspected leaking at the previous two shut-down but was reloaded due to the ambiguity of the test results obtained with the two detection methods.

Coolant activity data for cycle 20 confirmed that all leaking fuel assemblies had been removed from the core and I 131 as well as Xe 133 activity levels were in line with those for cycle 15.

4. *POOLSIDE EXAMINATION*

In 1990 the six defective fuel assemblies previously identified were repaired by replacing the defective fuel rods with stainless steel rods [Ref. 2]. Poolside TV inspection of the failed fuel rods established debris induced fretting at the first grid as the primary failure mechanism in five of the six cases. The following analysis is limited to these failures. Also there were one or more secondary failures visible on each failed fuel rod. Figure 4 shows the debris scars below grid 1 and the hydride blister between grid 4 and 5 of rod A08 of assembly 2019. Figure 5 shows the debris scars below grid 1 and the hydrided and cracked tubing at the top end plug of rod M12 of the MOX assembly M107. These pictures are representative of the failures due to debris fretting.

Fig 4 FUEL ASSEMBLY 2019, ROD A08

Fig 5 FUEL ASSEMBLY M107 ROD M12

5. *HISTORY OF FUEL FAILURE*

The following table sums up, for the successive cycles

CYCLE	PERIOD	CORE COMPOSITION	FAILED FUEL EVALUATION BY END OF CYCLE	FUEL FAILURES DEVELOPMENT HISTORY DEDUCTED FROM PRIMARY RADIOCHEMISTRY ANALYSIS FOR THE RESPECTIVE CYCLE
15	July 1985 to June 1986	121 U FAs	No leaking fuel rod	No leaking fuel rod
17	July 1987 to May 1988	121 U FAs	1 Xe/Kr burst but no failed fuel assemblies identified *	A primary failure 90 days after BOC
18	July 1988 to May 1989	109 U FAs +12 MOX FAs	U FA 2004 after 1 irradiation cycle found leaking by rod UT examination but not confirmed by sipping : reloaded for cycle 19 U FA 1904 after 2 irradiation cycles found suspected by sipping, but not by rod UT examination : reloaded for cycle 19	A secondary type failure 110 days after BOC
			MOX FA M107 : after 1 irrad. cycle found suspected by sipping but not by rod UT examination : reloaded for cycle 19	Primary type failures between 150 and 190 days
19	2 weeks in July 1989	97 U FAs +24 MOX FAs	U FA 2004 : leaking by sipping and rod UT examin.: removed. Not yet repaired. U FA 1904 : suspected by sipping not by rod UT examination : reloaded for cycle 19.A	A secondary type failure after 10 days
			MOX FA M107 : suspected by sipping, not by rod UT examination : reloaded for cycle 19 A	
19A	August 1989 to May 1990	97 U FAs +24 MOX FAs	U FA 2019 : after 1 cycle U FA 1926 : after 2 cycles U FA 1915 : after 3 cycles U FA 1704 : after 3 cycles failed by sipping and rod UT examination : removed, repaired in December 1990.	3 secondary type failures developed 40 days, 200 days and 250 days after BOC respectively
			MOX FA M107 : after 2 cycles failed by sipping and rod UT examination : removed, repaired in December 1990 and reloaded in cycle 21	Secondary type failures developed between 60 days and 190 days after BOC
20	July 1990 to May 1991	89 U FAs +32 MOX FAs	No leaking fuel rod	No leaking fuel rod
21	July 1991 to June 1992	85 U FAs +36 MOX FAs	Cycle not yet finished	No leaking fuel rod up to the date of issue of present paper

* normally only those fuel assemblies are leak tested which are unloaded definitively from the core

- the fuel failure development history as deduced from the primary water radiochemistry analysis
- the evaluation and decisions made at the end of the respective cycles, based on the on site inspections performed using plant sipping equipment and rod UT examination system.

The radiochemistry analysis of primary water has allowed to detect the time of occurrence of the main defects (secondary type defects), and provided the activity of the water is not too high, the time of occurrence of the primary type defects.

The analysis has also allowed to differentiate when the failure occurs in a MOX rod versus a uranium rod.

The defects were confirmed at the end of the cycles when high water activity has resulted in performing poolside examination (sipping tests and rod UT examination).

6 *ACTIVITY RELEASES RESULTING FROM U and MOX FUEL ROD FAILURES*

Figures 6 and 7 provide the beta and tritium activity evolution during cycles 15, 17, 18, 19 and 20 For the gamma activities, the representative examples of Xe 133, I 131, Cs 137 and Cs 134 are plotted in Figures 2 3 8 and 9 respectively since they are the main long life contributors to the activity of the coolant The beta activity provides an illustration on the total amount of fission products activity released to the coolant The tritium is incorporated also, since MOX fuel is known to generate more tritium by ternary fissions than U fuel

Superimposed on the graphs of Figures 10 and 11 are the primary and secondary failures determined as explained in the previous sections of this paper

The beta activity of the primary circuit increases slightly (up to a factor 2) due to fuel failures, with no influence of the type of fuel that failed The absence of a clear step increase at each failure is an indication that the coolant activity is predominantly affected by fuel released into the coolant by earlier failures

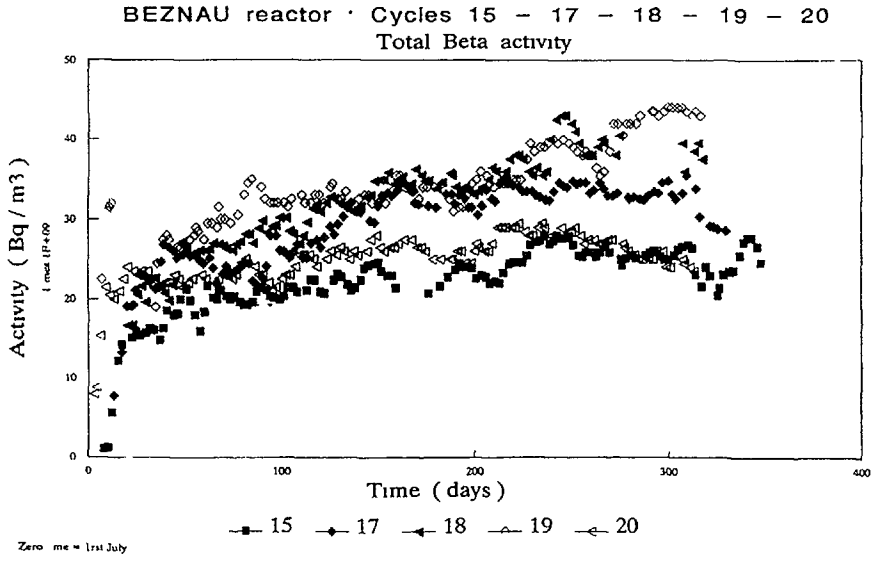

Fig 6

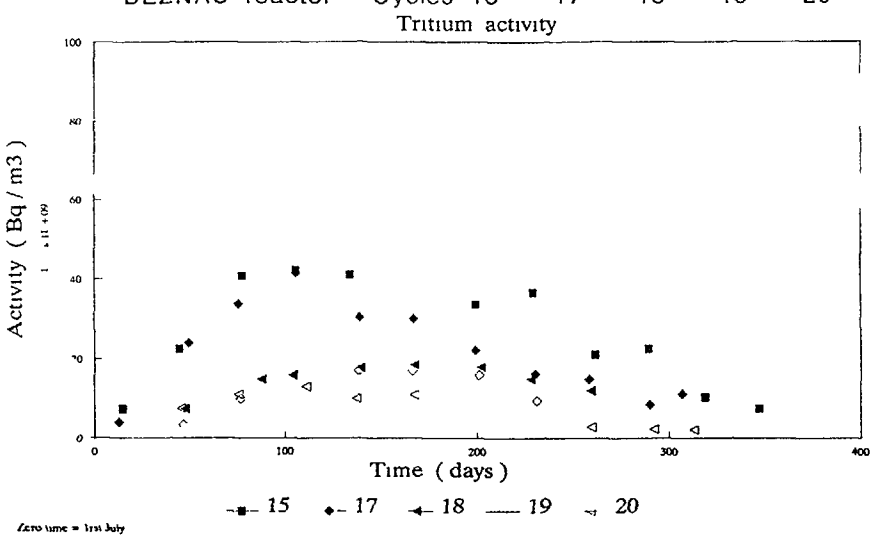

Fig 7

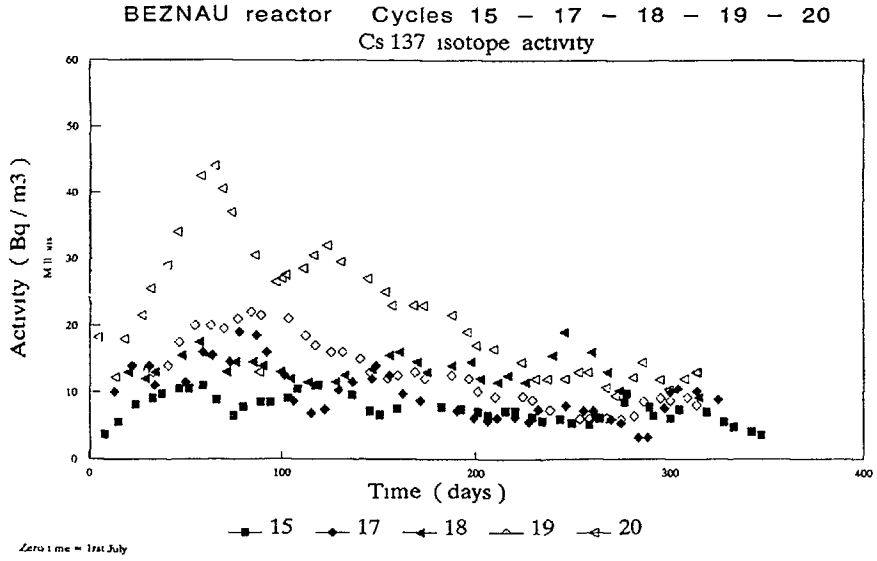

Fig 8

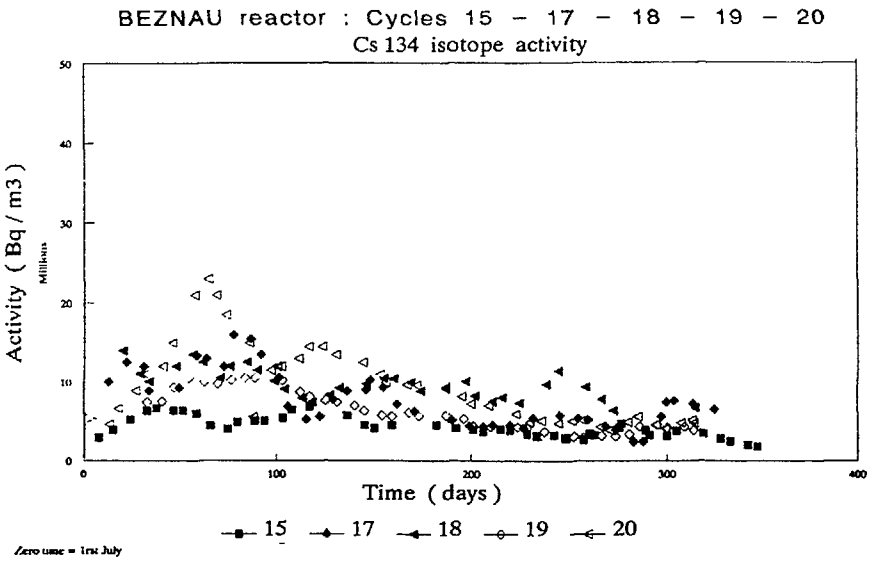

Fig.9

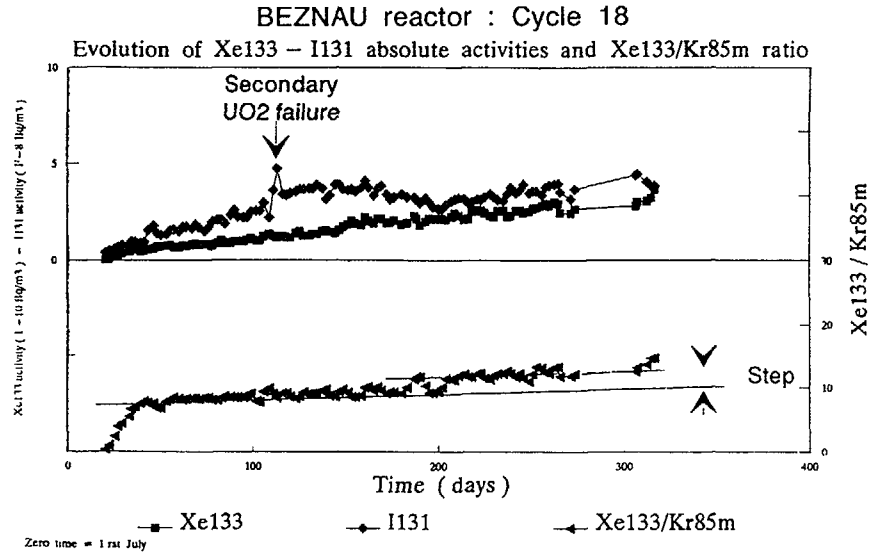

Fig.10

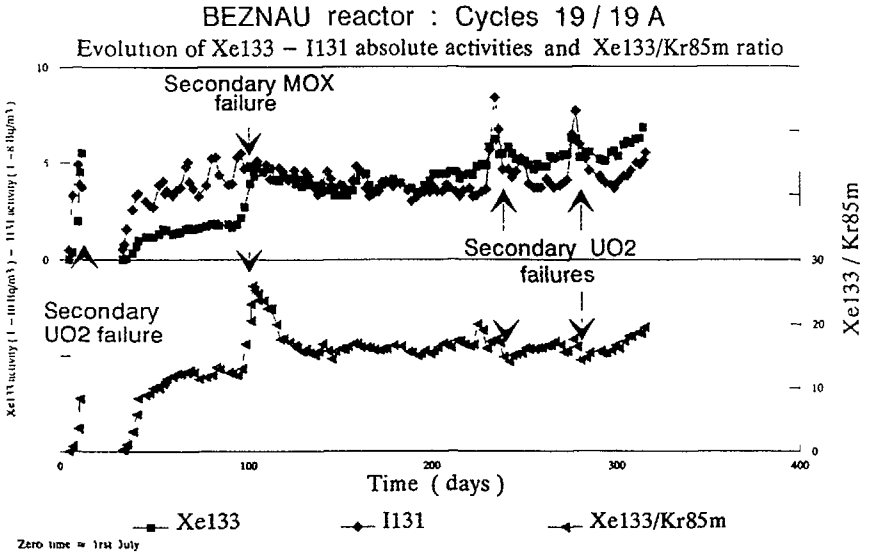

Fig.11

The typical increases of activity of the long life fission products for a primary and a secondary failure of both types of fuels is summarized in following Table. It shows that the two MOX failures induced an increase of coolant activity within the range observed for U failures and even indicate that, in this particular case, the effects were rather milder for MOX failures.

Fission product Half-life	Xe 133 5.3 d	I 131 8 d	Cs 137 30 a	Cs 134 2.1 a
Units	GBq/m^3	MBq/m^3	MBq/m^3	MBq/m^3
Primary failures				
U fuel	10	50	n d	n d
MOX fuel	5	n d	n d	n d
Secondary failures				
U fuel	20 (5-50)	300 (200-500)	5 (n d - 20)	3 (n d - 30)
MOX fuel	15	100	1	n d

n d : not detectable
(x - x) : range of values observed

The evolution of the tritium activity shows no influence of the failures of either U or MOX fuel. It confirms that the main source of tritium in the coolant is the transmutation of B of the boric acid.

7. *CONCLUSION*

The occurrence of debris induced failures affecting 5 U fuel rods and 2 MOX fuel rods indicated that the failure mechanisms are not affected by the type of fuel. This can be expected for the primary failures which are initiated from the water-side, but not necessarily for the secondary failures. The latter could indeed be affected by the fuel characteristics (density, in-pile densification rate, gap size, ...) and its propensity to be oxidized by water.

Lag time between primary defect detection and secondary defect occurrence ranges between 200 and 300 days and appears to be similar for both UO_2 and MOX fuel assemblies.

Not only have the failure characteristics found to be the same, but the activity releases were not worse for MOX failures than for U failures.

ACKNOWLEDGEMENT

The assistance of H.P. MEIER at the BEZNAU plant in collecting the chemistry data is greatly appreciated.

REFERENCES

[1] H. Bay, P. Deramaix, A. Charlier,
MOX Fuel Reloads in BEZNAU 1
IAEA TCM - Recycling of Pu and U in LWR Fuels,
Cadarache, 13 to 16 November 1989

[2] H. Bairiot, H. Bay, P. Deramaix,
Repair of MOX Fuel Assemblies -
A Practical Experience
IAEA TCM - Poolside Inspection,
Repair and Reconstitution of LWR Fuel Elements
Lyon, France - 21 to 24 October 1991

[3] M.E. Meek and B.F. Rider
Compilation of Fission Products Yields
Vallecitos Nuclear Center, 1974

SPECIFIC EXPERIMENTAL APPROACHES

(Session V)

Chairmen

T. OKUBO
Japan

J.R. STANBRIDGE
United Kingdom

MIXED OXIDE FUEL IN DEFECTIVE EXPERIMENTAL ROD EDITHMOX 1: IRRADIATION RESULTS AND METALLOGRAPHIC PIE

D. PARRAT
Direction des réacteurs nucléaires,
Commissariat à l'énergie atomique,
Centre d'études nucléaires de Grenoble,
Grenoble

Y. MUSANTE
Fragéma/Framatome Division Combustible,
Lyon

A. BRISSAUD
Service Etudes et projets thermiques et nucléaires,
Villeurbanne

France

Abstract

In connection with the normal refuelling of French Pressurized Water Reactors with mixed oxide (MOX) fuel assemblies, a comprehensive experimental programme has been developped by CEA, FRAMATOME and EDF. The objective of the new experimental data yielded by this programme is the validation of general design of MOX rod , leading to improve its performance.

An important point of this study is the behaviour of a defective MOX rod under irradiation, and especially the release rate of fission products. In France, a reactor cannot be in operation when primary coolant activity is beyond given thresholds, and necessitates an increase of surveillance when cladding defects occur. So it was necessary to verify that present activity limits, set up with UO_2 fuel, could be transposed without (or with minor) adjustments to MOX fuel.

In order to answer this question, an experimental defective MOX fuel rod, named EDITHMOX 01, has been recently irradiated in the JET POMPE irradiation loop in the SILOE research reactor at the CEA's Nuclear Research Center in Grenoble.

The experiment had two aims:

** determination of the experimental release rate of fission product from mixed oxide in a defective early in life rod. The cladding leak, located in front of the fuel pellets, had a high hydraulic conductance. The rod was irradiated at several steady-state power levels, similar to those found in normal operation of a PWR.*

** Comparison of these results with those obtained in the case of uranium oxide in the EDITH, CYFON and CRUSIFON programmes.*

The power levels conducted were in the region of 8, 15, 20 and 27 kW/m. Fission product release was measured by on-line gamma spectrometry and water sampling.

After irradiation, examinations were conducted to know the behaviour of the rod:

** Non destructive tests to appraise possible external changes and measure the internal fission products distribution.*

** Destructive tests to know the mixed oxide fuel's evolution under water conditions, essentially by means of metallographic sections and microstructure study.*

The results of this experiment show a release rate of fission products comparable to those obtained with uranium oxide. Metallographic analyses show an appreciable evolution of microstructure, with fission gas precipitation bubbles, due to fuel oxidation under water vapor conditions.

However, to cover the entire range of MOX fuel operating conditions in PWR's, these results should be validated for higher burn-up levels.

1. INTRODUCTION :

Since 1987, several French Pressurised Water Reactors are partially loaded with MOX (mixed oxide $(UPu)O_2$) fuel assemblies. At the end of 1991 in France, 216 MOX assemblies have been irradiated or were in irradiation.

The validation of general designs of MOX rod is made by means of a comprehensive experimental programme developped by CEA, FRAMATOME and EDF. This study includes post-irradiation examinations on irradiated rods in power reactors (during 1, 2 or 3 cycles), and analytical experiments in research reactors on short instrumented rods.

An important point of this programme is the behaviour of a defective MOX rod under irradiation, especially the release rate of fission products out of the pellet stack, and the behaviour of mixed oxide under water and vapor conditions. These data control the activity level observed in the primary coolant and its future evolution during the cycle at steady power levels and during transients.

Under normal operating conditions of a PWR the appearance of failures on fuel rod clads provoke the plant operator to realise a special surveillance of the primary coolant activity by means of gamma spectrometry. As regards the French PWR park, the frequency of such measurements is determined by operating technical specifications. It ranges from one measurement per week in the absence of failure to one or two measurements per day beyond a given activity threshold [1]. This strategy aims at complying with the primary activity limits provoking the reactor shutdown. So it was necessary to verify that present activity limits, set up with UO_2 fuel, could be transposed without (or with minor) adjustments to MOX fuel.

2. DESCRIPTION OF THE EDITHMOX 1 EXPERIMENT:

In order to answer this question, an experimental defective MOX fuel rod , named EDITHMOX 1, has been recently irradiated in the JET POMPE irradiation loop in the SILOE research reactor at the CEA's Nuclear Research Center of Grenoble

The aim of this experiment is to obtain the following informations

- determination of the fission product release rate from the oxide by means of a mixed oxide fresh fuel rod exhibiting a defect with high hydraulic conductance at the fuel stack, and irradiated at different steady-state reactor power levels ,

- comparison of these results with those already obtained for uranium oxide in the corresponding experiments of the EDITH, CYFON and CRUSIFON programmes at CEA/DRN/DTP [2] and with those published elsewhere [3].

3. DESCRIPTION OF THE EDITHMOX FUEL ROD (SEE FIGURE 1) :

The clad of the rod is of the Zircaloy-4, standard 17x17 design currently used in PWRs The fuel stack has a length close to 340 mm and comprises 27 mixed oxide pellets whose plutonium content is 7 1% There are a further two 5,1% enriched uranium oxide pellets located at the bottom end of the rod, which are used as a reference during gamma scanning Finally, an alumina pellet at each end of the pellet stack allows reproduction of the thermal effects normally observed at these locations in power reactor

The cladding defect is a cylindrical hole 0 3 mm in diameter The hole is drilled before rod loading and is located close to the core mid-plane and approximately at the mid-height of a mixed oxide pellet

4. EXPERIMENTAL IRRADIATION FACILITIES :

Irradiation took place in the JET POMPE test loop of the SILOE reactor (see figure 2) The thermodydraulic conditions of the irradiated section are close to those in a PWR reactor (water flow rate around rod 3 5 m/s, pressure 130 bar, temperature 280°C held steady irrespective of power level by a regulated electrical heater)

A bypass line routes the water from the test facility to the CEA/DRN Fission Product Analysis Laboratory, where its activity is continuously measured by on-line gamma spectrometry and by sampling on a regular basis

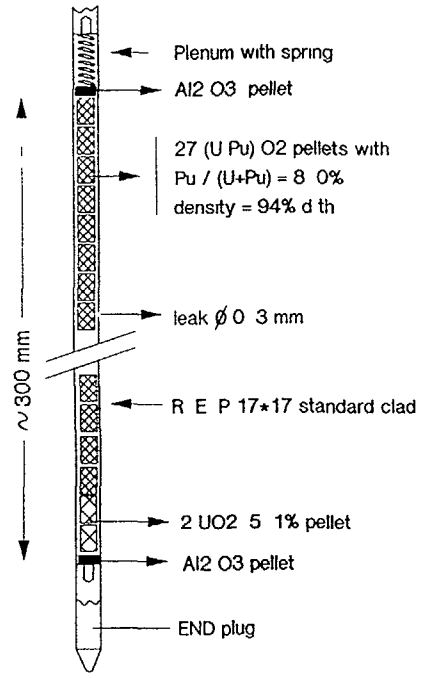

Figure 1 : The EDITHMOX 1 fuel rod

The analysed water is purified and gas-stripped, then routed again to the test loop The correct operation of the purification process is regularly checked by sampling

The absence of any change in fuel rod mechanical behaviour is also periodically checked by alpha spectrometry on water samples taken on a regular basis

5. PERFORMANCE OF THE EXPERIMENT - MAIN FINDINGS :

The rod was irradiated during three cycles of the Siloe reactor from May to August 1989, at steady-state power levels between 8 and 27 kW m^{-1} (see figure 3)

At the first power level (8 kW m^{-1}), fission gas and iodine release was studied with the fuel-cladding gap filled with water The power level was held at 25 kW m^{-1} at the beginning and end of irradiation to check release rates in the event of major

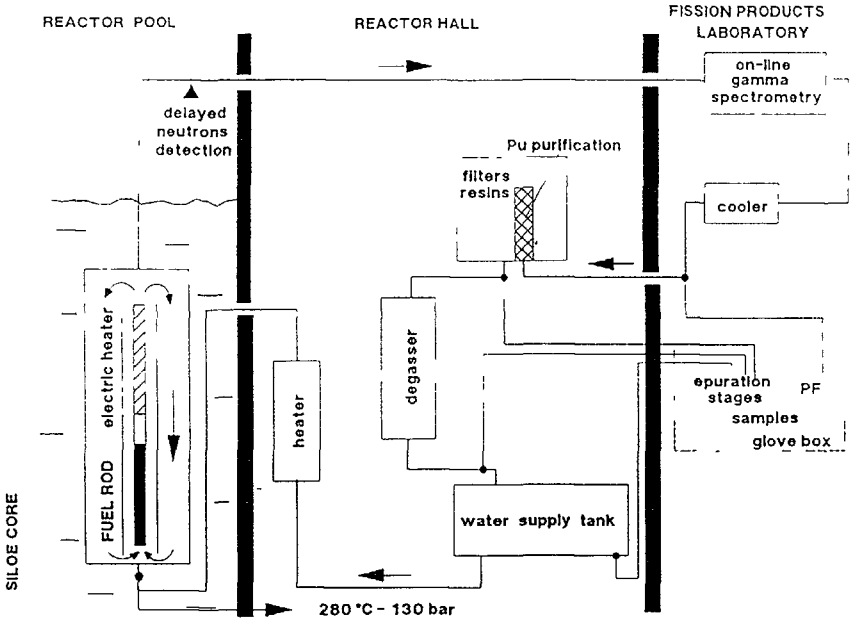

Figure 2 : JET POMPE irradiation loop

fuel densification. The 17 kW.m^{-1} power level was chosen because it is close to the unstable two-phase regime in the gap.

Each power hold lasted about 10 days.

A longitudinal gamma scanning examination was conducted at the end of the first cycle : no abnormal pattern was observed in fission product distribution and the linear power value supplied by neutron dosimetry was adjusted.

Since the excellent operation and the design of the test facility allow laboratory sampling after routing of the water at loop pressure and temperature, it is possible to closely monitor the emission of airborne or gaseous fission products from the rod up to a radioactive half-life of about 30 seconds.

Based on the specific activities measured in the bypass line fluid, calculation is made for each radionuclide of the release rate R/B defined below :

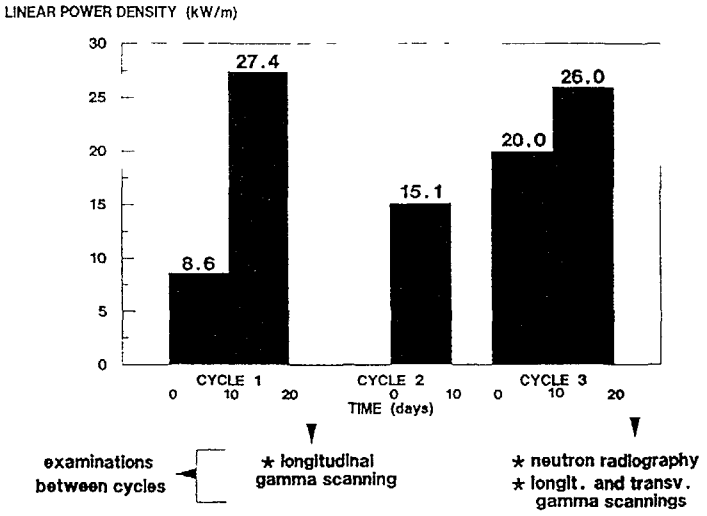

Figure 3 : Time History of irradiation

$$\frac{R}{B} = \frac{\text{Number of atoms emitted per second}}{\text{Number of atoms generated per second at radioactive equilibrium}}$$

The plot of release rates versus half-lives for each fission product is a straight line whose level and slope yield information on the mechanisms controlling release from the oxide and migration through the fuel/cladding gap.

An exemple of the EDITHMOX 1 findings is shown in figure 4.

Given the considerable hydraulic conductance of the cladding defect, the transit times through the gap are short and the R/B measurements are representative of release rates from mixed oxide, at least for gaseous fission products. For iodine, an in-gap partial retention and trapping mechanism is visible on the plots : iodine is released during the rod depressurisation-cooling sequence at the end of the cycle.

The mixed oxide release rate values versus rod linear power given by the EDITHMOX 1 experiment are plotted for ^{133}Xe, ^{85m}Kr, ^{131}I and ^{133}I in figures 5 and 6. They are clearly compatible with the "Recommended Values" established for uranium oxide on completion of the EDITH, CYFON and CRUSIFON programmes [2].

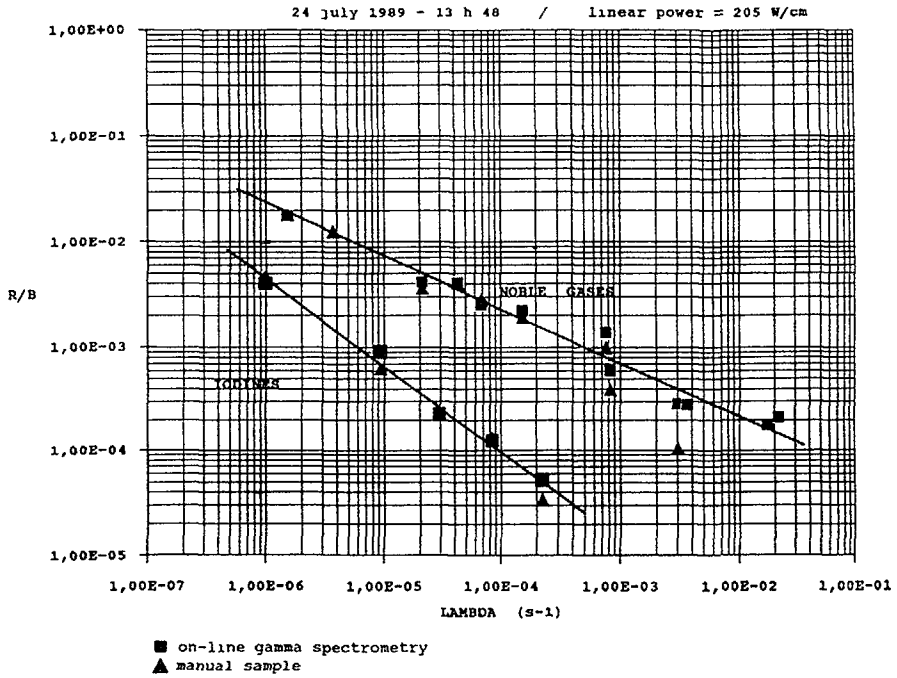

Figure 4 : Example of FP release rate obtained during irradiation

6. METALLOGRAPHIC POST IRRADIATION EXAMINATIONS :

After irradiation, several examinations have been performed on the rod.

* Non Destructive Examinations : visual and photographic inspection, Eddy Current and Metrology, and longitudinal gamma scanning.
* Destructive Examinations : two sections in the MOX pellets stack have been performed :

  - one at the level of the defect (mid - height of pellet 22) : cut Number a,
  - one at the bottom of the stack (mid - height of pellet 4) : cut Number b,

with the following examinations : metallographic analysis, alpha and (beta-gamma) radiography, section gamma scanning.

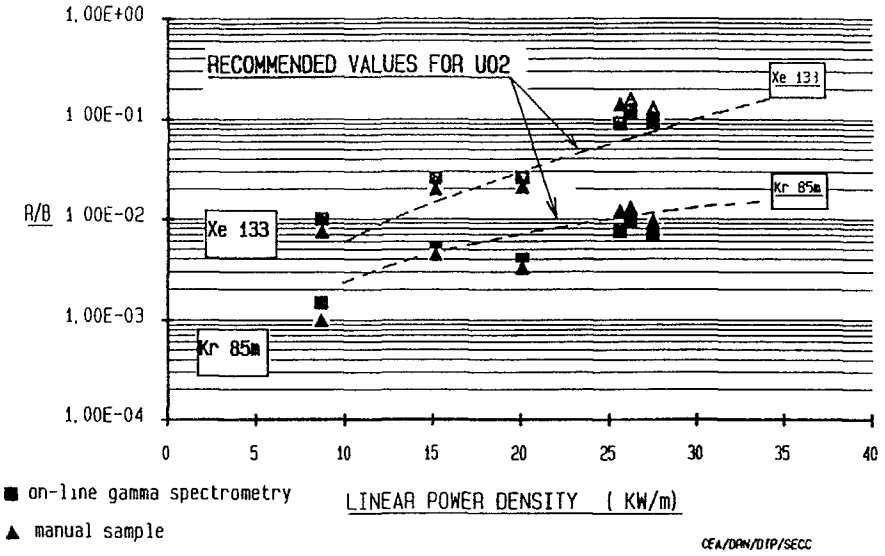

Figure 5 : Release rate of gaseous FP versus linear power

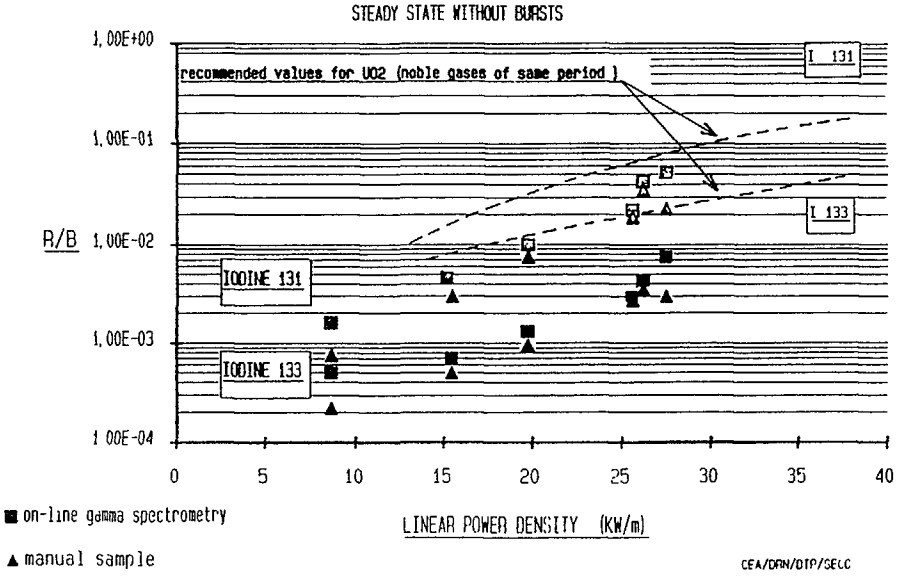

Figure 6 : Release rate of halogens versus linear power

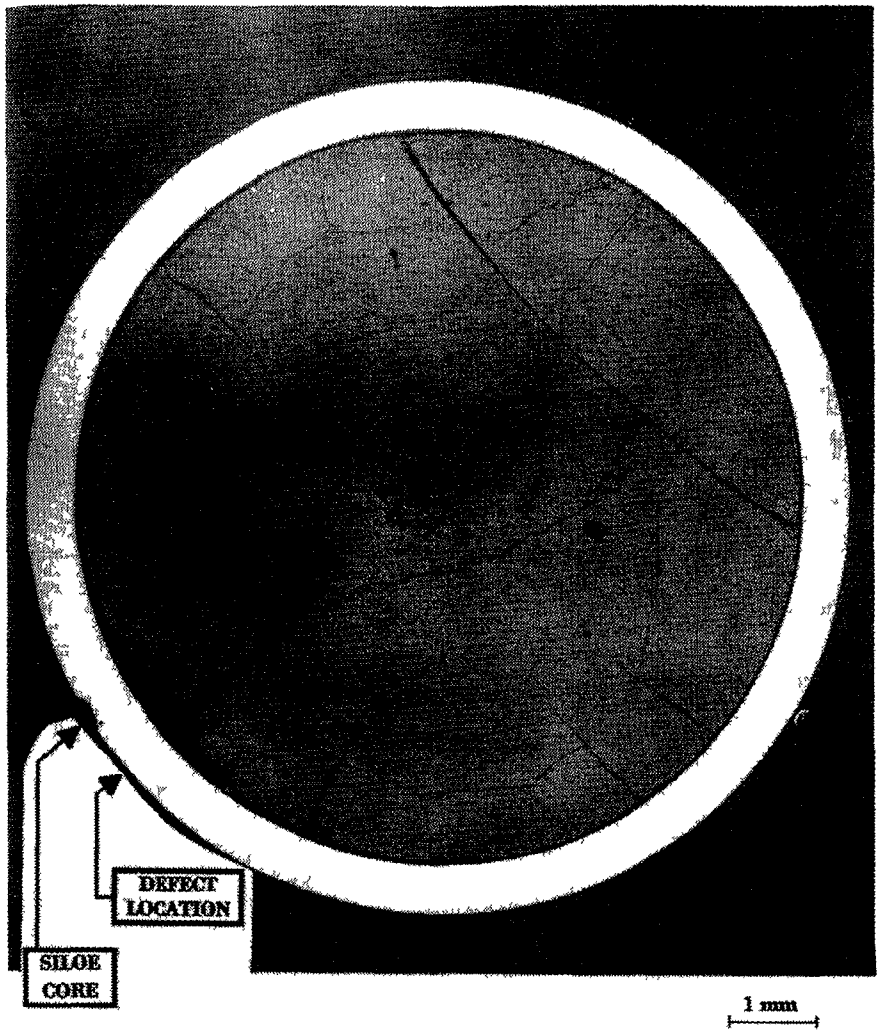

Figure 7 Metallographic section at the level of the defect

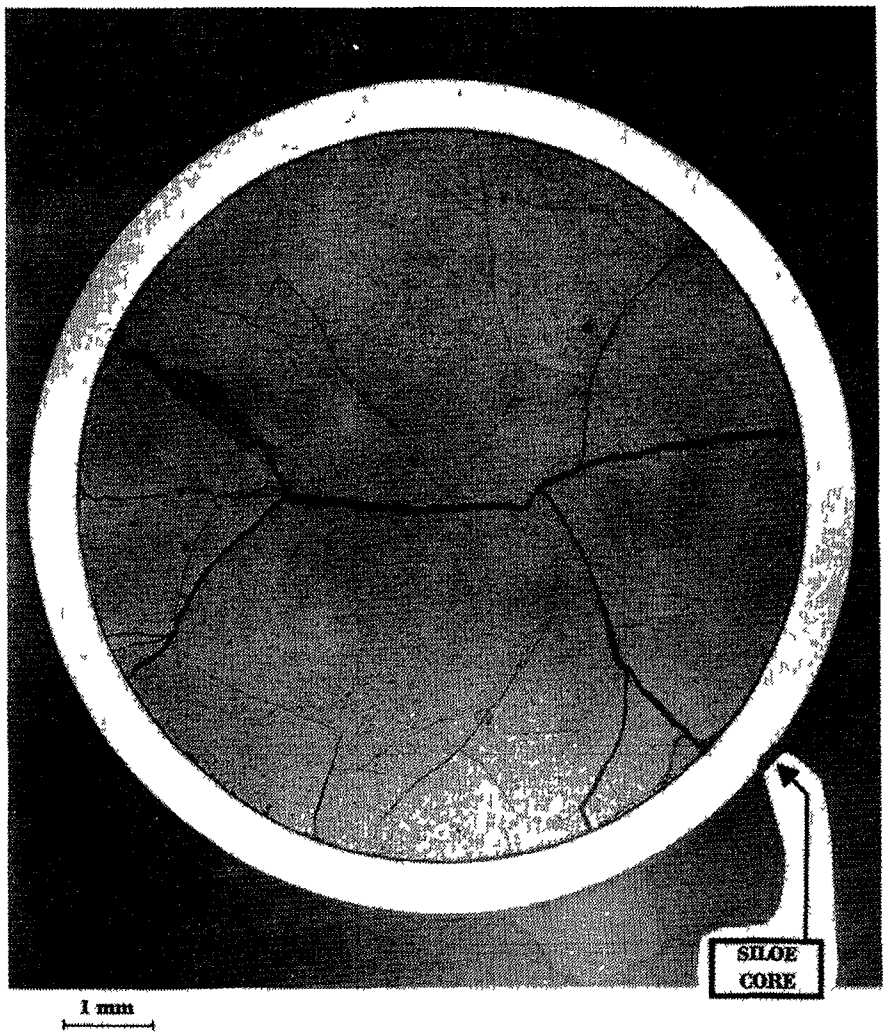

Figure 8 Metallographic section at the bottom of the MOX stack

The most interessant results are issued of the metallographic sections these cuts (see figure 7 and 8), and especially the cut Number a, show non-uniformity of microstructure, with gas bubbles precipitation at grain boundaries, and grain growth at the center of the pellet This evolution corresponds with a strong oxidation of the mixed oxide due to water vapor conditions These remarks are not usually observable on an early-in-life UO_2 pellet

7. CONCLUSIONS :

The successful performance of the EDITHMOX 1 experiment yielded values representative of gaseous and airborne fission product release rates from a mixed oxide fresh fuel stack under steady-state conditions, for power levels encountered in PWR

operation. These values are comparable with the findings of the uranium oxide experiments and fully compatible with the "Recommended Values" established for this type of fuel.

Metallographic examinations show an appreciable evolution of microstructure, with gas precipitation bubbles, due to fuel oxidation under water vapor conditions.

However, to cover the entire range of MOX fuel operating conditions in PWRs, these results should be validated for higher burn-up levels.

REFERENCES

[1] P. BOURNAY
Management of failed fuel during operation : French policy and experience.
IAEA Technical Committee Meeting on Fuel Failure in Normal Operation of Water Reactors ;
Dimitrovgrad, 26-29 May 92.

[2] H. SEVEON, C. LEUTHROT, P. CHENEBAULT, R. WARLOP, J.P. STORA.
Release of Fission Products by Defective Pressurised Water Reactor Fuel -
International Meeting on Nuclear Reactor Safety,
Karlsruhe, 10-13 septembre 1984.

[3] E. SCHUSTER, F. GARZAROLLI, K.H. NEEB, H. STEHLE.
Release of Fission Products from Defective Fuels Rods of Light Water Reactors.
AIEA Specialist' Meeting, Chalk River, Septembre 1979.

STUDIES IN THE R2 TEST REACTOR OF SECONDARY DAMAGE FORMATION IN LWR FUEL RODS WITH SIMULATED DEFECTS

H. MOGARD, M. GROUNES, H. TOMANI, G. LYSELL
Studsvik Nuclear AB,
Nyköping, Sweden

Abstract

Fretting type failures are pre-dominant causes of the very few fuel failures that have occurred in recent years in LWRs. These primary failures are sometimes followed by secondary failures which frequently cause considerably larger activity releases. In such cases the subsequent degradation of the defect fuel rods by internal hydriding of the cladding and by oxidation of the fuel are the common destructive mechanisms.

STUDSVIK NUCLEAR has introduceed an irradiation test scheme, adapted to the experimental conditions in the R2 test reactor, which offers the possibility of executing comparative investigations of the process of degradation of commercial types of LWR fuel under simulated primary defect conditions as well as of the mechanisms involved. In the new type of test the primary defect is simulated by a special device on top of the fuel rodlet containing an enclosed small reservoir of liquid water in such a manner that only water in the form of steam will communicate with the plenum volume and the interior of the rodlet.

Data from the first exploratory test are presented and show that the test method gives relevant data. A second experiment, now in progress, is described. A proposed third series of experiments will constitute an International Fuel R&D Project, the Defect Fuel Degradation Experiment (DEFEX). The objectives and extent of the proposed project are described.

1. BACKGROUND INFORMATION

1.1. INTRODUCTION

The operational reliability of LWR Fuel is currently less than desired [1]. Expressed in relative numbers the failure rate is very small, of the order of 10 in a million fuel rods. However, considering the economical consequences of the failures encountered the reliability is unsatisfactory [2].

The causes of the fuel failures in LWRs vary. Fretting type failures are predominant, in particular those caused by various types of loose objects, debris, accidentally appearing in the primary coolant system. However, irrespective of the causes of the primary failures, these are sometimes followed by a secondary failure which can cause considerably larger activity releases

than the original primary failure. In such cases the subsequent degradation of the defect fuel rods by internal hydriding of the cladding seems to be a common destructive mechanism. The hydriding leads to the formation of secondary failure, which typically gives rise to a steadily increasing release of radioactivity to the coolant. Occasionally fuel pellets are eroded and fuel particles which are spread in the primary water coolant system may persist for years as radioactive sources.

The secondary damage phenomenon is an important current fuel behavior problem and appears to be strongly dependent on the fuel design. Obviously, the ambitions of the nuclear industry are to take preventive measures against these failure occurrences. A better understanding of the mechanisms behind the fuel degradation process is called for in view of the fact that a variety of fuel designs are now being implemented. These designs might each react differently to the intrusion of water. Only a better knowledge of the degradation mechanisms can help us find the mitigating means required to minimize the consequences of a primary failure event.

The secondary damage formation phenomena and the underlying processes have been described in detail in a recent STUDSVIK NUCLEAR study, commissioned by the Swedish Nuclear Power Inspectorate (SKI) [3].

1.2. SWEDISH FUEL FAILURE EXPERIENCE

A number of fuel failures have occurred during the last few years in Swedish BWRs. Most of these fuel failures (60 %) have been identified as being caused by fretting debris [1]. The sequence of the fuel rod degradation stages, as observed visually, is schematically illustrated in Figure 1 and seems to follow the classical route of degradation as summarized by Pickman [3].

In some recent cases the fuel burnup level of the failed fuel rods was moderate, about 10 000 MWd/tU, which means that the pellet/cladding gap was still not fully closed. Three different stages of degradation can be distinguished (Figure 1). At stage 1 the fretting object penetrates the clad wall, coolant water flows into the open fuel rod volume and a fission product spike follows. After some time of continued power operation (stage 2) internal hydriding is initiated, and a secondary defect develops at some distance (0.3-0.4 m) away from the primary defect. However, the new defect is not being associated with any noticeable spike release of fission products. On continued power operation (stage 3), the internal hydriding continues at various spots in the lower section of the fuel rod, again at some distance away from the latest formed defect, until another penetrating defect develops. In the meantime the first formed secondary clad defect tends to open up as a result of local fuel pellet swelling. This causes the cladding to split up in the longitudinal direction, thereby exposing the UO_2 pellets to the eroding effect of the coolant water.

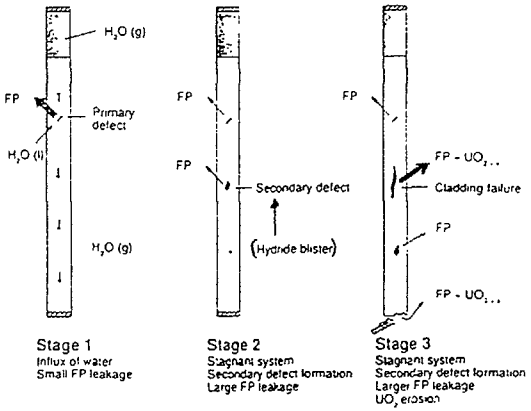

Figure 1

Observed secondary defect development.

A spectacular exception to this slowly progressing fuel rod degradation was seen in the failure event at the Oskarshamn 3 BWR a couple of years ago, when a single zirconium liner fuel rod failed under a large release of radioactivity and split up axially along almost its entire length [4]. A similar failure event has later been reported from the BWR Leibstadt unit in Switzerland [5]. In this case, an exceptionally large release of radioactivity was also noted. In both these cases it was stated that the operational mode during the degradation process was unfavorable to the defect fuel. In fact, other failure events with Zr liner fuel have resulted in only limited release rates quite similar to non-liner fuel failures [5]. In the autumn of 1991 extensive secondary defects were observed in the Wolf Creek PWR in the U.S. Such defects were found in 40 fuel rods in 3 fuel bundles [6].

The repeated failure incidents in the Swedish BWRs prompted the Swedish nuclear industry to look for plausible failure mechanisms and remedial measures. Various means to minimize the consequences of continued operation of defect fuel, especially in the case of internal hydriding, have in the meantime been introduced by ABB Atom e. g. 1) by lowering the linear heat rating through a shift to significantly smaller diameter rods as in the 10x10 fuel rod configuration and 2) by making the zirconium liner material more corrosion resistant [4].

1.3. THE MECHANISM OF CLAD INTERNAL HYDRIDING

The mechanism of clad internal hydriding in BWR type fuel has been theoretically evaluated by Davies [7]. According to his work the hydride formation is initiated when the water vapor,

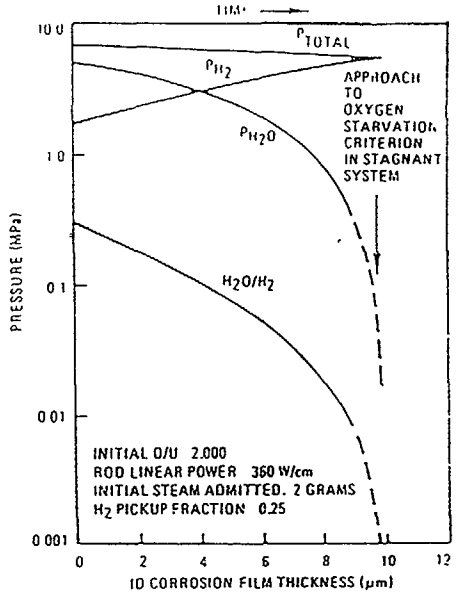

Figure 2

Development of H_2O and H_2 pressures in a defected fuel rod after Davies [7].

reacting with Zircaloy in a stagnant heated system, decreases in partial pressure to such a low value that the ratio of the partial pressures of water vapor and hydrogen produced by corrosion, p_{H2O}/p_{H2}, decreases into the range of about 0.01-0.10 (Figure 2). The critical conditions thus defined represent a kind of "oxygen starvation" situation within the closed system. Also, another critical condition should be fulfilled, i. e. the partial pressure of hydrogen P_{H2} should simultaneously exceed about 10-20 mm Hg, Figure 3.

Operational experience indicates that the rate of internal hydriding in a Zircaloy clad fuel rod decreases at lower heat rating. This is in line with the expectation that the rate of oxidation of the UO_2 (to form $UO_{2\pm x}$) as well as the radiolysis of the water decrease with lower fuel temperature. However, according to recent information, a long term exposure over three reactor cycles of a defect PWR fuel rod at such a low heat rating as 10 kW/m resulted in fuel oxidation and internal hydriding [8]. In that case Zr1%Nb cladding was used.

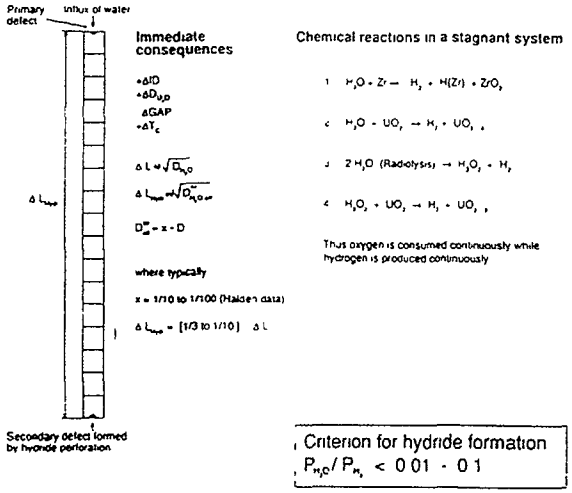

Figure 3

Secondary damage formation mechanism.

2. OUTLINE OF THE STUDSVIK FUEL TEST SCHEME

The outline of the new test technique differs on essential points from previous irradiation test schemes adopted for checking the potential degradation of intentionally defected test fuel. An appropriate revised test scheme, to be used at the R2 test reactor, has to fulfil certain experimental constraints i. e.

1 the length of the test fuel rodlets should not exceed the active core height (600 mm) of the R2 test reactor.

2 the release of fission products and fuel material from the defect fuel must be minimized in order that the contamination of the in-pile water loop circuit be tolerable.

Both these requirements can be met with the unique but simple test technique adopted. Instead of an artificial primary defect (drilled hole etc) the primary defect is now simulated by a special device at the top end of the fuel rodlet [9]. This device contains an enclosed small reservoir of liquid water in the "extension plenum", (Figure 4). This extra plenum is connected with the normal plenum volume of the rodlet through a tiny tube (the "steam snorkel") in such a manner that only water in the form of steam will communicate with the plenum volume and the interconnected void space of the interior of the rodlet. Heat is transferred to the enclosed water reservoir from the surrounding

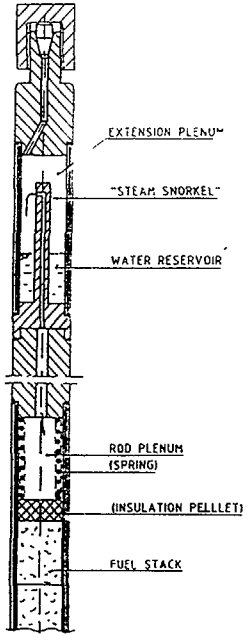

Figure 4

Array Simulating Primary Defects in Fuel Rods. (Patent pending).

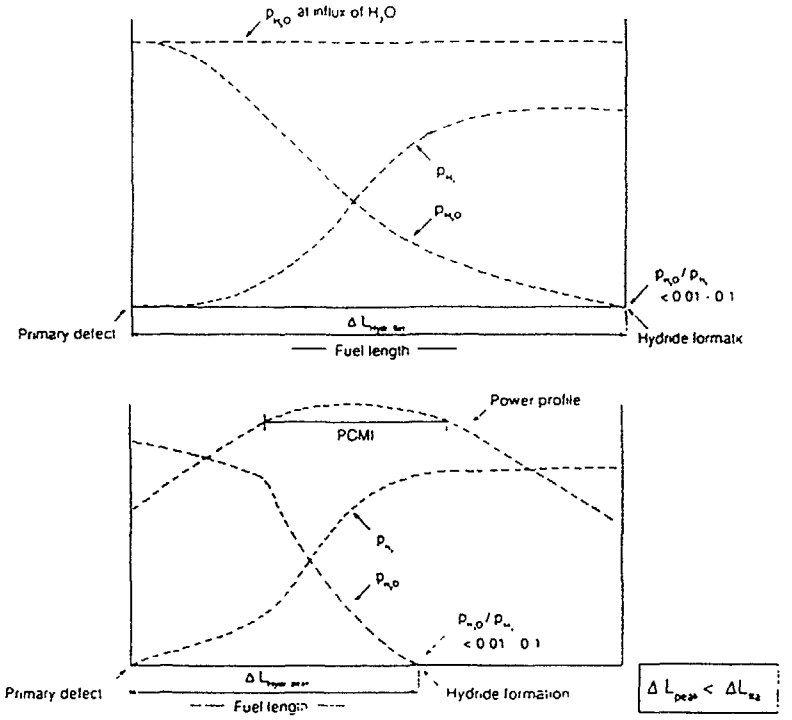

Figure 5

Partial pressures at flat power profile (top) and peaked power profile (bottom).

pressurized loop water at the start of the operation until the pressure and temperature of the whole system are in balance, simulating either BWR or PWR operating conditions.

An important experimental feature of this arrangement is the possibility of post-irradiation puncture and subsequent collection of released fission gases and hydrogen from the closed system of the individual rodlets being irradiation tested.

A test fuel rodlet is subjected to a modestly peaked axial power profile and the linear heat generation rate (LHGR) is maintained constant during the test period (one reactor cycle of about 16 days). The LHGR is kept sufficiently high to effectively close the fuel pellet/clad gap over the power peaked length section of the fuel rodlet, see Figure 5. The simulated single defect is located in the top plenum region where the steam is let in. By this arrangement the diffusional migration of H_2O and H_2 in the axial direction will be constrained to such an extent that axial concentration gradients and partial pressure gradients can build up and be maintained at a steady LHGR level until the termination of the test period. Hydriding is consequently expected to be initiated and to progress in the lower part of the fuel rodlet.

In addition to the two experimental constraints mentioned, it is considered desirable to reach hydriding conditions during one R2 operational cycle (lasting 400 hrs) in the majority of tests, both from an economic point of view and in order to maintain well-defined and undisturbed test conditions. Interrupted exposures or wider power variations downwards mean that water repeatedly enters all along the fuel length and eliminates the dynamic gas equilibrium conditions established during the steady operating power period and also interferes with the on-going chemical reactions in the system. However, in some cases, where hydriding has not initiated or is slow, it has been proposed that a few 2-cycle, or even 3-cycle irradiations might provide additional interesting data.

During the steady exposure the water tends to oxidize not only the inner surface of the cladding but also the UO_2 fuel pellets, which, as a result, tend to attain higher temperatures and swell. The thermal conductivity of the filler gas will, of course, also be affected. The rate of the thermal expansion and swelling is recorded by an on-line elongation extensometer, and the change in pellet-clad mechanical interaction can be followed by the use of the STUDSVIK power noise measuring technique during the exposure time [10].

3. EXPLORATORY TESTING OF PROMOTED/SUPPRESSED HYDRIDING

3.1. DEFECT FUEL EXPERIMENT NO. 1

The feasibility of creating internal hydriding conditions in the lower part of the fuel rodlet in the manner described was the primary objective of the first part of the irradiation test development. Another aim was to check if the reversed conditions could be created, i.e. to suppress hydriding, assuming that the primary objective was fulfilled.

For the first exploratory tests, financed by Swedish organizations, two unirradiated fuel rodlets of the 8x8 BWR type were available. However, they were not identical in details. One fuel rodlet was of the standard type and was originally manufactured for the past INTER-RAMP Project [11] (0.15 mm gap, L/D=1.1, dished pellets, no chamfer, density 10.17). The other rodlet (0.20 mm gap, L/D=1.1, dishing, slight chamfer, density 10.41) was provided with a "rifled" cladding [12] which is characterized by a large number (e.g. 40) of axially extending grooves of 10-15 microns peak depth in the interspace between the fuel pellet column and the multifaceted prismatic bore of the cladding during operation.

Both rodlets were subjected to a steady LHGR of 45 kW/m for the full duration of an R2 operational cycle (16 days). The axial rod power profile form factor (peak value to mean value) was close to 1.2. The intention was to operate under mechanically closed pellet-to-clad conditions, at least over the mid part of the fuel rodlets. The rifled clad fuel rodlet, however, retains its clad grooves open for axial gas migration even under mechanically closed gap conditions. The aim was to check if the availability of some unrestrained migration of H_2O and H_2 would suffice to suppress the onset of hydriding.

The experimental results so far show that both aims were successfully reached. However, about midway during the first test cycle a reactor scram occurred which to some extent disturbed the interpretation of the test results. Therefore, for the purpose of comparison, a simulated scram was imposed at about the same point in time during the irradiation of the second rodlet.

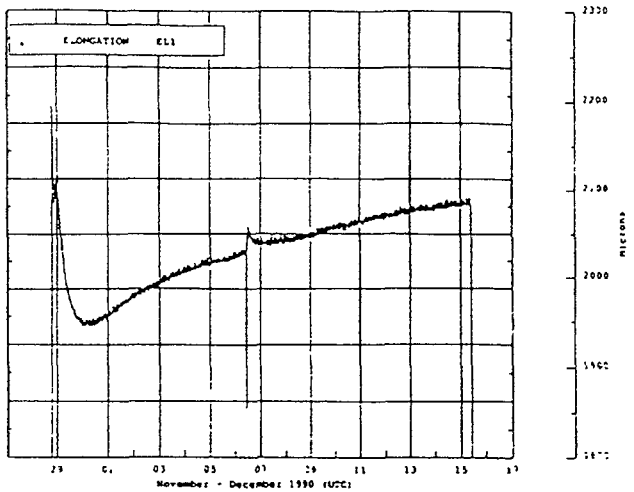

Figure 6

On-line elongation measurements, rod 1117 (standard cladding).

The fuel rod elongation measurements indicated approximately the same length change behavior for both rodlets during the constant power stage of the irradiation cycle. As expected an initial clad contraction was recorded in both cases, which was, however, of much shorter duration for the rifled clad fuel rodlet. What was not expected was the temporary reversal of the contraction after some 3 hours holding of the standard rodlet; see Figure 6. It has not yet been established whether this reflects e.g. a pellet hang-up or the onset of a major local hydriding.

Subsequent to the clad contraction period an immediate and substantial clad elongation commenced which then slowed down gradually during the constant power stage. Evidently an ongoing expansion of the fuel pellet column is reflected, indicating also a persistent hard mechanical pellet/clad interaction in both rodlets.

The subsequent eddy current examination clearly indicated defects in the bottom part of the standard type rodlet, one signal being very strong. However, no defects were recorded for the rifled clad rodlet. The definite proof of internal hydriding in the standard type rodlet was provided by neutron radiographs which showed that heavy hydriding had occurred in the standard type rodlet at the 6th pellet level from the bottom and minor hydriding at the 4th and 2nd pellet levels, Figure 7. Both hydrides and water may appear around the non-enriched bottom pellet and at

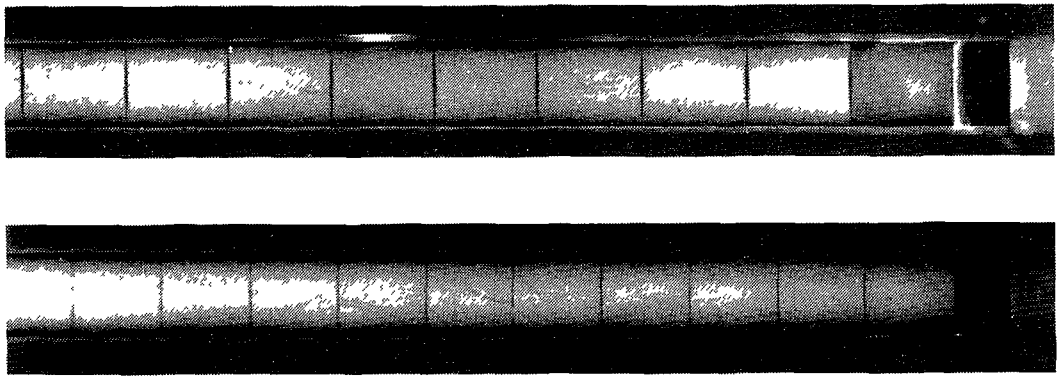

Figure 7

Neutron radiographs of standard cladding rodlet (top) and rifled cladding rodlet (bottom). Bottom end plugs to the right. White area at the sixth pellet shows hydrides.

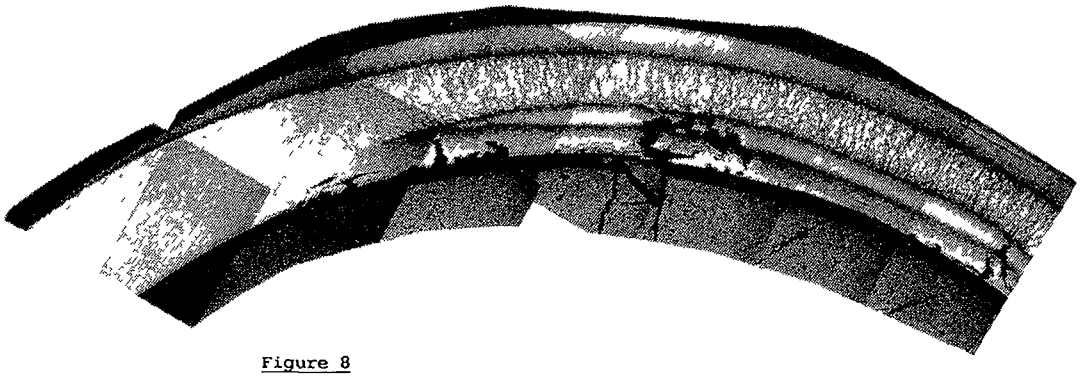

Figure 8

Micrograph of the standard cladding rodlet at the sixth pellet.

the end plug weld. In contrast, no hydriding was seen anywhere in the rifled clad rodlet, but there were possible indications of water at the bottom end plug.

The hydride concentration seen on the neutron radiograph of the rodlet with standard cladding (see Figure 7) was investigated by metallography, Figure 8. The hydrides are concentrated at both the inside and the outside of the cladding. The center region of the cladding is a zone where hydrogen is moving from the inside hydride rim to the outside rim. The hydrides in this region are seen to be radially oriented. This is caused by the large volumes of the inner and outer hydride rims thus stretching the zone between them in the tangential direction. The large cracks in the inside hydride rim are caused by shrinkage of the inside rim material compared to an earlier state when all the hydrogen now seen in the outside rim was still part of the inside rim forming one or more "sunbursts" at the inside.

3.2. DEFECT FUEL EXPERIMENT NO. 2

In this experiment three unirradiated fuel rodlets of the 8x8 BWR type were manufactured with the same type of pellets but with three different types of cladding:

- standard ("non-liner") Zircaloy-2
- Zircaloy-2 liner fuel, of the same type as used in the failed Oskarshamn 3 fuel rod discussed earlier [4]
- Zircaloy-2, rifled cladding.

These experiments are also financed by Swedish organizations and the actual irradiations are not part of the proposed international program outlined in Section 4 below. The experiments will be performed during 1992, and data from the test on the rodlet with standard cladding will be published as soon as possible; the remaining data will be made available to the actual participants in the international program.

3.3. CONCLUDING REMARKS ON THE EXPLORATORY TESTS

The irradiation test approach applied seems well suited for studying the initial phase of the degradation of experimental type fuel rodlets. The degradation process can be followed by non-intrusive on-line measurements like elongation measurements and noise measurements.

The rate of fuel rod degradation depends on the actual LHGR during operation. Preferably the LHGR should be kept constant during the test period in order not to complicate behavior and interpretation. Later studies of various non-steady operational schemes might, however, be justified since some operational modes might affect the mechanisms involved and accelerate the degradation process. The measured times until initiation of internal hydriding and through failures as a function of LHGR for a given fuel design can preferably be plotted in the form of a "modified Locke's diagram" (Figure 9). This would provide a method for comparing the propensity for secondary defect formation of different types of fuel.

4 A PROPOSED INTERNATIONAL PROGRAM

4.1. BACKGROUND

STUDSVIK NUCLEAR has since many years organized a series of internationally sponsored fuel R&D projects. During the last years an international program, the Defect Fuel Degradation Experiment (DEFEX), has been under discussion with interested parties (utilities, fuel suppliers, safety organizations and national research organizations in Europe, Japan and the U.S.).

4.2. OBJECTIVES

The objectives of the proposed DEFEX program would be:

* Investigate the various phenomena and design parameters which characterize and influence the degradation process and its time dependence during exposure of the test fuel at relevant heat ratings as regards in particular
  1. initiation of clad internal hydriding
  2. clad failure by hydriding and the effect of pellet and clad oxidizing
* Investigate the degradation process at
  1. near zero fuel burnup
  2. medium fuel burnup (10-20 MWd/kgU)
* Investigate under similar test conditions
  1. standard type fuel rodlets (BWR 8x8 and PWR 17x17)
  2. zirconium liner type fuel rodlets (BWR 8x8)
  3. potential remedy type fuel rodlets (BWR 8x8) (e.g. rifled cladding)
* Collect experimental data for defect failure modeling and make use of STUDSVIK NUCLEAR's special defect fuel modeling code
* Compare the experimental data, e.g. in a Locke's type failure diagram, in order to facilitate comparisons between different fuel designs.

4.3 FUEL RODS

Two main groups of fuel rodlets are under discussion:

Group A: Un-irradiated BWR and PWR fuel rodlets, specially made for the project: The following rodlets have been proposed:

BWR 8x8 type of rodlets with 0.15 mm gap, manufactured for the Project by ABB Atom and identical with the fuel rodlets tested in Defect Fuel Experiment No. 2.

* 2 rodlets with standard ("non-liner") Zircaloy-2 cladding
* 2 rodlets with zirconium liner fuel, of the same type as used in the failed Oskarshamn 3 fuel rod [4].
* 1 rodlet with rifled cladding.

PWR 17x17 type of rodlets with 0.12 mm gap, manufactured for the project

* 3 rodlets with standard ("non-liner") Zircaloy-4 cladding

This part of the program can to a large part be regarded as a generic water reactor program, of equal interest to BWR and PWR participants. However, it cannot be excluded that important differences in behavior may exist as regards the time of onset and the rate of degradation by hydriding between the BWR and PWR designs as a result of the differences in clad temperatures during operation. The rifled BWR type fuel rodlet is included for mechanistic reasons i.e. to investigate the effect of unconstrained axial migration. Also, it offers potential as a remedy design against degradation.

Group B: Irradiated BWR and PWR fuel rodlets, refabricated by the STUDFAB process from irradiated full-size LWR power reactor fuel rods with a burnup of about 10-20 MWd/kgU. It is assumed that two sets of BWR rods and one set of PWR rods will be selected, with 3 rodlets per set and with gaps of about 0.20 mm and 0.16 mm, respectively.

The selection of fuel rod parameters will be made in consultation with the prospective project participants.

4.4 IRRADIATION PROGRAM

All fuel rodlets will first be irradiated during one 400-hr cycle in an in-pile loop in the R2 test reactor (BWR rods in a loop operating under BWR temperature and pressure conditions and PWR rod in a loop operating under PWR conditions). After non-destructive examinations some selected rods will be irradiated further during a second (and possibly third) 400-hr R2 reactor cycle. Non-destructive examinations will be performed between cycles. The following program has been proposed:

Group A: Near 0 burnup (unirradiated rodlets to be irradiated during 400 or 800 or possibly 1200 hrs).

	Rod Type			LHR
	Non liner	Liner	Rifled	kW/m
	N	L	R	
BWR	x	x	1	45
rods	1	1	x	40
	1	1	x	35
PWR	1	x	x	45
rods	1	x	x	40
	1	x	x	35

Group B: Rodlets with 10-20 MWd/kgU burnup, refabricated by the STUDFAB process from irradiated full-size LWR power reactor fuel rods. Each of the three rod types would be irradiated at three different LHGR levels.

It is foreseen that some of these 17 fuel rodlets will not exhibit any hydride initiation during first 400-hr cycle in the R2 reactor. Some of them will then, after non-destructive examination, be exposed to a second (and possibly a third) 400-hr cycle.

ACKNOWLEDGEMENT

The experimental part of the work described was made possible through the support of the Swedish Nuclear Power Inspectorate (SKI), Vattenfall AB, OKG AB and Sydsvenska Värmekraft AB, which is hereby gratefully acknowledged.

REFERENCES

[1] Strasser A et al., Fuel for the 90's - A Utility Perspective. ANS/ENS International Topical Meeting on LWR Fuel Performance, Avignon, France 21-24 April 1991. Vol 1, p 2-16.

[2] Yang R L, Ozer O, Klepfer H H, Fuel Performance Evaluation for EPRI Program Planning. ANS/ENS International Topical Meeting on LWR Fuel Performance. Avignon, France, 21-24 April 1991. Vol 1, p 258-271.

[3] Pickman D O, Failure Development in Leaking LWR Fuel Rods - A Literature Survey. STUDSVIK/NF(R)-89/83. Studsvik AB, Sweden. 1989.

[4] Jonsson Å et al., Failure of a Barrier Rod in Oskarshamn 3. ANS/ENS International Topical Meeting on LWR Fuel Performance, Avignon, France, 21-24 April 1991. Vol 1, p 371-377.

[5] Davies J H, Potts G A, Post-Defect Behavior of Barrier Fuel. ANS/ENS International Topical Meeting on LWR Fuel Performance, Avignon, France, 21-24 April 1991. Vol 1, p 272-284.

[6] Reckley, W D, Summary of Meeting held on November 12, 1991 to discuss the Fuel Rod Failures Discovered during the Refueling Outage at Wolf Creek Generating Station. U.S. NRC Docket No. 50-482, November 25, 1991.

[7] Davies J H, Secondary Damage in LWR Fuel Following PCI Defection - Characteristics and Mechanisms. IAEA Specialists' Meeting on Defected Zirconium Alloy Clad Ceramic Fuel in Water Cooled Reactors. Chalk River, Canada, 17-21 September 1972. (IWGFPT/6, p 135-140).

[8] Hüttig W, Forberg M, Berndt R, Ergebnisse von Nachbestrahlungsuntersuchungen über das Hüllen- und Brennstoffverhalten in Brennstäben mit künstlichen Lecks. Jahrestagung Kerntechnik '91, Bonn, Germany. Proceedings, p 311-318.

[9] Tomani H, STUDSVIK AB, Pat. Pending.

[10] Oguma R, Bergdahl B-G, Schrire D, Application of a Recursive Identification Technique to Noise Analysis for Fuel Performance Study. Specialists' Meeting on Reactor Noise (SMORN-V), Munchen, Germany, 12-16 October 1987 Also Prog in Nuclear Energy 21(1988), p 357-360.

[11] Mogard H et al., The Studsvik INTER-RAMP Project - An International Power Ramp Experimental Program. ANS Topical Meeting on LWR Fuel Performance. Portland, Oregon, USA, April 29-May 3, 1979, p 284-294, (DOE/ET/34007-1).

[12] Mogard H, Kjaer-Pedersen N, Improved PCI and FGR Performance of LWR Fuel Using Rifled Cladding. IAEA Technical Committee Meeting on Fuel Performance at High Burn-up for Water Reactors. Studsvik, Sweden, 5-8 June 1980. (IWGPFT/36, p 147-159).

EXPERIMENTAL STUDY ON THE WWER FUEL BEHAVIOR IN RESEARCH REACTORS AND SHIELDED HOT CELLS

A F GRACHEV, V B IVANOV,
V V KONYASHOV, V P SMIRNOV
Research Institute of Atomic Reactors,
Dimitrovgrad, Russian Federation

Abstract

Some experimental results of post irradiation examination of VVER 1000 fuel are given A complex of technical means and methods, which are used for investigation of all stages of fuel defect appearance and development, is presented This complex comprises the SM 2, MIR and VK 50 reactors and the hot laboratory

The main source of the potential danger for radioactive contamination of the environment is burnt-up fuel of nuclear reactors and one of the radioactive debris propogation barriers is a fuel element cladding. Inspite of the fact that the relative amount of the WWER fuel elements failure is small from the point of view of the current safety concepts each event of the fuel element failure should be thoroughly considered in order to reveal and eliminate its causes. Taking into consideration a sufficiently wide range of the known causes and mechanisms of the defects appearance and development and asuming that there are also unknown ones, methods and equipment for investigation of the fuel element failure should meet various reqirements, i.e. they sould be universal. To cover all possible approaches of the failed fuel study the basis should involve as minimum:

- shielded hot cells (poolside test benches) with a complete set of methods and equipment for detection of the failure fact and location as well as for study of causes that led to cladding failure;
- test reactors provided with means for simulation of different operating conditions to perform investigations on standard fuel behavior and dynamics of the processes leading to fuel failure or direct experiments with irradiated fuel having artificial cladding defects in order to study dynamics of the defect development and primary sequences of such failure;
- shielded hot cells with a special rig for investigations performed on fuel behavior in the reactor under operation after primary loss of intergrity (boundary conditions of severe accedents);

Such choice of equipment allows for investigation of the LWR fuel.

1. Comprehensive failed fuel investigation program.

First of all it should be noted that the programs under realization involve the following types of fuel failure: changes of fuel element and assembly geometric dimensions and shape due to non-uniformity of irradiation strain, local thickness reduction of the fuel assembly wrapper or fuel element cladding caused by fretting corrosion, spacer grids geometry changes (crumpling, damage), formation of thick deposit layers on the fuel element cladding, local and extended corrosion areas, cracks and , finally, cladding perforation as a possible place for fission products release.

Primary investigations of standard fuel for commercial reactors performed in the hot cells are oriented to detection of anomalies or, if a fuel assembly is untight, search of defects. These investigations involve: visual inspection of the fuel assemly and its fragments; leak checking of fuel elements in the assembly based on gas release; measurement of the cladding and fuel element elongations; study of deformation; eddy-current flaw detection of fuel elements; axial gamma-scanning of fuel elements; neutron or x-ray radiography; analysis of gas quantity and composition in the fuel element free volume. The above methods and instrumentation allow, in most cases, for detection of all types of anomalies (by comparison with other fuel elements and designed characteristics) or verification of the perforation availability in a certain place of the cladding. In case when the primary investigations cannot provide exact determination of the causes of fuel failure or anomalies formation the following distructive investigation methods are used: metallo- and ceramography; quantity and composition analysis of interaction and deposit layers on the cladding; fuel density determination; gamma-scanning along the radius of polished samples; elementary microanalysis; x-ray structural analysis; measurement of the cladding strength properties.

Selection of standard fuel assemblies for investigations is performed on the basis of mutual discussion held by the representatives of the NPS chief designer, chief fuel production engineer and hot laboratory experts.

The investigations of standard fuel assemblies reveal failure causes but they do not always explain the machanism of the defect development under normal and what is more, under complicated operating conditions.

These tasks are being solved in the SM-2 and MIR research reactors of the institute and involve for each fuel type experiments for study of the fuel element behavior in the following operating conditions: transients; pulsed fuel nuclear heating; heat removal crisis; simultaneous reduction of the coolant flowrate and pressure; filling of the superheated fuel elements with cold coolant.

With these experiments it is possible to model practically all normal operating conditions and those of the designed accident. Both newly manufactured fuel elements(or their prototypes) and refabricated ones with irradiated fuel and claddings including those with artificial defects. The concrete parameters and type of the experiments are defined by the chief designer of the reactor and chief engineer of fuel production.

A number of experiments with failed fuel is performed with some restrictions in the VK-50 NPS with the boiling vessel-type reactor. These investigations are aimed at the determination of radiation sequences of the NPP operation with failed fuel elements, gaining of experimental data for further validation and improvement of the calculation methods for prediction of radioactive fission product (RFP) release from the fuel elements under water cooling conditions of the reactor. The investigation program comprises:

- study of the RFP background activity levels in the reactor circuit conditioned by the contamination of the fuel element cladding surfaces with fuel in the course of manufacturing;
- study of the RFP release from the failed fuel elements under the NPP operation, performance of separate experiments in transients;
- study of the RFP release from the fuel elements with artificial defects of different size under irradiation in various parts of the reactor core with different intensity;
- study of the RFP release from the failed fuel elements (including those after long-term storage) during their inspection in the out-of-pile stand for cladding leak testing, choice of the optimum inspection method and procedure;
- post-irradiation material science examinations of the fuel elements with artificial defects.

The comprehensive program involves investigations of temperature dependence of the fission product release from fuel. They are performed at special stands in the hot cells.

These investigations make it possible to understand in what quantities and what chemical forms the fission products release from fuel and to determine the dynamics of these processes. Such information is required in order to refine the physical models of the processes and to up-date the calculation program.

2. Methodical basis of the program and some data on the investigation experience

2.1. Detection of defects and measurement of their size

Detection of defects begins with visual inspection of the fuel assembly wrapper (for instance, those of WWER-440),bundle and single fuel elements. Visual devices with a magnification of 30 are used for this purpose. They are connected with photo-, videocameras and computers (Fig.1). In most cases surface anomalies and defects are successfully detected already at the visual inspection stage. As a rule they represent external cracks, corrosion spots, deposit, etc. (Fig.2).

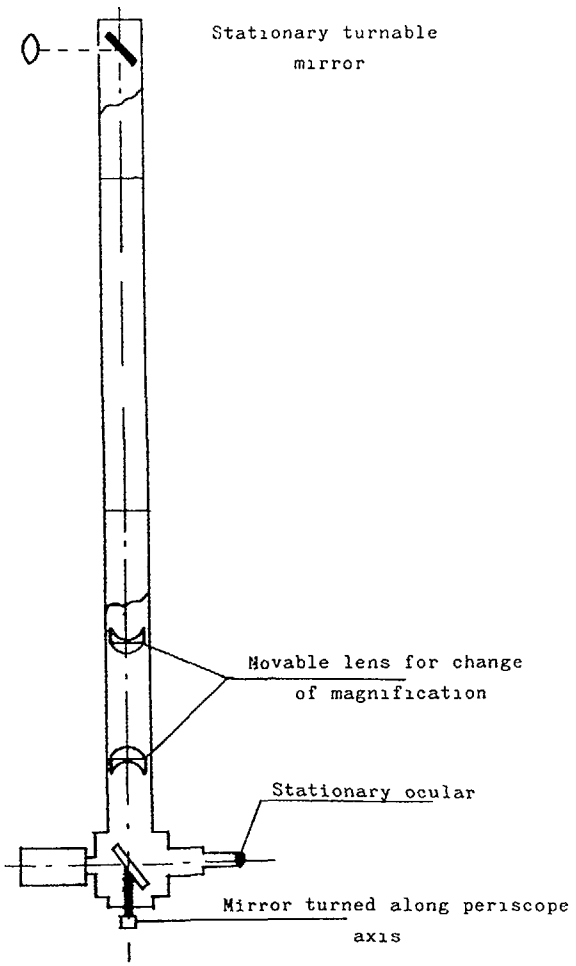

FIG 1 Periscope with variable magnification (the photograph is made through the flange at the top of the turnable periscope head)

THe investigation of the size of wrapper defects is performed with a device provided with three pairs of contact sensors, each of them defining the wrapper surface relative coordinate independent of the others [1]. The investigation results on deformation are presented in the form of vectors of the fuel assembly twisting and bending and also axial distribution of its transverse size (Fig.3).

The device allows for detection of prominences on the fuel assembly wrapper. The prominences in the minimum hexagonal dimensions correspond with the spacer grid locations and could be related to spacer grid striking against the wrapper walls in the process of the fuel assembly operation. The diameter of the spacer grid cells, providing horisontal fixation of fuel elements, is measured with gauges and presented in the form of specialized tables (Fig.4).

An external damage of the fuel element claddings is often observed in the places where the spacer grids are located or where the cladding comes in contact with other objects. In this case the anomalie and defects size can be defined by means of profilometry, visual inspection and metallography. Nowdays profilometry has found a wide application, the measurement error being + 5 m (Fig. 5) [2]. Metallography is the most reliable method for size determination of small defects.

Cracks, cladding hydrogination, including those connected with secondary defects, can be detected by the eddy-current flaw detection. Both pulse and harmonic excitation methods are used in the flaw detection. The minimum size of the defect recorded with certainty is 0.3 of the cladding thickness. Fig.6 presents the eddy-current diagram of the fuel element with a technological defect of 0.2 mm and secondary fuel element failure.

Cladding defects that make fuel release from the fuel element possible are detected by gamma-scanning. The same method is used for verification of the secondary defect accompanied by the cladding hydrogiation, thermal conductivity deterioration, increase of the fuel temperature and, as a result, cesium-137 migration from the defect area (Fig.7)

In some cases for the final verification of the defect availability the fuel element cladding is punctured with the laser beam and the analysis of the gases volume, pressure and composition is performed with the mass-spectrometer.

2.2. Study on the fuel failure causes and sequences

After the defect is detected the program of further investigations is worked out in accordance with its type. The information on the peculiarities of its production process and irradiation history are taken into consideration. The investigations make it possible to determine deposit thickness and composition by chemical, radiochemical and metallographic methods, to perform fuel ceramography (Fig.8) and study fuel structure and nuclide distribution along the radius by polished samples scanning method (Fig. 9,a) and tomography (Fig.9,b). The results of these methods permit evaluation of cladding thickness, level of its hydrotation and oxydation, fuel-cladding gap size, fuel-cladding interaction. The fuel and cladding structure gives information on the temperature distribution over the fuel element volume.

The welds state is examined by the x-ray radiography and matallography (Fig. 10). The fuel structure is evaluated from

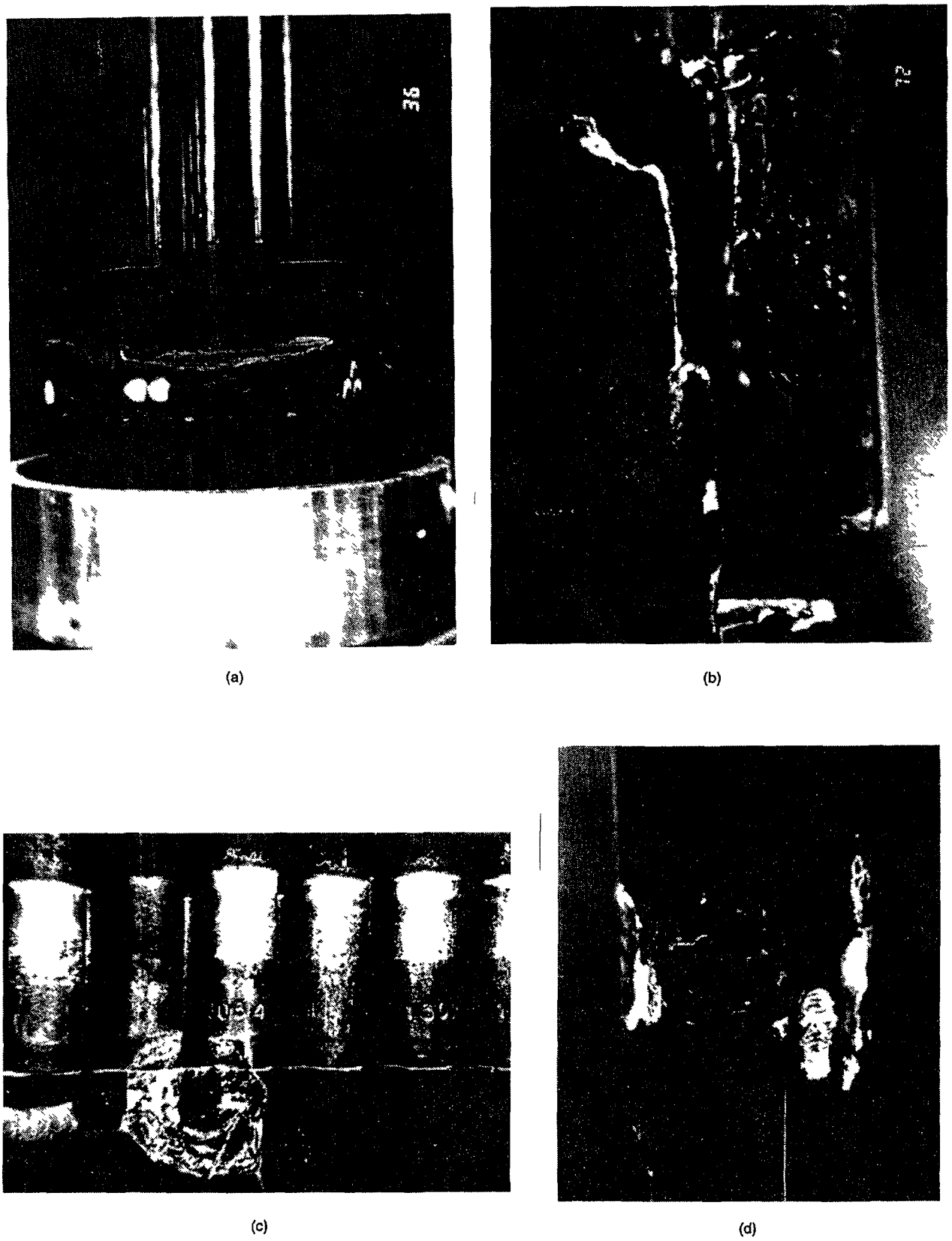

FIG. 2. Visually observed defects: (a) crumpled grid; (b) fuel element rupture; (c) grid defect; (d) nodular corrosion.

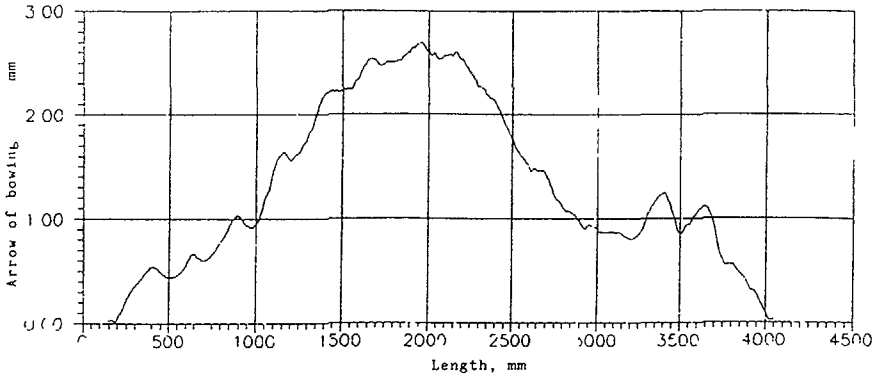

FIG 3a Arrow bowing of fuel assembly wrapper 0007

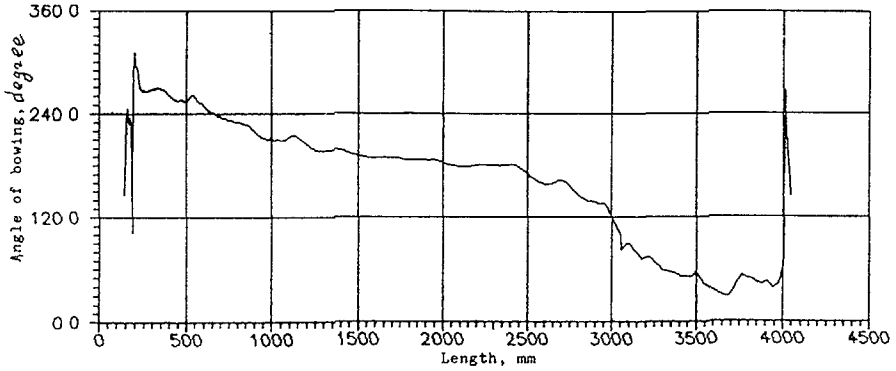

FIG 3b Angle of bowing of fuel assembly wrapper 0007

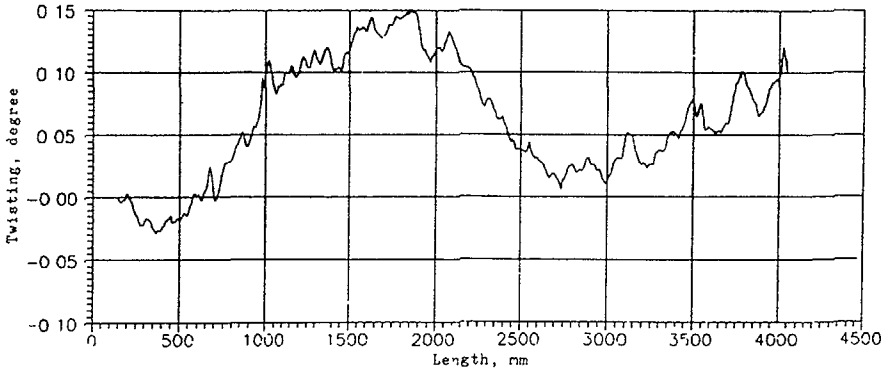

FIG 3c Twisting of fuel assembly wrapper 0007

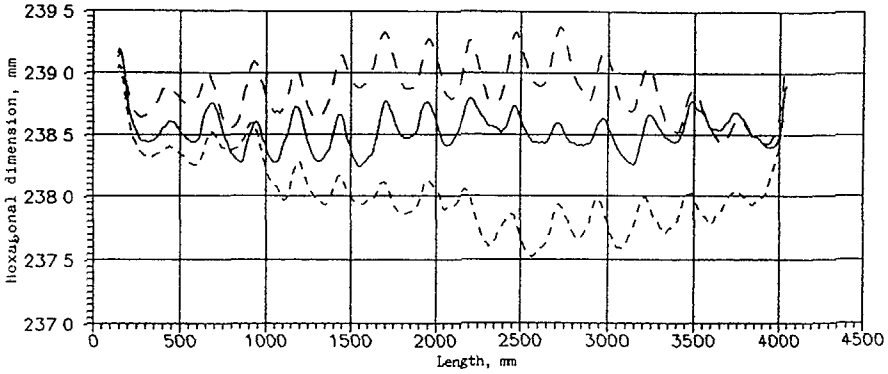

FIG 3d Average hexagonal dimension for rairs of sides of fuel assembly wrapper 0007

the neutron and x-ray radiography results (Fig.11) and refined form the ceramography results. The gap between pellets, pellet chops, size of the fuel column central channel are measured by the same methods.

Study of the fission product release dependence on the fuel temperature (Figs. 12, 13) is performed at the specialized rig. The results obtained permit evaluation of the fission products amount released in the coolant when cladding failure takes place as well as fuel temperature values in the process of operation.

There is a fuel element refabrication area in the hot cell intended for evaluation of the failed fuel behavior in the course of further operation. Fuel element models are manufactured there from the spent standard ones prepared for testing at the specialized rigs of the hot cells or in the research reactors.

2.3. Methodical basis of the in-pile experiments

The MIR reactor

The MIR reactor with the core of 1000 mm height comprises several loop facilities. Their type and parameters are determined by the experiment tasks. The loop channels are located in the second and third row of the core so, that each of them is surrounded with six channels loaded with operating fuel assemblies of the reactor (Fig. 14).

Each loop channel is surrounded with 3-5 regulating rods that allows operative power change of the fuel assembly under study with the minimum effect on the characteristics in the other loop channels. At present 5 water cooled loop facilities and another one with gas as coolant are being operated in the MIR reactor (Table 1).

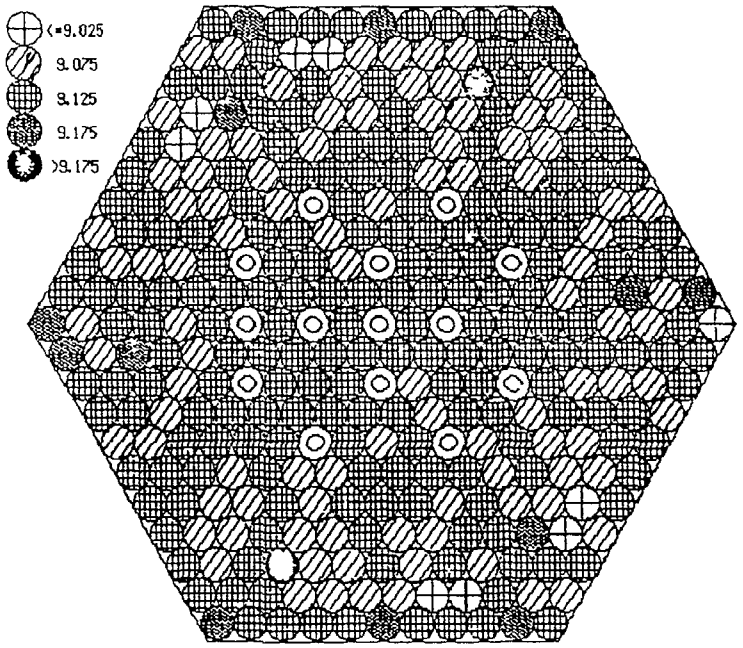

FIG. 4. Cartogram of diameter values for cells of spacer grid No. 2.

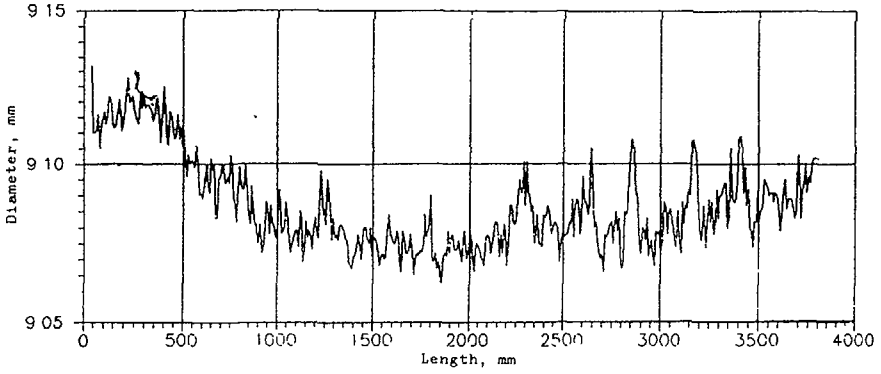

FIG 5. Average outer fuel element diameter of fuel assembly 0007.

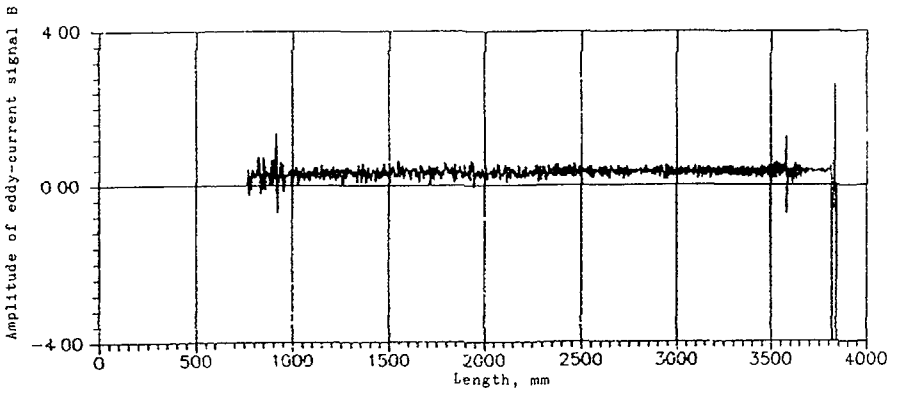

FIG. 6. Eddy current diagram of fuel element 139 in fuel assembly 0068.

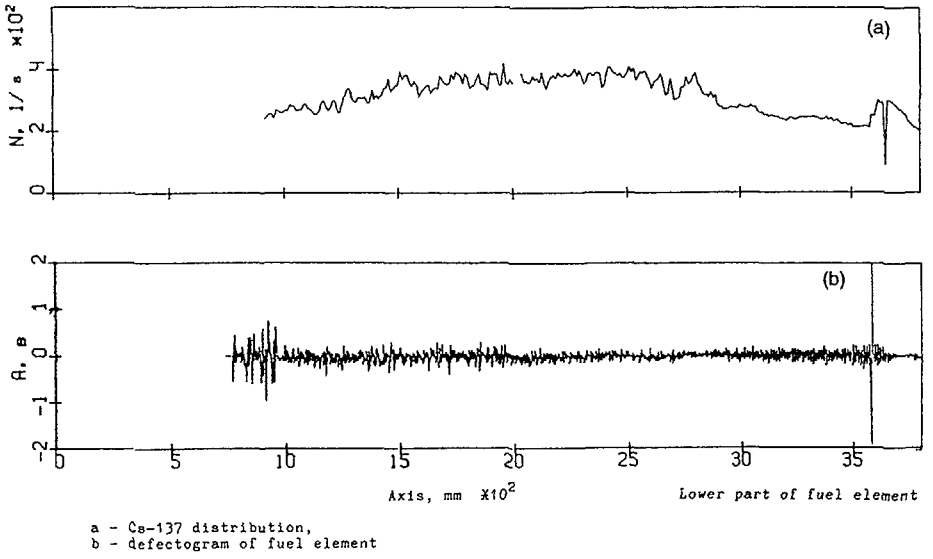

FIG 7. Distribution of Cs-137 concentration and signals of eddy current defectoscope along length of fuel element No. 139.

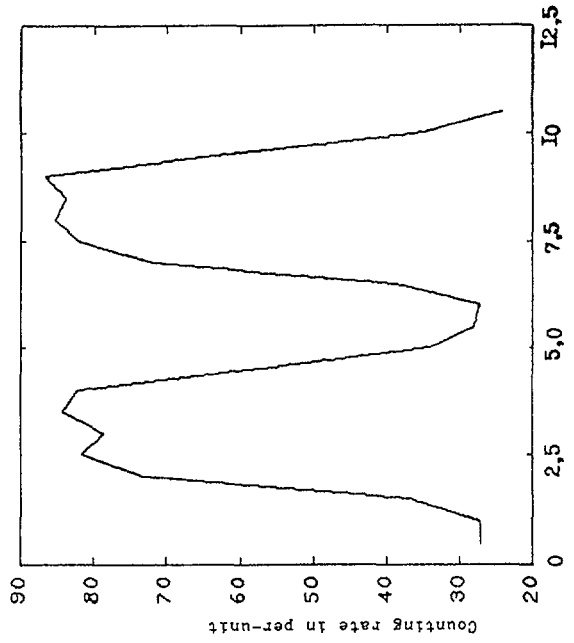

FIG. 9a. Cs-137 distribution along microsection diameter of VVER-1000 fuel element.

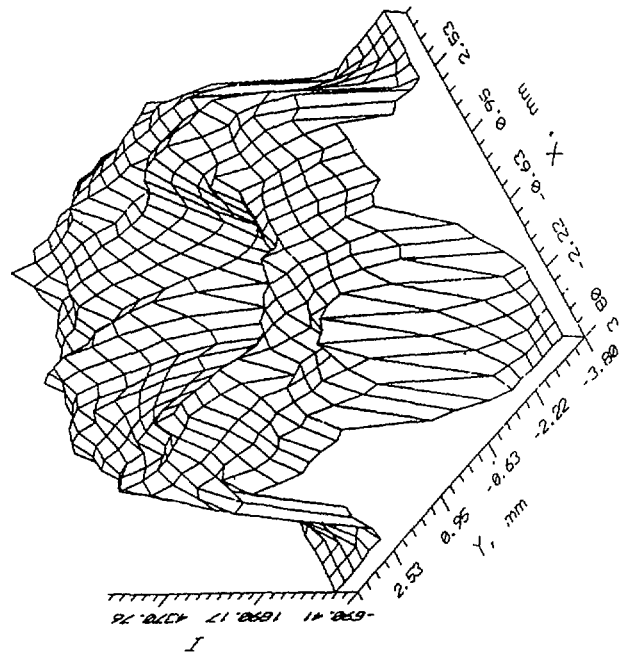

FIG. 9b.Emission tomograph for Cs-137

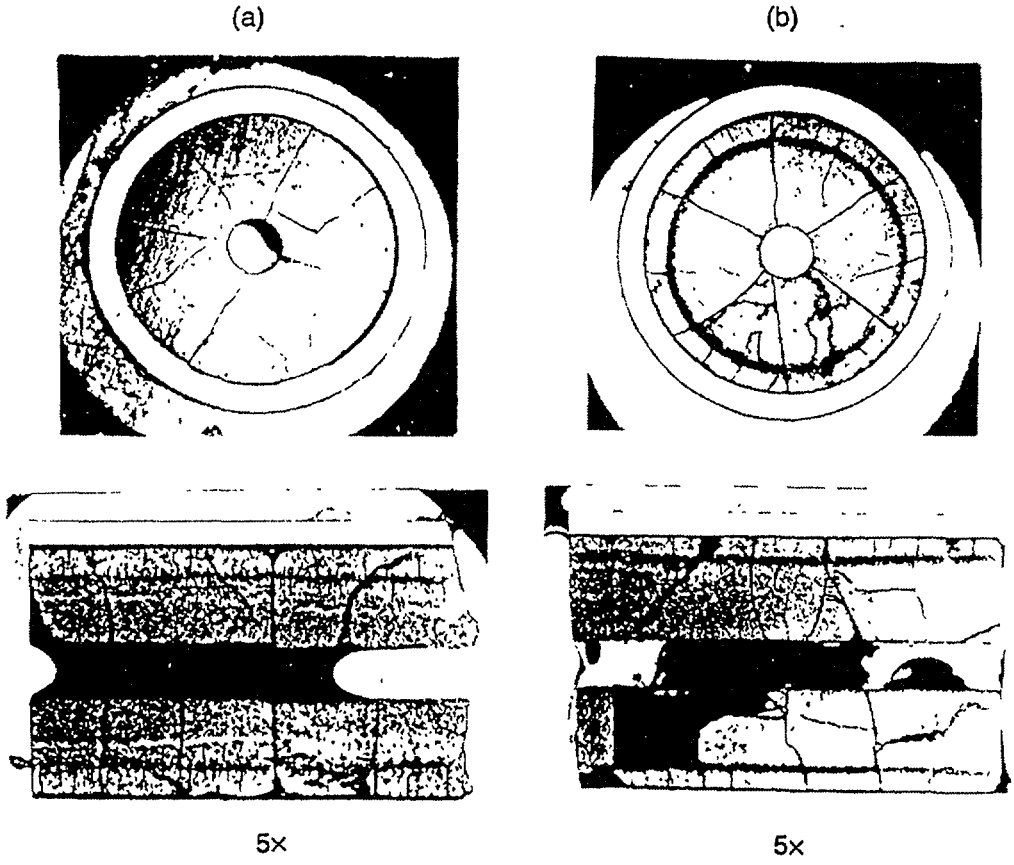

FIG. 8. (a) Metallography and ceramography of VVER fuel element; microstructure of fuel element Nos 122 (a) and 139 (b) longitudinal cross-section.

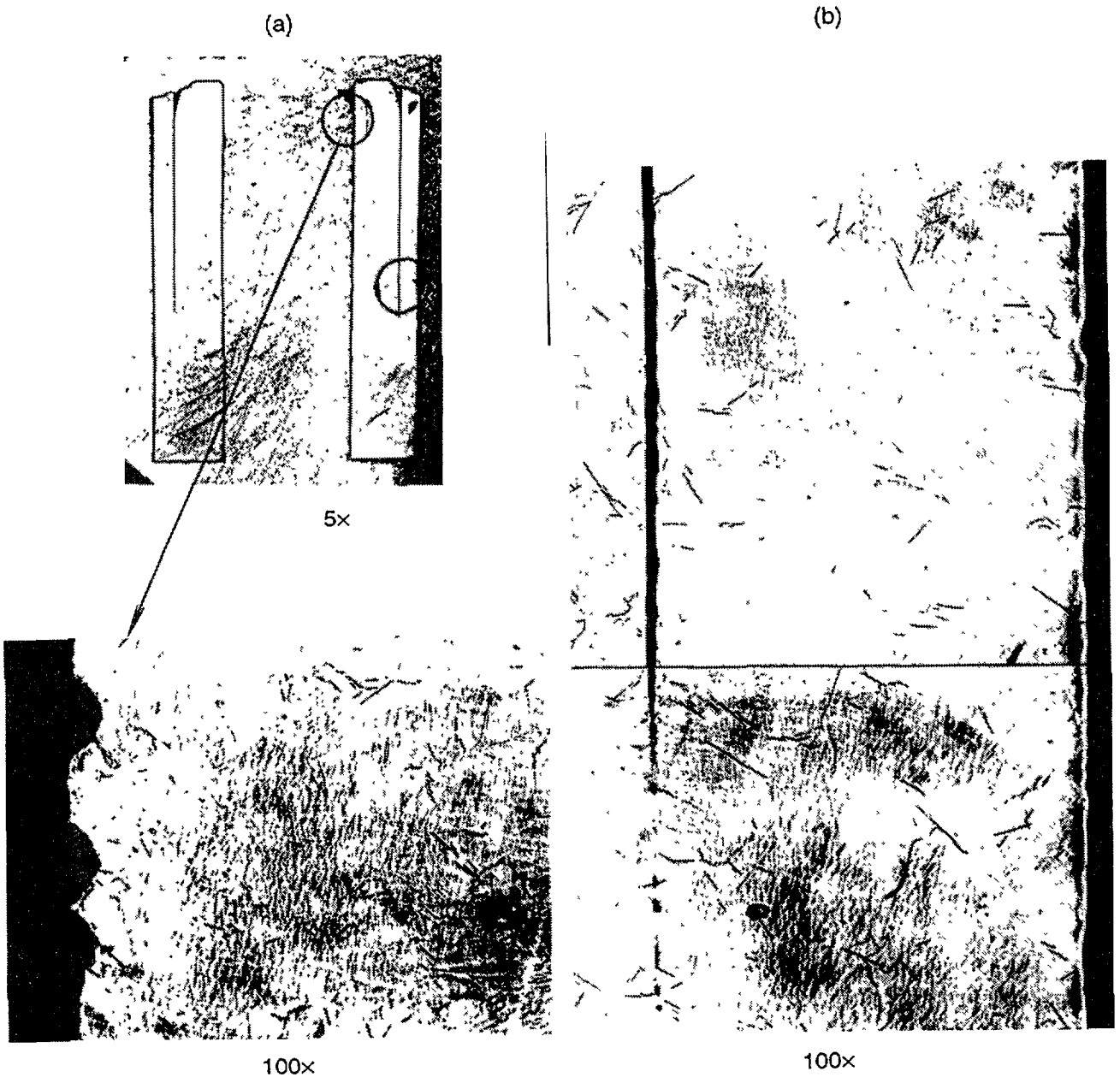

FIG. 10. Micro- and macrostructure of (a) lower welds and (b) upper welds of fuel element No. 139.

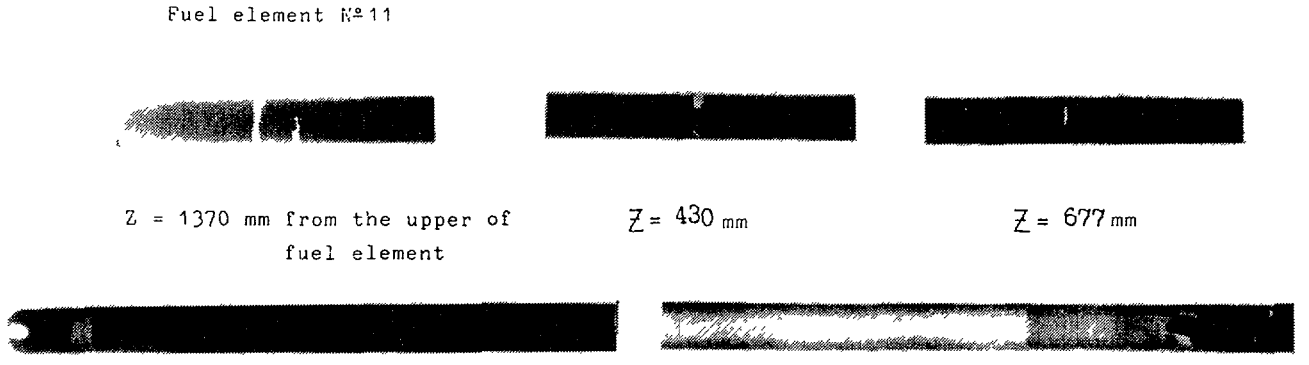

FIG 11. X ray and radiographic pictures of fuel element sections: (a) sections of fuel core in the region of local decrease of gamma activity; (b) shank, gas collector, locator and fragments of upper fuel pellets in fuel element No. 178.

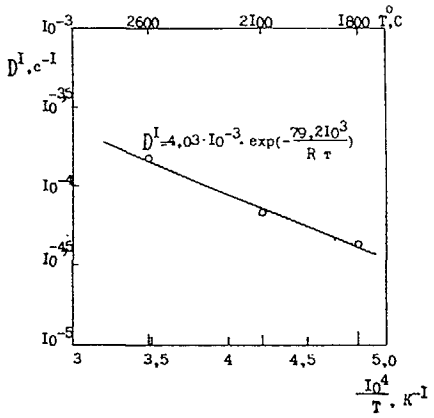

FIG. 12. Transformed factor of Cs diffusion for burnt up fuel of VVER 1000 (B = 44.7 MW·d/kg U).

TABLE 1. MAIN CHARACTERISTICS OF THE MIR REACTOR LOOPS

Parameter	Water loop WL-1 WL-2	Water boiling loop WL-1 WL-2	Vapour-water loop VWL-2	Gas loop GL-1	Organic loop OL-1
Coolant		Water	Water, Vapour-water mixture	Helium, its mixture with other gases	Ditholyl methane
Heat power, kW	2000	2000	2000	200	250
Coolant pressure, MPa	20	20	20	20	1.6
Max. outlet temperature, °C	300	300	500	500	300
Number of channels	4	4	1	1	1

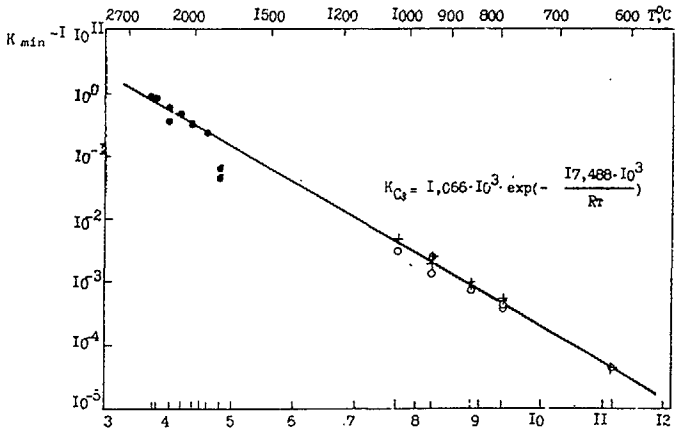

FIG. 13. Cs and Ru release in the atmosphere from the VVER burnt up fuel.

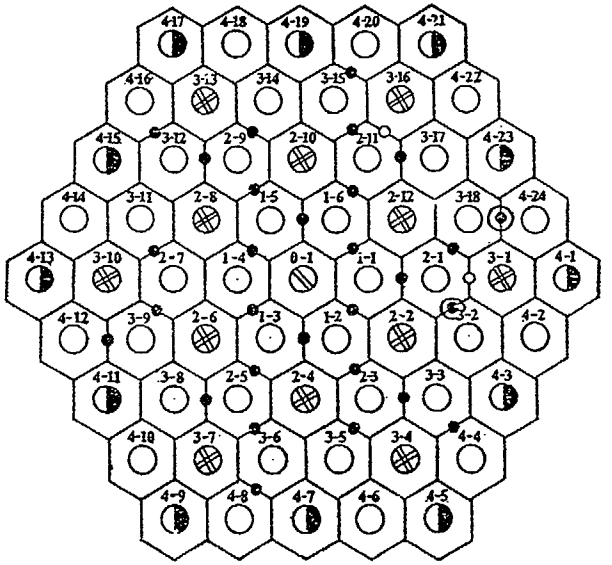

FIG. 14. Cartogram of the MIR reactor core: reactivity compensator; channels: with standard fuel assembly; loop channel with experimental fuel assembly; channels with TUE targets; shim safety rod; automatic control rod (digital designation of cell numbers).

Developed in the first years of the reactor operation the PV-1, PV-2, PVK-1 and PVK-2 loop facilities are used for testing of fuel elements before their failure. In this case one of the limiting factors of their operation is the coolant ultimate specific activity of 3.7x10 Bq/m (10 Ci/l). Life testing of fuel assemblies is performed in the loop facilities both under stationary and transient conditions.

Created in 1988 the PVP-2 loop facility is equipped with additional systems including those for activity localization and circuits decontamination that provides testing of not only tight fuel elements there but failed ones too up to a coolant specific activity of 3.7x10 Bq/m (1 Ci/l).

The PVP-2 flow-sheet allows fuel element testing both under stationary cooling conditions and also under those simulating accidental conditions with the pipe rupture followed by overflow of superheated fuel elements with cold coolant.

The SM-2 reactor

The SM-2 reactor with the core height of 350 mm comprises 3 water cooled loop facilities (Table 2). The VP-2 and VP-3 loop facilities are used for testing of power reactor fuel elements. Experimental channels are located in the berillium reflector surrounding the core (Fig.15) and used for fuel element testing. In accordance with the required conditions different channels can be connected to each loop. These channels differ in the neutron flux density value. The channel design permits output of a great number of various transducers that, in its turn, makes this reactor rather convinient for in-pile investigations. It was the SM-2 reactor where numerous experimental data have been obtained on fission product release and fuel element thermal-physical characteristics.

TABLE 2 MAIN PARAMETERS OF THE SM 2 REACTOR LOOPS

Parameter	WL-1	WL-2	WL-3
Maximum heat power, kW	2000	300	to 100
Coolant pressure, MPa	4 9	19 6	19.6
Inlet coolant temperature, C°	20-60	300	300
Total coolant volume of the first circuit, m^3	5 0	1 5	0 4
Total gas volume, m^3	0.5	0 9	0 4
Water flow-rate, m^3/h			
main & stand-by	200	8 0	8 0
emergency	30	8 0	8 0
Pump-induced pressure, MPa	0.94	0 94	8 0

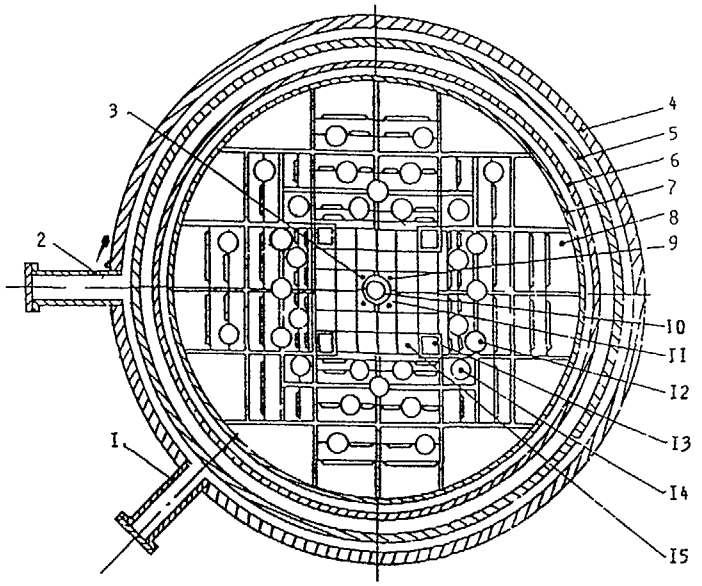

FIG 15 Sectional view of the SM 2 reactor 1, 2 – radial experimental channels, 3 – water trap, 4 – safety vessel, 5 – reactor vessel, 6 – shield, 7 – separator, 8 – beryllium reflector, 9 – absorbing rods, 10 – central shim, 11 – beryllium insert of water trap, 12 – automatic control rod, 13 – shim, 14 – cells of experimental channels, 15 – fuel assembly of active core

Experiments performed in transients

The MIR reactor can provide a significant power increase of the experimental fuel assembly at a sufficient rate and without use of special equipment by recompensation of the regulating rods.

For this purpose in the initial state the nearest to the loop channel regulating rods are located in the lower and intermediate positions but during ramping they are completely removed with the maximum velocity. Simultaneously in order to compensate the introduced positive reactivity the regulating rods in the other parts of the core are dropped. In this case the constant reactor power is maintained. The experiments performed were aimed at establishment of ultimate thermal loadings depending on the fuel burnup in ramping. They showed that this method allows for 2-2.5 times increase of the fuel assembly power in 8-10 minutes. It should be noted that ramping of the fuel element power with regulating rods requires prelimenary removal of several loop assemblies from the reactor. Therefore, not more than 3 experiments per year are performed in the MIR reactor by this method. The special

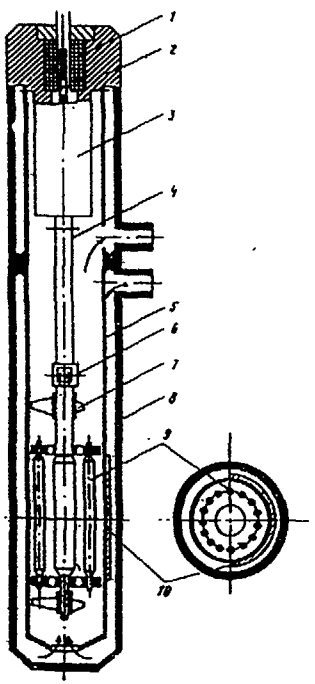

FIG. 16. Irradiator TC-2M: 1 – indicator of fuel assembly location; 2 – head; 3 – turnable mechanism; 4 – suspension rod; 5 – flow separator; 6 – hinge; 7 – spacer sprocket; 8 – vessel; 9 – fuel element; 10 – shield.

TZ-2M (Fig.16) irradiation rig is used for the fuel element tests with daily power cycling in MIR. The irradiation rig incorporates a method of the fuel assembly rotation in the non-uniform neutron field formed with stationary absorbing shielding. During operation of this rig 1000 cycles of the fuel element power change have been performed in the range 50...100% of nominal power value.

In the SM-2 reactor the TZ-SM irradiation rig and the RITM facility are used for power ramping and cycling. In the TZ-SM rig (Fig.17) fuel element power changes are realized by rotation of the neutron absorbing shield, in the form of a segment, round a fuel element and in the RITM facility they are realized by pressure change of H gaseous absorber in the annular gap round the fuel element. It should be noted that in the experiments performed with TZ-SM and RITM the fuel elements are equipped with pressure pick-ups for gas under the cladding, cladding and fuel column elongation sensors as well as with a thermal couple in the fuel column center.

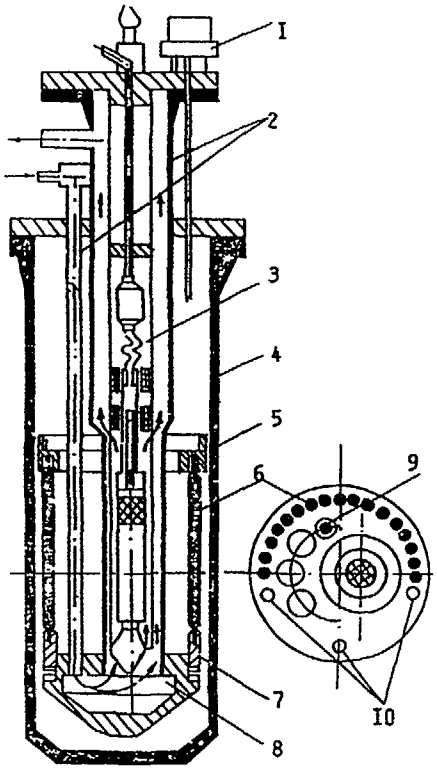

FIG. 17. Irradiation device TC-SM for fuel element testing under thermocycling conditions: 1 – electric motor; 2 – water lines; 3 – suspension rod; 4 – vessel; 5, 8 – upper and lower housings; 6 – rods of neutron absorber; 7 – fuel elements; 9 – direct charge detector; 10 – tie rods; 11 – collector.

Experiments with pulse nuclear heating.

In these experiments the fuel and cladding behavior has been studied depending on the accumulated heat value. They are performed in SM-2 with the help of "Impulse" irradiation rig and the RITM facility. In "Impulse" (Fig.18) the required nuclear heating change is achieved by the fuel element drop along the core through the neutron absorbing shield having an annular split. In the experiments performed with 21% enriched fuel elements the maximum amplitude was 30 - 40. The pneumatic drive of the rig provides a half-width of the pulse of 0.1-0.6 s. The maximum of accumulated heat in the experiments performed was 1200 kj/kg.

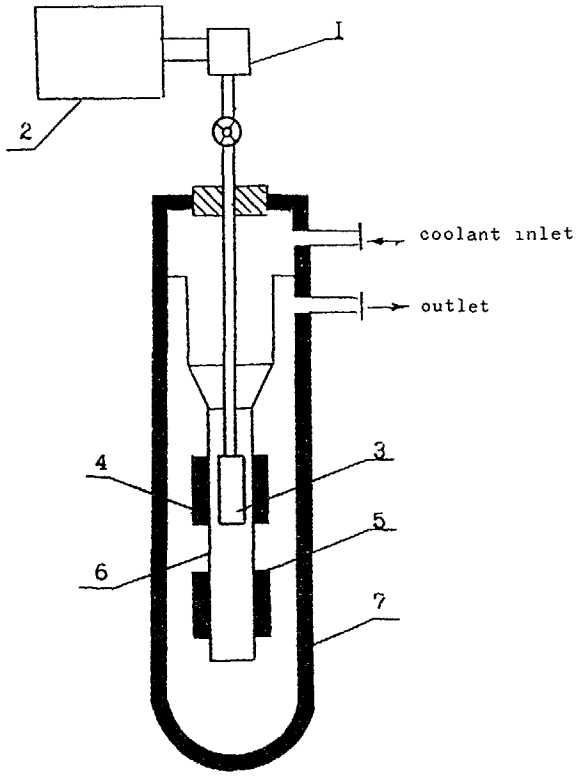

FIG 18 Irradiation device 'Impuls' 1 – transport unit, 2 – control and measuring block, 3 – fuel element, 4, 5 – cadmium screens, 6 – flux separator, 7 – channel vessel

In the RITM facility it is possible to achieve the power change amplitude of 20–30 s with a half-width of the pulse of 0.4 s.

Experiments with heat removal crisis.

These experiments are planned to be performed in SM-2 with single short (350 mm) fuel elements and assemblies (containing up to 7 fuel elements) as well as in MIR with assemblies containinf 18 fuel elements with a length of 1000 mm. The experiments performed in SM-2 with single fuel elements indicate that the most preferable method of the fuel element introduction in the heat removal crisis is not a decrease of the coolant flowrate at statinary power but, on the contrary, it is a smooth increase of the fuel element power at the stationary coolant flowrate.

In the heat removal crisis experimnets the temperature of the cladding and fuel column center is measured. In these experiments the efect of the short-term temperature increase is studied on the fuel element state on the whole.

Experiments with the primary circuit pipe rupture.

Although these experiments exceed the limits of the normal fuel operation they reveal possible sequences for fuel elements icluding those with defects.

The investigation on the fuel element behavior and cladding damage features under accidental conditions connected with the primary circuit pipe rupture are supposed to be performed in the PVP-2 loop facility of the MIR reactor. In this case rupture simulation is achieved by discharge of the loop coolant into a special tank. Regulation of the coolant discharge velocity allows simulations from small ruptures up to severe designed accident. The loop facility is eqipped with the emergency cooling system that could be used for simulation of the final accident phase connected with the overflow of superheated fuel elements with cold coolant.

2.4. Realization of the investigation program at the VK-50 NPS.

To realize the planned program at the VK-50 NPS the required experimental basis has been developed comprising: sampling system, measurement center, out-of-pile leak test stands. The realization of the investigation program of NPS operation with failed fuel elements would be impossible without efficient adsorbtion facility for decontamination of the turbine ejector gas release.

The schematic diagram of the VK-50 NPS with sampling locations and its operating parameters are given in Fig.19.

To obtain reliable and representative information on the RFP release from the fuel elements with the known defect size and location under long-term irradiation in the reactor core as well as during leakage testing at the out-of-pile stand experimental fuel assemblies (D-1 and D-2) have been manufactured and and loaded into the VK-50 core in succession. Each fuel assembly comprises 3 fuel elements having artificial cladding defects in the form of holes with the 0.9-1.0 diameter bored during fuel assembly manufacturing. Fig.20 presents the defect location and irradiation conditions of the fuel assemblies with artificial defects.

The long-term irradiation of the D-1 fuel assembly (during 5 years) showed that there is no significant washing out of fuel into the circuit. The gaseous RFP release from the fuel elements with artificial defects (D-1 and D-2 fuel assemblies) is described by the current calculation methods fairly well: the effect of the fuel-cladding gap size on the yield value is strong.

The D-1 and D-2 fuel asemblies have been tested at the out-of pile leak-test stand with all current methods. This work has led to the choice of the most reliable method and

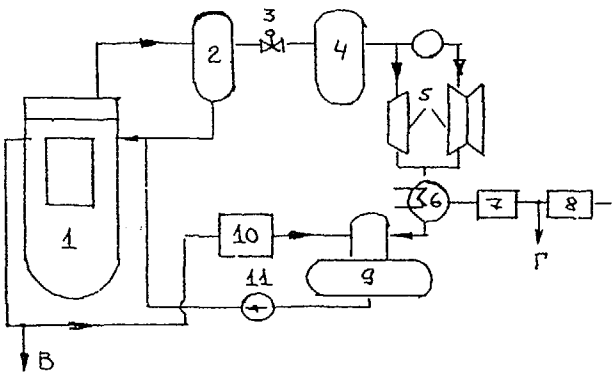

FIG. 19. Schematic diagram of VK-50 APS: 1 – reactor; 2, 4 – high and low pressure separators; 3 – throttle; 5 – turbine; 6 – turbine condenser; 7 – facility for hydrogen burning; 8 – facility for gas release decontamination; 9 – deaerator; 10 – facility for reactor water purification; 11 – points of water and gas samplings, respectively.

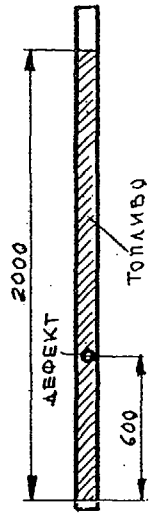

Characteristics	D-1	D-2
Defect diameter, mm	1.0	0.9
Fuel elements arrangement in fuel assemblies	inner row	outer row
Linear power of failed fuel elements, W/cm	50-70	90-120
Fuel burnup, MW d/kg U	16	11

FIG. 20. Scheme of arrangement of defects in fuel elements and characteristics of D-1 and D-2 fuel assemblies.

procedure of the test that would provide reliable detection of failed fuel elements and assemblies even after their storage for more than 10 years and determination of the defect size from the RFP activity in the circuit of the leak test stand.

Varying the artificial defect size is the next stage of the program. It is necessary for verification of the methods for determination of the defect size from the RFP activity in the circuit and for improvement of the calculation methods of the RFP release from failed fuel elements. In this case higher fuel element loadings are planned. The development of the out-of-pile leak testing stand methods is aimed at the improvement of the equipment and bringing of the methods for defect size determination to the standard level.

CONCLUSIONS.

Thus, in the Research Institute of Atomic Reactors a complex of technical means and methods have been developed and used that provides practically all kinds of investigations allowing investigation of all stages of fuel defect appearance and development under different operating conditions. This complex comprises the SM-2, MIR and VK-50 reactors and the hot laboratory.

REFERENCES

1. Dvoretzki V.G.,Ivanov V.B., Glushak N.S., Glushak S.M., Smirnov V.P. методика измерения геометрических размеров и формы чехла ТВСм Preprint, RIAR, 3(806), 1991.

2. Kanashov B.A., Alyoshechkin L.V. Анализ погрешностей измерения наружного диаметра цилиндрических изделий при различных способах их базирования. Moscow, CNIIATOMINFORM, Preprint, 1986.

3. Konyashov V.V. Shkokov E.I., Chechetkin Yu.V., E.K.Yakshin Экспериментальные исследования выхода радиоактивных продуктов деления из дефектных твэлов на АЭС с реактором ВК-50. Nuclear Power Stations, 5, -M.: Energoatomizdat, 1983, p. 185-189.

SEARCH FOR WAYS OF REDUCING VVER FUEL DAMAGE BY OPTIMIZING DESIGN AND OPERATING CONDITIONS

Yu.K. BIBILASHVILI, A V MEDVEDEV,
V.V. NOVIKOV, V.D. ONUFRIEV
Scientific Research Institute for Inorganic Materials,
Moscow

I N VASILCHENKO, E.D DEMIN
OKB 'Hydropress',
Podol'sk

G.L. LUNIN, V.N. PROSELKOV
I.V. Kurchatov Institute of Atomic Energy,
Moscow

A.F. GRACHEV, V.A. KUPRIENKO
Research Institute of Atomic Reactors,
Dimitrovgrad

A.G. IOLTUKHOVSKIJ
Research Institute for Nuclear Power Plant Operation,
Moscow

Russian Federation

Abstract

The paper discusses the main directions in improving VVER fuel through upgrading fuel element and assembly design, optimizing operation conditions in power reactor cores The existent designs of fuel elements and assemblies are shown to meet the requirements of operation reliability. At the same time they are prone to further backfitting to significantly improve serviceability, maintainability, neutron economy, to reduce limitations on operation conditions, and to increase burn-up and safety.

1. UPGRADING FUEL ASSEMBLIY DESIGNS

Operational reliability of power reactor fuel is controlled by both the properties of fuels and their operation conditions in FA. FAs can as a structural member of a core fail due to the following causes:

- fretting-wear in fuel spacing locations;
- fretting-wear due to debris getting into a fuel bundle;
- deformation and damage of elements due to inadequate accomodation of thermal and irradiation growth;
- deformation of absorber elements of ASS (automatic safety system) as a result of dynamic loads on scramming;
- damages due to a joint action of irregular handling and operation loads in a reactor.

Experience in VVER-440 and VVER-1000 operation shows that the chosen schemes of FA lay-out, the principle of fuel element spacing ensure the high operational reliability of FAs and their further upgrading.

VVER FAs are backfitted in the following main directions:

- reduction of parasitic neutron absorption through the use of zirconium grids and guide tubes, the use of zirconium of higher purity;
- use of integrated fuel burnable absorber- gadolinium;
- increase of efficiency and life-time of control rods;
- maintainability of FAs (reconstitutable ones);
- increase reliability of FAs for work under load follow conditions.

Besides, the base design of FA allows an increase the length of a fuel column to decrease the linear heating of a fuel element as well as introduction of a profiled fuel column.

Both FA designs, viz., the base one having steel grids and the backfitted one with zirconium grids are not subject to fretting wear. This is accounted for by adeguately rigid supports of fuel elements, and the selected pitch of grid location offsets the influence of possible gaps in fuel fixture cells.

FA dismantling for bench tests and post-irradiation investigations points to adequate fuel extractability from a bundle. All these qualities make this lay-out of a bundle optimal, meeting the reliability requirements both in a

reactor and during transport-technological operations. Therefore, this spacing principle is also retained in the backfitted FA, including the reconstitutable one.

It is expedient to increase the efficiency of control rods, primarily for the serial VVER-1000 reactor to lower the secondary criticality temperature.

The base and backfitting designs of FAs resolve this problem through using larger diameter of control rods.

The use of a combined absorbing element with hafnium nozzles increases the life-time of absorbing rods of ASS. Damping of the higher mass of ASS rods provided by a larger number of springs.

The post-irradiation investigations, as a rule, do not reveal any events of fretting wear due to presence of debris. This is ensured by the adequate filtration properties of the bottom grid of FA and cylindrical supprorts of a reactor well.

2. MAJOR DIRECTIONS IN IMPROVEMENT OF OPERATION RELIABILITY OF FUELS

The operation reliability of fuel elements is determined by their design and operation conditions.

Fuel failures are mainly due to the breach of the following criteria:

- cladding strength;
- cladding deformation including collapse under the action of pressure from outside;
- fuel melt-down;
- hydrogen pick-up by cladding.

Therefore, the design solutions and improvements are aimed at provision of the absolute compliance with the above criteria under all design basis normal operation conditions and on departure from normal operation conditions.

The presently employed VVER-1000 fuel elements have high operation reliability. The failure level does not exceed 0,005 -0,008%.

This is attained through the thorough analysis of actual operation conditions, optimized design and technological solutions.

To meet the above fuel reliability criteria in the best way specific design parameters of a fuel element were selected as optimized compromise solutions taking account of the complex mode of the effect of those parameters on the characteristics and processes taking place in a fuel element, see the table.

Table

Interrelation between Design Parameters and Fuel Element Characteristics and Processes

Design parameter	Parameter dependent characteristics and processes
Average pellet density: 10 6 g/cm3	No hydrogen pick-up by cladding, pellets strength, creep rate, extent of irradiation induced densification
Central hole of pellet: d - 2.2-2.4 mm	Margin to melt-down, swelling accomodation, volume for FG, reduced FPs getting to cladding
Pellet chamfers	Prevention of chips, lower PCI, free volume for FG
Fuel-cladding gap: 0.15-0.25 mm	Lower temperature drop between pellet and cladding, reduced stored energy, fuel behavior in LOCA, loading of pellets into cladding
Length of plenum	Gas pressure inside a cladding must not exceed coolant presure
Pressure of helium filler P=1.65-2 25 MPa	Lower gas release, elimination of collapse of free-standing cladding

The important influence on the fuel reliability is exerted by the acceptable operation conditions. Within the burn-ups reached this problem is known to be related to the fuel behavior in transients accompanied by linear heating ramps.

In practice power ramps are realized both on power changes of a reactor as a whole, and locally through power rating field variation. In the latter instance, the power ramp magnitude depends, as a rule, on methods and algorithms of a core control. Optimization of these methods is an important task in the total problem of power reactor core reliability.

The significance of the problem is illustrated by the following results of design studies.

As applied to a 24 hour load follow schedule two methods are considered: rigid and optimized one. As a rigid one an algorithm was spacifically selected that allows significant distortion of power rating field.

Fig. 1-4 illustrate the calculated data on variation of power density fields, specific loads and stresses of fuel cladding under 24 hour load follow conditions with a rigid

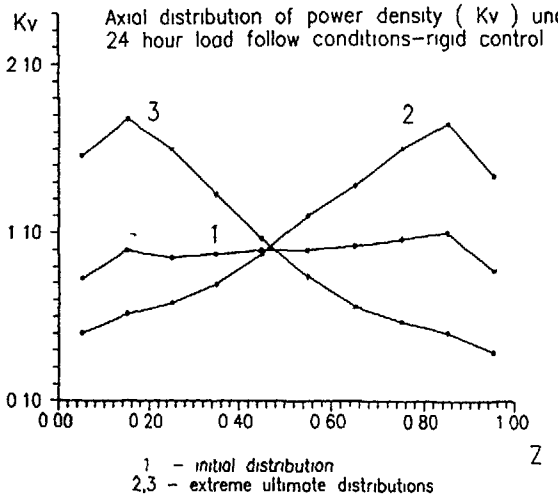

1 – initial distribution
2,3 – extreme ultimate distributions

Fig 1

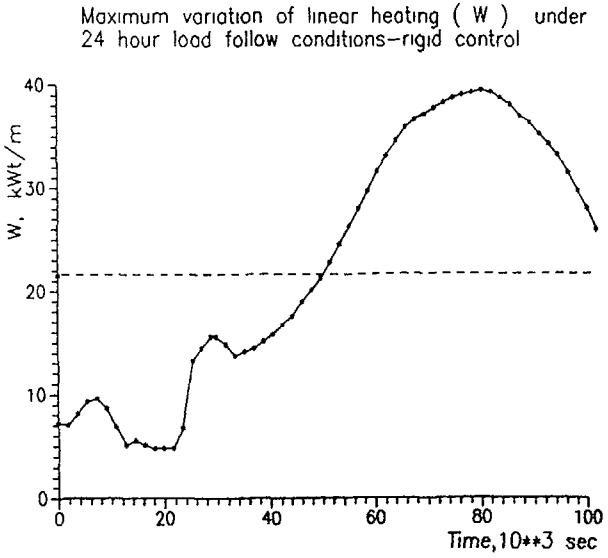

Fig. 2

core control. It can be seen that with a coarse control significant departure of power density fields from the steady-state form are possible. As a result of such non-optimized control high tensile stresses above the corrosion cracking threshold can be developed in a cladding giving rise to its significant damage, including a through defect formation.

Similar data on a 24 hour control shedule but with more optimized control algorithm are given in Fig. 5-8. A clear-cut dependence of the stressed state of a fuel element on the method of a core control is obvios. In this case, the stresses are significantly lower (115 MPa) and remain below their threshold value of the start of SCC process in Zrcladding. This allows any cladding damage in a single cycle and damage accumulation in the process of multiply power cycling to be avoided.

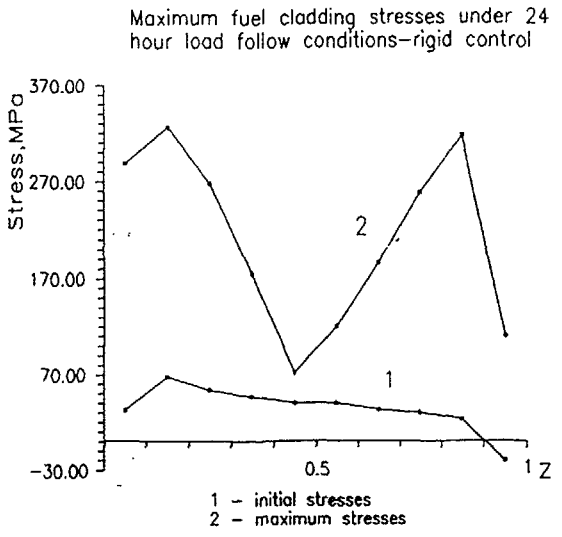

Fig. 3

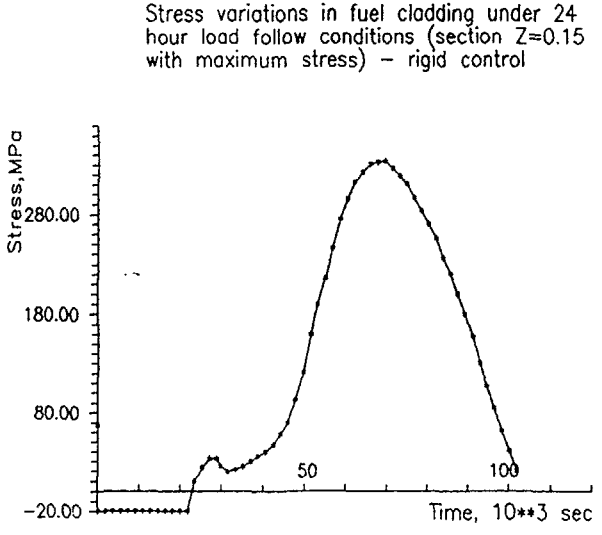

Fig. 4

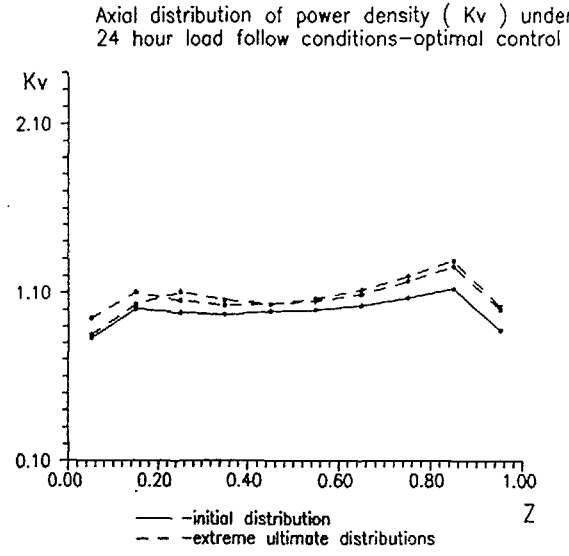

Fig. 5

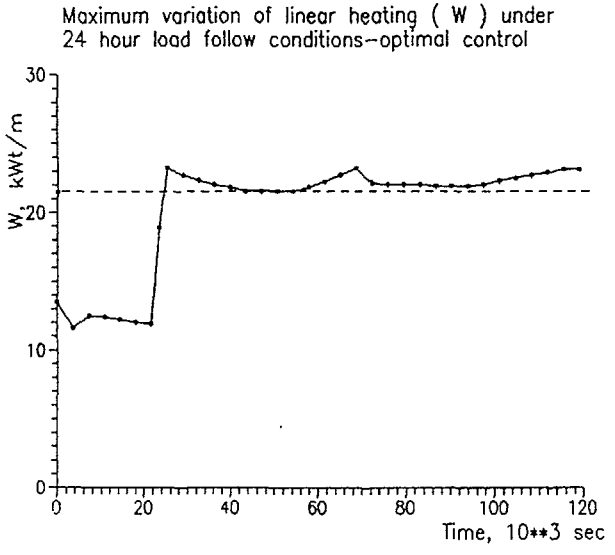

Fig. 6

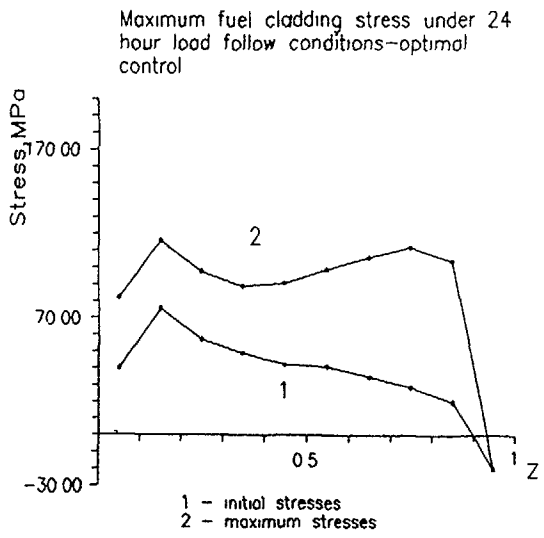

Fig 7

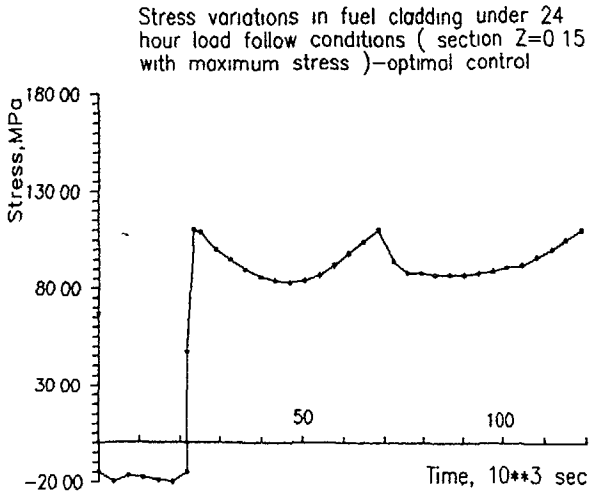

Fig 8

In Russia much experience has been gained in influencing the fuel serviceability by methods of control Optimized algorithms of core control have been worked out Their usage together with the improved design of fuel elements and assemlies will provide for the further improvement of fuel performance

It follows from the world-wide experience and domestic investigations that the major factor that limit the fuel serviceability under transient operation conditions is the strength of zirconium claddings under the action of aggressive fission products in presence of tensile stresses. The design-experimental studies permitted kinetic dependences for a SCC defect evolution in Zr-1%Nb cladding to be found, they make it possible to calculate the dinamics of a crack propagation process during fuel operation.

It is established that the rate of a crack evolution grows with its depth, thus the crack becomes unstable and the cladding strength is sharply reduced. Therefore, to guarantee the strength the designs establish the maximum permissible depth of an accumulated crack that is less than critical depth of its stable growth (60 μm).

Under this conditions the factor most important for cladding strength is the permissible depth of an initial as fabricated defect at the inner cladding surface.

Presently regulations for fuels in our country and abroad established 50μm for an as fabricated defect. Thus, there is only an insignificant margin to the critical depth of 60 μm.

Fig. 9 presents the strength of Zr-1%Nb claddings having initial defects of different depths. Fig. 10 shows the time to fracture of cladding as a function of an initial defect depth.

The data presented point to the expediency of adopting a more rigid requierment on the initial defect depth. At the same time the extent of tube defectiveness limitations must correspond to the process potentialities, quality control and economics.

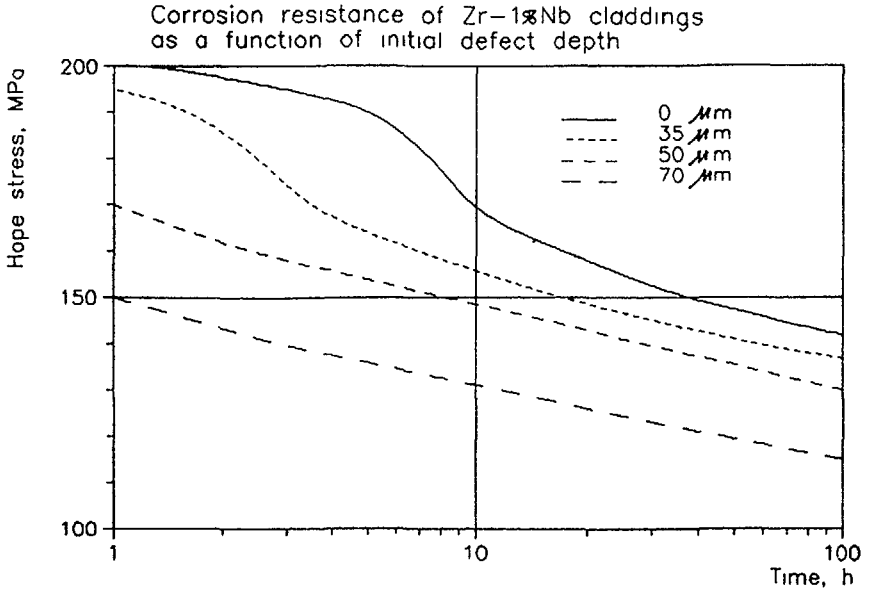

Fig 9

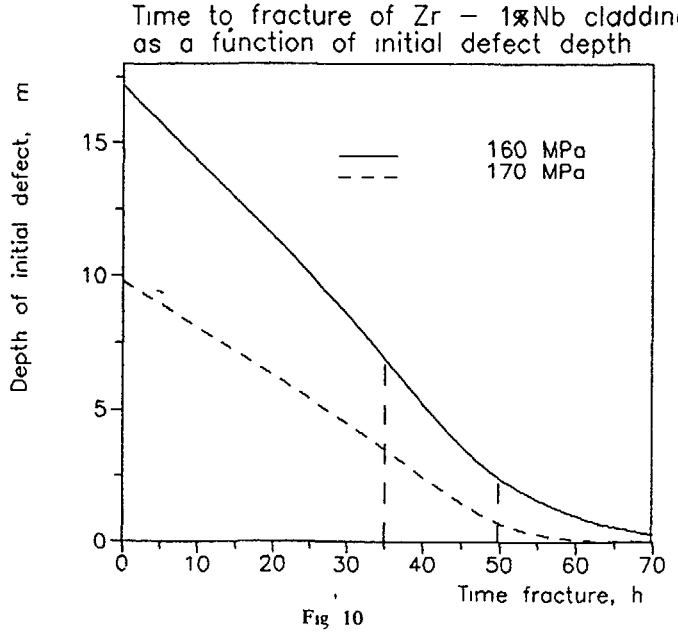

Fig 10

To date in Russia the work is nearing its completion to introduce fuel cladding tubes having an as fabricated defect not more than 35 μm into a commercial production.

Further upgrading the fuel design is aimed at improving its performance to provide its operation to extended burn-ups (the FA average discharge burn-up of 50-55 MWday/kgU) and under load follow conditions. At the first stage it is planned to employ bimetallic claddings with their inner surface coated with pure Zr. In future plastifiers containing fuel having a higher creep is suggested for use.

Backfitted fuel elements and assemblies, the optimal algorithms of control will provide the high reliability and practicability of cores of both the existent and new generation reactors.

STUDY ON STRESSS CORROSION CRACKING OF FUEL CLADDING TUBE

Y.H. KANG, W.S. RYU, K.S. RHEEM, S.H. KIM
Korea Atomic Energy Research Institute,
Daeduk, Republic of Korea

Abstract

Iodine-induced stress corrosion cracking (ISCC) tests on Zircaloy-4 CANDU- type tubes were carried out using a modified internal pressurization method to study the pellet cladding interaction (PCI) failure mechanism and its remedy. In the present test, the effect of various corrosion species including CsCl, CsI, FeI_2, CsOH and AlI_3 as well as I_2 on the SCC of Zry-4 tube specimens was investigated in terms of time-to-failure versus the concentration of species and the hoop stress of Zry-4 tubes. The results showed that the CsCl and CsI species were not active to SCC while the FeI_2, CsOH and AlI_3 species reduced the time-to-failure of SCC at the nearly same critical concentration of species as that of I_2. In order to study the effects of Zircaloy-4 tube fabrication processes on ISCC, two kinds of tubes from different commercial makers were also tested at the same condition for ISCC test. Two kinds of tubes showed a difference in threshold stresses of about 30 MPa which was attributed to the difference in texture and toughness of tubes. To find out the effects of brazing and welding process of CANDU-type fuel tubes, the time- to-failure of ISCC was measured in terms of hoop stresses. The threshold stress of spacer-brazed tube and end cap- welded parts was found to be reduced to about 70 % and 50 % of the stress of normal tubes, respectively. Either the annealing process after welding or a modified welding process reduced the susceptibility of SCC, indicating that the shape as well as residual stress of welding parts acted as an important role for controlling ISCC.When the inside of the tubes was coated with graphite, the tube didn't increase the ISCC threshold stress, although the critical concentration of iodine seemed to be shifted to a little higher concentration. On the other hand, siloxane-coating inside of tubes was found to increase the threshold stress for SCC failures.

1. INTRODUCTION

The stress corrosion cracking (SCC) of Zircaloy has been extensively studied in order to elucidate the mechanism of pellet-cladding interaction (PCI) failure, and to investigate the remedy [1-12]. It is known that the SCC of Zry-4 tubes is related to the combined effect of environment and mechanical stress. Iodine, which is produced as a fission product and which is present in various forms of compounds rather than elementary iodine, acts as one of the corrosive agents[1-3], and the ISCC was oftenly occured during the creep deformation of fuel tubes in reactors [4-6]. The critical concentration of iodine [7-9] and the threshold stress [10-12] are known to be very important to the ISCC of Zircaloy.

In an attempt to understand the SCC failure mechanism of Zircaloy-4 tubes under the various condition of variables including iodine concentration, manufacturing processes of tube, brazing and welding, and coating insides of tubes with graphite or siloxane, four kinds of SCC tests on Zircaloy-4 tube specimens were conducted in this study.

2. EXPERIMENTS

At first, the effect of various corrosive compounds of CsI, FeI_2, AlI_3, CsCl, and CsOH as well as I_2 on the SCC were examined as a function of their concentration versus time-to-failure. Second, to study the effect of manufacturing process on the ISCC, two kinds of tubes which were manufactured in different processes were examined by measuring the metallurgical properties and threshold stresses of tube for ISCC. Third, because the end cap welding part of tubes would have a potential risk of PCI in CANDU type fuels, the effects of welding process on the ISCC were measured on the Zry-4 tube specimens of various welding processes and annealing treatment.Finally, to improve the PCI failure resistance, the effect of graphite or siloxane coating inside of claddings was surveyed in terms of threshold stress and/or critical iodine concentration.

A tube-internal pressurization system [9] was used as the test apparatus in this experiment. A limited amount of iodine compound was loaded into the specimen using a small glass ampule, and an air-driven gas booster was used to pressurize the high purity argon gas into a tube specimen. The hoop stress of a specimen was calculated from the normal equation for thin wall tube, and the iodine concentration was defined as the amount of compound per surface area of a specimen. The fractograph of failure section was observed using SEM.

3. RESULTS and DISCUSSION

1) ISCC Susceptibility in the Environment of Various Iodine Compounds.

Figure 1 shows the ISCC susceptibility which is graphed in terms of time-to-failure versus the concentration and the hoop stress of Zry-4 tubes in the corrosive environments of CsI, FeI_2, AlI_3, CsCl, and CsOH as well as I_2. The I_2 species showed a typical ISCC behavior at a critical concentration of about 0.3 mg/cm^2 while the CsI and CsCl species were not so active to the SCC. Meanwhile, a ductile mode fracture

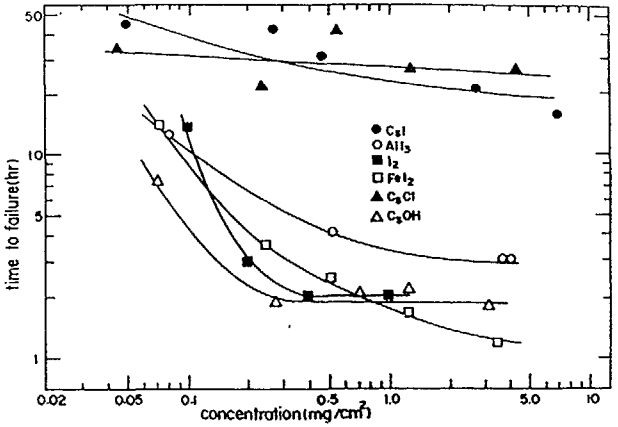

Figure 1 SCC Behavior with Various Corrosive Agents at 330 °C, 467 MPa.

with microvoid coalescence was observed in fractographs of the specimens. On the other hand, the CsOH species was found to be very corrosive like I_2 of which critical concentration was appeared at about 0.2 mg/cm². The fractographs of CsOH-reacted specimens showed cleavage features. In case of FeI_2, the value of time-to-failure of SCC gradually decreased with increase in iodine concentration, which was even lower than that for I_2 above 0.8 mg/cm². The fractographs related to FeI_2 did not also display any distinctive feature or any brittle-ductile transition mode. The reaction of AlI_3 showed a trend similar to that of FeI_2, but the value of time- to-failure for AlI_3 was higher. The AlI_3-related fractographs showed a brittle fracture mode without microvoids.

Even though identities of the corrosive sources to result in ISCC in fuel rods in reactors have not been clearly proven, AlI_3 or FeI_2 would be considered as a potential agent for SCC of Zircaloy-4 because Al and Fe can be present in pellets as an additive element or an impurity. CsOH can also be formed in operation by combinig Cs with moisture in the failed fuel rods, in which the SCC of Zircaloy-4 occurs.

2) Effects of Tube Fabrication Processes

Figure 2 shows the ISCC behaviors of two types of Zry-4 tubes at 330 °C and 0.8 mg I_2/cm². Curves of hoop stress versus time-to-failure showed typical behaviors of ISCC of two types of Zry-4 tubes which were fabricated in different processes. Tubes of supplier A were more resistant to ISCC than those of supplier B, resulting in higher threshold stress by about 30 MPa. Both types of commercial tubes were stress-relieved, of which chemical compositions are nearly same. The mechanical properties, however, were a little different. Tubes of supplier A had lower mechanical properties of ultimate tensile stress (UTS) and yield strength (YS) and elongation in longitudinal tensile tests, but had higher values of ultimate hoop strength (UHS) and total circumferential elongation (TCE) in burst tests than those of supplier B. The metallugical properties of both supplier's tubes were also a little different in

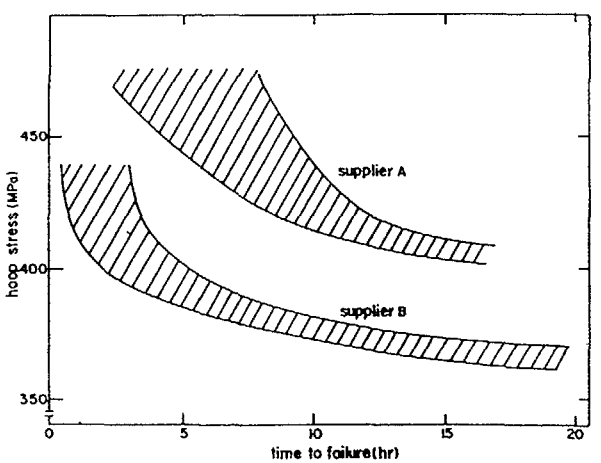

Figure 2 ISCC Behavior of Zircaloy-4 from Different Suppliers at 330 °C, 0.8 mg I_2/cm².

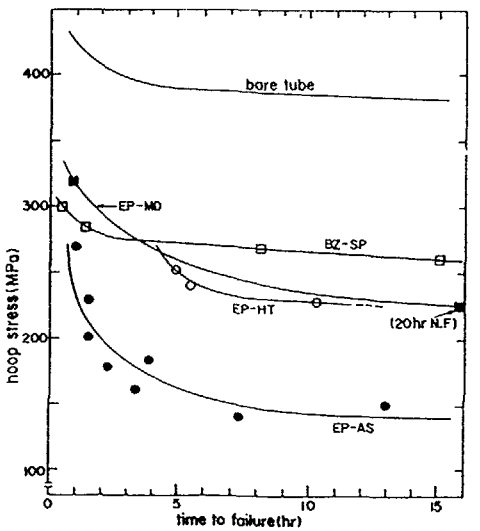

Figure 3 ISCC Behavior of Zircaloy-4 Tube with Appendices or End Plug at 330 °C.

texture. Hydride orientation in tubes of supplier A showed Fn numbers of less than 0.05 while the Fn = 0.1 in supplier B's tubes. This difference suggests that the ISCC susceptibility of Zircaloy-4 cladding tube is dependent on the tube fabrication process, especially the texture and the toughness in a circumferential direction rather than in an axial direction.

3) Effects of Welding and Brazing Processes

In the fabrication of CANDU-type fuels, a resistant welding has recently been used to seal the end caps, and a brazing process is employed to attach spacers and pads since it provides good mechanical properties as well as good metallurgical microstructures. But welded parts of a cladding tube have a potential risk of PCI failure under operation because they are located in a high flux region without plenum, and because welding-induced tensile stress or heat-affect zone makes welded parts susceptible to SCC. In fact, Figure 3 shows the ISCC susceptibility of welded parts in CANDU-type fuels. End cap welding also appeared to be very weak to ISCC, as shown in an EP-AS curve in Figure 3, resulting in a threshold stress less than 150 MPa of hoop stress which was 40% below of that of normal Zircaloy-4 cladding tubes. The ISCC was found to start at a notch formed between the tube and the weld upset during the welding process. The welding process, in general, produces residual stress, complexible microstructure and geometrical defects in a welded part. To remove the effects of residual stress, ISCC tests were carried out after annealing the welding part at 500 °C for 1 hour. Removing the residual stress in welded parts improved the ISCC resistivity up to 230 MPa of threshold stress, as shown in the EP-HT curve in the figure. However, the ISCC occurred at a notch in the welding part, and the

threshold stress was also only 60% of that of Zircaloy-4 tubes. A modified resistance upset welding process[13] was developed to produce a smooth upset, resulting in almost negligible notch effects. An EP-MD curve in the figure shows the ISCC behavior of the part welded by the modified welding process. It showed quite a good ISCC behavior, above 230 MPa of threshold stress, but the ISCC occurred again in the welded part.

In burst tests without a corrosive agent, axial cracks were found along the tube, never in the welded part. However, a welded part of an end cap should have a potential risk of ISCC under iodine atmosphere, even though an annealing treatment after welding and/or a modified welding process to reduce notch effects could result in high improvement in the ISCC resistance.

A brazing of spacers also had a potential risk of ISCC. ISCC occurred in the brazing part along an axial direction, and the threshold stress of ISCC was about 270 MPa, about 70% of that of Zircaloy-4 tubes, as shown in a BZ-SP curve in Figure 3. A main reason for this weakness would be metallurgical factors of coarse grains in the brazed part.

4) Effects of Graphite/Siloxane Coating

Graphite or siloxane is used as a coating material inside the cladding tube to improve the PCI failure resistance in CANDU-type fuels because coating materials are known to act as a lubricant, a getter of iodine and/or a protective barrier. In Figure 4, the ISCC behavior of graphite-coated tubes, which were baked at 300 °C for 1 hours after coating at room temperature, were compared with bare tubes at 330 °C, 0.8 mgI_2/cm^2. Graphite-coated tubes seemed to be a little better than bare tubes to ISCC resistance, but displayed almost the same behavior. The threshold stress of the graphite-coated tubes was about 360 MPa, comparable to the bare tubes. This result suggests that graphite coating may not be so effective as a protective barrier. On the other hand, graphite coating appeared to influence the critical concentration of iodine for SCC, even though the evidence was not so clear. As the iodine was supplied in a constant amount using an ampule in this study, it was not easy to get

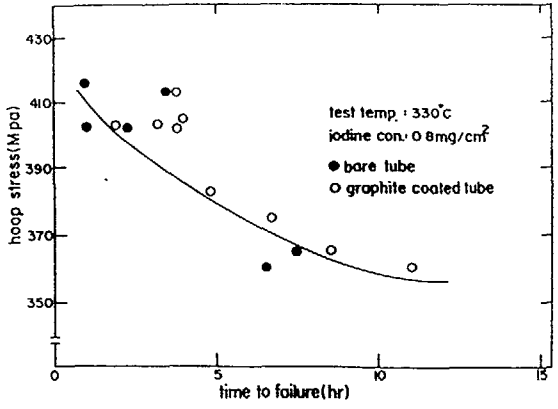

Figure 4 Failure Time of Graphited-coated and Bare Tubes as a Function of Hoop Stress.
(Baking Condition : 300 °C, 1 hr)

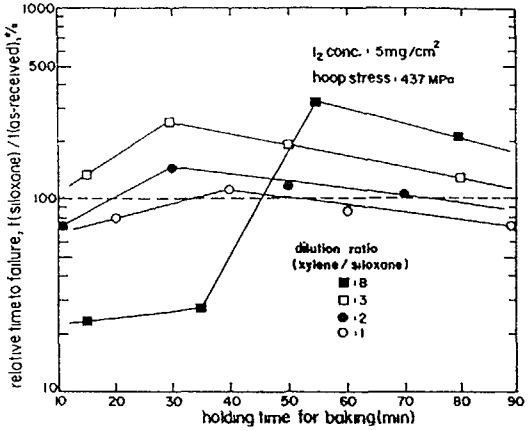

Figure 5 ISCC Resistivities of Siloxane Coated Zircaloy-4 Tube Specimens at 330 °C.

an accurate value of a critical concentration. However, in the range of of 0.3-0.5 mgI_2/cm^2 concentration which was just about or above the critical iodine concentration required in bare tubes, graphite-coated tubes displayed the same or better ISCC behaviors.

Considering that the friction coefficient of a graphite-coated tube is less than half of that of a bare tube, these results should lead to the conclusion that graphite-coating attributed to improving PCI/SCC failure by the roles of a iodine getter and/or a lubricant rather than a protective barrier.

Siloxane is known to be another candidate for a coating material to improve the PCI/SCC failure resistance. Since siloxane contains a large amount of hydrogen, the coating process is very important to keep the hydrogen concentration in Zry-4 tubes after baking it below the specification. In this study, an ISCC behavior of siloxane- coated tubes was investigated according to the dilution ratio of diluent to siloxane as well as baking time. Figure 5 shows the ISCC behavior of siloxane-coated tubes. ISCC resistance in the figure was represented using a relative time-to-failure which meant the ratio of time-to-failure of ISCC for a siloxane-coated tube, as compared with that for a graphite-coated tube. Both the dilution ratio and the baking time affected the ISCC resistance. In case of a low dilution ratio such as 1, the ISCC resistance was not better as compared with graphite-coated tubes, resulting from high concentration of hydrogen and from poor bonding with microcracks on the coating surface. For a high dilution ratio such as 8, however, the time-to-failure of ISCC was almost 3 times that of graphite-coated tubes. On the other hand, baking time was related to forming SiO_2 from siloxane, which gave a weak bonding force, so that the ISCC resistance versus baking time in the figure showed a peak at a certain baking time.

It is not known whether Siloxane plays a role as an iodine getter or a lubricant, thus, contrary to the case of graphite-coating, a protective barrier of siloxane-coating layer to ISCC should be of importance to improve the ISCC resistance.

4. SUMMARY

Iodine-induced stress corrosion cracking tests on Zircaloy-4 tubes were undertaken using an internal pressurization method to elucidate the mechanism and to find out remedies of pellet-cladding interaction failure. FeI_2, AlI_3 and CsOH acted as active corrosive agents for SCC of Zircaloy-4, showing almost the same critical concentration as that of I_2. CsI and CsCl, however, were found to be not active for SCC. The fabrication process of each company brought out certain characteristics of mechanical and metallurgical properties of Zircaloy-4 tubes, resulting in a different ISCC behavior. Tubes with high toughness in burst tests and with textures in a radial direction showed a good behavior of ISCC. In addition, the welding process made ISCC resistance decrease up to 40% as compared with that of tubes as-received. An annealing treatment and/or a modified welding process showed some effect to recovery the ISCC resistance, but welded parts still had a potential risk of ISCC. Graphite or siloxane was found to be so effective to improve the ISCC resistance which seemed to be act as a getter of iodine and/or a lubricant, or a protective barrier, respectively.

REFERENCES

[1] Peehs M., Stehle H. and Steinberg E., "Out-of-pile testing of iodine stress corrosion cracking in Zircaloy tubing in relation to the pellet-cladding interaction phenomenon", Zirconium in the Nuclear Industry (Proc. 4th Int. Conf. Stratford-upon-Avon, 1978), ASTM STP 681, ASTM, Philadelphia (1979) 244-260.

[2] Cubicciotti D., Syrett B.C. and Jones R.L., Stress Corrosion Cracking of Zircaloys, Rep. EPRI-NP-1329, Electric Power Research Institute (1979).

[3] Ryu W.S., Hong S.I., Choi Y., Kang Y.H. and Rim C.S., A study on the iodine-induced stress corrosion cracking of Zircaloy-4 cladding(I), J. Korean Nuclear Society 17 N3 (1985) 193.

[4] Roberts J.T.A. et al., "A stress corrosion cracking model for pellet-cladding interaction failures in light-water reactor fuel rods", Zirconium in the Nuclear Industry (Proc. 4th Int. Conf. Stratford-upon-Avon, 1978), ASTM STP 681, ASTM, Philadelphia (1979) 285-305.

[5] Kreyns P.H., Spahr G.L. and McCauley J.E., An analysis of iodine stress corrosion cracking of Zircaloy-4 tubing. J. Nucl. Mat. 61 (1976) 203.

[6] Choi Y., Kang Y.H., Ryu W.S. and Rim C.S., The slow strain rate dependence of Zircaloy-4 cladding tube in iodine atmosphere. J. Korean Nuclear Society 17 N3 (1985) 211.

[7] Hofmann P. and Spino J., Chemical aspects of iodine-induced stress corrosion cracking failure of Zircaloy-4 tubing above 500 °C. J. Nucl. Mat. 114 (1983) 50.

[8] Une K., Deformation and fracture behavior of Zircaloy-2 deformed at constant strain rate in iodine environment(I) (uniaxial). J. Nucl. Sci. Tech. 16 (1979) 577.

[9] Ryu W.S., Kang Y.H. and Lee J.Y., Effects of iodine concentration on iodine-induced stress corrosion cracking of Zircaloy-4 tube. J. Nucl. Mat. 152 (1988) 194.

[10] Jones R.L., Yaggee F.L., Stoehr R.A. and Cubicciotti D., Threshold conditions for iodine-induced stress corrosion cracking of unirradiated Zircaloy-4 tubing under internal pressurization. J. Nucl. Mat. 82 (1979) 26.

[11] Williford R.E., The iodine-induced strain rate sensitivity of Zircaloy fuel rod cladding. Nucl. Eng. Des. 78 (1984) 23.

[12] Ryu W.S., Lee J.Y., Kang Y.H. and Suk H.C., Strain rate dependence of iodine-induced stress corrosion cracking of Zircaloy-4 under internal pressurization tests. J. Mat. Sci. 25 (1990) 3167.

[13] Goh J.H. Lee J.W. and Jung S.H., Strain rate dependence of iodine-induced stress corrosion corrosion cracking of Zircaloy-4 under internal pressurization tests. J. Korean Nuclear Society 23 (1991) 1.

POSTER SESSION

EXPERIMENTAL INVESTIGATION OF OUT-REACTOR METHODS OF FAILED FUEL DETECTION

V P. ELIZAROV, V.V. KONYASHOV, A M KRASNOV
Research Institute of Atomic Reactors,
Dimitrovgrad, Russian Federation

Abstract

Results are reported on test and comparison for all known methods of out-reactor failed fuel detection: water, water-gas, air-lift, vacuum and dry. The D-1, D-2 experimental assemblies contained incl elements with initial defects in claddings as well as standard assemblies with failed fuel elements after 12 years keeping were investigated. Experimental devices and methods of tests are described.

Due to the uprated requirements to the NPS safety systems it was necessary to increase the efficiency of out-reactor method of failed fuel detection (FFD). To this end the all well-known methods were tested, compared and selected the more perspective onces. Both the fuel assembly D-1, D-2 with initial defects of fuel element claddings and the standard fuel assembly with typical operation defects of 12 years storage time were tested.

The experimental FFD stand (fig.1) involves can with hydraulic gear for plug closing, circulating pump, degasator and vacuum pump. The stand is connected to the system of compressed air and washing. It is equipped with the line of water sampling and gas supply from the degasator to the flow counter of ß-radiometer with 2 Bq/l sensitivity.

In testing a fuel assembly is placed in the can sealed with a plug. The can and stand are washed with distillated water, then the fuel assembly is controlled by one of known method The applied methods are as follows

1. Water method

The stand water is agitated with the circulating pump and the sample of water is taken for determination of fission products activity with the gamma-spectrometer of high resolution.

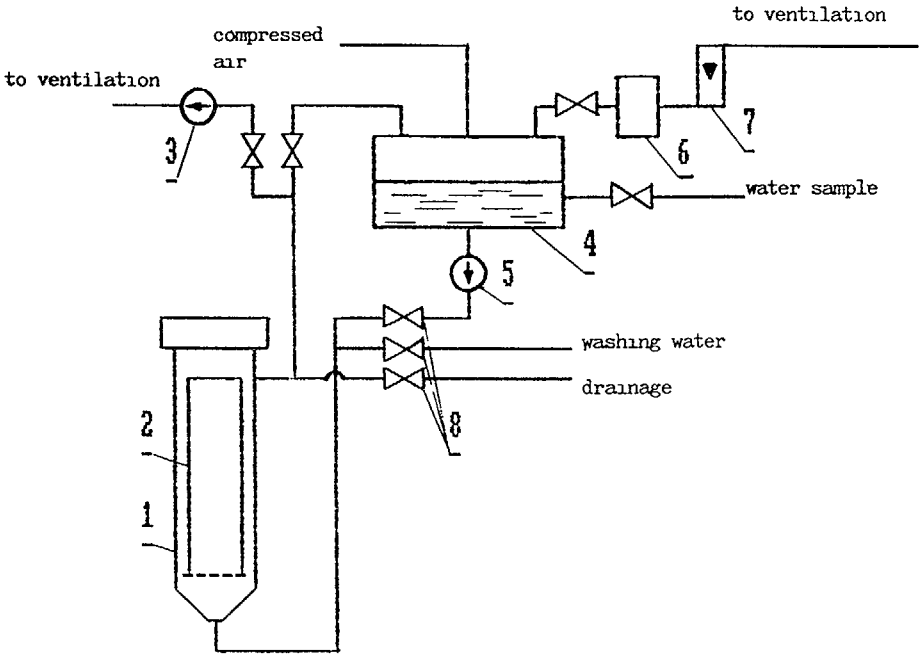

Fig.1 Principle schematic diagram of FFD stand

1 - can, 2 - fuel assembly, 3 - vacuum pump, 4 - degasator,
5 - circulating pump, 6 - flow ß-counter, 7 - rotometr,
8 - valve

To increase the rate of fission products release from the failed fuel elements into the circuit of FFD stand, the use is made of pressure pulses generated by compressed air.

2. Water-gas method

The stand water is agitated with the circulating pump and the sample of water is taken for determination of fission products activity. Also the fission products are degassed from water by a full-flow degasator with continuous supply of the measured gas into the ß-radiometer.

3. Airlifting method

Water is degassed by air entering into the lower sleeve of FFD can. Air is supplied through the upper sleeve into the flow counter to measure the fission gases activity.

4. Vacuum method

Vacuum generated in FFD can stimulates the fission products release from the failed fuel elements. Then can water is sampled or/and degassed with the following measurements of fission products activity.

5. Dry method

The FFD can is dried and blown air which is dispensed to the flow ß-radiometer.Process of fission gases release is intensified at the expense of fuel element heat-up.

An objective of investigation is a choice of the FFD method meeting the current requirements but siufficiently simple for realization.The current requirements are as follows: authentic information about existence and dimentions of defects in fuel element cladding within the range of dimensions (including microdefects), the possibility for the inspected fuel assembly to be returned into the reactor core. The more simple method was preffered.

As a result of numerous investigations the conclusions were made.

The authentic method allowing to obtain the repeated results (existence and dimension of defect) is a method in which all determinant parameters are constant and do not dependent on an operator. The following methods are not concerned with the authentic once: the dry method due to non-controlled heat-up of fuel elements and danger of their heat-up; the airlifting method due to nonuniform distribution of air flow on the fuel assembly section with water bubbling; the vacuum method due to data absence on water column height over defect determining the residual pressure within the range of defect. It is validated by the fact that results obtained by these methods are impossible to repeat. Some times fission products released from failed fuel elements change by several times. In addition, the method mentioned above are complex for realization.

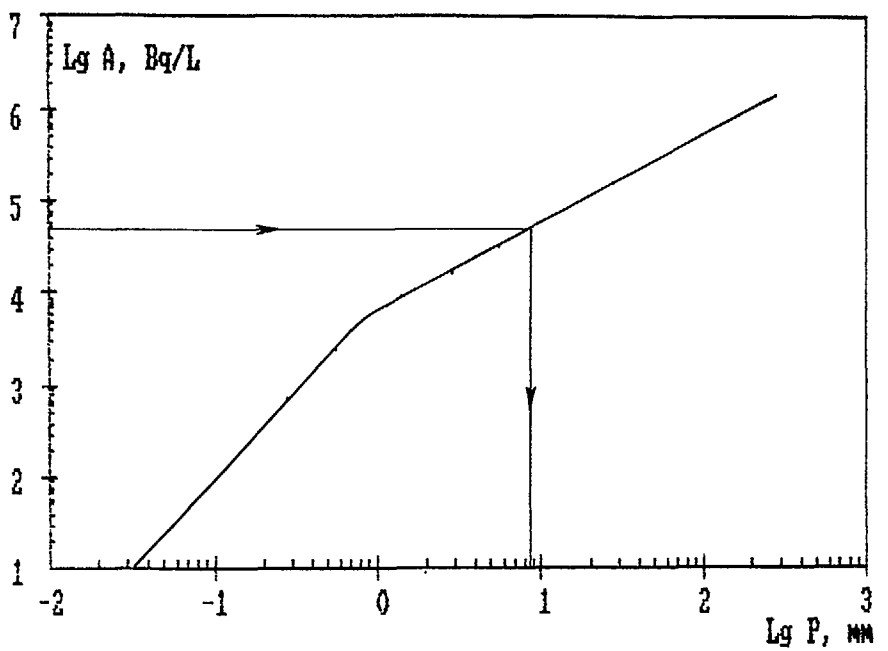

Fig.2. J-131 activity in stand water dependence on perimeter of defect

Time - 15 min.

Fuel element linear power - 74 W/cm

The water method do not meet the current requirements due to data absence about gas activity needed to control the microdefects in fuel element claddings.

The water-gas method is more suitable. For its realization an operator must start up the circulating pump after washing of the can, recording of flow ß-radiometer and water sampling in defined time; in comparison with other methods the obtained results are less dependent on linear power of fuel element, location of defects against fuel element height and fuel assembly cross section.

The sensitivity of the water-gas method meets the current requirements. The estimation obtained from the results of the D-2 fuel assembly control shows that cladding defects of 0.01 mm diameter will be recorded by increasing of gas-fission products activity with the flow ß-radiometer (control time - 15 min., time after reactor shutdown - 15 days, linear power of fuel element - about 100 Wt/cm). The high sensitivity of method was shown with control of the three VK-50 standard fuel assemblies with the failed fuel elements after 12 years storage. Excess of gas-fission products activity (krypton-85) over phone level was recorded during 15 min. The rate of Cs-137 release from defective fuel elements was controlled by measuring of water sample activity and reached 10^6Bq/h.

The most important advantage of the water-gas method is possibility for realization of diffusion mechanism of fission-products release from failed cladding that allows to determine the defective size by fission products activity in the FFD stand. This method is based on calculation of diffusive fission products release in the FFD stand for defects of different dimensions. The technique was validated by the VK-50 FFD stand with using of the D-2 fuel assembly with initial defects of known dimensions. (fig.2).

GEOMETRY VARIETY OF VVER FUEL RODS

B.A. KANASHOV, V.I. KUZMIN, G.D. LYADOV,
V.S. POLENOK, A.V. SMIRNOV, V.P. SMIRNOV, A.V. SUKHIKH
Research Institute of Atomic Reactors,
Dimitrovgrad, Russian Federation

Abstract

The classified experimental data are presented for study of dimensional stability of standard fuel rods for the VVER type reactors with UO_2 fuel core in Zr-1%Nb claddings. Dynamics of the length change, diameter and the gap between fuel and claddings was investigated for three fuel assemblies of the VVER-440 reactor and four fuel assemblies of the VVER-1000 reactors in dependence of the fuel burn-up 22-45 MWt day/kg of uranium.

Introduction

In the process of operation the power reactor elements are objected to the pronounced radiation, temperature and mechanical effects leading to irreversible changes of dimensions and shape. Having reached the definite values, these changes of construction parameters become the factor limiting their further operation. Thus, for the search of the new design decisions, promising materials and nominal operation modes the pronounced volume of works is carried out now on investigations of geometry of the spent fuel assemblies and their elements. In the paper the results are presented on the change of length, fuel element diameter and diametral gap between fuel and cladding during their operation in the VVER type reactors.

Characteristics of the tested fuel assemblies and elements

Three standard fuel assemblies of the VVER-440 reactors were selected for investigations together with four fuel assemblies of the VVER-1000 reactor. The main design parameters of the fuel rods are presented in Table 1 and the operation parameters are in Table 2.

Table 1

Constructive parameters of fuel elements

Parameters	Nominal value	
	VVER-440	VVER-1000
Fuel rod length, mm	2557	3837
Helium pressure, MPa	0.5-0.7	1.9-2.6
Cladding material	Zr-1% Nb alloy	
External diameter of cladding,mm	9.15	9.13
Internal diameter of cladding,mm	7.72	7.72
Fuel material	UO_2	UO_2
Length of fuel core, mm	2420	3530
Diameter of fuel rod,mm	7.60	7.53
Diameter of fuel rod hole,mm	1.2	1.4
Fuel rod diameter,mm	8-14	9-14

Value meanings of fuel rods are known within tolerance for production excluding fuel assembly №0007 for fuel rods with measured length and diameter in the state of the factory delivery.

It should be noted that during the production of one assembly the cladding tubes and fuel rods were used as a rule of several batches of delivery. This fact introduces the additionary variations into their geometrical values and initial features.

Methodics and measuring results

For measurement a combined method was used comprising measurement of various height of all the fuel rods directly in the bundle and absolute length of several fuel rods. For this sampling a calibration straight line was plotted in the coordinates "height difference vs absolute length of fuel rods. This line served as a basis for the length calculation of the rest fuel assembly rods

Table 2

Main characteristics of fuel assemblies and rods operation

Reactor type	NPS	FA number	Operation duration effec.day	Average burnup MWt d/kgU	Coolant pressure, MPa	Max.T°C of clad.
VVER-440	NV*	687	657	24.2		
	NV	809	1004	32.8	12.5	350
	R**	066	811	36.8		
VVER-1000	NV	0068	488	21.7		
	NV	0007	820	32.6	16	380
	SU***	0106	878	36.7		
	NV	1114	882	44.7		

* Novo-Voronezhskaya

** Rovenskaya

*** South-Ukrainian

Height difference was defined as the distance from the perpendicular axis of the fuel rod bundle of calibration platform up to their upper ends. Absolute length of the fuel rod was measured by comperison with the absolute length of the reference sample with cathetometer KM-6 or indicator head of round shape. Outer diameter of the fuel rod cladding in preset cross-section and in asimuthal orientation was measured by contact method using a convertor of magnetic scale type

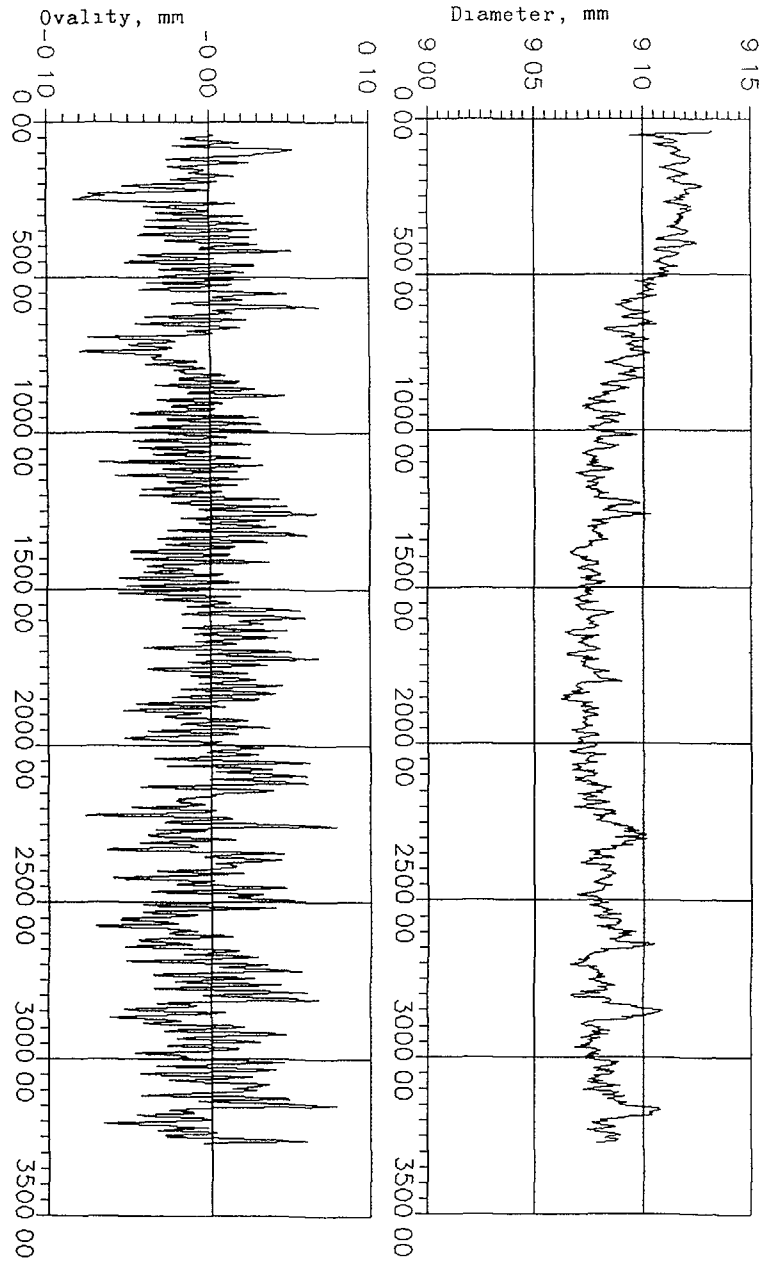

FIG 1
Average outer diameter (a) and ovality (b) of the VVER-1000 fuel rod

For calibration and sustaining of stable metrological characteristics of technical means and methods as a whole, the complex of standard samples of outer diameters was used The summerized ultimate error of a single measurement was $\pm$ 0.01mm.

The measurements were carried out in two mutually perpendicular orientations with a 2mm pitch.

Diametral gap $_{d}$ between the fuel core and cladding was measured on metallographic specimens perpendicular to the fuel rods axis The measurements were carried out with the remote microscope by comparison with the reference sample. The error for $_{d}$ was $\pm$30μm

In every fuel assembly a group of 30-60 rods was investigated in detail. The fuel rods were placed on three diagonals connecting the opposite ribs of a hexagonal tube. Metallographic investigations were carried out for 3-5 rods and the length measurements were carried out on the most number of fuel assemblies for all fuel rods.

Fig.1 presents the distribution of the average diameter and the cladding ovality along the VVER-1000 fuel rod length. Variety of the cladding diameter (absolute and relative) was determined in dependence of the initial diameter.

The general view of diagramms is characterized by the following:

- the greatest decrease of diameter is observed in central part of fuel rod
- in the process of operation practically all fuel rods become oval and the period of ovality is differing from rod to rod
- on diagramms of the average diameter the periodicity is observed and it is multiple of the length of a fuel core (11mm) for the fuel rod with burnup more than 35 MWt day/kgU.

The summerized results of fuel rods elongation (1) and diameter variety (1) investigations are presented in Tables 3 and 4 .

Table 3

Elongation of VVER-440 and VVER-1000 fuel rods

№ of FA	Quantity of tested fuel rods	Absolute elongation, mm				Relative elong-n,%	
		minimum	max.	average	RSS	Average	RSS
687	I26	3.0	7.0	4.9	0.8	0.I9	0.029
809	I26	5.0	9.2	6.7	0.9	0.26	0.033
066	I26	6.5	II.8	9.I	I.2	0.36	0.046
0068	3I7	2.2	II.4	6.2	I.2	0.I6	0.030
0007	3I7	3.6	I6.9	I0.0	I.7	0.26	0.044
0I06	44	6.3	I3.5	I0.3	I.6	0.27	0.042
III4	5I	8.7	I7.0	I3.2	2.0	0.35	0.052

Table 4

Average variety of diameter in central pert of fuel rods of VVER-440 and VVER-I000 reactors

№ of FA	Quantity of tested fuel rods	Absolute value, mm	RSS	Relative value, %	RSS
687	I4	-0,07	0.02	0.8I	0.24
809	24	-0.09	0.09	0.93	0.22
066	32	-0.I0	0.02	I.05	0.20
0068	52	-0.05	0.02	0.53	0.2I
0007	6I	-0.07	0.0I	0.79	0.I0
0I06	44	-0.09	0.02	I.02	0.23
III4	5I	-0.I0	0.02	I.07	0.22

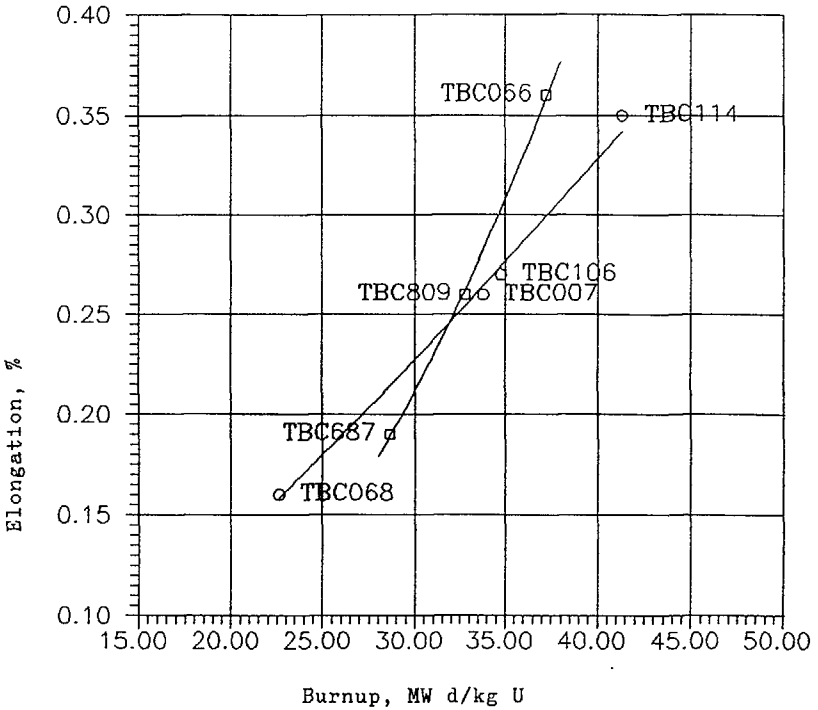

FIG. 2.
Dependence of relative elongation of fuel rods for VVER-440 (○) and VVER-1000 (□) on average burnup.

On the stage of regressive analysis the elongation l and diameter decrease d dependences from fuel burnup B were studied for all the investigated fuel assemblies. The results obtained show that the dependences between l and fuel burnup in VVER-440 and VVER-1000 fuel rods have a linear character and the inclination of the VVER-440 line is more tight (Fig.2).

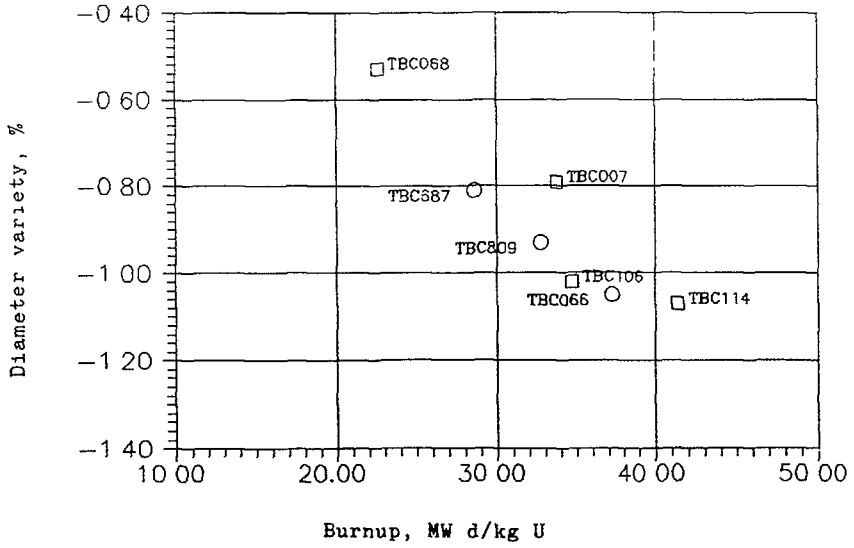

FIG 3
Dependence of diameter relative variety of fuel rods for VVER-440 (○) and VVER-1000 (□) on fuel burnup

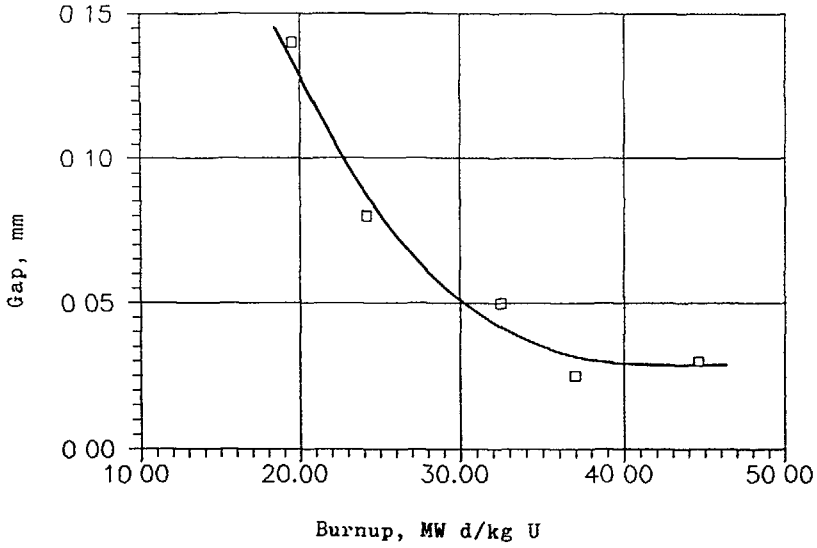

FIG 4
Dependence of diameter gap between fuel and cladding on fuel burnup

For all measured fuel rods of every fuel assembly the statistic connections between l and B, d and B were studied on the stage of preliminary analysis. In this case for one fuel assembly the correlation coefficient between the indicated parameters didn't exceed K=0.64. If the fuel rods of assembly №0007 belong to various technological batches of cladding, the correlation coefficient between elongation and burnup increases critically in every batch as well as between diameter decrease and burnup

Fif.3 shows the dependence of the averaged decrease of the cladding diameter in a central part of rods for the investigated assemblies. As seen from the figure, the points for VVER-440 and VVER-1000 are forming practically a common dependence, although there is a slightly greater effect of diameter decrease for VVER-440 fuel rods. When burnup is 35 MWt day/kgU, the rate of diameter decrease is tended to be lower and when burnup is about 40 MWt day/kg, the diameter decrease stops on the level of $\frac{d}{d_{init.}}$ = 1.1%.

Measurements of a diameter gap under the normal conditions (Fig.4) between fuel and cladding in the zone of the maximum burnup showed that in the range from 20 to 30 MWt day/kgU its values decrease monotonously from 0.11 - 0.17mm to 0.03-0.08mm. When burnup was more than 35 MWt day/kgU the diameter gap didn't exceed 0.02-0.04mm. Estimation of the difference between thermal expansions of the claddings and fuel values in radial directions under a nominal mode of operation showed that the value was 0 07-0.10mm. It is 0.03-0.08mm more than the minimum "cold" gap at the burnup exceeding 35 MWt day/kgU

thus, a part of pellets was pressed out by the cladding tightly during operation beginning from 30 MWt day/kgU burnup.

Mechanical pressure of fuel on the cladding compensated in some degree the coolant pressure and correspondingly decreased the pressing strength in it. As a result of it the cladding diameter decrease stopped at the values of burnup exceeding 35MWt day/kgU (Fig.3).

Conclusions

It is known, that with the absence of a contact between fuel and cladding the deformation may be a result of creep a radiation growth for the VVER fuel claddings. When the contact occures, the cladding is effected by the pressure of the swelling fuel and as a result of it the tensile quasistatic stress occures. Besides, when the reactor capacity changes, a short-term stresses take place leading to the cladding deformation by a ratchet-and-pawl type.

Assesment of the fuel cladding deformation caused by radiation growth can be carried out in the following way. Length and diameter of guiding tubes of assembly 0007 control rods were measured during post-reactor investigations. During in-pile operation the walls of the tube are pressed from all sides with the coolant pressure of about 16MPa. Under such conditions the component of the stressed state is absent which could cause a tube material creep. Consequently, the only mechanism of deformation is a radiation growth. Profilometry of the guiding tubes and the length measurement show that elongation in reference to niminal value was only 0 2mm and average diameter along the tubes length is changing within the limits of 0.3mm.

Thus, the radiation growth at the initial stage when the fuel burnup is 32.6MWt day/kgU, produces a small effect on the deformation of Zr-1%Nb tubes in the fuel assembly of VVER-1000.

The results obtained are not contrary to the literature data, according to which the radiation growth causes a pronounced rate of macrochanges beginning from fluence $2.2\ 10^{22}\ cm^{-2}$ (E 0.1MeV) by linear dependence during the irradiation of the cladding samples in spectrum of the BOR-60 reactor.

Evidently, for assembly 0007 the critical level of damage has not been yet reached in the tubes material, when the radiation growth rate increases sharply.

The fuel rod claddings are under another tensile state in comparison with the guiding tubes, as the gaseous pressure in the fuel rods doesn't put the coolant pressure in equilibrium. Calculation estimations show that because of the pressure difference the component of pressing stresses occures in tangential direction = 60MPa. Due to these stresses at the expence of creep,the fuel cladding diameter decrease takes place. On the site of the fuel core the diameter decrease is observed until the cladding is in contact with fuel cores. Complex results on the change of the cladding diameter and value of the diameter gap with burnup (Figs.3 and 4) show that the contact of fuel with cladding for VVER-1000 and VVER-440 occures at the burnup of B = 30MWt day/kgU. This is an averaged value and it depends on the following factors: initial diameter gap, fuel density and operation parameters. So for some fuel assemblies, fuel rods and even some parts of rods the burnup value can be differed from the indicated one in the case of the mechanical contact of the fuel core and cladding.

At the burnup exceeding B , the swelling fuel cores can deform the cladding, that was observed in some fuel rods of fuel assemblies 0662 and 1114.

Reference

1. G.P.Kobylyansky et al. Radiation form variety of the cladding and channel tubes of Zr alloys at high neutron fluences. Proceedings of International Conference on Radiation Material Science, Alushta, May 22-25, 1990, vol.4.

MEASUREMENT METHODS OF GAS FISSION PRODUCTS QUANTITY UNDER FUEL ELEMENT CLADDINGS BY MEANS OF DEEP COOLING

A.V. SUKHIKH, E.P. KLOCHKOV
Research Institute of Atomic Reactors,
Dimitrovgrad, Russian Federation

Abstract

Quantitative non-destructive expressive techniques for fission gas release analysis are described. The techniques use Xenon and Krypton low temperature condensation.

Barometry of fuel element gases is an integral component of all programs of post-reactor fuel element investigations. Pressure of gas fission products (GFP) possesses information about the tightness degree and fuel element operation regimes. Development of non-destructive methods of determining this value is one of the problems the priority of which seems obvious.

The investigations carried out in RIAR and aimed at solution of this problem allow the methods based on GFP transport to a condensed state to be recommended for such purposes.

The essence of the proposed methods lies in obtaining the GFP condensate and registering changes of the fuel element parameters in the area of gas collector using an external indicator appliance.

Fig.1 presents a block-diagram of the facility for performing the radioactive Kr-85 quantity determination in a hard GFP condensate using a gamma-spectrometer. Fig.2 illustrates the design of the facility for generating a Xe and Kr condensate in a local region of the fuel element gas collector. Fig.3 shows the spectrum region near the Kr-85 gamma-line with energy 514 keV prior to and after cooling of the fuel element. Metrological investigations demonstrated that the method gives an acceptable accuracy as early as at 0.01 MPa of the partial GFP pressure under the VVER fuel element cladding.

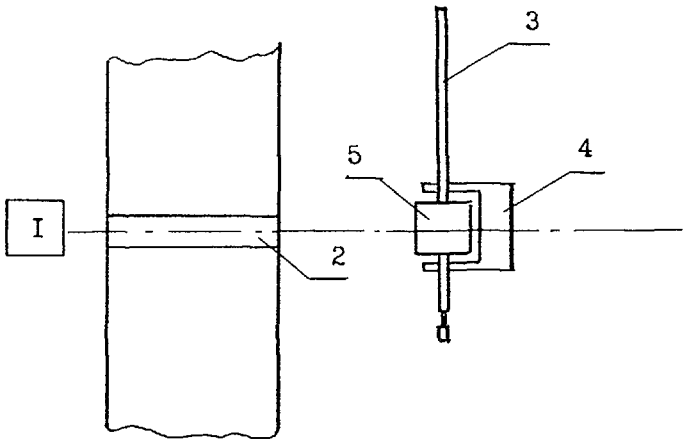

1 - Gamma-spectrometer detector
2 - Collimator in the shielded chamber wall
3 - fuel element under study
4 - fuel element adjustment mechanism
5 - cooling node

FIG. 1. Device for determining the quantity of radioactive Kr-85 in the GFP condensate.

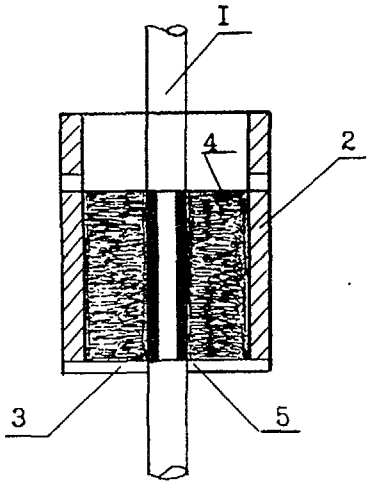

1 - fuel element
2 - devide vessel
3 - seal node
4 - liquid nitrogen
5 - Xe and Kr condensate

FIG. 2. Fuel elements cooling device.

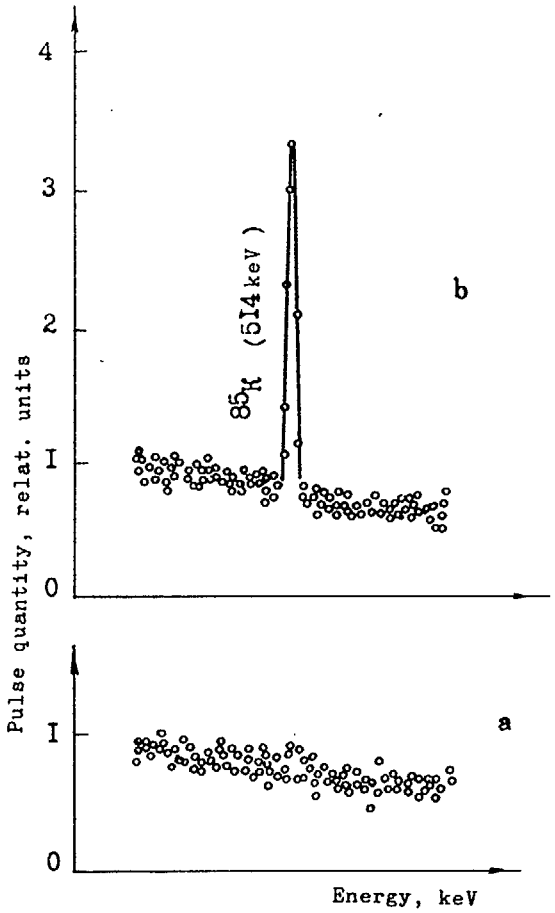

a) prior to cooling;
b) after cooling of fuel element

FIG. 3. Region of gamma spectrum within the fuel element gas collector.

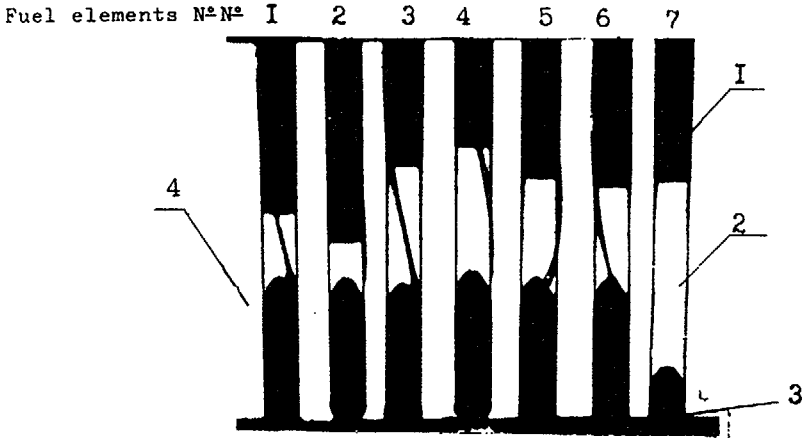

1 - fuel, 2 - gas collector, 3 - fuel element plug,
4 - Xe and Kr condensate

FIG. 4. X ray pictures of fuel element gas collectors after cooling.

GFP quantity can be estimated with the help of geometrical sizes of the condensate. Fig.4 presents an X-ray photograph of gas collectors of spent fuel elements after cooling. Absence of liquefied gases in fuel element №7 evidences of its untightness. Shape of the condensate meniscus observed in steel fuel elements is connected with the measuring scheme, namely, with fuel elements location at an angle 45° to the X-ray flux. Height of the condensate column being an informative parameter of GFP quantity can be easily measured with change of the angle up to 90° (Fig.5). The absorption method of determining the GFP quantity is characterized by high productivity and visuality of the results obtained. The sufficient measurement accuracy can be realized (using know-how) as early as at 1 n cm^3 of GFP under the fuel element cladding.

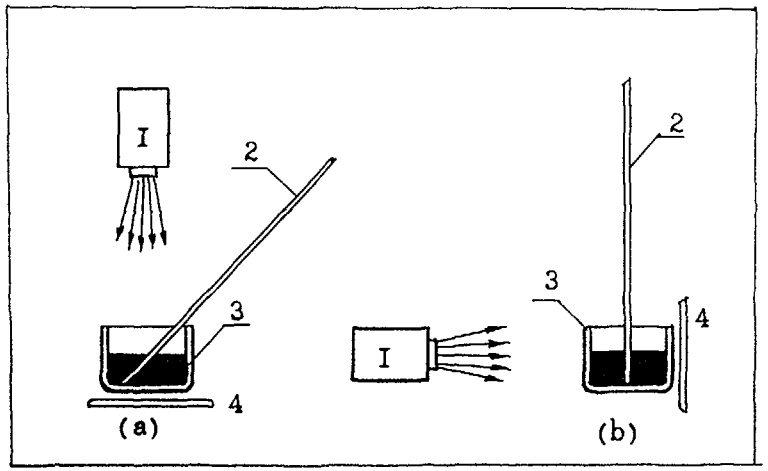

a,b - horizontal and vertical variant of X-ray aparatus location
1 - X-ray apparatus, 2 - fuel element, 3 - flask with cooling agent, 4 - X-ray film.

FIG 5 Scheme for realizing the method for GFP quantity determination according to geometrical sizes of its condensate

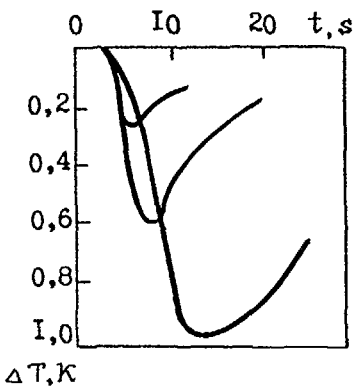

1 - 85% He + 15% air
2 - 70% He + 30% air
3 - 100% air, total mixture pressure $1 \cdot 10^5$ Pa.

FIG 6 Temperature jump value on the gas collector cladding of fuel element mock-up with different composition of helium–air mixture

The third measurement method of GFP partial pressure is based on fast cooling of a fuel element part and on registering change of cladding temperatures in the area of the gas collector using a special thermo-electrical converter. After cooling the pressure of gases in a fuel element falls abruptly due to adsorption and transport of some components of fuel element atmosphere to a new phase state. Drop of the pressure leads to cooling of gas and fuel element cladding outside the thermal perturbation area.

Fig.6 presents the measurement results for the cladding T of fuel element mock-ups with different content of the helium air atmosphere components. The value of a temperature jump depends on the fraction of air components in helium liquefying during cooling of the fuel element with liquid nitrogen.

All the enumerated methods can be used not only under shielded chamber conditions but also at posters of fuel element inspection in water cooling pools in investigations or repair works of demountable fuel assemblies. The cooling device in this case contains 2 sealing units and along with the channels for liquid nitrogen circulation via the chamber includes pipes for compressed air supply and discharge of water let into the system during recharging of the regular fuel element under control.

INVESTIGATIONS OF RADIOACTIVE FISSION PRODUCT RELEASE FROM FUEL ELEMENTS WITH INITIAL CLADDING DEFECTS DURING OPERATION OF THE VK-50 REACTOR

V P ELIZAROV, V.V. KONYASHOV, A.M. KRASNOV
Research Institute of Atomic Reactors,
Dimitrovgrad, Russian Federation

Abstract

Results are reported on measurement of fission product activity in reactor water and off-gas during D-1 and D-2 experimental assemblies irradiation. Every assembly contained three fuel elements with ⌀1 mm cladding holes in zone of maximum local power. Time of assembly D-1 is 5 years, that of D-2 - 2 years. Linear power of fuel elements in assembly D-1 reached 70 W/cm, in assembly D-2 - 100 W/cm. Fission products release from fuel elements with initial defects during irradiation was calculated on experimental data of fission products activity in the reactor circuit and compared with modelling calculations.

Experimental fuel assemblies with fuel elements possessing initial cladding defects have been irradiated at the VK-50 reactor since 1984 for experimental substantiation of calculation techniques of radioactive fission products (RFP) release from failed fuel elements in conditions of water-cooled reactor operation and in those of controlling the fuel assemblies with failed fuel elements after shut-down of a reactor. Experimental fuel assemblies D-1 and D-2 are manufactured according to the standard technology, but 3 fuel elements in each fuel assembly have through cladding defects in the form of holes, 0.9-1.0 mm in diameter, in the zone of maximum linear power (about 1/3 of the fuel element height) For D-1 the holes in fuel element claddings were drilled following the fuel element setting up, and for D-2 - following drilling of claddings the first step involved deburring inside the cladding and the second one - filling it with fuel pellets Fuel elements with initial defects in D-1 were located in the inner row, and in D-2 - in the penultimate outer one. The D-1 fuel assembly was irradiated in the VK-50 reactor with linear power of the fuel elements under study 50-70 W/cm for 5 years, fuel burnup in them achieved 18,000 MW d/t uranium. The D-2 fuel assembly is loaded into the reactor after the removal of D-1 and is irradiated the second year with linear power of the fuel elements under study 90-120 W/cm.

Prior to loading of the D-1 fuel assembly there were no failed fuel elements in the VK-50 reactor core and background RFP levels in the reactor circuit caused by surface contamination with fuel were carefully studied /1/. The equivalent core contamination with U-235, calculated due to the radionuclide activity of krypton, xenon and iodine, made up about 10 mg.

Control of the RFP activity in the NPP circuit was performed by means of the following method. Radioactive inert gases - krypton and xenon radionuclides were registered in fume-off of the turbine ejector at NPP, where more than 95% of their total amount are released. Other radionuclides are accumulated in the reactor water, and a part of them is transferred to the distillation decontamination facility with the reactor water. Samples of the ejector gas and reactor water were measured at the gamma-spectrometer with a semiconducting detector.

RFP release from fuel elements with initial defects (R/B) was calculated according to the measurements results of the RFP activity. The leakage rate (R) was determined by the RFP activity in samples, the formation rate (B) - by calculation of the known fuel element power.

Unfortunately, the condition did not allow the experiment with D-1 fuel assembly as at least 2 more failed fuel elements were formed in the reactor core in 1.5 years of irradiation which led to considerable growth of the gaseous radioactive fission products (GFP) activity (see Fig.1). In this case contribution of GFP, leaving the fuel elements with initial defects

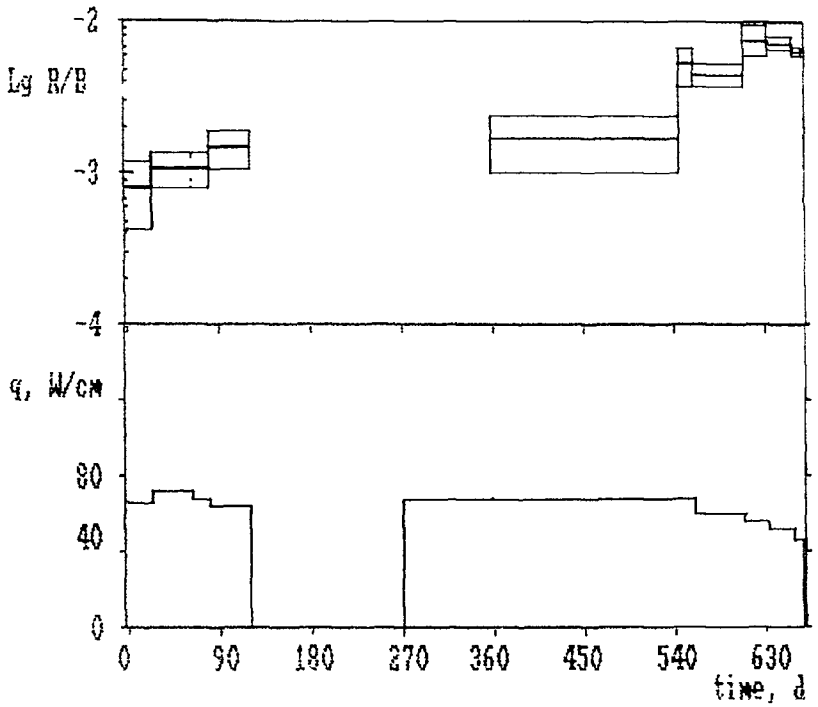

Fig.1. Change of Xe-133 release from fuel elements with initial defects during the D-1 fuel assembly irradiation

q - linear power of a fuel element with initial defect

of the D-1 fuel assembly, since that time made up, probably, no more than 20% of the total GFP activity. In fact, after the D-1 fuel assembly extraction from the core, the GFP activity in the reactor core did not practically change. GFP release from the fuel elements with initial defects was practically constant during the first 1.5 years of irradiation prior to defects formation in standard fuel elements. The data obtained coincides within the measurement errors with the results of model calculations (Tab.1, Fig.2).

The RFP activity levels in the reactor water during the D-1 fuel assembly irradiation for the first 1.5 years did not exceed their background values measured while operating without failed fuel elements. The estimations show that iodine radionuclides release from the fuel elements with initial defects

Table 1

Comparison of Calculated and Experimental Data about GFP Release during D-1 Fuel Assembly (f/a) Irradiation

Nuclide	GFP release, %				
	calculation				experiment
	from fuel			from f/e	from f/e
	recoil	diffusion	sum		
Xe-133	4.65E-2	1.83E-2	14.1E-2	13.7E-2	(11±3)E-2
Xe-135	4.65E-2	1.83E-2	6.48E-2	3.96E-2	(5.3±1.3)E-2
Kr-85m	4.83E-2	1.79E-2	6.62E-2	3.97E-2	(4.9±1.2)E-2
Kr-88	4.83E-2	1.41E-2	6.24E-2	3.01E-2	(2.4±0.8)E-2
Kr-87	4.83E-2	0.95E-2	5.78E-2	1.71E-2	(2.0±0.8)E-2
Xe-138	4.65E-2	0.41E-2	5.06E-2	5.08E-3	(6.0±2.7)E-3

Notes:

1. Pressure in the VK-50 reactor - 6.2 MPa, average linear power of the fuel element with initial defect - 70 W/cm.
2. Calculations of GFP release include
   - ratio of the fuel surface area to its volume is equal to 300 1/cm,
   - diffusion coefficient is equal to the sum of radiation-stimulated and thermal diffusion coefficients;
   - leakage coefficient of Xe-133 from under the cladding of a fuel element with initial defect makes up $7 \cdot 10^{-5}$ 1/s;
   - medium under the fuel element cladding - steam

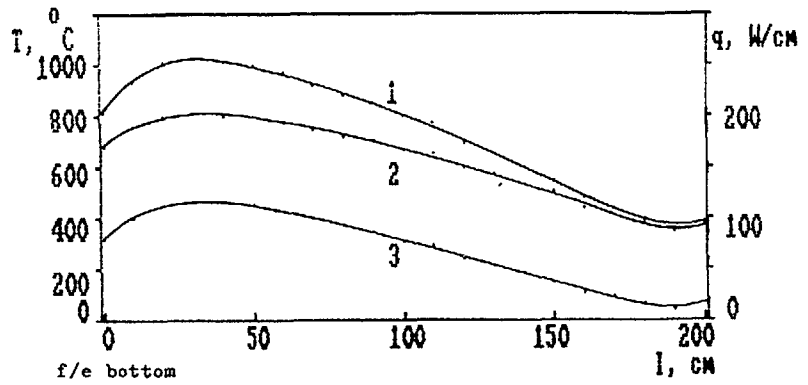

Fig.2a. Distribution of temperature and linear power along the fuel element with initial defect of the D-1 fuel assembly

1 – temperature in the centre of a fuel pellet
2 – temperature on the surface of a fuel pellet
3 – linear power (average value 70 W/cm)

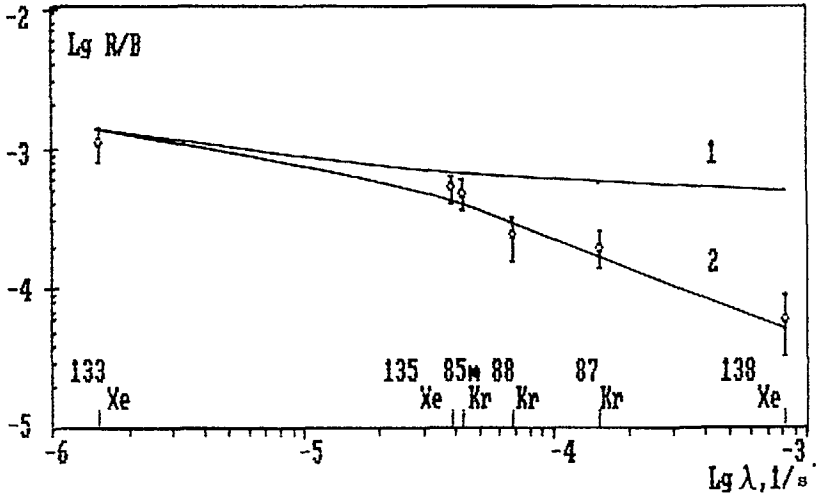

Fig.2b. GFP release from fuel and fuel element with initial defect of D-1 f/a versus the radioactive decay constant

1 – calculation of GFP release from fuel
2 – calculation of GFP release from f/e
I – experimental values

Table 2

Comparison of Calculated and Experimental Data about GFP Release during D-2 Fuel Assembly (f/a) Irradiation

	h, μm	q, W/cm	M, 1/s	GFP release, % Calculation from fuel recoil	from fuel diffusion	from fuel sum	Calculation from f/e	Experiment from f/e
Xe-133	80	95	4.E-5	2.78E-2	66.7E-2	69.5E-2	66.9E-2	(68+16)E-2
Xe-135				2.78E-2	13.1E-2	15.9E-2	7.98E-2	(7.0+1.6)E-2
Kr-85m				2.85E-2	12.7E-2	15.5E-2	7.51E-2	(8.3+2.0)E-2
Kr-88				2.85E-2	10.0E-2	12.9E-2	4.73E-2	(4.5+1.0)E-2
Kr-87				2.85E-2	6.74E-2	9.58E-2	2.23E-2	(3.1+0.7)E-2
Xe-138				2.78E-2	2.90E-2	5.69E-2	3.88E-2	(5.5+2.2)E-3
Xe-133	60	95	3.7E-5	2.85E-2	25.9E-2	28.8E-2	27.6E-2	(28+8)E-2
Xe-135				2.85E-2	5.11E-2	7.96E-2	3.83E-2	(4.0+1.0)E-2
Kr-85m				2.92E-2	4.93E-2	7.85E-2	3.64E-2	(2.5+0.8)E-2
Kr-88				2.92E-2	3.89E-2	6.81E-2	2.38E-2	(2.3+0.4)E-2
Kr-87				2.92E-2	2.62E-2	5.54E-2	1.21E-2	(1.3+0.3)E-2
Xe-138				2.85E-2	1.13E-2	3.98E-2	2.53E-2	(5.5+2.6)E-3
Xe-133	20	119	1.E-5	3.04E-2	11.4E-2	14.6E-2	12.6E-2	(10+3)E-2
Xe-135				3.04E-2	2.28E-2	5.31E-2	1.03E-2	(1.5+0.5)E-2
Kr-85m				3.1-E-2	2.20E-2	5.31E-2	1.00E-2	(1.0+0.3)E-2
Kr-88				3.12E-2	1.74E-2	4.85E-2	6.42E-3	(6.9+2.0)E-3
Kr-87				3.1-E-2	1.17E-2	4.29E-2	3.06E-3	(2.4+0.8)E-3
Xe-138				3.04E-2	0.50E-2	3.54E-2	0.75E-3	(1.7+0.9)E-3

Notes: 1. Pressure in the VK-50 reactor – 4 MPa.

2. Symbols in Table 2: h – gap; q – average linear power of the fuel element with initial defect; M – leakage coefficient of GFP from under the failed f/e cladding.

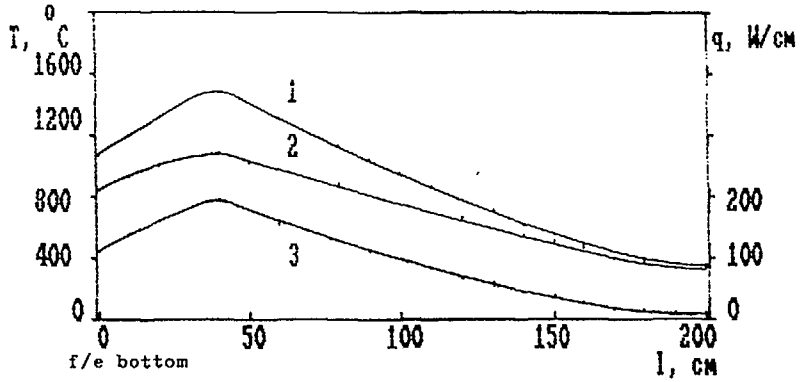

Fig.3a. Distribution of temperature and linear power along the fuel element with initial defect of the D-2 fuel assembly

1 - temperature in the centre of a fuel pellet

2 - temperature on the surface of a fuel pellet

3 - linear power (average value 95 W/cm)

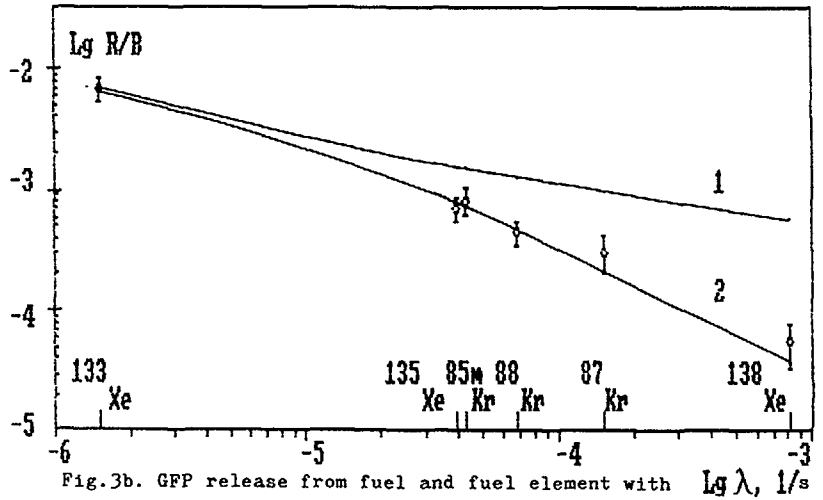

Fig.3b. GFP release from fuel and fuel element with initial defect of D-2 f/a versus the radioactive decay constant

1 - calculation of GFP release from fuel

2 - calculation of GFP release from f/e

I - experimental values

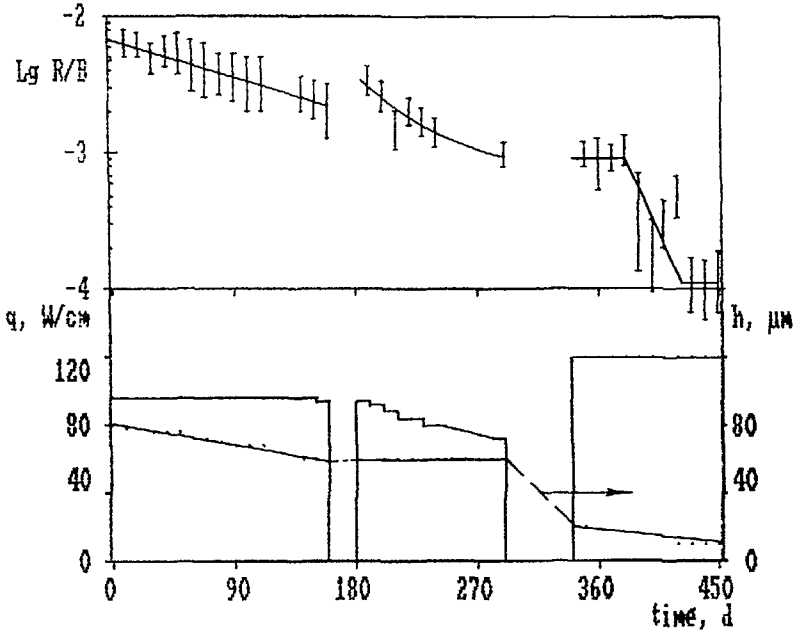

Fig.4. Change of Xe-133 release from fuel elements with initial defects during the D-2 fuel assembly irradiation

q - linear power of a fuel element with initial defect

h - value of the fuel-cladding gap (calculation)

is equal to less than 1% of the GFP release in the stationary operation of the reactor. This result was, perhaps, caused by imperfect production technology of initial defects and required additional investigations for the purpose of which the D-2 fuel assembly had been manufactured.

Fuel elements with initial defects of D-2 are irradiated at the linear power nearly 2 times greater than that of the same fuel elements in D-1 fuel assembly, so GFP release at the initial irradiation stage was 4-6 times higher (Tab.2, Fig.3). However,

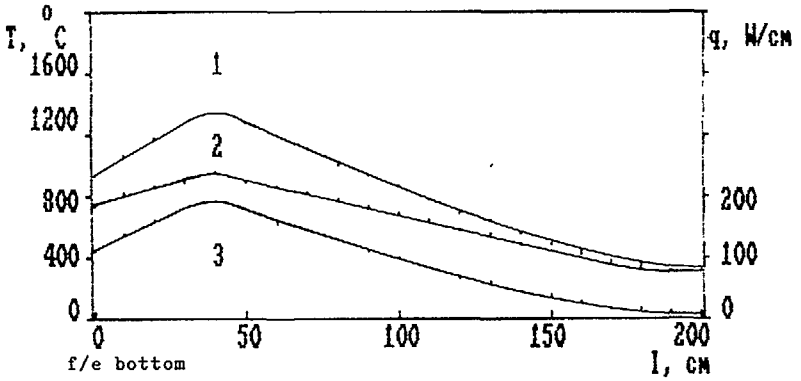

Fig.5a. Distribution of temperature and linear power along the fuel element with initial defect of the D-2 fuel assembly (gap 60 μm)
1 - temperature in the centre of a fuel pellet
2 - temperature on the surface of a fuel pellet
3 - linear power (average value 95 W/cm)

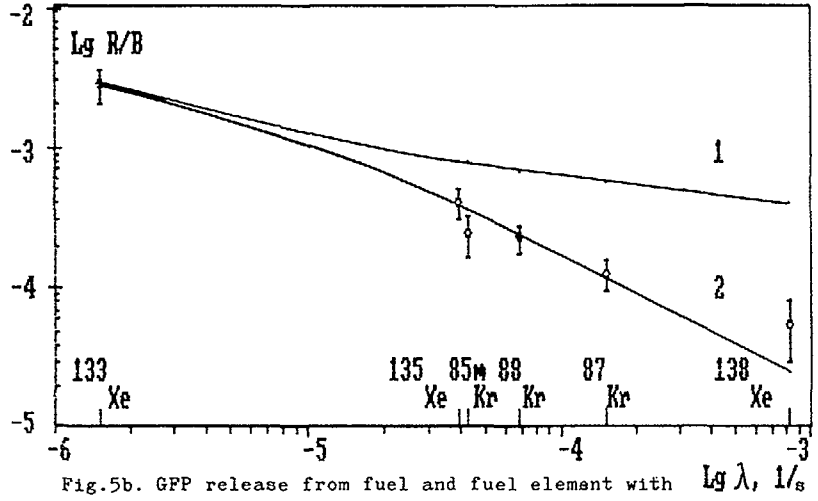

Fig.5b. GFP release from fuel and fuel element with initial defect of the D-2 f/a versus the radioactive decay constant
1 - calculation of GFP release from fuel
2 - calculation of GFP release from f/e
I - experimental values

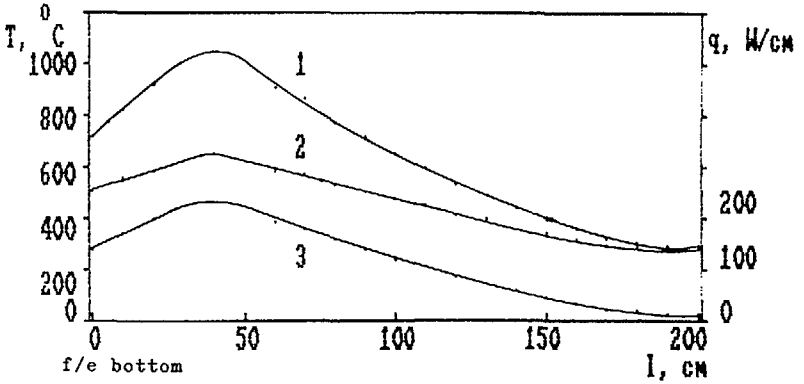

Fig.6a. Distribution of temperature and linear power along the fuel element with initial defect of the D-2 fuel assembly
1 - temperature in the centre of a fuel pellet
2 - temperature on the surface of a fuel pellet
3 - linear power (average value 119 W/cm)

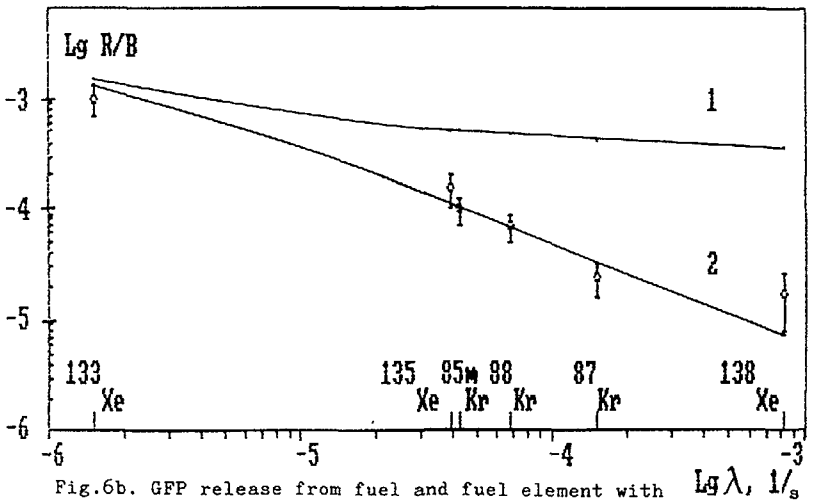

Fig.6b. GFP release from fuel and fuel element with initial defect of D-2 f/a versus the radioactive decay constant
1 - calculation of GFP release from fuel
2 - calculation of GFP release from f/e
I - experimental values

in the process of irradiation it gradually decreased, for example, Xe-133 release in 430 days of irradiation made up only about 2% of the original value (see Fig.4)

These experimental data can be explained supposing that at high fuel temperatures (more than 1700 K) the swelling fuel reduces the fuel-cladding gap which leads to decrease in the fuel temperature and, thus, to decrease in RFP release from the fuel Moreover, after reduction of the fuel-cladding gap to the critical value (about 20 μm) the pulsation mechanism of GFP transport under the failed fuel element cladding stops, and the diffusion mechanism presents considerably lower values of GFP release from under the gailed fuel element cladding to the coolant /2/. Tab.2 and Figs.3,5,6 show that with such suppositions there can be achieved good agreement of the experimental and calculated data.

At the first stage of the D-2 fuel assembly irradiation, release of I-131 with the value 5% of the corresponding value for Xe-133 was thoroughly registered from fuel elements with initial defects. Approximately the same relationship of these radionuclides release (about 1/10) was observed at the VK-50 NPP during operation with natural failed fuel elements /3/.

REFERENCES

1. Bordachev V.G., Vasilischuk A.V., Konyashov V.V., Yakshin E.K. Radioactive Fission Product Distribution within VK-50 Atomic Power Plant Circuit under Non-Defected Fuel Element Operation. Preprint RIAR-25(671) - M.: CNIIatominform, 1985.

2. Konyashov V.V., Krasnov A.M. Method for Calculation of Fission Product Release from Fuel-Cladding Gap of Failed Fuel Element to Coolant. Paper of the IAEA Technical Committee, 26-29 May, 1992, Dimitrovgrad.

3. Konyashov V.V., Shkokov E.I., Chechetkin Yu.V , Yakshin E.K. Experimental Investigations of Radioactive Fission Product Release from VK-50 Failed Fuel Elements.Atomic Electric Stations, Is.5, M.. Energoatomizdat, 1983, P.185-189.

METHOD FOR CALCULATING FISSION PRODUCT RELEASE FROM THE FUEL CLADDING GAP OF A FAILED FUEL ELEMENT TO THE COOLANT

V V KONYASHOV, A M KRASNOV
Research Institute of Atomic Reactors,
Dimitrovgrad, Russian Federation

Abstract

The model is presented for mathematical description of inert gas fission products release from failed fuel element cladding to coolant of a water cooled reactor. Results of calculations are reported on coefficient for different values of defect dimension and location, fuel-cladding gap, decay constant.

One of the most important problems of NPP safety is prediction of radioactive fission products (RFP) release from failed fuel elements to the primary circuit coolant. A lot of works are devoted to RFP release from fuel, but RFP release from the fuel-cladding gap of the failed fuel element was just slightly considered. An attempt was made in this paper to compensate this deficiency and to explain the available experimental data on RFP release from the failed fuel element fuel-cladding gap to the coolant using a calculated model with allowance for real processes under the fuel element cladding.

Let us consider a container fuel element of the water-cooled reactor with the fuel column length L consisting of pellets with diameter b and inner hole with diameter d, fuel element cladding r, the fuel-cladding gap thickness h, gas collector length a, with the fuel element defect having area S,located at distance l from the lower face of the fuel column.

Transport of the i-th radionuclide in the failed fuel element fuel-cladding gap is described by the equation

$$\partial C_i / \partial t = q_i - \mathrm{div}\,(\vec{J}_i + C_i \vec{v}) - \lambda_i C_i \qquad /1/$$

where C_i – local concentration of the i-th radionuclide,

q_i – rate of the i-th radionuclide release from fuel per a medium volume unit of the fuel-cladding gap;

$\vec{J}_i$ – flux density of molecular diffusion for the i-th radionuclide;

$\vec{v}$ – medium movement rate,

λ_i – decay constant of the i-th radionuclide;

Molecular diffusion is determined by a gradient of the concentration, temperature and pressure. The ratio for calculating the flux density of molecular diffusion is as follows:

$$\vec{J}_i = -D \left\{ \nabla C_i + \rho \left[k_t \nabla (\ln T) + k_b \nabla (\ln P) \right] \right\}, \qquad /2/$$

where ρ – medium density;

$k_t = D_t / D$, $k_b = D_b / D$ – thermodiffusion and barodiffusion ratio;

D, D_t, D_b – coefficients of concentration, thermo- and barodiffusion.

Equations /1/ and /2/ can be simplified: for fuel element of water-cooled reactors the gradient of temperature and medium pressures along the fuel element are small, i.e. contribution of thermodiffusion and barodiffusion can be ignored ($k_t \ll 1$, $k_b \ll 1$). Since under real conditions $L \gg d$, $l \gg d$, the equation of GFP transport in the fuel element fuel-cladding gap will be reduced to a one-dimensional one and the transport equation will be as:

$$\partial C_i / \partial t = q_i + \partial / \partial x \left(D\, \partial C_i / \partial x - C_i \vec{v} \right) - \lambda_i C_i \qquad /3/$$

Let us consider first of all the case when there is no convective transport $\langle v = 0 \rangle$, and the processes of GFP transport in the fuel element fuel-cladding gap are determined by molecular diffusion caused by their concentration gradient in the medium filling the fuel element. Equation /3/ will be as

$$\partial C_i / \partial t = q_i - \partial / \partial x \left(D\, \partial C_i / \partial x \right) - \lambda_i C_i \qquad /4/$$

Initial and boundary conditions are:

$$C_i(x,0) = C_{oi}\ ; \qquad /5/$$

$$\partial / \partial x \left[C_i (0,t) \right] = 0, \qquad /6/$$

$$D\, S\, \partial / \partial x \left[C_i (l,t) \right] = D\, S_o\, C_i (l,t) / r \qquad /7/$$

where S – area of the fuel-cladding gap cross-section;

S_o – area of the cladding defect.

Solution of equation /4/ for stationary state ($\partial C_i / \partial t = 0$) in case of uniform energy release distribution along the fuel element is as follows:

$$C_i = q_i \sum_{n=1}^{\infty} \frac{\frac{2 \sin \nu_n}{\nu_n}}{1 + \frac{\sin 2\nu_n}{2\nu_n}} \cdot \frac{\cos\left(\nu_n \frac{x}{l}\right)}{\lambda + \frac{D}{l^2} \nu_n^2}\ , \qquad /8/$$

where ν_n – root of equation $\mathrm{ctg}\,\nu_n = \nu_n / B_i$

$B_i = S_o\, l / S\, r$ – Bio criterium.

Integrating equation /8/ along the fuel element taking into account the given energy release distribution we shall find the number of atoms of the i-th GFP in the fuel-cladding gap (N_i), and using the expression for calculating the GFP flux through the defect from eq./7/ we shall define the GFP release rate from the failed fuel element (R_i). Then the leakage coefficient (M_i) determined as the R_i / N_i ratio can be calculated by simple formulas for microdefects ($B_i \ll 1$) and developed macrodefects ($B_i \gg 1$):

$$M_i = \left(S_o\, D / S_t\, r \right) \frac{\sum_{k=1}^{2} \frac{1}{\lambda_i + \alpha_k}}{\sum_{k=1}^{2} l_k \frac{1}{\lambda_i + \alpha_k}} \qquad \text{with } B_i \ll 1, \qquad /9/$$

$$M_i = \left(\pi^2 D\, S / 4\, S_t \right) \frac{\sum_{k=1}^{2} \frac{1}{l_k} \frac{1}{\lambda_i + \beta_k}}{\sum_{k=1}^{2} l_k \frac{1}{\lambda_i + \beta_k}} \qquad \text{with } B_i \gg 1, \qquad /10/$$

where l_1 , l_2 - distance from fuel element ends to the cladding defect,

S_t - area of cross-section of the fuel-cladding gap and central fuel hole:

$$\alpha_k = S_o\ D\ /\ S\ r\ l_k,$$

$$\beta_k = \pi^2\ D\ /\ 4\ l_k^2.$$

It follows from ratios /9/ and /10/ that for microdefects the GFP leakage coefficient from the failed fuel element fuel-cladding gap is in proportion to the defect area, and for developed macrodefects - it does not depend on it. Let us estimate the GFP leakage coefficient for the developed macrodefect. GFP diffusion coefficient in the fuel element fuel-cladding gap is equal to:

$$D = \frac{10^{-3}\ T^{1.75}}{P\ (V_1^{1/3} + V_2^{1/3})^{2/3}} \sqrt{m_1^{-1} + m_2^{-1}}, \qquad /11/$$

where V_1 , V_2 - volume of the GFP molecule and steam, repectively;

m_1, m_2 - mass of the GFP molecule and steam, respectively

T - steam temperature;

P - steam pressure.

At P = 60 atm, T = 600 K the average diffusion coefficient of krypton and xenon in steam makes up: D = 1 10^{-2} cm^2/s.

For the developed macrodefect in the middle of VK-50 fuel element (L=2m, h=10 μm): M (Xe-133) = 4 10^{-7} s^{-1}.

Under the VK-50 conditions there were also experimentally obtained far higher values of the GFP leakage coefficient from the failed fuel element fuel-cladding gap - up to $1 \cdot 10^{-4}$ s^{-1} /1/ which makes absence of GFP convective transport in the fuel-cladding gap doubtful. The reason of GFP convective transport under the failed fuel element cladding can be pressure pulsations of the coolant turbulent flux in the defect region. Periodical pressure pulsations in the coolant were observed by the authors of ref./2/ during tests of the VVER reactor

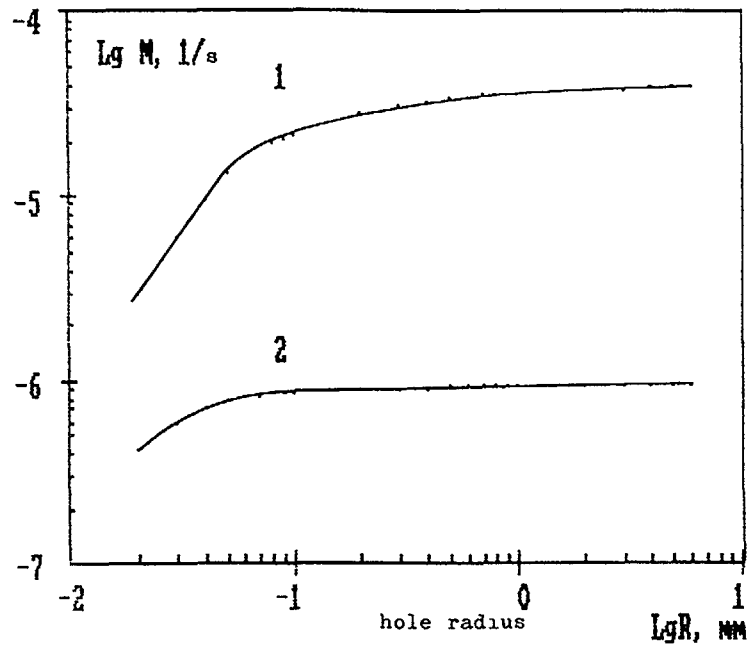

Fig.1. Leakage coefficient of Xe-133 from the VK-50 failed fuel element fuel-cladding gap (L=200 cm, h=30 μm, P=40 atm, l=60 cm) versus the defect raduis.
2 - diffusive transport;
1 - convective transport

failed fuel elements in the water loop: amplitude of pulsations was 0.04-0.06 atm, frequency - about 1 Hz.

Convective transport of GFP in the fuel-cladding gap is described in eq./3/ by the term $\partial / \partial x\ (C \cdot v)$. In all cases determination of the function v(x,t) is rather hard, however, if the amplitude of medium displacement under the fuel element cladding is considerably less than the fuel element length, then the problem of GFP transport can be reduced to solution of the diffusion equation. In this event pulsations of steam

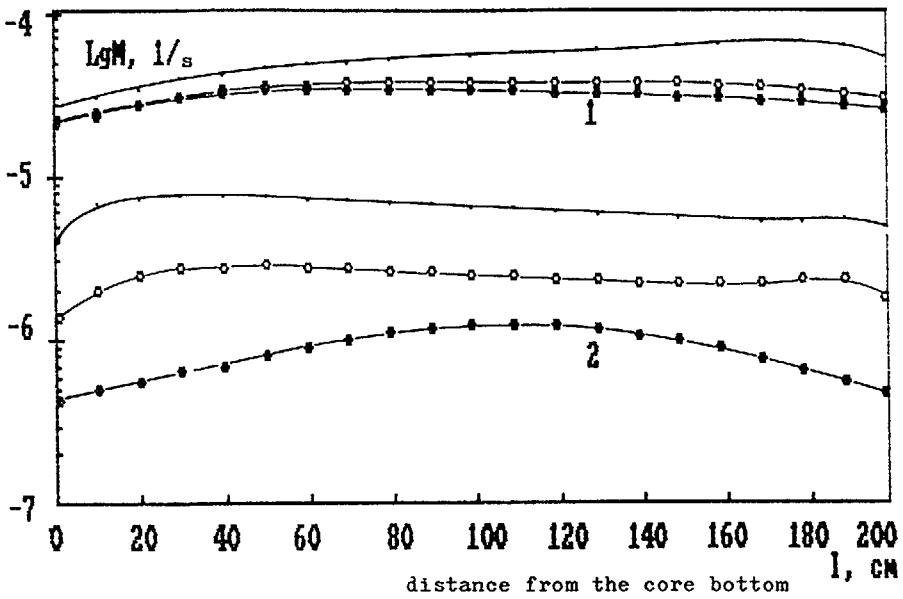

Fig.2. Leakage coefficient of GFP from the VK-50 failed fuel element fuel-cladding gap (L=200 cm, h=30 μm, P=40 atm) versus the defect location: 1 - diffusive transport; 2 - convective transport

• - Xe-133; ———— - Xe-138; o - Kr-88

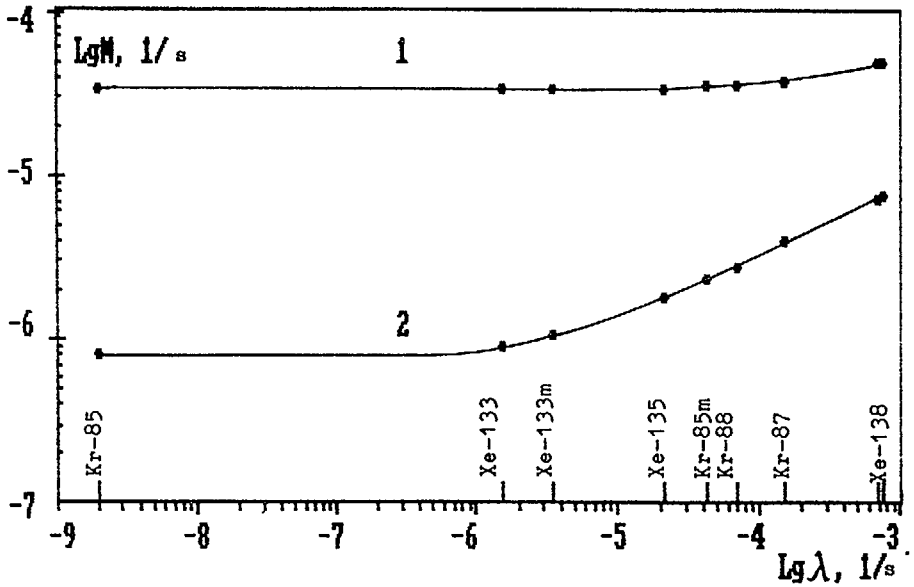

Fig.3. Leakage coefficient of GFP from the VK-50 failed fuel element fuel-cladding gap (L=200 cm, l=60 cm, h=30μm, P=40 atm) versus the radioactive decay constant
2 - diffusive transport mechanism;
1 - convective transport mechanism

under the fuel element cladding with amplitude A and frequency f lead to mixing of the medium within the pulsations amplitude range which is equivalent to increase of the diffusion coefficient:

$$D^* = D + D_k \,, \qquad /12/$$

where D^* - total diffusion coefficient;
D - molecular diffusion coefficient;
D_k - diffusion coefficient equivalent to steam pulsations.

Here: $D_k = A^2 f$

Amplitude of steam pulsations under the failed fuel element cladding is $A = \Delta P\, V / P\, S$,

where V - free volume under the fuel element cladding;
ΔP - amplitude of pressure pulsations.

For the defect located in the middle part of the VK-50 fuel element at f=1 Hz, P=0.06 atm, h=10 μm, P=60 atm, amplitude of steam pulsations under the fuel element cladding is 1.5 cm and the equivalent diffusion coefficient D^*=2 cm^2/s. In this case for the developed macrodefect we shall find due to formula /10/ that.

$M\ (Xe\text{-}133) = 7\ 10^{-5} s^{-1}$

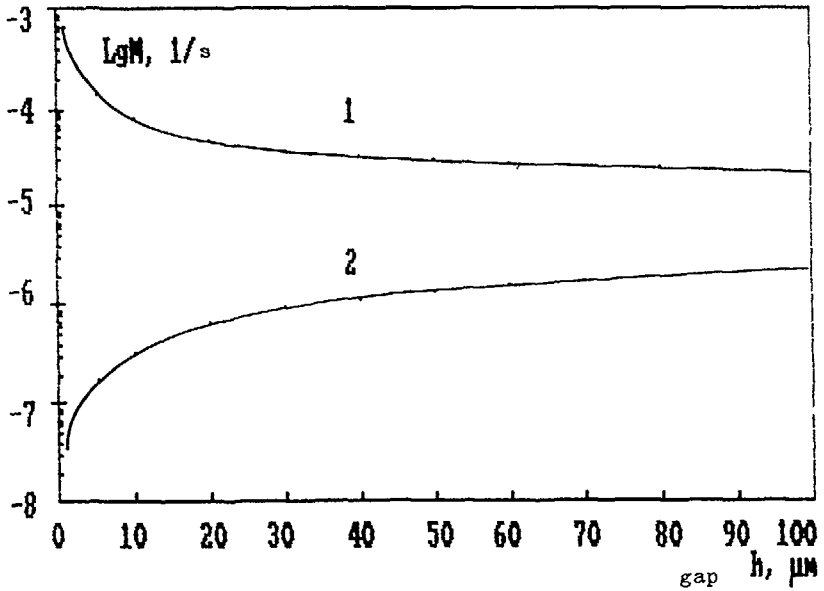

Fig.4. Leakage coefficient of Xe-133 from the VK-50 failed fuel element fuel-cladding gap versus the fuel-cladding gap thickness

2 - diffusive transport;

1 - convective transport

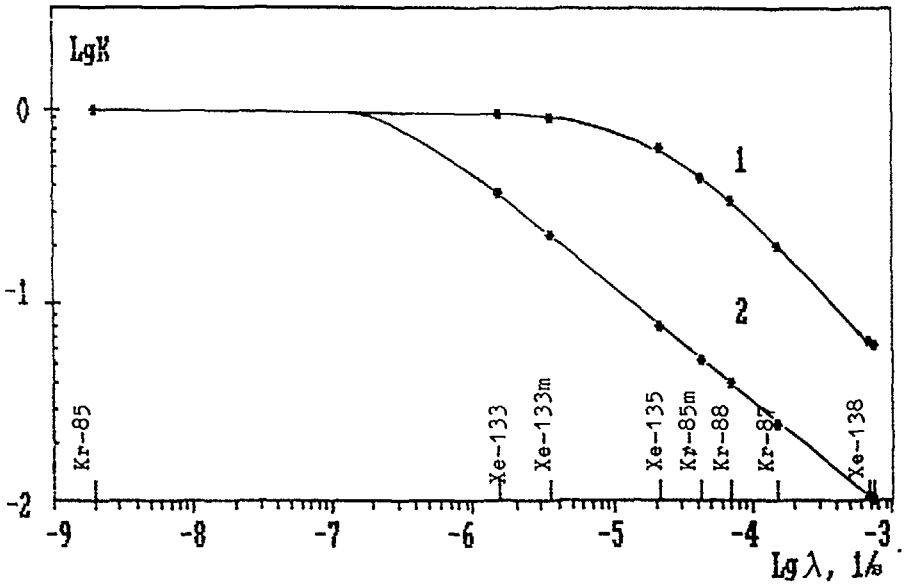

Fig.5. GFP release from the VK-50 failed fuel element fuel-cladding gap (L=200 cm, l=60 cm, h=30 μm, P=40 atm) versus the radioactive decay constant

2 - diffusive transport mechanism;

1 - convective transport mechanism

Therefore, the values for Xe-133 leakage coefficient from the failed fuel element fuel-cladding gap under the water-cooled reactor conditions can be within 10^{-7}-10^{-4} s^{-1} versus the GFP transport conditions under the fuel element cladding. So the possibility of convection emergence due to the coolant pressure pulsations is, probably, limited to dimensions of the defect and fuel-cladding gap in presence of a microdefect or pinch of the fuel-cladding gap the pressure pulsations do not propagate into the fuel element and there is no convection.

As an example Figs.1-4 present dependencies of the GFP leakage coefficient from the VK-50 failed fuel-cladding gap on size and location of the defect, nuclide decay constant and the fuel-cladding gap thickness. Fig.5 shows dependence of GFP release from the failed fuel element fuel-cladding gap on the nuclide decay constant. GFP release from the failed fuel element fuel-cladding gap (K_1) is defined from the ratio.

$$K_1 = M_1/(M_1 + \lambda_1)$$

REFERENCES

1. Konyashov V.V., Shkokov E.I., Chechetkin Yu.V., Yakshin E.K. Experimental Investigations of Radioactive Fission product Release from VK-50 Failed Fuel Elements. Atomic Electric Stations, Is.5, M.: Energoatomizdat, 1983, P.185-189.

2. Aksenov N.A., Samsonov B.V., Sulaberidze V.Sh., Frej A.K. Some Irradiation Regimes Investigations of WER-440 Failed Fuel Elements. - In book: Radiation Safety and Shielding of NPP, Is.6, M., Energoizdat, 1981, P.50-58.

SOME RESULTS OF POST-IRRADIATION INVESTIGATIONS OF VVER-1000 UNSEALED FUEL ASSEMBLY

K.P. DUBROVIN, A.V. SUKHIKH, V.I. KUZMIN,
A.V. MESTNIKOV, A.V. SMIRNOV, V.P. SMIRNOV
Research Institute of Atomic Reactors,
Dimitrovgrad, Russian Federation

Abstract

The results of post-irradiation tests of a fuel assembly are given The fuel assembly is from Unit I of the South Ukrainian NPP. 300 μm depth local corrosion of cladding was identified

In the beginning of the South-Ukrainian NPS operation (1 unit) a graphite bearing of the main circulating pump (MCP) failed. When MCP was repaired, the unit had been operating for a long time on the power close to nominal value. One of the fuel assemblies from the first charge after 3 cycles of operation (878 days with 36.7 MWt day/kg burnup) was transported to RIAR for assesment of its serviceability life-time and was investigated in the material science laboratory. After eddy-current examination one-third fuel rods were identified as those having the surfase defects of the cladding. Fig. 1 presents -scanogramm and eddy-current diagramm of one of the fuel rods from this assembly. Periodical minimums of the total -activity on the fuel rod length coincide with the position of the spacer grids (SG) of stainless steel The surface defects of the cladding were not higher than the fifth SG. The defects with the greater value of signals were observed near the first SG

The visual inspection of the damaged fuel surface revealed:

- white contrast spots;
- dark-grey graphite deposits of about 0.3 mm thickness partially covering the white nodular formations;
- graphite deposits 0.5 mm thick in the bottom of fuel rods.

White contrast spots were absent directly under SG but they localized partially or along the whole perimeter of the narrow belt 10-15 mm wide lower 1-5 SG.

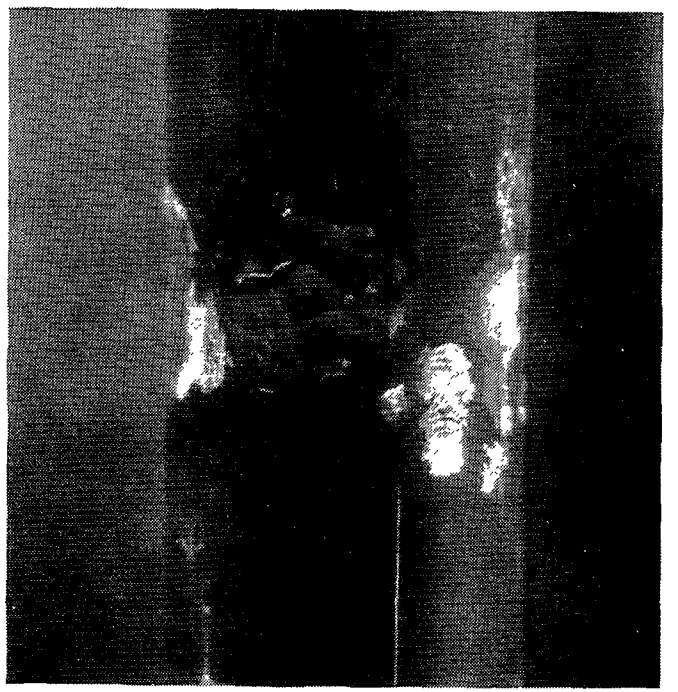

FIG. 2. Nodular corrosion of fuel rod cladding.

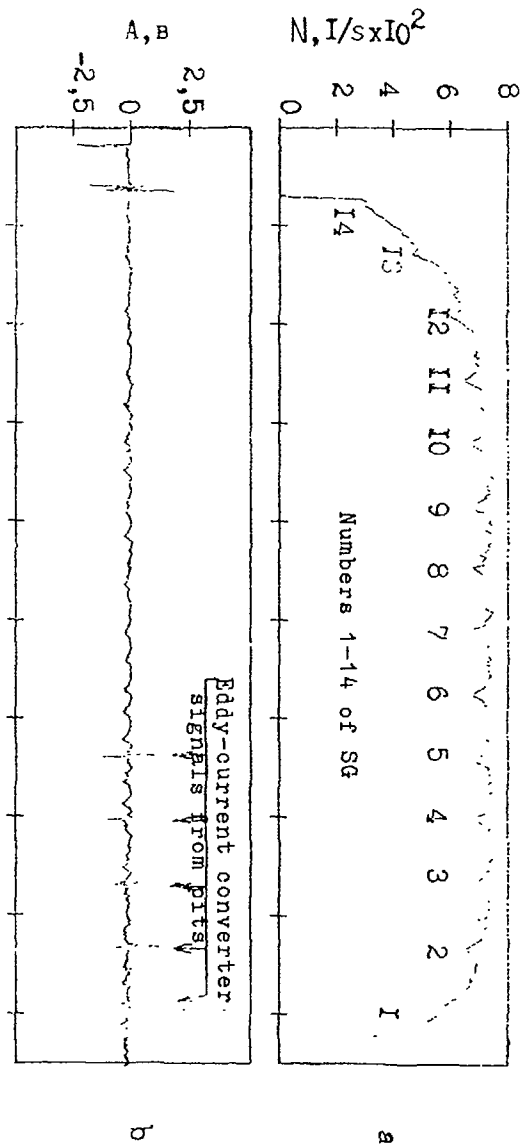

a - gamma-scanogramm b - eddy-current diagramm

FIG. 1. Location of corrosion nodules along the fuel rod.

After mechanical cleaning the corrosion nodules were discovered under the white spots (Fig 2)

Measurements of gas composition and pressure didn t reveal the elevated release of Xe and Kr from fuel in the fuel rods with graphite deposits. Under the cladding the portion of gaseous fissile products didn'exceed 0.4% from their quantity formed during the fuel rods operation.

Ceramographic investigations showed that the fuel microstructure wasn't changed. Metallographic research revealed the nodular corrosion of claddings 300 mkm depth from the side of coolant.

As it is known, the nodular oxidation of zirconium claddings is not typical for the fuel rods of the PWR and VVER reactors. Corrosion of this type is more typical for fuel rods of the BWR and RBMK reactors under conditions of the oxygen-containing coolant. Appearence of deposits on the surface of the fuel rods, local overheating and, as a result of it, the elevated rate of the cladding oxidation are the main causes of the nodular corrosion of CILC type (Crud Initiated Local Corrosion). The remainings of graphite deposit layer point to the possibility of the nodular corrosion formation by this mechanism in the investigated fuel rods. The layers were discovered above the white corrosion spots on the external surface of the claddings. Localization of the greater nodular oxidation on the first SG, where the neutron flux and energy release were lower than the maximum value, is explained by the greater thickness of deposits in the bottom of the fuel rods.

RESULTS OF POST-REACTOR INVESTIGATIONS OF VVER-1000 UNTIGHT FUEL ASSEMBLY

K P. DUBROVIN, A V SUKHIKH, V.I. KUZMIN,
A.V. SMIRNOV, V.P SMIRNOV
Research Institute of Atomic Reactors,
Dimitrovgrad, Russian Federation

Abstract

Results of post-reactor investigations of the VVER-1000 untight fuel assembly are given
The research results of structure, composition and properties of cladding are presented

Growth of the iodine radionuclides activity in the coolant was observed during commissioning to rated power of the reactor of the 5-th block at the New-Voronezh NPP after 3-weeks operation with 50% power (Fig.1). The untight fuel assembly found by the failed fuel detection (FFD) system was delivered to RIAR and investigated in a material science laboratory. The fuel assembly had been operated for 489 ef. days (4 and 5 fuel cycles) up to burnup 21.7 MW d/kg uranium. The maximum heat load on fuel rods did not exceed 240 W/cm.

In the process of fuel assembly dismantling at one of the central fuel rods bordering on the guiding tube of a control bar there were detected white spots of friable releases at 2 regions placed at marks 500 and 350 mm from the fuel rod top. While extracting the fuel rod out of fuel assembly spacer grids within the upper white spot, brittle break of the cladding took place (Fig.2). A through sickle-shaped defect of the cladding was revealed after decontamination of the fuel rod surface in the area of the lower white spot (Fig.3).

Figs.4 and 5 present the results of gamma-scanning and eddy-current flaw detection of the greater piece of the failed fuel rod. Fig.4 illustrates high-altitude distributions of energy release and residual fission products concentration. The energy release profile by the end of the 5-th fuel cycle was calculated according to the BIPR-7 programme

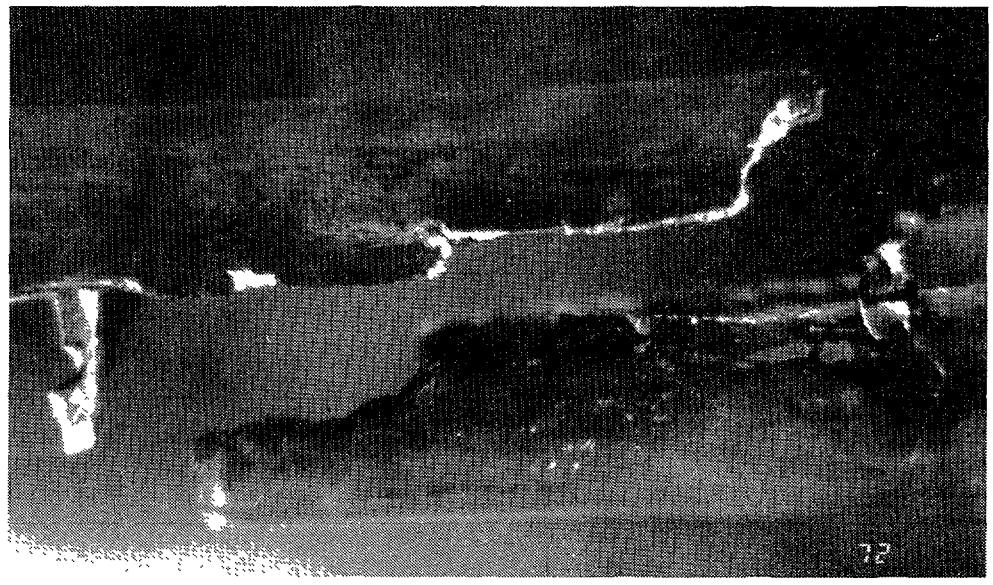

FIG. 2. Untight fuel element within the upper rupture of cladding.

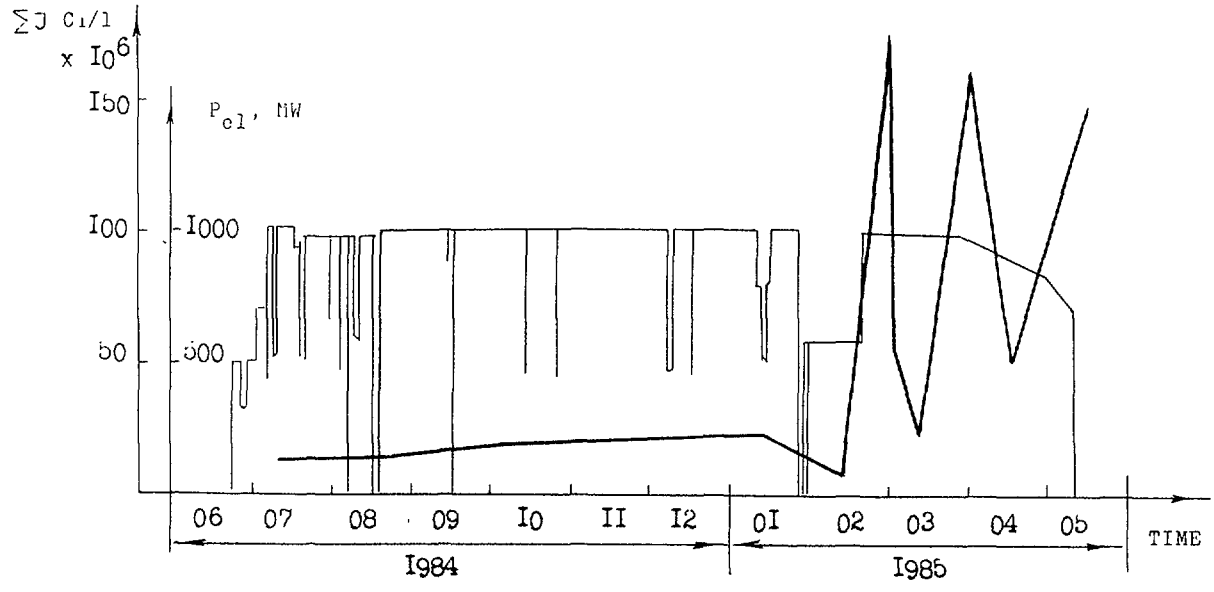

FIG. 1. Kinetics of change in the VVER-1000 reactor electric power and activity of iodine radionuclides in coolant during the 5th fuel cycle.

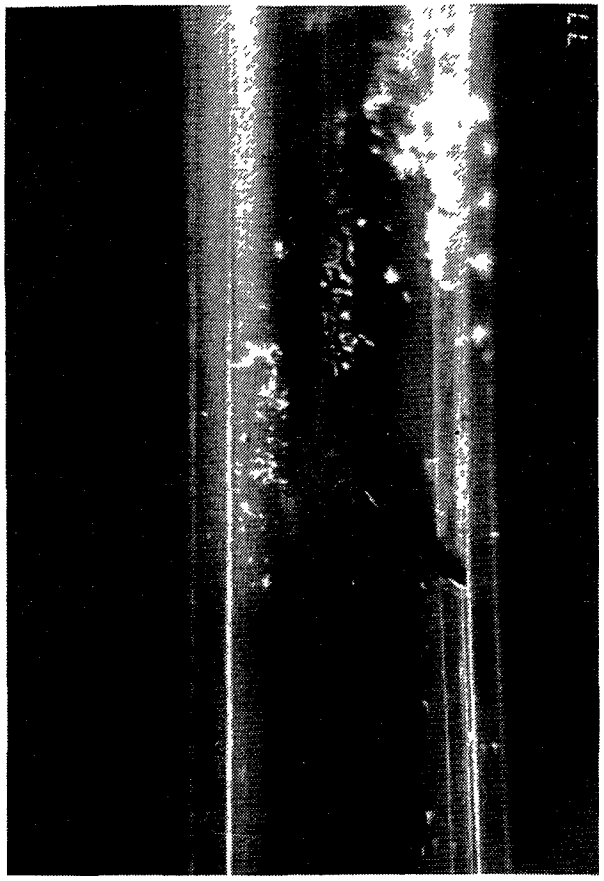

FIG. 3. Lower defect of cladding in the untight fuel element.

Analysis of the gamma-scanning results showed that about 35% of Cs accumulated during operation released from the failed fuel rod to the coolant. The greatest local decrease of Cs concentration (down to 50%) was observed in places of maximum energy release.

Amplitude-phase analysis of the eddy-current defect diagram signals (Fig.5) demonstrated that they are mainly connected with inner cladding defects the size of which is maximum near the place of the upper fuel rod destruction. Signals with the period divisible by the fuel bushing length were observed in the region with reduced Cs content (2800-3600 mm). A powerful signal from the through cladding defect (mark 3580 mm) did not disturb the periodicity of this distribution.

Material science investigations showed that tight fuel rods of a fuel assembly were in a satisfactory state. Maximum increase of the length and decrease of the fuel rods diameter made up 11.4 mm (0.3%) and 0.04 mm (0.41%), respectively. A fraction of inert gases (Xe and Kr) released from fuel did not exceed 2.3% of their quantity accumulated in the course of operation.

A uniform oxide film, 5 μm thick, was generated on the outer surface of all fuel rods. The oxide film thickness over the height and perimeter changed from 0 to 7 μm on the inner surface of tight fuel rods claddings. Hydrogen content in claddings did not exceed 5 10^{-3}% mass. Hydrides had predominantly a tangential orientation.

Mechanical properties of tight fuel rod claddings were at a sufficiently high level. The conventional yield strength $\sigma_{0.2}$ made up 300 MPa , and the ultimate strength - 330 MPa at the testing temperature 380°C. Uniform relative elongation changed within the range 3.5-4.0%, and the total relative elongation equaled 16.0-25.0%.

The fuel structure of tight fuel rods did not essentially change as compared to the initial state. Maximum swelling of UO_2 was 1.2%. Absence of growth in U dioxide grains and negligible number of released gas fission products evidenced of the fact that the maximum temperature in the centre of fuel did not exceed 1500°C.

The diameter of the central hole of fuel bushings in the failed fuel rod was close to the initial one. The diametric gap between fuel and cladding was not observed in an obvious form.

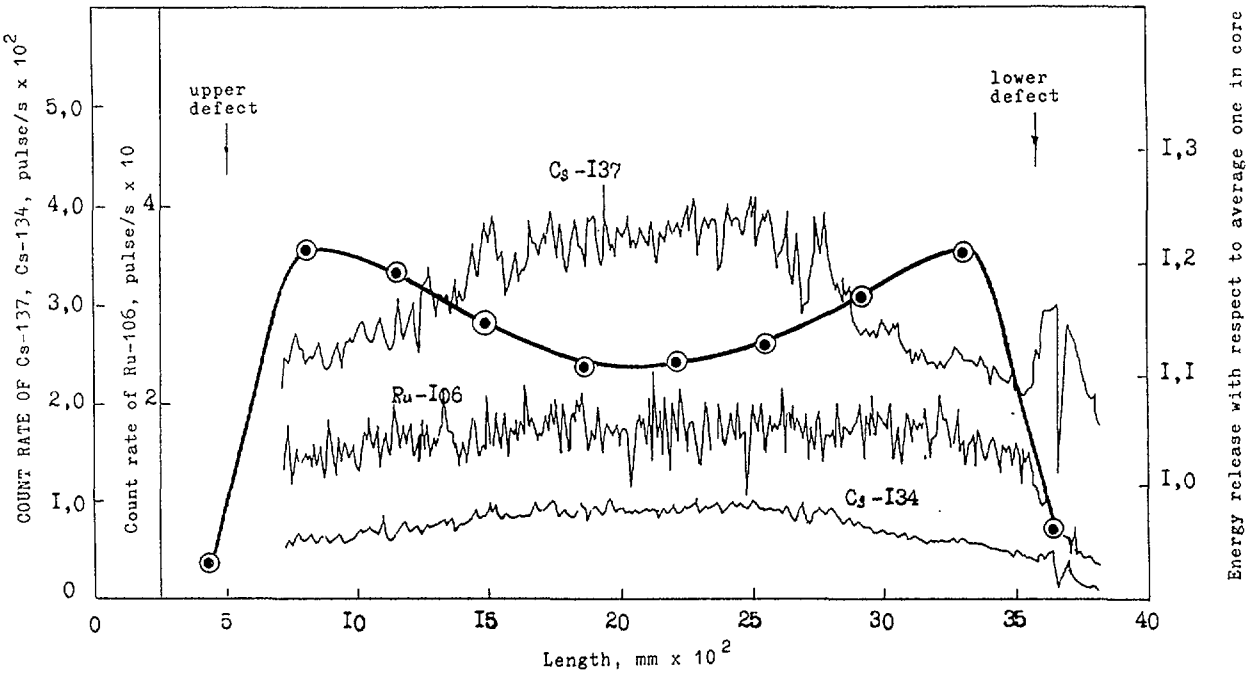

FIG. 4. Distribution of energy release (at the end of the 5th fuel cycle) and concentration of radioactive nuclides along the untight fuel element.

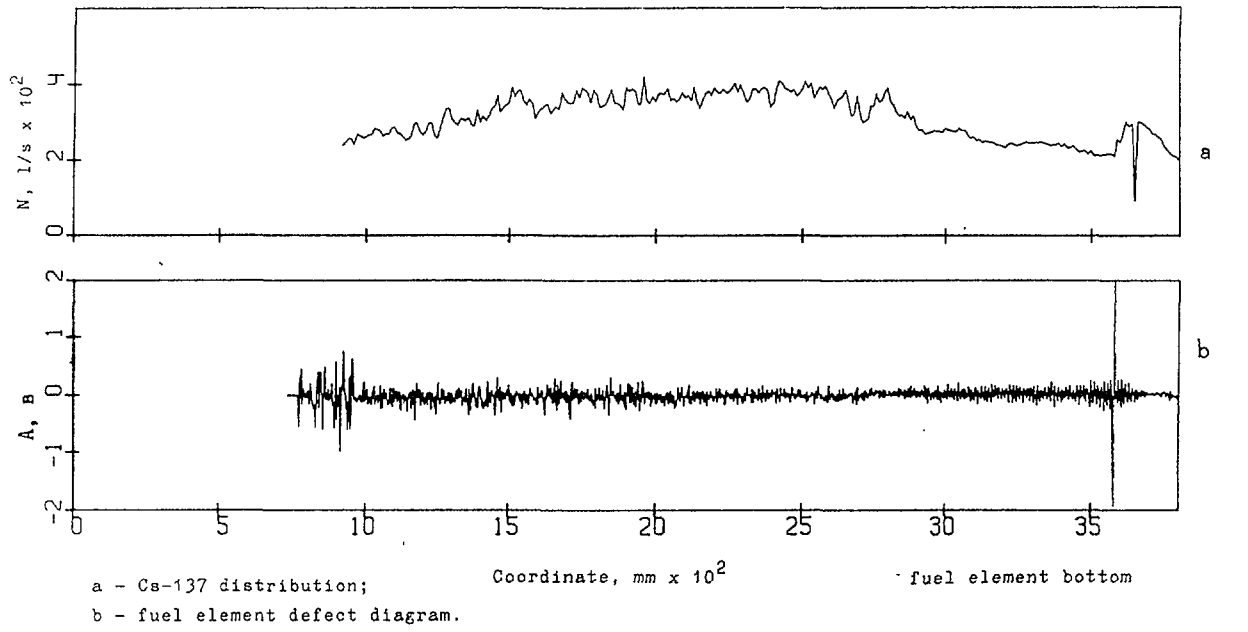

FIG. 5. Distribution of Cs-137 concentration and eddy current flaw detector signals along the untight fuel element.

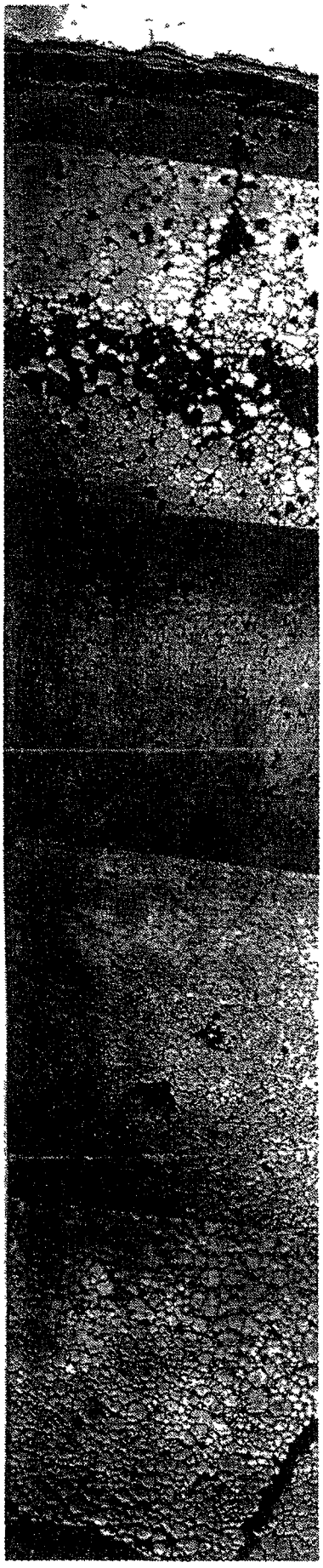

Region of column grains
after additional etching

FIG 6 Microstructure of fuel in untight fuel element (100×)

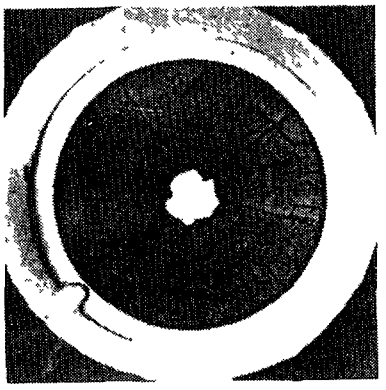

(a) 5×

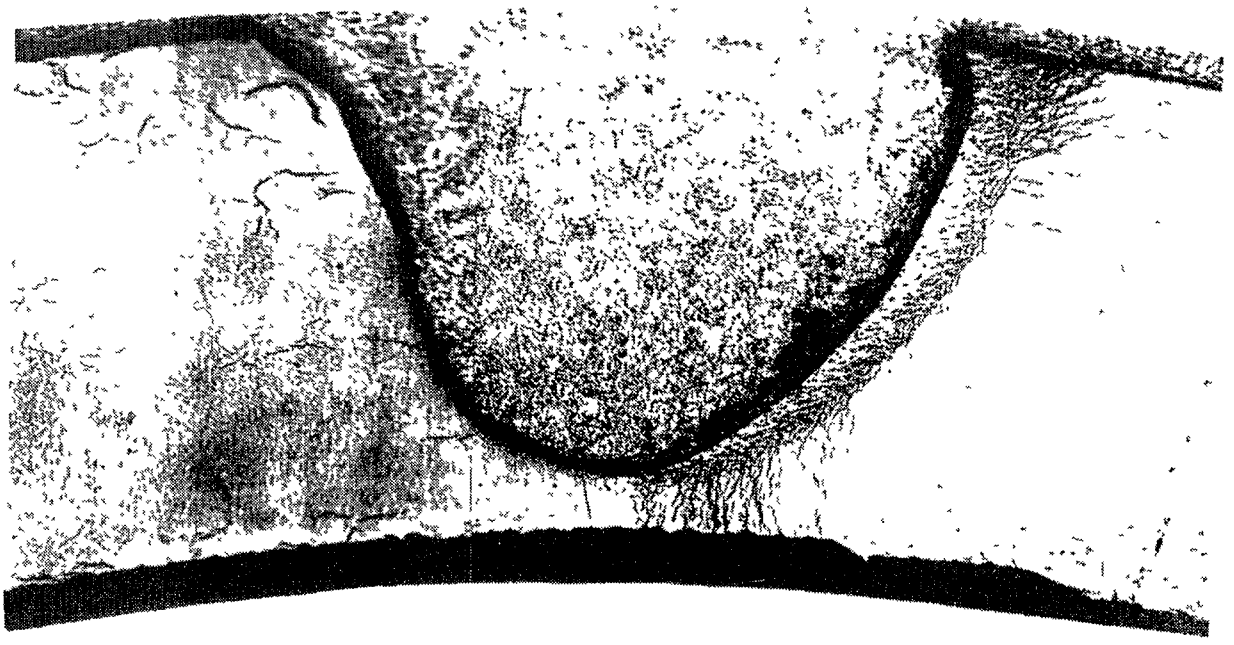

(b) 100×

FIG 7 Structure of fuel and cladding within the lower defect of untight fuel element

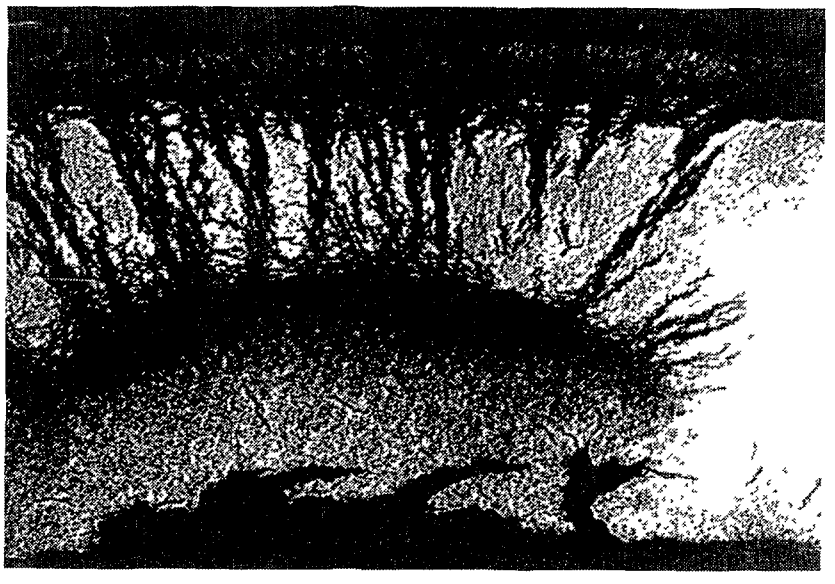

FIG 8 *Microstructure of cladding within the upper failure of fuel element*

It was, probably, filled with products of water interaction with fuel, cladding and fission fragments. Fine column grains of uranium dioxide were observed in some sections of the untight fuel rod. An interesting feature was location of the column grains area in the middle part of the fuel bushings wall (Fig.6).
Gaseous pores were generated in the central part of fuel bushings inside and on the surface of equiaxial grains, however, the grain size did not increase. Maximum decrease of the uranium dioxide density in the untight fuel rod was thrice greater than in tight fuel rods with the same fuel burnup.

Slight hydrogenation and oxidation from the side of the inner cladding surface occurred around the lower defect (mark 3580 mm) (Fig.7). Mechanical properties of the cladding in this region differed from mechanical properties of tight fuel rods claddings to a small extent.

Intensive local hydrogenation and oxidation of the cladding from the inner surface side took place in the area of upper destruction at mark 500 mm. Hydrogen concentration in this region rose up to 0.39%. The thickness of the continuous hydrides layer achieved 250-300 μm. "Sunburst" type hydrides were observed (Fig.8). Plate-shaped hydrides had predominantly a radial orientation. A great deal of through longitudinal cracks were noticed in claddings. Circular samples cut out of this area destroyed in a brittle manner at minor loads via mechanical tests.

The research results of structure, composition, properties of claddings indicate that the lower defect was primary, and cladding destruction in the upper fuel rod part was the result of local hydrogenation affected by the coolant entering under the cladding via the primary defect.

EFFECT OF INNER SURFACE PRELIMINARY OXIDATION ON STRESS CORROSION CRACKING SUSCEPTIBILITY OF Zr-1%Nb TUBING

Yu.K. BIBILASHVILI, Yu.N. DOLGOV, V.V. NOVIKOV
Scientific Research Institute for Inorganic Materials

A.P. GRYAZEV
Physics Engineering Institute

Moscow, Russian Federation

Abstract

Internally pressurized claddings of VVER-1000 fuels were tested under iodine SCC conditions at 653 K in a laboratory unit equipped with an automated acoustic-emission system. Zr-1%Nb claddings were pre-coated with ZrO_2 0.5-10 μm thick. Cladding time to failure is given as a function of oxide layer thickness. Oxide film growth is shown to lead to a sharp reduction of time to failure of claddings subject to iodine corrosion. Areas of failure were studied fractographically and diagrams of recorded acoustic emission (AE) signals that accompanied major stages in crack evolution are interpreted. Also discussed is the influence of cladding inner surface oxidation on mechanism of SCC resistance degradation with fuel burnup.

1. INTRODUCTION

PCI is one of the main factors that determines power reactor fuel serviceability under transient conditions. Loss of tightness by fuels results from SCC effected by chemically aggressive fission products, particularly iodine. Aside from other factors SCC process also depends on cladding inner surface condition. Fuel burnup process is known to result in both irradiation induced damage of cladding inner surface with fission product fragments and its oxidation. The former takes account of possible embrittlement of cladding surface and, hence, higher susceptibility of metal to iodine induced cracking. The influence of the latter factor is related to fuel released oxygen forming an oxide film at cladding inner surface. The results of some studies to estimate oxide layer thickness were tabulated (see the table below) [1,2].

Table 1. Observed oxide thickness on the inner surface of fuel cladding [1, 2]

Authors	Burnup (GWd/t)	Oxide Thickness (μm)	Remarks
F.H. Megerth, et al.	23.9-26.6	1 - 6 (avg. 3 - 4)	uniform
	27.3-37.4	4 - 9 (avg. 8)	some are uniform others are nonuniform
N. Fuhrmah, et al.	13	4 - 6	nonuniform, only found in the area of fuel bonding
R.F.Mattas, et al.	27 - 30	0.5 - 7	nonuniform
	10.6 - 14	1 - 4	nonuniform
	8.5 - 11	0.5 - 6	nonuniform
	7.2	3 - 4	uniform (unbreached)
	8.4	3 - 4	nonuniform (breached)
	24	0.5 - 18	nonuniform
F.Garzarolli, et al.	< 20	negligible	at higher burnups, oxidation starts locally and becomes a thin continuous film
H.Lindroth and R.Terasvirta	42.9-45.9	0 - 13 (avg. 8.2)	cladding material - Zr-1%Nb

Data available on the influence of oxidation on SCC show that an oxide film can both improve and degrade resistance to SCC [3]. Therefore to determine the influence of cladding inner surface oxidation on SCC and mechanism of cladding damage during PCI experiments were planned to study claddings having ZrO_2 films of different thickness.

2. EXPERIMENTAL MEANS AND METHODS

2.1. Specimens under study

Internally pressurized tubular Zr-1%Nb specimens were investigated. Their chemical composition and strength were practically similar to those described [4]. At their inner surface the specimens had a pre-applied ZrO_2 film 0.5, 1, 2, 5 and 10 μm thick.

The sequence of specimen preparation was as follows.

1. Tubes 150 mm long, 9.15 mm outer dia and 0.7 wall thickness cut from unirradiated VVER-1000 fuel cladding were subjected to air oxidation in a resistance furnace at 773 K. The tubes were arranged horizontally in a specially designed container. The container with the tubes was located into the heated furnace and unloaded out of the heated furnace. Following oxidation for 2, 8, 100 h and subsequently after each 100 h the specimens were weighed to determine weight gain. Through calculation of weight gain per unit area the thickness of ZrO_2 layer was found.

2. Claddings as oxidized were grooved in the middle over 40 mm length to produce a higher stress area. The average thickness of the thinned cladding was 350±15 μm.

3. The end plugs were electron beam welded. To assure the needed quality of the welds the oxide layer near the tube ends at the inner and outer surfaces over 5-6 mm length was removed.

4. The specimens as pre-evacuated were filled with an inert gas (argon). Iodine as loose crystals was inserted in the amount of 0.2 mg/cm². The specimens were sealed with resistance spot welding. The argon pressure under the cladding was 6.5 MPa at room temperature and was controlled with a gauge as well as by weighing specimens before and after filling.

2.2. Laboratory unit

The specimens were tested in a laboratory unit "KROT" (Corrosion Cracking of Fuel Claddings) equipped with an automated AE-system CAMAS (Computer Added to Multi-channel Acoustic System). The unit is shown schematically in fig.1. The unit allows a simultaneous performance of experiments in 4 heaters with an autonomous selection of temperature conditions in air or an inert gas environment. A tubular ampule type specimen 1 is placed vertically inside an electric resistance furnace 2. The temperature of the middle part of the working zone is measured with thermocouple the signal of which is controlled with digital voltmeter 7. The communication of the power circuits of the heater is accomplished with a block of thyristor amplifiers 4 switched in the circuit of high precision temperature controller 5. The discrete AE-signals arising in a specimen subject to SCC are transferred over rod waveguide 6 to primary converter 8 in the body of which a piezoconverter and pre-amplifier are installed. The piezoconverter material is zirconate of lead titanate, that of waveguide is stainless steal of X18H9T type.

Conversion of AE and temperature transducer signals into a digital code and their subsequent processing were accomplished with CAMAS system consisting of functional CAMAC modules 9-18 operating under the control of microcomputer 19. Under laboratory conditions CAMAS system provides for the following:

- separate recording by each measuring channel of time dependencies of specimen temperature as well as count rate and total count of AE-signal flow that accompanies nucleation of corrosion damages in a cladding;

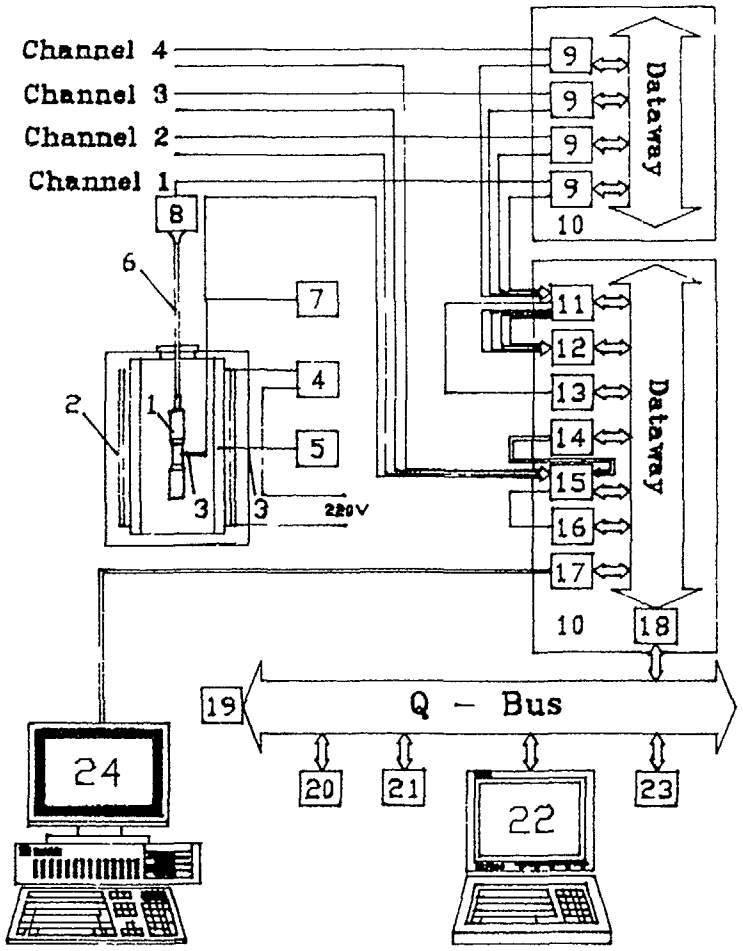

Fig.1. Schematic of automated AE-system:

1 - specimen; 2 - electrical furnace; 3 - thermocouple; 4 - thyristor amplifier; 5 - temperature controller; 6 - rod waveguide; 7 - voltmeter; 8 - remote probe; 9 - active filter amplifier; 10 - crate CAMAC; 11 - 4-channel amplitude discriminator and analog multiplexer; 12 - 4-channel quad scaler; 13 - pulse ADC; 14 - output register; 15 - relay multiplexer; 16 - isolated A/D converter; 17 - serial interface; 18 - SM-3 CAMAC interface; 19 - processor MC1201.02; 20 - RAM; 21 - floppy drive; 22 - monitor; 23 - printer; 24 - IBM PC/AT.

- statistical analysis of AE-signal flow along one of measuring channels selected according to the program or at will of a user, programmed setting of statistical processing conditions and control of amplitude selection level
- accumulation, preliminary processing and display of experimental information, recording of results on computer external memory devices,
- audible and visual signalling an excess threshold value of count rate recorded in any measuring channel,
- flexible interaction with a user and control of system functioning with the help of a menu

To improve the efficiency of the multi-channel AE-system a personal computer IBM PC/AT 24 was incorporated, it is used for archiving, processing and systematization of investigated results The personal computer and the microcomputer of the CM type are connected with a serial interface module 17, installed in crate CAMAC Software support of heterogeneous local network is provided by a complex of program products

2.3 Experimental technique

Counting off the time to cladding failure was started from the moment the specimen reached the test temperature that was held constant at the accuracy ±3 K until fracture Under steady-state conditions the axial temperature gradient over 150 mm did not exceed 12 K and in a 40 mm long area of higher tensile stresses it was 4 K The specimen was heated for 1 hour, held at the constant temperature for (7 12) h If the rupture did not take place during this time, the test were interrupted to measure the hoop strain of the cladding at room temperature and then continued in the same sequence

The hoop stresses of the cladding were calculated by the known relation

$$\sigma\theta = P\,(1 + c^2/r^2)\,a^2/(c^2 - a^2) \qquad (1)$$

where P is a gas pressure under cladding at testing temperature, a and c are inner and outer radii of cladding, r = (a + c) / 2 is a coordinate of a point where the stress is calculated

In the course of the experiment the time dependencies of the specimen temperature, count rate and total count of AE were recorded

3 EXPERIMENTAL RESULTS

3 1 Tests of pre-oxidized claddings

The oxidation temperature of 773 K was chosen based on time of specimen holding that is needed for the maximum oxide layer of 10 μm to form Some specimens were oxidized at T=673 K The difference in the oxidation temperature did not affect the results of cladding testing under SCC conditions

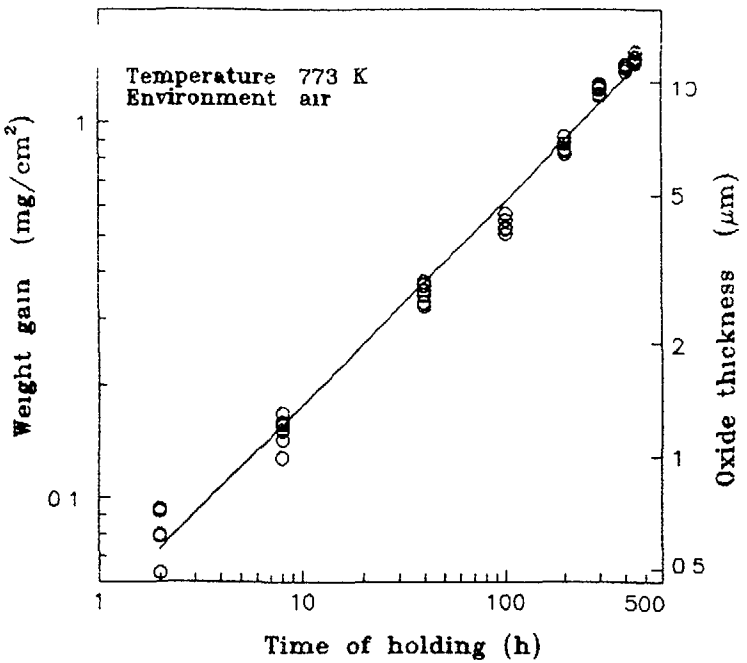

Fig.2 Sample weight gain and calculated ZrO_2 layer thickness.

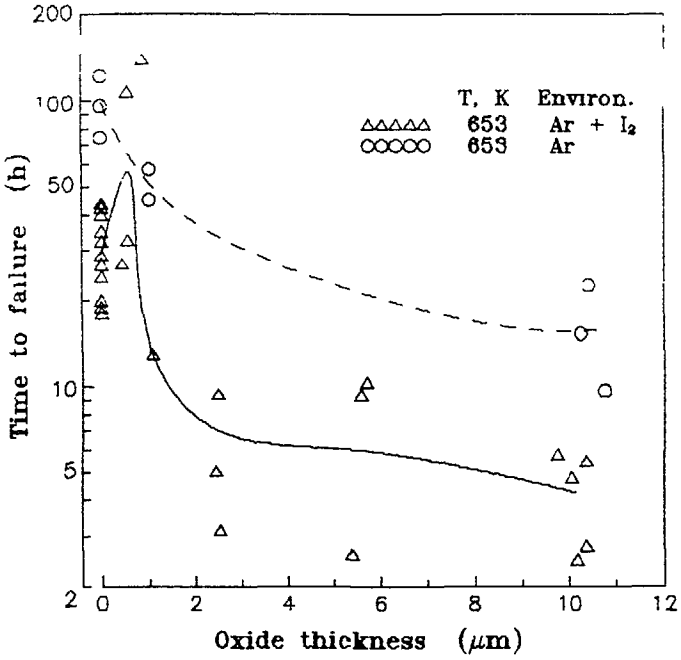

Fig.3 Influence of ZrO_2 at cladding inner surface on time to failure in iodine (△) and inert gas (○).

Fig 2 shows the kinetic dependencies of specimen weight gain in air at 777 K and the oxide thickness for Zr-1%Nb calculated assuming similar rates of outer and inner surface oxidation According to the appearance the resultant ZrO2 can be divided into three types

1) a black strongly adherent film up to 2-2 5 μm thick,
2) a grey more loose film likely to contain a larger amount of defects from 2 to 10 μm thick,
3) a spotted film more than 10 μm thick with light spots 1-3 mm in size against the grey background of the oxide

Alloy oxidation in each of the three indicated ranges can proceed by different mechanisms We did not specially study the structure of the oxide layer, however, the approximation of the experimental data by the power dependence showed that the parabolic law describes the results at an adequate accuracy in the thickness range 0 25 - 10 μm

$$\Delta m = 0\ 0675\ \sqrt{t},\ T=773\ K,\ \ 2 < t < 450 \qquad (2)$$

$$\delta = 0\ 457\ \sqrt{t} \qquad (3)$$

where Δm is the amount of oxygen reacted, mg/cm², δ is thickness of ZrO2 layer, μm, t is holding time, h

Pressurised tube test was conducted at 673 K The concentration of iodine under the cladding was 0 2 mg/cm², control specimens without iodine were also used Hoop stresses calculated from relation (1) were 165 MPa, i e , were close to the yield stress $\sigma_{0\ 2}$ of Zr-1%Nb claddings at the test temperature

The oxidation conditions were selected in such a way that the whole batch of tubes could be divided into groups of 6 specimens that had an essentially equal oxide film thickness at the inner surface of the cladding The testing conditions were carefully controlled, however, the scatter in the time to failure was significant within a single group of 6 specimens

Table 2. Influence of oxide thickness on the inner surface on VVER cladding time to failure

Test conditions	Oxide thickness (μm)	Average time to failure (h)
T=653 K CI=0.2mg/cm²	initial	29.1
	0.5	55.8
	1.0	13.1
	2.5	6.22
	5.6	7.48
	10.1	4.27
T=653 K specimens without iodine	initial	98.6
	1.0	51.4
	10.6	15.9

The experimental results are shown in fig.3 and tabulated in table 2. The claddings as supplied without an oxide film at their inner surface tested at the iodine concentration 0.2 mg/cm² had the mean time to failure t_f = 29 h. The oxide layer 0.5 μm thick increased the mean time to failure to 56 h under iodine corrosion conditions. With a further increase of ZrO_2 thickness from 1 to 10 μm a smooth decrease of the cladding life time was observed from 13 to 4-5 h. For specimens without iodine the mode of the time to failure vs ZrO_2 thickness dependence was approximately the same. The time to failure of the specimens containing iodine was on the average a factor of 3-4 less than that for the specimens without iodine both for the claddings with the initial inner surface and the ones having ZrO_2 layer 10 μm thick.

Two types of fracture are characteristic of loss of tightness by claddings: narrow axial splits at low hoop strains and cladding ruptures at high plastic strains. The analysis of the fracture types shows that with an increase of the oxide layer thickness the rupture fraction becomes prevailing.

3.2. Acoustic emission and fractographic studies

Fig.4 illustrates the influence of oxide layer thickness on the mean intensity of AE that was assumed to be a gain in the total count ΔN during exposure at constant temperature divided by the testing time t. Each point on the graph corresponds to a single specimen, therefore if the tests were conducted for several days additional averaging was performed for all day cycles. It can be seen that the AE intensity increases with ZrO_2 growth essentially by the linear law; no significant differences in the mean signal intensity for the specimens with and without iodine were revealed. It is likely that the main factor that determines the extent of the specimen damage is the oxide layer thickness.

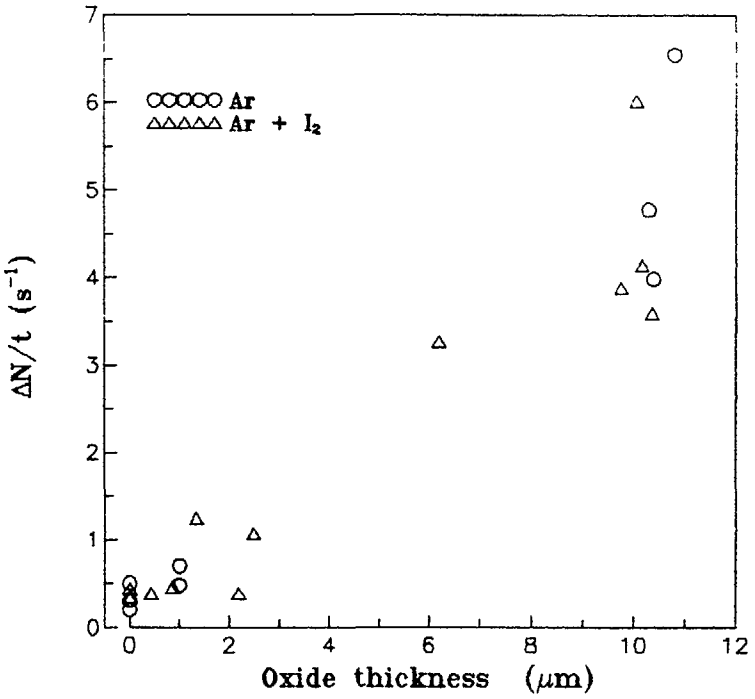

Fig.4 Mean intensity of AE-signals in samples with ZrO_2 layer of different thickness at cladding inner surface.

The concentration of iodine, particularly in the amount of 0.2 mg/cm² is of secondary importance for recorded AE-signals, although the time to failure of specimen is certainly affected by the availability of iodine under cladding.

Fig.5 shows a characteristic example of the time dependence of cladding temperature T, total count N and count rate of AE $\dot{N}$ in the course of testing one of the specimens; fig.6 illustrates the results of fractographic studies of the same specimen the fracture of which is described by an axial crack at the strain of 5.2%. The joint analysis of the fractographic and AE studies allows one to assume that SCC process can be divided into three stages.

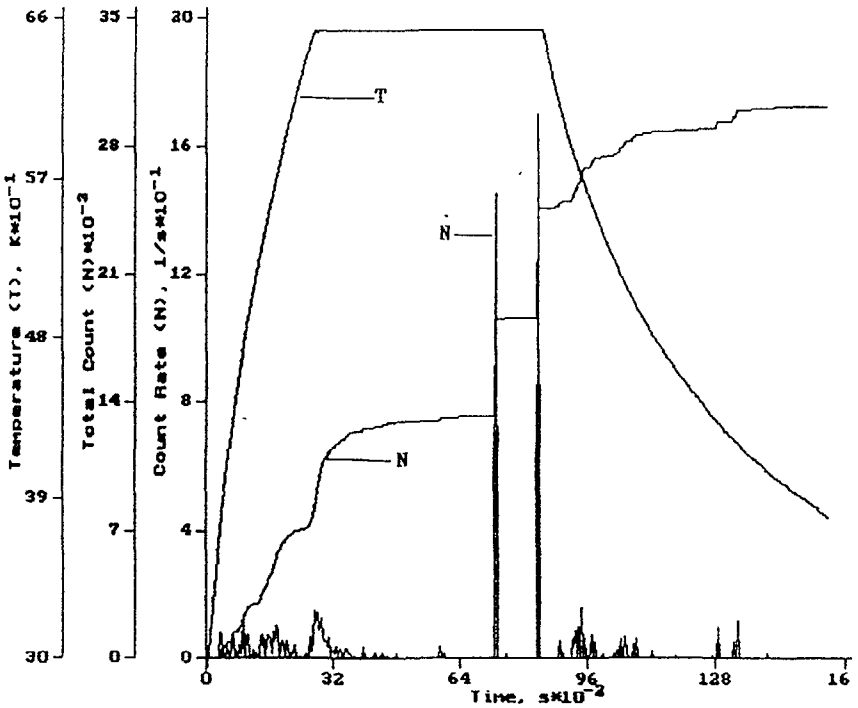

Fig.5 Time dependencies of specimen temperature T, total count of AE N and count intensity $\dot{N}$, recorded during testing cladding with oxide layer at its inner surface under SCC conditions.

At first stage beginning from the moment the testing temperature is reached to the first peak in the count rate of AE (see fig.5) there was a slow crack growth until a 90 μm depth was attained. This stage is paralleled by area 1 in fig.6; it is described by a mixed inter-and-transgranular type of fracture. The duration of the first stage varies in a wide range depending on a specimen and is 60 to 90 % of the total time to failure. The mean rate of crack propagation is about 5 x 10^{-3} μm/s at this stage.

At the second stage that is located between two intensity peaks the crack surface had areas of ductile fracture (area 2 in fig.6), and its propagation rate was higher and equal to ≈0.07 μm/s for the specimen studied. The duration of this stage in different specimens varied from 1000 to 5500 s.

The third area of fracture is paralleled by a zone located at the outer cladding surface. The fracture pattern at this stage is that of a transgranular shear with characteristic ridges produced by a plastic rupture. The count rate of AE at the moment of loss of tightness by a specimen (the second peak) can be 2-3 orders of magnitude higher than all the other ones recorded before.

The fracture surface at the inner cladding surface is shown in fig.7; the thickness of ZrO_2 layer well discernible in the photograph coincides with the calculated value determined from the oxidized specimen weight gain.

4. DISCUSSION

The tests indicated a sharp reduction in the cladding time to failure from 56 to 4 h with an increase of oxide layer thickness at the inner surface. To identify the cause of this cladding behaviour in an iodine environment the use is made of the concept of failure time as a sum of two items: t_1 is the time of crack nucleation and t_2 is time of its propagation. The results of some work [5,6] and our preliminary investigations show that under conditions of internally pressurized claddings the time of a crack nucleation is up to 90 % of the total time of fracture. It is apparent that oxide film formation effects significant changes in the first stage of iodine induced corrosion. These changes include:

1) oxide film cracking giving rise to characteristic microcracks at cladding surface;

2) growing permeability of oxide films for iodine related to increased oxide thickness;

3) stresses appearing in cladding surface layer that are induced by cladding tension under the action of resultant oxide due to a difference in volumes of Zr and oxide;

4) changes in surface layer mechanical properties as a result of oxygen diffusion.

In our opinion of highest significance are the first and third factors as they can result in local stresses in a cladding surface layer and, hence, in a sharp reduction of time of a slow crack growth. The contribution of stresses by an oxide film to a fracture process is evidenced also by a large fraction of a transgranular shear observed in fractographic studies.

With due account of the results of the study the known reduction in SCC resistance of fuel claddings irradiated to 30 MWd/kg is likely to be related to an oxide film formed at the inner cladding surface during burnup. Certainly one cannot neglect other phenomena affecting SCC, e.g., dislocation channelling.

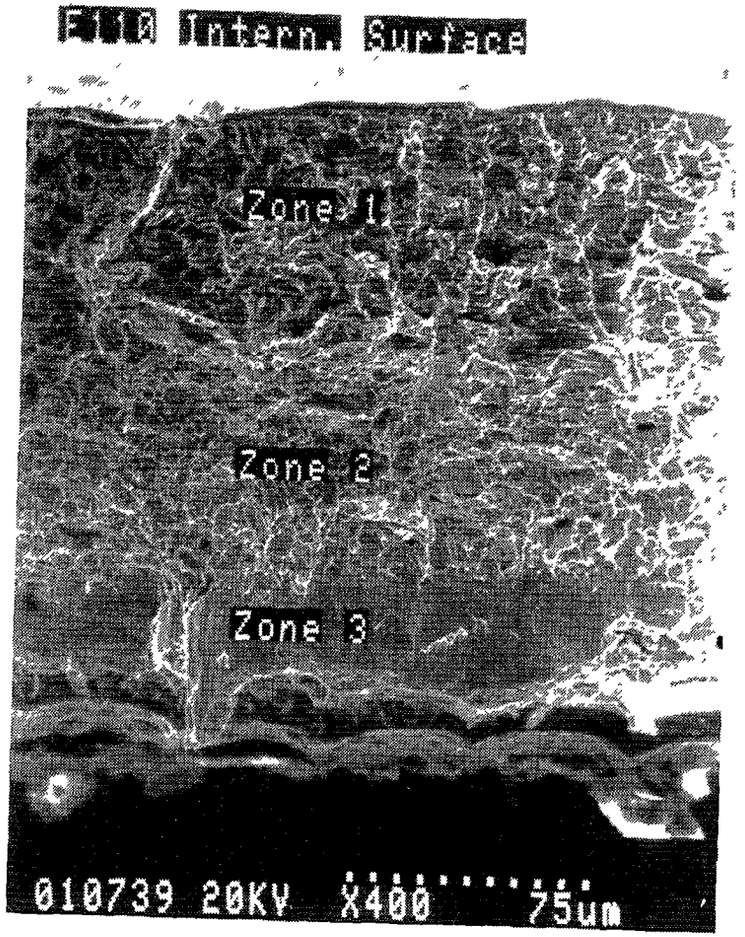

Fig.6a Fracture surface in penetrating crack area: zone 1 - essentially transgranular fracture in iodine environment; zone 2 - ductile fracture; zone 3 - ultimate fracture

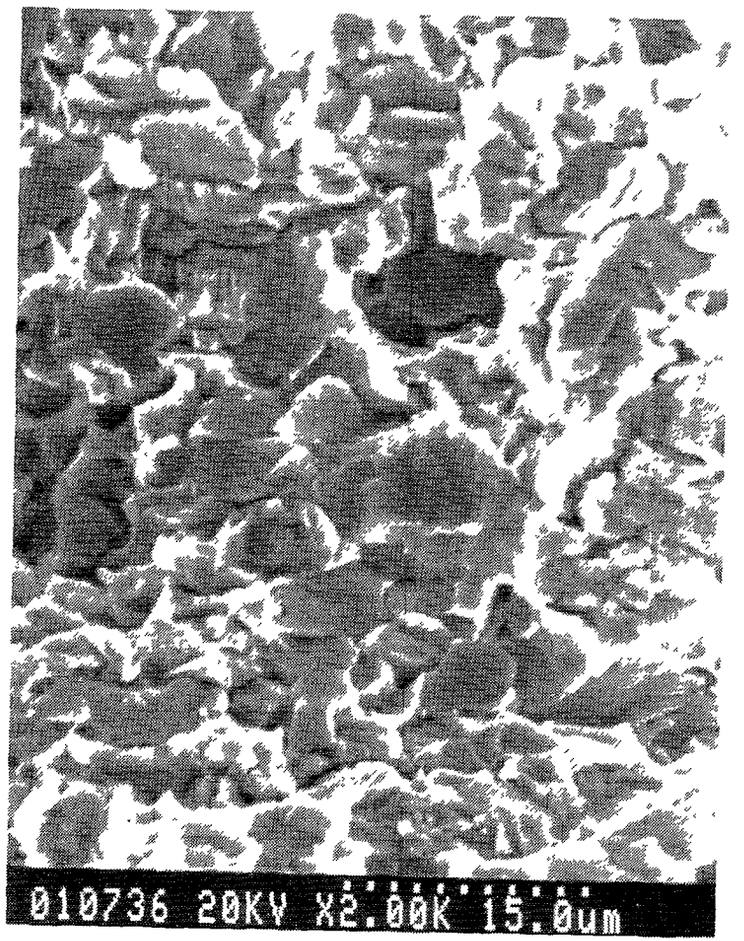

Fig.6b Area of transgranular zone 1.

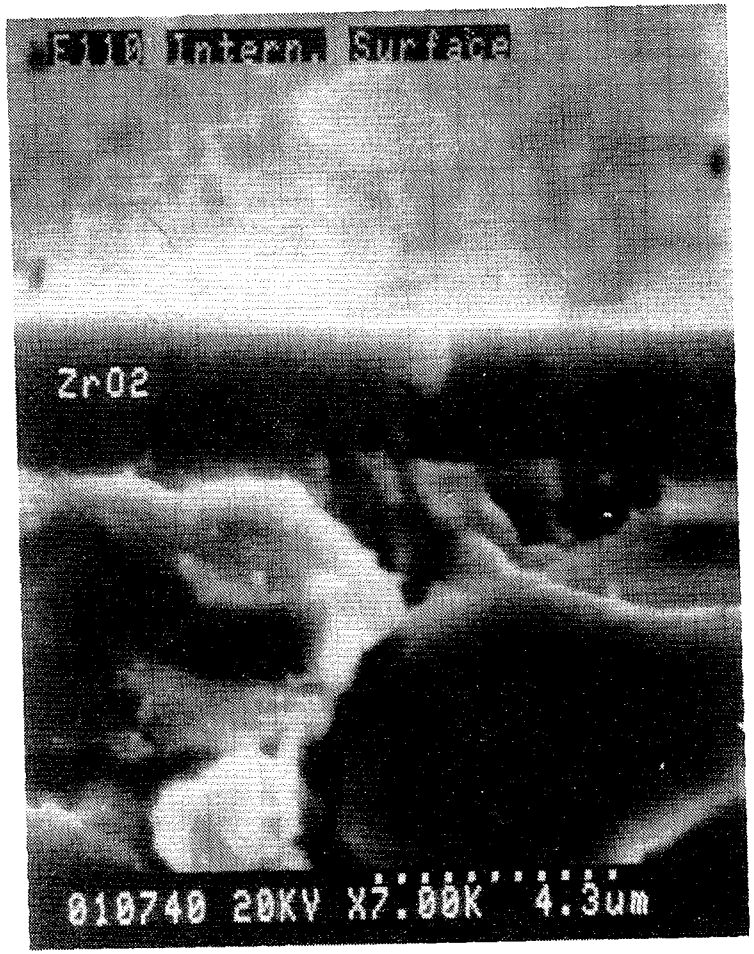

Fig.7a Start of fracture at inner surface of cladding.

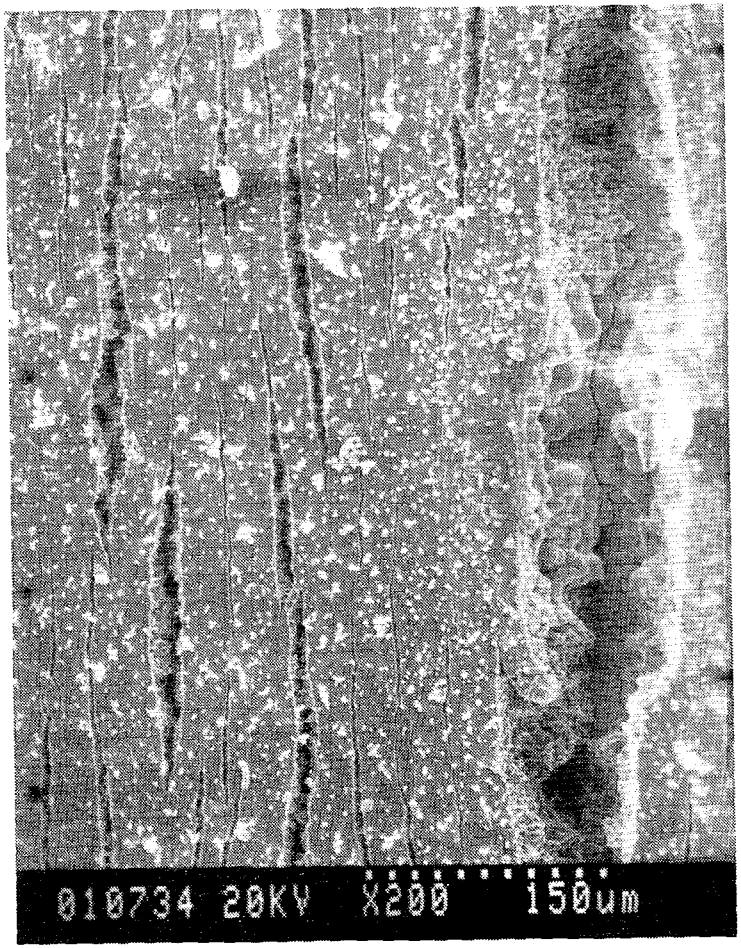

Fig.7b Appearance of inner surface area near penetrating crack.

However, dislocation channelling in claddings irradiated without fuel and having no oxide film formed at the inner surface leads to a reduction in SCC resistance to ≈ 350 MPa. At the same time claddings irradiated to high fuel burnup show a sharper reduction (≈200 MPa) [7-9]. The results of the study indicate that in the validation of fuel serviceability criteria under transient conditions one should take account of the physico-chemical condition of the inner cladding surface.

5. CONCLUSIONS

1. Internally pressurized VVER fuel simulators were tested under iodine SCC conditions. Zr-1%Nb claddings had a ZrO_2 layer of different thickness at their inner surfaces. Using AE-method and fractographic analysis it is shown that a crack has a three-stage propagation in cladding thickness beginning with transgranular shear in iodine the time of which constitutes the major fraction of the whole time until loss of tightness by cladding.

2. An increase of oxide film thickness at the inner cladding surface from 0.5-1.0 μm results in a sharp reduction of time to failure both in iodine and inert gas conditions.

REFERENCES

1. Nagai M., Shimada S., Nishimura S., Amano K. and Yagava G. Elucidating the Iodine Stress Corrosion Cracking (SCC) Process For Zircaloy Tubing, in: Pellet Cladding Interaction in Water Reactor Fuel. Proc. of IAEA Specialist's Meeting, Seattle, USA, 3-5 October 1983, pp.89-102.
2. Lindroth H., Terasvirta R. Post Irradiation Examinations of High-Burnup Fuel and Leaking Fuel of Loviisa NPS, in: Poolside Inspection, Repair and Reconstitution of LWR Fuel Elements. Proc. of IAEA Technical Committee Meeting, Lyon, France, 21-24 October, 1991.
3. Tsing-Tyan Yang and Chuen-Horng Tsai On the Susceptibility to Stress Corrosion Cracking of Zircaloy In an Iodine Containing Environment. J. of Nucl. Mater., 166(1989) N3, pp.252-264.
4. Reshetnicov F.G., Bibilashvili Yu.K., Golovnin I.S. et al. Problems of VVER-1000 Fuel Design for Operation under Load Follow Conditions and at Extended Burnup. Atomnaya Energiya 64(1988) N3, pp.258-266 (in Russian)
5. Videm K., Lunde L., Hollowell T. et al. Cracking of Cladding Tubes Caused by Power Ramping and by Laboratory Stress Corrosion Experiments. J. Nucl. Mater., 87(1979), pp.259 - 271.
6. Nagai M., Shimada S., Nishimura S. et al. Evaluation of SCC Crack Behavior in Zirconium and Zircaloy-2 Using Nonlinear Fracture Mechanics Parameters. Nucl. Eng. and Design, 88(1985), pp.319-326.
7. Wood J.C. and Kelm J.R. Effects of Irradiation on the Iodine-induced Stress Corrosion Cracking of CANDU Zircaloy Fuel Cladding. Res Mechanica, 8(1983), pp.127-161.
8. Onchi T., Kayno H. and Higashiguchi J. Inhomogeneous Plastic Deformation and its Relevance to Iodine Stress Corrosion Cracking Susceptibility in Irradiated Zircaloy-2 Tubing. J. Nucl. Mater. 116(1983), pp.211-218.
9. Tomalin D.S. Localized Ductility of Irradiated Zircaloy-2 Cladding in Air and Iodine Environments, in: Zirconium in the Nuclear Industry, ASTM STP 633, A.L. Lowe, Jr. and G.W. Parry, Eds., American Society for Testing and Materials, 1977, p.557-572.

MECHANISMS OF FUEL CLADDING FAILURE IN PCI

V.V. NOVIKOV
Scientific Research Institute for Inorganic Materials,
Moscow, Russian Federation

Abstract

The report suggests an iodine induced cracking model for LWR fuel.

The kinetics of a crack growth is considered; conditions are shown under which the cladding fracture mode is changed. The influence of irradiation and some other factors on the cladding resistance to SCC is discussed.

1. INTRODUCTION

SCC studies of Zr-alloy claddings were started in 60-ies in connection with fuel failures under transient conditions. As it pointed out by Cox, barrier fuel, i.e., claddings having a Zr coat at their inner surfaces, decreased the interest for SCC, and hence, the number of published papers despite some gaps in comprehension of this phenomenon, including the validation of using Zr-barrier claddings [1]. Among them is the mechanism of SCC in iodine. Wood and Cox were the first to discuss mechanisms of SCC; they chose adsorption and diffusion models for the analysis [2, 3].

The paper reviews the existent concepts of iodine induced cracking mechanism and the model of SCC failure is suggested that takes account of the influence of stresses on intensity iodine induced embrittlement of fuel claddings.

2. IODINE-ZR CLADDING INTERACTION IN SCC

In an iodine environment a crack can propagate as a result of the following processes (fig. 1):

1 — gas transport of iodine molecules (or I-containing molecules) in a crack volume;

2 — physical adsorption and migration of iodine along a crack surface;

3 — chemical adsorption;

4 — conversion to a dissoved state in a metal volume;

5 — diffusion to a fracture nucleation site and embrittlement of an area beyond a crack tip.

This scheme is likely to be the most general for the analysis of the embrittlement effect of an environment on a metal, although it is possible that not all of the indicated stages of "active environment - metal" interaction will take place in the process of iodine induced cracking of Zr-cladding. (The scheme shows a mouth of a propagating crack, however, the stages of I-Zr interaction are also retained for a crack nucleation).

The embrittlement process starts at the stages of volume or surface diffusion of I molecules to a crack nucleation site. These stages are followed by the physical adsorption of I with a metal induced by Van der Walls forces; during the adsorption gas molecules do not dissociate into atoms. It is possible that in our instance there can be no physical adsorption since it is usually characteristic for low temperatures.

When molecular I gets to a Zr surface then as a result of chemical adsorption that is, effected by the forces of the chemical affinity of gas molecules to metal atoms, the lather exchange electrons to for the covalent or ionic bond. With a temperature rise the amount of the adsorbed gas is always decreased (at the constant pressure), but in this case the temperature rise accelerates the chemical adsorption process.

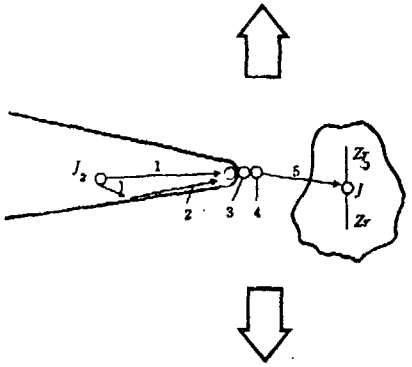

Fig.1. Stages of J-Zr interaction (see the text).

The pressure dependence of the amount of the gas adsorbed at the constant temperature is graphically presented as curves called adsorption isotherms. Theoretically the isotherms are described with equations according to which the extent of coverage is increased with a gas pressure.

Langmuir isotherm for I and Zr has the following form $Q=P_R/(1+P_R)$ where $P_R=log_{10}(P/P_C$ P - is pressure $ZrJ_4(Pa)$, P_C — critical pressure of the start SCC equal to 10^{-2} Pa.

Cubicciotti has studied the I chemosorption on Zr. The enthalpy of chemosorbed I formation proved equal to -146 kJ/g — atom [4]. It is also shown that on interaction with I iodides (not only those of Zr but also of other metals, e.g., Fe and Al) can generally form Zr iodide followed by a chemosorbed layer formation according to [4, 5]:

$$\frac{1}{n}MJ_n(g) + ZrJ(s) = ZrJ(s) + \frac{1}{n}M(s)$$

Therefore, it is not suprising that metal iodides induce a corrosion fracture of Zr.

If desorption is not taken into account the rate of Zr coverage with I is

$$\frac{dn_a}{dt} = 2.363 \cdot 10^{20} \frac{P}{\sqrt{MT}} f$$

where $\frac{dn_a}{dt}$ — coverage rate (molecule / cm^2 s)

P — pressure, Pa

M — molecular weight,

T — absolute temperature,

f — sticking coefficient

According to Williford, the chemosorption time at a pressure Zr J_4, equal to 27 Pa and the coverage extent $Q = 0.75$ is estimated to be 3.9×10^{-3} s, i.e., the time of this process does not control the totaltime of Zr cladding fracture [6].

In the end the chemical adsorption of I (or iodide) molecular results in their disintegration into atoms that are absorbed by a metal.

I as adsorbed by Zr can be in different states:

a) as dissolved in the metal;

b) as segregated on defects of crystal structure, grain boundaries included;

c) as adsorbed at the surface of microdiscontinuities and interphase boundaries;

d) in interaction with alloying elements and secondary phases.

The brittleness of a metal can be due to

1) adsorption induced crack nucleation due to a decrease of surface energy

2) adsorption induced crack nucleation as a result of I dissolution and reduced cohesive strength of area adjacent the metal surface,

3) critical I concentration in the maximum tensile stress area as a result of pre — transport of I to this area

Since the experimental data revealed the feasibility of a long slow stage of intercrystalline cracking the investigations were focused to studying this stage of a crack nucleation This stage of a crack evolution takes the path of 2—3% to 10 % of a cladding thickness, according to Videm and Lunde its duration can be 75—90% of the total time to fracture For the analysis of the nucleation mechanism the adsorption model was preferred

The process of embrittlement was considered either in terms of the surface energy reduction (Williford) or decohesion (Cubicciotti) Williford divided the iodine corrosion induced fracture into four stages [8].

1) microc ck nucleation,
2) crack formation,
3) crack growth,
4) cladding fracture.

The first stage implied a nucleation of a small surface defect or defective area and defect growth into a crack, for which the use of fracture mechanics is possible. The second and third stage implied the critical crack opening displacement and growth that then at the fourth stage transform to fracture According to Williford model the nucleation process results from the higher rate diffusion of vacancies to form intergranular voids as a result of surface ene gy decrease through iodine chemosorption with Zr However, this model was not confirmed experimentally intergranular voids were not revealed Williford model did not either explain a crack nucleation having essentially no incubation period and described by transgranular cleavage (Cubicciolti, Peehs, Cox, Shann, Miller et al, [3—5, 9, 10]) Cracking without the incubation period, i.e , crack initiation during 10—20s and the subsequent approximately one minute period prior to the full fracture of cladding was also observed in some fuel tests under nsient conditions [11]

Cubicciotti assumed this mode of fracture without a long incubation phase to be related to adsorption (chemosorption) leading to a metal surface strength degradation through decohesion It is known that on chemosorption the binding forces of surface atoms change, they are redistributed as a result lattice parameters grow and the fracture becomes easier In support of this viewpoint Cubicciotti presented data that indicated that crack nucleation was revealed in sites enriched in impurities such as Fe, Si and Ti Interaction between impurity segregations and I resulted in local decohesion and facilitated the rupture of bonds between Zr atoms Since these segregations were concentrated along grain boundaries, according to Cubicciotti the intergranular microcraks appeared due to this fact

It should be noted that a decrease in cohesion force reduces the strength and improves the plasticity But if the cohesion strength is reduced in local volumes, the localized plastic flow can give rise to a premature fracture at a lower plasticity which is in fact observed

The decohesion mechanism is preferred in this case compared to the adsorption effected decrease of the surface energy Thus, the surface energy decrease cannot explain why I effects embrittlement while oxygen does not, although it can be also actively chemosorbed by the Zr surface (According to the data of Cubicciotti and Scott the kinetics of Zr reactions with iodine and oxygen are very close at temperatures below 500°C) [12] The experimental data on the influence of temperature are not in favour of the surface energy hypothesis The temperature rise above 100—200°C increases Zr

Table I.
Coefficients and Parameters of I-125 Volume and Grain Boundary Diffusion in Zr - 1% Nb [14]

Method of calculation	Diffusion coefficient, cm^2/s	Temperature, TK			Q^*, eB (kcal/mole)	D_0^*, cm^2/s
		873	843	693		
		time of anneal, s				
		3.6×10^5	12.24×10^5	16.56×10^5		
	D_v^*	$(2.3\pm0.4)\times10^{-15}$	$(1.6\pm0.4)\times10^{-16}$	$(1.3\pm0.2)\times10^{-17}$	1.46±0.11 (33.5±2.6)	$(0.4\ ^{+1.6}_{-0.3})\times10^{-6}$
	D_{eff}^*	$(1.4\pm0.1)\times10^{-13}$	$(9.2\pm0.6)\times10^{-15}$	$(3.1\pm0.3)\times10^{-16}$	1.55±0.54 (35.6±12.4)	$(4.68\ ^{+1.25}_{-4.67})\times10^{-5}$
T Suzuoka	sD_{gb}^* (δ= 0.5 nm)	$(1.4\pm0.2)\times10^{-11}$	$(9.6\pm1.2)\times10^{-12}$	$(7.0\pm1.0)\times10^{-14}$	1.58±0.09 (36.4±2.0)	$0.022^{+0.058}_{-0.016}$

susceptibility for iodine induced embrittlement However it is known that adsorption is reduced with a temperature rise therefore the increased susceptibility is apparently due not to the surface interactions between I and Zr

Assuming the hypothesis of the decohesion effect of I on Zr strength the the decohesion area problem should be discussed (fig 1) If the decohesion area is related to the subsurface material it is apparent that chemosorption will be the last stage for the I transport in Zr. In another version the critical area must be at some distance from the surface that can be surmounted by iodine as a result of diffusion. An attempt at attracting the diffusion mechanism was made not only in connection with the discussion of one more model of fracture The data of the iodine induced corrosion experimental studies cannot be explained based on changes in surface properties of Zr These results are to include the delayed fracture of Zr cladding in an iodine environment at the constant load, the existence of a threshold (critical) factor of stress intensity and several stages of crack propagation rates in an iodine environment, the effectiveners of a Zr layer Considerable experience gained in investigations of the influence of environments on embrittlement and corrosion cracking of metals and alloys allows one to attract the diffusion model of Zr and its alloy fracture in iodine to explain the above regularities The main obstacle to the development of the above mechanism was apparently the viewpoint that iodine cannot or can penetrate Zr to a very low depth that was also corroborated by some experimental data (Cox, Haddad and Wood [2, 3, 13])

However, our experiments revealed the parameters of volume and grain boundary diffusion of I in Zr-1% Nb alloy (table 1) [14]. The values of the parameters proved to be low therefore the model took account of the fact that I transport to a fracture area is controlled by the hydrostatic stress gradient The analysis of the mechanism revealed some regularities in the fracture of fuel claddings in an iodine environment, that will be discussed below

4. INFLUENCE OF STRESSES ON CRACK GROWTH IN IODINE ENVIRONMENT

To analyze the influence of stresses at a crack tip on iodine diffusion use a chemical potential that is specifically related to a mechanical stresses gradient [15]:

$$\mu = \mu_o + RT\ln C + \mu_\sigma \qquad (1)$$

where C is concentration,

μ_o is a chemical potential in absence of stresses,

$\mu_\sigma = -V_J(\sigma_1 + \sigma_2 + \sigma_3)/3$

V_J is a partial molar iodine volume in a metal.

Taking account of the fact that an iodine flow to a metal is defined by the expression

$$J = -\frac{DC}{RT}\nabla\mu \qquad (2)$$

using (1) one obtains

$$J = -D\nabla C - \frac{DC}{RT}\nabla\mu_\sigma \qquad (3)$$

where D is a diffusion coefficient.

Diffusion equation for a stress field will be the following

$$\frac{\partial C}{\partial t} = D\nabla^2 C - \frac{DV_J}{RT}\nabla C\nabla\sigma \qquad (4)$$

To solve these equations one needs to know the diffusion coefficient and stress distribution at a cr tip. As iodine diffusion in zirconium is rather a slow process (the diffusion results are available and a be published) it will basically concentrate only in the area of the hydrostatic stress gradient act

Determination of stresses at a crack tip is one of the main tasks of fracture mechanics and we shall s the available solutions given, e.g., by Rice and McMeeking [15, 16]. As is known there is a plastic r at a crack tip, the approximate size of the former can be estimated e.g. from an expression for plane strain

$$r = K_1^2 / 2\pi\sigma_y^2 \qquad (5)$$

where K_I is a stress intensity factor;

σ_y is yield strength

It is shown that

1) in this area stresses grow starting from the values not less than the yield strength at a crack tip to attain maximum at a distance from the tip approximately equal to the doubled crack opening

$$2\delta \approx K_1^2 / E\sigma_y \qquad (6)$$

2) the higher is strain hardening coefficient the higher is the maximum stress and the maximum is displaced to the left closer to the tip (i.e., the stress gradient is increased)

At the strain hardening factor n≈0 the stress maximum is displaced to the right and the rate of a stress increment is lowered.

The above features of the stressed state in the tip area give an indication of the fact that the maximum iodine concentration may be reached not at a crack tip but inside a plastic area at a distance appropriate to the maximum stress (fig. 2)

The iodine delivery to a potential fracture area results in zirconium embrittlement According to the suggested model the loading type and, hence, the stressed state scheme is the most important factor that determines the intensity of iodine induced embrittlement As is known, for many metallic materials (iron, nickel etc base alloys) the conception of an embrittlement reaction as a chemical interaction resulting in new compounds is not considered to be an actual fact for a wide range of operation conditions, i.e., embrittlement of metals of this kind is a result of a relatively quick physical interaction the mechanism of which is not yet clear The embrittlement is suggested to be almost instant if iodine enters a critical area. Thus, the iodine induced crack growth in zirconium or its alloys is controlled not only by the material properties but also by the specific features of iodine transfer and local accumulation processes.

This fact is responsible for a significant difference between the crack growth process under consideration and the static loading effected brittle fracture under conventional when the time dependence of the fracture process, i.e., a progressive increment of a crack, is so weak that it may be neglected without any large detriment to the adequate description of the phenomenon

Evidently the iodine induced fracture sets in when stresses are in excess of zirconium strength lowered by iodine, i.e., when the concentration becomes critical

$$C(\vec{R},\Delta t) = C_\sigma(\sigma) \qquad (7)$$

where $\vec{R}$ is a coordinate in a microfracture area at a crack tip

Under the action of a stress gradient iodine diffuses to an area beyond the crack tip where tensile stresses are at a maximum The structure of equation (4) suggests that the major portion of iodine should concentrate in some neighbourhood of the stress maximum, the iodine accumulation beyond this

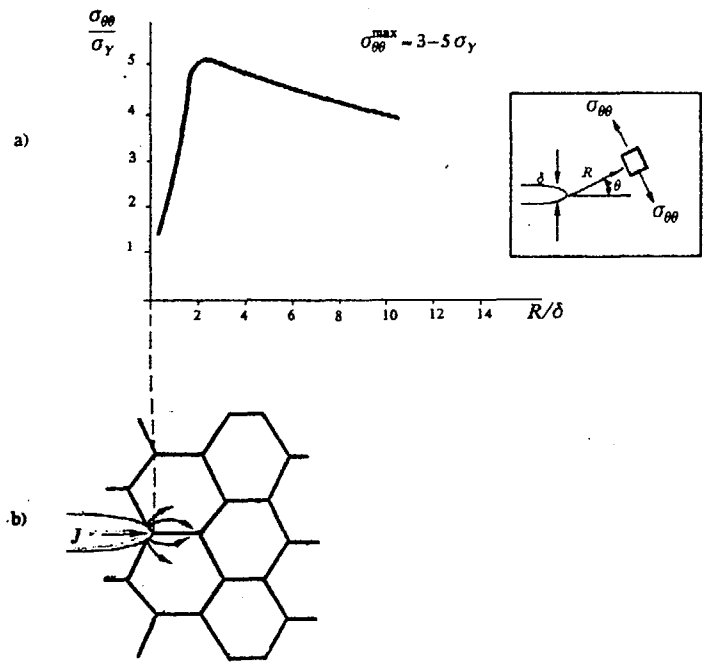

Fig.2. Stress distribution at tip of crack propagating (a) as a result of iodine induced embrittlement (b)

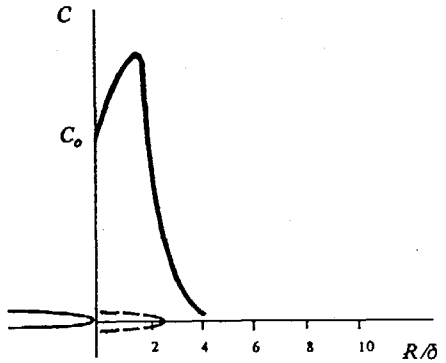

Fig.3. Variation of iodine concentration in stress field at crack tip.

maximum is prevented by the negative stress gradient. This kind of a diffusion flow distribution makes it reasonable to assume the type of the concentration distribution shown in fig. 3. When the critical iodine concentration is reached a microfracture takes place and the resultant microcrack merges to the main one to effect its growth. After an abrupt change in the crack the significant portion of iodine localized in the maximum will be found in a new area not related to the stress field near the tip. Hence, studying the crack growth process one can assume a crack to propagate in sequential jumps the length of which is determined by a distance between the tip and the microarea inside a plastic zone within which the critical iodine concentration is reached during the time Δt.

Since the components of stresses and strains nucleated at the crack tip are specific functions of the coordinate of point the stress intensity factor equation (7) can be presented as

$$C(\vec{R},\Delta t) = C_{cr}(K) \tag{8}$$

Equations (1)-(4) were used to analyze a crack propagation in iodine that brings about zirconium alloy embrittlement. However, those equations that describe an iodine diffusion in a metal are applicable to any stress field including the cladding surface where corrosion induced cracks nucleate. It is apparent that it is the level of stresses and the mode of their distribution in the cladding surface layer that determine the kinetics and the mode of the corrosion effected cracking onset.

5. RATE OF IODINE INDUCED CRACK GROWTH

Structural studies of SCC propagation showed that depending on the stress intensity factor a crack can be either inter-or transgranular. Based on the above mechanism of an iodine effected fracture consider the condition under which the mode of a crack propagation is altered.

It is apparent that for a fracture to be transgranular iodine should penetrate a depth not less than a grain size. Otherwise, the fracture will be intergranular. For this change-over the critical stress intensity factor according to (6) is found as follows:

$$K \geq \sqrt{2\delta E \sigma_y}$$

where $2\delta = d$ is a grain size;

E is an elastic modulus;

σ_y is yield strength.

By substituting the relevant values into this inequality (d=5 μm, E=7.3×10^4 MPa, $\sigma_{0.2} \approx$ 170 MPa) one obtains K ≥ 8 MPa m$^{1/2}$ for Zr-1% Nb claddings at t=350°C. For zircalloy-2 (at $\sigma_{0.2} \approx$ 200 MPa) one has K ≥ 8.5 MPa m$^{1/2}$. The found stress intensity factor above which a transgranular fracture is to take place well agrees with the values found experimentally (K=8-8.5 MPa m$^{1/2}$) for zircalloy-2 [7, 17].

At K < 8 MPa m$^{1/2}$ a crack will propagate along grain boundaries and iodine will be supplied to a pre-fracture area from a crack tip. In this case the stress maximum will be within a grain and a crack jump will not be in excess of a grain size. Evaluate the crack propagation rate using the approach suggested in [18]. If v is an average rate of iodine atoms, 2δ is a length of an iodine accumulation area apart from a crack tip, Δt is time after which a crack jump takes place, the critical concentration will be determined as follows:

$$C_{cr} = C_o + \frac{C_o v \Delta t}{2\delta} \tag{9}$$

According to relation (3)

$$v = -D\frac{\nabla C}{C} - \frac{D}{RT}\nabla\mu_\sigma \qquad (\ldots)$$

or approximation.

$$v = \frac{D}{RT}V_J\frac{d\sigma}{dx} \qquad (11)$$

(since we deal with intergranular cracking $D=D_{gb}$).

From relations (9) and (11) one finds that

$$\Delta t = \frac{C_\sigma - C_o}{C_o}\frac{2\delta}{v} \qquad (12)$$

To evaluate $d\sigma/dx$ use the mean-value theorem and present the ascending branch of the stress dependence at a crack tip (fig. 2) as

$$\sigma = \sigma_y\left(1 + \frac{2}{ln\,(1+2\delta)}ln\,(1+x)\right) \qquad (13)$$

(This relation does not take account of the strain hardening of a metal).

Then

$$\overline{\frac{d\sigma}{dx}} = \frac{1}{2\delta}\int_0^{2\delta}\frac{2\sigma_y}{ln\,(1+2\delta)}\frac{1}{1+x}dx \qquad (14)$$

or after transformation

$$\overline{\frac{d\sigma}{dx}} = \frac{\sigma_y}{\delta} \qquad (15)$$

Using (11), (12), (15) one obtains for the time of a crack jump

$$\Delta t = \frac{C_\sigma - C_0}{C_0}\frac{RT}{DV_J}\frac{\delta}{\sigma_y}2\delta \qquad (16)$$

or

$$\Delta t = \frac{C_\sigma - C_0}{C_0}\frac{RT}{DV_J}\frac{1}{\sigma_y}2\delta^2 \qquad (17)$$

Since during this time the crack propagates to $\sim 2\delta$, the mean rate of its propagation is determined with the following expression.

$$\frac{da}{dt} = \frac{2\delta}{\Delta t} = \frac{C_0}{C_\sigma - C_0}\frac{DV_J}{RT}\frac{\sigma_y}{\delta} \qquad (18)$$

Taking into consideration that the crack propagates within a grain, i e , $2\delta = \alpha d$, d is a grain size one has ($\alpha \leq 1$)

$$\frac{da}{dt} = \frac{2C_0}{C_\sigma - C_0}\frac{DV_J}{RT}\frac{\sigma_y}{\alpha d} \qquad (19)$$

It follows from the above analysis that the rate of a crack growth should increase with alloy strengthening (including irradiation induced strengthening) A larger grain size and strength reduction will favour a lower rate of corrosion effected cracking Another not less important conclusion is that

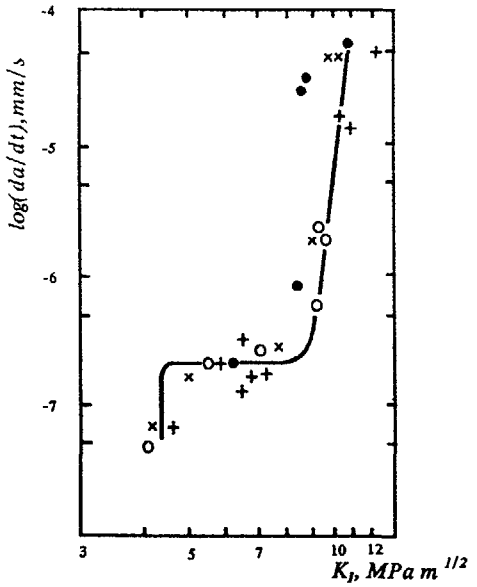

Fig.4. Rate of crack growth in zircalloy-2 claddings as a function of stress intensity factor [17].

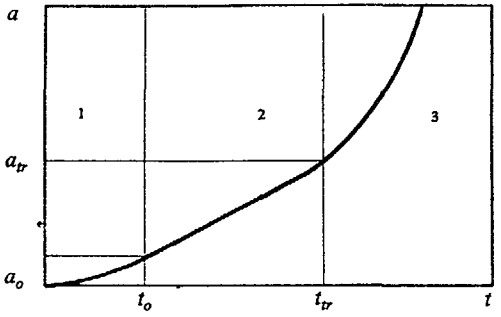

Fig.5. Crack growth in cladding thickness as a function of time (according to the suggested model)

1 — crack nucleation at the depth a_o during time t_o;

2 — crack growth at constant rate propagation,

3 — acceleration of crack growth (with conversion to transgranular fracture (a_{tr}))

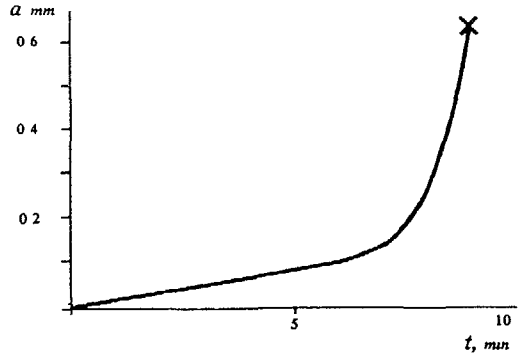

Fig.6. SCC of internally pressurized cladding [19]

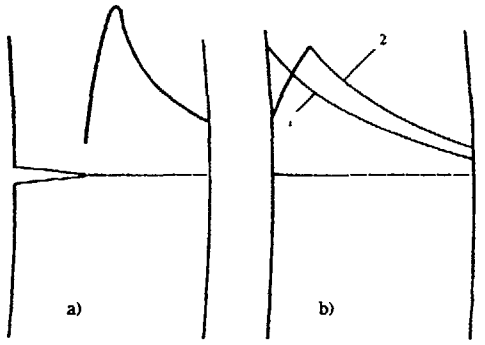

Fig.7. Stress variation in cracked cladding thickness (a) and as well as on elastic (1) and elastic-plastic (2) loading without a crack (b)

according to relation (19) the crack growth proceeds at a constant rate essentially independent of the stress intensity factor (at K < 8 MPa $m^{1/2}$) This feature of a crack growth can be experimentally observed in fig 4 [17] for the parameter K varying within ~4—8 MPa $m^{1/2}$ Taking into account the above analysis of the inter- and transgranular fracture of cladding the crack growth rate vs parameter K will apparently have the form shown in fig 4 Based on the results obtained the crack propagation process can be presented as follows On condition the parameter K is within 4—8 0 MPa $m^{1/2}$ the nucleated crack will grow deep into cladding at a constant rate (according to equation (19)) In this case the crack will propagate along grain boundaries An increase of the intensity factor (K> 8 MPa $m^{1/2}$) will be described by transgranular or mixed cracking The cracking rate will grow with the stress intensity factor according to the relation of the type $da/dt \sim K^n$ Hence, the crack evolution has three stages the first one is nucleation, the second one is a growth at a constant rate independent of the stress intensity factor, the third one is accelerated cracking after K reaches the value characteristic of the transition to a transgranular fracture (fig 5). The fractions of the latter two stages can be different depending on metal properties and stress level

The results of the experiments to studding the fracture process in iodine corrosion of Zry internally pressurized claddings corroborate this mode of a crack evolution [19] (fig. 6) The stress intensity factor at which the constant rate crack growth in a cladding is finished on condition that the hoop stress σ_θ = 313 MPa and the crack reached the depth of ~100 μ is equal to~ 6 MPa $m^{1/2}$ This magnitude is within the range of the factors K for which, as is shown above, the crack growth rate does not depend on this parameter

6. CRACK NUCLEATION AT INNER FUEL CLADDING SURFACE

According to equation (3) the penetration of cladding by iodine is accelerated at the positive stress gradient. As it is shown above this gradient results at a crack tip in a plastic strain area It is known that stress changes in the plastic area of a crack tip are similar to stress distribution in members subject to elastic-plastic load (fig 7) The positive stress gradient resulting from the plastic state (for example during fuel cladding interaction or under internal pressurization etc) of an area abjacent the inner cladding surface produces conditions favourable for an accelerated iodine accumulation in this area

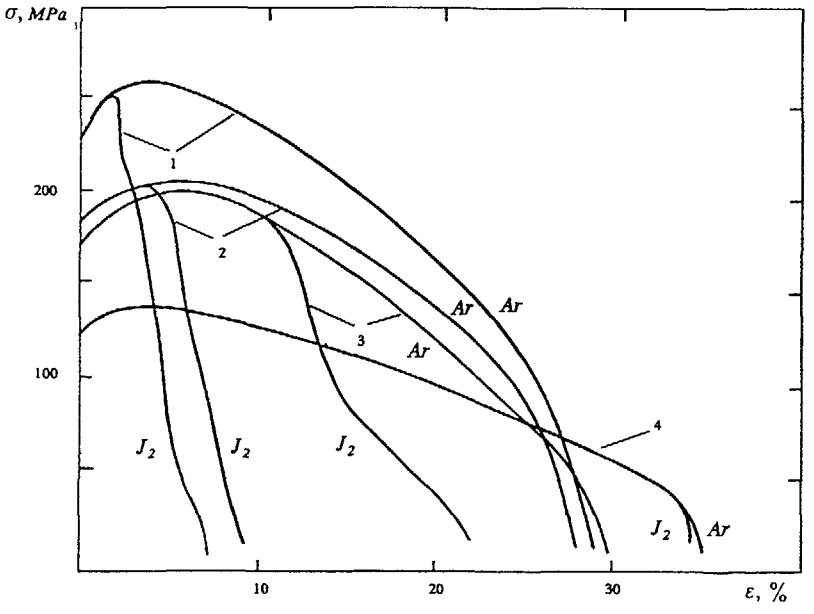

Fig 8 Zr-alloy deformation in iodine and argon (1 — Zry4, 2 — Zry2, 3 — Zr—1% Nb, 4 — Zr) under $\varepsilon = 2\ 10^{-5}\ s^{-1}$, T = 623K

According to equation (7) a surface crack is nucleated when the critical concentration of iodine is reached. Hence, for a surface crack to nucleate no defects of inner cladding surface are needed. It is apparent that the nucleated crack can be trans- or intergranular.

Possibility of a transgranular fracture is realized on condition if the stress level and iodine concentration are adequate for a grain cleavage. In any case for a quick nucleation of a crack the iodine concentration of a surface layer must reach the critical value in rather a short time. Apparently, it is this mechanism that can explain the quick nucleation of cracks observed in power ramp experiments as well as in laboratory studies of iodine induced cracking that model a fuel-cladding interaction [11, 20]. Thus, a transgranular crack ~20 μm long was nucleated [20] at the 5 sec load pulse. The crack initiation in 10—20 sec and its full penetration in about a minute were attained in tests of fuels under transient conditions [11].

When analyzing the causes related to a surface crack nucleation one cannot neglect the influence of a local surface segregation of impurities, inclusions as well as residual internal stresses or defects [4, 21—23]. The above factors can accelerate the diffusion flow of iodine; the rate of iodine accumulation in a metal can be significantly increased thus reducing the time of a crack nucleation. The influence of inner surface accumulated impurities or alloying elements on corrosion induced cracking is indicated in [4, 21]. It is shown that a removal of a surface layer 60 μm thick increased the time to fracture by a factor of 20 [22].

Thus, the elastic plastic-condition of cladding allows an acceleration of iodine induced cracking. The rate of the penetration of the surface zone by iodine will be controlled by the stress gradient that is in its turn dependent on the metal strength and strain hardening. A higher strength will increase the rate of iodine transport to the cladding material both at its surface and in the area of the tip of a propagating crack and, hence, accelerate the metal fracture as compared to that of low strength alloys. Thus, the time to fracture and the strain of Zry-4 turned out to be less than those of either Zry-2 or Zr-1% Nb (fig. 8).

The highest resistance to SCC was demonstrated by zirconium that has a plasticity and the lowest among Zr-alloys strength (fig. 8).

At the end of the analysis of a crack nucleation consider a loading version when cladding is elastic. The typical hoop stress distribution in the cladding thickness is shown in fig. 7 (b).

In this case the iodine accumulation in the area adjacent the inner cladding surface will be inhibited by the negative stress gradient. Apparently, it is the load level at which the cladding will still retain the elasticity will determine the threshold stresses below which as is shown experimentally, the corrosion induced cracking does not take place for the actually forseable time. The suggested scheme does not consider the polycrystal material straining non-uniformity related to the orientation of grains to one another and to the direction of the load applied. During loading variations in deformation of adjacent grains can effect the stress concentration at their boundaries which in its turn will govern the site of both the intergranular nucleation of microcracks and the transgranular cleavage.

7. INFLUENCE OF IRRADIATION ON CLADDING IODINE CORROSION RESISTANCE

An important but least studied is the problem of elucidating the effect of irradiation on iodine SCC.

Consider the possible factors capable of influencing the cladding resistance in an iodine environment. They are:

1) irradiation effected hardening and structural changes in Zr alloys;

2) irradiation induced damage of inner cladding surface with fission product fragments;

3) oxidation of cladding inner surface.

If irradiation brings about hardening then according to the above arguments iodine will accumulate at a crack tip at higher rates and the crack growth will be accelerated. The experiments to assess the crack

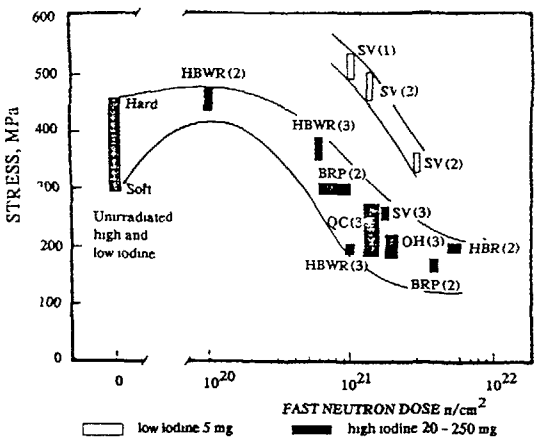

Fig 9. Failure stress corresponding to 1—3 h failure time in tube pressurized SCC tests of irradiated material as function of neutron fluence [26]

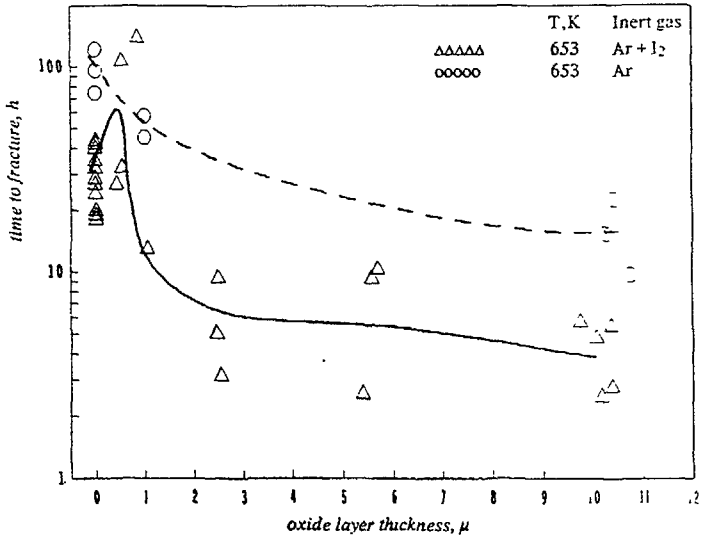

Fig 10. Influence of ZrO_2 at cladding inner surface on stress rupture in iodine (Δ) and inert gas (o) [33].

growth rate in irradiated and unirradiated Zr claddings depending on the stress intensity factor corroborate this conclusion However, when assessing the full time to fracture one should not forget the process of a crack nucleation. Irradiation induced increase of Zr alloy strength will lead to longer time of a crack nucleation as compared to unirradiated alloy at the same stress level, i e , irradiation should improve the resistance to iodine corrusion [24, 25] None the less this tendency of improving the iodine corrasion resistance with fluence was not always reasized after the dose of $\sim 10^{20}$ n/cm^2 [26, 27] Thus the results of irradiated (burn-up ~30 MW day/kg UO_2) cladding specimen testing pointed to a reduction in iodine corrosion resistance at neutron fluence of $2—6 \times 10^{21}$ n/cm^2 to a level still lower than that observed for unirradiated claddings [27] (fig. 9)

To account for this effect an idea was suggested that dislocation "channeling" leads to an oxide film fracture, thus, facilitating the onset of corrosion cracking [28] However dislocation channeling while accelerating iodine corrosion rate, leads to a resistance to SCC in irradiated claddigs reduced to only −350 MPa, not to −200 MPa, as it was obtained for irradiated fuels [27, 29] In this connection, assess the two remaining factors that possibly influence iodine SCC

The former cannot be apparently excluded taking account of cladding surface embrittlement with fission product fragments, and, hence, also an increase of metal susceptibility to cracking in iodine [30] However, no direct experimental proof was given that would corroborate the decisive role of a cladding surface damaged to a depth of ~10 μm in iodine corrosion

The influence of the latter factor is related to oxygen released on fuel fission to form a Zr oxide film at the inner cladding surface The ZrO_2 thickness as measured in post-irradiation studies varies in wide ranges depending on burn-up and linear heating and reaches 18 μm [31] Tests of Zry [32] and Zr — 1% Nb claddings showed that their SCC resistance is sharply decreased with the oxide thickness (fig 10) [33] The stimulating effect of an oxide film for SCC is likely to be induced by stresses that the oxide film creates in a metal due to differences in volume changes between Zr alloy and this oxide The growth of a Zr oxide film in likely to lead to tensile stresses which when added to stresses effected by an external load produce a fracture at a higher rate than in case of unoxidiged claddings

The analysis showed that the irradiation effect on iodine embrittlement of fuel claddings shows up not only as irradiation produced hardening but also as an influence of the cladding inner surface condition depending on fuel burn-up

8. CONCLUSION

The major element of the suggested theory of iodine — induced cracking of claddings in the action of stress field on iodine diffusion to a pre-fracture area of a metal. The model assumes that fracture takes place as a result of a decrease of Zr cohesion strength depending on stress level and I concentration thus defining the phenomenon under study as iodine induced embrittlement. The analysis of the cracking process revealed the feasibility of predicting the influence of material strength as well as irradiation on fracture of fuel claddings in an iodine environment.

Analysis of published data on claddings of water cooled reactor fuels showed that their behaviour under aggressive conditions is quite adequately explained by the suggested mechanism.

REFERENCES

1 B Cox. J Nucl. Mater., 172 (1990) p 249
2 J C Wood J Nucl. Mater , 45 (1972/1973) p 105
3 B Cox and J C Wood, in Proc. Electrochemical Society Symp on Corrosion Problems in Energy Conversion and Generation. Ed C S Tedmon Jr (ECS, New York, 1974), p 275
4 D Cubicciotti, R L. Jones and B C Syrett Zirconium in the Nuclear Industry Fifth Conference ASTM, STP754, Boston, 4—7 Aug., 1980 Ed. American Society for Testing and Materials 1982 p 146
5 S H Shann and D R Olander J Nucl Mater , 113 (1983) p 234
6 R E Williford Nucl Eng Design, 78 (1984) p 23
7 K Videm, L.Lunde Proc 4th Intern Symp on Zirconium in the Nuclear Industry Stratford upon Avon, UK, June 1978, ASTM STP681, p 229
8 R E Williford J Nucl Mater , 132 (1985), p 52
9 M Peehs, H Stehle and E Steinberg, in [7] p 244
10 A K Miller H Ocken, A Tasoon J Nucl. Mater , 99 (1981) p 254
11 H Mogard U Bergenlid S Djurle, G Lusell, G Ronhberg "Intern Trans Ramp I Fuel Project" Proc of IAEA Technical Committee Meeting,Karlsruhe, 11—15 November 1985 (IWGFPT/25), p 157
12 J Cubicciotti and A.C Scott J of the Less-Common Metals, 77 (1981) p 241
13 3 Cox and R Haddad Zirconium in the Nuclear Industry Seventh Intern. Symposium ASTM STP939, 1989, p 713
14 Gladkov V P , Smirnov E A , Petrov V.I , Svetlov A B , Temshev V I , Bibilashvili Yu K Novikov V V To be published in Atomnaya Energiya (in Russian)
15 P Sofronis and R M Mcmeeking J Mech. Phys Solids, 37 (1989), p 317
16 J.R Rice Corrosion, 32, January (1976) p 22
17 K. Norring, Y Haag and C Wikstroom J Nucl Mater , 105 (1982) p 231
18 Gerberich W W , Chen Y T and John C St Metallurgical Transactions 6A (1975), p 1485
19 M Nagai, S Shimada, S Nishimura, H Ueda, G Yagawa Nucl. Engn. Design, 88 (1985) p 319
20 R Haddad and B Cox J Nucl Mater , 138 (1986), p 81
21 D Cubicciotti, S M Howard and R L. Jones J Nucl Mater , 78 (1978), p 2
22 Syrett B C , Cubicciotti D and Jones R L. J Nucl Mater , 92 (1980) p 89
23 T Kubo, Y Wakashima, H Imahashi and M Nagai J Nucl Mater , 132 (1985), p 126
24 T Onchi, H Kayano M Narui J of Nuclear Science and Technology, v 19 № 9 1982 p 740
25 Stupina L.M , Shamardin V K , Kobylyansky G P Novikov V V , Bibilashvili Yu K Sotnikov A.S "Irradiation effect on corrosion cracking of VVER fuel element claddings in iodine and cesium iodine medium" in Proc Intern Conf on Radiation Materials Science, Alushta USSR May 22—25, 1990, v 8, p 41
26 Lunde L., Videm K. J Nucl. Mater , 95 (1980), p 210.
27 J C Wood and J R Kelm Res Mechanica, 8 (1983), p 127
28 Onchi T , Kayno H and Higashiguchi J J Nucl. Mater 116 (1983), p 211
29 Tomalin D S in Zirconium in the Nuclear Industry, ASTM STP 633, 1977, p 557
30 I Schuster and C Lemaignan J Nucl Mater , 151 (1988) p 108
31 M Nagai, S Shimada, S Nishimura, K. Amano and G Yagawa Proc of IAEA Specialists Meeting, Seattle, USA, 3—5 October, 1983, p 89
32 Tsing-Tyan Yang and Chuen-Horng Tsai J Nucl Mater , 166 (1989) p 252
33 Bibilashvili Yu K., Dolgov Yu N , Novikov V V , Gryazev A P "Effect of inner surface preliminary oxidation on stress corrosion cracking susceptibility of Zr — 1% Nb Tubing" II s meeting.

ANALYSIS OF TRENDS IN FUEL ROD DEPRESSURIZATION AND DETERMINATION OF 'GAS LEAK' AND 'PELLET–WATER INTERACTION' TYPE FAILURES USING RADIATION MONITORING TECHNIQUES OF FUEL ROD LEAK TIGHTNESS

E.A. PANOV, Yu.M. SHESTAKOV, V.N. MIGLO
Research Institute for Nuclear Power Plant Operation,
Moscow, Russian Federation

Abstract

Analysis of fuel rod failures in the Light Water Reactor operation is presented. Analysis includes the mechanism of formation and development of fuel rod cladding failure until through-wall defects appear (welding defects; inner hydriding defects; pellet-cladding interaction; crud deposit - intensified corrosion) as well as factors that determine defects propagation after fuel rod depressurization (metal condition in the vicinity of defect determined by the mechanism of formation and propagation defect; operational transients; degree of core cooldown after depressurization during preventive maintenance).

Possibilities of in-service monitoring of fuel rod through-wall crack propagation using normal tools of cladding bak-tightness monitoring are addressed and used in the course of analysis. Characteristics and values are presented for radiation parameters for fuel assemblies during propagation of defects with different degree of rod depressurization, including "gas leak", cladding crack and "open pellet-water interaction" with potential particulate fission product release from the damaged rods as well as after formation of recurring defects.

Based on experimental data on specific activity of different iodine isotopes in the primary coolant, a mathematical model to analyse defect propagation trends has been developed. The model describes the rate of radionuclide release from depressurized rods and the rate of nuclear fuel fission processes in the vicinity of defects. The model and results of analysis are illustrated by experimental and statistical data on depressurization of VVER (PWR) and RBMK (BWR) reactor fuel rods.

Possibility to solve the problem of predicting defect propagation is considered.

1. Processes of Clad Failure and the Fission Product Leakage Model

The present version "Nuclear Safety Rules for Nuclear Power Plants" [1] establish the operation limits for fuel rod failure and the safety operation limits for guantity and size of fuel rod damage. This limits established for failure "gas leak" and "open pellet-water interaction" (tabl.1). However, it's

Table 1

Operation Limits of Fuel Element Failure and Limits of Nuclear Safety Operation by Number and Size of Fuel Element Defects (Appendix 1,2,3,4 [1, p.56-60])

Type of Reactor	Type of Fuel Rod Defects	Operation Limits of Failure	Limits of Nuclear Safety Operation
VVER (PWR)	Gas leak	0,2 % fuel rods	1 % fuel rods
	Pellet-water interaction	0,02 % fuel rods	0,1 % fuel rods
RBMK (BWR)	Gas leak	0,2 % fuel rods	1 % fuel rods
	Pellet-water interaction	0,02 % fuel rods	0,1 % fuel rods
BN (FBR)	Gas leak	0,05 % fuel rods	0,1 % fuel rods
	Pellet-water interaction	0,005 % fuel rods	0,01 % fuel rods
AST	Gas leak	In technical project of reactor construction	0,1 % fuel rods
	Pellet-water interaction		0,01 % fuel rods

necessery following measure for safety operation fuel assemblies (FAs) with depressuriziation: in the first plase, to realize the inspection to nuclear fuel conditions; in the second plase, to prediction the development of failure and take out in time a fuel assemblies with depressurization fuel rods (FRs).

Process of clad failures have many stage: 1. the rousing of cladding failures; 2. the development of damage to throught-way; 3. the gladding leakage; 4. the development of first micro-damage to macro-damage; 5. the rousing ,the development and the appearance of second throught-way damage; 6. the accelerated development of second damage to destroy of cladding.

The special any nuclear power plants - it is practical impossible during operation directly to inspection to cladding failure development. Only with inderect radiation methods of fuel integrity inspections (FII) may to assess a degree of failed cladding with initial the cladding leakage include a releasing of current and a leakage monitoring of fission product from the FR failed.

Based on experimental data of iodine radionuclide specific activity in primary coolant are chose matematical model.

It is allow to assess a development of FRs through-wall crack propagation with first cladding leakage stage. The model define the radionuclide relase rate from depressurized FRs and the nuclear fuel fission process rate in the defect region.

The radionuclide relase rate from the failed FRs are determined from equations describing fission product generation and transport in the material system-the reactor primary coolant:

$$dA(t)/dt = S(t)\cdot C_2\cdot\lambda(t) / M - \left[\lambda(t) + \nu(t)\right]\cdot A(t) \qquad (1)$$

where $S(t)$ is the t-radionuclide release rate from failed cladding, atom/s; $A(t)$ is the specifical activity of t-radionuclide in the primary coolant, Ci/kg; M is mass of water in the reactor coolant system, kg; $\lambda(t)$ is decay constant of t-radionuclide, 1/s; $\nu(t) = (G/M)\cdot(E-1)/E$ is the t-radionuclide release rate from the primary coolant by clean on the cleaned filter,1/s; G is the water expenditure through of the cleaning filter, kg/s ; E is the cleaning filter effectivning; $C_2 = 3.7\cdot10^{+10}$ decay/(s*Ci) is constant.

The release rate on constant condition is it:

$$S(t) = A(t)\cdot M\cdot C_2\cdot\left[1+\lambda(t)/\nu(t)\right] \qquad (2)$$

As a rule, it is better used by the releasing relativly rate which are determined from parametr $S(t)$ by difine on the radionuclide rousing rate $B(t)$ in the FR:

$$F(t) = S(t) / B(t), \qquad (3)$$

where $B(t) = (W / n_{twel})\cdot C_1\cdot æ(t)$, 1/s; W is the reactor power, W; n_{twel} is number of the FRs in reactor core; $C_1 = 3.1\cdot10^{+10}$ decay/(sW); $æ(t)$ is the t-radionuclide summary releasing by fission heavy nuclear, atom/decay.

This matematical model was used for calculation of releasing relatived rate from failed cladding in the reactor core Nuclear Power Plant - 2 " Lovisa" (Finland) [2]. The dinamic development of FRs leakage is reflected in fig.1. It is had meanings of the relasing relativly for different levels of the cladding leakage: 1 - pressurization FRs, when only sourse of the fission product appearance in primary coolant are turned up the uranium fission processes on outside surfase of FRs; 2 - once leaking FR in the development stage of gas and iodine leak; 3 - once leaking FR with gas and iodine leak; 4 - two leaking FR what's more once FR - with gas and iodine leak and other - with claddihg leakage and pellet-water interaction. Under the circumstances for the short lived radionuclides ^{132}I and ^{134}I the release rate was increased strong (curve 4).

The stowing regularity give confidence for saying that the existing methods of cladding leakage degree assess by the short lived and specific activity balance based on real the releasing process of fission products from cladding leakage. By further development this methods could be improved quality of the assess

Relative Release Rate of Iodine Nuclides
out of Leaker Fuel Rods
(2 Unit Loviisa, Finland)

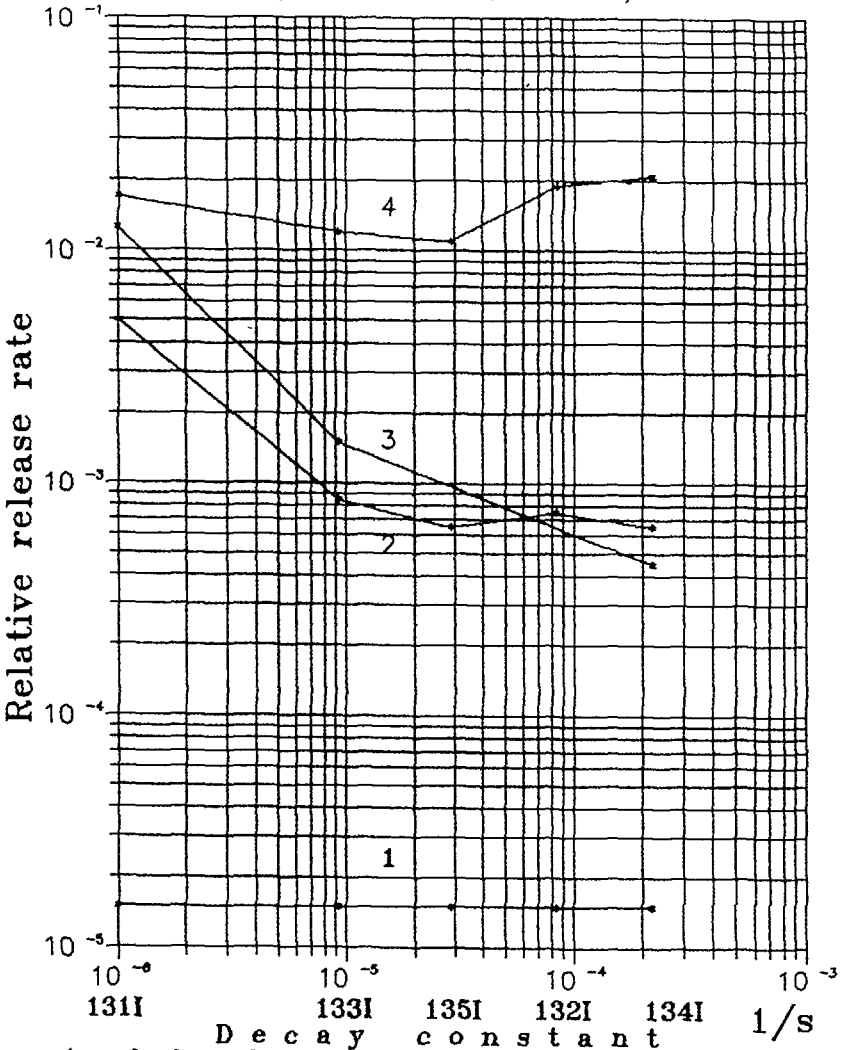

1 – leak–tight rods; 2 – measured 05.03.87;
2 – measured 06.03.87; 4 – measured 24.07.89.
Fig.1

Release Rate of Iodine Nuclides out of
Leaker Fuel Rods in Primary System of
RBMK Reactor

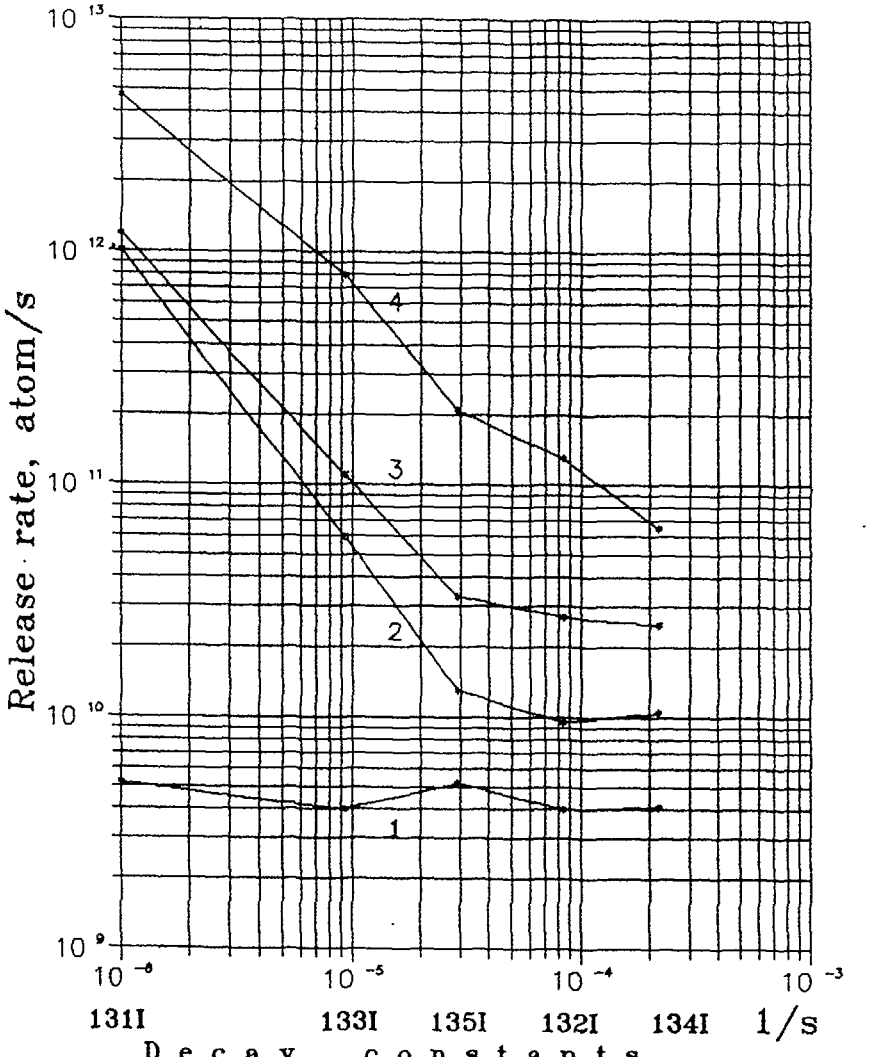

1 – leak–tight rods; 2 – leaking of 1st Degree;
3–leaking of 2 and 3 Degree; 4–leaking of 4 Degree.
Fig.2

and calculated quantity on reactor core the FRs with gas and pellet-water type failure.

It will be noted that researchs of the activity fission products on primary coolant are contemporary for learning of FR failure process in constant and change conditions of operation (by the reactor power changing).

In particular the such measurement was maked on NPP "Loviisa " [3] and showed two manner of FRs failure development: 1 - quick increasing of activity and seting of activity level smaller of peak activity; 2 - quick increasing of activity in 5/10 of magnitude and seting of activity level smaller of peak activity for 15/45 o'clock. It will be noted that sometimes the iodine and the gas activitys were increase quick for time, in other case - the iodine activity was increase only later the delay period.

The showing of regularity is characteristic of for reactors RBMK that is showing in fig.2 [4].

2. Structural-Dinamic Analysis of Damage Reasons

2.1 The Damage Mechanisms and Block Diagram of Analysis

However, the knowledge of FRs failure process, of cladding leakage degree and of FRs failure development is not enough for failed cladding development prediction. It possible only in a way *establiching of mechanism* and reasons which is defined of failure process.

Analysis of damage reasons of the water coolant FRs with zirconium alloy cladding was showed that is know nine damage mechanisms. The design reason of FRs are determined possibility constriction of cladding, denselyty of fuel pelletelongation and buchling of fuel elements and fretting-corrosion. The technological deficiencies are determined folloing a damage mechanisms - inner hydriding, different of pellet enrichment and welding defects. The outward corrosion which is increased from deposit of corrosion products on the clad FRs and mechanical

Block Diagram of Information Processing under Fail-Safe Control of Fuel Assemblies

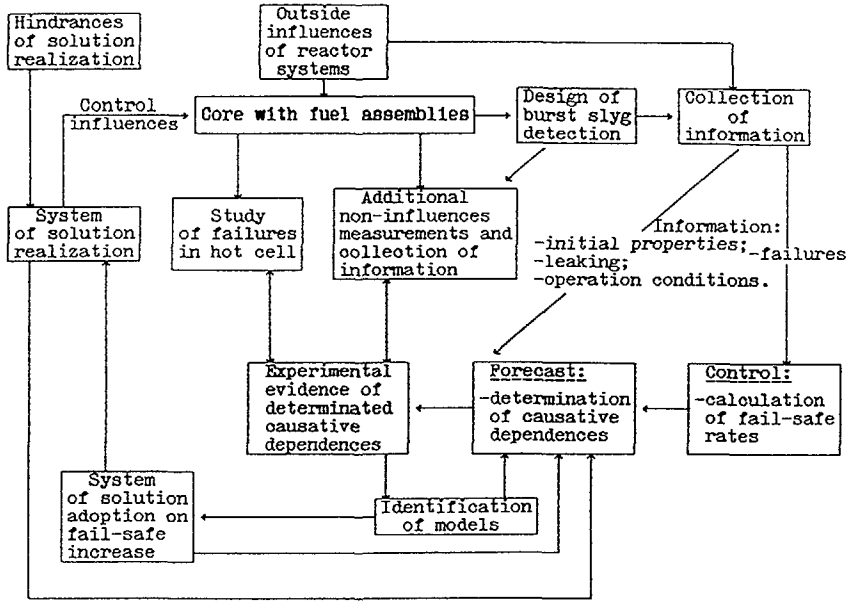

Fig.3

interaction of fuel and clad which is intensity of fuel fission products.

On fig.3 is showing block diagram of information processing under analysis of FRs reasons. The using this block diagram are make it possible to establich of reasons regularitys of parameters values which is characteristic of FR- failure degree, whith similarity of parameters values of real quality and FRs operation conditions.This method are have the systematic analysis which are allowed to influence on FRs work include the action of relatively constant factors and of dinamic factors which is changed in time. It is gived the FRs defects development prediction possibility and to choose and to change a parameters, what are decreased the FRs failure number.

Table 2

The Basic Mechanisms and Causes for Failure of Fuel Element Claddings from Zirconium Alloys in Water-Cooled Reactors

Mechanisms for Failure	Causes		
	Construction	Fabrication	Operation
1	2	3	4
Clad collapse under effect of fission product gases (FPG) and pressure of coolant (PWR)	-differential pressurized; -relation of wall thickness to diameter; -firstling local circularity; -gap with fuel pile.	-size of grains; -microstructure of metal and impurity elements; -head-end cold deformation; -annealing regime; -mechanical properties.	-temperature; -neutron current.
Pellet densification leading to reduction of heat-remov and local pulses of power (PWR,BWR)	-density of pellets; -microstructure of pellets.		-temperature; -neutron current.
Fuel rod/fuel assembly growth and bowing leading to local limitation of coolant flow, reduction of heat-transfer and magnifing cladding corrosion (PWR)	-mituality of fuel rods and spacer grids; -distance between spaser grids; -moment of inertia for cladding axial section; -pressing(widening) force; -thickness of cladding.	-creep and elongation of claddings.	-gradients of temperature and neutron current.
Clad fretting (BWR)	-sizes of fuel rods -distance between spaser grids; -physical and electrochemical properties of contacting metals; -load at contact interface.		-turbulence and pulses of coolant pressure (frequency, amplitude, a general number of vibration circuit); -corrosion environment.

Continuation of Table 2

1	2	3	4
Local hydriding of ZR (PWR, BWR)	-presence of weldes and zones of their heat influence.	-leaving of moisture and organic substance in fuel; -impurities of chemical catalysts neutralizing protection properties of oxide film	-termodiffusion of hydrogen to greater cold walls; -decontamination of oxides under PSI; -lessen oxygen quantity lower of critical size.
Enrichment errors (BWR)		-lask of γ-scanning of fuel pins.	
Welding defects (PWR, BWR)		-faulty welds are missing to control	
Outside corrosion is intensifing crud/scale deposition corrosion products on fuel rod cladding surfaces (BWR)		-outside and inside dirty of metall for nitrogen and oxidate deposits; -non-optimum thermal process.	-temperature; -time; -thickness of oxide film; -neutron current; -chemical properties of coolant; -heat current; -boiling regime; -deposits of Fe,Cu,Si -materials of circuit
Mechanical pellet/cladding interaction (PCI) is intensifing effect of fuel fission product (PWR, BWR)	-density of pellets; -microstructure of pellets.	-peculiarities of pellet fabrication technology.	-cracking of pellets; -creep of cladding; -lessen gup; -burnup of fuel; -level of linear power under chugging; -speed of linear power increase; -time of functioning under big power; -air of transient regimes; -namber of cicuit; -stress corrosion cracking in effect of fission product.

2.2 The Fuel Failure Characteristics at RBMK. Analysis of Damage Reasons

The design of reactors RBMK are allow in every assemblie and unloaded them from reactor immediate in time of work. On exemple of experience RBMK may have desided problems of cladding defects development prediction.

Discovering of FAs with the FRs failure, sistematic observation for them using methods of the cladding bak-tighness monitoring and comparing results of observation with results of the primare coolant sample radio-chemical monitorings and with changing of the gas fission products (GFPs) in steam of the separator-drums are allowed to distinguish several stages of FRs failure. It is haved the events with gradually development of cladding defects and with quick development of defect sizes which is accompany sharp of the GFPs activity increasing in the steam separator-drums. Based on this observation, of FAs operation experience, of FRs failure degree definition by experimental values of monitoring systems and of FAs inspection results are maked the classification of the cladding defect values in depending on failure degree [5].

The fuel failure characteristics of the RBMK-1000 FRs are introduced in tabl.3. Analysis of FAs distribution with FRs

Table 3

Descriptions and Values of Radiation Parameters for RBMK-1000 Fuel Assemblyes (FAs) with Different Leaking Degree.

Title and Size up of Parameter	Leak-Proof FAs	Leaking Degree				
		1st Degree POINT DEFECT, MICROCRACK	2nd Degree CLOSED MACROCRACK	3rd Degree OPEN MACROCRACK	4th Degre DEVELOPED DEFECT	5 Degree SECOND LEAKEGE DEFECT
1. Description of defect	There is not defect	Gas and iodine leaking	Leakage of cladding	Pellet-water interaction	Pellet-water interaction. Destruction of pellets in fuel element	Either second in either first defect from 1st to 4 Degree
2. Sizes of probe away design detectors At, imp./s	0-100	200-1000	1000-2500	2500-5000	2500-5000	>5000
3. Specific activity of radionuclides in primary coolant, Cu/kg:						
- $^{131}I, ^{132}I, ^{133}I, ^{134}I, ^{135}I$	10^{-8}	$(1,1-1,3)\times 10^{-6}$	$(1,2-2,0)\times 10^{-6}$	$2,0\cdot10^{-6}$	$(0,8-1,0)\times 10^{-5}$	Any from 1st leaking Degree to 4th Degree.
- ^{131}I	$2\cdot10^{-9}$	$4\cdot10^{-7}$	$4,5\cdot10^{-7}$	$6\cdot10^{-7}$	$(0,6-1,7)\times 10^{-6}$	
- ^{239}Np	is not	is not	is not	$(3-4)\cdot10^{-7}$	$(3-4)\cdot10^{-7}$	

lailure by GFPs activity decreasing effect after them inloadeding from reactor core (fig.4) and comparing with results of classification are allowed to make folloing conclusion. The development of failures from gas and iodine to macro-failures by the GFPs activity increasing in the steam separator-drum to 2500 imp/s are occured apparently without water geting under clad. Open pellet-water interaction and following dectruction of fuel are due to second distribution peak from 2500 to 5000 imp/s.

The FR failure with unloadeding effect over 5000 imp/s are corresponded always sharp the GFP. activity sharp increasing. However, in this case the activity increasing are not occured frequently by the activity increasing another radionucleus that is haved with the FR failure 4-degree (tabl.3). Therefore, the GFP activity increasing over 5000 imp/s are connected with appearing the FR second through-wall failure at certain distance from first. Appearing second failure is leaded to increase of the GFP short half-life leacage from cladding because of the pressure differance along FR. It case,if first and second failures have level of gas leak only the steam phase is

Distribution of Discharging Leaking Fuel Assemblies with 2,0% Concentration (n) by Decrease Activity Effect in Steam Separator-Drums (SSD) after Discharge (ΔA_{SSD}) (Kursk NPP)

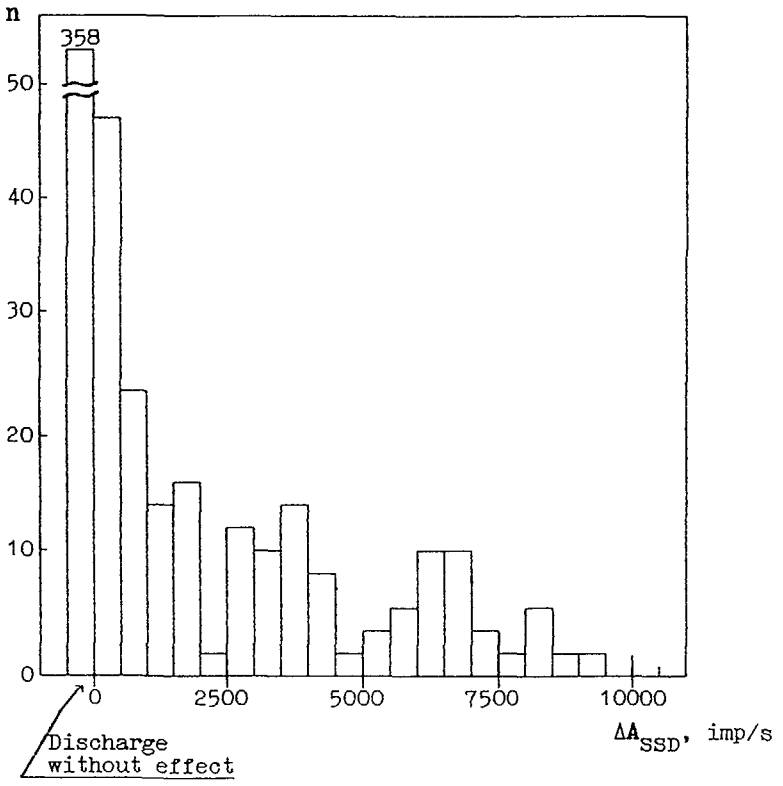

Fig.4

contacted with fuel and it is contacted with fuel and it is not leaded to fuel destruction and leakage of hard fission products in reactor system.

The probability curve of work without failure and of assemblies RBMK-1000 failure intensity, which is determined in moment of FRs failure discovering is showing in fig.5. Analysis this curve by realibility theory and structural-dinamic analysis of failure course was allowed make the conditional classification of the FRs failures mechanisms.

Cladding leakage in burnhap interval to 300 MWd/FA is stipulate for initial manufactoring defects and in burnhap interval from 300 to 900 MWd/FA-with inner hydriding process. Cladding leakage in burnhap over 900 MWd/FA is defined of operation factors and besides is taked please of failure mechanisms.

Probability of Functioning without Leaking (P′) and Leaking Intensity (λ′) of Fuel Assemblies (FAs) at the 1st and 2nd Units of Kursk and Chernobyl

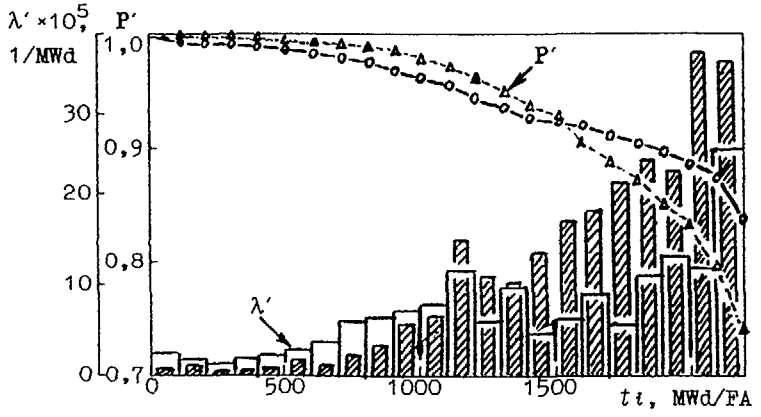

Concentration: 1,8% ▨, – –Δ– –; 2,0% □, ——o——.

Fig.5

The first mechanism is determined of the corrosion products large-scale particle separation along the primary reactor system horizontal collectors for inlet to core canal. Particles is accumulated in reactors under them interruption for repairing work fulfiment. They is precipitated under liffing reactor power on FRs, which is coolant from the collector final share. The accomulation of the corrosion product large-scale particle is took plase in presense the coolant raising mixing (on the spacer glids and on the FAs entrance). In this plase is realised possible the wick-effect of aggresive admixture concentration of water (chlorine - ione alcali) and the conception of cladding uncer corrosion local process. It may be leaded to the fuel leakage for two-three years.

The second operation mechanism of failed cladding is determined by mechanical interaction of fuel and clad, that is due to the energy control deficiency, to transients expenditure oscillation through of technological canal with FA.

Cladding leakage over 1500 MWd/FA may be connected also with FR wear, that is determined of any mechanisms combination of failed cladding.

2.3 Conditional Probability of Cladding Failure Development

From the showing classification is calculated the conditional probability of cladding failure development for worked interval, which is connect with fuel leakage suitable mechanisms (fig.6-9).

The FA refusal probabilitys becouse of them failure and unload from core in burnhap intervals 0-300 and 300-900 MWd/FA is reached 70% (fig.6,7).The fuel leakage in this work intervals is connected with the FRs construction and origin in regions of strains concentration on FR cladding and of cover welding seams, which is plased at core centre. That is why of the FA intensive refusal at once after them failure, when take plase the increasing velositys of defects development in region of first defect (curves 2,3). When moisture penetreting into cladding and hydrogenation in region of welding seams is appeared grate

Failure Probability (F) and Failure Intensity (λ) of Fuel Assemlies (FAs) on Condition of their Leaking under Burnup Interval t_p (0-300) MWd/FA

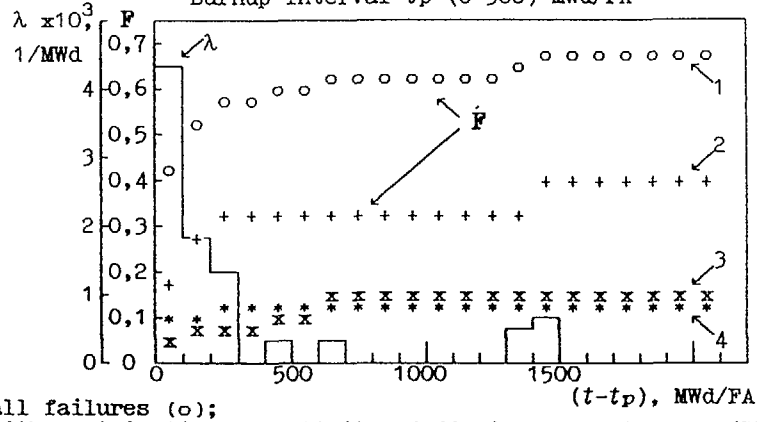

1-all failures (o);
2-with contribution to activity of fission product gases (FPG) in steam separator-drum (SSD) (0-2500) imp/s (+);
3-with contribution to activity of FPG in SSD (2500-5000)imp/s (x);
4-with contribution to activity of FPG in SSD ⩾ 5000 imp/s (*).

Fig.6

Failure Probability (F) and Failure Intensity (λ) of Fuel Assemlies (FAs) on Condition of their Leaking under Burnup Interval t_p (300-900) MWd/FA

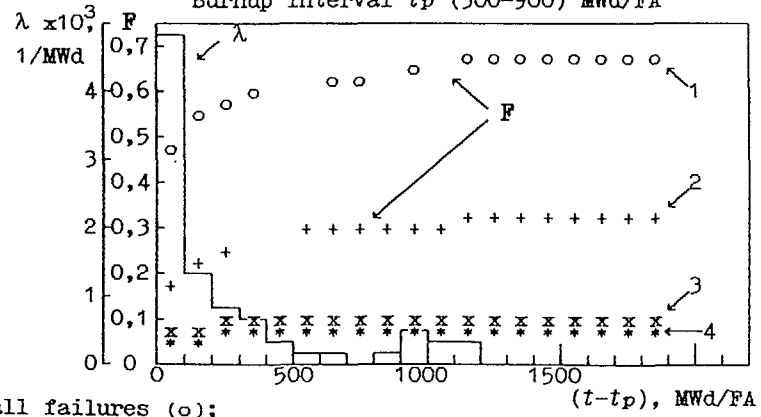

1-all failures (o);
2-with contribution to activity of fission product gases (FPG) in steam separator-drum (SSD) (0-2500) imp/s (+);
3-with contribution to activity of FPG in SSD (2500-5000)imp/s (x);
4-with contribution to activity of FPG in SSD ⩾ 5000 imp/s (*).

Fig.7

Failure Probability (F) and Failure Intensity (λ) of Fuel Assemlies (FAs) on Condition of their Leaking under Burnup Interval t_p (900-1500) MWd/FA

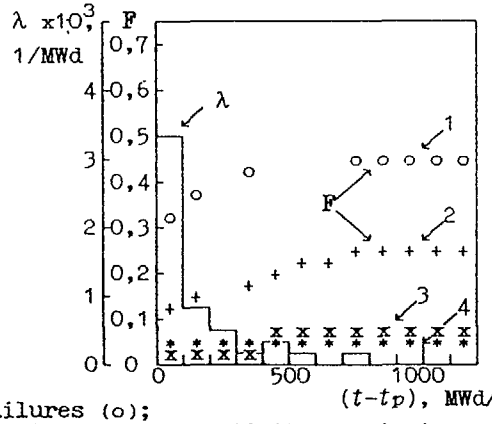

1-all failures (o);
2-with contribution to activity of fission product gases (FPG) in steam separator-drum (SSD) (0-2500) imp/s (+);
3-with contribution to activity of FPG in SSD (2500-5000)imp/s (x);
4-with contribution to activity of FPG in SSD ⩾ 5000 imp/s (*).

Fig.8

Failure Probability (F) and Failure Intensity (λ) of Fuel Assemlies (FAs) on Condition of their Leaking under Burnup t_p ⩾1500 MWd/FA

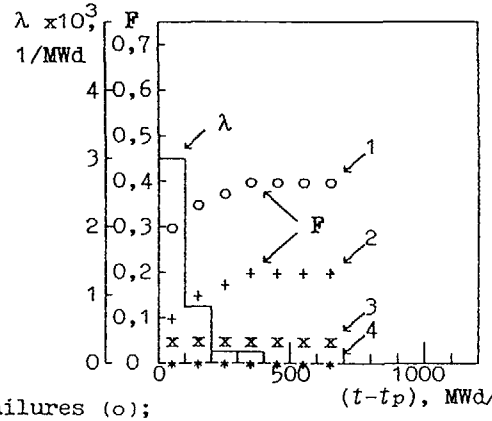

1-all failures (o);
2-with contribution to activity of fission product gases (FPG) in steam separator-drum (SSD) (0-2500) imp/s (+);
3-with contribution to activity of FPG in SSD (2500-5000)imp/s (x);
4-with contribution to activity of FPG in SSD ⩾ 5000 imp/s (*).

Fig.9

probility of second defects on some distance from the first defect (curve 4).

The FA refusal probabilitys by burnhap intervals 900-1500 MWd/FA and above 1500 MWd/FA (fig.8,9) is not increased 45% and 40% accordingly. The defect development probability of gas leak (curve 2), of pellet-water interaction (curve 3) and of second defects (curve 4) is being considerably smaller. The FR cladding leakage becouse of unser local corrosion is not had of reasing strains and it is possible to propose, thet the velosity decreasing development of second defects is discovered exactly for this failure mechanism. On the contrary, under mechanical interaction fuel and clad is increase the strains concentration in plases of failure and it is appeared the crack. Therefore, the second defects development on failed cladding under the burnhap over 900 MWd/FA is took plase under the first defects becouse of the mechanical interaction fuel and clad.

It must be borne in mind, that at least mechanisms and factors of beginning and of the cladding defect development is connected with the metal state in defect. region however it is not defened them. The defect development after failure is determined also possibly of moisture penetrating under cladding, which is depend on the trancients operation number and the cooling degree of core under the reactor stop. It is being the possibility to the second defects beginning and the second defects development in region of first defect becouse of inner hydrogenation.

In conclusion is added, that the FRs with gas leak defects may be quite opereting, that is provided of the them state monitoring possibility and of the defect development prediction possibility operation choosihg. The FA operation with the greater cladding defects is limited and them unloading is as a rule regulated of standardized documents.

REFERENCES

[1] Nuclear safety rules for NPPs. (Rules and standart at atomic power engineering) M.:EAP,1991. - 60p.

[2] Moisio J.M. et.all. Experience of Operation with Leaking Fuel at Loviisa NPS an Examination of Leaking Assembly //International Topical Meeting "Fuel for the 1990's",Ovinion, France, April 1991. - Proceeding, Vol.1, 465-477.

[3] Moisio J.M., Terasvirta R.P.VVER-440 Fuel Performance at Loviisa // Jornal of ENS. - Nuclear Europe Worldscan. - NO.1/2 January/February 1991,9-10.

[4] Panov E,A. Practical Gamma-Spectroscopy at Nuclear Power Plants. -M.:EAP,1990. - 200p.(Library of NPPs woker; Vol.28). ISBN 5-283-03838-6

[5] Panov E.A. Fuel Rods Leakadge Degree Classification. Fission Products Exit Model from Fuel Rods Failled Cladding Characteristics of Defects // NPPs Operation Level Perfection. -M., 1989. -p.207-219

OPERATION AND RADIATION MONITORING OF WATER COOLED REACTORS WITH FAULTY FUEL RODS

Yu.M. SHESTAKOV, E.A. PANOV
Research Institute for Nuclear Power Plant Operation,
Moscow, Russian Federation

Abstract

Typical operation peculiarities of fuel assemblies (FAs) with faulty fuel rods of Soviet pressurized water reactors (VVER) and one-circuit pressuretube boiling water reactors (RBMK) are addressed. Operation of FAs with faulty fuel rods is considered for steady state plant operation, for transients and shutdowns. The methods of radiation monitoring of rod cladding bak-tightness in the course of operation, radiation leak-tightness criteria and the creed for discharging failed fuel rods from reactor are considered. General reliability indicators describing fuel element cladding leak-tightness in the core and criteria of current plant radiation safety are presented. Possibility to solve the problem of choosing optimum operation regime in the presence of failed fuel rods in the core is considered.

1. VVER Fuel

1.1. Burst Slyg Detection

Burst slyg detection (BSD) of VVER type FAs is made during the preventive maintanance. Water sumplings were being taken away without defuelling fuel rods out of core in the initial period of WWER type reactor operation. Then FAs were become to load into canned casks with water being in fuel pool or refueling machine with aim to enhanced of sensibility. Water sumplings were being taken away after being of FAs in casks [1, p.190].

Presence of defects in fuel rod claddings is determined results of fuel rod cladding leak-tightness testing (LTT) during reactor operation and after their defuelling from core in LTT fluid-sampling apparatus at present (table 1).

1.2. Radiation Criteria of Fuel Rod Leaking and the Creed for Discharging Failed Fuel Rods (Table 1)

Fluid-sampling apparatus and FAs are washed from depositions of fission and corrosion products with aim to find all FAs with leaking fuel rods including defects of "gas leak" type. After that water circulates in closed circuit of fluid-sampling apparatus with five minute cycles under differential pressure in fuel cask and water samplings are taken away (table 1). Activity values (A_j) of choice nuclides in samplings for group of studied n-FAs are re-determined to the moment of reactor shutdown (A_j).

Mean value of activity ($\bar{A}$) and standard deviation (σ) are determined:

$$\sigma = \sqrt{\sum_{j=1}^{n}(A_j-\bar{A})^2/(n-1)} \qquad (1)$$

If specific activity of choice nuclide (^{131}I) overbalances mean value of activity for group of FAs greater than to 3σ and activity of corrosion products (through ^{54}Mn) differes from mean value less than to 3σ, then this fuel assembly is been leaking for VVER-1000 type reactors. If fuel assembly with leaking rod has been found then count is repeated for remaining fuel assemblies with the exception of leaking FAs. Count is repeated until all FAs with leaking fuel rods have been found.

FAs with activity of corrosion products differing from mean value greater than to 3σ are put to the revision test in LTT fluid-sampling apparatus. If through ^{131}I finding of leaking FAs is difficulted, then values of ^{134}Cs and ^{137}Cs specific activities are processed too.

Like criterion of fuel rod leaking is used for VVER-440 type reactors including abroad of our country (table 1).

Table 1

The Methods of Radiation Monitoring of Fuel Rod Cladding Bak-Tightness, Radiation Leak-Tightness and Failure Criteria of Fuel Rods and the Creed for Discharging Failed Fuel Assemblies (FAs) from Reactor are Used for VVER-Type Reactors

Condition of Reactor	The Method of BSD		Reactor Type	Radiation Criteria of Fuel Rod Leaking	The Creed for Discharging FAs. Failure Criteria.
	The Method of BSD Testing	Regim of Measuring			
1	2	3	4	5	6
The reactor operates to stationary power	Control of the fission products in primary circuit water	Water sumplings are taken away	VVER -440	Specific activities of ^{131}I and ^{133}Xe exceed greater than 4/10 times according $3,1 \cdot 10^{-8}$ Ci/Kg and $3,0 \cdot 10^{-6}$ Ci/kg activities through uranium dirt on fuel rod claddings	Failure of reactor through radiation safety function: activity of dried precipitate $\geq 10^{-2}$ Ci/kg every 2 hour past sumpling water
		Continuous current of coolant			
		Water sumplings are taken away	VVER 1000	Specific activities of ^{131}I and ^{134}I exceed greater than 4/10 times according $1,2 \cdot 10^{-7}$ Ci/kg and $5,0 \cdot 10^{-6}$ Ci/kg activities through uranium dirt on fuel rod claddings	Failure of reactor through radiation-safety function: activity of 131-131 iodines sum is $\geq 1,5 \cdot 10^{-2}$ Ci/kg in moment sumpling water
		Continuous current of coolant			
	Section loop monitoring of rod cladding bak-tightness	Continuous	VVER -440	-	-
			VVER 1000		
Changes of power, cum local changes are caused movement of the absorber-type control rods	Continuous control of the fission products (FP) in water of primary circuit and/or preheat section loop monitoring of fuel rod cladding bak-tightness		VVER -440	Increase of activity equal to or greater than 5 times every 30/60 minutes past reactor-down. Increase of latent neutron flux near primary circuit pipes.	-
			VVER 1000		

Continuation of table 1

1	2	3	4	5	6
The reactor had been chuted down at preventive maintetenance	Specific activities of ^{131}I, ^{34}Cs, ^{137}Cs FP and ^{54}Mn corrosion products are measured in cask water of CLTT fluid-sumpling apparatus after washing of apparatus and FAs, and circulating of water by 5 minutes cycles under differential pressure:	Until 40 days past shutdoun: 1-0,3 MPa 2-0,05MPa 3-0,3 MPa -watere sumpling is taken away.	VVER -440	$A_j \geq \bar{A} + K_q \cdot \sigma$, where A_j is choice nuclide activity in sumpling of j - FAs, $\bar{A}$ is mean value of activity for group of tested n-FAs, σ is standard deviation, K_q is Student distribution kvuntil	To momert of reactor shutdown $A_j(^{131}I) \geq 10^{-4}$ Ci/kg
		From 40 days to 7 month. two sumplings past 1st cycle- A'_j past 3rd cycle- A_j		For ^{134}Cs and/or ^{137}Cs $A_j \geq \bar{A} + K_q \cdot \sigma$ (1) and $A_j > A'_j$. If $A_j \sim A'_j$, revision test; if relations maintain, then FAs leaking, in another way-conclusion by(1)	-
		Two sumplings 1st past 0,4 MPa cycle, 2nd past 0,05 MPa cycle.	VVER 1000	If for I: $A_{j2} > \bar{A}_2 + 3 \cdot \sigma_2$ (2) and for ^{54}Mn: $A'_{j2} \leq \bar{A}'_2 + 3 \cdot \sigma_2$ then count is repeated for remaining FAs until all leaking FAs have been found. If $A_{j2} \approx \bar{A}_2 + 3 \cdot \sigma_2$, then results of ^{134}Cs and ^{137}Cs are processed too.	To moment of reactor shutdown: $A_j(^{131}I) \geq 10^{-4}$ Ci/kg

1.3. Fail-Safe Rates (Table 2)

The fail-safe rates describing condition (leak-tight) of reactor 1st protective border had been introduced for assessing of NPPs safety standart in 1991 (Table 2). They are defined activity values of fission products being in primary coolant circuit. The fail-safe rates of fuel rods are determined activities of iodine nuclides are measuring cladding leak-tightness testing system (LTTS) in primary coolant for stable state of reactor and power equal to or greater than 85% of nominal power.

The fail-safe rates of fuel rods in month are determined as mean of measuring activity during month. Rate characteristics for a period greater than one month are determined as mean values of rates in every month.

1.4. Current Radiation Safety Criteria for VVER Power Plants

Month-mean equilibrium specific activity for the iodine nuclide sum PII(I) is radiation rate of fuel rod total leaking.

This value describes halogen (iodine, bromine) release out of faulty fuel rods and it determines leaking degree of fuel rods, putting to dirtting of coolant. If it is reaching critical value $4.3 \cdot 10^{-4}$ Ci/kg, then it is necessary to wath on a weekly basis measuring nuclide composition in primary coolant. On reaching the total iodine nuclide specific activity of $1.0 \cdot 10^{-3}$ Ci/kg, i.e. the second critical level, analysis of the isotopic composition has to be performed on the dayly basis and possibilities of the unit operation without changing of power are studied with a view to decrease rate of specific activity increase. In case of exceeding the limiting level of the total iodine nuclide specific activity, which is equal to $1.5 \cdot 10^{-2}$ Ci/kg, a reactor has to be shut down and FAs with faulty rods have to be discharged.

Table 2

Fail-Safe Rates of Fuel Rods for Assessing of Safety Standard of VVER Units

Title of Fail-Safe Rate	Formulas for Count of Fail-Safe Rates
1	2
1. Mean equilibrium ^{131}I specific activity of primary coolant for stable states of reactor that is normalized to design speed of coolant cleaning - A(131I), Ci/kg	$A(131I)=\frac{1}{n}\cdot\sum_{i=1}^{n}\left(A(131I,t)\cdot\frac{\lambda_{131}+\nu_{СВО}}{\lambda_{131}+\nu_{пр}}\right)$, where A(131I,t) is ^{131}I specific activity of primary coolant for t stable states of reactor that is normalized to design speed of coolant cleaning (Ci/kg); λ_{131} is ^{131}I decay constant, it is equal to $1.0 \cdot 10^{-6}$ 1/s; $\nu_{СВО}=\frac{Q}{M}$ is coolant real cleaning speed for water-cleanup filters (WCF) (1/s), $\nu_{СВО}=0$ if filteres are turned off; Q is coolant flowrate in WCF (kg/s); M is primary coolant mass with exception of water mass in pressure compensator (kg), it is equal to 165 kkg for VVER-440 and it is equal to 214 kkg for VVER-1000; $\nu_{пр}=\frac{Q_{пр}}{M}$ is coolant design cleaning speed for WCF, it is equal to $3.4 \cdot 10^{-5}$ 1/s for VVER-440 and it is equal to $3.9 \cdot 10^{-5}$ 1/s for VVER-1000; $Q_{пр}$ is design coolant flowrate in WCF (kg/s), it is equal to 20 t/hr for VVER-440 and 30 t/hr for VVER-1000.
2. Mean equilibrium ^{134}I specific activity of primary coolant for stable states of reactor that is normalized to design speed of coolant cleaning - A(134I), Ci/kg	$A(134I)=\frac{1}{n}\cdot\sum_{i=1}^{n}\left(A(134I,t)\cdot\frac{\lambda_{134}+\nu_{СВО}}{\lambda_{134}+\nu_{пр}}\right)$, where A(134I,t) is ^{134}I specific activity of primary coolant for t stable states of reactor that is normalized to design speed of coolant cleaning (Ci/kg); λ_{134} is ^{134}I decay constant, it is equal to $2.2 \cdot 10^{-4}$ 1/s; $\nu_{СВО}$, Q, M, $\nu_{пр}$, $Q_{пр}$, n are as well as division 1.

Continuation of table 2

1	2
3. Mean equilibrium iodine nuclide sum specific activity of primary coolant for stable states of reactor - PI(I), Ci/kg	$PI(I)=\frac{1}{n}\cdot\sum_{i=1}^{n}A(I,t)$, where A(I,t) is total iodine equilibrium specific activity of $^{131}I, ^{132}I, ^{133}I, ^{134}I, ^{135}I$ nuclide sum in primary coolant for stable states of reactor (Ci/kg).
4. Mean relative release rate of ^{131}I nuclide out of leaker fuel rods to primary coolant - F(131I), rel.units	$F(131I)=\frac{S(131I)}{B(131I)}$, where $S(131I)=A(131I)\cdot C\cdot M\cdot\frac{\lambda_{131}+\nu_{пр}}{\lambda_{131}}$ is average during month equilibrium release rate of ^{131}I nuclide out of leaker fuel rods to primary coolant (atom/s); λ_{131}, $\nu_{пр}$, A(131I), M are as well as division 1; $C = 3{,}7 \cdot 10^{10}$ dis/sCu is constant; $B(131I)=D\cdot\text{æ}(131I)\cdot\frac{1}{n}\cdot\sum_{i=1}^{n}Wt$ is average during month formation speed of ^{131}I in reactor core (atom/s); $D = 3{,}1 \cdot 10^{10}$ div/sW is constant; $\text{æ}(131I) = 2.774 \cdot 10^{-2}$ atom/fis is cumulative bearing of ^{131}I atoms during fission; Wt is heat power of reactor at t measuremet moment (W).
5. Mean relative release rate of ^{134}I nuclide out of leaker fuel rods to primary coolant - F(134I), rel.units	$F(134I)=\frac{S(134I)}{B(134I)}$, where $S(134I)=A(134I)\cdot C\cdot M\cdot\frac{\lambda_{134}+\nu_{пр}}{\lambda_{134}}$ is average during month equilibrium release rate of ^{134}I nuclide out of leaker fuel rods to primary coolant (atom/s); λ_{134}, $\nu_{пр}$, A(134I), M are as well as division 1; $B(134I)=D\cdot\text{æ}(134I)\cdot\frac{1}{n}\cdot\sum_{i=1}^{n}Wt$ is average during month formation speed of ^{134}I in reactor core (atom/s); $\text{æ}(134I) = 7.176 \cdot 10^{-2}$ atom/fis is cumulative bearing of ^{134}I atoms during fission; C, D, Wt are as well as division 4.
6. Campaign-mean failure rate of fuel assemblies through leaking fuel rods - W, 1/effective day	$W_{ОТ}=N_{ОТ}/E_{эфф}$., where $E_{эфф}$. is fuel-residence live time of unit during its campaign (effective day of heat power); $N_{ОТ}$ is the FAs number with leaking fuel rods of a failure criterion leaking degree these are detected at the end of campaign.
7. Campaign-mean leaking rate of fuel assemblies - $W_{НГ}$, 1/effective day	$W_{НГ}=N_{НГ}/E_{эфф}$., where $N_{НГ}$ is the FAs number with leaking fuel rods of a radiation criterion leak-tightness degree these are detected firstly at the end of campaign; $E_{эфф}$. is as well as division 6.

If month-mean equilibrium specific activities of primary coolant for stable states of VVER-1000 reactors are equal to $1.2 \cdot 10^{-7}$ Ci/kg of ^{131}I and $5.0 \cdot 10^{-6}$ Ci/kg of ^{134}I then all fuel rods in core are canned. For VVER-440 reactors such specific activities are equal to $3.1 \cdot 10^{-8}$ Ci/kg of ^{131}I and $2.7 \cdot 10^{-6}$ Ci/kg of ^{134}I. These activity levels are determined only manufacturing uranium dirt on the fuel rod cladding surfaces. Activity of more longer lived ^{131}I nuclide exceedes 4/10 times mentioned levels on appearing in the core the first fuel rod with beginning "gas-leak" type failures. Increase of the specific activity of more short-half life ^{134}I nuclide arises from next propagation of cladding defects.

Rates of month-mean relative release rate of iodine nuclides out of leaker fuel rods to primary coolant, i.e. F(131I) and F(134I), determine leaking degree of all fuel rodsin core. They were introduced with aim comparing the fail-safe rates of fuel rods in different units and reactor types.

1.5. Peculiarities of Operation of VVER Type Reactors with Faulty Fuel Rods

Depressurization of fuel rods hardly ever takes not place on high manufacturing quality of VVER-440 and VVER-1000 fuel rods as well as stable operation conditions of cores. Less than one or two fuel rods with defects of "gas leak" type are found during one compaign.

Such case appearing one "gas leak" fuel rod has been submited in figure 1. Activity value of more longer lived ^{131}I nuclide approximately equel $7 \cdot 10^{-6}$ Ci/kg and exceedes greater than 4/10 times its specific activity from dirt on the fuel rod cladding surfaces. The specific activity of ^{134}I at 3 unit of Zaporozhye NPP grew also in April/May. This arose from developing of cladding defect in "gas leak" limits.

During the last years high depressurization VVER fuel rods through manufacturing defects was watched only at 4 unit of Novovoronezh NPP (figure 2). Eight FAs with leaking fuel rods were discharged during three campaigns, four of theirs had

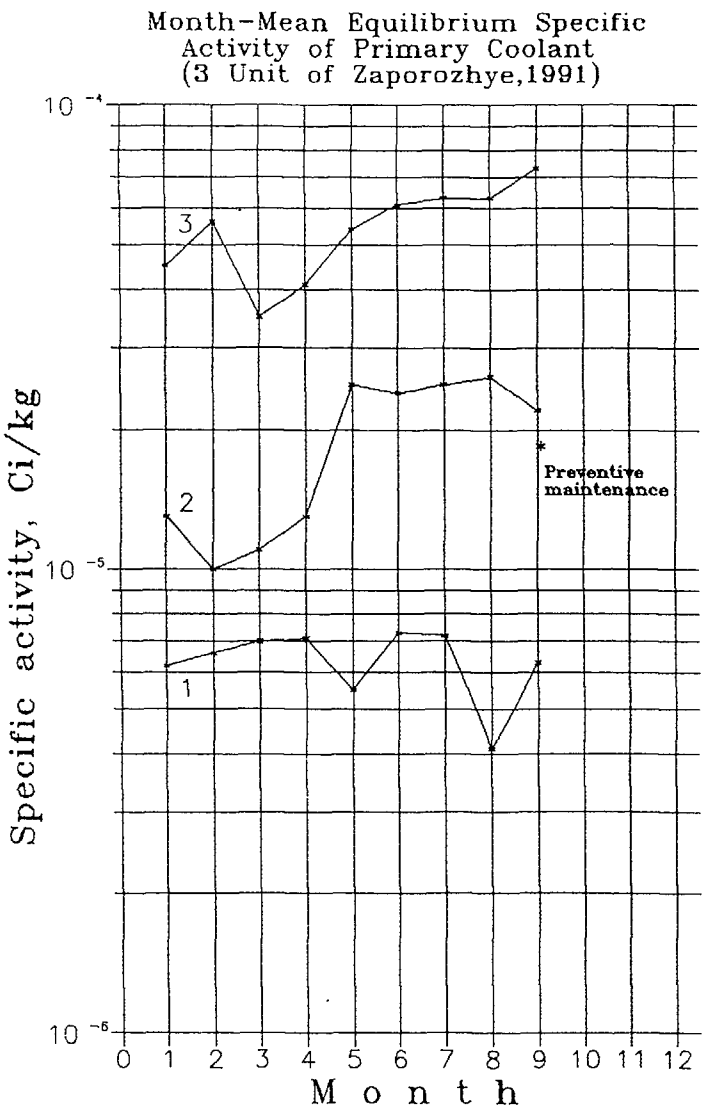

1 - 131 I, 2 - 134 I, 3 - iodine sum;
* - 80 per cent of nominal power.

Fig.1

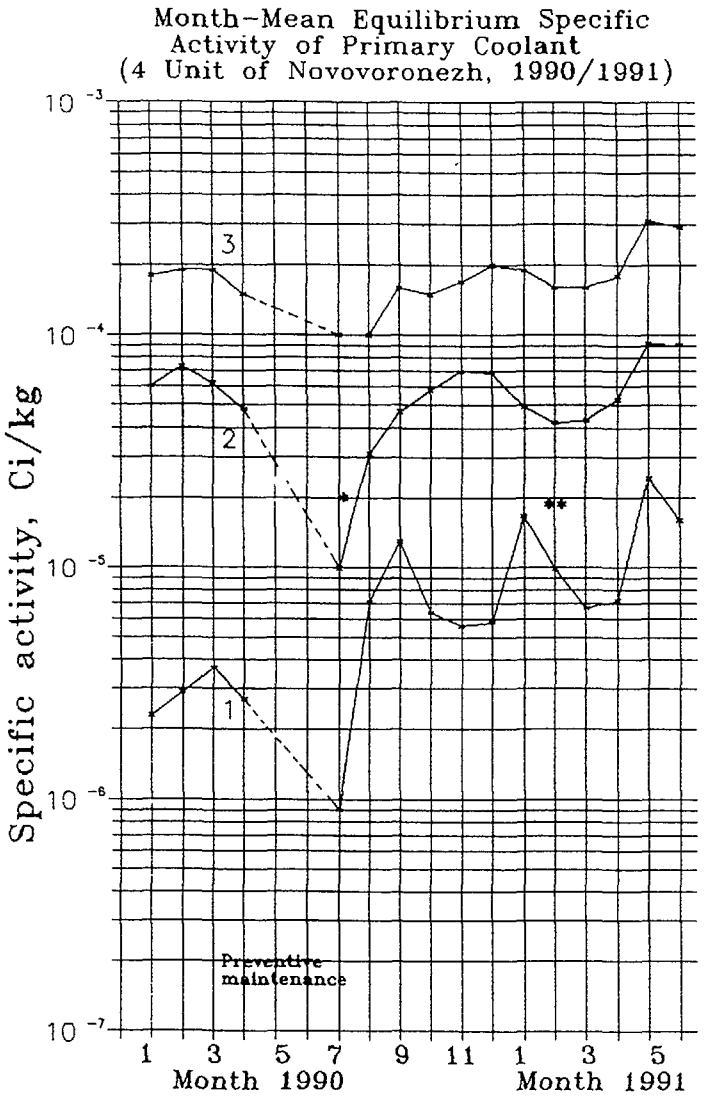

1 - 131 I, 2 - 134 I, 3 - iodine sum;

* - 75 per cent of nominal power;

** - 77 per cent of nominal power.

Fig.2

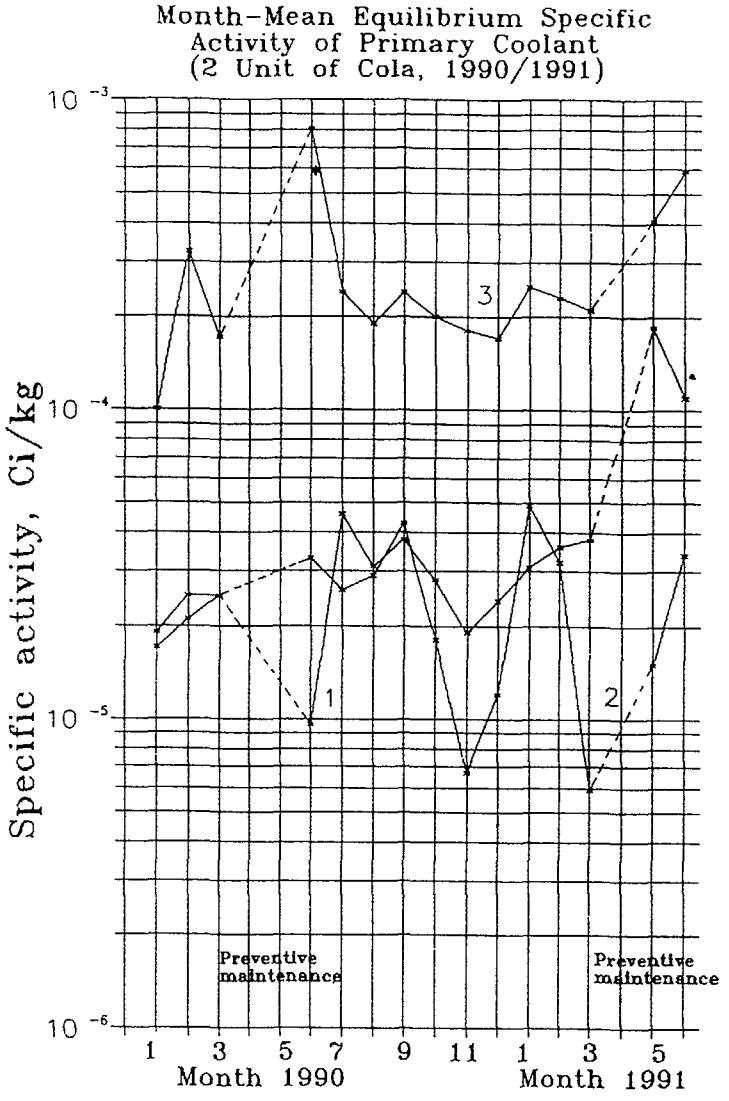

1 - 131 I, 2 - 134 I, 3 - iodine sum;

* - filter of water cleaner is turned off.

Fig.3

the"gas leak" type defects and four of theirs had more large defects. All these FAs belong to one experience party with contact welding of fuel rod claddings and their lids. One FAs of this party was discharged with failure defect of fuel rod after the first campaign in 1989. In 1990 during the preventive maintenance one more FAs of this party was discharged with failure defect of fuel rod. As a result happening depressurization of this party fuel rods two more failure FAs and four FAs with "gas leak" type defects were discharged out of reactor in July 1991.

Faulty of fuel rods by virtue of operation condition violations was observed in 2 unit of Cola NPP (figure 3). In 1990/1991 eight FAs with failure defects of fuel rod claddings were discharged out of the reactor on account of depressurization (5 FAs in April 1990 and 3 FAs in April 1991). At that considerable growth of ^{131}I activity in comparison with ^{134}I activity results from appearing a large quantity of "gas leak" fuel rods. Their depressurization had been connected with deposits of corrosion product crud particles and organic substance. This substance probably have appeared in primary circuit as result destroing of organic filter. High thickness of these deposits is observed on claddings in the region of the lower spacer grids (into the zones with the high flow turbulence). These deposits can to put into nodular (pitting) corrosion and depressurization of fuel rods.

Increase of primary coolant activity was watched in both cases for VVER-440 however the equilibrium total activities of primary coolant were less than $4.3 \cdot 10^{-4}$ Ci/kg, i.e. the first critical level.

Fop the WWER-1000 reactors insignificant increase of fuel rod depressurization was noted only during the first three campaigns of unit operation and it had been connected with non-stationary regime of FAs refueling and enhanced intensities of unit power changes and emergency protection activations in that period. However there were no difficulties with operation of leaking fuel rods because in the main only "gas leak" type defects were noted.

For the VVER-440 reactors difficulties with operation of leaking fuel rods arise in two cases: 1. if it was necessary to deactivate the water-cleanup filteres for supporting reactivity during boron control at the end campaign of unit operation; 2.during unit chutdown in the preventive maintenance and primary circuit depressurization leading to increase of fission product release.

Experimental data show that the fission product activity in primary coolant every 30/60 minutes after power shutdown equal to or greater than 5 times activity size befor reactor shutdown. Continuous measurements of the coolant activity changes in primary circuit of VVER-440 units were carried out systematically in Finland at Loviisa units [2]. These measurements also have shown that during reactor shutdowns doubling times of iodine activity shanged of about 0,5 to 1,5 hours compared to the literature data for the western reactors of 10±3 minutes. The reason for this is reduction the gap from pellet fragments until fuel rod cladding as high as the values approximately equal mean free path of iodine atoms. It increases considarably time of fission product escape out of cladding, in particular it putes into disintegration of short-half life iodine nuclides in case of the first stadium of "gas leak" type defect propagation.

2. RBMK Fuel

2.1. Peculiarities of Burst Slyg Detection

Design of RBMK type reactor makes it possible to conduct some kind of fuel rod leak-tightness testing (LTT). Fission product escape out of faulty FAs is recorded through activity of: 1. fission products carring coolant from each FAs through the correlative pipe of water-steam communications (WSC) (measurements can be carried out during: reactor operation under stationary power and transient regimes; beginning of coolant circulation after reactor shutdown and being present water in canal with FAs without circulation; refueling FAs out of

Table 3

The Methods of Radiation Monitoring of Fuel Rod Cladding Bak-Tightness, Radiation Leak-Tightness and Failure Criteria of Fuel Rods and the Creed for Discharging Failed Fuel Assemblies (FAs) from Reactor are Used for RBMK-Type Reactors

The Method of BSD			Condition of Reactor	Radiation Criteria of Fuel Rod Leak-Tightness (Radiation Monitoring Signal)	The Creed for Discharging Failed FAs from Reactor
Monitoring Design	The Method of Testing	Regim of Measuring			
1	2	3	4	5	6
Any-Canal Monitoring Design	Movement of NaI scintillation detectors along WSC tube rows	"Negativ" 1.1/3.1 MeV	Stationary power	$Z_t \geqslant 1000$ imp/s	$Z_t \geqslant 1000$ imp/s during two weeks or increase greater than 500 imp/s in 24 hr
		0.3/1.5 MeV		$Z_t \geqslant 700$ imp/s	-
		0.5/1.5 MeV		$Z_t \geqslant 600$ imp/s	-
		0.25/0.75 MeV		$Z_t \geqslant 500$ imp/s	-
		Automatic with "negativ" 0.3/1.5 MeV and $E_\gamma \geqslant 4.6$MeV		$\Delta Y_t \geqslant 2\sigma + 2{,}85 \cdot \frac{t}{t_H}$, where σ is standart deviation, t_H and t are rated and real burnup of the fuel assembly	E<1200 MWd/FAs, $\Delta Y_t \geqslant (2.0\text{-}2.5)\sigma$ E>1200 MWd/FAs, $\Delta Y_t \geqslant (3.0\text{-}3.5)\sigma$
	Movement of NaI scintillation detectors along WSC tube rows with quick speed and recording	Integral: 0.25/0.75 MeV	Transient regime	$(Y_t - \bar{Y}) \geqslant 1000$ imp/s, where $\bar{Y}$ is mean for row of 115 WSC tubes	-
		Integral: 0.25/0.75 MeV	After reactor shutdown and being present water in canal with FAs	$A = \frac{1}{2T_H} \cdot \sum_{k=1}^{n} (Y_k - Y_0) \cdot (t_k - t_{k-1})$, $A \geqslant 200$imp/min, where T_H is water exposure time in canal with FAs, Y_0 and Y_k are count rates without and after start coolant circulation during k-passing of detector, t_k is time of k-passing.	-

Continuation of table 3

1	2	3	4	5	6
Any-canal monitoring design	Stop of NaI scintillation detector beside individual WSC tube	"Negativ" 0.25/0.75 MeV	Stationary power	Periodical pulses with $Z_k \geqslant 700$ imp/s	-
		Integral: 0.25/0.75 MeV	After reactor shutdown and being present water in canal with FAs	$B = \frac{K \cdot l \cdot S_{MBK}}{T_H (t_{MAX} - t_0)} \int_{t_1}^{t_2} [Y(t) - Y_0]dt$, $B \geqslant 10^{-7}$Ci/s, where K is coefficient (Ci.s/imp.m^3), l is WSC tube length from core to detector (m), S_{MBK} is area of WSC tube (m^2), T_H is water exposure time without circulation(s), ($t_{MAX} - t_0$) is time from start of coolant circulation until measuring maximum signal, t_1 and t_2 are times of start and finish measuring, Y_0 and $Y(t)$ are count rates without and after start circulation in WSC, imp/s	-
		"Negativ" 0.25/0.75 MeV or 1.1/3.1 MeV	During refueling FAs out of operation reactor	Continuous pulse of gamma-radiation intensity is with $\Delta Z \geqslant 1000$ imp/s above background radiation intensity.	-
Steam sampling out of SSD	Figure and analogue recording	Until and after discharging FAs	Discharging FAs at stationary power	$\Delta\Pi \geqslant 700$ imp/s	-
Any-canal and Steam sampling designs	Stop of detector beside WSC tube. Analogue recording	"Negativ" 0.3/1.5 MeV and analogue signal of SSD changes	Local power decline in region of control rod insertion	Correspondence of FAs power decline for 5/7 % and signal increases of both designs is determined leaking of "gas leak" type.	Correspondence of FAs power decline for 5/7 % and signal decrease of both designs is determined pellet-water interaction
Water sampling out of SFP casks	Water sampling	Specific activities of ^{131}I, ^{137}Cs and ^{239}Np	FAs is in casks of spent fuel pool	After discharging FAs from power core: $A(^{131}I) > 5 \cdot 10^{-5}$Ci/kg, $A(^{137}Cs) > 5 \cdot 10^{-6}$Ci/kg	Failure criterion: $A(^{131}I) > 10^{-3}$Ci/kg, $A(^{137}Cs) > 10^{-4}$Ci/kg, $A(^{239}Np) > 10^{-5}$Ci/kg for any nuclides.

operating reactor); 2. fission product gases (FPG) in steam of four steam separator-drums (SSD) joining trough pipes of WSC in quarters core canals with FAs (during reactor operation under stationary power cum as until and after discharging the FAs from core as the local power changes in the time of control rod insertion); 3. fission product nuclides in coolant of primary circuit; 4. fission product nuclides in water of spent fuel pool (SFP) casks with FAs (table 3).

Low energy gamma-radiation of fission product in WSC coolant is recorded against the radiation background of activation and crud activity of coolant and radiative deposits of fission and corrosion products on the WSC walls. Radiation of short-half life ^{16}N niclide being activation product of oxigen in water by fast neutron especially prevents through considerable Compton distribution in its apparatus spectrum. For canal design of fuel rod cladding leak-tightness testing system signal Z_t of FAs leaking characteristics forms as subtraction, i.e. "negative" counts in low energy range Y_t (main range equals 1.1/3.1 MeV) and high energy range (with gamma-radiation energy

greater than 3.1 MeV) in order to compensate this ^{16}N radiation during operation of reactor in stationary power:

$$Z_t = X_t - k*X_t. \quad (2)$$

where $k=(Y_t/X_t)_{min}$ is minimal value of compensation coefficients chosen out of their values for row of 115 WSC tubes and t (t=1,2,...115) is number WSC tube in row.

2.2. Radiation Criteria of Fuel Rod Leaking and the Creed for Discharging Failed Fuel Rods (Table 3)

Possibilities of leaking fuel rod detection and discharging during RBMK reactor operation conditioned to develop the criteria for leak-tightness location and discharging FAs before they have deteriorated (table 3). Criteria of fuel rod leak-tightness are defined geheral to all RBMK-1000 reactors: 1. for different operation situation and movement methods of LTT detectors along WSC tube rows; 2. for methods locating leak-tightness fuel rods in the time of LTT detector stop beside individual WSC tube; 3. for method locating leak-tightness during discharging FAs; 4. for method of fuel rod leak-tightness final confirmation in spent fuel pool casks with FAs.

The creed for discharging leaking fuel rod out of core and its reasoned operation was determined situations of practical necessary discharging failed fuel rod: 1. for preventing its accident destruction, 2. for limitation of radio-active fission product release to environment in maximum permissible level limits, 3. for preventing radio-active contamination of primary system and NPP facilities.

In the first place criteria for discharging the faulty FAs are definitions for parameter values describing realization one of the tree above-mentioned situations of necessary discharging FAs. In the second place they are criteria for some more effective LTT methods describing location of fuel rods with correlative failure leaking degree. In the third place the leaking criteria of different LTT methods were broken up into preferable order of discharging FAs with maximum leaking degree. *Ad hoc* in case of equal leaking degree for some FAs was determined need discharging FAs with maximum burnup and earlier located fuel rod leak-tightness of the last FAs.

Failures of fuel assemblies as a result depressurization their fuel rods were suggest to consider all leaking FAs with refueling according to mentioned criteria for discharging leaking fuel rods and their failures were confirmed fuel rod cladding bak-tightness tests in SFP casks (table 3).

2.3. Peculiarities of Operation of RBMK Type Reactors with Faulty Fuel Rods

Possibilities of location and discharging FAs with leaking fuel rods during operation of core are made it possible to operate RBMK-1000 reactors with "gas leak" fuel rods almost without risk of their shutdown through radio-active contamination of primary system or exceeding maximum permissible levels of fission product release to environment. Incident in the initial period RBMK-1000 operation happened operating in core at the same time about 250 FAs with "gas leak" fuel rods. At the present time as a result improving the quality of manufacturing and operating fuel assemblies the numbers of "gas leak" fuel rods in RBMK cores are less than 25/50.

Steady-state regime of unit operation is necessary condition for operating FAs with leaking fuel rods. Transient regimes and especially continual shut-downs lead to leakage damps into cladding of leaking fuel rods. Soon after as propagation of the primary defect as appearance of the recurring defects are possible as results internal hydriding and pellet cracking.

2.4. Fail-Safe Rates (Table 4)

For assessing of NPPs safety standart the fail-safe rates of RBMK fuel rods are defined as activity values of fission products in primary coolant as for VVER fuel rods. RBMK reactor is one-circuit and pressuretube boiling water reactors. A few rates are used because of this. They describe possibilities of

Table 4

Fail-Safe Rates of Fuel Rods for Assessing of Safety Standard of RBMK Units

Title of Fail-Safe Rate	Formulas for Count of Fail-Safe Rates
1	2
1. Mean relative activity of fission product gases (FPG) in steam condensate of k-steam separator-drum (SSD) - $\Pi(k)$ and its standard deviation - $\sigma(k)$, imp/s	$\Pi(k) = \sum_{i=1}^{n} \Pi(k,i)/n,$ where $\Pi(k,i)$ is relative activity of FPG in steam condensate of k-SSD on a hourly basis measuring for stable states of reactor (imp/s); n is measurement number at stable states of reactor during month.
2. Unit-mean relative activity of FPG in steam condensate of all SSD - РП(FPG), imp/s	$РП(FPG) = \sum_{k=1}^{4} \Pi(k)/4,$ where $\Pi(k)$ is as well as division 1.
3. Mean equilibrium iodine nuclide sum specific activity in primary system for stable states of reactor - РП(I), Ci/kg	$РП(I) = \frac{1}{n} \cdot \sum_{i=1}^{n} \left[\sum_{k=1}^{2} A(k,i)/2 + \sum_{k=3}^{4} A(k,i)/2 \right] \Big/ 2$ A(I,i) is total iodine equilibrium specific activity of $^{131}I, ^{132}I, ^{133}I, ^{134}I, ^{135}I$ nuclide sum in k- SSD water for stable states of reactor (Ci/kg).
4. Specific activity of ^{239}Np nuclide in system for stable states of reactor - РП(Np), Ci/kg	$РП(Np) = \frac{I}{n} \cdot \sum_{i=1}^{n} \sum_{j=1}^{2} B(j,i) / 2$ where B(j,i) is ^{239}Np specific activity in primary coolant of both loop circuit for stable states of reactor; n is measurement number at stable states of reactor during month.
5. Mean during reactor operation period the failure rate of fuel assemblies through leaking fuel rods - $W_{от}$, 1/effective day	$W_{от} = N_{от} / Е_{эфф}.$, $Е_{эфф}.$ is fuel-residence live time of unit during its operation periods (month, three month, year) (effective day of heat power); $N_{от}$ is the FAs number with leaking fuel rods of a failure criterion leaking degree are discharged during period.
6. Mean during reactor operation period the leaking rate of fuel assemblies - $W_{нг}$, 1/effective day	$W_{нг} = N_{нг} / Е_{эфф}.$, $N_{нг}$ is the FAs number with leaking fuel rods of a radiation criterion leak-tightness degree are detected firstly during period; $Е_{эфф}.$ is as well as division 5.

different fission product fractions to release out of cladding versus types of fuel rod defects. The fail-safe rates of fuel rods for RBMK NPPs are presented in table 4.

The rates of month-mean relative activity of fission product gases (FPG) in steam condensate each of the four steam separator-drums (SSD) - $\Pi(k)$ and unit-mean relative activity of FPG in steam condensate of all SSD - РП(FPG) can are used only as relative characteristics of their trends in unit. With a view to fulfil the IAEA requirements for comparison between values of fail-safe rates of different type NPPs it is necessary to organize metrological normalization of the SSD sampling LTT system and to establish absolute normalized coefficient for measured activity of fission product gases. In this case the radiation rate will assume the form:

$$РПА(FPG) = K \cdot \sum_{k=1}^{4} \Pi(k) \; / \; 4 \; , \qquad (3)$$

where $K=[A(^{138}Xe) + A(^{88}Kr)]/ \Pi(k)$ is normalized connection coefficient for spesific activities - (A) of ^{138}Xe and ^{88}Kr nuclides in primary coolant (Ci/kg) with measured values of the SSD sampling LTT system (imp/s). It is approximately equal to $(3,3^{+2.15}_{-1.3}) \cdot 10^{-9}$ sCi/imp.kg

2.5. Current Radiation Safety Criteria for RBMK Power Plants

Counting result analysis of mean relative FPG activities in steam condensate each of k=1,2,3,4 SSD (imp/s) - $\Pi(k)$, their standard deviations - $\sigma(k)$ and month diagrams of statistical distributions are fixed tasks of: 1. fuel rod leak-tightness control FAs group with single SSD joining through pipes of WSC in quarters the core canals and 2. rapid assessing contribution of this FAs group in FPG release to environment.

If part of the $\Pi(k)$ values overbalance mean of the statistical distribution on month diagram greater than to $3\sigma(k)$, then leaking fuel rods appeared in the core canals of k-SSD. If FAs with these leaking fuel rods were not discharged from

reactor and their operation is lasted, then $\Pi(k)$-mean next month increases greater than to $3\sigma(k)$.

If part of the $\Pi(k)$ values overbalance mean of statistical distribution greater than to 3000 imp/s or $\Pi(k)$-mean next month increases greater than to 3000 imp/s, then depressurization of fuel rod led to failure of "pellet-water interaction" type and destruction of fuel pellets with possibility their release in primary system. It is necessary in time to find FAs with such defects and to discharge their from reactor. Increase of corresponding $\Pi(k)$ values to (2000-3000) imp/s correlates with appearance fuel rod defects with macro-crack and cladding leakege. Increase of $\Pi(k)$ to (200-2000) imp/s correlates with appearanse defects of fuel rod with micro-crack and "gas leak" or "iodine leak" type.

Unit-mean relative activity of FPG in steam condensate of all SSD, i.e. РП(FPG) is relative radiation rate of fuel rod total leaking. It characterizes release of FPG out of faulty fuel rods and determines their release to atmosphere. Critical value of its is to (3000-4000) imp/s. In this case it is necessary to apply all LTT methods for location FAs with maximum defects of fuel rod claddings and theirs discharging from reactor. That is necessary with a view to prevent overbalance of activity release into environment greater than permissible limits and under the necessity shutdown.

Month-mean equilibrium specific activity of the iodine nuclide sum in primary coolant, i.e. РП(I) is radiation rate of fuel rod total leaking. This rate can characterize halogen release out of faulty fuel rods and leaking degree of fuel rod sputting to dirtting of primary system. Specific activity increase of iodine nuclides (especialy short-half life nuclides) with activity limits: for iodine sum to $1.0 \cdot 10^{-5}$ Ci/kg, for ^{131}I to $1.0 \cdot 10^{-6}$ Ci/kg and for ^{134}I to $2.0 \cdot 10^{-6}$ Ci/kg characterizes accident destruction of fuel rod and propagating defects on fuel rod cladding. This leades to pellet-water interaction. In that case it is necessary to discharge FAs with maximum leaking degree of fuel rods.

Specific activity critical value for ^{239}Np nuclide in primary system, i.e. РП(Np) is equal to $4.0 \cdot 10^{-7}$ Ci/kg. It characterizes appearance propagating defect of fuel rod cladding with release of fissible material into primary coolant and accident destruction of fuel rod.

Notation

Descriptions of RBMK fuel rod defects, analysis results of theirs depressurization causes and possibility to solve the problem of predicting defects propagation are presented authors in separate work.

References

[1] Овчинников Ф.Я., Голубев Л.И., Добрынин В.Д. и др. Эксплуатационные режимы водо-водяных энергетических ядерных реакторов. М.: Атомиздат, 1979.

[2] J.M.Moisio and R.P.Terasvirta. VVER-400 Fuel Performance at Loviisa. Journal of ENS. Nuclear Europe Worldscan. NO.1-2 January/February 1991, p.10.

INFLUENCE OF WATER CHEMISTRY REGIMES ON FUEL CLADDING FAILURE IN LWRs

V.G. KRITSKIJ
Research, Design and Process Association 'VNIPIET',
Saint-Petersburg, Russian Federation

Abstract

Some statistical data on cladding failure in the RBMK-1000 and WWER-1000 fuel rods have been collected and studied. A model has been developed, based on the correlation between the quantity of clad defects and water chemistry parameters. The model shows the possibility of twofold reduction in fuel failure rates for some NPPs.

Under normal nuclear reactor conditions some portion of fuel rods develops cladding defects. The probability of cladding failure depends among other factors also on the water coolant quality. In the general case interactions at the coolant-cladding interface result in deposition, corrosion (general and local) and hydriding processes.

Penetrating defects in fuel claddings (clad failure) may be induced by any of the above processes, all of them having one feature in common, however their intensity increases sharply with the clad temperature growth. In addition, the deposition of itself induces the clad temperature growth. The formation of deposits is caused by precipitation of construction material corrosion products (mainly of ferrous origin). Therefore, when analyzing the clad failure probability one should consider complex effect of the deposits formed [1]. The deposition processes in pressurized water (PWR and WWER) and boiling water (RBMK and BWR) regimes obey different relationships; a generalized relationship is, however, possible.

Let,

$$f(n)=f(\Delta T) + f(\lambda) \qquad (1),$$

where $f(n)$ is the clad failure probability; $f(\Delta T)$ is the clad failure probability due to overheating under the influence of water chemistry conditions; $f(\lambda)$ is the probability of manufacture defects.

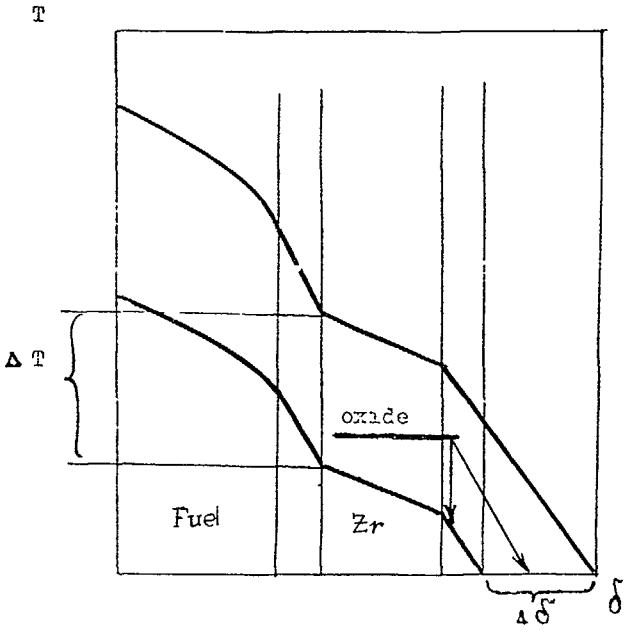

Fig.1. Change of fuel cladding temperature at cladding-coolant interface with surface oxide thickness growth.

Fig.1 shows change in the fuel-clad-coolant interface temperature with the surface oxide thickness growth.

Changing in ΔT with the increment $\Delta\delta$ in the oxide thickness can be described as

$$\Delta T = \frac{q}{\lambda}\Delta\delta, \qquad (2)$$

where q is heat flux and λ is the thickness of thermal conductive layer.

All parameters in relationship (2) vary with time.

We have shown [2], that the precipitation of corrosion products (CPs) from the coolant environment onto the fuel surface may result in the formation of a porous oxide film distinguished for great thermal resistance. The cladding temperature is then defined by the rates ratio of colloids fixation and dehydration as well as compact layer formation processes.

Normally these processes are under the influence of the CP transport rate towards the heat transfer surfaces.

Experimental measurments of the clad temperature growth rate show the period of the temperature stabilization in RBMK-1000 may achieve 10-20 days [2].

Corrosion products coming into the reactor core undergo random distribution, which process results in nonuniform CP deposition over different core areas. The nonuniform CP distribution along the fuel rod length is caused by fluctuations in the thermal physical and chemical properties of the cooling environment, surface and corrosion products. The coefficient of nonuniformity in the CP distribution over the core areas might be due to the combination of occasional factors and is equivalent in essence to a certain coefficient describing extra deposition of CPs on the fuel rod surfaces.

Let

$$n_\tau = f(\Delta T)\ N, \qquad (3)$$

where n is a number of fuel assemblies failed during the time period τ, N is the total number of fuel asemblies in a reactor.

In the physical sense

$$f(\Delta T) = \alpha\ \Delta\bar{T}, \qquad (4)$$

where α is the nonuniformity coefficient, ΔT is the clad temperature growth due to the CP deposition (averaged over the reactor).

From eq.(2) it follows that

$$\Delta\bar{T} = \frac{\bar{q}}{\lambda}\Delta\bar{\delta} \qquad (5)$$

where $\Delta\bar{\delta}$ $f(\Delta m)$ is a function of the tolal amount of CPs entering the core during the time τ.

By combining (2)-(5) we get

$$n_\tau = \alpha\ \frac{\bar{q}}{\lambda_\tau}\ \Delta m_\tau\ N$$

If $\alpha\ \frac{\bar{q}}{\lambda_\tau}\ N \approx \text{Const}$, we have:

$$n_\tau \approx m_\tau \qquad (6)$$

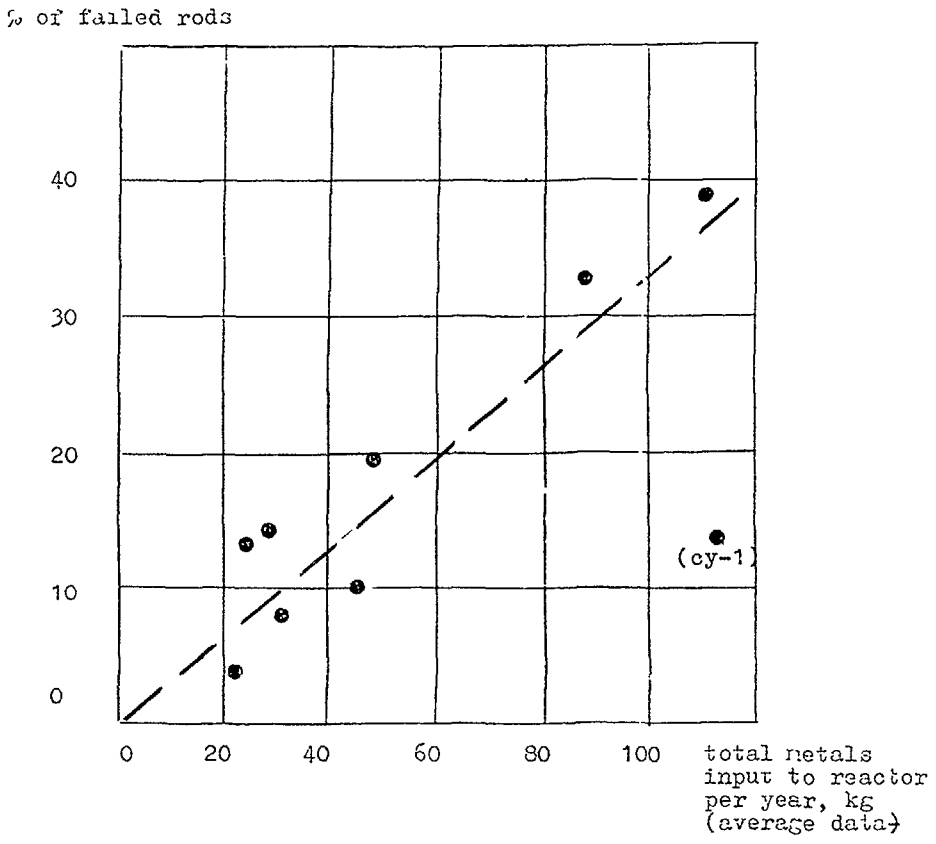

Fig.2. Percentage of failed fuel rods as function of total metals input to BWR reactor /3/.

Hence, one would expect a correlation exists between the failed fuel quantity and that of CPs entering the core (with the feed water in BWRs or accumulated in the primary circuit in PWRs).

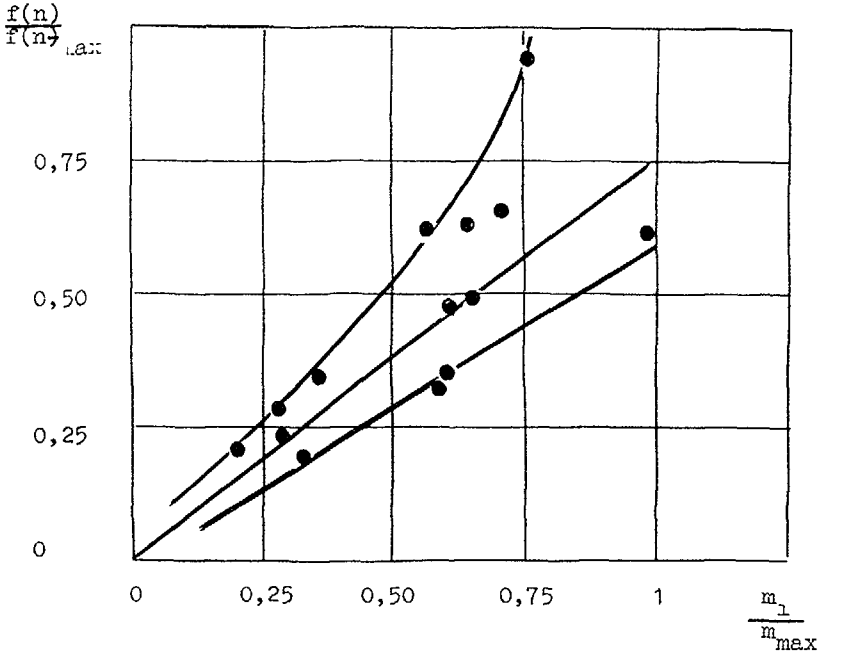

Fig.3. Fuel cladding failure probability f(n) as function of total metals input to RBMK reactor.

Fig.2 shows percentage of failed assemblies discharged from Indian BWRs as function of ferrous impurties transported to the reactor core with the feed water during a fuel cycle [3].

Fig.3 shows a number of fuel assemblies discharged from four RBMK-1000 units during 5 years, plotted as function of the CP quantity transported to the reactor. The data are normilized on the maximum value in the data set.

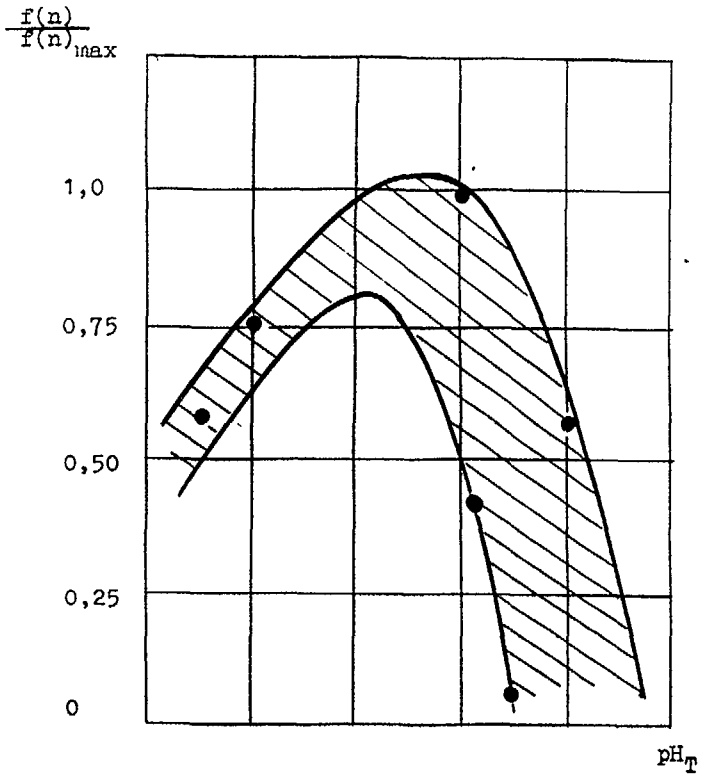

Fig.4. f(n) as function of pH_T for primary circuit of WWER.

It is known [4] that the precipitation rates of CPs in PWRs depend on C_{cp} and $\Delta Fe(T)$.

$$\frac{d\delta}{d\tau} = K_d C_{cp} + K_{d-d} [Fe(T_1) - Fe(T_2)] - R_d \delta, \qquad (7)$$

where δ is the surface concentration of particles, K_d is the deposition coefficient, K_{d-d} is the dissolution-deposition coefficient, Fe(T) - the iron solubility at T; T_1 - the coolant temperature; T_2 - the surface temperature; R_d - the deposit release coefficient.

C and $\Delta Fe(T)$ are functions of pHт. It follows, therefore, that $\delta(T)$ is a complex nonlinear function of pHт. Fig.4 shows a plot of f(n) against pHт, obtained from the data averaged over the 5-year operation of 7 WWER-1000 units.

It follows from Figs 3 and 4, that optimal water chemistry control results in the decrease of $f(\Delta\tau)$. At some power units the intensity of fuel failure can be reduced at least by a factor of two.

References

1. V.I.Solyany, Yu.K.Bibilashvili, G.I.Sukhanov, Yu.V.Pimenov "Some aspects of influence of coolant water chemistry on reliability of WWER- and RBMK- type fuels"/IWGFPT/17. Influence of water chemistry on fuel element cladding behaviour in water cooled power reactors", IAEA,Vienna,1983

2. В.Г.Фрицкий и др. К вопросу о формировании отложений на поверхности твэлов РБМК-1000. А.Э. т.59, вып.6, декабрь 1985, с.405

3. K.S.Venkateswarlu, G.Venkateswaran "Evaluation of and improvements in the performance of zircaloy cladding during and after its residence in water cooled nuclear power reactors"/IWGFPT/24.External cladding corrosion in water power reactors., Vienna,1986,

LIST OF PARTICIPANTS

BELGIUM

H Bairiot
FEX
Lijsterdreef 24
B-2400 Mol

P Deramaix
BELGATOM
Avenue Ariane 7
B-1200 Brussels

C. de Paepe
BELGATOM
Avenue Ariane 7
B-1200 Brussels

CANADA

T.J. Carter
AECL Research
Chalk River Laboratories
Chalk River, Ontario K0J 1J0

CZECH REPUBLIC

O. Bárta
CHEMCOMEX
Azalkova 1137
102 00 Prague

F. Pazdera
Nuclear Research Institute
250 68 Řež nr. Prague

M. Valach
Nuclear Research Institute
250 68 Řež nr. Prague

FRANCE

P. Bournay
Service de la production thermique
Electricité de France
Tour Atlantique – 20e étage
F-92080 Paris – La Defense Cedex 06

A. Brissaud
Service Etudes et projets thermiques et nucleaires
Electricité de France
12-14, avenue Dutriévoz
F-69628 Villeurbanne Cedex

A. Dumont
FRAGEMA/FRAMATOME Division Combustible
10 rue Juliette Récamier
F-69006 Lyon Cedex

C Leuthrot
Direction des reacteurs nucléaires
Departement d'études des combustibles
Commissariat a l'énergie nucleaire
Centre d'etudes nucléaires de Cadarache
F-13108 Saint-Paul-lez-Durance Cedex

D Parrat
Centre d'etudes nucléaires de Grenoble
Commissariat à l'energie atomique
F-38041 Grenoble Cedex

GERMANY

R. von Jan
Siemens AG/KWU
Dept. BT4
Hammerbacherstrasse 12+14
D-W 8520 Erlangen

JAPAN

Y. Hayashi
Nippon Nuclear Fuel Development Co Ltd
2163 Narita-cho, Oarai-machi
Higashi-Ibaraki-gun
Ibaraki-ken 311-13

T Okubo
Sophia University
Faculty of Science and Technology
Kioi-cho 7-1, Chiyoda-ku
Tokyo 102

K Ono
Nuclear Fuel Industries, Ltd
950 Oaza-Noda, Kumatori-cho
Sennan-gun, Osaka

KOREA, REPUBLIC OF

Y H Kang
Nuclear Mechanical Test Department
Korea Atomic Energy Research Institute
P.O. Box 7, Daeduk Danji
Daejeon City

NORWAY

C Vitanza
OECD Halden Reactor Project
Institutt for Energiteknikk
Os Alle 13
N-1750 Halden

RUSSIAN FEDERATION

V G Aden	Research and Design Institute of Power Engineering P O Box 788 10100 Moscow
A D Bakunyaev	Ministry of Atomic Energy Staromonetny per 26 109180 Moscow
Yu K Bibilashvili	Scientific Research Institute for Inorganic Materials St. Rogov 5 123479 Moscow
B.V Budylin	Ministry of Atomic Energy Staromonetny per 26 109180 Moscow
K.P. Dubrovin	I V Kurchatov Institute of Atomic Energy pl. Acad. Kurchtov, 1 123182 Moscow
A.A. Egorov	Ministry of Atomic Energy Staromonetny per. 26 109180 Moscow
A.G Ioltukhovskij	Research Institute for Nuclear Power Plant Operation Ferganskaya 25 109507 Moscow
V B. Ivanov	Research Institute of Atomic Reactors 433510 Dimitrovgrad, Ulyanovsk Region
V.A. Nikolaev	Research and Design Institute of Power Engineering P.O Box 788 10100 Moscow
V.D. Onufriev	Scientific Research Institute for Inorganic Materials St. Rogov 5 123479 Moscow
V N Prosselkov	I V. Kurchatov Institute of Atomic Energy pl Acad. Kurchtov, 1 123182 Moscow
V P Smirnov	Research Institute of Atomic Reactors 433510 Dimitrovgrad, Ulyanovsk Region
I N Vassilchenko	OKB 'GIDROPRESS' Ordzhonikidze Sreet 21 142103 Podol'sk, Moscow Region
I V Zhukov	Research and Design Institute of Power Engineering P O. Box 788 10100 Moscow

SWEDEN

M Grounes	Studsvik Nuclear AB S-61182 Nykoping
L Hallstadius	ABB Atom AB S-721 73 Västerås
L Lundholm	ABB Atom AB S-721 73 Västerås

SWITZERLAND

R.W. Stratton	Paul Scherrer Institute CH-5232 Villigen
G Bart	Paul Scherrer Institute CH-5232 Villigen
S Lundberg	Kernkraftwerk Leibstadt AG Leibstadt CH-4353 Leibstadt

UNITED KINGDOM

R J. White	Nuclear Electric Berkeley Nuclear Laboratories Berkeley, Gloucestershire GL139PB
J.R. Stanbridge	British Nuclear Fuels plc B-382 Springfields Works Salwick, Preston, Lancashire PR4 OXJ

UNITED STATES OF AMERICA

A A. Strasser	The S.M Stoller Corporation 485 Washington Avenue Pleasantville, N Y 10570

UNITED STATES OF AMERICA (cont.)

H.W. Wilson — Commercial Nuclear Fuel Division
Westinghouse Electric Corporation
P O. Box 355
Pittsburgh, PA 15230-0355

INTERNATIONAL ATOMIC ENERGY AGENCY

J.L. Zhu — Division of Nuclear Fuel Cycle and
Waste Management
International Atomic Energy Agency
P O. Box 100
A-1400 Vienna, Austria

G. Sukhanov
(*Scientific Secretary*) — Division of Nuclear Fuel Cycle and
Waste Management
International Atomic Energy Agency
P.O. Box 100
A-1400 Vienna, Austria